AN EXPERIMENTAL STUDY AND FINITE ELEMENT ANALYSIS OF PUNCHING SHEAR FAILURE IN STEEL FIBRE-REINFORCED CONCRETE GROUND-SUSPENDED FLOOR SLABS

WAFA ABDELMAJEED LABIB

School of the Built Environment

Liverpool John Moores University, Liverpool, UK

A thesis submitted in partial fulfilment of the requirements of Liverpool John Moores University for the degree of Doctor of Philosophy

August 2008

TABLE OF CONTENTS

LIST OF TABLES

LIST OF FIGURES

DECLARATION

This is to certify that;

1. This thesis embodies the author's research
2. The originality (and contribution to knowledge) rests solely with the author

Signature of candidate:.....

Date:.....

ACKNOWLEDGMENTS

I would like to express my deepest gratitude to my supervisor Dr. Nicholas Eden for his invaluable guidance, comments, endless encouragement and his patience in correcting both my stylistic and scientific errors throughout the project. I am also grateful to Dr. Glynn Rothwell and Dr. Andrew Ross for their professional guidance, invaluable advice and continuous support.

I would like to extend my thanks to Dr. William Atherton and other technical staff in the concrete and structural laboratory of the department of Built of Environment for their helpful technical support and ready assistance during the experimental work.

A special thank to my parents for their endless support. You never gave up on your dream for me, your encouragement, love, determination and sacrifices over the years have made it all possible, and whose blessings will always light my heart. Thank you for always praying for me and my family, which helps us remain focused and enjoy the goodness that God has given us. I am also grateful to my brothers and sisters, for their love and unfailing support during this research.

I am grateful to my father and mother in-law, whose kindness and assistance on numerous occasions will always be cherished.

Above all, I would like to express my deepest love and gratitude to my husband for his love, understanding, encouragement and support he always offered. I am so blessed to have you in my life. Your generosity, wisdom and untiring support enable me to put my best efforts into this research. I will never forget your kindness, care, and invaluable advice throughout my work and life. You have always given me a push when I need it most. To you I will always be indebted. "***From the day that we met I knew you were the one***".

I am also grateful to my loving baby who allowed mom to follow her dreams, I'm all yours now.

ABBREVIATIONS

The following notation is used throughout this thesis. When more than one meaning is being assigned to a symbol, the correct definition will be evident from the context in which it is used. Those symbols not defined below are explained in the relevant part of the text

ACI	American Concrete Institution
ACIFC	Association of Concrete Industrial Flooring Contractors
ASTM	American standard for testing material
BS	British Standard
D	Diameter of column stub
d	Fibre diameter
E_c	Modulus of elasticity of concrete
f'_c	Concrete compressive strength
f_{cm}	Cylinder compressive strength
f_{ct}	Tensile strength
f_{cu}	Cube compressive strength
FEA	Finite Element Analysis
f_{sp}	Split-cylinder strength
h	Slab thickness
k	Modulus of subgrad reaction
l	Fibre length
l/d	Fibre aspect ratio
l_c	The span length between the edge of the columns
l_o	The span length from centre to centre of the column
LVDT	Linear Variable Differential Transformers
OPC	Ordinary Porlan Cement
P	Concentrated nodal force vector
PCA	Portland Cement Association
P_u	Ultimate punching shear strength
q	Applied surface tractions
SFRC	Steel Fibre-Reinforced concrete
SPSS	Statistical Package for Social Science
UK	United Kingdom
V_c, V_f, V_m	Volume of composite, fibre, matrix
VIF	Variance Inflation Factor
W_f	Fibres content expressed as a percentage of the concrete weight
W_f	Weight of fibres as a percentage of total composite weight
x_c	The distance between the zero bending moment position and the edge of the column along the column line
x_o	The distance between the zero bending moment position and the centre of the column along the column line
α_c	x_c/l_c
α_o	x_o/l_o
γ_m	Work of failure
δ	Displacement at any point
ε	Strain

η_b	Bond efficiency
η_c	Concrete type factors
η_L	Efficiency factor depending on the fibre length
η_θ	Efficiency factor depending on the fibre orientation
ν	Poisson's ratio
σ	Stress
σ_{cu}	Ultimate post cracking tensile strength of composite
σ_f	Stress in fibre
σ_{fu}	Failure stress of fibre
σ_t	Tensile stress
σ_{tu}	Ultimate tensile stress
τ_{fm}	Fibre matrix interfacial bond strength
ψ	Angle of dilation

ABSTRACT

The present research is concerned with investigating the structural effect of using steel fibre-reinforcement on the punching shear behaviour of ground-suspended slabs with internal columns. The main objectives of this research were to develop a constitutive model for steel fibre-reinforcement (SFRC), to study experimentally the punching shear behaviour of SFRC with no longitudinal reinforcement and to develop a finite element model that can accurately predict the behaviour of SFRC slabs subjected to punching shear.

In this respect, a literature review of the work undertaken by previous researchers on punching shear behaviour of concrete slabs is presented. After that, a constitutive model for SFRC was developed. This is followed by a preliminary finite element analysis (FEA) and experimental study of SFRC slabs. Finally, a finite element model was developed.

The literature review revealed that little work has been carried out to study the effect of fibre-reinforcement on the punching shear capacity of concrete slabs. Furthermore, currently no guidance is available on the shear capacity of steel fibre concrete and there are still no generally accepted theories to explain the punching shear mechanism in SFRC structures, hence a thorough investigation in this area was mandatory.

A constitutive model for SFRC in post-cracking stage was developed. This enables one to estimate the tension stiffening behaviour of SFRC based on a simple beam bending test and a statistical model developed in this research, this constitutive model was used later on in modelling of the SFRC slabs using FEA.

In the preliminary FEA, sufficient information for the size and the design of test specimens that were used in the experimental programme was produced. In the experimental study, eight steel fibre-reinforced concrete slab-column connection specimens were tested. The variables of the test specimens include the concrete compressive strength, fibre dosage and fibre aspect-ratio. The deflection along the diameter of the slab and strains in concrete were measured and analysed and conclusions were drawn on the extent to which the steel

fibre affects the ultimate load capacity, load-displacement behaviour, crack pattern, failure mode and the angle of punching cone.

Finally, these test specimens were analysed by the finite element method in order to, numerically demonstrate the possibility of reproducing the structural behaviour of the slabs. Hence, finite element model implementing an axi-symmetrical element was developed in this research. The punching failure in SFRC slabs were successfully simulated allowing the parametric analysis to be performed. Therefore, parametric studies were carried out in which the influence of material and geometrical properties on the punching behaviour is studied.

In this manner, the present work provides a finite element model that has the capability to identify the key influencing factors and express the extent of their effect on the punching shear capacity. This model gives a good prediction of the behaviour of SFRC slabs failing in punching shear and can be used with confidence in practice.

CHAPTER ONE
INTRODUCTION

1.1 Research Background

The concrete industrial ground-floor slab is a key structural element in most industrial enterprises. It is a foundation that sustains the operational loads from loaded racking systems, goods stored directly on the floor, fork-lift truck wheel loads and transfers them to its supports (i.e. soils, piles, beams, columns and walls) without any structural failures or unaccepted settlements. Hence, there is a great need to take advantage of the appropriate methods available to achieve good long-term performance of the ground-floor slabs.

The punching failure of flat ground-floor slabs supported on piles is a serious problem that often governs their collapse, as in these slabs, the upper and lower surface are plane, and there are no beams, drop panels or column heads. Punching shear is a brittle failure: it occurs in slabs suddenly with little or no warning prior to collapse. It often couples with bending and cracking, and changes the post-peak behaviour drastically (Prisco and Felicetti, 1997) by a decline of load after the peak stress point.

The use of shear reinforcement (e.g. stirrups, stud rails and other proprietary reinforcement) has been applied extensively to increase the punching shear capacity of a slab-column connection by providing a means to prevent widening and propagation of the inclined cracks. Li et al (1993) observed that concrete cracks induced by punching shear load can be quite large in width and can reduce the long-term durability of a structure even with the use of stirrups. Moreover, it is labour demanding and can lead to rebar congestion (Swamy and Ali, 1982). Furthermore, some design codes, i.e. British Standard BS 8110:1997 and Euro code 2 EC2:2004 have a lower limit of 200 mm on the slab-depth below which shear reinforcement ought not to be used.

Consequently, for improvement, durability and structural safety, it would be necessary to design structural connections subjected to punching shear loads with a material, which have enhanced tensile strength, strain and fracture energy properties (Killu, 2002). Fibre reinforcement had long been known to enhance the material and mechanical properties of concrete. In addition, with the advent of fast-track systems (i.e. laser screeders machine) in the construction industry, concrete flooring has had to meet quicker construction programmes. Therefore, fibres are often specified instead of conventional mesh due to the inconvenience of positioning individual mats of mesh immediately in front of the laser screeding machine as the machine progresses (Knapton, 1999).

Floor construction methods involving the addition of fibres into the concrete have become commonplace in the UK. Moreover, over the past ten years, the use of steel fibres as the only reinforcement within structural concrete slabs have been developed and is now in routine use for applications such as industrial ground-floor slabs resting on a grid of piles (Destree, 2005).

Despite an extensive amount of experimental research work on shear strength of reinforced concrete slab, little work has been carried out to study the effect of fibre-reinforcement on punching shear capacity of concrete slabs. Furthermore, currently no guidance is available on the shear capacity of steel fibre concrete with no longitudinal reinforcement (Beckett, 2004).

1.2 Problem Statement

It is clear that there is a growing demand for steel fibre-reinforced concrete (SFRC) ground-suspended floor slabs for different commercial and industrial applications. There is a lack of understanding of the philosophy and principles on which a unified design method of this fundamental structural element should be based. However, the dominant criterion that normally governs the design of concrete ground-suspended floor slabs is their resistance to punching shear around the pile heads (TR 34, 2003).

Although, it is estimated that 20% of industrial concrete floors are pile-supported (ground-suspended), currently in UK, there are no documents dealing specifically with ground-suspended floors (Eddy, 2003). Publications such as TR34 Concrete industrial ground floors – a guide to design and construction, ITN11 the design of ground-supported concrete industrial floor slabs and TR550 Design of floors on ground, deal comprehensively with the design and construction of ground-supported floor slabs.

In the UK, the common practice in designing ground-suspended floor slabs follows the requirements appearing in building design code BS8110 so that, they are treated as fully suspended slabs. Although ground-suspended floor slabs are designed as fully suspended, their behaviour is different due to the presence of the underlying soil. Such slabs will initially act as hybrid supported/suspended slabs, so that stresses induced due to loading in a suspended slab on ground may be much lower than the normal design predicts because inevitably the underlying ground will provide some support. This means that the actual bending moments and shear forces could be much less than the structural design predicts. Moreover, whether or not steel fibre is effective in arresting crack propagation in a brittle fracture process such as punching shear in ground-suspended concrete floor slabs without any longitudinal reinforcement is yet to be investigated.

Therefore, the industry has shown that it requires guidance in this topic so that, the Association of Concrete Industrial Flooring Contractors (ACIFC) are committed to provide an introductory guide to the design and installation of concrete ground-suspended floor slabs (Eddy, 2003). It is intended that the document will provide expert, wide-ranging direction and impartial information that will enable clients, designers and contractors to fully understand the processes involved and to select the appropriate solution for their project.

To this end, the aim of the present research was to improve the understanding of the punching shear behaviour of SFRC ground-suspended floor slabs. This can allow more durable slabs to be built. More importantly, it will allow for a unified design philosophy, which gives the owner and the designer a clear set of gains with regard to safety, serviceability and economy.

1.3 Aims and Objectives

The research objectives that were derived from this aim can consequently be presented as follows:

- To build-up an understanding on the current theoretical theories on punching shear behaviour of concrete slabs, and to identify the main influential factors affecting punching shear.

- To identify the concrete models used in finite element programme ABAQUS, the main features of it, and whether it is suitable for the current investigation.

- To develop a constitutive model for SFRC, namely in post-peak tension using inverse analysis on experimental results of beams under bending tests carried out in different laboratories.

- To identify the test set-up of the tested specimens.

- To conduct a series of experimental tests on eight SFRC slabs having various concrete compressive strength, fibre dosage and fibre aspect-ratio.

- To further investigate the experimental programme aiming at producing a finite element model that is capable of describing the punching shear behaviour of SFRC slabs. This model can then be extended to allow for parametric studies, by means of axi-symmetric model, in order to asses the effect of various variables on punching shear. The variables included are concrete compressive strength, tensile strength, tension stiffening, column size effect and slab size effect.

- To determine the structural effect of using steel fibre-reinforcement on the punching shear failure of concrete slabs and their role in the failure process.

1.4 Purpose and Scope of the Current Investigation

This investigation is carried out to assess the effect of steel fibre-reinforcement in the punching shear behaviour of ground-suspended floor slabs.

The research in this project includes both an experimental and theoretical study.

1.4.1 Experimental Study

Since there are still no generally accepted theories to explain the punching shear mechanism in SFRC structures, experimental study remains an important means to the shear study of reinforced concrete slab systems.

In this research, eight slab-column specimens of SFRC slabs have been tested. A detailed description of specimens and the test programme is given in Chapter 6.

Also, considering the availability of the working space and other equipment in the laboratory needed for the tests, it was decided to use specimens similar to the commonly adopted traditional slab-column specimens. Furthermore, the dimensions of the specimens were determined based on the results of extensive preliminary Finite Element Analysis (FEA) using the ABAQUS finite element package, as discussed in Chapter 5. The concrete models in this package will be discussed in detail in Chapter 3.

The variables of the test specimens include the concrete compressive strength, fibre dosage and fibre aspect-ratio.

1.4.2 Theoretical Study

Due to limitations of cost and time, experimental programmes cannot cover all the factors that influence the punching shear strength of SFRC slabs. Therefore, a theoretical study is still necessary as a supplement to the experimental work.

As was pointed out before, there are still no well established theories at present that can be employed to explain the punching shear behaviour of SFRC structures. A theoretical study using numerical structural analysis with the help of modern electronic computers can help in this respect.

In this research programme, the finite element analysis (FEA) package ABAQUS, has been used to carry out all the FEA. ABAQUS is a powerful FEA package which can be adopted to perform various kinds of structural analyses.

Moreover, a series of parametric studies was conducted to study the effect of concrete compressive strength, tensile strength, tension stiffening and the effect of slab depth and column size on the punching shear behaviour of SRFC slabs. Based on the information from experiments and from FEA, a comparatively deeper understanding of the punching shear performance of SFRC slabs can be achieved.

1.5 Research Area (Types of Ground-Floor Slabs)

Concrete floors are divided into two main structural types; Ground-supported floors rest on the ground and are supported by it and suspended floors are supported by other building elements. Most suspended floors are above ground level, supported by columns, beams or walls. Other suspended floors are at ground level, so that, not every floor at ground level is ground-supported, some are in fact suspended floors, supported by piles.

1.5.1 Ground-Supported Slabs

The slabs rest directly on the ground and are supported by it. Structural design in this case is a matter of ensuring that the floor slab has enough flexural strength to transfer them to the sub-grade without cracking. This type of slabs has been extensively studied by Abbas (2002). The design of ground-supported slabs is beyond the scope of the present research.

1.5.2 Suspended Floor Slabs

The vast majority of industrial floors are ground supported, but there are occasions when a suspended floor may be necessary whether on the ground (ground-suspended/or pile-supported) or elevated.

1.5.2.1 Ground-Suspended Floor Slabs

Ground-suspended floor could be required where weak soils with low bearing capacity exist that cannot carry the required loadings and/or there is a high risk of excessive floor settlement, and thus the slab is usually supported by piles. Ground-suspended and ground supported floors are designed according to fundamentally different structural principles. All slabs discussed hereinafter, in the present research, are of this type. In addition, the slabs studied here are assumed to be of flat type, as there are no beams, drop panels or column heads.

1.5.2.2 Elevated Floor Slabs

Elevated floor could be required where poor ground conditions exist that cannot carry the required loadings and/or where industrial floor slabs are required above ground level, the most common type is a mezzanine floor installed in a single-story industrial building (Simpson, 2004). The design of elevated slabs is beyond the scope of the present research.

1.6 Thesis Layout

Chapter Two presents a review of the literature concerning all aspects of the proposed project. The themes covered include different current theories for punching shear behaviour of concrete slabs and the key factors affecting the punching shear failure. A detailed overview on the fibre reinforcement historical use, fibre types, composition and quality, placing, finishing and curing, strengthening mechanism, factors influencing effectiveness of fibres and its mechanical properties are presented in this chapter. Chapter two seeks to

develop an understanding of the related research that has been previously conducted and to identify its major shortcomings as a starting point for this research.

Chapter Three discusses the various features of the concrete models offered by FEA package ABAQUS to model the behaviour of reinforced concrete structures. Moreover, it discusses how the selected material model suitable for the analysis of SFRC structures. The selected material model with the theory behind it is also explained in details.

Chapter Four illustrates the development of constitutive model, namely the behaviour of SFRC in post-peak tension. This was based on the inverse analysis of experimental results from the literature using FEA.

Chapter Five presents the preliminary FEA that was conducted in order to determine the experimental test set-up and the size of the slab required for the current investigation. This was based on linear analysis to select the line of contra-flexure and to assess the effect of the presence of the underlying soil on the ultimate load capacity of the slab.

In **Chapter Six** the properties of materials used to manufacture the test specimens for this work are discussed. The methods applied for casting, preparation and/or fabrication of the test specimens, set up of the testing equipment, instrumentation, measurement and test procedure. Also the results obtained from tests with the analysis and discussion of the general behaviour of the tested slabs and the test results are summarised.

Chapter Seven presents a finite element model that has the capability to predict the punching shear behaviour of SFRC slabs. This method showed good agreement with experimental results, therefore, a parametric study to asses the influence of various parameters on the punching shear behaviour of SFRC slabs was carried out.

Finally the major conclusions are presented in **Chapter Eight,** together with a list of suggested recommendations for further research.

CHAPTER TWO

STATE OF THE ART AND REVIEW OF PREVIOUS WORK

2.1 Introduction

Nowadays, much literature on punching shear behaviour of flat slabs over many decades is available for reference. However, most of them are from studies of flat slabs with conventional reinforcement. Very little of them have considered the punching shear behaviour of flat slabs reinforced with steel fibres. In this chapter a brief summary of the development of mechanical and analytical models of punching shear theory is presented. This chapter also describes the parameters which influence the behaviour and punching shear strength of concrete slabs as studied from experimental observations and models. It is followed by a detailed overview on the fibre reinforcement and a review of the past research on the mechanical properties of fresh and hardened steel fibre-reinforced concrete. Finally, emphasis is given to the experimental and theoretical work on punching shear of flat slabs with steel fibres.

2.2 Mechanical Models for Punching Shear

Models for punching shear can be classified into two groups, namely theoretical and analytical models. Theoretical models include models based on different approaches such as, Kinnunen and Nylander (1960), elastic, plastic, flexural capacity, strut and tie and post-fractured, whereas the analytical models include the finite element method and the finite difference method. In the following section, a detailed review of these models is presented to illustrate the dependence of the punching resistance on the influential parameters.

2.2.1 Theoretical Approach

Most research on the punching shear strength of flat slabs has been concerned with the generation of experimental data and the development of empirical equations, only a limited number of theoretical analyses have been carried out predicting the ultimate punching strength of a flat slab-column connection.

To date, the Kinnunen and Nylander (1960) model seems to be the most rational model for predicting the punching shear failure of reinforced concrete slabs. This model has been used by many investigators. They modified it to cater for different types of situations. For example; Brooms (1990) modified it to include unsymmetrical punching, Marzouk and Hussein (1991b) modified it to analyse high-strength reinforced concrete slabs. Different versions of Kinnunen and Nylander model will be discussed in the following sub-sections.

2.2.1.1 The Development of Kinnunen and Nylander Model (1960)

The original slab equilibrium model was developed by Kinnunen and Nylander, about 48 years ago to study the shear failure of slabs without shear reinforcement as the first real attempt to establish a theoretical method of analysis. This model is based upon observations of tests on circular slabs, centrally supported on circular columns, and loaded at the free edges. Two radial crack lines, a part of the initial circumferential crack and the slab boundary divide the slab, see Figure 2.1.

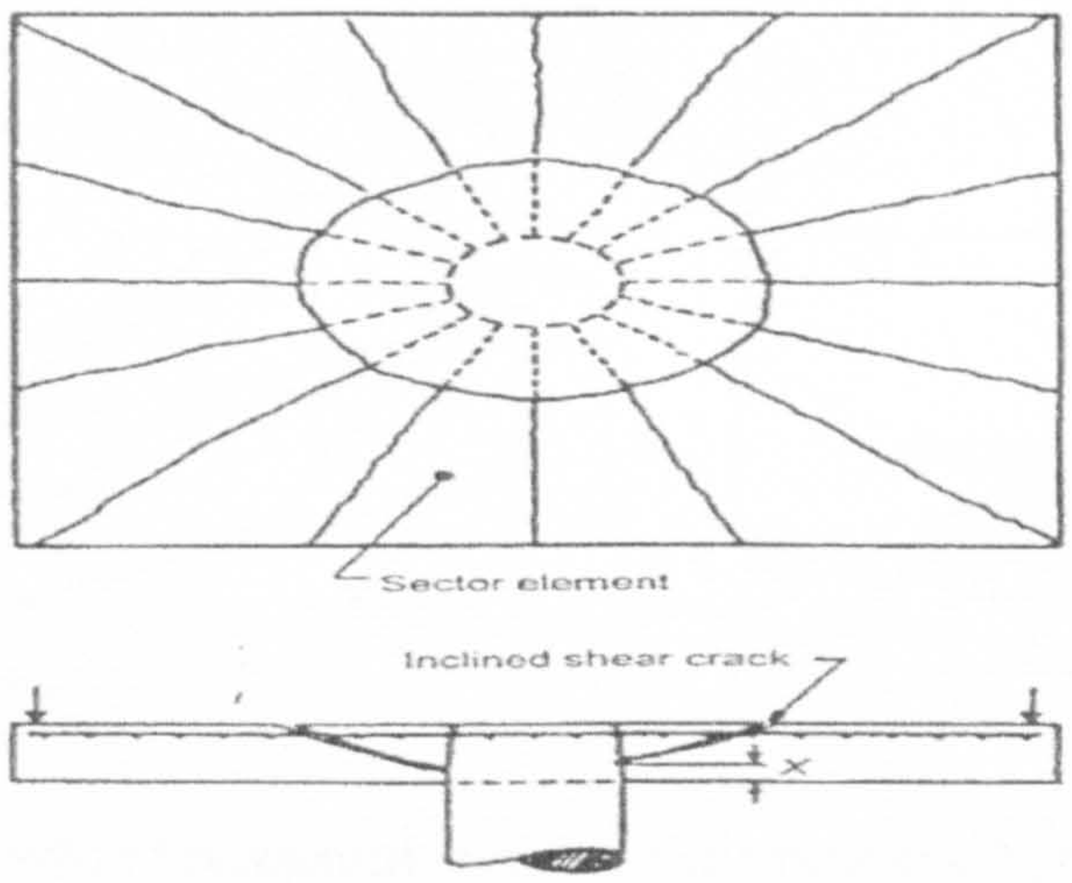

Figure 2.1: Kinnunen and Nylander punching model

The theoretical method of analysis was based on the mechanical model shown in Figure 2.2. When subjected to load, each rigid segment rotates about the apex of the inclined crack and to be supported on the imaginary conical shell which is in turn supported on the column. They derived expressions for the forces acting on each sector; it is supposed that these forces, except the load and reaction, are proportional to the angle of rotation of the slab. The shear strength is evaluated from the condition of equilibrium at failure. The

failure criteria is defined by the ultimate shear expansion of the concrete at the bottom surface of the slab (ε_c = 1.96%). In their tests on slabs with two-way reinforcement, all measured values of ultimate load were higher than the calculated values. The difference between these values varied from 10 to 25%. This deviation can be attributed to the development of dowel forces, which are not taken into account in this study. This approach has been extensively presented in Regan and Braestrup (1985). The Kinnunen and Nylander model shows that punching load of slab is governed by the compressive strength of concrete, column size, slab thickness and flexural reinforcement ratio. The influence of these parameters on the failure load of slab will be discussed in section 2.3.

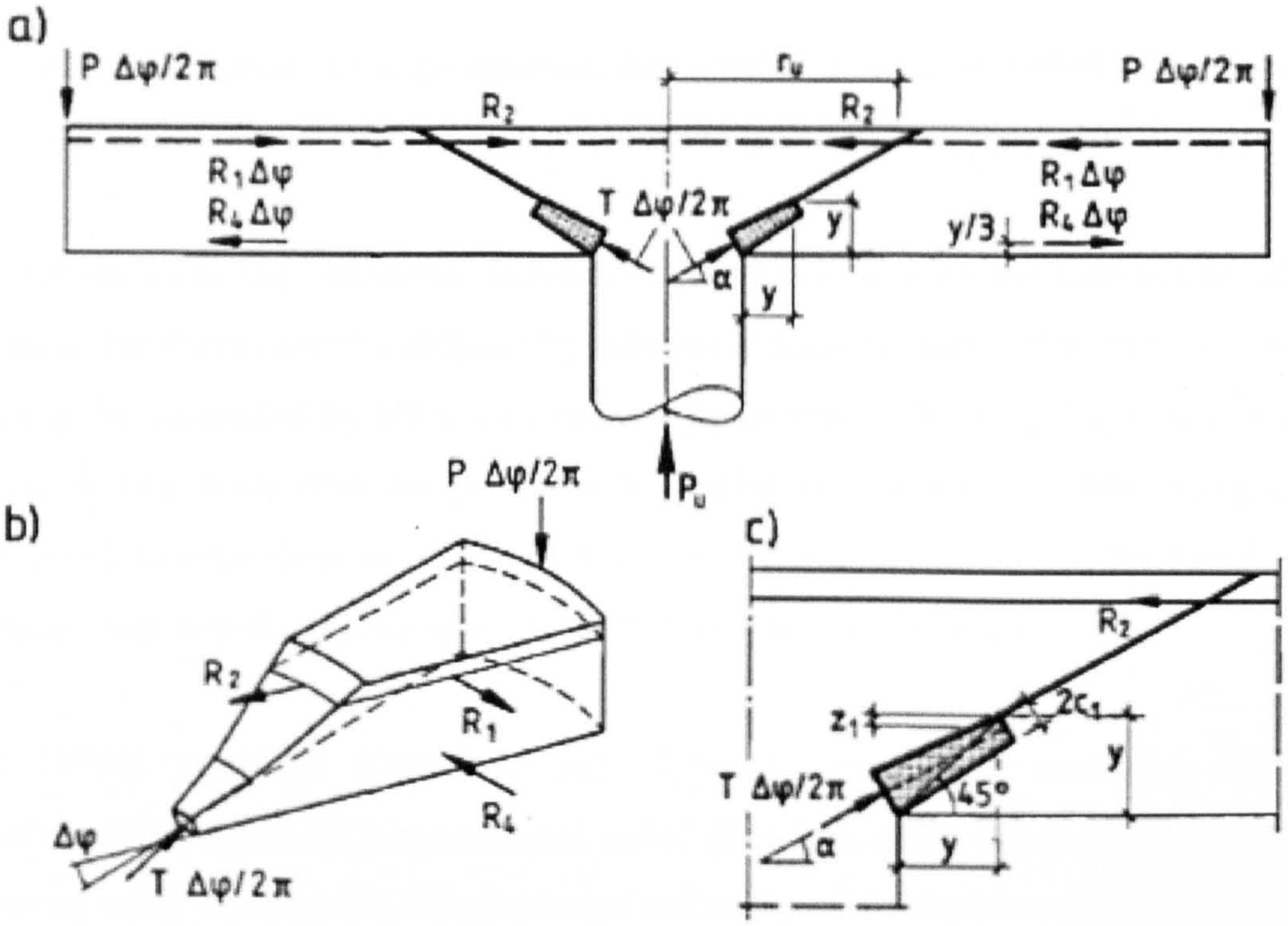

Figure 2.2: Mechanical model of Kinnunen and Nylander

The original theory developed by Kinnunen and Nylander is derived for slabs with ring reinforcement. Kinnunen (1963) expanded the theory to include the effect of dowel forces, the vertical component of the reinforcement forces and the deviation of a two-way reinforcement pattern from polar symmetry.

Shehata and Regan (1989) modified Kinnunen and Nylander model by treating punching failure in a similar manner but utilising the generally recognised values for concrete

properties and different failure criteria. Punching failure is considered to take place either by splitting under principal tensile stresses or by crushing in the radial or tangential direction. The failure criteria are defined as follows:

- Failure by splitting of the concrete is assumed to occur when the angle α of the compressive force at the column face reaches 20°.
- If the average radial strain on the compressed face reaches a value of 0.0035 in the plastic length starting from the column face, there is radial crushing of the concrete. Based on experimental ultimate rotations, Shehata assumed the plastic length as 150mm.
- If the tangential strain of the compressed face reaches a value of 0.0035 at a distance x from the column face, there is a tangential crushing of the concrete.

This model indicates that punching failure is caused not only by the destruction of the conical shell, but it may also be initiated by a diagonal tension crack. Thus punching shear strength may be controlled by the tensile strength of concrete. While giving easier method of calculation, this model does not present a convincing failure criterion. For example, for two-way reinforcement there is no justification for 150 mm to be taken as the length over which the average radial concrete strain is limited to a determined value.

Brooms (1990) modified Kinnunen and Nylander model by assuming different compression zone heights for tangential and radial directions strain failure mechanisms and using normal value for concrete ultimate stress and strain. This model was then extended to include unsymmetrical punching for interior slab with moment transfer.

Marzouk and Hussein (1991a) adopted the model modified by Shehata, but excluded the failure criterion for tensile splitting. They made this assumption probably due to the following reasons:

- They observed that the angle of the failure surface for high strength concrete slabs varied between 32° and 38°. This indicated that the contribution of tensile stress to the

punching strength is less than the punching strength based on α=20°. i.e. the effect of tensile strength is less significant.

- Although the ratio of tensile strength to compressive strength for high strength concrete is smaller than for normal strength concrete, still the absolute value can be large.

The model indicates that the influence of tensile strength on punching capacity is less important for high strength concrete.

Andersson (1963) used the test results as a basis for a theoretical model for slabs with shear reinforcement. The failure criterion adopted by him led to a pessimistic view of the potential of shear reinforcement.

Gomes and Regan (1999) proposed another theoretical model for analysing the punching resistance of reinforced concrete flat slabs with shear reinforcement for concentric loading. Kinnunen and Nylander's and Shehata's treatments of slab without shear reinforcement and Andersson's theoretical model for slabs with shear reinforcement together with the results of tests found in the literature and those made by Gomes and Regan (1999) constitute the basis of the proposed model.

In this model, two failure criteria were proposed. The first one is for the case of a failure surface reaching to the column, which is assumed to occur when a local mechanism is formed and the shear stress in this region reaches the sliding resistance. The second failure criterion is for the failure surface occurring outside the shear reinforcement region. This is assumed to occur when the maximum principal stress at a section 1.35d (an empirical number) outside the shear reinforcement region reaches the splitting strength of the concrete. Gomes and Regan concluded that more tests are needed to corroborate the failure criterion adopted for the concrete adjacent to the column. The criterion used seems very plausible. They also found that the 1.35d used to determine the critical section for a failure surface outside the shear reinforcement may require a slight revision.

Finally, the model proposed by Kinnunen and Nylander was extended by Marzouk et al in 2002 to include the crack size and size effects based on the fictitious crack model

assumptions and equilibrium equations in order to predict the punching load and the deformations of reinforced concrete slabs. Concrete strength, aggregate type, reinforcement ratio as well as the fracture strength properties were taken into account in developing this model.

2.2.1.2 Elasticity Theory Based Model

Long and Bond (1967) presented a theoretical method of analysis for the calculation of the punching load of a flat slab-column connection with two way reinforcement and no shear reinforcement. This is based on elastic thin plate theory from which the stresses in the compression zone are derived, assuming a linear distribution of stress. An octahedral shear stress criterion of failure is used to find the corresponding failure stresses. The analysis does not include the case of transfer of moment between column and slab combined with a direct punching load. The load found by this analysis was multiplied by a factor of 1.3 to take into account the dowel action effect. Tests were carried out on one-fourth-scale slab-column connection and test results were in good agreement with those predicted by their analytical method. Examination of their theoretical analysis leads to the following critical remarks, the use of elastic theory to find the relationship between the column load and the induced moments means that the effect of both flexural and shear cracks is not taken into account, which may change the stress distribution and cause a redistribution in the internal tensile and compressive forces in the slab. In addition, the assumption of constant shear stress distribution between the neutral axis and the reinforcement is questionable since the flexural cracked part of the slab does not contribute any resistance to shear.

Many years later, Long (1973) extended the above theory to include the case of the punching load for a slab-column connection subjected to shear and transfer moment. Shear loading and pure transfer of moment were considered separately and because the method of analysis is basically elastic these can be superimposed to apply to the general case of shear and moment transfer. A factor of 1.3 was also applied to the punching load to take into account the dowel action effect.

2.2.1.3 Plasticity Theory Based Model

The theory of plasticity has mainly been used to determine upper bound values for the punching load. It was originally proposed by Braestrup and Nielsen (Nielsen et al, 1978) and later by Jiang and Shen (1986). In this model concrete is considered to be a perfectly rigid-plastic material and a modified coulomb failure criteria was adopted. The reinforcement is assumed to be capable of carrying longitudinal tensile and compressive stresses only and to be a rigid-plastic material. The ultimate punching strength can be found as an upper bound solution, by using the work equation i.e. by equating the external work done by the load for a given failure mechanism to the internal work dissipated in the structure. The following critical remarks were observed, the assumption about concrete means that elastic deformations are neglected in the analysis and that unlimited ductility is implied. However this is a drastic simplification of the behaviour of concrete since the deformation of concrete is very limited, especially in tension. Moreover, the assumption about reinforcement means that the dowel effect as well as the vertical component of the reinforcement force is neglected.

An extension to this theory was made by Kuang & Morely (1993) who developed a plastic theoretical model for the punching shear failure of laterally restrained concrete slabs, in which a parabolic Mohr's failure criteria for concrete was adopted. The proposed method allows for the effect of a compressive membrane action and a membrane-modified flexural theory of elasto-plasticity was used to calculate the compressive membrane forces.

Later on Nielsen (1999) presented the well-known plasticity model, which was initially developed by Nielsen et al (1978) in long equations, by convenient design charts. This new form is quite straightforward to use.

On the other hand, lower bound solutions were discussed by Braestrup in Regan and Braestrup (1985), and among them the lower bound approach by Pralong (1982), cited in CEB-fib (2001), which involves the tensile strength of concrete.

2.2.1.4 Flexural Capacity Approach

Moe (1961) developed a model in which the punching shear strength of reinforced concrete slabs was derived from the flexural capacity. Moe's work had a very important influence on the formulation of code provisions on the shear design of concrete slabs in ACI Building Code up to present. In his study, the principal variables considered were: the effect of openings near the surface of the column, the effect of concentration of tensile reinforcement under the column, the effect of column size, the effect of eccentricity of the applied load, and the effectiveness of various types of shear reinforcement. From his study, Moe concluded that:

- The critical section governing the ultimate shear strength of slabs and footings should be taken along the perimeter of the loaded area.
- The shear strengths of slabs and footings are dependent on flexural strength.
- The triaxial state of stress in the compression zone at the critical section affects the shear strength of that section considered.
- The shear strength of concrete increases as the column size relative to the thickness of the slab decreases.
- Concentration of flexural reinforcement in narrow bands across the column did not increase the shear strength. However, such concentration was beneficial in the sense that it increased the flexural rigidity of the slabs, and so increased the load at which yielding began in the tension reinforcement.

2.2.1.5 Strut and Tie Models or Truss Models

Truss models or strut-and-tie models with concrete ties describe the load transfer in the slab and thus may be classified as smeared models. The cracks are not explicitly addressed but may only be considered in one or the other failure criterion, like a reduced value for the concrete compressive strength. Pralong (1982), cited in CEB-fib (2001), proposed truss models with concrete ties for punching.

2.2.1.6 Post-Fractured Based Model

In 1999, Yankelevsky and Leibowtiz developed a new model, based on rigid post-fractured behaviour, opposed to the rigid-plastic behaviour which had been assumed by Nielsen et al. (1978), utilising the post fracture properties of concrete at the rough crack interfaces that are developed. The model uses post fracture properties of concrete and considers both the equilibrium and the kinematics of the system. Therefore, it may predict the force – displacement resistance during punching, the stress distributions along the failure surface as a function of displacement as well as the shape of the punched concrete plug. They showed that compressive strength of concrete as well as the shape of the failure surface as a function of displacement govern punching shear load of the slab. The surface may be determined by its smaller diameter d (which is equal to the column diameter) and the larger diameter D on the other side of the slab, or alternatively by the angle θ (the angle between the failure surface and the vertical plane of column face). It has also been shown that an average angle of 60° yields good results for a wide range of parameters (reinforcement ratio, concrete strength and diameter to thickness ratio)

The proposed model implements the fictitious crack model principles and the fracture energy as illustrated by Hillerborg (1985) to determine the crack growth in tangential directions of slabs. The forces of the reinforced concrete slab in tangential and radial directions are calculated using strain compatibility and equilibrium equations.

2.2.2 Numerical Methods and Fracture Mechanics

Since 1985 models based on numerical analysis and fracture mechanics have increasingly been proposed to predict the behaviour of slabs with complex shapes and boundary conditions. Basically, there are two kinds of numerical analysis methods available to analyse slab structures: "Finite Difference Method" and "Finite Element Method". The method of finite differences was the first numerical technique developed for the purpose of analysing the slab structures. In this approach, the analytical solution procedure is replaced by setting up and solving a set of linear simultaneous equations. Although the finite

difference method has had a very long history, the restrictions of this method in implementing general fully automatic solutions of complex structures has led to a decline in its popularity. On the other hand, the finite element method is capable of handling very complex situations such as orthotrophy, varying depth, edge beams and various kinds of practical loading and boundary conditions with little difficulty. It is generally recognised as the most powerful and versatile of the numerical techniques currently available for structural analysis, especially for complex engineering structures. The finite element technique is a particularly valuable tool for the analysis of structures with material nonlinearities.

Nowadays, there are many finite element packages commercially available. Some of them incorporate the material model of concrete to allow for the behaviour peculiar to concrete structures, such as concrete cracking, tension stiffening etc.

An overview of the application of the finite element method for the simulation of punching failure in reinforced concrete slabs is given in CEB-fib Bulletin technical report (CEB-fib, 2001). As was presented in the technical report Ozbolt and Voke (1999), Marzouk and Jiang (1996), Beutel and Hagger (1998) used 3-D elements in their simulation of the punching shear behaviour. Menetrey (1994), Gonzalez et al (1988) and Hallgren (1996) used axisymmetric elements. However shell elements were used by Gastmeyer (1994) and Polak (1998).

In addition to the above models, some FE models have been revealed in the literature. A brief review of these researches on the prediction of the shear strength of the slab using finite element includes the following:

Jofriet & McNeice (1971) studied experimentally and numerically a slab where the corners were prevented from lifting and subjected to a point load at the centre. They used plate element for their numerical analysis. This slab was subsequently analysed by many other investigators. The main emphasis was on predicting behaviour in flexure.

De Borst & Nauta (1984) using axisymmetric element with smeared crack model, in which a crack is modelled by changing the material property matrix or (D-matrix) instead of altering the mesh conectivities, analysed two simply supported slabs subjected to concentrated load which were tested at Delft University.

Gonzalez et al. (1991) used 20 node solid elements with smeared crack model to investigate a plain concrete prism, a reinforced concrete beam and a reinforced concrete slab.

Abbasi et al. (1992) investigated the effect of flexural reinforcement ratios and edge restraints on punching capacity of reinforced concrete slabs. They used a multilayered plate element with smeared crack to analyse slabs tested by Taylor and Hayes (1965).

Marzouk & Chen (1993) used shell element with layered approach to study the behaviour of high strength concrete slab. The post-cracking behaviour of concrete was represented by smeared crack model. They analysed fourteen slabs tested by Marzouk and Hussein (1991a).

Menetrey (2002) developed a model to reproduce the different states of stress, characterising punching failure so that the triaxial failure criterion developed by Menetrey and William (1995) was considered. The concrete cracking phenomenon is described with the smeared crack model using the strain-softening formulation. The fictitious crack model developed by Hillerborg et al. (1976) is considered for which the reduction of the tensile stress σ_t is controlled by the crack opening along the line of exponential decohesion process.

2.2.3 Discussion of the Punching Shear Models

From the above discussion, it has been concluded that over many years researchers were trying to include different constitutive models for concrete in their models to modify the prediction of punching shear load capacity of concrete slabs. Moreover, these models show that the punching load of slab is governed by influential parameters such as concrete

strength, column size (loaded area), slab thickness, reinforcement ratio, in plane restraint and the angle of punching cone.

However, the most recent developed models are based on the finite element method. Hence, the concrete constitutive models native to ABAQUS is used in this investigation. The model is based on the theory of plasticity for concrete and the post-cracking behaviour of concrete was represented by smeared crack model (as presented in Chapter 3). As a result, it is expected that this model can lead to reliable results when used as an analytical tool in order to predict the punching shear behaviour of SFRC ground-suspended floor slabs as well as force-displacement resistance during punching.

2.3 Factors Affecting Punching Shear Strength of Concrete Slabs

The extensive theoretical and experimental studies of many years revealed some primary factors that have influencing effects on predicting the punching shear. The following is a detailed discussion of the most important factors and their effects on the punching shear strength of concrete slabs. These factors include concrete strength, slab size, size of loaded area (column), shape and type of the loaded area, in-plane restraints, angle of the punching cone, ratio of the flexural reinforcement, arrangement of the flexural reinforcement, compression reinforcement and fibre reinforcement.

2.3.1 Concrete Strength

In the current ACI Building Code (1989), the shear strength is related to the square root of cylinder compressive strength. This is originally based on Moe's work (1961). Moe selected the square root expression because tensile strength is generally assumed to be proportional to the square root of the cylinder compressive strength and he believed that shear failures of concrete are controlled primarily by tensile strength of concrete.

Based on the tests for interior slab with moment transfer, Hawkins (1971a) concluded that the shear strength of concrete is more likely to be proportional to the cubic root of concrete strength. The same result was arrived at by Regan (1986) after testing six circular slabs

with different concrete compressive strength; he concluded that it is reasonable to assume that the punching resistance is proportional to the cube root of the concrete compressive strength. Marzouk and Hussein (1991b) analysed the behaviour of 17 slabs characterised by a compressive strength in the range of 30-80 MPa, and confirmed that the cube root of the concrete compressive strength is a better assumption for predicting punching shear for slabs made of high-strength concrete.

2.3.2 Size Effect (Span-Depth Ratio)

The effect of the slab depth on the punching shear strength was studied by Regan (1986). He tested six specimens of reinforced concrete slabs, the effective depths were 80, 160 and 250mm. His results also agree reasonably well with the size factor $\sqrt[4]{l/d}$ used in BS 8110. Regan quoted that the range of the slab depth in his test was limited but the tests carried out by Kinnunen et al. (1978) at KTH Stockholm on slabs with effective depths up to 619mm also correlate satisfactorily with the fourth root relationship.

John and David (1990) tested a series of slabs of constant thickness (100mm) with varying span-depth ratios. They concluded that the punching shear strength was significantly increased for the span-depth ratio below six. The strength enhancement may be due to the development of compression struts forming an arch mechanism in the slabs and in plane compressive forces resulting from friction at the support.

2.3.3 Size of the Loaded Area (Column)

Recognition of the dependence of shear strength of concrete slabs on the ratio of a characteristic dimension, c, of column or loaded area to the effective thickness of slab, d, was first proposed by Elstner & Hognestad (1956). They tested three slabs with different sizes of the column stub. As would be expected, the increase in column size increased the slab stiffness and thereby increased the slopes of the load-deflection curves. Moe (1961) reported that the shear strength of slab-column connection tends to increase with the increase of the ratio of c/d; this is because for a given effective depth of the slab and given shape of the loaded area, the perimeter of the critical section becomes greater as the loaded

area increases, resulting in an increase in shear strength. He assumed a linear variation in shear strength with the side dimension of the column based on test data when the side length of the loaded area was between 0.75d and 3.0d, where d is the slab thickness. After testing five slabs by Regan (1986), where the loaded area is the only significant variable, the test results confirmed the linear relationship for the loaded dimension provided that it exceeds 0.75d. When the loaded area is very small (side dimension less than about 0.75d), the slab failed in local crushing and therefore the strength of slab is far below that predicted by the linear relationship. Abbasi et al. (1992) concluded that as the patch size increases the full punching mechanism corresponding to the asymptotic value of the failure load requires greater energy to mobilise a larger portion in the compression shear, thus allowing the radial cracks to propagate leading to a combined flexure shear failure.

2.3.4 Shape and Type of Loaded Area

The majority of available test data from the literature indicated that even with the same c/d ratio, slabs loaded through circular areas exhibit higher strengths than those loaded through square areas. However, the extent of relative effects are influenced by many factors such as the c/d ratio, the reinforcement pattern, and the support conditions. The ultimate shear stress also varies with the rectangular nature of the loaded area. The shear strength decreases with the increasing rectangularity. This is because the shear stresses are not uniformly distributed around the column. There is the tendency for the shear stresses to be concentrated at the ends of the elongated column section (Hawkins et al, 1971).

Regan (1986) tested two sets of slabs one was loaded by plates on the surfaces of the slabs and the other was loaded through monolithic column stubs in order to simulate conditions arising where the heads of piles penetrate a suspended ground slab. The difference was believed to have had no effect on punching resistance.

2.3.5 In-plane Restraints

Kuang and Morley (1993) examined the punching shear behaviour of twelve restrained reinforced concrete slabs; they concluded that edge restraint had a significant effect on the

ultimate punching load of a concrete slab, resulting in a great increase in the shear resistance and enhancement of the load-carrying capacity of the slab. Its magnitude depends on the degree of lateral restraint, the stiffer the lateral restraint the higher the enhancement.

Abbasi et al. (1992) found that the support constraint enhances the punching capacity, yet the beneficial affect tapers off with increasing steel ratio. The also found that weakly reinforced slabs exhibited a significant reduction in radial cracking, undergoing a transformation in the behaviour from pure flexural mode to a flexure shear mode and at the same time reduces the ductility of the slab. Thus the overall effect of the support restraint is to reduce the zone of cracking damage (by virtue of in-plane compressive forces) and allow a greater percentage of the true punching capacity to be mobilised.

It is apparent that the restraint can considerably enhance the load carrying capacity of a slab, but reduce its ductility. However, the degree of enhancement in strength due to the membrane action is difficult to quantify since it depends on the in-plane restraint provided by the surrounding structure.

2.3.6 Angle of Punching Cone

Over many years, punching tests were conducted on concrete slabs with distances between loads and supports short enough for the shapes of the failure surfaces to be defined by specimen geometry, in order to provide a relationship between the ultimate punching resistance stress and the angle θ between the failure surface and the mean plane of the slab. Regan (1984) concluded that there is a dependence of punching resistance upon the angle θ. When the clear shear spans were very short, $\theta = 70°$. Yankelevsky and Leibowitz (1999) reported that the angle θ increases with concrete strength and also found that an average angle of 60° yields good results for a wide range of parameters. Gomes and Regan (1999) tested twelve flat slabs. All the slabs failed by punching but with two different modes of failure. In the first, the failure surface was inclined at about 65°. In the other, the failure surface was outside the region of shear reinforcement.

2.3.7 Ratio of Flexural Reinforcement

Shear strength is expected to increase with increasing flexural reinforcement ratios. Regan (1971) suggested that the flexural reinforcement may influence the punching resistance of a concrete slab in different ways. First, with the increase of flexural reinforcement, the depth of the compression zone will be increased and thus a larger area of un-cracked concrete will be available to resist the shear forces. Also the increase of flexural reinforcement could reduce the width of cracks, thus improving the transfer of forces by aggregate interlock. Furthermore, more reinforcement will also enhance the dowel action in the slab. Dowel forces normally develop progressively where the inclined cracks cross the longitudinal flexural reinforcement. Kinnunen and Nylander (1960) tested a number of slabs with ring reinforcement in which steel ratios was equal to those tests with two-way reinforcement. By comparisons, they concluded that dowel action carries about 30% of the total shear.

2.3.8 Arrangement of Flexural Reinforcement

Elstner & Hognestad (1956) and Moe (1961) conducted tests on slabs with flexural reinforcement concentrated in the column region. Both tests indicated that the concentration of reinforcement does not increase the ultimate load of the slab. In some slabs, concentration of reinforcement even reduced the ultimate load of the slab. Hawkins et al (1974a) concluded that the concentration causes a slight decrease in strength and a reduction of ductility.

Alexander and Simmonds (1992) studied the effects of concentration of reinforcement by adding extra reinforcement placed over the column strip. They found that considering the densities of reinforcement, decreasing the spacing increases the load capacity but decreases ductility. However, the concentration of flexural reinforcement in the column region (critical perimeter) is to be encouraged because it improves the behaviour of the slab in the service load range. Concentration increases the stiffness of the slab, increases the load for the first yielding of the flexural reinforcement, and consequently results in smaller maximum crack widths for a given loading.

2.3.9 Compression Reinforcement

As far as compression reinforcement is concerned, it has a negligible effect on the ultimate strength, provided that the failure is controlled by the shear rather than by flexure (Elstner & Hognestad, 1956). However, when the failure modes change from shear to flexure the increase of the compression reinforcement area from zero to an amount equal to tension reinforcement area, could result in an increase of the ultimate capacity by about 30 percent (Manterola, 1966).

Pan and Moehle (1992) tested slabs under combined gravity and lateral loads. They observed that if the compression reinforcement in the slab continues through the column, then it could act as a suspension net, hold the slab to the column and thus support some load after punching. Top steel is not effective in providing post-punching resistance because it tends to tear out of the slab when punching occurs due to concrete cover over this steel splitting off. Therefore, properly detailed bottom reinforcement in the slab may prevent catastrophic failure.

2.3.10 Fibre Reinforcement

Before investigating the effect of using fibre reinforcement on punching shear behaviour of concrete slabs, a detailed overview on the historical use of fibre reinforcement, fibre types, composition and quality, placing finishing and curing, strengthening mechanism, factors influencing the effectiveness of fibres and its mechanical properties are presented in the following section.

2.4 Fibre Reinforcement

Although concrete as a building material has a high compressive strength and is very cheap and durable, it possesses some well known deficiencies such as: low tensile strength, low ductility and low fracture toughness. The low tensile strength and brittle character of concrete have been bypassed by the use of reinforcing rods in the tensile zone of the

concrete since the middle of the nineteenth century (ACI Committee 544, 1986). Moreover, patents have been granted since the turn of the century for various methods of incorporating discontinuous steel reinforcing elements such as, nails, wire segments or metal chips into concrete.

2.4.1 Historical Use of Fibres

The use of fibres in brittle matrix materials has a long history going back at least 3500 years when sun-baked bricks reinforced with straw were used to build the 57 m high hill of Aqar Quf near Baghdad (Newman & Choo, 2003). In addition, horsehair was used to reinforce masonry mortar and plaster (ACI Committee 544.1R, 1996). After that, asbestos fibres have been used to reinforce cement products for about 100 years. This material known as "asbestos Cement" has found wide application for the manufacture of corrugated roofing sheets, cladding panels and pipes. However, primarily due to health hazards associated with asbestos fibres, alternate fibre types were introduced throughout the 1960s and 1970s.

During the early 1960s in the United States, the first major investigation was made to evaluate the potential of steel fibres as a replacement for concrete (Romualdi & Baston, 1963). The Portland Cement Association (PCA) investigated fibre reinforcement in the late 1960s (Monfore, 1968). In the early 1960s, experiments using plastic fibres in concrete with and without steel reinforcement were conducted (Goldfein, 1963; Williamson, 1965). Experiments using glass fibres have been conducted in the United States (Goldfein, 1963), the United Kingdom (Majumdar and Ryder, 1968; Grimer and Ali, 1969; Majumdar, 1970; Majumdar and Ryder, 1970) and Russia (Biryukovich et al, 1965). Later on, structural synthetic fibres were developed. However there is still little research in this area. Synthetic fibre reinforced concrete utilises fibres derived from organic polymers which are available in a variety of formulations (ACI Committee 544.1R, 1996).

Similarly, over the past 40 years, a number of applications have been recommended for the use of fibre reinforced concrete including road and floor slabs, refractory materials and concrete products (ACI Committee 544, 1986). Since then, a substantial amount of

research development, experimentation, and industrial application of fibre reinforced concrete has occurred.

More recent references have been made to the use of metallic and non-metallic fibres in hybrid systems (Ohama et al, 1985; Qian and Stroeven, 2000) and their advantages over single fibre matrices (Benture and Mindess, 1990) though the research work carried in this area is somewhat limited. Ohama et al (1985) concluded that the fibre hybrid reinforced concrete using steel and polyethylene fibres has much better properties such as flexural toughness and maximum tensile strain than the concretes reinforced with only one type of fibres.

2.4.2 Types of Fibres

According to the ACI Committee 544 (1986) fibres could be defined as reinforcing elements that have a discontinued and discrete nature. Continuous meshes; woven fabrics and long rods are not considered to be discrete fibre reinforcement in this respect. A convenient numerical parameter describing a fibre is its aspect ratio (l/d), defined as the fibre length (l) divided by the fibre diameter (d). In the case of non-circular fibres the equivalent diameter may be used (ACI Committee 544, 1986, Ramakrishnan, 1988).

There are numerous fibre types, in various sizes and shapes, available for commercial and experimental use. The fibres that are currently being used in concrete can be classified into two types. Low modulus high elongation fibres, such as nylon, polypropylene, and polyethylene, are capable of large energy absorption characteristics; they do not lead to strength improvement, but they impart toughness and resistance to impact and explosive loading. High strength, high modulus fibres such as steel, glass, asbestos and carbon, on the other hand, produce strong composites of higher strength and stiffness than the matrix itself, and to a lesser extent improve the dynamic properties.

However, the most common reinforcing material in ground-suspended floor slabs is steel fibre. The next section will discuss the types of steel fibres available in the market as well as their effect on the behaviour of concrete.

2.5 Steel Fibres

Industrial floors and pavements are major applications for steel fibre concrete. In the United Kingdom, several million square meters of steel-fibre-reinforced slabs have been installed over the past ten years, both for ground-supported and pile-supported floors. It has been estimated that about 2,000,000m^2 of pile-supported floors have now been constructed in the UK (TR 63, 2006).

The stresses occurring in a concrete slab are complex as they depend on the type of load. There are, in addition, stresses that are difficult to quantify, arising from a number of causes such as sharp turns from fork lift trucks, shrinkage and thermal effects, and impact loads (Knapton, 2003). These fibres, compared to traditional fabric reinforcement, have a tensile strength typically 2-3 times greater and a significantly greater surface area to develop a bond with the concrete matrix (ACIFC, 1999).

2.5.1 Types of Steel Fibres

Many efforts have been made in recent years to optimise the shape of steel fibres to achieve improved fibre-matrix bond characteristics, and to enhance fibre dispersibility in the concrete mix. ASTM A 820 provides a classification for four general types of steel fibres based on the product used in their manufacture (ACI Committee 544.1R, 1996):

- Cold-drawn wire
- Cut sheet
- Melt extracted
- Other fibres

A few of the more common types of steel fibres are shown in Figure 2.3 (Knapton, 2003). Rounded straight and hooked steel fibres are produced by cutting or chopping wire, typically having diameter between 0.25mm and 1.0mm. Flat, straight steel fibres having typical cross sections ranging from 0.15mm to 0.41mm thickness by 0.25 mm to 1.14 mm

width are produced by shearing sheet or flattening wire. Crimped and deformed steel fibres are produced either with full length crimping or bent or enlarged at the ends only. Some fibres are deformed by bending or flattening to increase bonding and facilitate handling and mixing (TR34, 1994). Some fibres have been collated into bundles to facilitate handling and mixing. During mixing, the bundles separate into individual fibres. Fibres are also produced from cold drawn wire that has been shaved down in order to make steel wool. Moreover, steel fibres are produced by the melt-extraction process (ACI Committee 544.1R, 1996).

The ultimate tensile strength of steel fibre ranges from 345-1700 MPa, whereas the length ranges from 19 to 60 mm, the aspect ratio (length/diameter) ranges from 30 to 100 and the Young's modulus is 205 MPa.

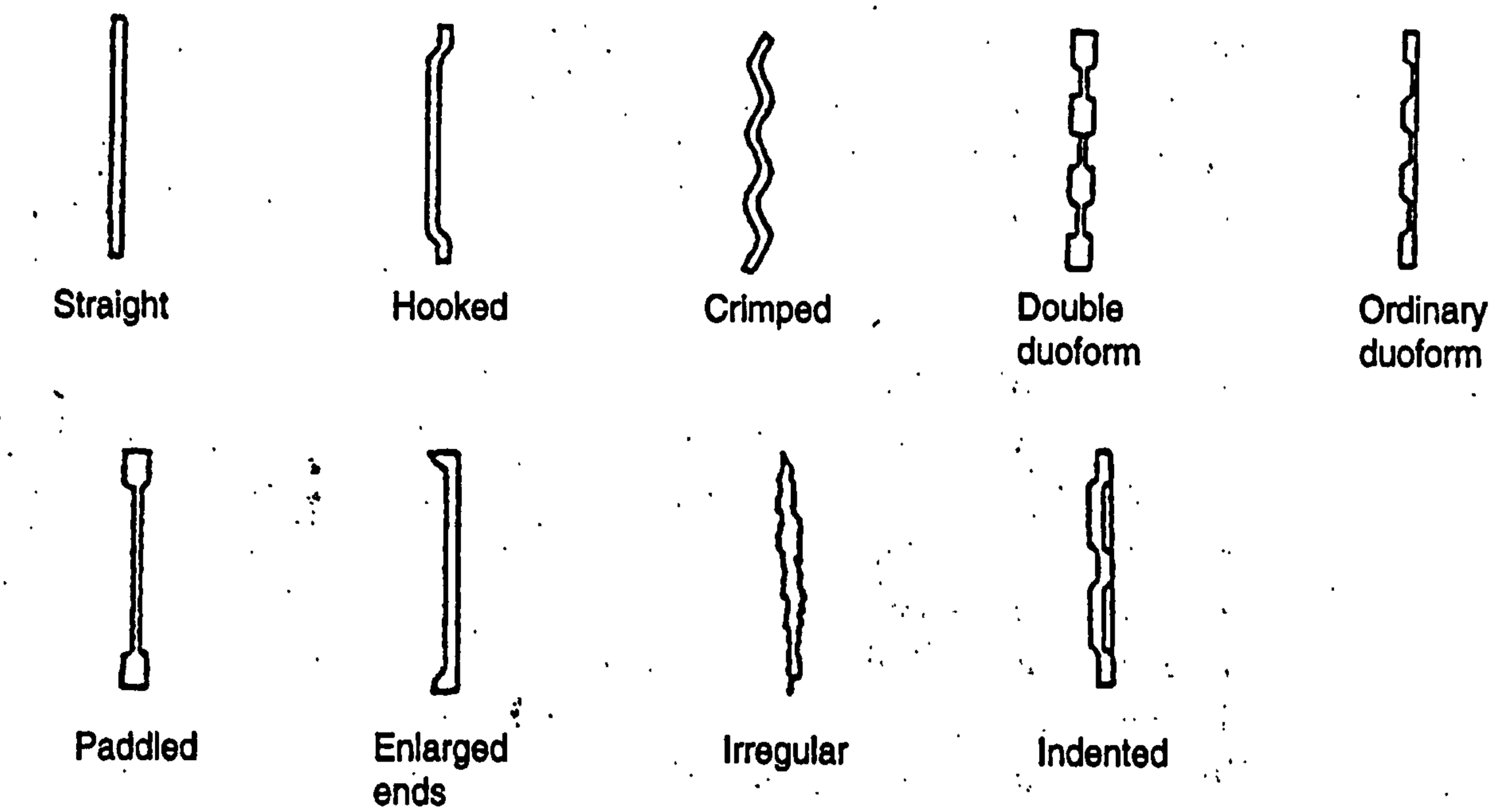

Steel fibre shapes

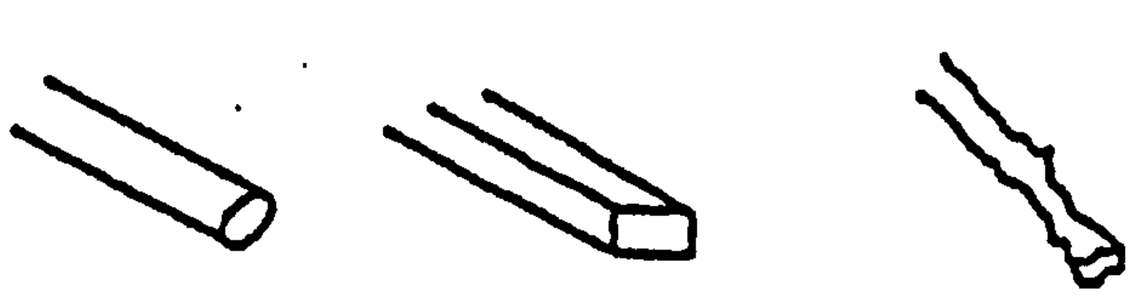

Steel fibre cross sections

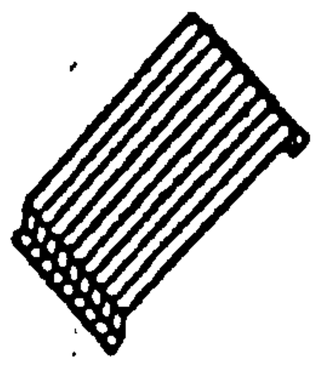

Fibres glued together in a clip

Figure 2.3: Steel fibres cross sections (After Knapton, 2003)

2.5.2 Composition and Quality

Compared to plain concrete, fibre reinforced concrete mixes generally have higher cement and fine contents and smaller aggregates. The slump decreases as the fibre content increases. (Newman and Choo, 2003; ACI Committee 544.1R, 1996). So, in order to obtain steel fibre-reinforced concrete that is easy to pump and to work, with minimum shrinkage, a steel wire manufacturer specifies the following (Bekaert, 1990):

- Quantity of cement should be between 320 and 350 kg/m^3.
- 750-850 kg/m^3 good quality zero to 4mm well graded sharp sand should be used.
- Use a continuous aggregate grading with a maximum size of 28mm for rounded gravel and 32 for crushed stone. Limit the fraction larger than 14mm to 15-20%.
- Characteristic compressive strength of at least 25 N/mm^2 should be used.
- Water/cement ratio should be about 0.50, and should not exceed 0.55.
- The use of superplasticizer is permitted to obtain the necessary workability. Superplasticizers should be used mainly as an aid to increase the workability of standard mixes, or to reduce the w/c ratio of a high workability mix in order to achieve adequate strength and durability in the hardened state (ACI Committee 544, 1986).
- Admixtures of chloride or chloride containing concrete additives are not permitted

2.5.3 Placing Finishing and Curing

Good quality and economic construction with steel-fibre reinforced concrete requires approved mixing, placing, finishing and quality control procedures to be followed (ACI Committee 544.1R, 1996). It is good concrete practice to place concrete as near to its final position as possible. This is even truer for SFRC because of its reduced flow characteristics (Unwalla, 1982; Swamy, 1974).

Conventional tools, equipment and procedure may satisfactorily be used for placing, finishing and curing steel-fibre reinforced concrete (Knapton, 1999; Killen & Dalgleish, 1997; Swamy, 1974 and ACI Committee 544, 1993). After compaction and levelling, anti-wear products and cement are often spread on top of the concrete surface (Knapton, 2003). SFRC should be cured and protected by the same methods and techniques as plain concrete. Inadequate curing methods can produce plastic and shrinkage cracking encountered in conventional concrete (Knapton, 1999; ACI Committee 544, 1993; Swamy, 1974)

2.5.4 Fibre Strengthening Mechanics

Failure in concrete subjected to loading occurs as a result of coalescing and propagation of micro-cracks which are inherent in concrete Li et al (1991) as a result of drying shrinkage and thermal mismatch between aggregates and the matrix during the curing process (Neville, 1995). The fibre reinforcing action is assumed to occur through the fibre/matrix interfacial bond stress. When the composite strain exceeds the cracking strain of the matrix the latter will crack and since the fibres are stiffer than the matrix, they will deform less and as a result will exert less pinching forces at the crack tip. Generally, steel fibres in concrete act to prevent failure by two distinct mechanisms:

- By impeding, coalescing and subsequent growth of micro-cracks into macro cracks.
- By stress transfer across a crack (crack bridging mechanism) once the macro-cracks have formed.

As far as the punching shear in SFRC is concerned, the crack bridging mechanism is more important as it defines the ultimate tensile strength, ductility and energy absorbing characteristics of the concrete composite. The crack bridging efficiency of steel fibres depends on its length, interfacial properties and geometry, as well as the steel fibre properties such as yield strength and ductility.

2.5.5 Factors Influencing the Effectiveness of Fibres

The effectiveness of the reinforcing fibres depends on the fibres' modulus of elasticity, orientation, geometry, shape and length, aspect ratio, volume content and bond strength of the fibre-matrix interface. These parameters are discussed in more details in the following sub-sections.

2.5.5.1 The Modulus of Elasticity of the Un-cracked Composite

It is generally accepted that the modulus of elasticity E_c of fibre reinforced concrete is governed by the law of mixture (Kelly, 1973; Keer, 1984; Hannant, 1978). Hence, prior to the matrix cracking it may be assumed that:

$$E_c = \eta_L \eta_\circ E_f V_f + E_m V_m \qquad \ldots.2.1$$

Where E_c is the modulus of elasticity, V is the volume fraction, c is the composite, f is the fibre, m is matrix, $\eta_\circ$ is efficiency factor depending on the fibre orientation and η_L is the efficiency factor depending on the fibre length. However length and orientation factors are discussed in more details in the succeeding section.

2.5.5.2 Critical Length, Length Efficiency Factor and Orientation Factor

The effect of fibre length on the behaviour of a composite reinforced with discontinuous fibres can be viewed in terms of a parameter referred to as the critical length l_c. It is the minimum length of the fibre required to achieve the full-length capacity (maximum fibre stress, σ_f) of the fibre. However, as the length of the fibre decreases, its crack bridging efficiency decreases.

The value of maximum fibre stress on failure of the composite depends upon the length of the fibre; if the fibre length is long enough, the fibre tensile stress will vary from zero to the fracture stress, σ_{fu}. For a fibre with a length equal to a critical length, the stress σ_f will be equal to σ_{fu} only at the centre point of the fibre, whereas for a short fibre the stress σ_f will not reach the fracture stress and fibre pull-out or de-bonding will occur.

If the fibre length is less than the critical length, failure in composites will be initiated by failure of the matrix surrounding the fibre and subsequently the fibres will pullout. Otherwise, the composites will fail by fibre fracture. So, there is a minimum fibre length required for the fibre stress σ_f to reach the fracture stress σ_{fu} without slipping occurring.

Moreover, considering the strength of a discontinuous fibre composite, two efficiency factors must be introduced, the orientation factor and the length efficiency factor. The orientation factor describes the effect of fibre orientation on the composite strength. The length efficiency factor describes the effect of the fibre length on the efficiency of the reinforcement. The values of the orientation factor, η_0, and the length efficiency factor, η_L, depend on the method of analysis used but some typical values are given below

a) Fibre Orientation

The direction of the fibre orientation relative to the direction of the applied load is an important factor to be considered when determining the efficiency with which the randomly oriented fibres can resist stresses. Although the fibres may be oriented randomly in three dimensions in the mixer, this is seldom the case after vibration and compaction have taken place (Hannant, 1978). For example when using table vibration, the fibres tend to align in planes at right angles to the direction of vibration or gravity.

Krenchel (1974) has used a value of $\eta_0 = 1$, $\eta_0 = 3/8$ and $\eta_0 = 1/5$ for 1-D, 2-D, and 3-D, respectively.

b) Length Efficiency

The length efficiency factor for a given type of concrete depends on whether the fibre length is greater or less than the critical length.

Laws (1971) and Allen (1975) proposed the following values for the length orientation factor:

- When the fibre length is less than the critical fibre length:

$$\eta_L = \frac{l_f}{2l_c} \quad \textbf{for } l_f < l_c \qquad \textbf{....2.2}$$

- When the fibre length is greater than the critical fibre length:

$$\eta_L = 1 - \frac{l_c}{2l_f} \text{ for } l_c < l_f < 2l_c \qquad \text{....2.3}$$

Where the critical fibre length is given by:

$$l_c = \sigma_{fu} \frac{d_f}{4(\eta_b \eta_c \tau_{fm})}$$

Where d_f is the fibre diameter, τ_{fm} is the fibre matrix interfacial bond strength, η_b and η_c are bond efficiency and concrete type factors. The interfacial bond strength is obtained by fibre pull-out tests on fibre embedded in concrete at different orientations. A value for τ_{fm} of 4.14 MPa, η_b of 1.12 and η_c of 0.85 have been proposed by Theodorakopouls and Swamy (1999).

2.5.5.3 Fibre Aspect Ratio (Length/Diameter)

Edgington et al (1974) have shown that the fibre aspect ratio has a crucial influence on the volume of fibres which can be included in the mix while retaining relatively easy compaction. Hannant (1978) suggested that if a number of long thin fibres of aspect ratio greater than 100 are shaken together, they will interlock to form a mat or a type of bird's nest from which it is very difficult to dislodge individual fibres by vibration only. On the other hand, short fibres with an aspect ratio less than 50 are not able to interlock and can easily be dispersed by vibration. Similar effects were observed when fibres were dispersed in mortar or concrete (Hannant, 1978).

2.5.5.4 Content of Fibre

Edgington et al (1974) established a simplified equation which enables an approximate estimate to be made of this fibre content for mixes containing aggregates of normal density.

$$W_f < \frac{600(1 - A_g)}{l/d} \qquad \text{....2.4}$$

Where,

W_f = weight of steel fibres, as a percentage of the concrete matrix, which can be compacted with normal site techniques.

A_g = weight of aggregate greater than 5mm/total weight of concrete.

l/d = fibre aspect ratio.

Swamy (1974) suggested that for SFRC, fibre addition in excess of 4% by volume is difficult to achieve, but most practical mixes rarely contain more than 2% by volume of fibres.

2.5.5.5 Bond Strength of Fibre-Matrix Interface

One of the most important factors influencing the properties of a fibre composite is the bond resistance between steel fibres and cementitious matrix. The steel fibres used in composites are plain, crimped, duoform, and hooked fibres. They have either circular or rectangular cross-section, with length and aspect ratio ranging from 20 to 65 mm and from 40 to 150, respectively.

For a given fibre-matrix system, various indirect and direct methods can be used to determine the bond strength. In the direct methods either a single fibre model or a group of fibres embedded in a block of a matrix material can be used. The value of bond strength is calculated directly from the measured failure load. In the indirect methods, a relative value of bond strength is obtained from the material properties of the composite materials. With steel fibres, the bond strength is a combination of adhesion, friction and mechanical interlocking.

2.5.5.6 The Failure Strain of the Matrix

The failure strain of the matrix is defined as the strain at which cracks propagate unstably across the cross section of a tensile specimen (Keer, 1984). Hannant (1978) believes that the failure strain of the matrix is not affected by the presence of fibres and consequently the cracking stress of fibre is not significantly increased by the presence of fibres. Aveston et al. examined the energy requirements for a crack to form in the matrix and suggested that

the matrix will fail either when it reaches its normal cracking strain, ε_{mu}, or when the strain reaches a value ε_{muc}, whichever is greater. ε_{muc} is given by:

$$\varepsilon_{muc} = \left\{ \frac{12\tau 2_m E_f V_f^2}{E_c E_m^2 r V_m} \right\}^{1/3} \quad \text{....2.5}$$

Where, τ is the fibre-matrix frictional stress transfer, γ_m is the work of failure and r is the fibre radius.

The theory of Aveston et al. (1974) is now considered to give a lower limit to the strain that must be exceeded for cracking to occur.

2.5.6 Mechanical Properties of Fibre Reinforced Concrete

The inclusion of fibres may significantly alter the properties of concrete in both the fresh and hardened states. However, its main contribution is to enhance the properties of hardened concrete such as compressive, tensile and flexural strengths and flexural toughness (Maidl, 1995; ACI Committee 544, 1986, and Keer, 1984).

The extent to which the addition of fibres alters the mechanical properties of concrete is influenced by the fibre type, geometry, volume, and orientation and the bonding between the concrete matrix and the fibres (ACI Committee, 544,1988a).

In the following section the important effects of steel fibres upon the properties of fresh and hardened concrete are discussed.

2.5.6.1 Mechanical Properties of Fresh Steel Fibre-Reinforced Concrete

The inclusion of the fibres into the concrete mix influences its workability, with an increase in the fibre volume and aspect ratio leading to decreased workability (Hannat, 1978; Swamy, 1974; and Edington et al, 1974). Achieving adequate workability is one of the most important problems generated when using steel fibre reinforced concrete. Accordinglt

the ACI Committee report in 1996, reported that in the typical ranges of volume fractions used for steel-fibre reinforced concrete (0.25 to 1.5 volume percent), the addition of steel fibres may reduce the measured slump of the composite as compared to plain concrete in the range of 25 to 120 mm. Incorporation of super-plasticizer is essential to maintaining a good level of workability (120-150 mm) slump. In addition to the above consideration, the balling of fibres must be avoided.

It is generally accepted that SFRC requires more compaction energy than plain concrete (Swamy, 1974; Maidl, 1995). Even though several types of vibration may be employed (Hannant, 1978) external mould vibration is preferable to internal vibration (Swamy, 1974; ACI Committee 544, 1986). The type and direction of vibration can have a critical effect on the fibre orientation relative to the future direction of loading (Edgington and Hannant, 1972; Edgington et al, 1974; Hannant and Spring, 1974; Swamy and Stavrides, 1975) and hence on the properties of the hardened state (Swamy, 1974; Hannant, 1978; and Maidl, 1995).

2.5.6.2 Mechanical Properties of Hardened Steel Fibre-Reinforced Concrete

a) Compressive Behaviour

The compressive strength of concrete is relatively less affected by the presence of fibres as compared to the tensile strength. It has generally been concluded that steel fibres do little to enhance the compressive strength of concrete with increases in strength ranging from zero to a maximum of 30% depending on fibre shape and content. (Ezzeldin and Lowe, 1991; Febrillet et al., 2000; Johanston, 1974; Williamson, 1974). However, the steel fibres do provide increased ductility (energy absorption), which may prove advantageous in a compressive failure (Fanella and Naaman, 1985; Hughes and Fattuhi, 1977; Swamy and Al-Noori, 1975 and Barros and Figueiras, 1999). The typical influence of steel fibres on the compressive stress-strain curve for concrete is illustrated in Figure 2.4.

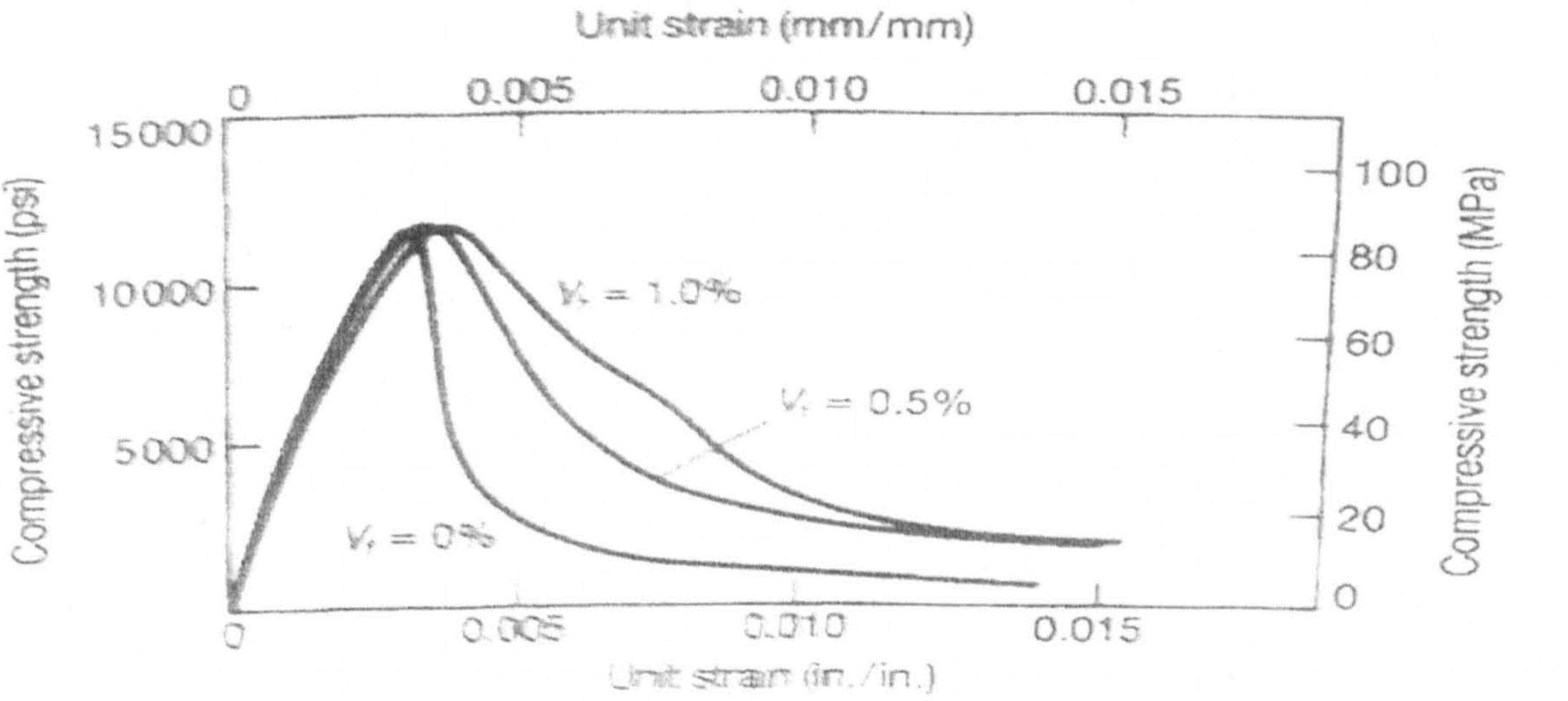

Figure 2.4: Compressive response of fibre strength concrete (After Nawy, 1996)

b) Tensile Behaviour

Steel fibres are used basically to enhance the tensile capacity and energy absorption characteristics of plain concrete, which is weak in tension. A typical tensile response of SFRC is shown in Figure 2.5. The response can generally be divided into three stages depending on volume fraction of fibres and fibre characteristics.

Stage I, before cracking, the composite can be described as an elastic material with a stress-strain response similar to that of a plain concrete matrix. Naaman (1987) used the mechanics of composite materials to predict the tensile stress at cracking by the equation shown below.

$$\sigma_{cc} = \sigma_{mu}(1 - V_f) + \eta_b \eta_\circ \tau_{fm}(V_f l_f / d_f) \qquad \ldots.2.6$$

Where σ_{mu} is the tensile strength of the un-reinforced matrix, V_f and l_f/d_f are the volume fraction and the aspect ratio of fibres respectively and τ_{fm} is the fibre-matrix interfacial bond stress. η_b and $\eta_\circ$ are bond and orientation efficiency factors.

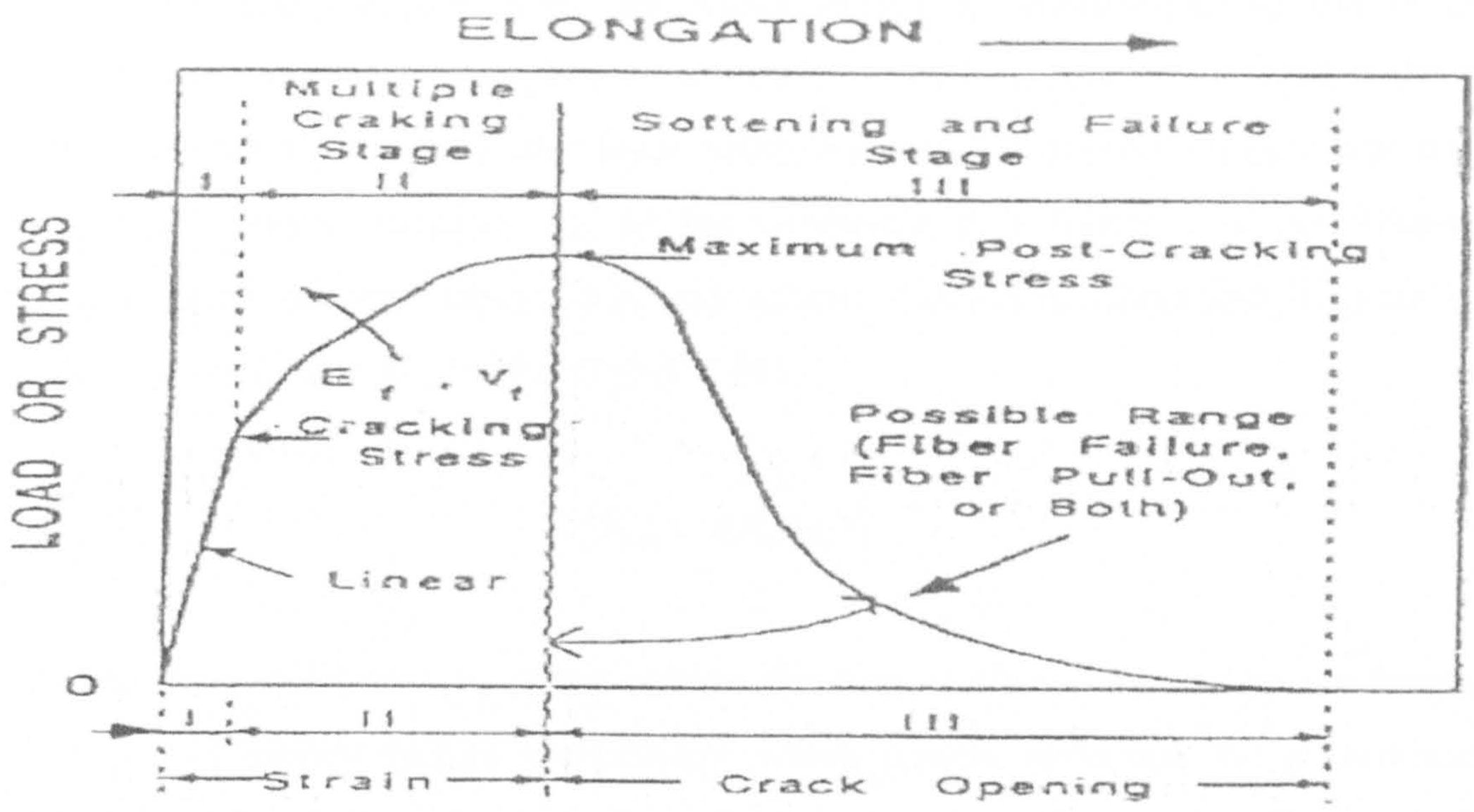

Figure 2.5: Typical load – elongation response of fibre reinforced concrete in tension (After Naaman, 1987)

Stage II, after cracking, the load initially carried by the composite is transformed to the fibres and further cracks develop in the vicinity of the first crack. This stage is referred to as multiple cracking stages and will occur if the fibres are capable of carrying the entire load transformed from the matrix without pulling out or fracturing suddenly.

Multiple cracking may occur when the fibre volume is greater than the critical volume; this is a desirable situation because it changes a basically brittle material with a single fracture surface and low energy requirement to fracture, into a pseudo-ductile material which can absorb transient minor overloads and shocks with little visible damage. Hanannt (1978) defined this as the volume of fibres, which after the matrix cracks will carry the load that the composite sustained before cracking and is given by:

$$V_{fcrit} = \frac{E_c \varepsilon_{mu}}{\sigma_{fu}} \qquad \text{....2.7}$$

Where V_{fcrit} is the critical volume of fibres, ε_{mu} is the strain at which the matrix cracks, σ_{fu} is the failure stress of the fibres, and E_c is the modulus of elasticity.

Stage III, beyond the peak point and characterised by gradual pulling out of and/or fracturing of fibres along a single critical crack. Ductile failure is observed if the fibres pulling out gradually. On the other hand, brittle behaviour is observed if the fibres fracture. The ultimate tensile strength, σ_{ctu} of the composite is a function of the fibre-matrix interfacial bond strength, aspect ratio and volume fraction of fibres and is given by the equation below (Zia et al., 1995 and Hull, 1981).

$$\sigma_{ctu} = \eta_o \eta_L \sigma_{fu} V_f \qquad \text{....2.8}$$

σ_{fu} is the fibre stress and V_f is the volume fraction of fibres, η_L and η_o are length and orientation efficiency factors respectively which greatly influence the performance of SFRC as was discussed in the preceding section.

c) Post-Cracking Behaviour in Tension

The failure strain of a reinforcing fibre is generally substantially higher than that for the matrix. Consequently, significant benefits can be gained if full use is made of the ductility of the fibre component (Keer, 1984).

Ductility is usually determined by the ratio of deflection at ultimate load or at any specified point in the descending part of the load-deflection curve, to the deflection at first crack load.

Once the brittle matrix cracks, a fibre cement or concrete may exhibit three types of post-cracking behaviour in tension:

- The composite fails as the fibres fracture immediately under the increased stress
- The composite can carry a decreasing load as the fibres pull out from the cracked surfaces. After the matrix cracks, the tensile strength of the composite is not increased. However, the strain at complete failure is increased and there can be a considerable increase in the toughness of the composite as measured by the area under the complete

stress-strain curve. This type of behaviour is typical of some short, randomly oriented steel fibre composites (Keer, 1984).

- With a sufficient volume of continuous (or long) steel fibre reinforced cement the material behaves in a pseudo-ductile fashion so that the composite continues to carry an increasing tensile stress and multiple cracking of the matrix accurse (Keer, 1984).

d) Flexural Behaviour

Steel fibres have a much greater effect on the flexural strength of SFRC than on either the compressive or tensile strengths, with increase of more than 100% having been reported (Johanston, 1974). Furthermore, the fibres volume fraction and aspect ratio are the most important factors affecting the flexural strength, with increase in these parameters leading to higher flexural strength. Although, a linear relationship was suggested by many investigators among them, Hannant (1978) a unique relationship could not be established between these parameters due to the wide variability in the published data, such as differences in the matrix strength, the bond strength or the fibre orientation. More recent studies (Soroushian and Bayasi, 1991; Ramakrishnan, 1988; Sri Ravindrarajah and Tam, 1984 and Ramu, 1983) have suggested that deformed (hooked) steel fibres produce similar increases in flexural strength but at lower fibre volumes due to their improved bond characteristics.

e) Flexural Toughness

As was implied in the previous sections, steel fibres are generally added to concrete not necessarily to improve the strength, but rather to improve its toughness or energy absorption. The flexural toughness was found to be affected by the fibres volume fraction and aspect ratio, as in the case of flexural strength (Barros and Figueiras, 1998; Beckett, 1990; and Hannant, 1978). Some researchers among them Ramakrishnan (1988) and Ramu (1983) reported that fibres with better bond characteristics gave higher toughness values than smooth straight fibres at the same volume concentrations.

f) Durability

The long-term stability under various environmental and exposure conditions is the most important property that need to be established for any construction materials and in particular for new materials.

The corrosion of steel fibres has been reported not to cause a durability problem or a substantial change in the properties of the composite with time (Schupack, 1986). Based on tests conducted on normal weight and lightweight concrete cylinders in the un-cracked state placed on three sites covering mild exposure, marine conditions and a polluted industrial atmosphere, over a period of about three years, Edgington et al (1974) reported that the corrosion of fibres within the concrete is unlikely to cause major problems. Steel fibre concrete also shows excellent freeze-thaw resistance, based on short-term studies (Balaguru and Ramakrishnan, 1986). Obviously, long-term results are necessary to establish the performance of steel fibre concrete, but considering that one of the essential properties of the fibres is to enhance the crack control characteristics of the composite, it is unlikely that such composite will be less durable than ordinary concrete.

2.5.7 Investigation of Punching Shear Behaviour of Concrete Slabs with Steel Fibre-Reinforcement

The effect of steel fibre reinforcement on the punching shear capacity of concrete slabs will be discussed extensively in this next section. Although much research has been carried out on SFRC, little attention has been focused on the punching shear behaviour of SFRC slabs. As a result, the full economical benefits of steel fibres in such applications may not be realised. Presented below are some of the notable works previously done in this field and also some relationships currently available to estimate the punching shear strength of concrete slabs as a function of fibre parameters. For design purposes, the absolute punching shear capacity of steel fibre reinforced concrete slabs can be obtained by adding the ultimate shear resistance of conventional slabs (without fibres) and the incremental increase in shear strength due to the presence of fibres.

Seven slab-column connections were tested by Patel (1970). The size of the slab specimen was taken as 1.22x1.22m, 101 mm thick with a column stub of 203mm in diameter in the centre. The steel fibres were flat strips 0.25x0.56 mm cross-section and 19-25.4 mm long. Two percentages 0.574% and 1.20% by volume were used. The strength of all seven specimens was controlled by flexure. The maximum column load was reported as 56.93kN obtained by a slab without fibres, which has a tensile reinforcement ratio of 0.32% and a similar slab with 1.2% fibres. Inclusion of fibres was noted to increase the load needed for visible flexure cracking of the slab. As the amount of steel fibres was increased, the cracks become finer, whereas the crack pattern was observed to be almost the same. Due to the fact that only flexure failures were observed, he concluded that the fibres were effective in preventing shear type of failures.

Criswell (1974) tested four one-third scale 0.635 x 0.635 m, 51 mm thick, with 114 mm square column stub. Two steel reinforcement ratios of 1.04% and 1.88% with 1.0% by volume steel fibres or no fibres were used in the four slabs. The steel fibres were flat strips 0.254 x 0.56 mm of cross section and 26.4 mm long. The strength of the two slabs with 1.04% steel ratio was controlled by flexure and the two slabs with 1.88% ratio by punching. He concluded that percentage increases in strength and deflection at failure were larger for the specimens with the lower percentage of steel bars. The inclusion of fibres also improved the residual resistance remaining after punching failure.

To study the shear behaviour of SFRC slabs, Swamy and Ali (1982) investigated 19 full-scale slabs. The main variables in their investigation were, fibre content ranging between 0 – 94.2 kg/m^3 corresponding to 0-1.2% volume fraction and percentage of flexural and shear reinforcement. They observed that, the addition of fibres reduced the slab deformations at all stages of loading, particularly after cracking and also increase its ductility and energy absorption. Furthermore, they concluded that although bent-up shear reinforcement was more effective in resisting punching shear, it was four times as labour intensive as fibre reinforcement.

Alexander and Simmonds (1992) tested six square slab-column connection specimens. The dimensions of the slab specimens were of square shape with 2750 mm side length and

155mm slab depth. The main variable investigated was fibre quantity. Corrugated steel fibres 50mm in length with quantity ranging between 0 kg/m^3 to 69 kg/m^3 were used. They concluded that the addition of fibres increased the punching shear capacity of the specimens by 20 to 30 percent.

Shaaban and Gesund (1994) tested thirteen slab specimens the dimensions of which were 1600 mm square by 82.5mm total depth. The concrete used had a compressive strength ranging between 22.0-47.6 MPa. They used corrugated steel fibres 25 mm in length with a nominal tensile strength of 1200 MPa. In their experiments, the quantity of the fibres was the only variable and ranged between 0 – 140 kg/m^3 (0 - 6% of the weight of the concrete matrix). From statistical analysis of their experimental results, they came up with empirical equation shown below for predicting the punching shear resistance of a fibre-reinforced slab.

$$P_u = (3.95e^{-0.05w_f} + 0.025e^{0.45w_f})f_{sp} \quad \text{....2.9}$$

Where P_u is the ultimate punching shear strength (kN), W_f is the fibre content expressed as a percentage of the concrete weight and f_{sp} is the split-cylinder strength (MPa).

Tan and Paramasivam (1994) found that increasing the volume fraction of fibres led to increase in the punching shear capacity of the slab. They also concluded that the critical punching shear perimeter was found to occur at some distance away from the loading plate. Measurements on both the top and bottom surfaces of the slabs indicated that the critical perimeter formed on average, at a distance of about 4.5 times the effective depth from the perimeter of the loading plate. The shear plane was inclined at an angle varying from 20° to 60° to the plane of the slab. Moreover, the results of their work showed that the value of the span to depth ratio does not affect the cracking, yield and ultimate load significantly. This is because the curvature of the slab is proportional to the applied load and independent of the effective span of the slab. The ultimate load was found to increase as the slab depth increases.

Harajli et al (1995) tested twelve simply supported square small-scale isolated slab-column connections. The specimen's side length was 650mm and their depth ranged from 55 to 75mm. The load was applied through a 100mm square column cast monolithically with the slab. Hooked end steel fibres were used with a concrete compressive strength ranging from 22.0-32.2 MPa. Several parameters were investigated such as slab depth, fibre content and fibre aspect ratio. They observed that steel fibres substantially improved the ductility of the slab-column connections and modified the mode of failure from punching to flexure. An increase in the ultimate punching shear capacity was also observed to vary linearly with the steel fibre content. From a linear fit of the experimental data, they proposed the following equation for predicting punching shear:

$$p_u = (0.54 + 0.009V_f)b_o d\sqrt{f_c} \qquad \text{....2.10}$$

Where P_u is the ultimate punching shear strength (kN), V_f is percentage of fibres by weight of content, f_c is the concrete compressive strength (MPa), b_o is the critical punching perimeter and d is the effective depth of the slab in mm, herein defined as the distance from the tension face of the slab to the average position of the orthogonal flexural reinforcement. They also found that the increase in punching shear as steel fibres increased was not very sensitive to the span-depth ratio of the slabs and that steel fibres decreased the angle of shear failure plane of the slabs and hence pushed the failure surface away from the column face. This resulted in increasing their punching shear resistance. The distance of the outer edge of the cracked surface to the column face varied between 2.3 x h and 2.82 x h (h = slab thickness), in steel fibre slabs, as compared to 1.82xh in conventional slabs.

Prisco and Felicetti (1997) tested fifteen fixed supported circular slabs. The slabs were originally cast as square slabs of length 330mm and height 70mm, then were sawn into circular shape, and the height was reduced by grinding to 55mm. Hooked end steel fibres of length 30mm and diameter 0.5mm were used in the mix with the fibre content ranging between 19.2kg/m^3 and 62.7kg/m^3 which corresponds to 0.25% - 0.8% volume fraction. They observed that low fibre contents had little effect on the ultimate punching shear strength but high fibre contents (0.8 %) increased the peak load and the energy dissipated significantly. It should be noted that with the support conditions they had, it is very

difficult to single out and quantify the effect of the steel fibres on the behaviour of the specimens as compressive membrane action comes into play.

2.5.8 Current Methods Dealing with Punching Shear in SFRC Slabs

Punching shear capacity is determined in accordance with design codes by checking the shear at the face of the contact area and the critical parameter distance (ranged between 0.5d to 2d, where d is the effective depth).

Design codes are written on the bases of conventional reinforcement and hence they are not suitable to be implemented in the current study. However, Concrete Society in their technical report TR34 (TR34, 2003) proposed a design formula for punching shear capacity of SFRC slabs.

Based on RILEM guidance (RILEM TC 162-TDF, 2002) the presence of steel fibres will increase the design shear capacity over that of the plain concrete by an amount v_f given by:

$$v_f = 0.12 R_{e,3} f_{ctk.fl}$$

Where,

$R_{e,3}$ = Equivalent flexural strength ratio

$f_{ctk,fl}$ = Characteristic flexural strength of plain concrete

The draft Eurocode EC2 gives a minimum shear capacity of 0.035 $k_1^{3/2}$ $f_{ck}^{1/2}$. Thus for steel fibre reinforced concrete the slab load capacity, P_p, is given by:

$$P_p = \left(0.035 k_1^{3/2} f_c^{1/2} + 0.12 R_{e,3} f_{ctk,fl}\right) u_1 d \qquad \text{.....2.11}$$

Where:

$k_1 = 1 + (200/d)^{0.5} \leq 2$

u_1 = The length of the perimeter at a distance 2d from the loaded area

d = The effective depth of the slab

2.5.9 General Discussion

From the above discussion on the theoretical and experiential work done to date in the area of punching shear of concrete slabs, parameters such as concrete strength, column size (loaded area), column type, column shape, slab thickness, slab span-to-depth ratio, in plane restraint and the angle of the punching cone, ratio of flexural reinforcement, ratio of compression reinforcement and ratio of fibre-reinforcement are the influencing factors affecting the punching shear behaviour of flat slabs. However, As this research focused on studying the behaviour of steel fibre-reinforced concrete slabs subjected to punching shear without taking into account any longitudinal reinforcement, the effect of all the parameters mentioned above except the ratio of flexural and compression reinforcement will be taken into account in the conducted parametric study using FE analysis as is discussed in chapter four.

Based on experimental studies some proposed equations for predicting punching shear are available in the literature (i.e. equations 2.9 and 2.10), these equations are limited to a certain type of steel fibres and slab geometry. Moreover, the tested slabs were reinforced with conventional steel bars. So that, these proposed equations are inappropriate to be implemented for the current study.

Although the formula proposed by the TR34 (TR34, 2003), see section 2.5.8, take into account the effect of steel fibres on punching shear capacity of concrete slabs, it was developed for slabs reinforced with both conventional bars and steel fibres, so that it is also inappropriate to be applied in the current study.

2.6 Concluding Remarks

It is clear from the reviewed literature presented in this chapter that there is no theoretical or analytical model developed for punching shear behaviour of SFRC slabs with no longitudinal reinforcement, which indicates that more research is needed in this field. Hence, it is mandatory to develop a new model by using a modern computational

technique, such as the FE method, and to provide an updated set of guidelines if necessary. It is also clear that this research is needed in order to study the structural effect of introducing steel fibre reinforcements on the punching shear capacity of concrete slabs, especially after cracking takes place.

The present literature survey, on the other hand, enables one to obtain useful data on the developed model for punching shear of flat slabs as well as, the influencing factors of the punching shear capacity of flat slabs.

As the need for further research was outlined, the FE analysis of the beams and slabs are described in the following chapters.

CHAPTER THREE

FINITE ELEMENT METHOD AND ABAQUS CONCRETE MODELS

3.1 Introduction

To an increasing degree, computational modelling of reinforced concrete structures is being employed to understand more fully their behaviour considering the complex interactive effects of various parameters. Finite Element Method is one of the promising methods as applied to reinforced concrete structures.

Finite element method and material modelling of concrete has been extensively covered (Zienkiewicz and Taylor, 1989; Bathe, 1996; Hinton, and Owen, 1989; Bangash, 1989; Kotsovos and Pavlovic, 1995 and Chen, 1982). However, the nonlinear behaviour of reinforced concrete such as concrete cracking, tension stiffening and concrete plasticity have been extensively studied by various researchers and constitutive laws have been proposed (ASCE, 1982; Chen, 1982; Vecchio and Collins, 1986). Therefore, an increasing number of researchers are using finite element to study the behaviour of reinforced concrete structures. This chapter described the choice of the material model utilised in the current research. In addition, the main features available in the selected model are presented.

3.2 General Description of the Finite Element Method

The actual number of degrees of freedom in any continuum system is infinite, and hence an exact analysis is impossible unless a closed form solution is available. In the finite element method, the continuum is divided by imaginary boundaries into a set of smaller regions known as finite elements, the elements are then assumed to be interconnected at a finite number of nodal points at element corners or on element boundaries. The division process is called discretization. However, there is no unique way of discretizing a structure. This will have to rely on the analyst's experience to choose an appropriate finite element mesh.

The fundamental variable of formulating finite element stiffness matrices for structural analysis is the nodal displacement. Therefore, in this formulation one will be seeking to express the element responses (i.e. displacement, stress, and strain) in terms of the nodal displacement. However, the displacement is assumed to have unknown values only at the nodal points so that the variation within any element is described in terms of the nodal values by means of interpolation functions or shape functions.

$$\{u\} = [N]\{d\} \qquad \text{.....3.1}$$

Where {u} is the matrix of displacements within the elements, {d} is the nodal displacements matrix and [N] is the shape function matrix.

The strains within the element can be expressed in terms of the element nodal displacement by differentiating shape functions.

$$\{\varepsilon\} = [\partial]\{u\} = [B]\{d\} \qquad \text{.....3.2}$$

Where {ε} is the element strains matrix and $[B] = [\partial]\{N\}$.

Stress σ may be related to the strain by use of an elasticity matrix D as:

$$\{\sigma\} = [D]\{\varepsilon\} \qquad \text{.....3.3}$$

Where {σ} is the element stresses matrix and [D] is the matrix of constitutive relations. Now substituting (3.2) into (3.3) yields

$$\{\sigma\} = [D][B]\{d\} \qquad \text{.....3.4}$$

The governing equilibrium equations for structural applications can be obtained by minimising the total potential of the system. The total potential, π, can be expressed as:

$$\pi = 0.5\int_v \{\sigma\}^T\{\varepsilon\}dv - \int_v \{\delta\}^T\{p\}dv - \int_v \{\delta\}^T\{q\}ds - \{P\}\{\delta\}^T \qquad \text{.....3.5}$$

Where σ and ε are the stress and strain vectors, respectively, δ is the displacement at any point, **p** is the body force per unit volume, **q** is the applied surface tractions, and **P** is the concentrated nodal force vector. Integration is carried out over the volume v of the structure and the loaded surface area s. The first term on the right hand side of equation 3.5 represents the internal strain energy and the remaining terms are the work contributions of the external forces p, q and P, respectively.

The total potential energy of the continuum will be the sum of the energy contributions of the individual elements. Thus

$$\pi = \sum \pi_e \qquad \text{.....3.6}$$

Where, π_e represents the total potential energy on an element *e*. By using equation 3.5, π_e can be written as:

$$\pi_e = 0.5\int_{v_e} \{\delta^e\}^T [B]^T [D]^T [B]\{\delta^e\} dv - \int_{v_e} \{\delta^e\}^T [N]^T \{p\} dv - \int_{s_e} \{\delta^e\}^T [N^T]\{q\} ds \qquad \text{.....3.7}$$

Where, v_e is the element volume, s_e is the loaded element surface area. Minimisation of π_e for element e with respect to the element nodal displacement δ_e results in:

$$\frac{\partial \pi_e}{\partial \delta^e} = \int_{v_e} [B]^T [D]^T [B]\{\delta^e\} dv - \int_{v_e} [N]^T \{p\} dv - \int_{s_e} [N]^T \{q\} ds \qquad \text{.....3.8}$$

$$= [K^e]\{\delta^e\} - \{F^e\} = 0$$

$$\text{Where, } \{F^e\} = \int_{v_e} [N]^T \{p\} dv + \int_{s_e} [N]^T \{q\} ds \qquad \text{.....3.9}$$

Are the equivalent nodal forces for the element, and

$$[K^e] = \int_{v_e} [B]^T [D]^T [B] dv \qquad \text{.....3.10}$$

is termed element stiffness matrix. The summation of the terms in equation 3.8 over all the elements, when equated to zero, results in a system of equilibrium equations for the complete continuum, i.e.

$$\{F\} = [K].\{\delta\} \qquad \text{.....3.11}$$

Where $\{F\}$ is the equivalent nodal forces for the continuum, $[K]$ is the global stiffness matrix of the continuum and $\{\delta\}$ is the nodal displacement of the continuum.

These equations are then solved by any standard technique to yield the nodal displacements. Once the displacements are determined, the strains and thereafter the stresses in each element can be evaluated by using equations 3.2 and 3.3, respectively.

3.2.1 Non-linear Analysis

When large displacements or material non-linearties are considered, the true structural behaviour is non-linear, being characterised by non-proportional variation of displacements with loading. As pointed out in section 3.3, due to the nature of concrete at the material level, the behaviour of a concrete structure is highly non-linear. The constitutive models that depict the behaviour will be outlined in section 3.2. A non-linear problem is solved by a search process based on repeated solutions (iterative) of linear systems until a specified degree of accuracy (convergence tolerance) is achieved.

If there is concern about material non-linearity, geometric nonlinearity or an unstable response as in the case of the current FEA, ABAQUS uses the modified Riks method (Riks, 1972; Park, 1975; Powell and Simons, 1981; Ramm, 1981 and Crisfield, 1981) to perform the analyses of the structure. This method assumes proportional loading and develops the solution by stepping along the load-displacement equilibrium line with the load magnitude included as an unknown, see Figure 3.1. Therefore, another quantity must be used to measure the progress of the solution; ABAQUS uses the arc-length, along the static equilibrium path in the load-displacement space. You need also to provide an initial increment in arc length along the static equilibrium path, when you define the step. This

approach provides solutions regardless of whether the response is stable or unstable. When the Riks method is used, the relative magnitudes of the various loads given on the data lines specify the loading pattern. The actual magnitudes are computed as part of the solution. The user must prescribe loads and provide solution parameters that will give a reasonable estimate of the initial increment of the load. If the response is linear, this first increment of the load will be the ratio of the initial time increment of the time period, multiplied by the actual load magnitude. If the response is nonlinear, the initial load increment will be somewhat different, depending on the degree of the nonlinearity. For more information about this method the reader should refer to, The Riks procedure described and presented in the ABAQUS Theory Manual (ABAQUS, 2006b).

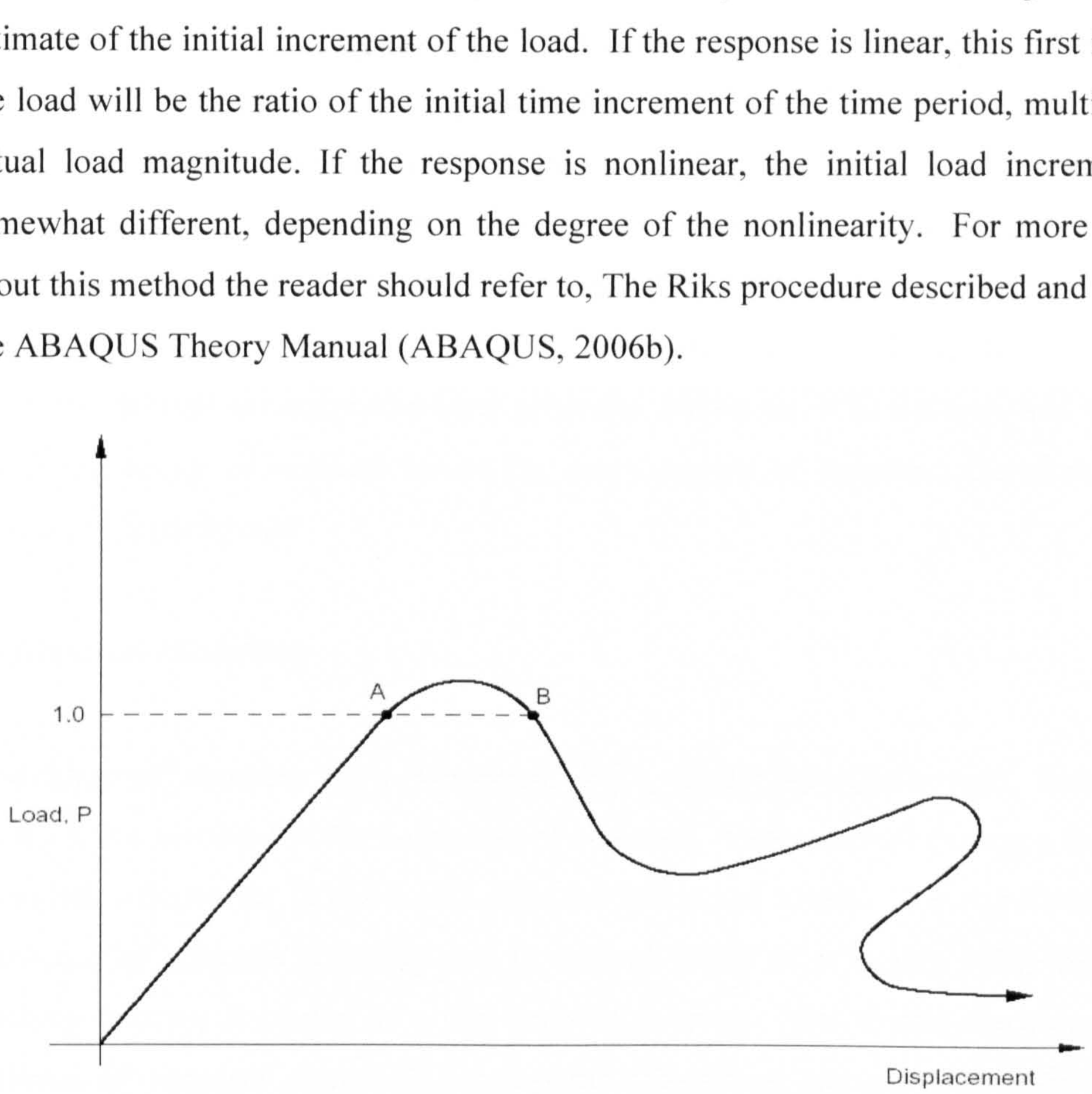

Figure 3.1: The modified Riks method: Proportional loading with unstable response (after ABAQUS 2006a)

However, the solutions of non-linear problems by the finite element method are usually attempted by the incremental-iterative method. The details of this method are described elsewhere (Zienkiewiez and Taylor, 1989; Bathe, 1996; Hinton and Owen 1989; Kotsovos and Palvlovic, 1995). The incremental/iteration procedure is adopted in this study. In this method, the load is applied in increments and the solutions are obtained iteratively until equilibrium is achieved to an acceptable level of accuracy. The stiffness is calculated by using the secant modulus approach (because the concrete constitutive law requires the use

of secant modulus) as a starting value for the iterative process. The stiffness is then updated at the second iteration of each increment.

The equilibrium conditions are checked by evaluating "residual forces". The basic technique of this method is that, at any stage, a load system evaluated from the stress in the structure is checked against the applied load system. The difference between these two will result in a set of residuals. These residuals are then applied to the structure to restore equilibrium. The process is then continued to dissipate the residual forces to a sufficiently small value. Therefore, it is important to include reliable convergence criteria which will ensure the gradual elimination of the residual forces and terminate the iterative process when the desired accuracy has been achieved. However, it is difficult and expensive to check the decay of residual forces for every degree of freedom; therefore, an overall evaluation is preferable.

3.3 Material Modelling

Modelling of concrete in a non-linear FEA is not straightforward, because of the complexities involved in the behaviour of concrete. Experimental evidence shows that the behaviour of concrete is non-linear even for low stress levels. The significant non-linear behaviour of concrete is mainly due to various forms of softening behaviour, especially cracking because it occurs at a low level of loading. The tensile cracking reduces the stiffness of concrete structural components. Therefore, the use of continuum damage mechanics is necessary to accurately model the degradation in the mechanical properties of concrete. An appropriate finite element model of cracking is essential to get satisfactory results.

The cracking process can be represented by two approaches. The first approach uses the discrete crack representation model, which is based on the stress-displacement (σ-w) concept. The discrete crack approach is usually based on the fracture mechanics theory. This means that the criteria for crack propagation and, eventually, the prediction of the direction of propagation come directly from this theory, which is, mostly, based on the energy criteria. Discrete crack models perceive the individual cracks as actual

discontinuities in the topology of the FE mesh. For more details about this approach and its use in ABAQUS, the reader can refer to (Vitali & Zanatelli, 1994 and Gasser & Holzapfel, 2005).

Concrete models native to ABAQUS are based on the second approach, which is the smeared crack approach (σ-ε method). The smeared crack approach is always based on the continuum mechanics theory, in the sense that the criteria for crack propagation and the prediction of the direction of propagation come directly from this theory, which is, mostly, based on failure criteria expressed in terms of stresses or strains. In this type of cracking models, the cracked material is assumed to remain a continuum and the mechanical properties (stiffness and strength) are modified to account for the effect of cracking, according to the evolving states of strain and/or stress. This method was first introduced by Rashid (1968) and then enhanced by Leibengood et al (1986) considering the effects of shear retention, Poisson's ratio and tension stiffening due to reinforcement.

There are three established models for reinforced concrete offered by ABAQUS, Cracking Model for Concrete, Concrete Damaged Plasticity Model and Smeared Cracking Model. The choice of suitable material model for the current study is discussed below:

The Cracking Model for concrete is designed for applications in which the behaviour is dominated by tensile cracking using the smeared crack approach to represent the discontinuous brittle behaviour in concrete. However, in this model the compression behaviour is always linear elastic, which makes the modelling of non-linear plastic compression behaviour impossible. Hence, this model was inappropriate for the current study.

The concrete Smeared Cracking Model is a traditional concrete model. It consists of an isotropically hardening yield surface with associated flow that is active when the stress is dominantly compressive and the independent crack detection surface that determines if a point fails by cracking, see Figure 3.2. A damaged elasticity concept is also used to describe the reversible part of the material's response after cracking failure.

The damaged Plasticity Model consists of non-associated hardening plasticity and isotropic damaged elasticity to describe the irreversible damage that occurs during the fracturing process. It also allows for stiffness recovery effects during cyclic load reversals. However, Damaged Plasticity Model was preferred over the Smeared Cracking Model for the following reasons:

- The Damaged Plasticity Model allows for stiffness recovery effects, while the Smeared Cracking Model cannot. This is an important feature when modelling SFRC structures. As in such structures, during failure the cracks are initially bridged by fibres. Further damage is mostly caused by fibre pull-out; however, some of the fibres also break. Damage is localized in a softening zone perpendicular to the loading direction. This softening zone is also referred to as the crack band, which is a zone of distributed micro-cracks, which consequently link up during strain softening. The key features of the material behaviour should be the development of a strain softening yield surface, permanent (plastic) deformation, as well as stiffness degradation and recovery.
- A distinguishing difference between the Smeared Cracking Model and the Damaged Plasticity Model is that the first model assumes an associated potential flow (which defines the directions of the flow of plasticity) and yield (hardening) functions, while the second model assumes a non-associated potential flow function and utilises an independent yield function. Using a non-associate (i.e. independent) potential flow and yield functions as opposed to associated functions is aimed at providing a more realistic simulation of the concrete material. Park and Kim (2005) used a non-associative flow rule in conjunction with a Damaged Plasticity model to describe the dilatancy due to the compressive damage.
- A preliminary work carried out at the early stages of this research showed that there is a difficulty in getting a converging solution in both beam and slab models using the Smeared Cracking Model, whereas the same problem was not encountered when using the Damaged Plasticity Model.

Accordingly, the Damaged Plasticity Model has been selected to be the most appropriate concrete models for the purpose of this study. The use of this model has been supported by

other recent researchers including Robinson et al (2004) and Taylor and Robinson (2004). More details of this model are presented in the following sections.

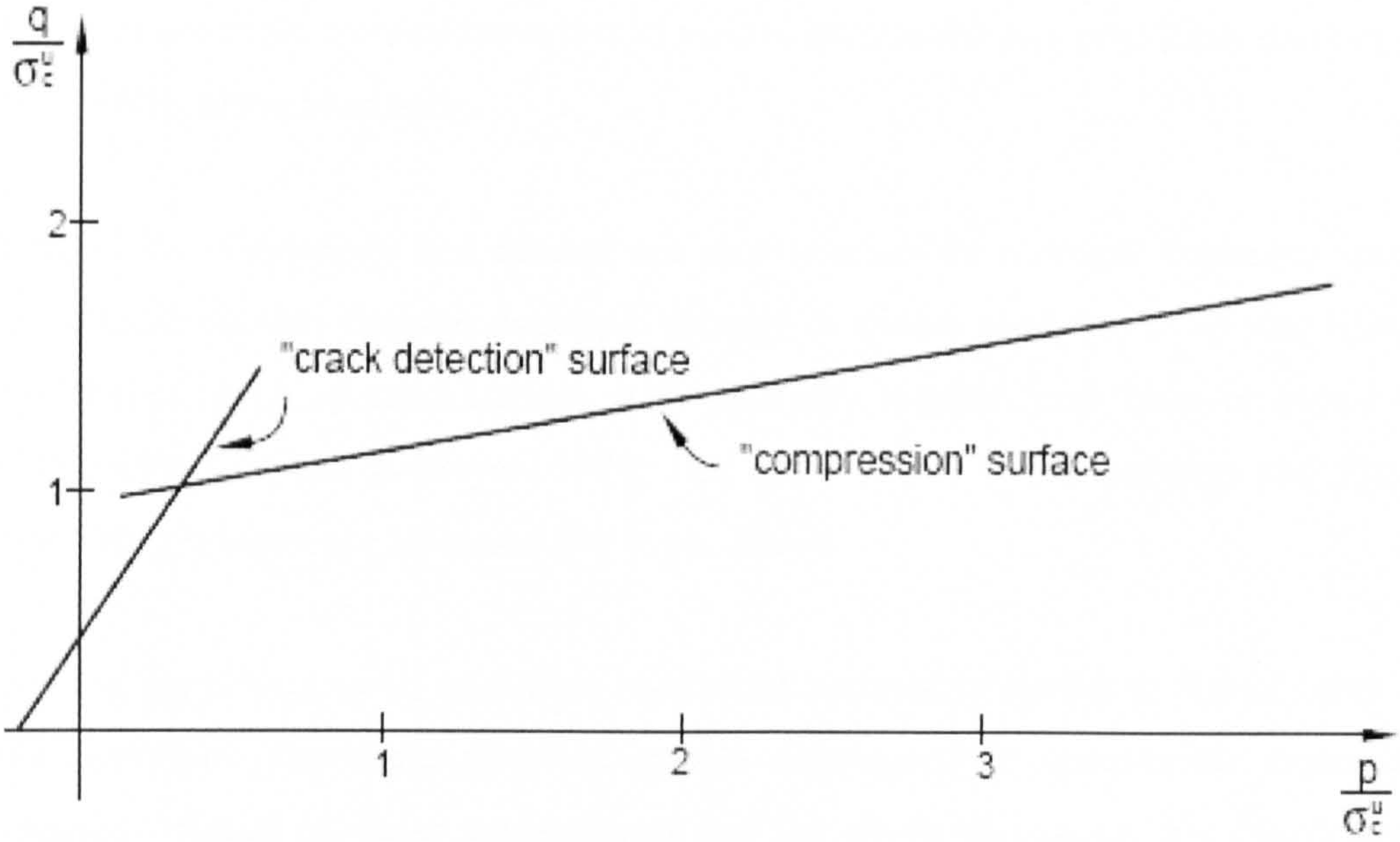

Figure 3.2: Yield and failure surfaces in the (p-q) plane, smeared crack model (After ABAQUS 2006a)

3.4 Reasons for Using the Damaged Plasticity Model

Plasticity theories have been used in modelling the behaviour of concrete by many researchers among them (Chen and Chen, 1975; William and Warnake, 1975; Bazant, 1978; Dragon and Mroz, 1979; Schreyer, 1983; Chen and Buyukozturk, 1985; Onate et al., 1988; Voyiadjis and Abu-Lebdeh, 1994; Karabinis and Kiousis, 1994; Este and Willam, 1994; Menetrey and Willam, 1995 and Grassl et al., 2002). However, using only plasticity to characterise the concrete behaviour failed to address the degradation of the material stiffness due to micro-cracking. On the other hand, Loland, 1980; Ortiz and Popov, 1982; Krajcinovic, 1983; Krajcinovic, 1985; Resende and Martin, 1984; Simo and Ju, 1987a; Simo and Ju, 1987b; Mazars and Pijaudier-Cabot, 1989 and Lubarda et al., 1994 have used the continuum damaged theory alone to model the material nonlinear behaviour such that the mechanical effect of the progressive micro-cracking and strain softening are represented by a set of internal state variables which act on the elastic behaviour (i.e. decrease the stiffness) at the macroscopic level. However, there are several facets of

concrete behaviour (e.g. irreversible deformations, inelastic volumetric expansion in compression and crack opening/closure effects) that cannot be represented by this method. Since both micro-cracking and irreversible deformations contribute to the nonlinear response of concrete, a constitutive model should address the two physically distinct modes of irreversible changes equally.

Combinations of plasticity and damage are usually based on isotropic hardening combined with isotropic (scalar) damage. Isotropic damage is widely used due to its simplicity such that different types of combinations with plasticity models have been proposed in the literature (Yazdani and Schreyer, 1990; Lee and Fenves, 1998; Gatuingt and Pijaudier-Cabot, 2002; Jason et al., 2004 and Wu et al., 2006).

Moreover, the behaviour of steel fibre reinforced concrete is similar to that of other quasi-brittle materials. Therefore, material models developed for quasi-brittle materials are considered. Based on these requirements and the above discussion, the Plastic-Damage model proposed by Lubliner et al. (1989) and extended by Lee and Fenves (1998) has been chosen for the present study. This model was developed for quasi-brittle materials like concrete, rock and ceramics. It captures the material behaviour using both classical plasticity and continuum damage mechanics. Therefore, this model is supposed to have a wide range of applicability and can serve as an appropriate material model for the present material.

3.5 Damaged Plasticity Model

The concrete Damaged Plasticity Model is intended to provide a general capability for the analysis of concrete structures under static, cyclic and/or dynamic loading. The model is also suitable for the analysis of concrete and other quasi-brittle materials such as rock, mortar and ceramics. The Plasticity Model can be considered as an upgraded version of the traditional Concrete Smeared Cracking Model.

This model assumes that the main two failure mechanisms are tensile cracking and compressive crushing of the concrete material. The evolution of the yield or failure surface

is controlled by two hardening variables, $\tilde{\varepsilon}_t^{pl}$ and $\tilde{\varepsilon}_c^{pl}$, linked to failure mechanisms under tension and compression loading, respectively. These variables are referred to as tensile and compressive equivalent plastic strains, respectively.

The main components and assumptions about the mechanical behaviour of concrete are discussed in the following sections.

All the figures and descriptive information of the various features offered by ABAQUS have been extracted from the software manufacturer's documentation (ABAQUS 2006a, b)

3.5.1 Uniaxial Condition

The model assumes that the uniaxial tensile and compressive behaviour of concrete is represented by damaged plasticity, as shown in Figure 3.2. Under uniaxial tension the stress-strain behaviour follows a linear elastic relationship until the value of the linear stress, σ_{to}, is reached. This failure stress corresponds to the start of micro-cracking in the concrete material. Beyond the failure stress, the formation of micro-cracks is represented microscopically with a softening stress-strain response, which induces strain localisation in the concrete structure, unlike the traditional Smeared Cracking model, which does not track individual macro cracks. Under uniaxial compression, the behaviour is linear until the value of initial yield, σ_{co}, is reached. In the plastic regime the response is typically characterised by stress hardening followed by strain softening beyond the ultimate stress, σ_{tu}. This representation, although somewhat simplified, seems to capture the main features of the behaviour of concrete.

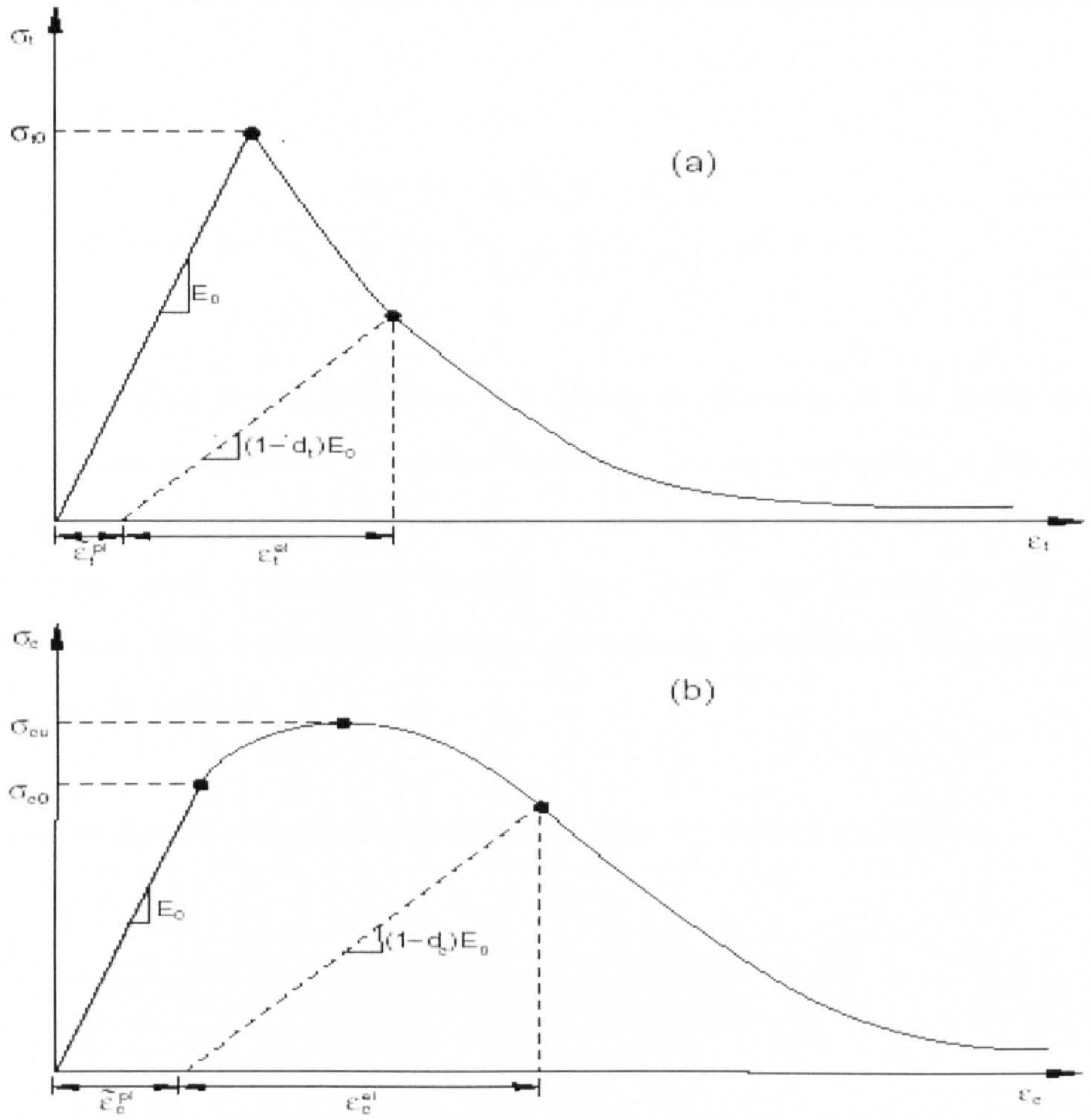

Figure 3.3: Response of concrete to uniaxial loading in tension (a) and compression (b) (After ABAQUS 2006a)

As shown in Figure 3.3 when the concrete is unloaded from any point on the strain softening branch of the stress-strain curves, the unloading response is weakened, i.e. the elastic stiffness of the material appears to be damaged or degraded. The degradation of the elastic stiffness is characterised by two damage variables, d_t, and, d_c, which are assumed to be function of the plastic strains:

$$\mathbf{d_t = d_t\left(\tilde{\varepsilon}_t^{pl}\right),\quad 0 \le d_t \le 1} \qquad \text{.....3.12}$$

$$\mathbf{d_c = d_c\left(\tilde{\varepsilon}_c^{pl}\right),\quad 0 \le d_c \le 1} \qquad \text{.....3.13}$$

The damage variables can take values from zero, representing the undamaged material, to one, which represents total loss of strength. If E_o is the initial (undamaged) elastic stiffness

of the material, the stress-strain relations under uniaxial tension and compression loading are, respectively.

$$\sigma_t = (1 - d_t) E_o \left(\varepsilon_t - \tilde{\varepsilon}_t^{pl}\right), \qquad \text{.....3.14}$$

$$\sigma_c = (1 - d_c) E_o \left(\varepsilon_c - \tilde{\varepsilon}_c^{pl}\right) \qquad \text{.....3.15}$$

Under uniaxial loading cracks propagate in a direction transverse to the stress direction. The nucleation and propagation of cracks, therefore, causes a reduction of the available load-carrying area, which in turn leads to an increase in the effective stress. The effect is less pronounced under compressive loading since cracks run parallel to the loading direction; however, after a significant amount of crushing, the effective load-carrying area is also significantly reduced.

The effective tensile and compressive cohesion stresses are defined as follows:

$$\bar{\sigma}_t = \frac{\sigma_t}{(1 - d_t)} = E_o \left(\varepsilon_t - \tilde{\varepsilon}_t^{pl}\right) \qquad \text{.....3.16}$$

$$\bar{\sigma}_c = \frac{\sigma_c}{(1 - d_c)} = E_o \left(\varepsilon_c - \tilde{\varepsilon}_c^{pl}\right) \qquad \text{.....3.17}$$

The effective cohesion stresses are important since they determine the size of the yield (or failure) surface.

3.5.2 Multiaxial Behaviour

The plastic-damage concrete model assumes that the elastic stiffness degradation is isotropic and characterised by a single scalar variable, d:

$$D^{el} = (1\text{-}d)\, D^{el}_0; \quad 0 \leq s_t, s_c \geq 1 \qquad \text{.....3.18}$$

The definition of the scalar degradation variable d must be consistent with the uniaxial monotonic responses (d_t and d_c), and it should also capture the complexity associated with degradation mechanisms under cyclic loading.

3.5.3 Compressive and Tensile Damage

In the Plastic-Damage model, stiffness degradation due to damage is embedded in the plasticity part of the model. In order to account for different effects under tensile and compressive loading, damage is represented by two independent scalar damage parameters: one for compression (d_c) and a second for tension (d_t) such that the total stress is decomposed into tensile and compressive components. This is done because quasi-brittle materials show different damage mechanisms in tension and compression. In tension the damage is associated with cracking while in compression it is associated with crushing. The initial undamaged state and final damaged state of the material under tension and compression are indicated by $d_t = d_c = 0$ and $d_t = d_c = 1$ respectively. Any intermediate value indicates a partially damaged state. Apart from this, a stiffness recovery scheme is used for simulating the effect of micro-crack opening and closing. The effect of damage is embedded in the plasticity theory and all stress definitions (true stress) are reduced to the effective stress. This enables the decoupling of the constitutive relations for the elastic–plastic response from stiffness degradation (damage) response. Consequently, the numerical implementation of the model becomes much simpler.

3.5.4 Tension Stiffening

The post-failure behaviour for direct straining is modelled with tension stiffening, which allows you to define the strain-softening behaviour for cracked concrete.

Tension stiffening is required in the concrete damaged plasticity model. It can be specified by means of a post-failure stress-strain relation or by applying a fracture energy cracking criterion. However, a post failure stress-strain relation was used in the current research.

In reinforced concrete, the specification of post-failure behaviour generally means giving the post-failure stress as a function of cracking strain, $\tilde{\varepsilon}_t^{ck}$. The cracking strain is defined as the total strain minus the elastic strain corresponding to the undamaged material; that is, $\tilde{\varepsilon}_t^{ck} = \varepsilon_t - \varepsilon_{0t}^{el}$, where $\varepsilon_{0t}^{el} = \sigma_t / E_o$, as illustrated in Figure 3.4.

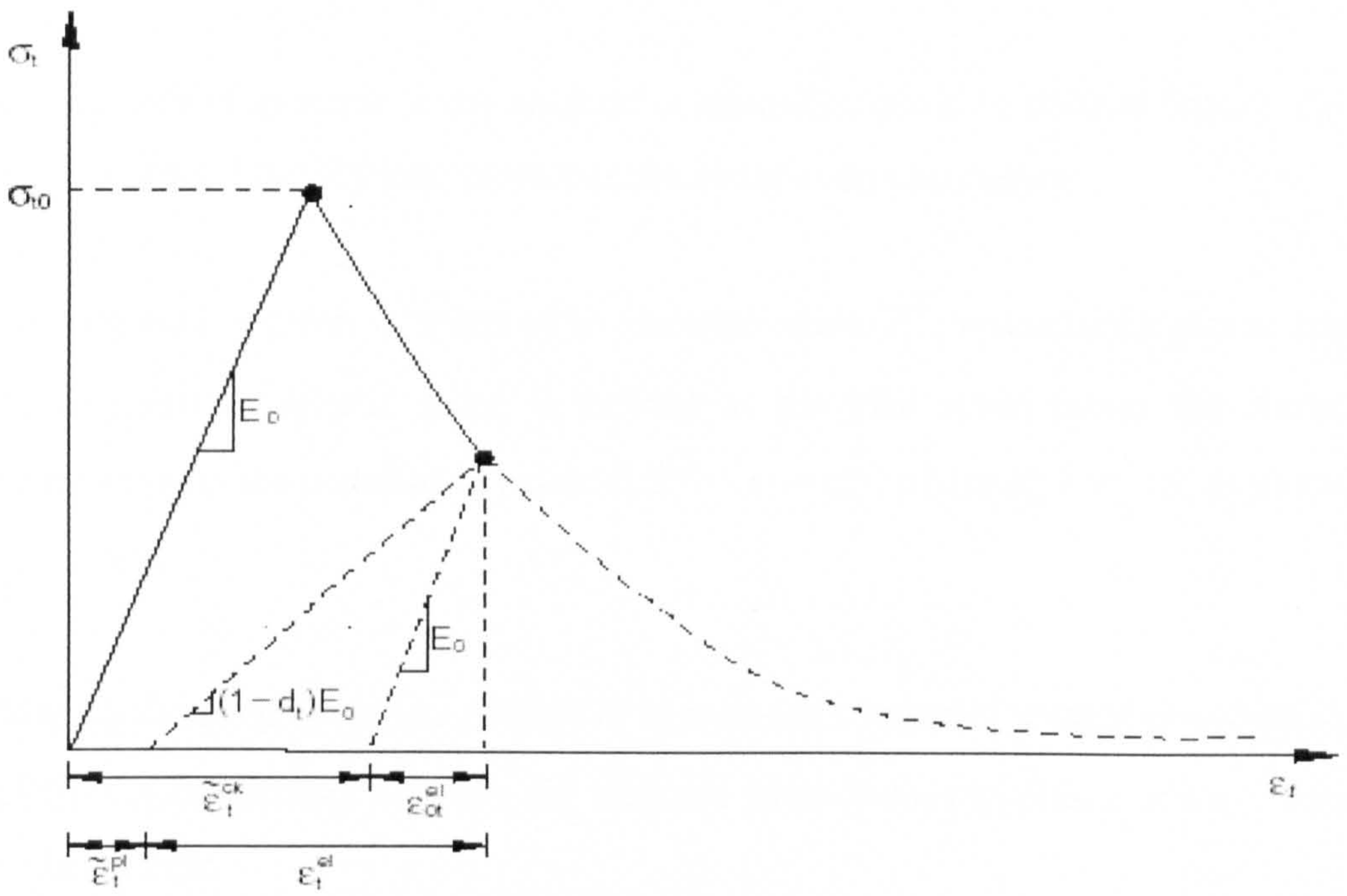

Figure 3.4: Illustration of the definition of the cracking strain used for the definition of tension-stiffening data (After ABAQUS 2006a)

Tension stiffening data are given in terms of the cracking strain, $\tilde{\varepsilon}_t^{ck}$. When unloading data are available, the data are provided to ABAQUS in terms of tensile damaged curves, d_t - $\tilde{\varepsilon}_t^{ck}$ .ABAQUS automatically converts the cracking strain values to plastic strain values using the relationship:

$$\tilde{\varepsilon}_t^{pl} = \tilde{\varepsilon}_t^{ck} - \frac{d_t}{(1-d_t)} \frac{\sigma_t}{E_o} \qquad \text{.....3.19}$$

The choice of tensile stiffening parameters is important since, generally, more tension stiffening makes it easier to obtain numerical solutions. Too little tension stiffening will

cause the load cracking failure in the concrete to introduce temporarily unstable behaviour in the overall response in the model. Few practical designs exhibit such behaviour, so the presence of this type of response in the analysis model usually indicates that the tension stiffening is unreasonably low.

3.5.5 Defining Compressive Behaviour

The behaviour of concrete in the uniaxial compression could be defined outside the elastic range and beyond the ultimate stress into the strain-softening regime.

Hardening data is given in terms of an inelastic strain, $\tilde{\varepsilon}_c^{in}$, instead of a plastic strain $\tilde{\varepsilon}_c^{pl}$. The compressive inelastic strain is defined as the total strain minus the elastic strain corresponding to the undamaged material, $\tilde{\varepsilon}_c^{in} = \varepsilon_c - \varepsilon_{0c}^{el}$, where $\varepsilon_{0c}^{el} = \sigma_c / E_o$ as illustrated in Figure 3.3(b).

Unloading data is provided to ABAQUS in terms of compressive damage curves, $d_c - \tilde{\varepsilon}_c^{in}$. ABAQUS automatically converts the inelastic strain values to plastic strain values using the relationship:

$$\tilde{\varepsilon}_c^{pl} = \tilde{\varepsilon}_c^{in} - \frac{d_c}{(1-d_c)} \frac{\sigma_c}{E_o} \qquad \text{.....3.20}$$

ABAQUS will issue an error message if the calculated plastic strain values are negative and/or decreasing with increasing inelastic strain, which typically indicates that the compressive damage curves are incorrect. In the absence of compressive damage if damage was not specified,

$$\tilde{\varepsilon}_t^{pl} = \tilde{\varepsilon}_t^{ck} \text{and} \quad \tilde{\varepsilon}_c^{pl} = \tilde{\varepsilon}_c^{in} \qquad \text{.....3.21}$$

3.5.5.1 Concrete Plasticity

This option is used to define the flow potential and yield surface for the concrete Damaged Plasticity model.

a) Plastic Flow

The concrete Damage Plasticity model assumes non-associated plastic flow. The flow potential G used for this model is the Drucker-Prager hyperbolic function,

$$G = \sqrt{(\varepsilon\sigma_{to}\tan\psi)^2 + \bar{q}^2} - \bar{p}\tan\psi, \qquad \text{.....3.22}$$

Where,

ψ is the dilation angle measured in the p-q plane at high confining pressure

σ_{to} is the uniaxial tensile stress at failure, taken from the user-specified tension stiffening data

ε is a parameter, referred to as the eccentricity, that defines the rate at which the function approaches the asymptote (the flow potential tends to be a straight line as the eccentricity tends to be zero)

This flow potential ensures that the flow direction is always uniquely defined. The function reaches the linear Drucker-Prager flow potential, (ABAQUS, 2006b), asymptotically at high confining pressure stress and intersects the hydrostatic pressure axis at 90 degrees.
The default value for the flow potential eccentricity was 0.1, which implies that the material has almost the same dilation angle over a wide range of confining pressure stress values (i.e. the analysis will not be sensitive to the dilation angle).

b) Yield Function

The model makes use of the yield function of Lubliner et al (1989), with the modifications proposed by Lee and Fenves (1998) to account for the different evolution of strength under tension and compression. The evolution of the yield surface is controlled by the hardening variables $\tilde{\varepsilon}_t^{pl}$ and $\tilde{\varepsilon}_c^{pl}$. In terms of effective stress, the yield function takes the form:

$$F = \frac{1}{1-\alpha}\left(\bar{q} - 3\alpha\bar{p} + \beta\left(\tilde{\varepsilon}^{pl}\right)\left\langle\hat{\bar{\sigma}}_{max}\right\rangle - \gamma\left\langle-\hat{\bar{\sigma}}_{max}\right\rangle\right) - \bar{\sigma}_c\left(\tilde{\varepsilon}_c^{pl}\right) = 0 \qquad \text{.....3.23}$$

With

$$\alpha = \frac{\left(\sigma_{b0}/\sigma_{c0}\right) - 1}{2\left(\sigma_{b0}/\sigma_{c0}\right) - 1}; \quad 0 \le \alpha \le 0.5$$

$$\beta = \frac{\bar{\sigma}_c\left(\tilde{\varepsilon}_c^{pl}\right)}{\bar{\sigma}_t\left(\tilde{\varepsilon}_t^{pl}\right)}(1-\alpha) - (1+\alpha)$$

$$\gamma = \frac{3(1-K_c)}{2K_c - 1}$$

Where,

$\hat{\bar{\sigma}}_{max}$ is the maximum principal effective stress

σ_{b0}/σ_{c0} is the ratio of initial equibiaxial compressive yield stress to initial uniaxial compressive yield stress (the default value is 1.16)

K_c is the ratio of the second stress invariant on the tensile meridian, $q_{(TM)}$, to that on the compressive meridian, $q_{(CM)}$, at initial yield for any given value of the pressure invariant p such that the maximum

principal stress is negative, $\hat{\sigma}_{max} < 0$; it must satisfy the condition 0.5 < Kc ≤ 1.0 (the default value is 2/3)

$\bar{\sigma}_t\left(\tilde{\varepsilon}_t^{pl}\right)$ is the effective tensile cohesion stress

$\bar{\sigma}_c\left(\tilde{\varepsilon}_c^{pl}\right)$ is the effective compressive cohesion stress

Typical yield surfaces are shown in Figure 3.5 on the deviatoric plane and in Figure 3.6 for plane stress conditions.

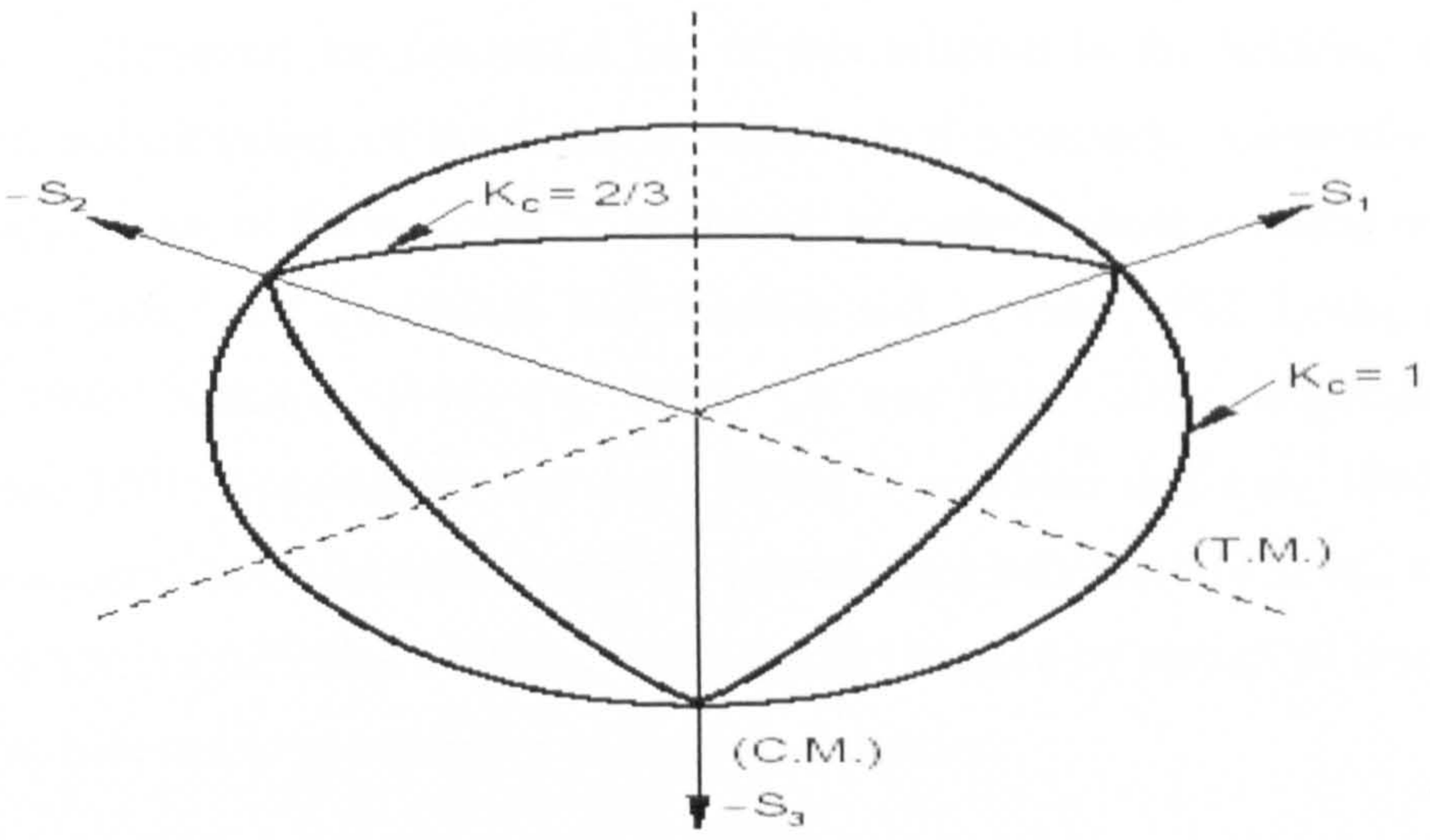

Figure 3.5: Yield surfaces in the deviatoric plane (After ABAQUS 2006a)

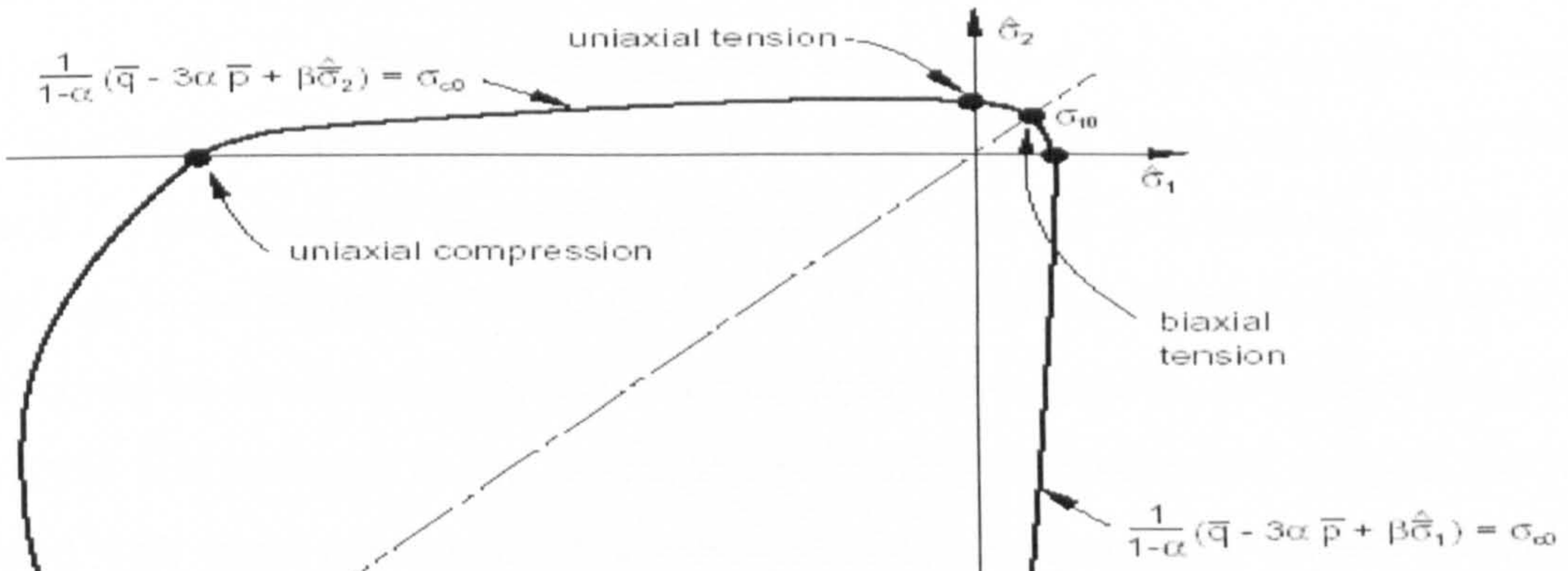

Figure 3.6: Yield surface in plane stress (After ABAQUS 2006a)

CHAPTER FOUR

A CONSTITIUTIVE MODEL FOR STEEL FIBRE REINFORCED CONCRETE

4.1 Introduction

As discussed earlier in Chapter two, SFRC has been used extensively in industrial floors. However, for successful use of this material in the building industry, a fundamental understanding of the material behaviour is necessary. Generally, the most important application of fibres would be to prevent or control tensile cracking occurring in concrete structures (ACI Committee 544; Banthia and Trottier, 1994; Leung and Geng, 1998; Li, 1998; Nataraja, 1999; Oh, 1992; Oh and Kim, 2003; Goparalatnam and Wecharatana, 1991; Souroushian and Lee, 1990a; Soroushian and Lee, 1990b). It is, therefore, necessary to realistically model the postcracking behaviour of SFRC members in tension. The tension stiffening diagram, which can be obtained by numerical investigations, describes the post-cracking behaviour of concrete in tension.

The Finite Element Method is one of the promising numerical methods applied to reinforced concrete structures. Numerous general-purpose finite element computer programs are available for the analysis of reinforced concrete structures. However, modelling the effect of fibres in concrete, fibre bond/slip and the bridging effects across cracks have still not been taken into account in FEA of SFRC structures in any of these programs. Therefore, this research was intended to develop a constitutive model for material non-linear analysis of SFRC members. The main characteristics induced by fibre reinforcement are simulated in the material constitutive laws, namely, the tension post-peak stress-strain relationship. In the model, the poly-linear approximation analysis method combined with finite element method was used for determination of tension stiffening diagrams. This method belongs to the inverse methods. Experimental data of simply supported SFRC beams tested under 3-point and 4-point bending in different research laboratories were used to develop the model. Consequently, the finite element results enabled a statistical model for the tension stiffening behaviour of SFRC to be determined, which is an important parameter in the design of SFRC members.

In the finite element model, nonlinear material properties have been used for concrete using the Damaged Plasticity Model native to ABAQUS as presented in Chapter three.

In the following, the assumptions and constitutive relationships used in modelling the flexural response of SFRC is discussed first. Then inverse method assumptions used to determine the post-cracking behaviour and the development of the finite element model with the determination of material parameters for SFRC as required for the simulations are presented. Finally, a statistical model-predicted tension-stiffening behaviour of SFRC is given.

4.2 Constitutive Model for SFRC

Results obtained from FEA for concrete structures are largely dependent on the stress-strain relationships, failure criteria used and modelling of cracking and post cracking behaviour. However, proper simulation of the behaviour of concrete, particularly post cracking behaviour is somewhat difficult, although it is the parameters most likely to affect FE predictions (Kotsovos and Pavlovic, 1995).

The experimental research has revealed that the post-peak behaviour of SFRC both under tension and under compression is much more ductile than the corresponding behaviour of plain concrete (ACI544.IR-96, 1996; Barros and Figueiras, 1999). However, there is a complete lack of proper post-peak characteristics in compression and tension. Generally, the peak stress in compression is never actually reached in a structure. Thus, even if any strain softening relations in compression were to be included in the analysis, they would make no difference to the results. On the other hand, descending branches in tension do not have a reliable experimental basis. In quasi-brittle materials such as concrete and rock, and certain brittle matrix composites reinforced with fibres, the tensile behaviour after peak strength may be represented by a tension-stiffening curve.

While pre-peak stress-strain behaviour and associated mechanical properties of fibre composites have been extensively studied (Aveston et al., 1971; Buixansky et al., 1986),

the post-peak tension-stiffening behaviour of fibre-reinforced composites has not been adequately investigated.

In recent experimental studies, Wang et al. (1990a, b) found that the tension-stiffening curve of cement mortar can be significantly enhanced by the inclusion of a small volume percentage of fibres. However, several models to represent the tension-stiffening effect have already been proposed, ranging from simple to very refined models with great degree of complexity (Branson, 1968 and Cosenza, 1990). There are more complex models based on the bond-slip mechanism and on localized phenomena (Floegl and Mang (1982), Gupta and Maestrini (1990), Wu and Tanabe (1991) Russo and Romano (1992) Choi and Cheung (1996) and Kwak and Song (2002). These complex models, also known as "microscopic models", depend on a series of parameters that are usually difficult to obtain, requiring specific experiments for each particular member, hence they are not usually applied to full-scale problems.

For nonlinear finite element analysis of reinforced concrete structures, quite a few models that modify the constitutive equation of concrete after cracking have been proposed, (including Scanlon and Murray, 1974; Lin and Scordelis, 1975; Collins and Vecchio,1986; Stevens et al., 1987; Balakrishnan and Murray, 1988 and Massicotte et al, 1990). Generally, the models that modify the constitutive equation of concrete, in which the descending branch of the tensile stress–strain curve of concrete is modified to take into account the tension-stiffening effect in an average way, are more widely used. These so-called "macroscopic" models are easier to implement and, by being simpler than the "microscopic" ones, they can be readily applied to analyse full-scale structures.

However, most macroscopic models oversimplify the tension-stiffening effect by considering only one equation to describe the post-cracking range of the tensile stress–strain curve. Therefore, this research developed a statistical model of the tension-stiffening behaviour of steel fibre-reinforced composites based on the FEA and the inverse method technique.

4.3 Inverse Method

Seeking a simple model that can represent the tension-stiffening effect more realistically and at the same time be easily implemented into finite element programs, inverse analysis of experimental results on 3- and 4- point bending test on SFRC beams were used. In this method, the tension stiffening diagram is extended step by step as shown in Figure 4.1. The extended part of the tension stiffening diagram is chosen so that a stress-strain can be found that will equate the analytical load-displacement curve of the beam under bending with the experimental one. This method is called "back calculation" or "inverse analysis" for the determination of the stress-strain characteristics.

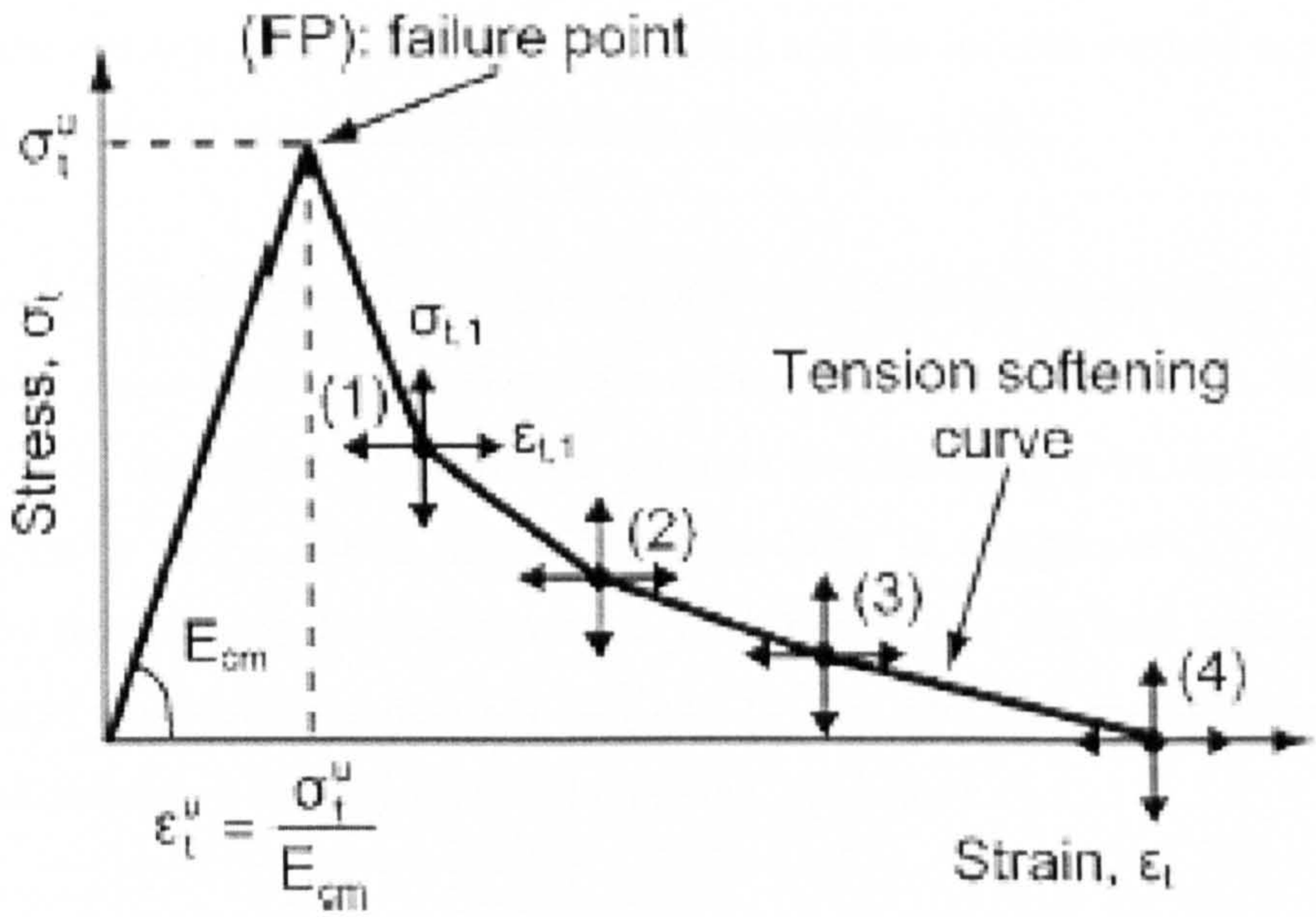

Figure 4.1: Tension softening model adopted in FE analysis (after Tlemat et al., 2006)

Several researchers have used an iterative model to derive either a σ-ε or σ-w characteristic by employing what is called the "inverse analysis" of experimental results using the different FEA packages (e.g. DIANA, ATENA, ANSYS and ABAQUS). Among them, Dupont and Vandewalle (2002) used the ATENA FEA package in order to derive the σ-w characteristics. Due to restrictions in the ATENA package, the post-cracking σ-ε characteristics were modelled with a linear drop. This model was found to be a simple way

of simulating the behaviour of SFRC. On the other hand, Ostergaard et al. (2002) used an inverse analysis based on the bi-linear σ-w law model implemented in DIANA to simulate the non-linear behaviour of an imaginary hinge in the crack zone. Stang (2002) used non-linear springs between element nodes to simulate the crack. Both methods resulted in good agreements with experimental data but no σ-ε law model was proposed. The ANSYS FEA package was used by Hemmy (2002) to analyse the same problem. He added the effect of fibres by introducing smeared reinforcement in 3-D since ANSYS does not allow much flexibility in defining the characteristics of concrete in tension. His attempts did not reach a successful conclusion. Tlemat et al. (2006) has chosen ABAQUS in order to avoid the problems encountered by previous researchers, because it allows the user to define the strain-softening behaviour for cracked concrete in as many stages as needed. A good correlation between the analytical and the experimental results was found.

As a result, the ABAQUS FE package was adopted and the inverse method approach was implemented in order to get a reliable constitutive model for SFRC.

In this study the tension softening is simulated by a poly-linear descending curve. The gradient of the stress-strain curve along the softening region is varied as illustrated in Figure 4.1. Up to the failure point one the concrete is considered to be uncracked, having an elastic modulus of E_{cm} (same as the initial modulus in compression). This point is established by determining the first deviation from linearity of the load deflection curve. After this stage, subsequent points (2), (3) and (4) are obtained by iteration, until the complete load deflection curve is followed relatively accurately.

An overview of the FE model will be discussed in details in the following section.

4.4 Finite Element Model

The experimental work carried out Barros and Figueiras (1999), Farhang and Vogt (2000) for SFRC beams tested under 3- and 4-point bending is used to develop the tension stiffening model using the Inverse method. The selection of these experimental works was due to the similarity with the current research in the type of steel fibre used (Dramix

hooked-end steel fibre). Table 4.1 shows details about the selected tested beams. However, more details about Dramix steel fibres are presented in Chapter six.

Table 4.1: Fibre type and contents for all analysed beams

Beam No.*	Fibre type	Fibre content Kg/m^3
B1	ZP30/.50	30
B2	ZP30/.50	30
B3	ZP30/.50	45
B4	ZP30/.50	45
B5	ZP30/.50	60
B6	ZP30/.50	60
B7	ZP30/.50	60
B8	ZP30/.50	60
B9	ZP30/.50	60
B10	ZP30/.50	60
B11	ZP30/.50	60
B12	ZX60/.80	30
B13	ZX60/.80	30
B14	ZX60/.80	45
B15	ZX60/.80	45
B16	ZX60/.80	60
B17	ZX60/.80	60
B18	ZX60/.80	60
B19	ZX60/.80	60
B20	ZX60/.80	60
B21	ZX60/.80	60
B22	RC 65/60 BN	30
B23	RC 65/60 BN	30
B24	RC 65/60 BN	30
B25	RC 65/60 BN	30
B26	RC 65/60 BN	30
B27	RC 65/60 BN	30
B28	RC 65/60 BN	40
B29	RC 65/60 BN	40
B30	RC 65/60 BN	40
B31	RC 65/60 BN	40
B32	RC 65/60 BN	40
B33	RC 65/60 BN	40

* Beams B1 to B21 tested by Barros and Figueiras (1999), Beams B21 to B33 tested by Farhang (2005)

Taking the advantage of the symmetry only half the beam is modelled. To simulate the notch along the symmetry axis, nodes within the notch's height are unrestrained. This means that the notch is modelled physically as a discontinuity in the beam. A mesh with 66

elements was used to optimize the results as suggested by Tlemat et al. (2006). The mesh consisted of 11 concrete elements along the length and 6 elements over the depth. The mesh employed for the study is square and had an element length of 25mm. Figure 4.2 shows the mesh size used and the boundary conditions applied.

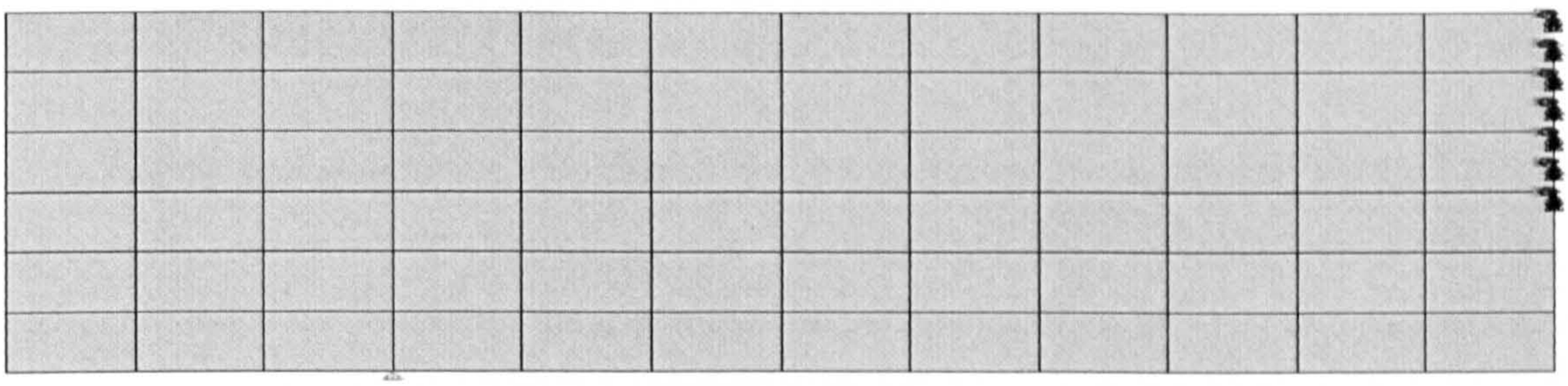

a. Three-point bending test

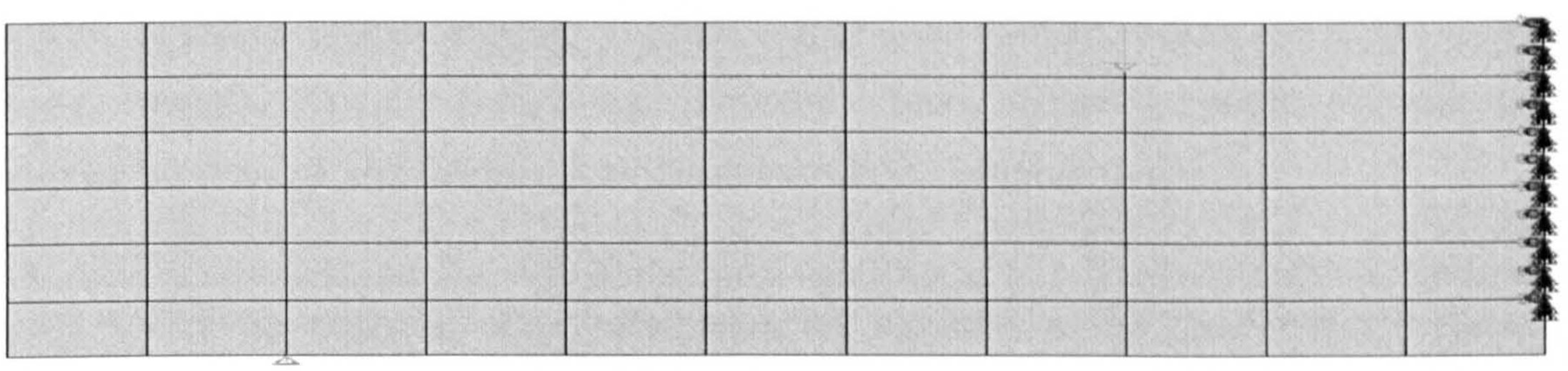

b. Four-point bending test

Figure 4.2: mesh size and boundary conditions, a. (3-point bending test), b. (4-point bending test)

A two-dimensional solid biquadratic plane stress element (CPS8) with eight-nodes having two degrees of freedom per node (X, Y) was chosen to simulate the structural behaviour of the SFRC beams. A full integration rule over the element plane was adopted. Since considerable nonlinearity is expected in the response of the analysed beam, incremental loading performs the analysis with integration in each increment using the Riks method. More details about this method were given in section 3.2.1. The termination condition for the analysis is set in this case by specifying a maximum required displacement in the middle of the step as 5 mm. This is enough to ensure that a limit condition is reached.

4.5 Sensitivity Analysis

Various parameters have different degrees of influence on the numerical results for the behaviour of SFRC beams. Therefore, it is necessary to perform sensitivity analyses of the parameters involved in the model.

The following parameters are considered for investigation to determine whether their influence on the results is significant and to determine their suitable values for the subsequent analysis. Generally, these parameters can be classified into two categories. The first category contains numerical parameters such as convergence tolerance, the size of initial load increment and the size of the arc length in the Riks method, mesh size and element type. The second category contains material parameters such as compressive and tensile strengths, Young's modulus, Poisson's ratio, dilatancy angle, tensile and compressive damage and failure envelope under biaxial compression.

In the sensitivity analysis, other parameters are assumed to be fixed when a certain parameter is varied and thus its effects on the numerical outputs can be investigated. The values of the parameters chosen are based upon those giving the best comparison with the experimental results. The comparison between the experiments and the predicted values was based on the load-deflection response. As the number of variations is large, the comparison will be confined to one typical beam B13. Table 4.1 shows a detailed description for this beam.

4.5.1 Numerical Parameters

The main purpose of studying of the effect of numerical parameters on slabs behaviour is to choose the values of parameters to achieve an accurate and at the same time economical solution for the non-linear analysis. Four parameters which have a significant effect on the computational cost and Finite Element prediction were studied. These parameters are:

1. Convergence tolerance

2. Size of the arc length
3. Size of the initial load increment
4. Mesh density

After having chosen the best values for the concrete model, all the analysis will use this set of parameters for the analysis of the remaining tested beams.

4.5.1.1 Convergence Tolerance, Size of Arc Length and Initial Size of Arc Length

In the numerical procedure, the structural responses in terms of load-displacement behaviour are practically identical for the different values of convergence tolerance, size of arc length and size of initial arc length as shown in Figures 4.3 to 4.5. The effect of these parameters on the number of increments and the computational cost, see Table 4.2, is discussed below.

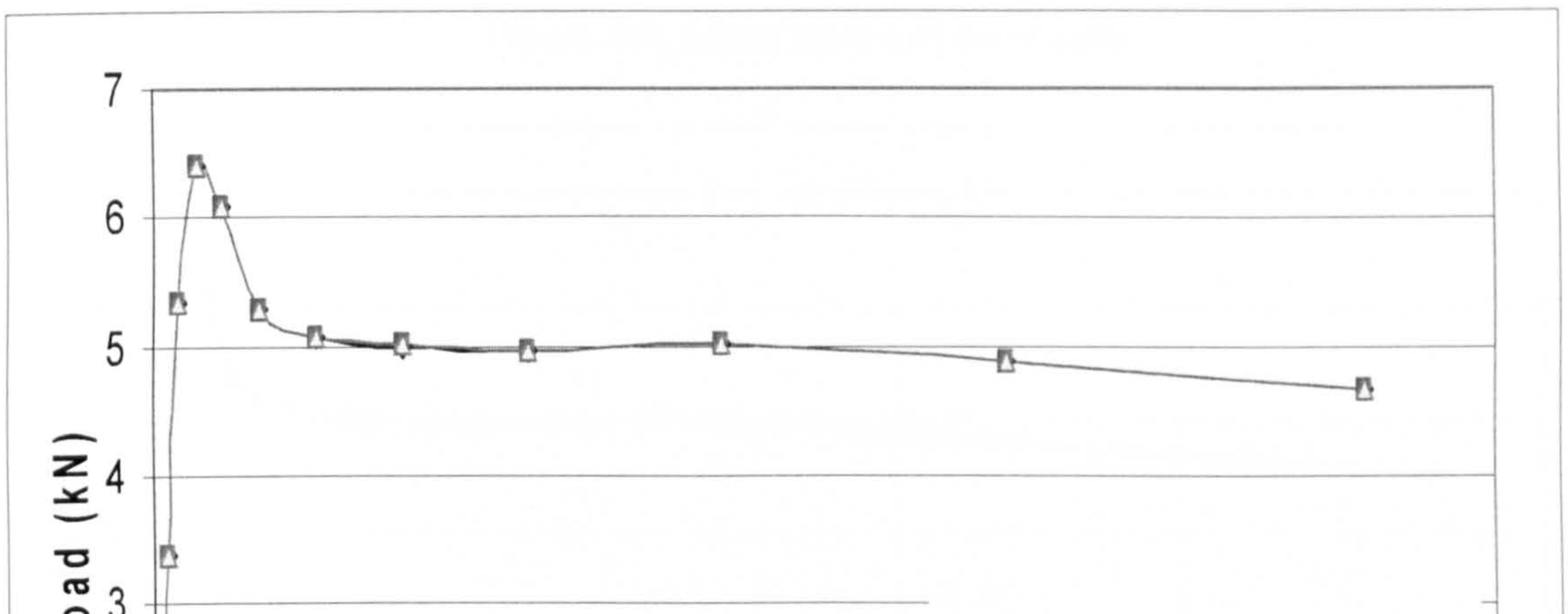

Figure 4.3: Effect of convergence tolerance

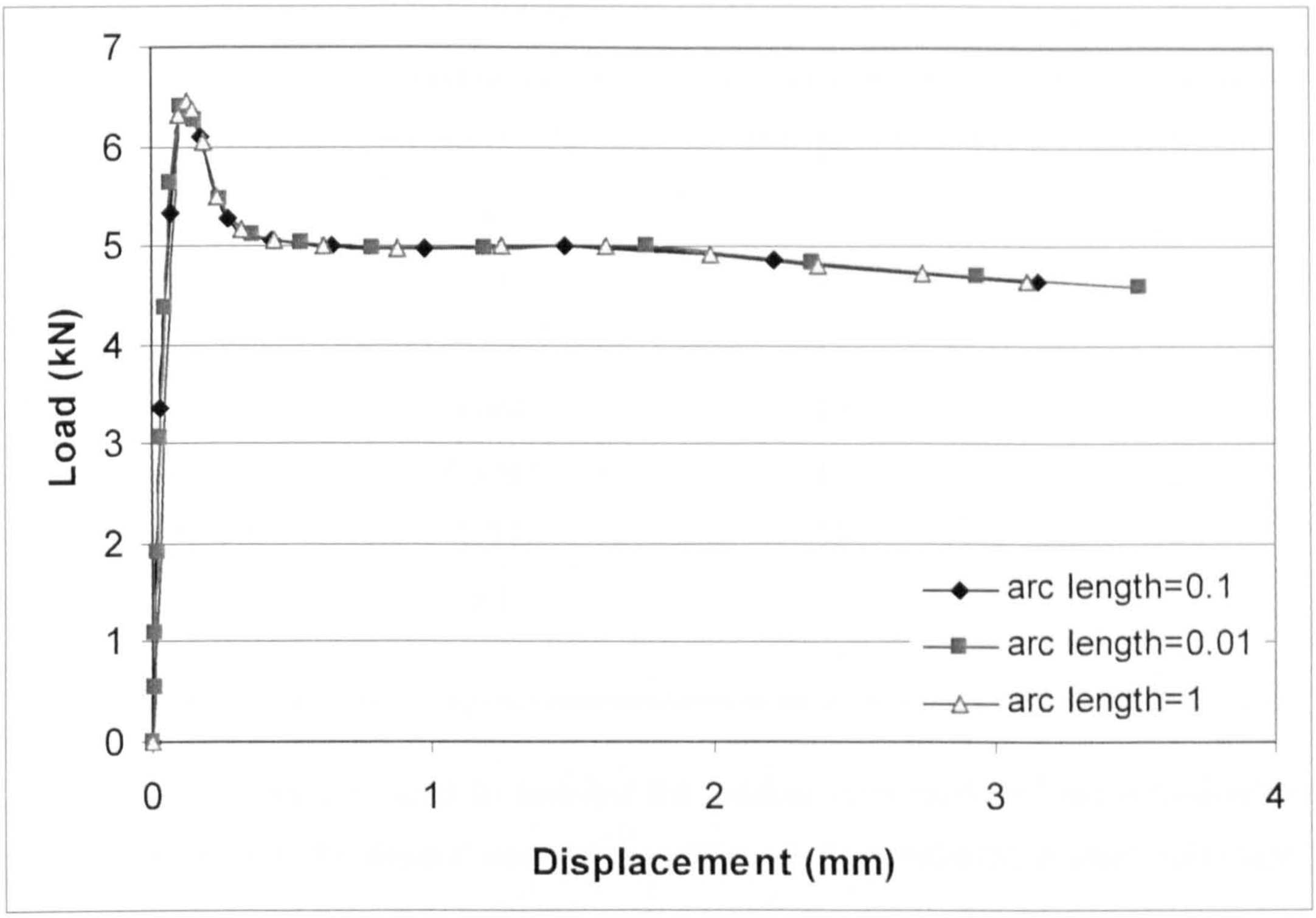

Figure 4.4: Effect of size of arc length

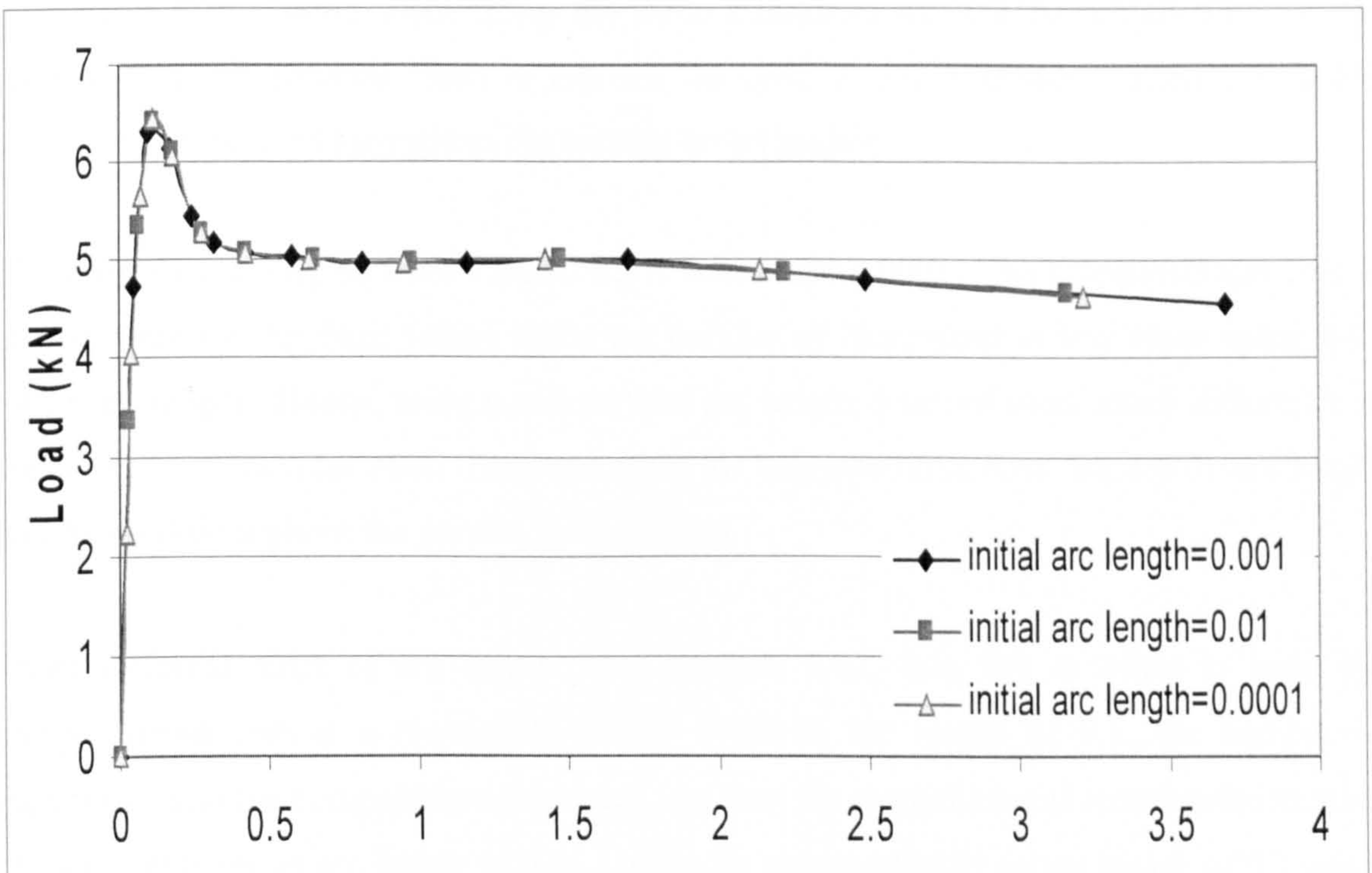

Figure 4.5: Effect of size of initial arc length

Table 4.2: Effect of numerical parameters

Numerical parameters	Percentage (%)	No. of increment	Total time (secs)
Convergence	1	12	14
tolerance	5	12	12
	10	12	13
Size of initial arc length	0.1	12	12
	0.001	12	12
	0.0001	13	12
Size of arc length	0.01	18	14
	0.1	12	12
	1	16	14

Convergence tolerance is used to monitor the gradual elimination of the out-of-balance residual forces until the desired accuracy is achieved. Theoretically, a small tolerance is required but it can be very expensive because it requires a large number of increments. For this study, three tolerance factors were studied 1%, 5% and 10%. The number of increments is the same when using the three tolerances but the computational cost (as measured by the solution time) is less for the case of 5% tolerance. Therefore, a 5% tolerance will be used throughout the present investigation.

Three initial arc lengths were studied 0.01, 0.001 and 0.0001. The computational cost is almost same for the three values while the number of increments is less when using 0.01 initial arc length. Hence, using smaller initial arc length does not show much difference in the structural behaviour other than increasing the computational cost. So, a 0.01 arc length will be used throughout the present investigation.

Three different sizes of arc length were studied: 0.01, 0.1, 1.0, in order to keep the computational cost at a reasonable level. With an arc length of 0.1, the number of increments and the computational cost was less than the computational cost and the number of increments for an arc length of 0.01. It can be concluded that an arc length of 0.1 could be used in the current analysis, in order to get reasonably good results and to reduce the computational cost.

4.5.1.2 Mesh Density

A mesh sensitivity study was performed using three meshes as shown in Figure 4.6. As expected, mesh (a) leads to an increase in the post-crack energy absorption capacity, whilst mesh (c) underestimates the capacity after cracking. In concrete modelling with the smeared crack approach, the choice of mesh is influenced by the energy dissipated in tension, which also depends on the aggregate size. Mesh b was chosen for further analysis, since it was on the lower limit of the dimensions allowed for this particular concrete. However, Tlemat et al.(2006) developed a method, which is able to derive the stress-strain curves for any mesh sizes, when the optimum stress-strain curves for a given mesh size is known. This method allowed an amount of energy to be dissipated in a crack irrespective of element size.

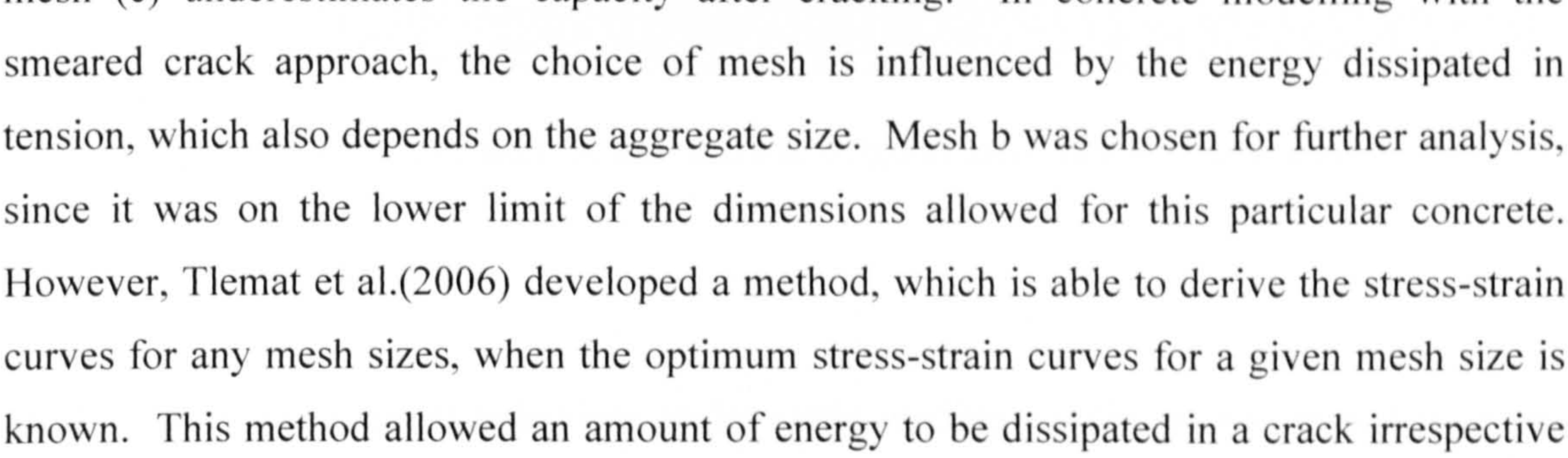

a. fine mesh

b. original mesh

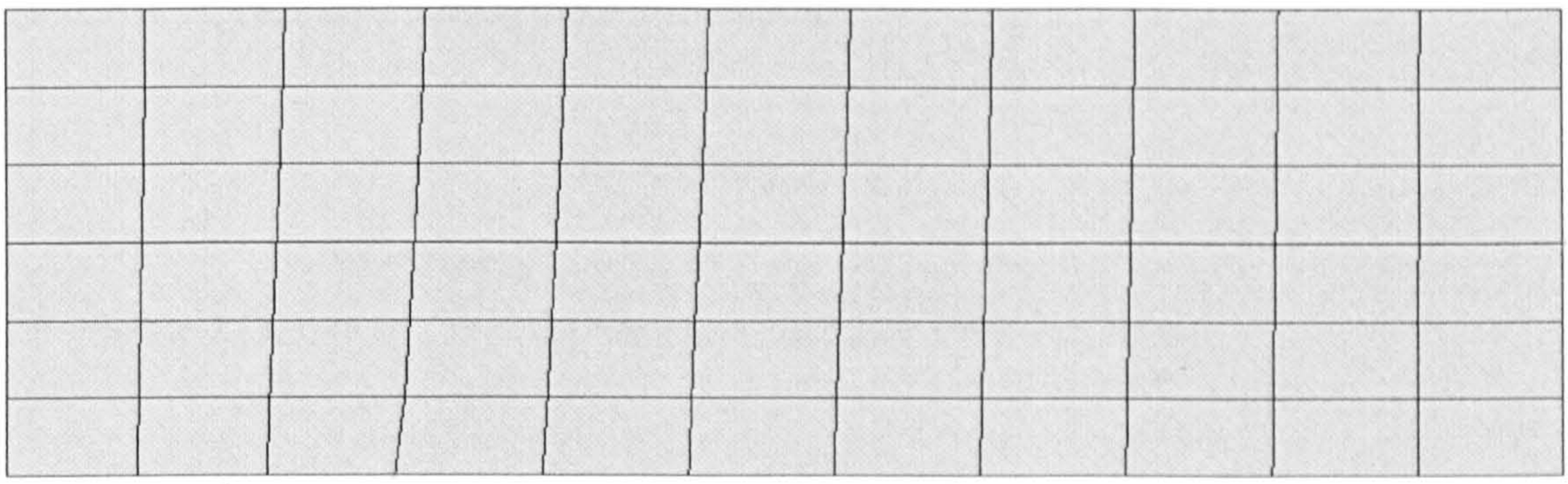

c. coarse mesh

Figure 4.6: mesh sizes (a. fine mesh b. original mesh and c. coarse mesh)

4.5.2 Material Parameters

Modelling of the material behaviour under static loading conditions has been performed using the finite element software ABAQUS with its existing Plastic-Damage material model. This model is primarily used to simulate quasi-brittle materials such as concrete, rock, mortar and ceramics. The material parameters required for the model can be categorized into three types, namely elasticity, plasticity and damage. The elasticity parameters are Young's modulus and Poisson's ratio. For plasticity and damage, strain softening and damage evolution curves are required. In addition to these parameters, a further material constant called the dilation angle ψ is necessary. In the following the determination process of the above mentioned parameters are discussed.

4.5.2.1 Modulus of Elasticity

The initial modulus of elasticity of concrete E_c is highly correlated to its compressive strength. This property is only marginally changed by the fibre reinforcement (Barros and Figueiras, 1999) and can be calculated with reasonable accuracy from the empirical equation proposed in the design codes. Three design code formulas were adopted in the current sensitivity analysis as described below:

1. CEB FIP Model Code 1990 (CEB-FIP, 1993) recommendations,

$$E_c = 21{,}500\left[f_{cm}/10\right]^{\frac{1}{3}} \qquad \text{.....4.1}$$

2. RILEM TC162-TDF (2003) recommendations,

$$E_c = 9500(f_{cm})^{1/3} \qquad \text{.....4.2}$$

3. Eurocode 2 Design of Concrete Structures (BS EN 1992-1-1:2004)

$$E_c = 22{,}000\left[f_{cm}/10\right]^{0.3} \qquad \text{.....4.3}$$

where f_{cm} is the cylinder compressive strength in MPa.

Figure 4.7 shows the load-displacement curve obtained using the three formulas. The structural response is very similar for the different values of modulus-of-elasticity. Hence, the formula proposed by CEB FIP Model Code 1990 (CEB-FIP 1993) is used.

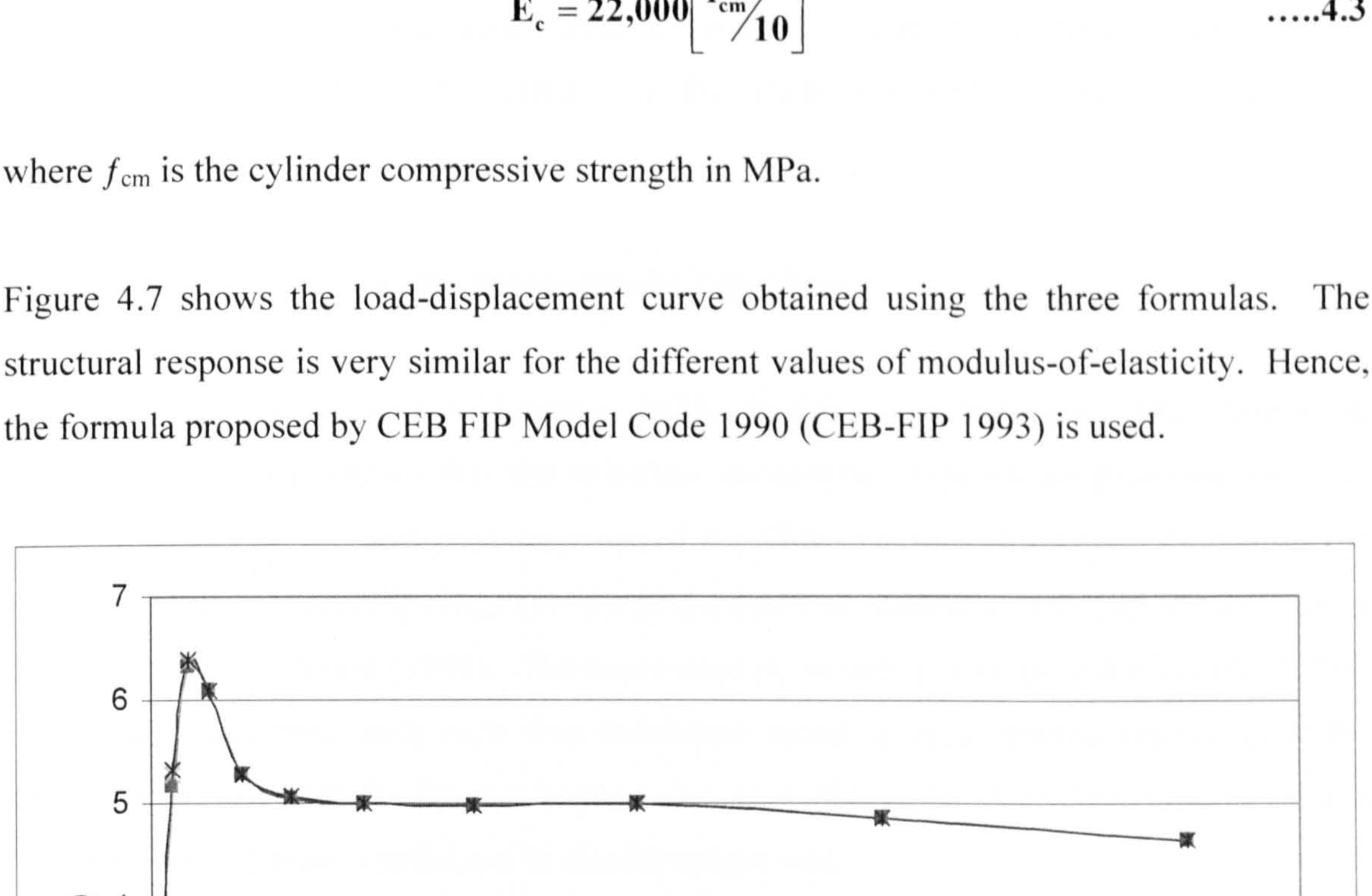

Figure 4.7: Effect of modulus of elasticity

4.5.2.2 Poisson's Ratio

Generally the value of υ for normal-weight and light-weight concretes lies in the range of 0.15 and 0.25 when determined from measurements taken in the static modulus-of-elasticity tests (Neville, 1995). On the other hand, the Poisson's ratio υ_c of concrete under uniaxial compressive stress ranges from about 0.15–0.22, with a representative value of 0.19 or 0.20. However, such small variability in υ will not greatly affect the results, hence, this parameter need not to be varied. In this study, the Poisson's ratio of concrete is assumed to be 0.2.

4.5.2.3 Uniaxial Compressive Stress-Strain Behaviour

Previous work (Fanella and Namman 1985; Ezeldin and Balaguru 1992; Barros & Figueiras, 1999) has shown that the complete stress-strain expressions proposed for plain concrete cannot fit the post-peak response of the fibre concrete. However, the expression proposed by Barros and Figueiras (1999) is based on one parameter only like the expression of Ezelden and Balaguru (1992). The expression proposed by Barros and Figueiras (1999) is used in the current study as it was developed based on experimental results on SFRC beams reinforced with the Dramix hooked end steel fibres (the same fibre type as used in the experimental study carried out in this investigation).

The expression is based on the following stress-strain relationship:

$$\sigma_c = f_{cm} \frac{\frac{\varepsilon_c}{\varepsilon_i}}{(1-p-q)+q\left(\frac{\varepsilon_c}{\varepsilon_i}\right)+p\left(\frac{\varepsilon_c}{\varepsilon_i}\right)^{(1-q)/p}} \qquad \text{.....4.4}$$

With

$$q = 1-p-\frac{E_{c1}}{E_{ci}}, p+q \in]0,1[, \quad \frac{1-q}{p} > 0$$

This was proposed by Vipulanandan and Paul (1990) for polymer and plain concrete and used by Mebarkia and Vipulanandan (1992) for glass fibre reinforced polymer concrete.

The strain at peak stress ε_{c1}, the average compression strength f_{cm}, and the ratio between the secant modulus of elasticity E_{c1}/E_{ci} ($E_{c1}/ f_{cm}/ \varepsilon_{c1}$) for each type of fibre is expressed in function of the fibre percentage. The parameter p, which takes a value in the range of 0 – 1, is obtained by Barros and Figueiras (1999) by applying the method of least squares to the results, The following expression for ZP30/.50 fibres were obtained:

$$\varepsilon_{c1} = \varepsilon_{c10} + 0.0002W_f \qquad \text{.....4.5}$$

$$p = 1.0 - 0.919\exp(-0.394W_f) \qquad \text{.....4.6}$$

For ZX60/.80 fibres

$$\varepsilon_{c1} = \varepsilon_{c10} + 0.00026W_f \qquad \text{.....4.7}$$

$$p = 1.0 - 0.722\exp(-0.144W_f) \qquad \text{.....4.8}$$

Where ε_{c10} = strain at peak for plain concrete and W_f= fibre weight percentage in the mixture.

This study was carried out in order to investigate whether the complete stress-strain behaviour proposed for plain concrete can fit the post-peak response of the fibre concrete or not. In addition to the compression stress-strain relation developed by Barros & Figueiras (1999) for fibre-reinforced concrete, including a concrete compression-softening, the EC2 compression stress-strain relation for plain concrete was used, see Figure 4.8a. The effect of using these two approaches on the load-deflection response of the beam is shown in Figure 4.8b. The results show that the compressive stress-strain equation proposed by Barros and Figueiras (1999) gives an almost identical response for the load-deflection curve as the EC2 does. This result is expected due to the fact that the peak stress in compression is never actually reached in a structure. Thus, if any strain softening relations in

compression were included in the analysis, they would make no difference to the results (Kotosovos & Pavlovic, 1995).

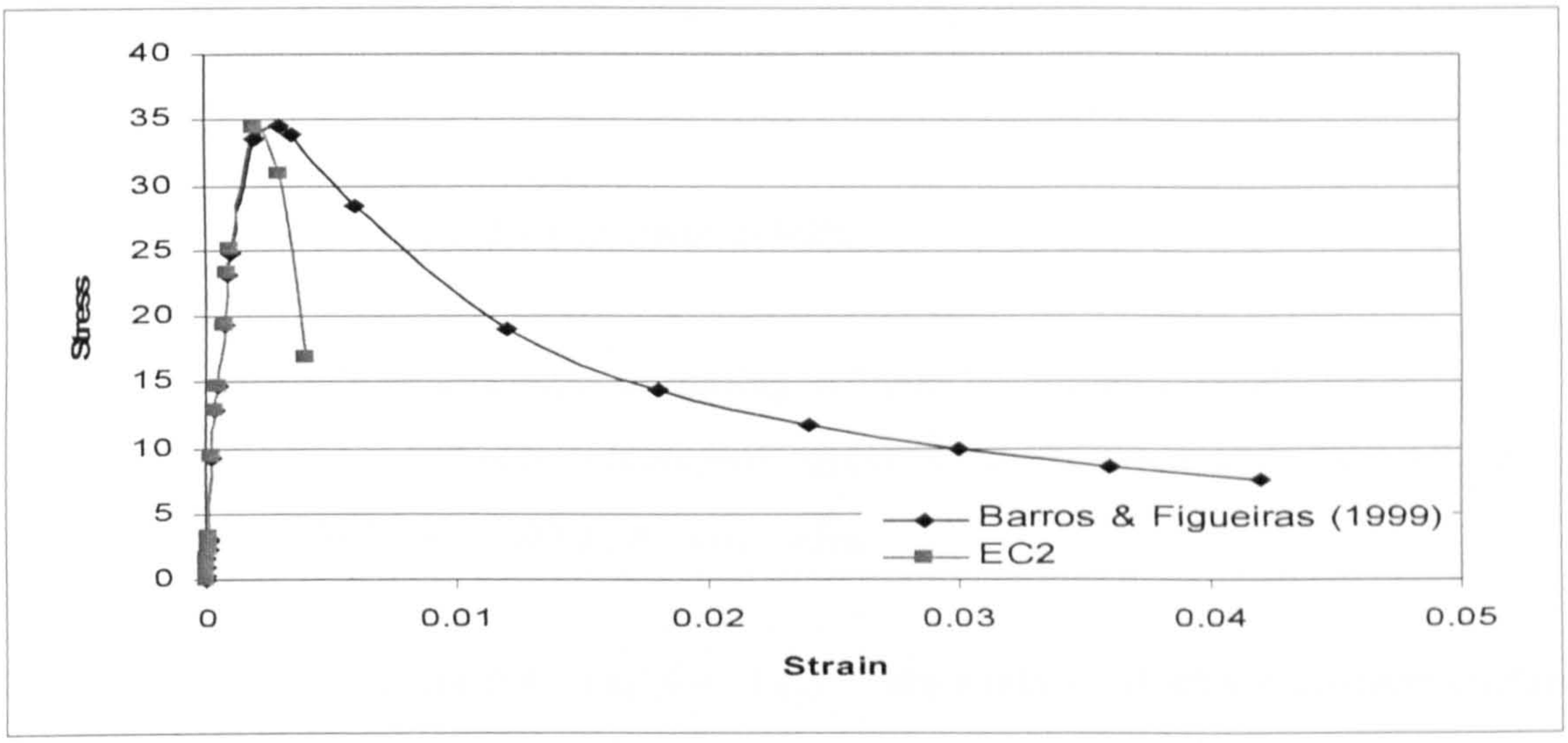

Figure 4.8a: Stress-strain behaviour of concrete in uniaxial compression according to Barros and Figueiras (1999) and EC2

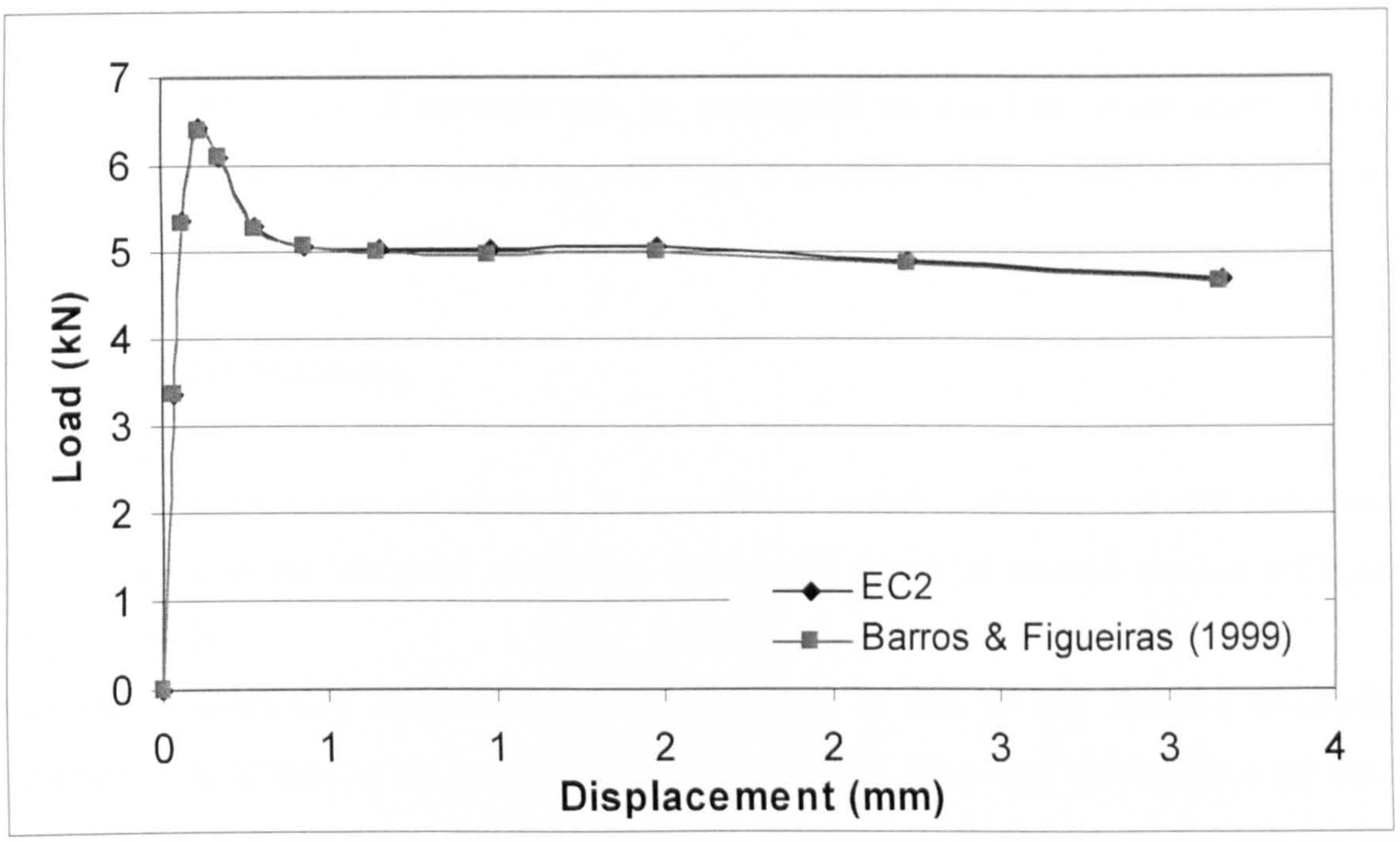

Figure 4.8b: Effect of uniaxial compression stress-strain behaviour

The EC2 Stress-strain behaviour of concrete in uniaxial compression is assumed to be linear up to a stress value of $0.4f'_c$ and thereafter, it is assumed to be

$$\frac{\sigma_c}{f_{cm}} = \frac{k\eta - \eta^2}{1 + (k-2)\eta} \qquad \text{.....4.9}$$

Where:

f_{cm} = cylinder strength of concrete in MPa.

$\eta = \varepsilon_c / \varepsilon_{c1}$

ε_{c1} = the strain at peak stress according to Table 3.1 in the EC2 code, the strain at which the maximum compressive stress occurs is taken as 0.0022-0.0023 for f_{cm} = 30-40MPa, $K = 1.05\, E_c \times |\varepsilon_{c1}| / f_{cm}$

This expression is valid for $0 < |\varepsilon_c| < |\varepsilon_{cu1}|$ the strain at which the concrete crushes, ε_{u1} is taken as 0.0035.

4.5.2.4 Behaviour of Concrete in Tension

The tensile behaviour of concrete can be reasonably assumed as linear elastic before cracking. However, the post cracking behaviour of concrete can be modelled using tension stiffening curve as discussed below.

4.5.2.5 Tension Stiffening

It is known that the cracked concrete of a reinforced concrete element can still carry some tensile stress in the direction normal to the crack, which is termed tension stiffening (ASCE, 1982).

The tension-stiffening diagram of concrete, which is one of the fracture mechanics parameters, is defined as the relationship between tensile stress and tensile strain (or crack width) in the fracture zone. The fracture energy is obtained as the area under the tension-stiffening diagram. The tension-stiffening diagram can describe the post-cracking behaviour and express the resistance of concrete against crack development. So, the tension stiffening diagram and the fracture energy seem to be effective as indices for the

evaluation of properties of SFRC including the post-cracking behaviour (Kurihara et al., 2000).

Steel fibre reinforced concrete (SFRC) is superior to plain concrete in toughness, which is the energy absorption at fracture. The performance of SFRC is influenced by the properties (geometry and strength) of fibre, the fibre contents, the fibre distribution, the performance of the matrix concrete. The performance of SFRC such as the crack resistance and deformability cannot be appropriately expressed with only the strengths.

In order to simplify the constitutive model, the tension stiffening of concrete after cracking can be simulated by linear, bilinear, tri-linear or poly-linear descending curves. A simple descending line is usually used to model this tension-stiffening phenomenon for plain concrete. The default value of the strain ε^* at which the tension stiffening stress reduced to zero is $\varepsilon^*=0.001$ (ABAQUS, 2006a).

Moreover, RILEM TC162-TDF (2003) proposed a tension stiffening diagram for SFRC based on the residual flexural tensile strength $f_{R,i}$. The residual flexural strength is an important parameter characterizing the post-cracking behaviour of SFRC and could be determined by the deflection control bending test. The load value F_L is determined by drawing a line at a displacement of 0.5 mm and parallel to the load axis of the load-displacement diagram and taking as F_L the highest load value in the interval of 0.05 mm. Two residual tensile strengths are used to define the tension-stiffening diagram as shown in Figure 4.9. The residual tensile strengths $f_{R,1}$ and $f_{R,4}$ respectively, are defined at the following mid span deflection $\delta_{R,1} = 0.46$ mm, $\delta_{R,4} = 3.00$ mm.

$$f_{R,i} = \frac{3F_{R,i}L}{2bh_{sp}^2} \quad \text{.....4.10}$$

Where: b = width of specimen (mm), h_{sp}= distance between tip of the notch and top of cross section, L = span of the specimen (mm), $F_{R,i}$= load recorded at $\delta_{R,i}$ (N).

However, in the diagram shown in Figure 4.9, the stresses are defined according as follows:

$$\sigma_1 = 0.7f_{fctm}(1.6-d)\ \ (N/mm^2)\ \text{and (d in m)}\ \ \varepsilon_1 = \frac{\sigma_1}{E_c} \qquad .....4.11$$

$$\sigma_2 = 0.45f_{R,1}\kappa_h \quad (N/mm^2) \qquad \varepsilon_2 = \varepsilon_1 + 0.1\% \qquad .....4.12$$

$$\sigma_3 = 0.37f_{R,4}\kappa_h \quad (N/mm^2) \qquad \varepsilon_3 = 25\% \qquad .....4.13$$

$$E_c = 9500(f_{fcm})^{1/3} \quad (N/mm^2) \qquad .....4.14$$

Where,

$f_{fctm,fl}$: is the mean value of flexural strength in N/mm^2

f_{fcm} : is the mean value of compressive strength in N/mm^2

κ_h : is the size factor = $1.0 - 0.6\left(\frac{h[cm]-12.5}{47.5}\right), \qquad 12.5 \le h \le 60\ \ (cm)$

In addition, the poly-linear model developed using the inverse analysis was used.

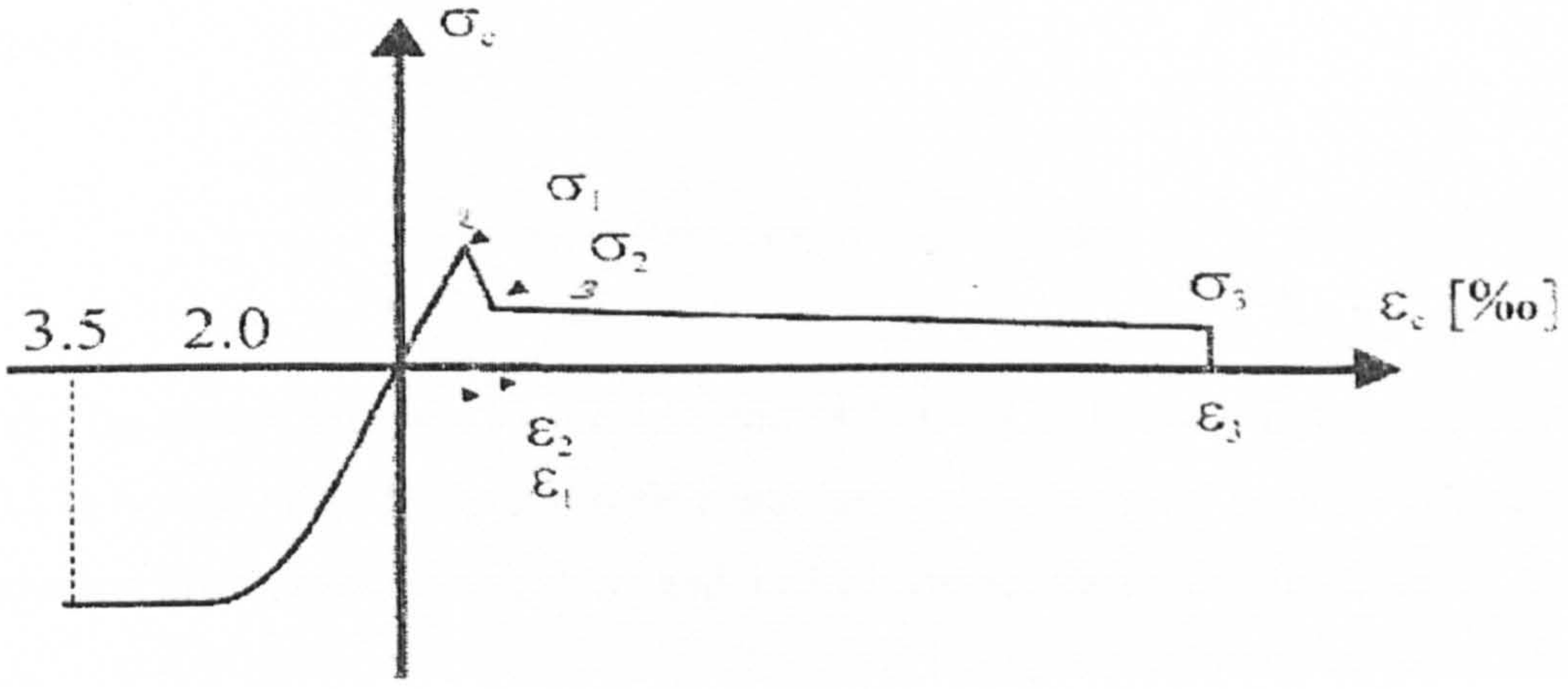

Figure 4.9: Tension stiffening model for SFRC (after RILEM TC162-TDF, 2003)

Figure 4.10 shows the load-deflection results. It can be concluded that while the linear model, proposed for plain concrete, underestimates the behaviour of fibre reinforced concrete in post-tension, the RILEM TC162-TDF (2003) tension stiffening diagram model

does not fit the experimental results. As a result, the use of an inverse analysis method was mandatory.

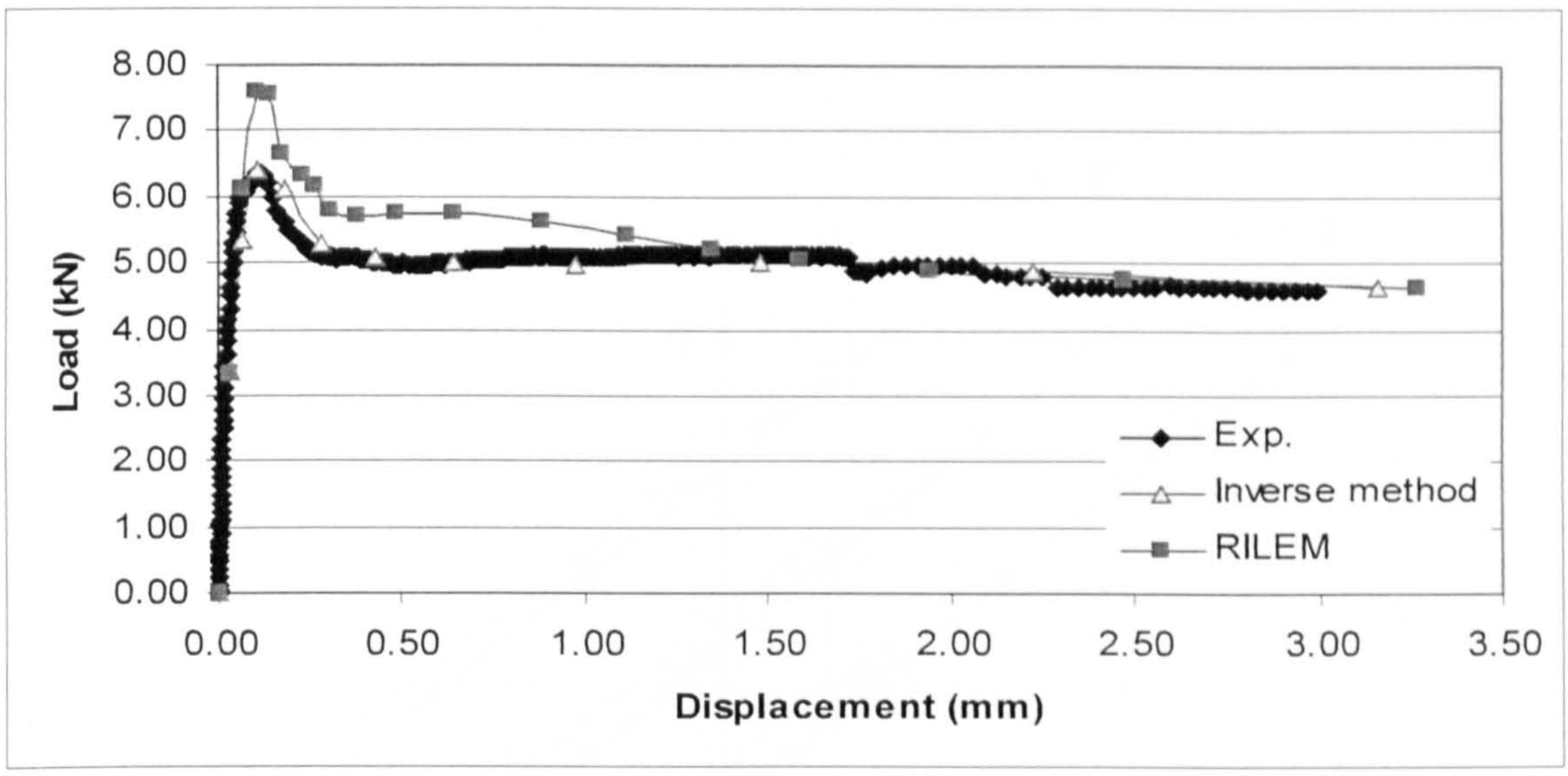

Figure 4.10: Effect of tension stiffening

4.5.2.6 Dilatancy Angle

The dilation angle ψ controls the orientation of the flow potential function G, which is defined as

$$G = \sqrt{(\varepsilon\varepsilon_{t0}\tan\psi a^2 + \bar{q}^2} - \bar{p}\tan\psi \qquad \text{.....4.15}$$

where, the eccentricity (see Figure 4.11 and (ABAQUS, 2006a) for further explanations), ε = 0.1 (a typical value for quasi-brittle materials). σ_{to} is the yield strength in tension. The equivalent effective deviatoric stress and the hydrostatic stress are defined as:

$$\bar{p} = -\frac{1}{3}\bar{\sigma} : \underline{I} \quad \bar{q} = \sqrt{\tfrac{3}{2}\bar{S} : \bar{S}} \qquad \text{.....4.16}$$

where I is the unit matrix and S the effective stress deviator.

It is not possible to obtain ψ directly from the results of the static experiment. As a result of previous numerical tests on plain concrete cylinders, the constant values $\psi = 10^{o}$ were assumed (Snezana and Alendar, 2008). The same value was used earlier by Menetry (1994) in his analysis for the punching shear behaviour of concrete slabs.

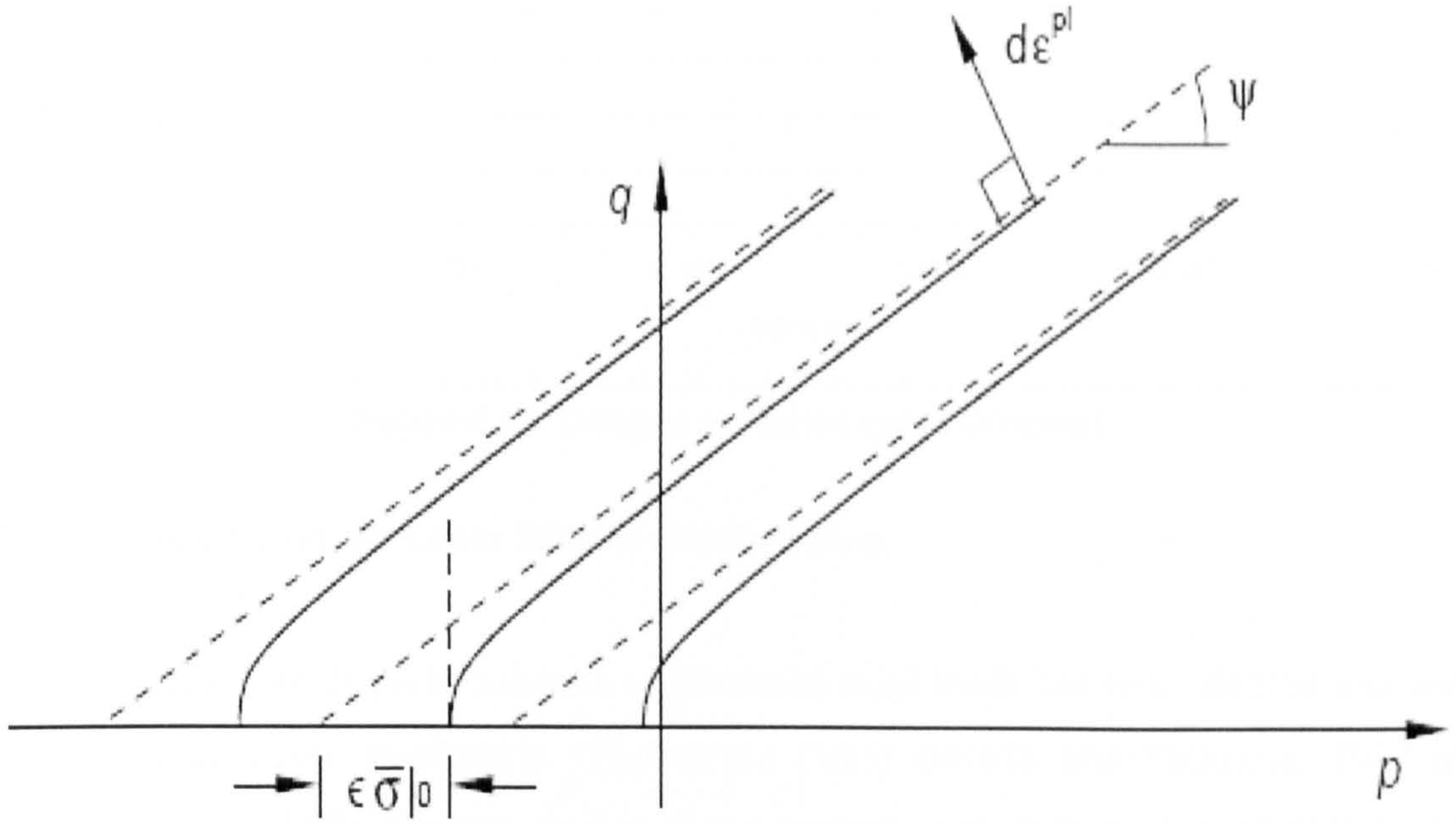

Figure 4.11: Illustration of: (a) yield surface and flow potentials and (b) dilation angle (after ABAQUS, 2006a)

4.5.2.7 Tension and Compression Damage

Since there is no information available in the literature on what is the proper damage value for eroding the concrete materials in numerical simulation, the evolution of damage has been assumed to be the same as in quasi-brittle materials such as concrete. The damage evolution is given as damage versus plastic strain relation. From the damage evolution curve shown in Figure 4.12, a pronounced increase in tension damage occurs initially and later gradually approaches 1. This is consistent with the experimental observation that the matrix in fibre reinforced cracks near the tension yield point and most of the load carrying area is lost. At a later state of loading in the post-peak regime, fibre breaking and pull-out occurs gradually and the rate of damage development is decreased. On the other hand, the compression damage was assumed to increase linearly until it approached 1.

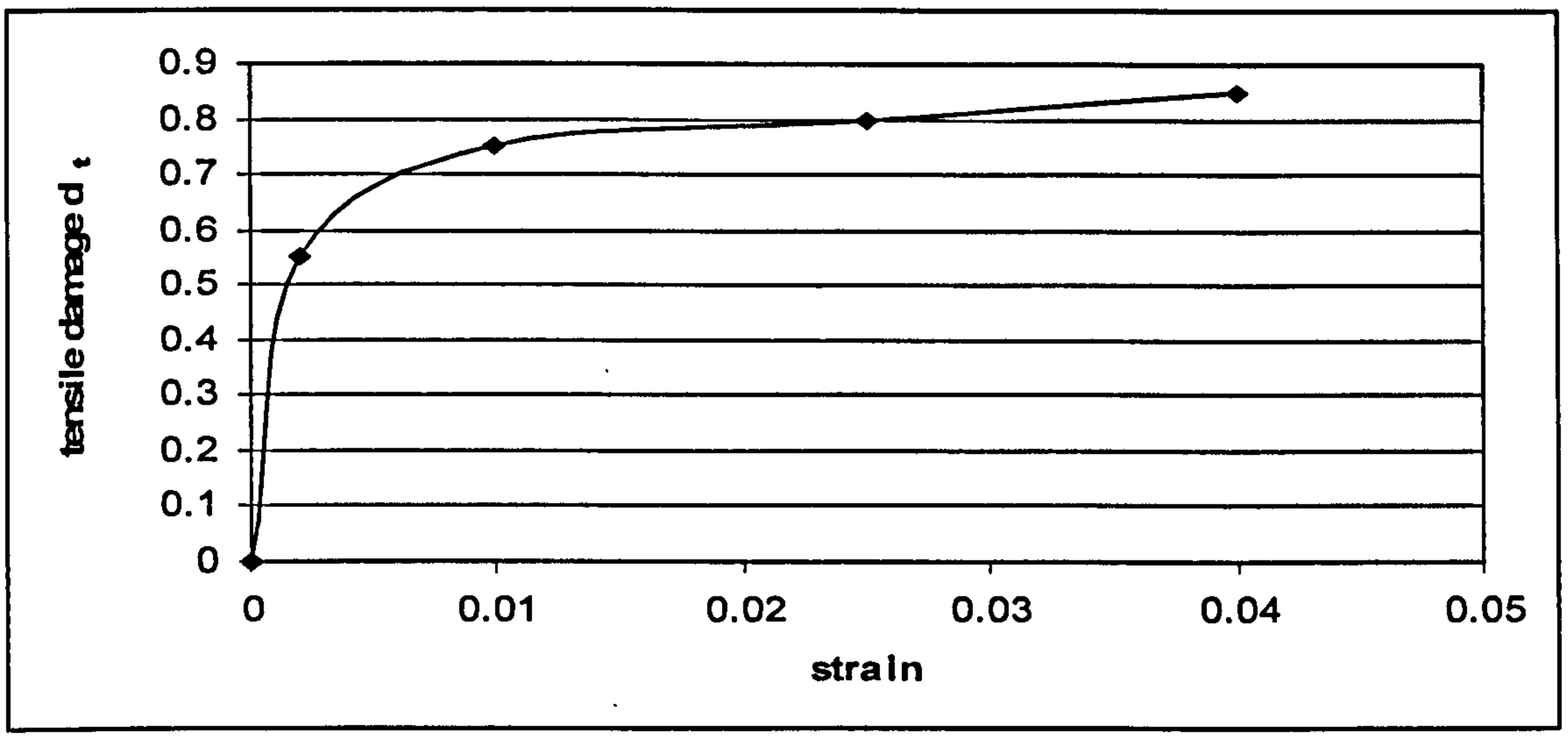

Figure 4.12: Damage evolution curve (tension)

4.5.2.8 Failure Envelope under Biaxial Compression

While the behaviour of plain concrete under multi-axial loads has been studied and well-documented by many researchers (Tho et al., 2003; Darwin and Pecknold, 1977 and Candappa et al., 1999), limited studies in the strength and deformation of SFRC when subjected to multi-axial loads have been reported. Chern et al. (1992) and Pantazopoulou and Zanganeh (2001) reported the experimental triaxial behaviour of SFRC. On the other hand, Nielsen (1998) proposed a bilinear failure criterion for high-strength steel fibre-reinforced mortar under axi-symmetrical loads, while Hu et al. (2003) developed a biaxial failure curve which may be modified to fit the different failure envelopes of SFRC containing varying amounts and types of fibre. Murugappan et al. (1993) developed an analytical approach to determine the biaxial compressive strength envelope for SFRC. The approach characterizes the influence of the fibres by means of the postcracking tensile strength. Traina and Mansour (1991) and Yin et al. (1989) have studied the biaxial behaviour of SFRC. The experiments demonstrate that the biaxial envelope of SFRC has different shape from that of plain concrete. However for the content of fibres usually applied in industrial floors, the differences are marginal (Barros and Figueiras, 2001). Hence, the value suggested for plain concrete (Kotsovos and Pavlovic, 1995) could be used. To this end, the ratio of the biaxial to uniaxial compressive stress was taken as 1.15.

4.5.3 A summary of the Recommendation stemming from the Sensitivity Analyses for the Present FE Analysis

For this analysis, the following parameters were kept constant for all the beams analysed.

- The convergence criteria based on the residual forces tolerance is 5%.
- The size of the arc length is 0.1.
- The size of the initial load increment is 0.01.
- For the mesh density, 66 square elements had an element length of 25mm were used.
- The Poisson's ratio is kept constant at 0.2.
- Young's modulus, $E_c = 21{,}500\left[f_{cm}/10\right]^{\frac{1}{3}}$.
- For uniaxial stress-strain characteristics, expression proposed by Barros & Figueiras (1999) is used.
- For post-cracking behaviour in tension, the inverse method is used.
- The dilatancy angle at the ultimate uniaxial compression strength $\psi = 10°$.
- The ratio of the biaxial to uniaxial compressive strength =1.15.
- Compression damage is varied linearly, while tensile damage is as shown in Figure 4.13.

4.6 Data for the Numerical Analysis

The proposed computational model is performed using results from two experimental programs reported in the literature and bending beam results obtained from this research (see Chapter Six, section 6.4.2). Experimental program "A" was conducted at the University of Minho Azurem, Portugal. Recent tests (Barros & Figueiras, 1999) on 4-point-bending beams all made with Dramix hooked-end steel fibres provide comprehensive benchmark data for numerical investigation. Twenty one SFRC beams with identical dimensions were tested under four-point bending test on notched beam. Dramix steel fibres with two fibre aspect ratios were used, ZP30/.50 and ZX60/.80 with different steel fibre-reinforcement ratios (30, 45, 60) kg/m^3. Eleven of the beams were reinforced with ZP30/.50 Dramix steel fibres, while the other ten beams were strengthened by Dramix steel

fibre ZX60/.80. Experimental program "B" has been documented in Report no. 2005-95 (Farhang and Vogt, 2005) and was conducted on SFRC beams subjected to three-point bending at the Swedish Cement and Concrete Research Institute. Twelve specimens of identical dimensions each reinforced with Dramix hooked-end steel fibre RC 65/60 BN were tested. Two dosages of 30 and 40 kg/m^3 were used in this study.

Experimental program "C" has been carried out on SFRC beams subjected to three-point bending by the researcher. Twelve specimens with identical dimensions each reinforced with Dramix hooked-end steel fibre ZP30/.50 and RC 65/60 BN were tested. Two dosages of 20 and 40 kg/m^3 were used in this study.

The load-displacement responses of all programs (i.e. "A", "B" and "C") were monitored using LVDTs and used to validate the computational model. The material properties of the test specimens used in the experimental programs "A" and "B" are given in Table 4.1. The material properties of the test specimens of experimental programme "C" are presented in Chapter Six Table 6.3.

The FE model for the SFRC beam was set using the same dimensions as the experimental SFRC beam tests described in experimental programmes "A" B"" and "C" and the objective here was to simulate the geometry and materials in order to model their load versus mid-span deflection behaviour.

4.7 Results and Comparisons

The FE analysis gives a detailed picture of the complete behaviour of the beams from elastic to ultimate load. The input tension-stiffening curve was modified until the calculated load versus mid-span-deflection curve agrees with the results obtained from the experimental tests. Hence, an analytically based computational tool for modelling the behaviour of a SFRC member is developed. This analytical model could be used to describe the tension-stiffening behaviour of SFRC which enables a more reliable finite element analysis. Data for tension stiffening diagrams determined from the experimental load-displacement curves for experimental programmes "A" and "B" are shown in Table 4.3 and

for experimental programme "C" is shown in Chapter Seven, Table 7.1. The simulated load-displacement curves of Series "A" and "B" using the determined tension stiffening diagrams through the poly-linear approximation method are shown in Figures A.1 to A.32 (Appendix A), and for series C are shown in Chapter Seven, Figures 7.2 to 7.7. The simulated load-displacement curves agreed with the experimental ones.

Table 4.3: Data for tension stiffening diagrams

Beam No.	E_{cm} (GPa)	σ_t^u (N/mm^2)	$\sigma_{n1}/\varepsilon_1$	$\sigma_{n2}/\varepsilon_2$	$\sigma_{n3}/\varepsilon_3$	$\sigma_{n4}/\varepsilon_4$
B1	33.28	3.3	1.5	1.3	1.1	0.9
B2	33.28	3.6	1.5	1.3	1.1	1.0
B3	33.28	3.8	2.4	2.0	1.8	1.5
B4	33.28	3.2	1.8	1.8	1.8	1.4
B5	32.45	3.4	2.2	2.0	2.0	1.6
B6	32.45	3.4	2.2	1.5	1.1	1.0
B7	32.45	2.8	1.85	1.8	1.8	1.4
B8	32.45	3.5	1.4	1.2	1.2	1
B9	32.45	3.2	1.8	1.5	1.3	0.9
B10	32.45	3.2	1.8	1.65	1.4	0.95
B11	32.45	2.5	1.75	1.45	1.45	1.0
B12	32.14	3.0	1.3	1.2	1.15	1.15
B13	32.14	3.0	1.45	1.5	1.55	1.35
B14	32.14	3.0	2.7	2.3	1.5	1.3
B15	32.14	3.3	1.8	1.8	1.8	1.4
B16	32.14	3.2	1.8	1.8	1.5	1.15
B17	32.14	2.9	2.25	2.0	2.3	2.0
B18	32.14	2.9	3.2	3.3	1.8	2.3
B19	32.14	3.2	2.5	2.85	2.45	1.8
B20	32.14	3.2	3.15	3.2	3.0	2.5
B21	32.14	3.0	4.9	4.2	3.2	2.8
B22	.....	3.2	1.6	1.3	1.2	1.05
B23	.....	3.4	0.6	0.8	0.85	0.8
B24	.....	3.0	2.0	2.3	2.3	1.8
B25	.....	3.25	1.2	1.55	1.3	1.25
B26	.....	3.25	1.2	1.1	1.3	1.1
B27	.....	3.5	1.55	1.7	1.7	1.35
B28	.....	3.6	1.5	1.8	1.8	1.5
B29	.....	3.0	1.4	1.4	1.3	1.25
B30	.....	3.6	1.8	2.1	1.9	1.5
B31	.....	3.8	1.7	2.3	2.3	1.75
B32	.....	3.0	1.5	1.4	1.6	1.3
B33	.....	3.2	1.3	1.0	1.1	1.0

4.8 Regression Model for Tension-Stiffening

As discussed earlier in section 4.5.2.4, the residual flexural strength is an important parameter characterising the post-cracking behaviour of SFRC. It could be determined by the deflection control bending test. Although the displacement controlled flexural tests do not give a direct result, it is a simple alternative to direct tensile tests, such a test is not easy to perform due to the localisation of the strain introduced by cracks. Results from flexural tests can be used to develop the stress-strain or stress-crack width characteristics for FEA modelling. RILEM TC162-TDF (2003) proposed a tension stiffening diagram for SFRC based on two residual flexural tensile strength $f_{R1,}$ and $f_{R,4}$. The residual tensile strengths $f_{R,1}$ and $f_{R,4}$ respectively, are defined at the following mid span deflection $\delta_{R,1}$ = 0.46 mm, $\delta_{R,4}$ = 3.00 mm.

The FEA in section 4.5.2.5 shows that the formula proposed by RILEM TC162-TDF (2003), see Figure 4.10, is not able to predict the behaviour of SFRC beam under bending test. Therefore, this research was intended to propose a procedure to determine the tension-stiffening diagram for SFRC beams, using results of FEA. The plastic strains ε_1, ε_2, ε_3 and ε_4 were determined at values of 2‰, 10‰, 25‰, and 40‰, respectively. The input parameter for the stresses at plastic strain ε_1, ε_2, ε_3 and ε_4 were changed step-by-step until the analytical load-deflection curve equate with the experimental one. The values for σ_{n1}, σ_{n2}, σ_{n3} and σ_{n4} are shown in Table 4.3. As proposed by Tlemat et al. (2006) the strain limit 25‰, suggested by RILEM TC162-TDF (2003) corresponds to a deflection of about 2mm, and is not sufficient to describe the full load deflection characteristics. Therefore, the use of strain limit 40‰ was mandatory. This value gave a good correlation with the experimental results when used by Tlemat et al.(2006).

The regression statistics model was utilised to investigate the relationship between the stresses (σ_{n1}, σ_{n2}, σ_{n3} and σ_{n4}) as dependent variables and (σ_{tu}, f_L, f_{R1}, f_{R2}, f_{R3} and $f_{R,4}$) as independent variables, which is normally represented by the following equation:

$$Y = C + b_1X_1 + b_2X_2 + \cdots + b_nX_n, \qquad \text{.....4.17}$$

Where Y is the normalized stress, and X_1, X_2... X_n are measures of distinguishable factors that affect the prediction of Y. For example, X_1 could be the residual flexural strength at mid span deflection of 0.46 mm, X_2 the residual flexural strength at mid span deflection of 3.0 mm, etc., C is constant, and b_1, b_2.... b_n are the coefficients estimated by regression analysis, given the availability of some relevant data. The Statistical Package for Social Science (SPSS) stepwise techniques was used to develop the regression model. Only the statistically significant parameters (regression coefficient) i.e. $\rho < .05$, VIF (Variance Inflation Factor) <10, were selected to establish the final relationship. The following relationships were found:

$$\sigma_{n1} = 0.055 - 0.14\,\sigma_{tu} + 0.486 f_{R1} \quad \text{.....4.18}$$

$$\sigma_{n2} = 0.193 - 0.082 f_L + 0.46 f_{R2} \quad \text{.....4.19}$$

$$\sigma_{n3} = 0.347 - 0.236 f_L + 0.489 f_{R3} + 0.17\,\sigma_{tu} \quad \text{.....4.20}$$

$$\sigma_{n4} = 0.344 - 0.076 f_L + 0.378 f_{R4} \quad \text{.....4.21}$$

This regression model enabled one to predict the post-cracking stress-strain characteristics of SFRC by knowing the load at four mid-span deflections $\delta_{R,1} = 0.46$ mm, $\delta_{R,2} = 1.31$ mm, $\delta_{R,3} = 2.15$ mm and $\delta_{R,4} = 3.00$ mm.

4.9 Conclusion

This chapter emphasises upon the development of a constitutive law for modelling the post-peak behaviour of SFRC in tension. This was achieved by using the poly-linear approximation analysis method with a nonlinear finite element method to model the flexural response of SFRC beam sections, described in Barros and Figueiras (1999) and Farhang and Vogt (2005) and in this research (see Chapter six). This method is an inverse method. However, it was found that a model which has components embedded to simulate damage due to tension cracking, compression yielding and crushing of concrete such as the Damaged Plasticity Model native in ABAQUS seems to simulate the transformation of the load-displacement curves resulting due to the variation in steel fibre dosages realistically. The FE results have also been utilised to formulate a simplified tension-stiffening model and a good correlation with the experimental results has been obtained. There are two

major motivations for the development of this constitutive model, one is to guide the optimisation of the material behaviour by tailoring the types and forms of the constituent components, and the other is to predict the mechanical response of the end products made of such materials. Moreover, this constitutive model could be used in predicting the behaviour of SFRC slabs subjected to punching shear, as will be discussed in Chapter Seven.

CHAPTER FIVE

DEVELOPMENT OF TEST SPECIMENS AND PRELIMINARY FINITE ELEMENT ANALYSIS

5.1 Introduction

As was pointed out earlier in Chapter Two, experimental study remains a very important means to predict the punching shear of SFRC slabs. This is because due to the complexity of the problem, there are still no generally accepted theories to explain their shear failure mechanisms. This means that the acceptability of any analytical model developed to describe the punching shear behaviour of flat slabs relies to some extent on experiment results. Despite, the far-reaching development of numerical methods and material models for concrete, finite element simulations are not yet able to fully replace the information from actual punching tests. However, a numerical analysis might be helpful to design the test setup or the geometry of the punching tests as well as details of the test specimen, e.g. the boundary conditions (CEB-fib, 2001) which can be used to model the flat slab system satisfactorily. This chapter presents a preliminary FEA which was carried out in order to determine the scale and size of the specimens that are appropriate to the present research. In addition, a study on the effect of underlying soil on the loading capacity of ground-suspended floor slabs using FEA is also discussed.

5.2 Test Set-ups for Testing Slab-Column Connection

Since testing of real structures is not feasible, specimens are tested to study the behaviour of slab-column connections in a real structure. In order to model the slab-column interaction of the flat slab structure under shear loading, there are two main types of set-ups which have been used for testing interior slab-column connection. These are single column tests and slab-column sub-systems.

Most of the tests on slab-column connections are single column tests often referred to as isolated slab-column connections. The test specimen consists of a column or a column stub surrounded by a portion of the slab. The dimensions of the slab portion are chosen to

model the points of contra flexure or the zone of negative moments of the real slab as shown in Figure 5.1. This isolated slab-column connection model has been used extensively as an expedient way to study the response of the slab-column area in more complex slab systems. On the other hand, it is believed that slab sub-system is more realistic than single column test (CEB-fib, 2001). However, both test set-ups have their limitations which are discussed in the section below.

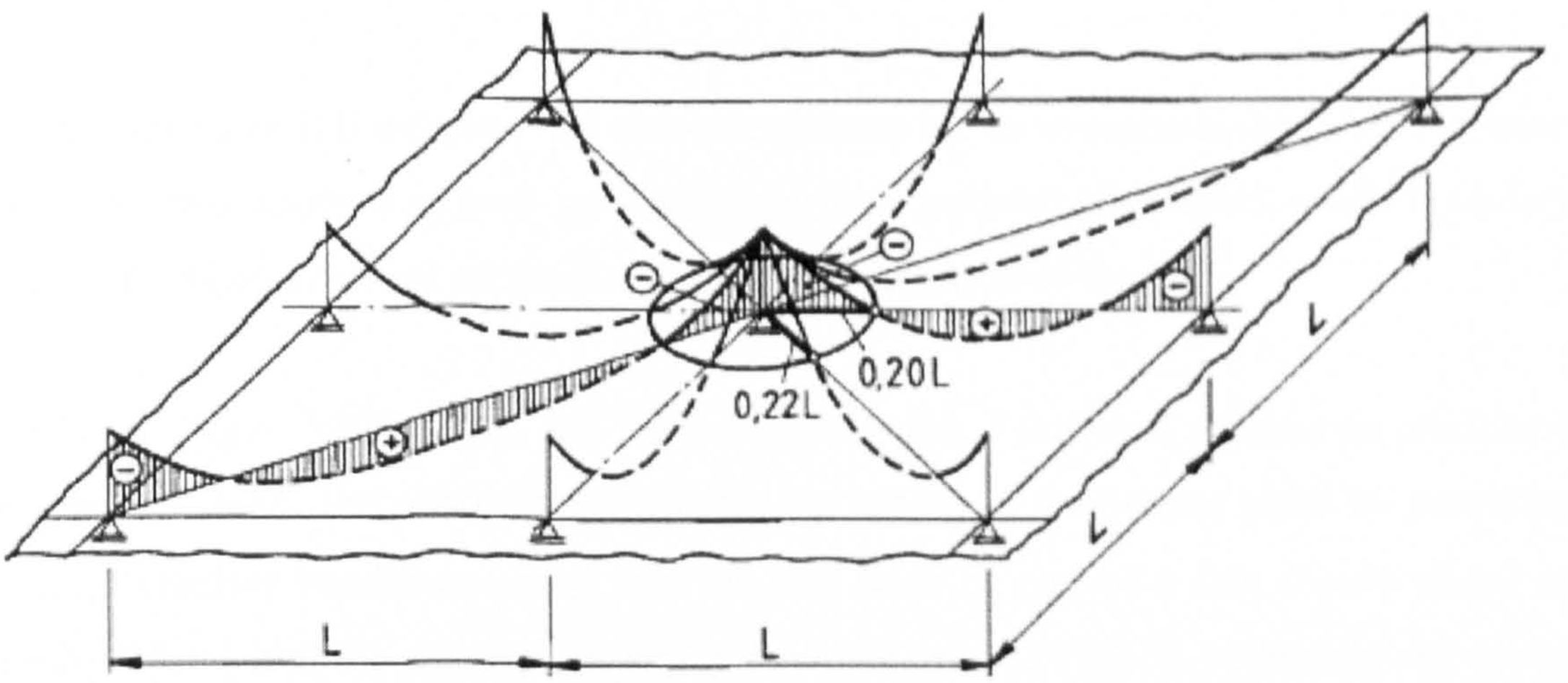

a. Distribution of the radial moments of point supported flat slab under dead load on an internal column

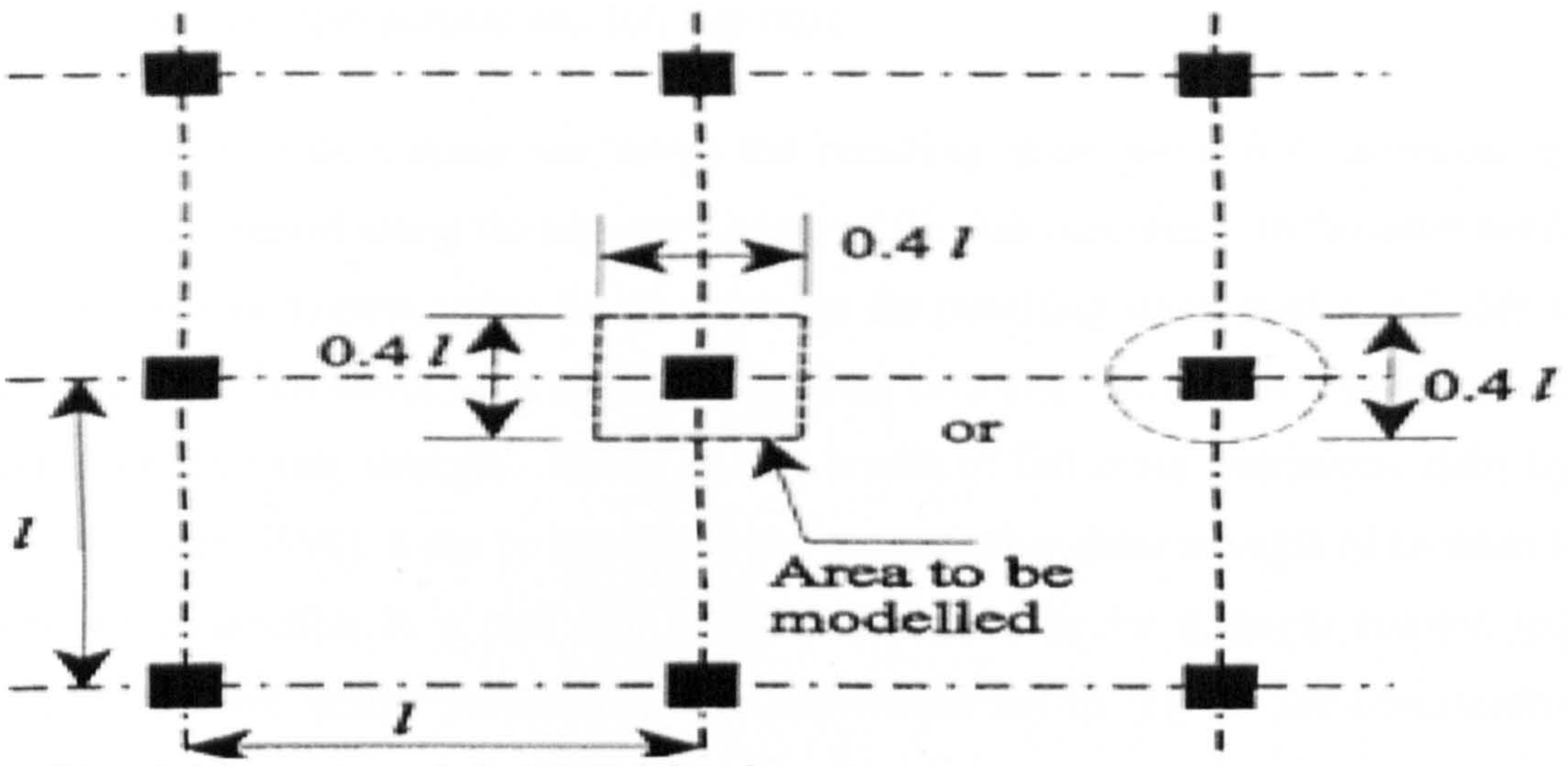

b. Size of slab specimen in isolated slab-column tests

Figure 5.1: a. Distribution of the radial moments of point supported flat slab under dead load on an internal column, b. Size of slab specimen in isolated slab-column tests (after CEB-fib, 2001)

5.2.1 Test Set-ups Limitations

Although an isolated slab-column connection model is relatively inexpensive and permit testing of full-scale specimens, it cannot exactly reproduce the conditions existing in the continuous and highly redundant flat slab system. It fails to represent the real structures in the effects of boundary conditions, confinements and in-plane forces (membrane forces). Moreover, load redistribution is not possible.

On the other hand, it is believed that slab sub-systems are more realistic than single column tests. The only concern in such system is that the supported edge could create boundary forces with unknown effect on the punching shear resistance of the slab.

Sherif and Dilger (1998) tested full scale 150mm thick, 5.0m span continuous reinforced concrete flat slabs. The test set-up facilitates the testing of continuous slabs by providing realistic boundary conditions along lines of zero shear of part of a slab centred about an exterior column and the adjacent interior column (Figure 5.2 (a)). A schematic test set-up is shown in Figure 5.2 (b). Based on the results of the tested slabs, Sherif and Dilger (1998) concluded that the punching shear strength of interior slab-column connections is the same for isolated slab-column and full slab tests.

To sum up, in a single column test set-up the punching shear strength is increased by boundary forces created along the supported edges of the slab specimen. On the other hand, the compressive membrane action which enhances the punching strength of a real slab is not accounted for. However, in a real slab restrained shrinkage introduces tensile stresses which reduce the shear strength. Based on test results of full scale continuous slabs by Sherif and Dilger (1998), it can be concluded that the punching shear strength of an interior slab-column connection in a real slab is about the same as for a single column test specimen. Thus, for design purposes it is recommended not to rely on the compressive membrane action in order to increase the punching shear strength of an interior slab-column connection.

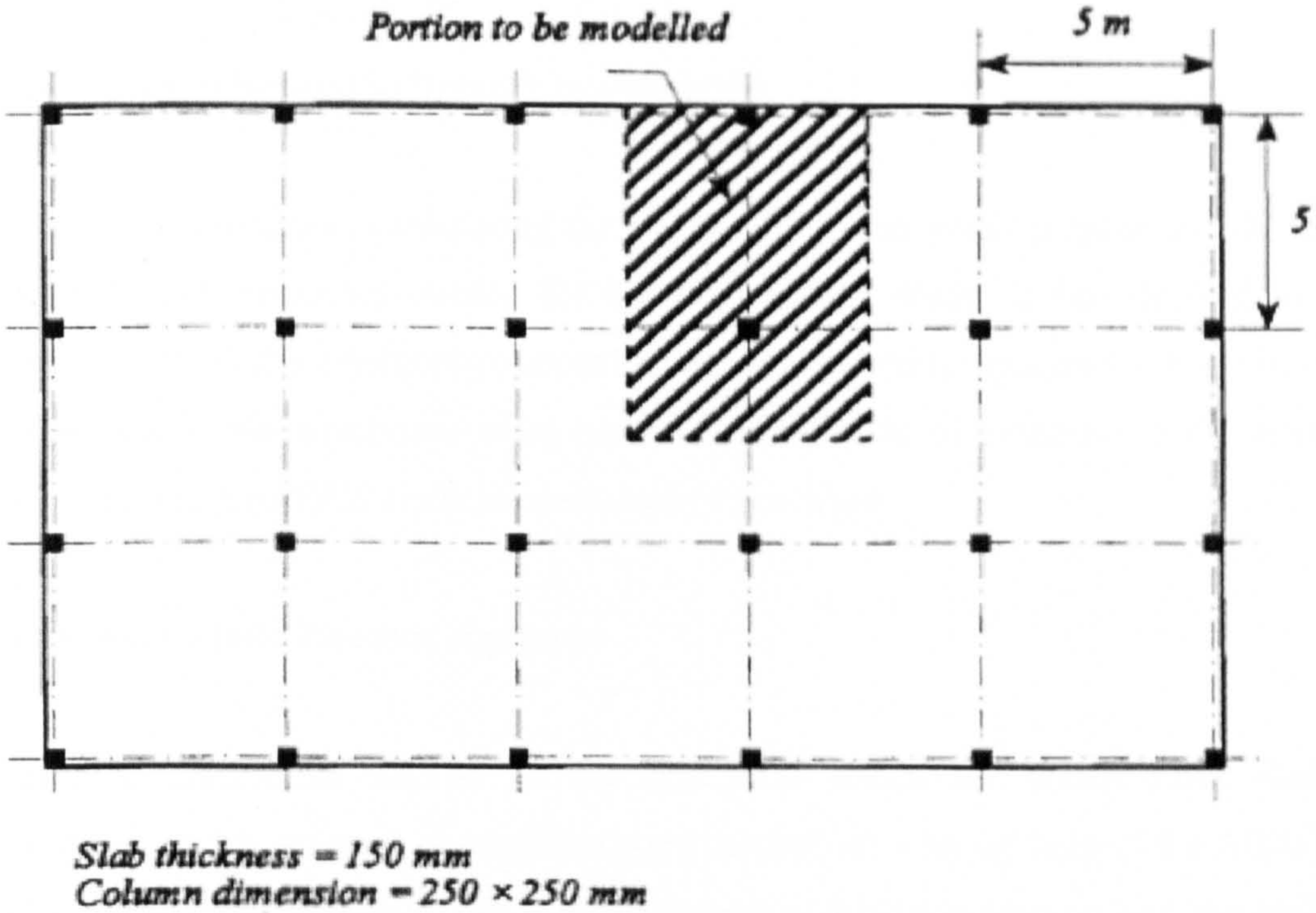

a. Plan of a typical flat slab floor

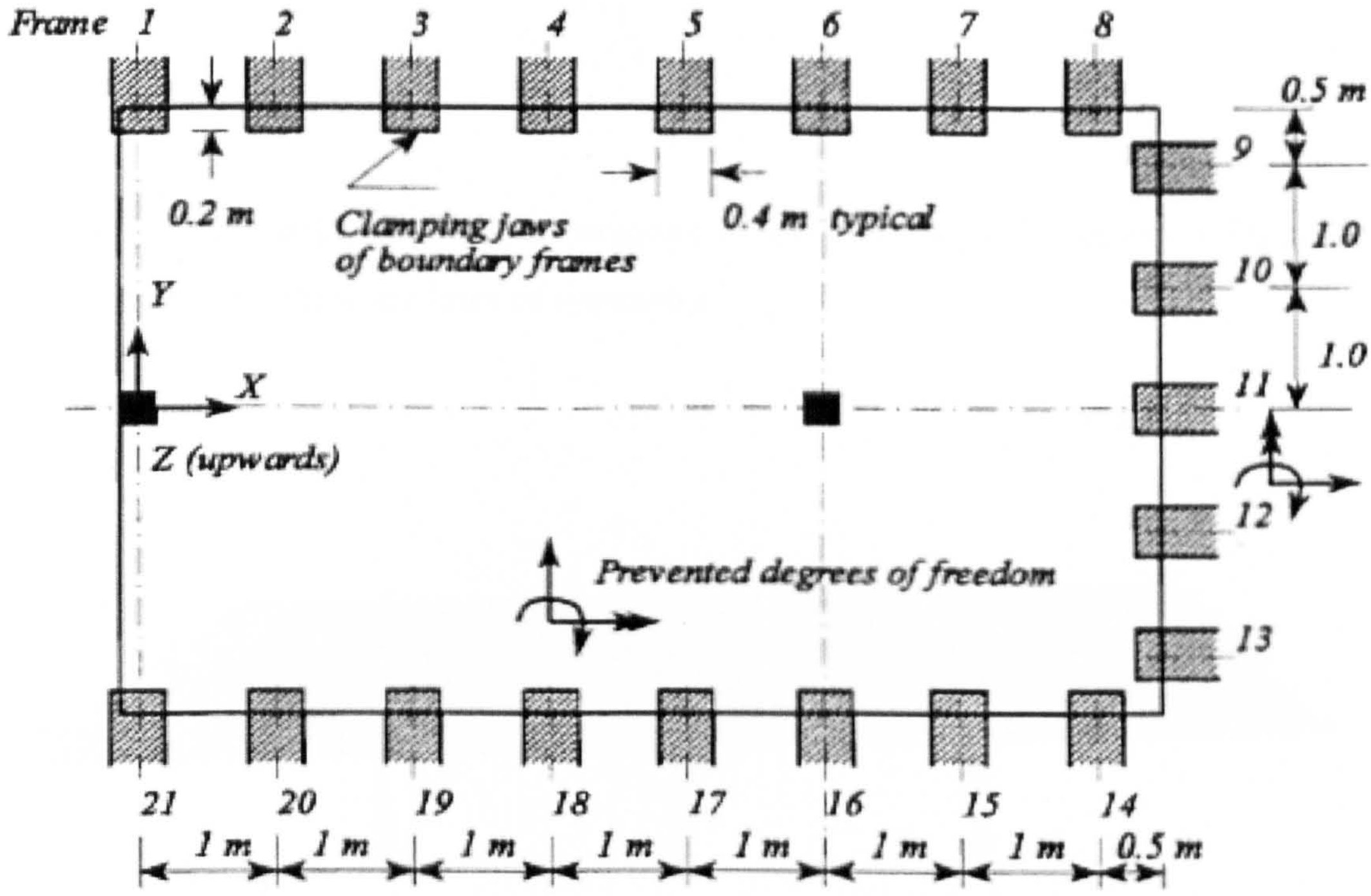

b. Boundary conditions of symmetry provided by the boundary frames

Figure 5.2: Full-scale continuous slab (after Sherif , 1996)

5.2.2 Specimens to be used in Present Investigation

In the present investigation, considering the availability of the working space and the other equipments in the laboratory needed for the experimental study, it was decided to use specimens similar to the commonly adopted isolated slab-column specimens. Furthermore, the dimensions of the specimens were based on the results of extensive finite element analyses using the ABAQUS finite element analysis package.

5.3 Preliminary Finite Element Analysis

In order to determine the size of the test specimens effectively, elastic finite element analyses based on the un-cracked condition were carried out with the help of the ABAQUS finite element analysis package. The main objectives at this stage were to find the position of the lines of contra-flexure in the slab around the internal columns and the effect of the presence of the underlying soil on the slab's ultimate capacity.

5.3.1 Size of Slab

A typical internal panel of the flat slab structure which was analysed is shown in Figure 5.3. In the internal panel there are lines of symmetry.

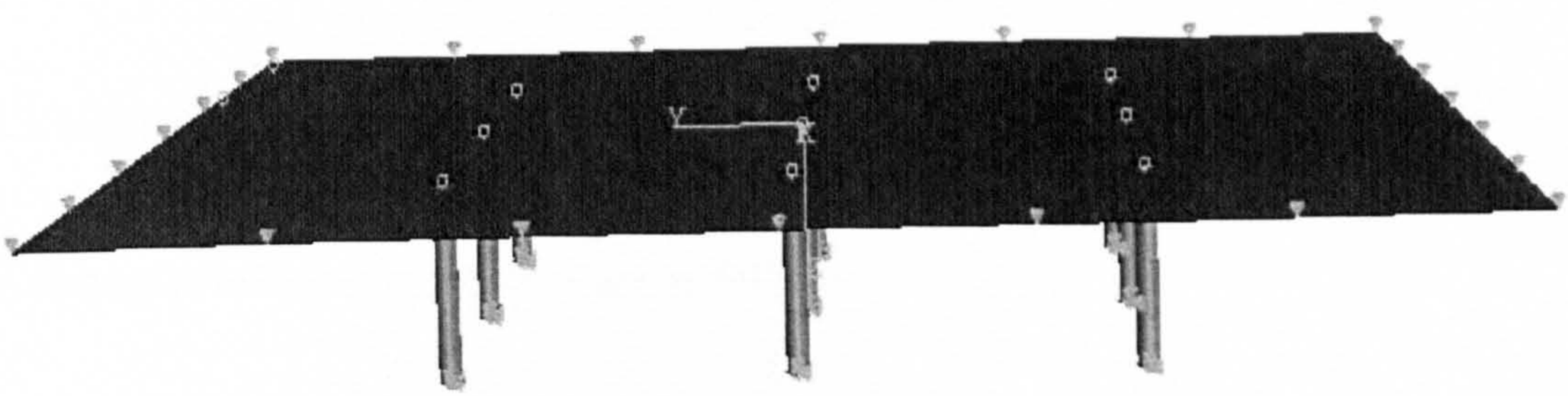

Figure 5.3: A typical flat slab on a grid of columns (12 x12 m, span L=3m) and the boundary condition

In order to take advantage of this symmetry to reduce the cost and computer running time of the analysis, only a part of the panel consisting of a single column with surrounded slab was analysed as shown in Figure 5.4.

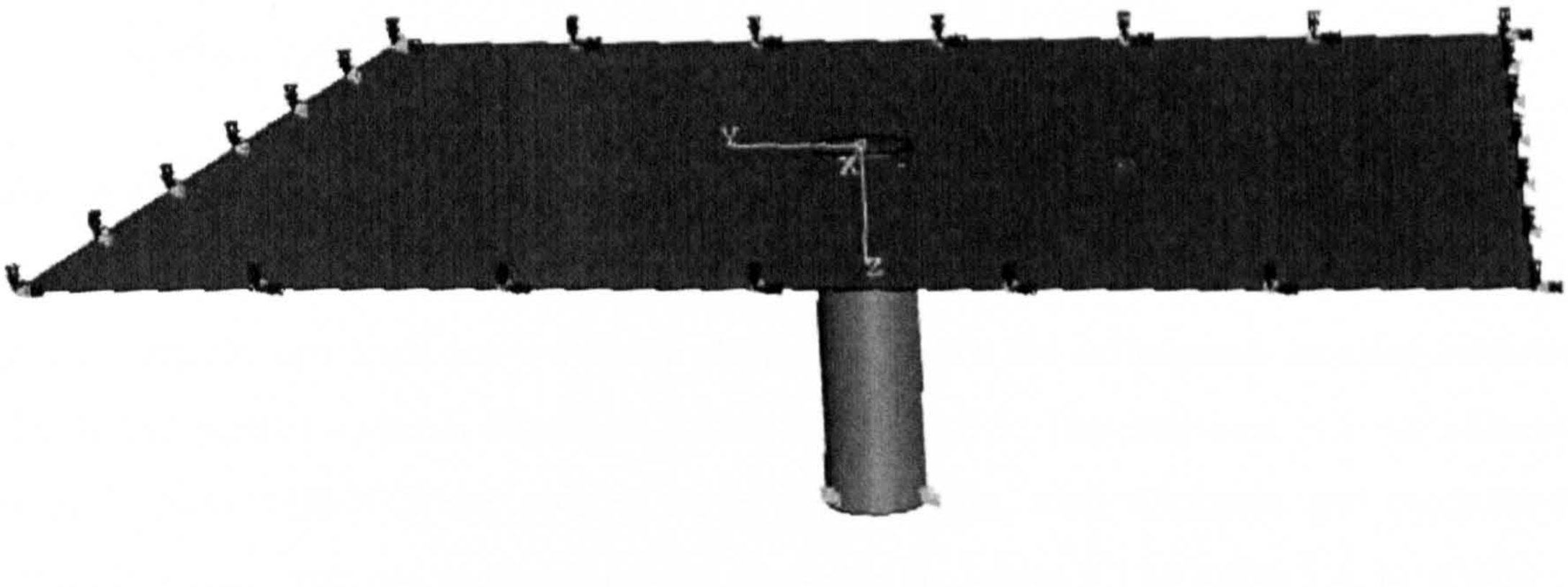

Figure 5.4: A typical slab-column connection (a single column with surrounded slab)

In the analyses, the slab was modelled with the eight-node quadrilateral shell elements designated as element type S8R. In order to study the effect of the column sizes on the position of contra-flexure lines in slabs, the twenty-node three dimensional solid elements, element type C3D20, were adopted.

Different column sizes, spans of the panel and slab thicknesses were studied in the current FEA. Moreover, the effect of modulus-of-elasticity of concrete was also studied. More details about these factors are presented below.

5.3.1.1 Factors Considered in the FEA

The factors considered in the FEA are as follows:

1. Size of column, four different column sizes namely, 100, 200, 300 and 400mm diameters were considered in the FEA.

2. Span of the panel, slab with three different spans L=3m, L=4m and L=5m from column centre to centre, were analysed.
3. Slab thickness, the practical range of slab thicknesses h = 150 mm to h = 300 mm were studied. The actual thicknesses adopted for the present study were: 150 mm, 200 mm, 250 mm and 300 mm.
4. Concrete modulus-of-elasticity, two values for the modulus-of-elasticity were studied, E_c=30GPa and E_c=36GPa.

5.3.1.2 Contra-Flexure Lines in Flat Slabs

The contra-flexure lines are the lines of contra-flexure for orthogonal bending moments (i.e. those parallel to panel edges) as shown in Figure 5.5. The positions of contra-flexural lines in slabs with different column sizes, span lengths, slab thickness and modulus-of-elasticity of concrete are summarised and presented in Tables 5.1 to Table 5.4, in which:

x_o is the distance between the zero bending moment position and the centre of the column along the column line.

x_c is the distance between the zero bending moment position and the edge of the column along the column line.

l_o is the span length from centre to centre of the columns

l_c is the span length between the edges of the columns

$\alpha_o = x_o/l_o$

$\alpha_c = x_c/l_c$

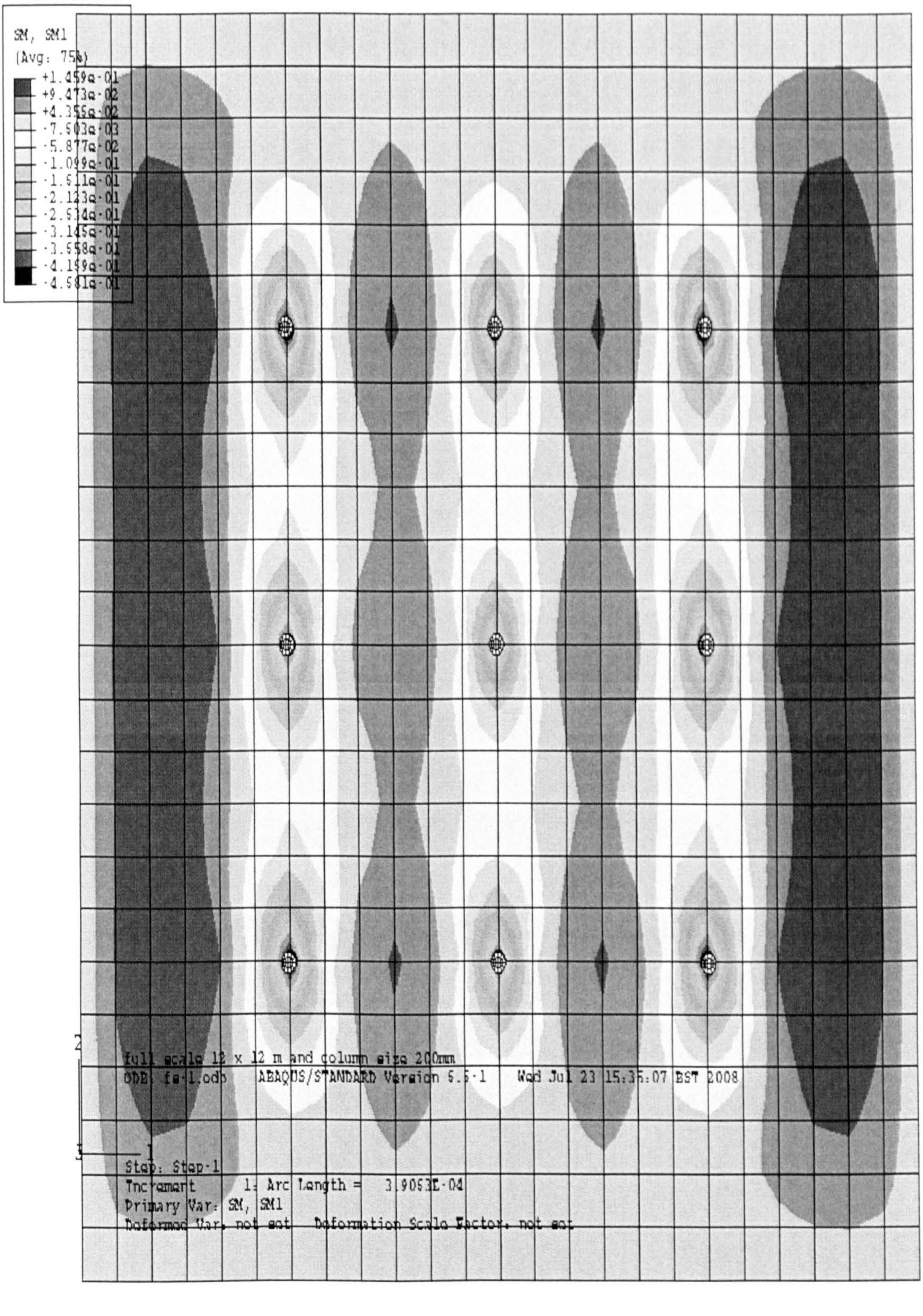

Figure 5.5: Section moment as it appears in the plan view of the flat slab shown in Figure 5.3 (a. section moment SM1 and b. section moment SM2)
a. Section moment SM1

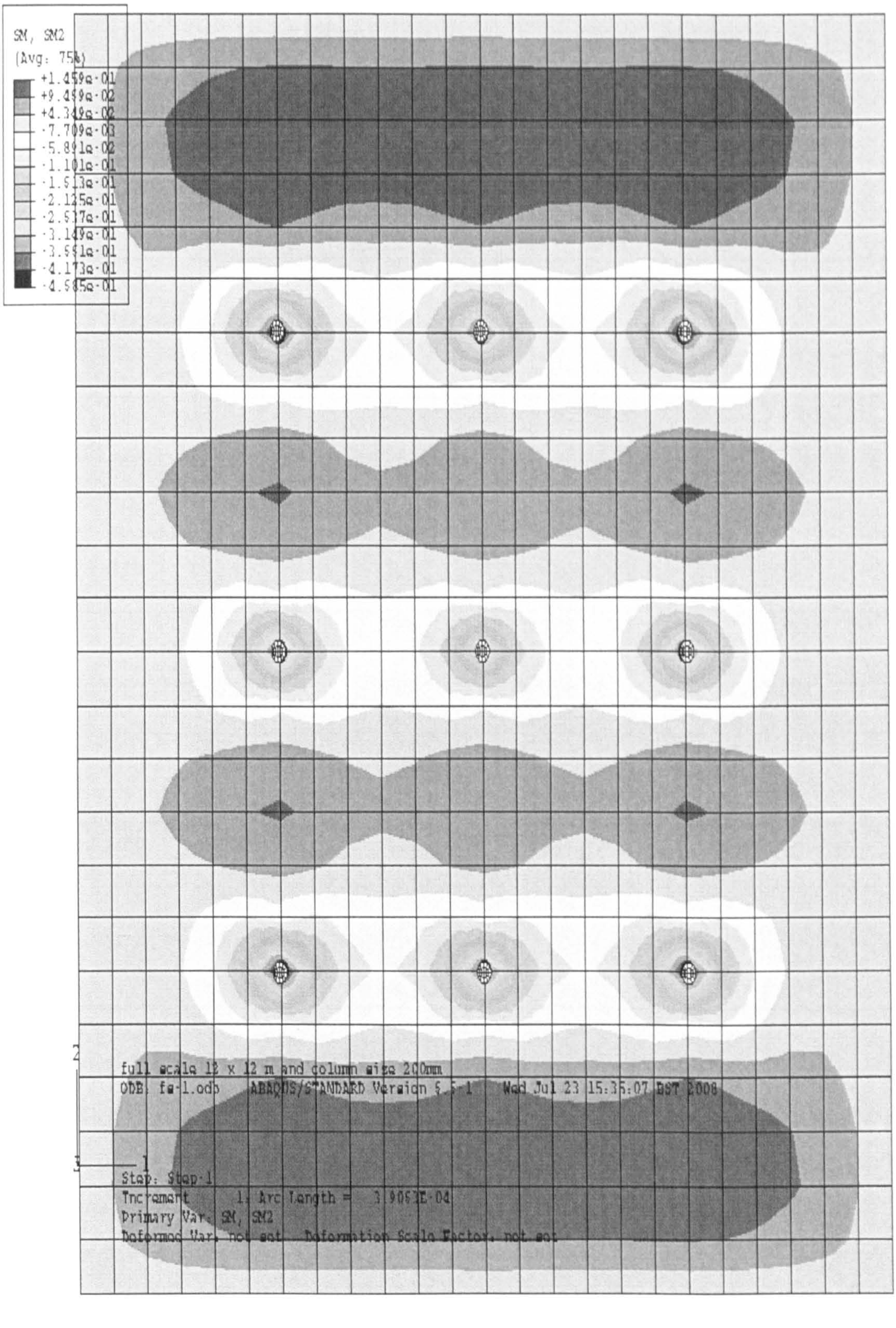

Cont' Figure 5.5: Section moment as it appears in the plan view of the flat slab shown in Figure 5.3 (a. section moment SM1 and b. section moment SM2)
b. section moment SM2

Table 5.1: Positions of contra-flexure lines of slabs (L=3 m)

Slab thickness	h=150mm				h=300mm			
Column size (mm)	x_o	x_c	α_o	α_c	x_o	x_c	α_o	α_c
100	610	560	0.203	0.193	610	560	0.203	0.193
200	618.75	518.75	0.206	0.185	618.75	518.75	0.206	0.185
300	625	475	0.208	0.176	625	475	0.208	0.176
400	640	440	0.213	0.169	640	440	0.213	0.169

Table 5.2: Positions of contra-flexure lines of slabs (L=3 m)

Concrete modulus-of-elasticity (GPa)	x_o	x_c	α_o	α_c	x_o	x_c	α_o	α_c
E=30	610	560	0.203	0.193	610	560	0.203	0.193
E=36	610	560	0.203	0.193	610	560	0.203	0.193

Table 5.3: Positions of contra-flexure lines of slabs (L=4m, h=150 mm)

Column size (mm)	x_o	x_c	α_o	α_c
100	820	770	0.205	0.197
200	825	725	0.206	0.191
300	823.5	475	0.208	0.184
400	840	640	0.21	0.178

Table 5.4: Positions of contra-flexure lines of slabs (L=5m, h= 150mm)

Column size (mm)	x_o	x_c	α_o	α_c
100	1020	970	0.204	0.198
200	1025	925	0.205	0.193
300	1030	880	0.206	0.187
400	1040	840	0.208	0.183

From Table 5.1 and 5.2 it can be seen that in slabs with a span length of 3m, and a column diameter of 100mm, the contra flexure lines are always located at a distance of 610mm from the centre of the column regardless of the thickness of the slab and the modulus of elasticity of concrete. This means that the slab thickness and the value of the modulus of elasticity in flat slabs do not seem to affect the position of contra-flexure lines. In slabs with the span length L=4m and L=5m, the contra-flexure lines are located respectively at a distance 820mm and 1020mm from the centre of the column. Therefore, it can be suggested that the location of contra-flexure lines vary with the span lengths.

Tebbett and Harrop (1979) pointed out that the column size had some significant effects on the distribution of bending moments in slabs. It seems, however, that the column size does have little influence on the positions of contra-flexure lines. This can be seen clearly from the FEA results presented in Tables 5.1, 5.3 and 5.4. The data listed in these Tables show that within each span length of slab, the positions of zero bending moments vary little with the different sizes of columns.

$\alpha_o = x_o/l_o$ was used as a parameter to define the positions of contra-flexure lines in slabs. For L = 3m slabs, α_o is in the range of 0.203 to 0.213. While for L = 4m slabs, α_o is 0.205-0.21 and for L=5m slabs, α_o is 0.204-0.208. Therefore, for commonly used flat slabs, the value of α_o should lie somewhere between 0.203 and 0.213. This definition and value are very similar to those proposed by CEB-fib, (2001) for flat slabs in which the α_o is defined as 0.2, see Figure 5.1a.

5.3.2 Effect of Soil

As was pointed out earlier in Chapter One, the common practice of designing suspended ground-suspended floor slabs in the UK follows the requirement appearing in the building design code BS8110 (1997) which treated them as fully suspended slabs.

Although ground-suspended floor slabs are designed as fully suspended, their behaviour is different due to the presence of the underlying soil. Such slabs will initially act as hybrid supported/suspended slabs, so that stresses induced due to loading in a suspended slab on ground may be much lower than the normal design predicts because inevitably the underlying ground will provide some support. This means that the actual bending movements and shear forces could be much less than the structural design predicts. On the other hand, a slab on the ground can only dry out from the top surface, because the lower portion of the slab acts as restraint to the top. Another restraint arises also from the supporting piles. This means that there can be considerable tension forces induced by the restraint contraction particularly at the top of the slab. Consequently, the dominant stress at the top of a ground-suspended slab could be the restrained contraction stress, which could result in no compression at the top of the slab at mid-span (Simpson, 2004).

As a result, more research is needed to re-examine the effect of the underlying soil on the ultimate load of the SFRC slabs. FEA was carried out, in order to assess the extent to which the presence of soil affects the ultimate capacity of a concrete slab.

5.3.2.1 Modelling of Concrete Slabs with Underlying Soil

A finite element analysis was carried out to predict the effect of the presence of underlying sub-grade soil on the ultimate punching shear capacity of slabs. Although, in the last two decades there has been a rapid development of numerical simulation of concrete structures, numerical simulation of a slab supported on soil remains a difficult task (Barros and Figueiras, 1998). Accurate simulation of the behaviour of this kind of structures is only feasible if the numerical model takes into account, in an appropriate way, the behaviour of both the concrete and the soil.

As this research aimed at modelling circular slabs subjected to symmetrical punching shear without moment transfer, circular slab with underlying soils were modelled. Due to polar symmetry, the slab and soil were modelled with axi-symmetric isoparametric eight-node solid elements with nine integration points.

Due to axi-symmetry, only one-half of the slab with the underlying soil will be taken, with the origin at the centreline. The punching load is applied by imposing vertical displacement restraints throughout the loaded area (at the bottom of the column stub), Figure 5.6 shows the slab, soil, and column with the boundary conditions adopted in this analysis.

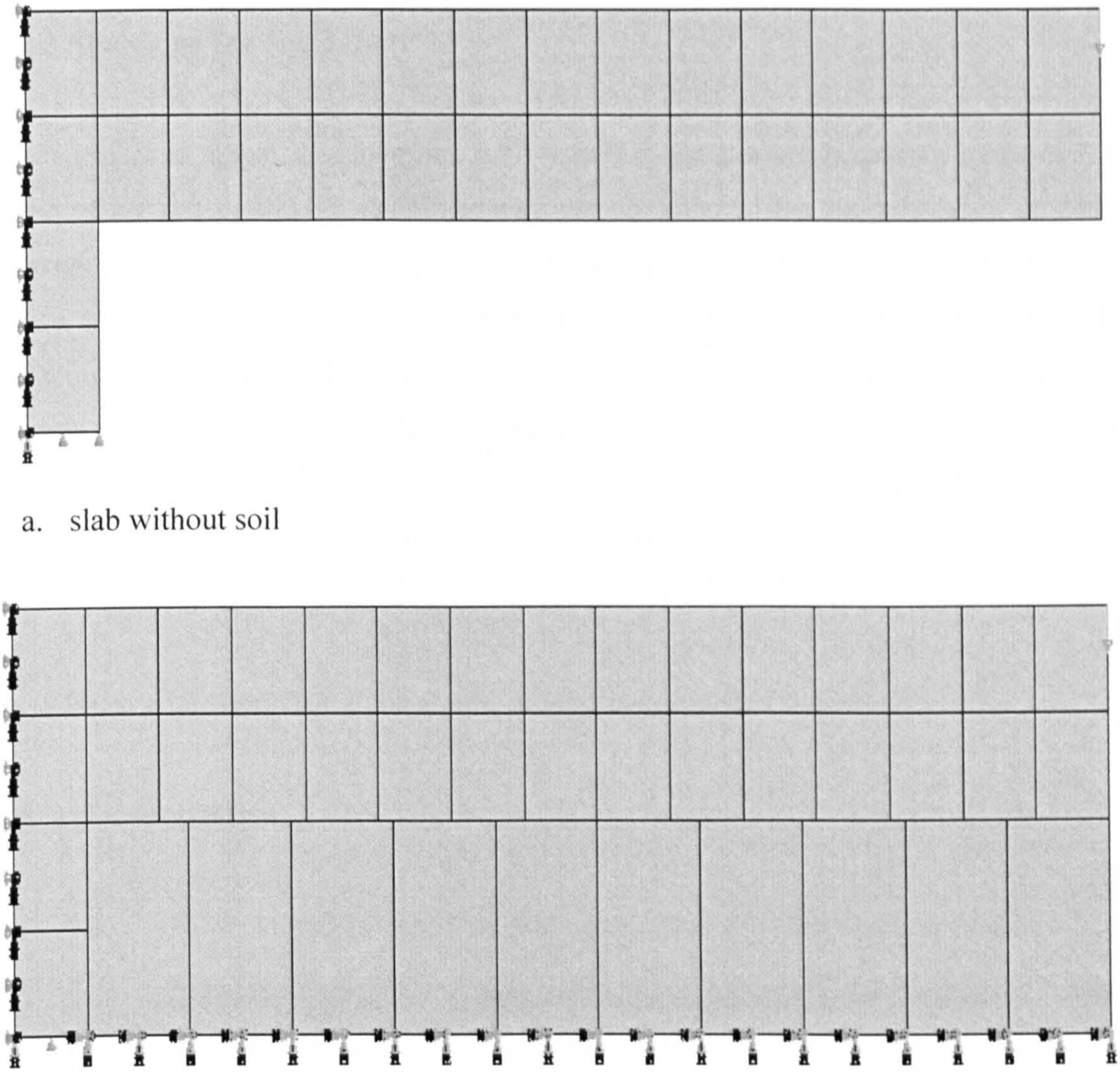

a. slab without soil

b. slab with soil

Figure 5.6: Mesh and boundary conditions adopted in the FEA (slab without soil and b. slab with soil)

Due to the fact that this part of investigation was carried out at the early stages of this research and due to lack of experimental results on SFRC slabs, the elastic material properties of the concrete slab were incorporated into the concrete Damaged Plasticity Model.

5.3.2.2 Modelling the Sub-Grade

It is important to make an assumption with regard to the sub-grade bearing pressure at the bottom of the slab. Three main models are usually adopted for the purpose of modelling sub-grade elastic deformational behaviour. These are: the Winkler foundation, the Semi-infinite elastic half space and the modified Winkler model. Other methods aimed at improving the Winkler model by depicting the continuity of the sub-grade were carried out by many researchers and are described elsewhere (Selvadurai, 1979). The focus of these methods was on providing mechanical interaction between the individual springs. Plastic and nonlinear models are also used for the foundation-structure interaction problem, but they are beyond the scope of the present research.

The stiffness characteristics of the elastic models are described below.

a) Winkler foundation

The Winkler (1867) model is based on the assumption that the reaction pressure in the foundation is proportional at every point to the deflection occurring at that point and is independent of the pressure deflection produced elsewhere in the foundation. This can be expressed mathematically as follows:

$$p \alpha \delta \qquad \text{.....5.1}$$

Where p is the reaction pressure in the foundation and δ is the deflection at that point. The lack of continuity in the supporting medium can be physically represented by rows of closely spaced, but independent, elastic springs.

The Winkler model provides the simplest mathematical model leading to reasonable estimates of the response of a beam resting on a soil medium (Hetenyi, 1946). The popularity of the Winkler foundation model is due to its simplicity. It is a single-parameter model that depends only on the constant of proportionality of the spring and yet has proven

to be reliable and effective in solving many soil-foundation interaction problems (Selvadurai, 1979). The spring constant, which is known as the modulus of sub-grade reaction k, is readily available from equation 5.1 as the constant of proportionality, i.e.

$$k = \frac{p}{\delta} \qquad \text{.....5.2}$$

The Winkler model is accurately applicable for fluid-structure interaction problems, while for foundation-structure interaction problems it is only a practical approximation. However, it is extremely useful in many types of soil-foundation interaction analyses (Davis and Selvadurai, 1996). The main deficiency of the model is the lack of continuity between the springs. However, this is true only if the load is applied directly on the sub-grade without foundation, in which case the spring directly under the load will be deformed while the neighbouring springs will remain unaffected. On the other hand, introducing the foundation will provide continuity among the group of springs representing the sub-grade and thus make the Winkler model more applicable in modelling soil-foundation problems. Though it is mathematically simpler than the elastic-half space model, one should not regard it, as some investigators do, as an "elementary" solution for the elastic soil foundation, because it has its own physical characteristics and significance (Hetenyi, 1946). From the design perspective, it is more efficient and does not require the knowledge of the thickness of the sub-grade layer and the value of k can be determined by a simple field test.

Many researchers have used the Winkler assumption to simulate the soil in finite element modelling, among them Shentu et al. (1997), Abbas (2002) and Al-Nasra (1997). It was concluded that using such an assumption can give good correlation when compared to experimental results. However, for the analysis of industrial ground floor-slabs Panak and Rauhut (1975) adopted the Winkler model. It can be concluded, therefore, that the present model is applicable for normal loading and geometry conditions, as is the case with ground-floor slabs.

b) Semi-infinite Elastic-Half Space

The foundation here is assumed to behave as an isotropic and homogeneous elastic solid. Therefore, its deformational behaviour can be sufficiently defined by the modulus of elasticity E_s and Poisson's ratio υ. Unlike the Winkler model, it represents the case of complete continuity in the supporting medium.

This type is usually referred to as a "semi-infinite elastic half space" and is based on the pioneering work of Boussinesq (1878), who calculated the stress profile through the thickness of a multi-layer elastic soil due to a point load at the top of the soil. The model is good for modelling sandy soils (Selvadurai, 1979), but does not give equally good results for clay soils whose deformational behaviour are predominantly plastic. Under heavy loads, significantly high stresses develop in an elastic-half space, which would cause the real soil to yield or "flow", i.e., the soil would tend to shift its behaviour from that of an elastic solid to that of a dense liquid (Ioannides and Korovesis, 1992). For FE solutions that adopt this model for the soil, the solution is dependent on two additional parameters, namely the sub-grade thickness and the plan dimensions. The lateral support boundary conditions on the sub-grade edges might also affect the solution. Therefore, adopting this model for FE analysis might be useful if a specific soil type is to be investigated.

c) Modified Winkler Model

An improvement to the Winkler model was proposed by Abbas (2002). He utilised the developed model to analyse and design the ground floor slabs using a finite element method.

In this case, the sub-grade is modelled as a group of 1-D springs that have stiffness in one direction only, along the sub-grade thickness. In order to partly overcome the discontinuity deficiency, the springs were connected together along the vertical sides (i.e. common nodes in the vertical directions). In addition to the continuity provided at the top by the slab (i.e. common horizontal nodes between the slab and the sub-grade). Thus, the present finite

element model is very slightly different from, and constitutes a small improvement over, the "pure" Winkler model used by Westergaard. The only parameter needed to define the spring stiffness is the modulus of sub-grade reaction k. In order to incorporate this model in the FEA, the value of k was bypassed by means of an equivalent modulus of elasticity for the Winkler sub-grade (E_w). The material model adopted was an anisotropic elastic material that has one elastic constant (E_w) along the thickness. This model was used throughout the current investigation. The relationship between the constant k and E_w was derived as described below.

Assume that a spring of length H is fixed at the base. The spring is loaded on the top by the pressure from the slab, which is equal to the sub-grade reaction p. Hence, the deflection δ of the element with an infinitesimal area dA can be computed from simple strength-of-materials principles by noting that the axial stress σ_A of the element is

$$\sigma_A = \frac{pdA}{dA} = p \qquad \text{.....5.1}$$

and the axial strain

$$\varepsilon_A = \frac{\delta}{H} \qquad \text{.....5.4}$$

So that the modulus of elasticity of the anisotropic material through the thickness E_w is

$$E_w = \frac{\sigma_A}{\varepsilon_A} \qquad \text{.....5.5}$$

By substituting eq. (5.3) and eq. (5.4) into eq. (5.5) yields

$$E_w = \frac{p.H}{\delta} \qquad \text{.....5.6}$$

Now, recalling eq. (5.2), the modulus of the sub-grade reaction k is, by definition

$$\frac{p}{\delta} = k$$

and by substituting eq. (5.2) into eq. (5.6), one obtains

$$E_w = k.H \qquad \text{.....5.7}$$

It is worth noting that the constant in eq. (5.7) is k, while the equivalent E_w is dependent on the spring length H.

The anisotropic stress-strain relationship adopted for the sub-grade material is

$$\begin{bmatrix} \sigma_x \\ \sigma_y \\ \sigma_z \\ \tau_{xy} \\ \tau_{xz} \\ \tau_{yz} \end{bmatrix} = \begin{bmatrix} 2G+v & v & v & 0 & 0 & 0 \\ v & 2G+v & v & 0 & 0 & 0 \\ v & v & 2G+v & 0 & 0 & 0 \\ 0 & 0 & 0 & G & 0 & 0 \\ 0 & 0 & 0 & 0 & G & 0 \\ 0 & 0 & 0 & 0 & 0 & G \end{bmatrix} \begin{bmatrix} \varepsilon_x \\ \varepsilon_y \\ \varepsilon_z \\ \gamma_{xy} \\ \gamma_{xz} \\ \gamma_{yz} \end{bmatrix} \qquad \text{.....5.8}$$

Where σ_x, σ_y, σ_z, τ_{xy}, τ_{xz}, τ_{yz} and ε_x, ε_y, ε_z, γ_{xy}, γ_{xz}, γ_{yz} are the direct and shear stresses and strains, respectively, while G and v are the shear and Lame's moduli. The latter can be defined as

$$v = \frac{\mu E}{(1+\mu)(1-2\mu\mu)} \qquad \text{.....5.8a}$$

By substituting eq. (5.7) into eq. (5.8) gives

$$\begin{bmatrix}\sigma_x\\ \sigma_y\\ \sigma_z\\ \tau_{xy}\\ \tau_{xz}\\ \tau_{yz}\end{bmatrix}=\begin{bmatrix}0&0&0&0&0&0\\0&0&0&0&0&0\\0&0&kH&0&0&0\\0&0&0&0&0&0\\0&0&0&0&0&0\\0&0&0&0&0&0\end{bmatrix}\begin{bmatrix}\varepsilon_x\\ \varepsilon_y\\ \varepsilon_z\\ \gamma_{xy}\\ \gamma_{xz}\\ \gamma_{yz}\end{bmatrix} \qquad \text{.....5.9}$$

Eqs. (5.8) and (5.9) can be used to obtain a transition formula between a Winkler sub-grade with a modulus of sub-grade reaction k and an elastic half-space sub-grade with a modulus of elasticity E_s and Poinsson`s ratio μ_s. By equating the stiffness in the z-direction in both, one obtains

$$k.H = E_s \frac{(1-\mu_s)}{(1-2\mu_s)(1+\mu_s)} \qquad \text{.....5.10}$$

Eq. (5.10) reduces to eq. (5.7) when μ_s =0. It is also interesting to note that k tends to ∞ when μ_s =0.5, which is the case with a liquid sub-grade.

The base of the proposed spring is fixed at all directions, i.e. an infinitely rough and rigid base below the sub-grade is assumed. Furthermore, common nodes are used at the interface between the top of the spring and the bottom of the slab as the effect of vertical lift off and horizontal slip is considered insignificant and beyond the scope of the present FEA.

5.3.2.3 Parameters Considered for the FEA

As explained earlier, the main objective of the present finite element analysis was to determine whether or not the presence of the underlying soil affects the punching shear capacity of the concrete slab. In this respect, the parameters considered in the present FEA were:

- Modulus of elasticity of concrete (E_c)
- Modulus of sub-grade reaction (k)

- Thickness of the sub-grade

a) Modulus of Elasticity of Concrete

A typical range of the values of E_c (Neville and Brook, 1994, BS8110: Part2:1985) is presented in Table 5.5 which also shows the values adopted for the present sensitivity analysis for concrete after 28 days casting. However, in order to study the effect of the underlying soil prior to 28 days, different moduli of elasticity of concrete were used. Five values for the modulus of elasticity 6.3, 11.97, 16.92, 25 and 36 GPa were used in the analysis.

Table 5.5: Typical range of values of 28-days static modulus of elasticity for normal weight concrete, according to BS8110: Part2:1985

Grade (28 days cube compressive strength in MN/m^2)	C30	C40	C50	C60
E_c (GN/m^2) typical values	20-32	22-34	24-36	26-38
E_c (GN/m^2) mean values	26	28	30	32
E_c (GN/m^2) values adopted for present analysis	32	34	36	38

b) Modulus of Sub-Grade Reaction

Different values for the modulus of sub-grade reaction were used in the present study. The work of the previous investigators points to the fact that the tensile stresses induced in the slab by point loads are not greatly affected by small variations in the value of k (Westergaard, 1925; Kelley, 1939b; Chandler and Neal, 1988 and Beckett, 1999). This does not imply that the values of the stresses remain the same for any value of k, but it does suggest that the whole range of soils used in practice can be represented by a handful of values of k rather than continuous values. Consequently, an adequate estimate of k may be obtained by means of a typical value for each type of soil, rather than varied and unnecessary detailed values for the same type of soil.

Typical values of k are defined in BS 5930 (1999) and in the British Cement Association Interim Technical note 11 (Chandler and Neal, 1988), where typical soils were divided into for sub-grade groups, namely: “enhanced”, “good”, “poor”, and “very poor”. Based on this

classification, the following values of k were adopted for the present study in order to represent the whole range of sub-grades:

- 14 MN/m^3, which represents a very poor sub-grade.
- 27 MN/m^3, which represents a poor sub-grade.
- 54 MN/m^3, which represents a good sub-grade.
- 82 MN/m^3, which gives allowance for an enhanced sub-grade.

c) Thickness of the Subgrade

Since the subgrade is modelled as a group of springs (Winkler model), the solution is independent of the thickness of the subgrade i.e. the length of the spring. The only parameter that needs to be defined is the spring constant k. As explained earlier, a given value of k is denoted by adjusting the value of an equivalent modulus of elasticity E_w according to the value of the thickness of the subgrade chosen initially. Therefore, it is clear that the present FEA is independent of the value of the thickness of the subgrade. However, for the purpose of carrying out the analysis, a value of 0.15 m was adopted for the thickness of the subgrade.

5.3.2.4 Discussion of the Results

A series of finite element runs were performed to investigate the effect of E_c on the values of ultimate load capacity of the concrete slabs. For these runs slabs of thicknesses 200 mm and span of 1600 mm were adopted, which represent a flat slab with span length = 4 m. These results were arrived at from the FEA, as discussed and presented in section 5.3 and Table 5.3. Furthermore, the values for the modulus of subgrade reaction of 10 MN/m^3 and 27 MN/m^3 were used. This represents a soil with very poor and poor conditions, respectively. The rationale behind the selection of these two types of soil is that the soil, in the case of ground-suspended floor slabs, is not expected to be in a good condition.

However, a case which represents no soil effect has been studied for comparison purposes. The effect of modulus of elasticity and modulus of sub-grade k on the ultimate load is

presented in Table 5.6 and Figures 5.7 and 5.8. The results showed that the values of ultimate load remain almost the same regardless of the modulus-of-elasticity of the concrete. It was also found that the modulus of the subgarde reaction slightly affected the values of the ultimate load with a maximum increase of 3% and 9% due to the presence of subgrade with a modulus of subgrade reaction of 10 MN/m^3 and 27 MN/m^{3,} respectively.

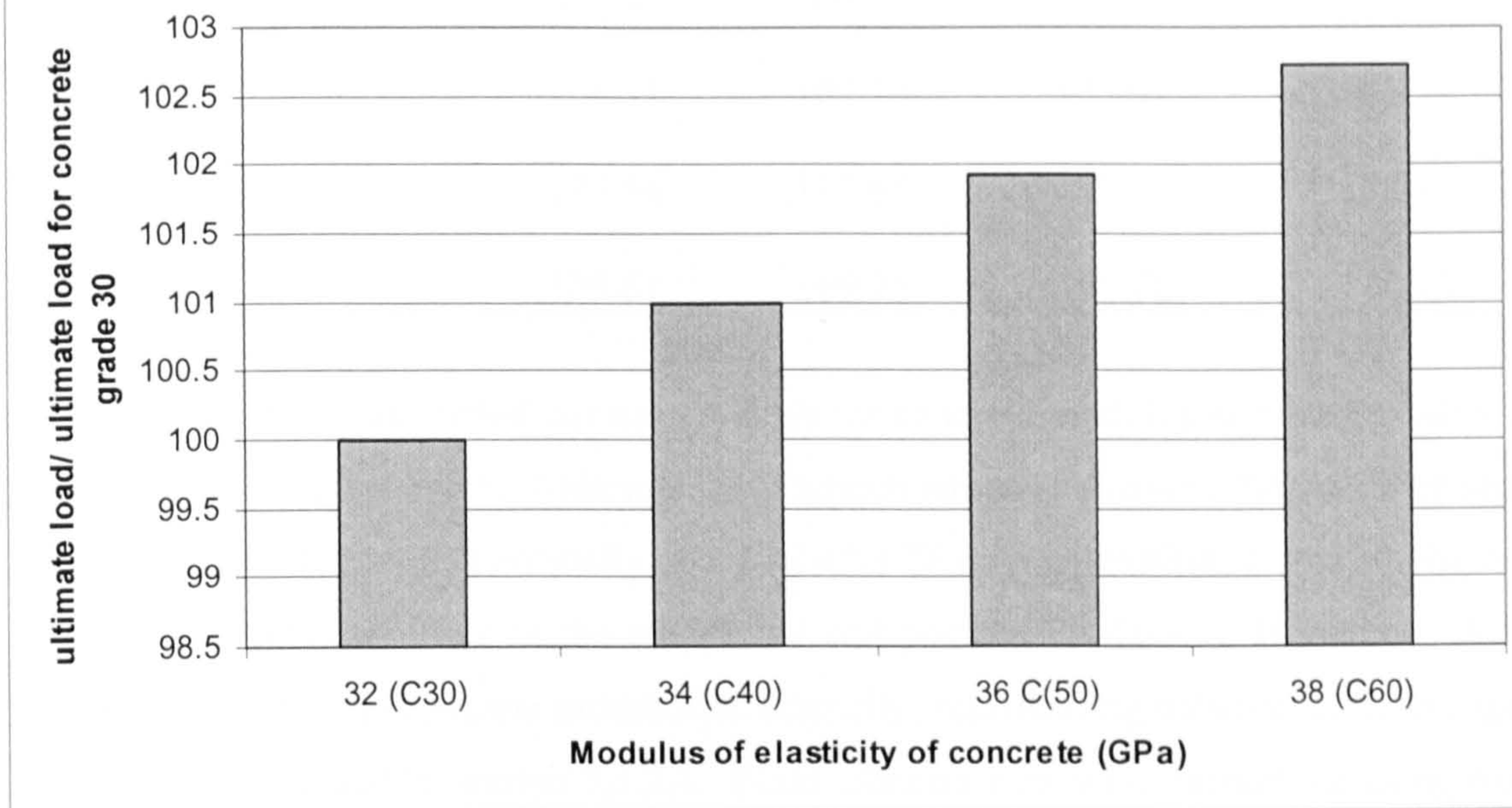

Figure 5.7: Effect of modulus of elasticity of concrete on the values of ultimate load

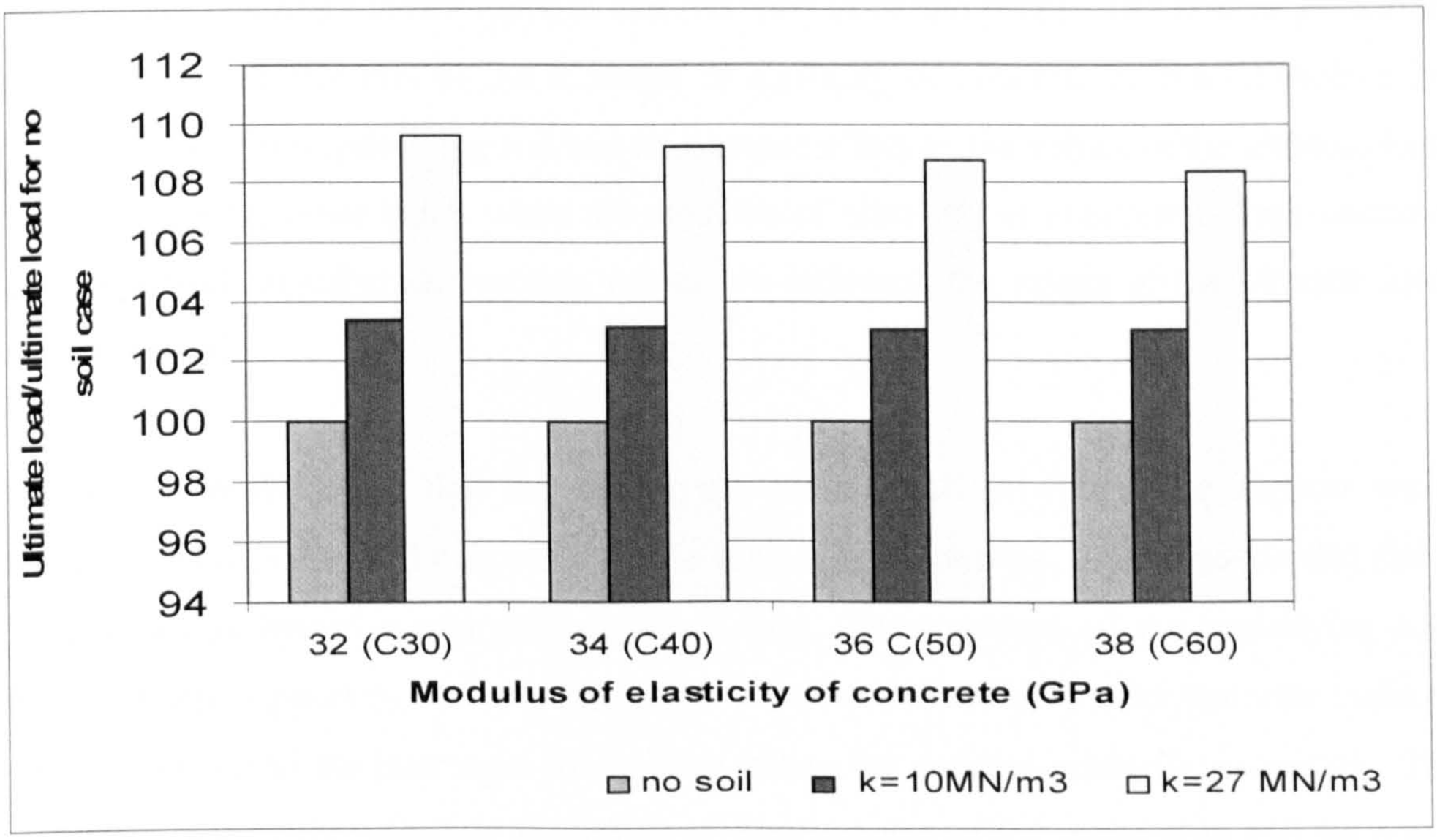

Figure 5.8: Effect of modulus of elasticity on the values of ultimate load at different values of k.

Table 5.6: Effect of modulus of elasticity on the values of ultimate load.

E (GN/m^2)	32 (C30)	34 (C40)	36 (C50)	38 (C60)
K (MN/m^3)				
No soil	160.15	161.73	163.25	164.53
10 MN/m^3	165.5	166.77	168.27	169.61
% no soil	103.34	103.12	103.07	103.09
27 MN/m^3	175.54	176.65	177.55	178.39
% no soil	109.61	109.22	108.76	108.42

The above analysis was carried out using values for concrete modulus of elasticity after 28 days of casting, see Table 5.5. Although this research aimed at studying the punching shear failure of SFRC slabs which normally occurred after 28 days of casting, it also emphasised upon investigating the effect of the underlying soil prior to 28 days. In order to do so different values for the concrete modulus of elasticity, representing different concrete ages, were used as presented in section 5.3.2.3. Finite element runs were carried out using these values for the modulus-of-elasticity with the two values for the modulus of subgrade reaction, representing the two types of soil (i.e. very poor and poor). The results, presented in Table 5.7, indicate that as the modulus of elasticity of concrete decreased (before 28 days) the role of the underlying soil had an increase effect on the values of the ultimate load capacity. On the other hand, when the modulus of elasticity of concrete is kept constant and the moduli of subgrade reaction values are increased the values of the ultimate load were increased.

The above results show that the underlying ground will provide some support were expected. This is due to the fact that, in the early age of concrete, ground-suspended slabs initially act as hybrid supported/suspended slabs. The presence of the underlying soil provides more support in the early age of the concrete (immediately after concrete casting) when compared to the later ages of concrete where the support gradually decreases. 28-days after casting the concrete, the effect of the presence of the underlying soil becomes

minimal, as was discussed in the above paragraph, with a maximum 9 % increase in the ultimate load due to the presence of soil with a 27 MN/m^3 modulus of subgrade reaction.

Table 5.7: Effect of modulus of elasticity on the values of ultimate load.

E (GN/m^2)	36	25	16.92	11.97	6.3
K (MN/m^3)					
No soil	163.25	153.42	143.44	134.1	116.87
10 MN/m^3	168.27	159.74	151.36		131.97
% no soil	103.07	104.12	105.52		112.92
27	177.55	171.18	165.88	161.95	161.18
% no soil	108.76	111.58	115.64	120.77	137.91

5.4 Conclusions

An experimental study is a very important means of investigating the behaviour of a concrete slab under shear loading. In the experimental study, one of the most important things is to determine the type and size of the specimens to be adopted in order to model the slabs properly. The choice of the type and size of the test specimens is dominated by many factors, such as the working space available in the laboratory, the requirements for the experimental set up, and the requirements for the capacity of the loading equipment etc.

In the present investigation, based on the considerations of many aspects, the specimens similar to the commonly used isolated slab-column model are adopted.

From the preliminary FEA, the locations of the contra-flexure lines with respect to different sizes of columns, span lengths of the panels, thicknesses of the slab and concrete modulus-of-elasticity are obtained. Also, the effect of the underlying soil was studied.

The information stemming from this preliminary analysis forms the basis on which the test specimens are designed.

One of the aims of this research was to experimentally investigate the effect of the underlying soil on the ultimate load capacity of the concrete slabs. However, this FEA demonstrated that the presence of soil with modulus of subgrade reactions of 10 and 27 MN/m^3 have minimal effect on the ultimate load capacity of the slab after 28 days casting. The presence of soil affects the ultimate capacity of the slab more at the early age of casting (before 28 days). Moreover, the physical restraints on experimentally investigating the effect of underlying soil on the ultimate load capacity of concrete slabs, which, include time and cost restraints in addition to the difficulties in obtaining the required modulus of sub-grade reaction, made it difficult to carry out this investigation. Hence, the present research will not take into account the presence of the underlying soil, when designing the set-up of the specimens used in the experimental study.

CHAPTER SIX

EXPERIMENTAL PROGRAMME

6.1 Introduction

As it has been pointed out in Chapter Two, the literature review shows that there is no current sound theory that could be used to predict the punching shear behaviour of fibre reinforced concrete slabs. Moreover, it reveals that the current design practices are mainly based on experimental studies of conventional slab-column connections where very little research has considered the effect of the fibres.

There are many parameters that can affect the punching shear strengths in SFRC slabs, including concrete strength, size effect (span-depth ratio), size of loading area, shape and type of the loading area, in-plane restraint, steel fibre type, dosage and aspect ratio (length-to-diameter ratio). Since there is a dearth of systematic experimental studies on punching shear behaviour of SFRC slabs with no longitudinal reinforcement, it is important to study the effect of all these factors on punching shear strength in SFRC. However, due to time constraints, funding and laboratory limitations, it becomes impractical to cover all these parameters in this research. Accordingly it was decided to investigate the effect of key parameters on the punching shear behaviour in SFRC slabs. These parameters include concrete strength, fibre dosage, and fibre aspect ratio.

In this chapter, details of the materials used to manufacture the test specimens including the concrete and the steel fibres are presented. The loading and supporting methods together with testing procedure are illustrated and described. It is also the intention of this chapter to analyse and discuss the overall performance of each of the factors considered in the experimental programme on the punching shear strength of the SFRC slabs.

6.2 Scale and Summary of Test Specimens

The prototype on which the test specimens were based is a typical internal panel of a multi-panel flat slab. The scale effect is one of the problems concerning the model test of

concrete structures. Whenever the model test is involved, the first thing to do is to justify its validity in serving the purposes of the test and to make sure that no size effects exist on the results of the test. If there is any size effect, it must be allowed for in the interpretation of the test results.

Some model studies of bridge structures (Clarke et al., 1985) show that scale effects are not significant provided all the constituent materials are scaled properly. This fact has been confirmed by tests on both 1/4 and 1/6 scale models used to investigate the punching shear failure at internal columns. Hawkins et al. (1974) also pointed out from the comparative tests of models and prototypes that there is no effect of size on the shear strength with the use of approximately scaled concrete mixes.

In the present experimental study, one third scale models were considered appropriate for reasons of economy and laboratory constraints. Based on the above argument by (Clarke et al., 1985 and Hawkins et al., 1974) this scale is felt to be able to reasonably model the behaviour of SFRC slabs in the region of the hogging bending moment around an internal slab column connection and is large enough that it will not involve any problem of size effects. Moreover, this has also been supported by other research including Narayanan and Darwish (1987), Xiang (1993) and Killu (2002) who tested at the same scale and obtained meaningful results.

Eight circular SFRC slabs were tested. The slabs were identical in size and shape. The slab dimensions were obtained by scaling down from those slabs of the prototype designed and presented in Chapter Five, using the scale factor of 1/3. The diameter of the slabs was 600mm and the diameter of the circle along which the load was uniformly distributed was 550mm. The total depth of the slab was 75mm. A specimen of this size represents, with good approximation, the region of negative bending around an interior supporting column of a one-third-scale model flat-plate floor slab. Assuming the points of contraflexure to be about 0.206 times the span from the zero bending moment position to the centre of the column at the column line (as presented in Table 5.3), the span of the floor represented by these specimens would be about 4.0m. A thickness of 225 mm would probably be the minimum required for such a span.

The fibre percentage, fibre aspect ratio and the concrete compressive strength were the main variables that were changed to evaluate their influence on the behaviour of the SFRC composites analysed. Figure 6.1 illustrates the plan view of the slab specimens, which can be further seen in more details in Table 6.1.

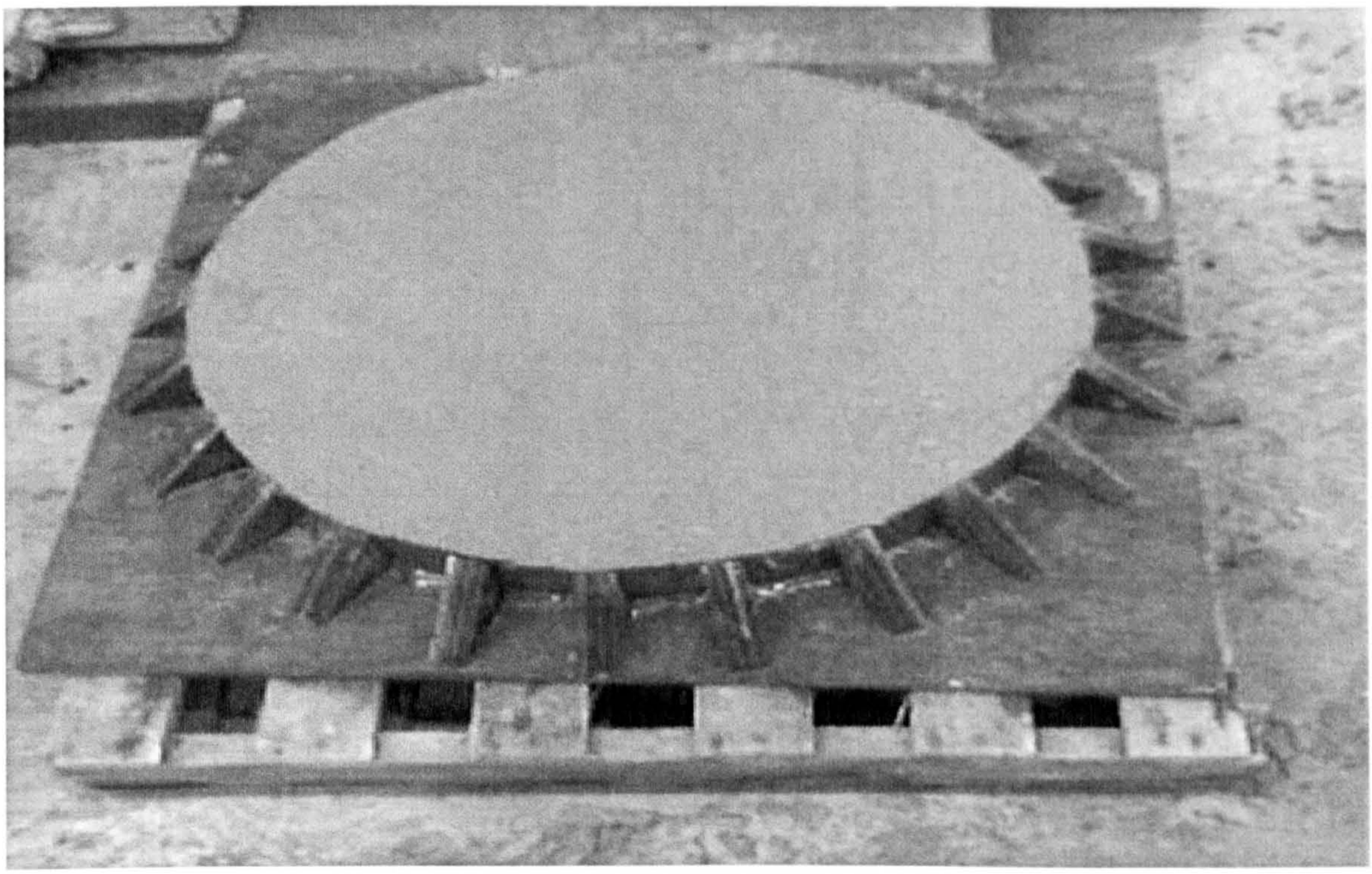

Figure 6.1: Plan view of test specimen

Table 6.1: Details of slab specimens

Specimen no.	Fibre type	Fibre dosage kg/m^3	Fibre aspect-ratio (length/diameter)	Characteristic compressive strength MPa
S1	-	-	-	30
S2	ZP30/.50	20	60	30
S3	ZP30/.50	40	60	30
S4	RC65/60BN	20	67	30
S5	RC65/60BN	40	67	30
S6	-	-	-	40
S7	ZP30/.50	40	60	40

S8	RC65/60BN	40	67	40

6.3 Materials and Fabrication of Test Specimens

This section presents the details of the materials used to manufacture the test specimens used in this study. The methods adopted for the materials and the specimen's preparation and fabrication are also described.

6.3.1 Concrete Mix Design

Several procedures are available for proportioning SFRC mixes, with emphasis on good workability (Killeen and Dalgleish, 1997; Schrader, 1989; ACI Committee 544, 1986; Schrader and Munch, 1976 and Edgington et al., 1974). However, in many projects, steel fibres in particular have been added without any changes to the conventional mixture proportions although, where large percentages of fibre volume are used, some adjustments are advisable (ACI Committee 544, 1986 and Swamy, 1974). To provide better workability, SFRC demands more paste and in essence a greater proportion of fine materials than plain concrete. Normal concrete contains between 25-35 % of paste of the total volume of concrete, whereas, for SFRC this becomes 35-45 %, depending on the fibre geometry and fibre volume (ACI Committee 544, 1993 and Swamy, 1974).

As with any other type of concrete, the mix proportions of SFRC depend upon the requirements of each project, in terms of strength and workability. The ACI Committee 544 (1993) advises that the usual amount of steel fibres ranges from 0.25% to 2% by volume.

Trial mixes were performed to obtain the right concrete mix with the desired strength and the appropriate workability for use during this investigation. This included performing slump tests (according to BS EN 12350-2: 200) as well as cube compressive strength tests.

The concrete mix was designed to produce a concrete that would give characteristic compressive cube strength of 30 N/mm^2 and 40 N/mm^2 at 28 days and a medium

workability, in terms of the slump, of 70 to 120 mm. According to fibre manufactures, these are expected and acceptable values for fibre reinforced concrete. Water reducing admixture (super-plasticizers) was used to improve the workability of SFRC mixes.

Based on the results obtained from the trial mixes, two different mix proportions were selected to be used in the casting to give two different characteristic compressive cube strengths as shown in Table 6.2. The materials used in the mix are described below.

Table 6.2: Mixture proportions

Component and characteristics	Series 1					Series 2		
Specimen no.	S1	S2	S3	S4	S5	S6	S7	S8
Ordinary Portland cement (kg/m3)	345						345	
Fine aggregate (kg/m3)	685						685	
Course aggregate (kg/m3)	1,165						1,165	
Water (kg)	14						12.42	
Super-plasticizer (g)	62.1						208	
Dramix steel fibres ZP30/50	0	20	40	---	---	---	40	---
Dramix steel fibres RC65/60BN	---	---	---	20	40	---	---	40
Characteristics								
W/C	0.45					0.4		
Additive in weight of cement %	0.2					0.7		
Fibre content in volume %	0	0.25	0.5	0.25	0.5	0	0.5	0.5
Fibre content in weight %	0	0.83	1.66	0.83	1.6	0	1.66	1.66

a) Cement

Ordinary Portland cement supplied by Travis Perkins was used throughout the test programme. All the cement was from a single batch acquired at the beginning of the project.

b) Coarse Aggregate

The coarse aggregate used had a nominal maximum size of 10 mm down to 5 mm, chosen so as to model 20 mm aggregate in a real structure. The reason for selecting such a relatively small-size aggregate was to improve the efficiency of fibre reinforcement and distribution, as well as to improve the workability of the mix. The coarse aggregate was crushed limestone and was supplied by Travis Perkins. This was used throughout the test programme.

c) Fine Aggregate

The fine aggregate used had a nominal maximum size of 5mm down to 0 mm. This was supplied from Travis Perkins and was used throughout the test programme.

d) Plasticizing Admixtures

The plasticity of the mix is important to ensure the proper dispersion of fibres. The cohesive properties of the matrix can be improved by the incorporation of liquid admixtures, which also reduce the inter-particle friction between the steel fibres and between the steel fibres and aggregates (ACI Committee 544, 1986; and Swamy and Stavrides, 1979).

A commercially available concrete superplasticising admixture supplied by RMC under the brand name CSP313 was used. It complies with the European standard EN934-2.

CSP313 is an admixture based upon high molecular weight polycarboxylate type materials, and is free from chloride and low alkali (RMC Admixtures, 2007). The admixture was added to the concrete mixes containing fibres in order to increase the workability of the mixes and to reduce the water cement ratio w/c of the mixes to achieve adequate strength and durability in the hardened state.

e) Steel Fibre

Hooked-end steel fibres of trademark Dramix ZP30/.50 and RC65/60BN were used (Bekaerts, 1998). Dramix steel fibres are widely used in pile-supported floor slabs. The ZP30/.50 fibres were 30 mm in length and 0.5mm in diameter and had a strength of about 1,250MPa, whereas, RC65/60BN fibres were 60 mm in length and 0.9 mm in diameter and had a strength of about 1,150 MPa. The hooked-end steel fibres were supplied bundled together into plaquettes using water-degradable glue to avoid balling of fibres when mixing, and to enhance uniformity in distribution. Fibres were introduced into the concrete mix at two different dosages 20 and 40 kg/m^3. This is the recommended dosage rate of steel fibres for concrete floor construction (Knapton, 2003 and Vassou, 2003).

6.3.2 Control Specimens

In order to determine the mechanical properties of the SFRC slabs, control specimens were made from the same batch of concrete from which the slab specimens were cast. Three 150 mm x 150 mm x 150 mm cubes and two 150 mm x150 mm x 600 mm beams were cast. The cubes and beams were cast and tested according to the guidelines of BS EN 12390-3: 2000 and RILEM TC 162-TDF (2003) respectively.

6.3.3 Casting Moulds

The moulds for the casting of the slab specimens were made of a square plywood baseboard and a deformable plastic strip of 600 mm diameter surrounded by triangular wooden supports.

The slabs were, as illustrated in Figure 6.2, cast in a wooden mould. For the convenience of making the moulds and casting the concrete, the column stubs were not cast with the slabs. The load was applied through a circular steel loading stub placed in the centre of the slabs

simulating the action of the columns. The cubes were cast in the standard steel moulds while the beams were cast in a wooden mould.

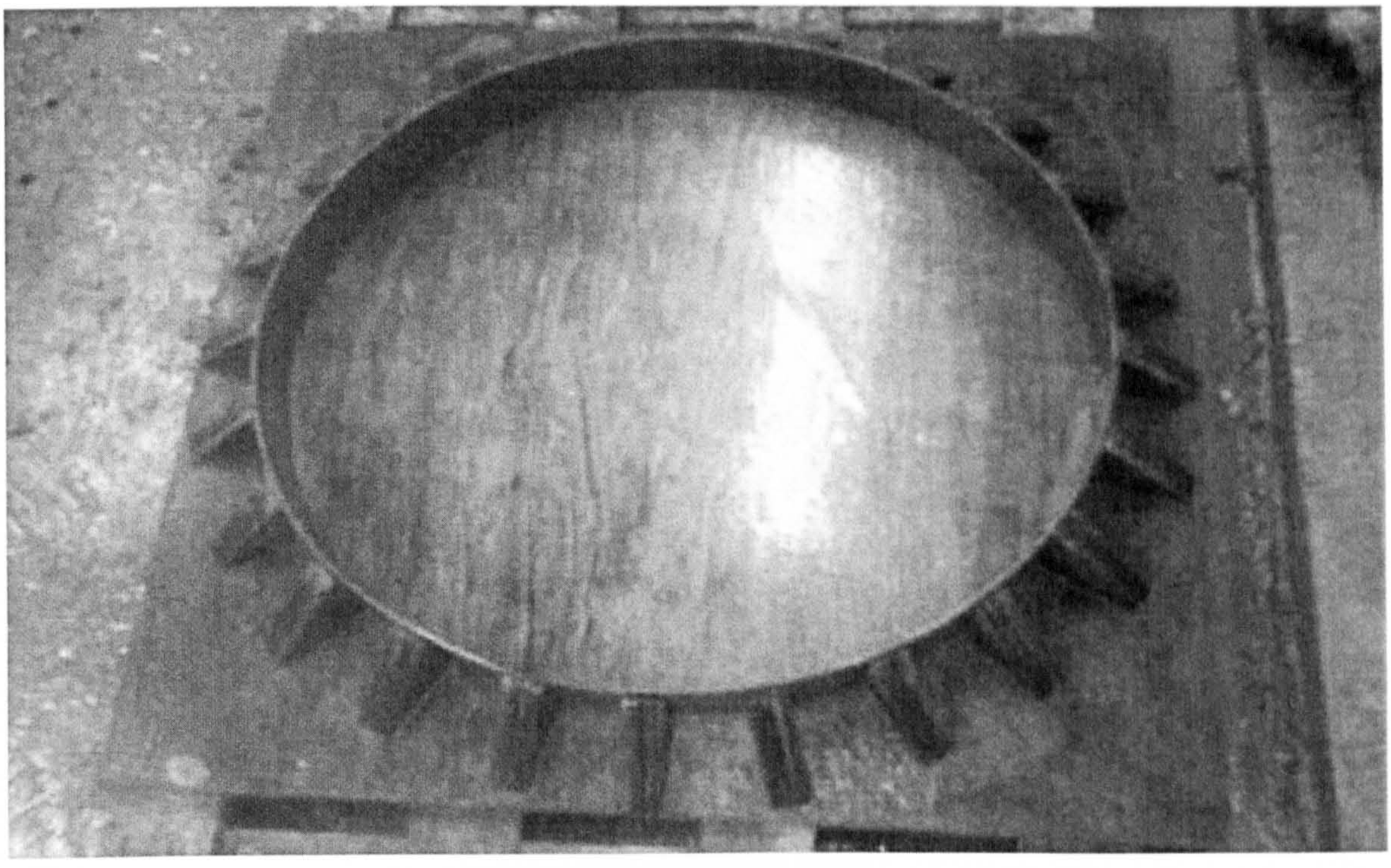

Figure 6.2: Cast mould for slab specimens

6.3.4 Mixing, Casting and Curing the Specimens

It is important that fibres are dispersed uniformly throughout the concrete mix in order to prevent balling. A variety of methods are available for introducing steel fibres into the concrete mixer, either to the dry constituents or to the wet mix (Cao & Chung, 2001; Knapton, 1999; Maidl, 1995 and Unwalla, 1982). These techniques range from charging the aggregate conveyor with fibres (Gregory et al., 1975 and Gray and Rice, 1972), sieving fibres directly into the mixer drum (Johanson and Nephew, 1975), sieving fibres and blowing them into the drum (McCurrich and Adams, 1973). The fibre used in this research was developed to be glued together with a water-soluble adhesive, into units similar to staples (Bekaerts NV Ltd, 1998), which enables it to be dispersed into the mixer as normal aggregate and subsequently they separate in the mixing process.

The constituent materials of the concrete mix for each slab were weighed in advance in the prescribed mix proportions and were put into a mixer. The dry materials (i.e. the OPC, the

steel fibres, the sand and the coarse aggregate) were turned over for about 2 minutes before the required quantity of super-plasticizer and water was gradually added. The concrete was then mixed for an additional two minutes and then transported to the casting bed.

The slab specimens were cast in the normal position as it would be in the real structure. Before casting, the plywood mould was cleaned and the mould oil was applied to facilitate the strip off of the side and the base plywood after casting.

Two identical slab specimens were cast for each input variable (i.e. concrete compressive strength, fibre type and dosage) the first one was used in testing while the other one was kept as a spare in case of any damage when testing the first slab.

The slump test was carried out immediately before the casting of the test slab and the control specimens. The test slab and the control specimens were cast at the same time from the same batch of concrete mix. Conventional tools, equipment and procedures may satisfactorily be used for placing and finishing SFRC (Killeen and Dalgleish, 1997, Unwalla, 1982 and Swamy, 1974). During the casting of the slab, concrete was compacted by steel rod. Finally, a tamping board was used to ensure that the top layer of concrete was properly compacted and the slab surface was trowelled to give a smooth finish. The control specimens (i.e. cubes and beams) were cast in the standard steel moulds and wooden moulds respectively.

All cubes, beams and slabs were cured covered with polythene sheets, to prevent the moisture from escaping, during the first day after the casting. The moulds of the cubes and beams and the formwork of the slabs were removed after 24 hours. The cubes and the beams were cured in water continuously until testing. The slabs were cured, covered with burlap sacks during the first five days and then finally, placed in the indoor climate of the laboratory. The curing temperature for all specimens was about 20°C, both in water and in air.

6.4 Testing of Control Specimens

6.4.1 Compressive Strength

The compressive strength of the concrete was measured on cubes. The strengths of the concrete cube were obtained at the time of testing the model. The average results of three cubes for each slab are presented in Table 6.3. The compressive tests followed the British standard BS EN12390-3:2002 which is given in British standard for concrete testing (2002). The cubes had the side length of 150 mm and were wet cured, as described earlier.

Table 6.3: Compressive strength of test specimen

Specimen no.	Cube compressive strength f_{cu} (MPa)	Cylinder compressive strength f_{cm} (MPa)
S1	32.12	25.70
S2	35.53	28.42
S3	40.7	32.60
S4	32.36	25.89
S5	38.63	30.90
S6	40.5	32.40
S7	51.63	41.30
S8	44.36	35.49

6.4.2 Tensile Strength

The tensile strength of concrete was determined by flexural test on SFRC beams (see Figure 6.3). Figures 6.4 to 6.11 show the load versus centre deflection plot of the beams. Flexural tensile strengths, of all beams, were measured at the time of the slab tests. The test followed the RILEM standard, which is given in RILEM TC 162-TDF (2003). The beams had height, width, and length of 150 mm, 150 mm and 600 mm, respectively. The beams were tested by three-point bending and the length between the supports at testing was 500

mm. Beams were wet cured as described in section 6.3.5. The tests were performed under displacement control conditions testing system using a deflection rate of 0.2 mm/sec.

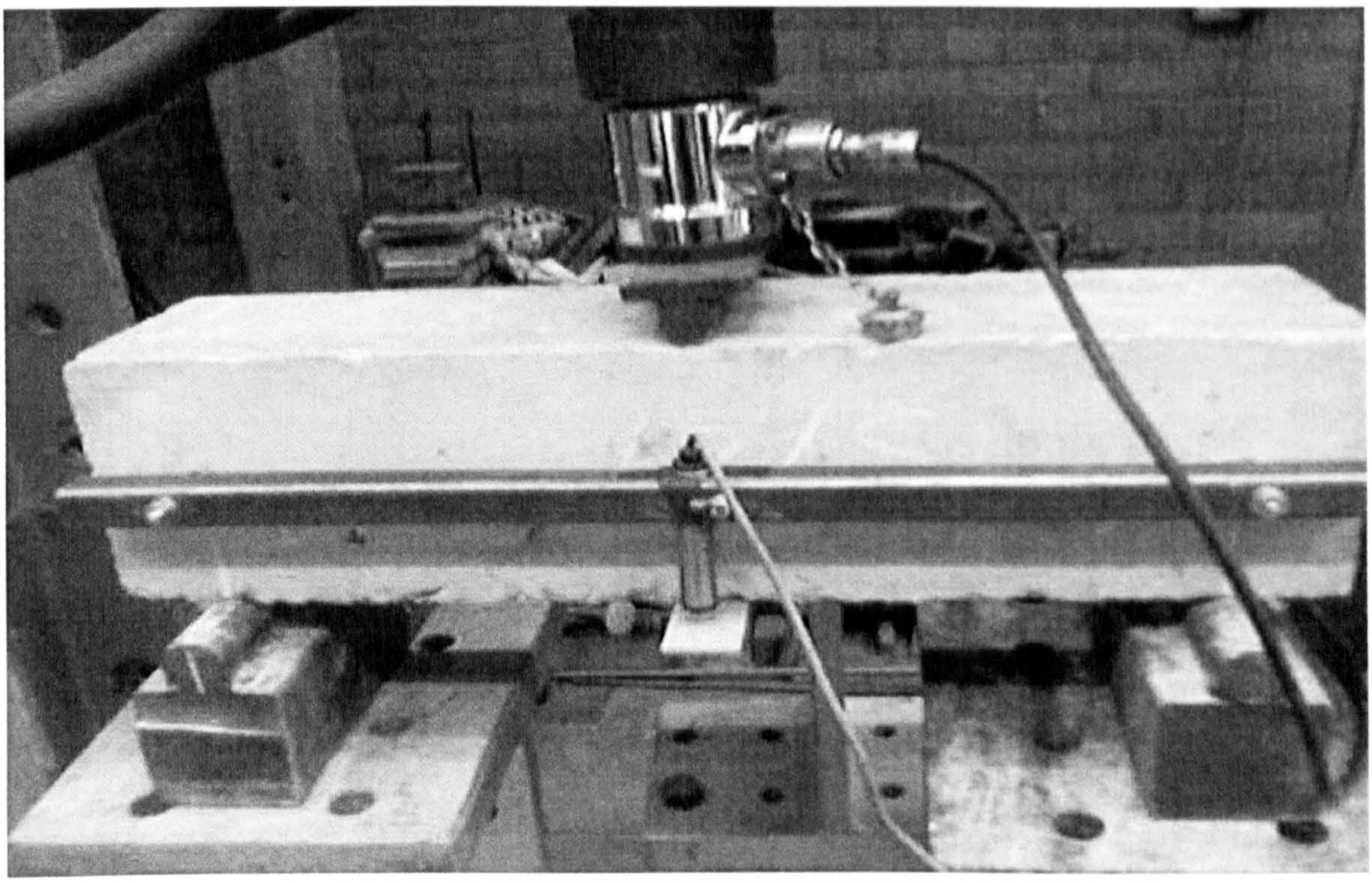

Figure 6.3: Beam under three-point bending test

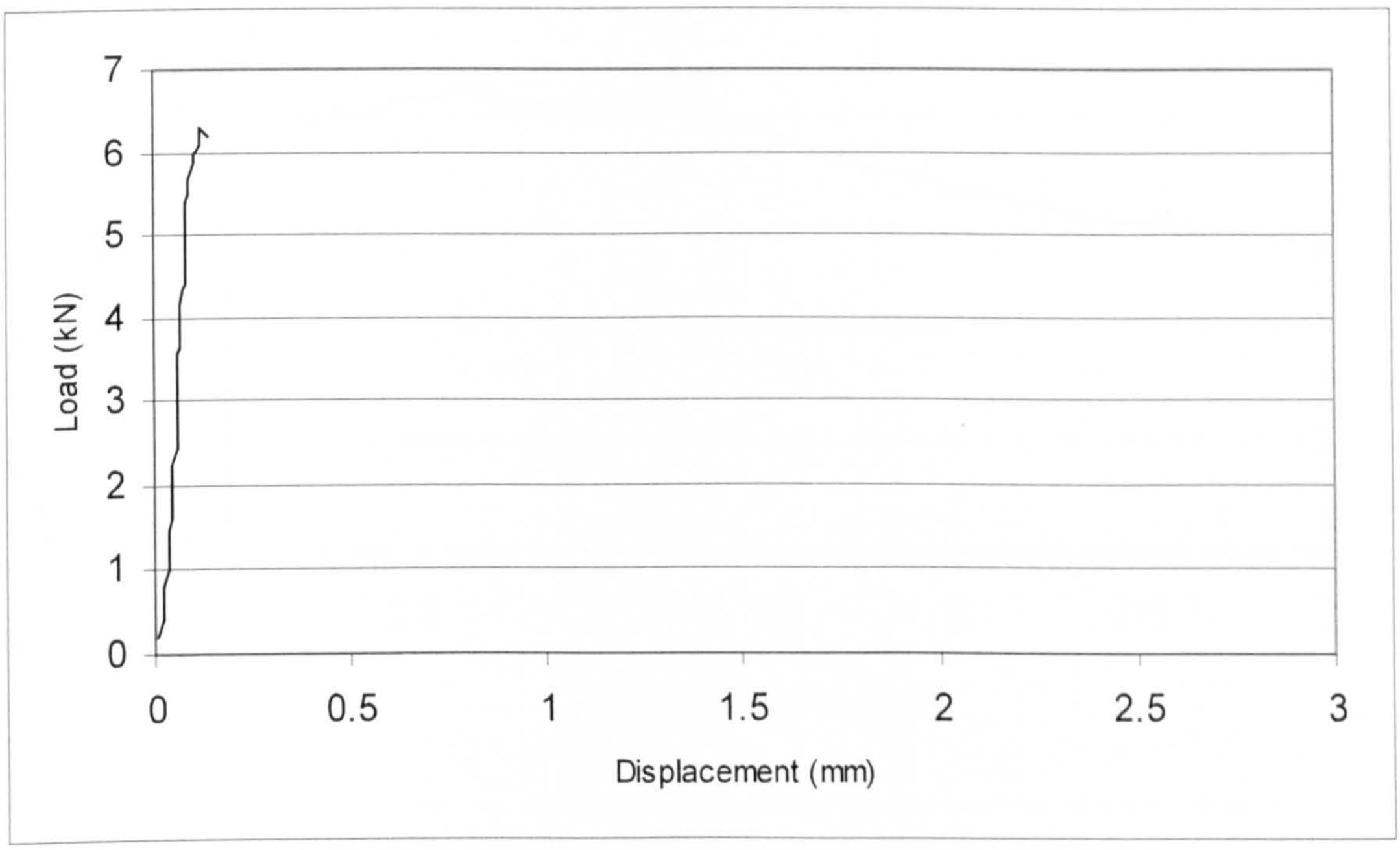

Figure 6.4a: Load-displacement curve of beam 1 - slab S1

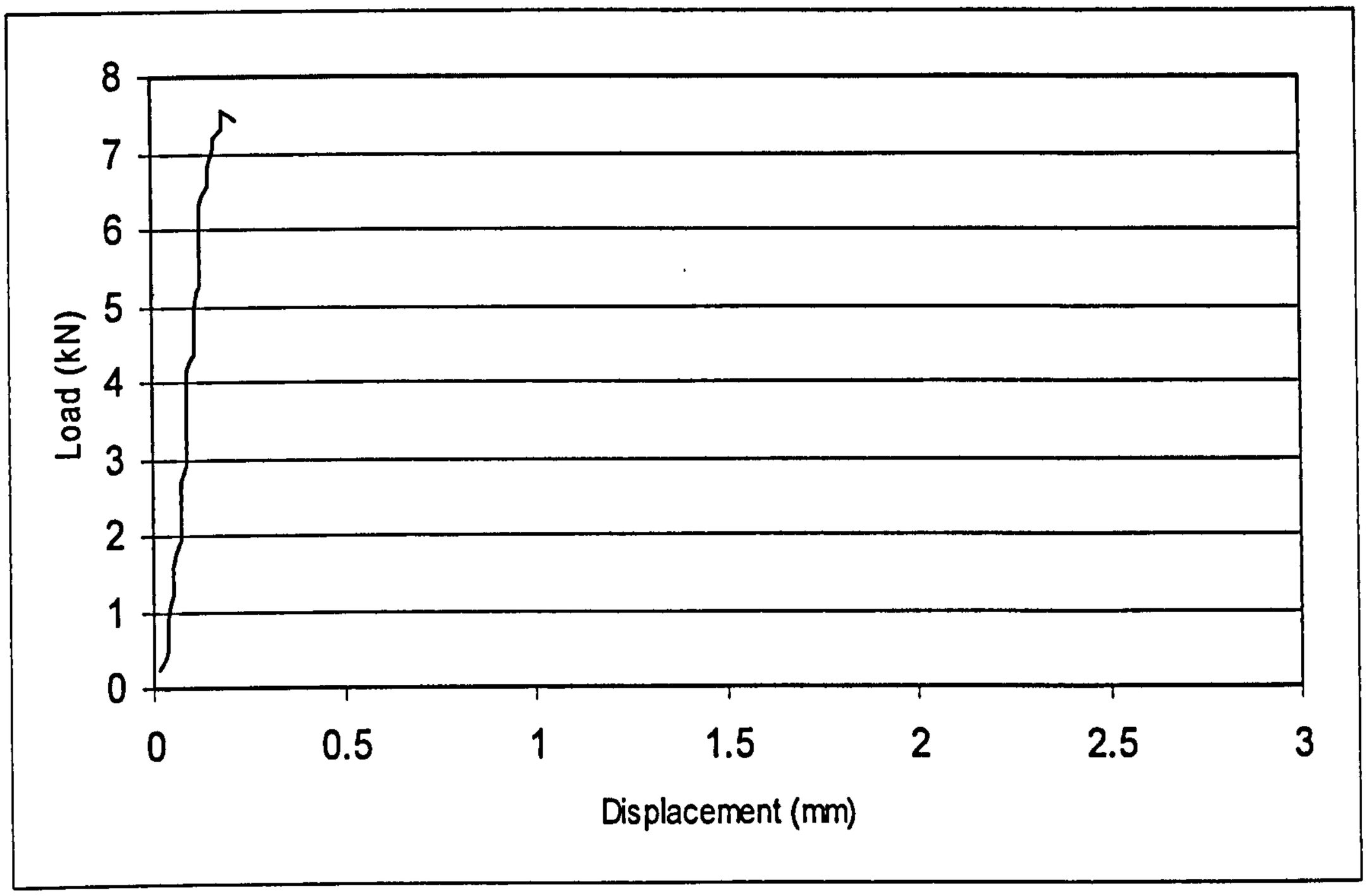

Figure 6.4b: Load-displacement curve of beam 2 - slab S1

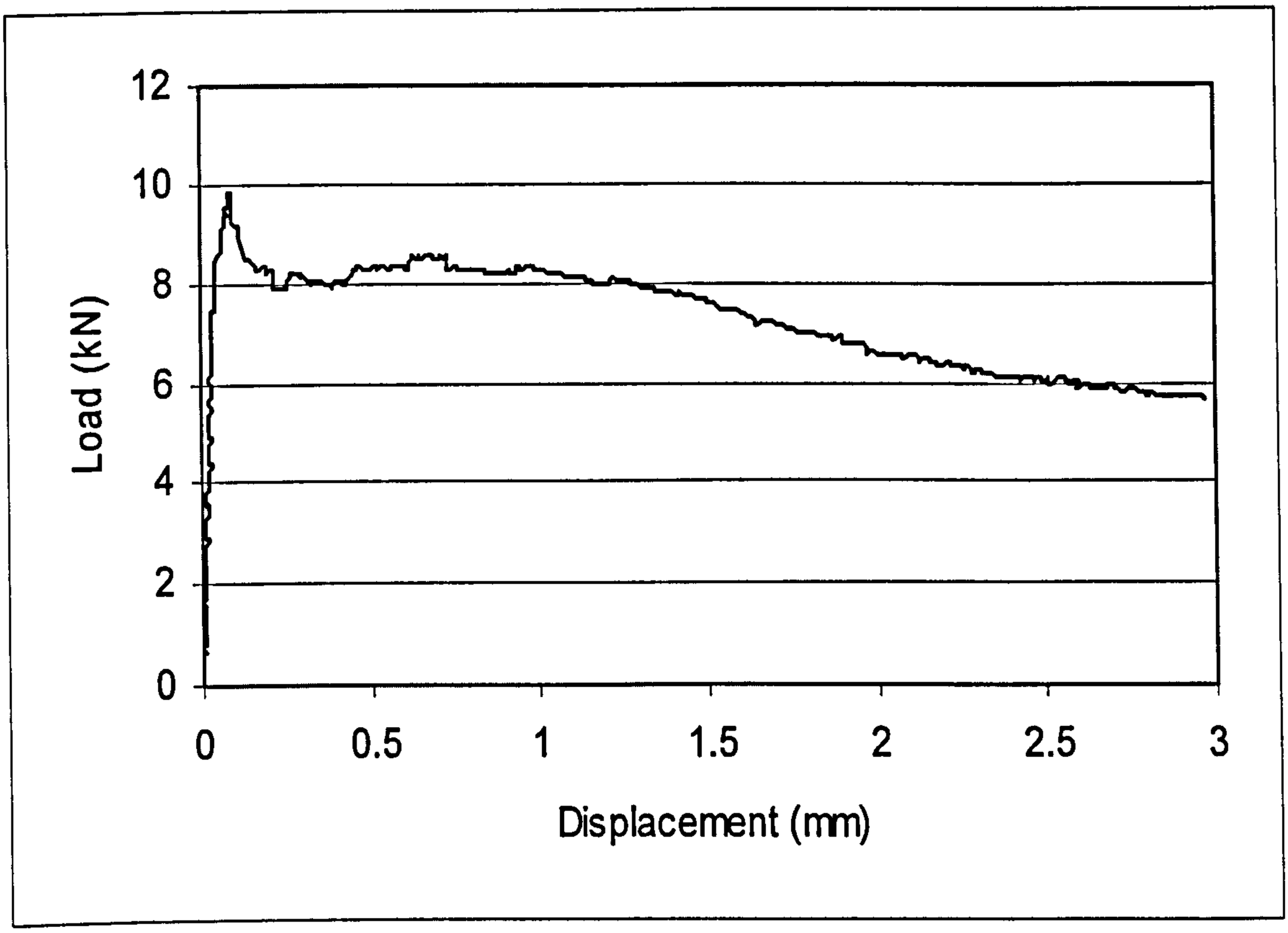

Figure 6.5a: Load-displacement curve of beam 1 - slab S2

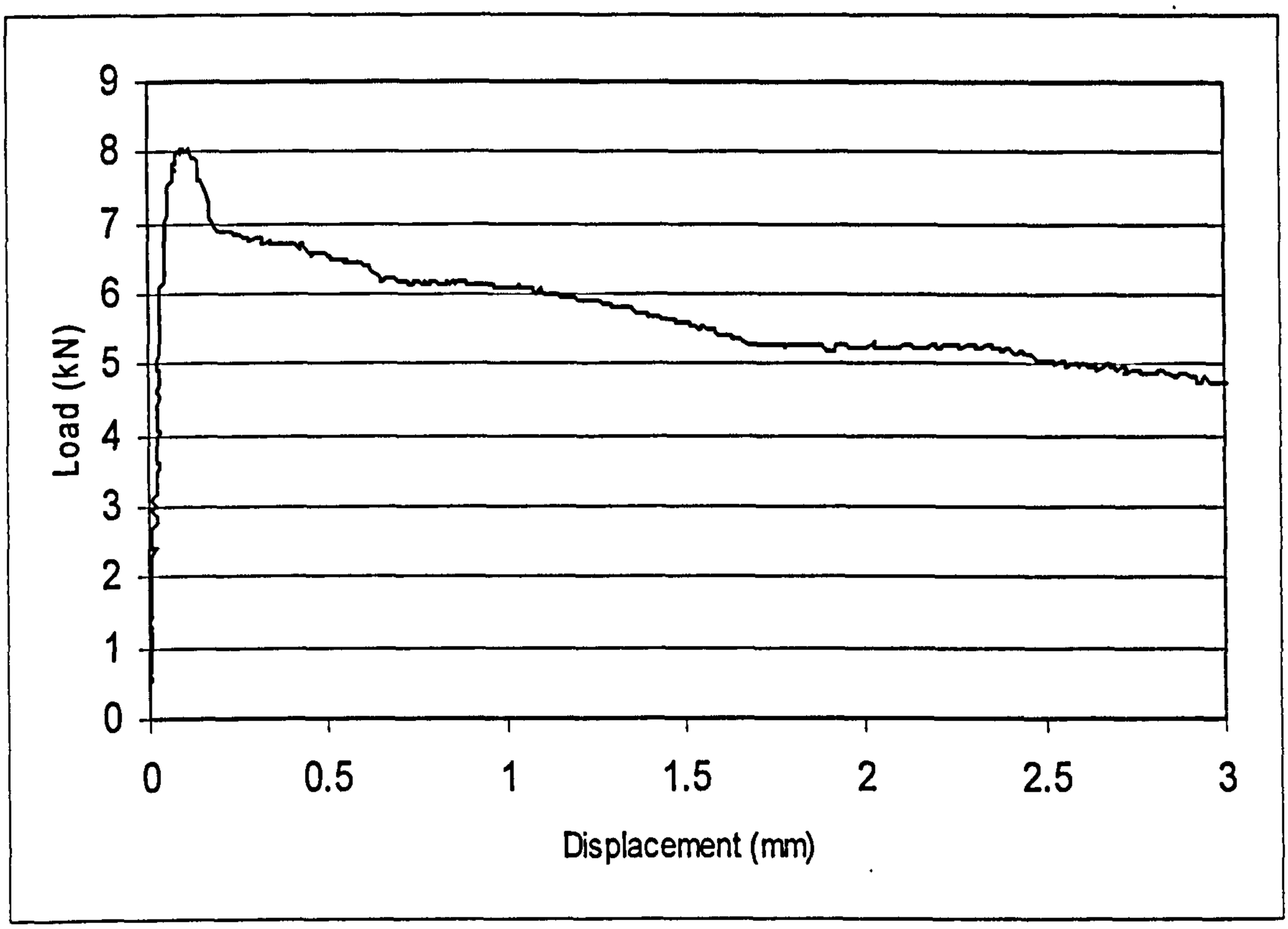

Figure 6.5b: Load-displacement curve of beam 2 - slab S2

Figure 6.6a: Load-displacement curve of beam 1 - slab S3

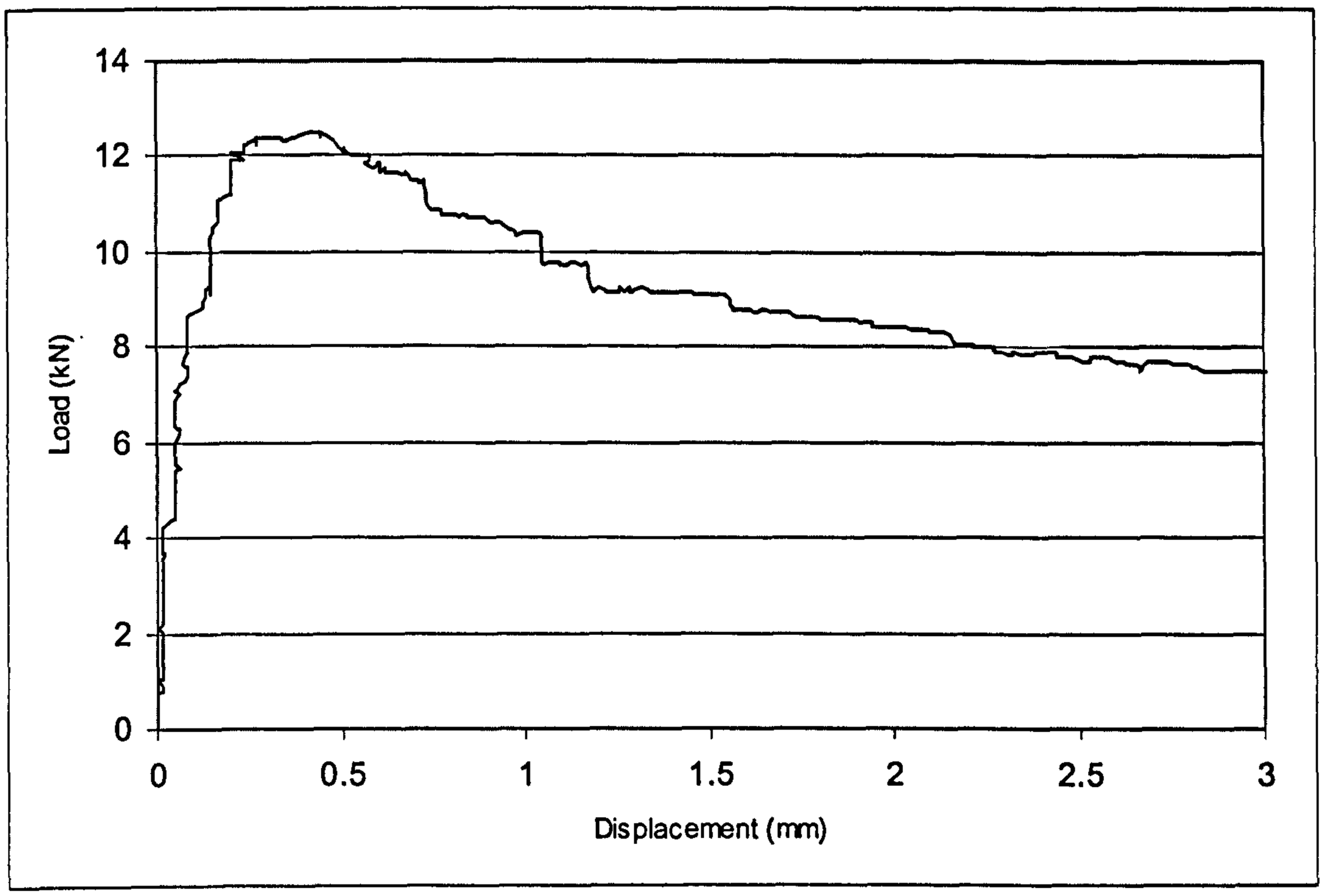

Figure 6.6b: Load-displacement curve of beam 2 - slab S3

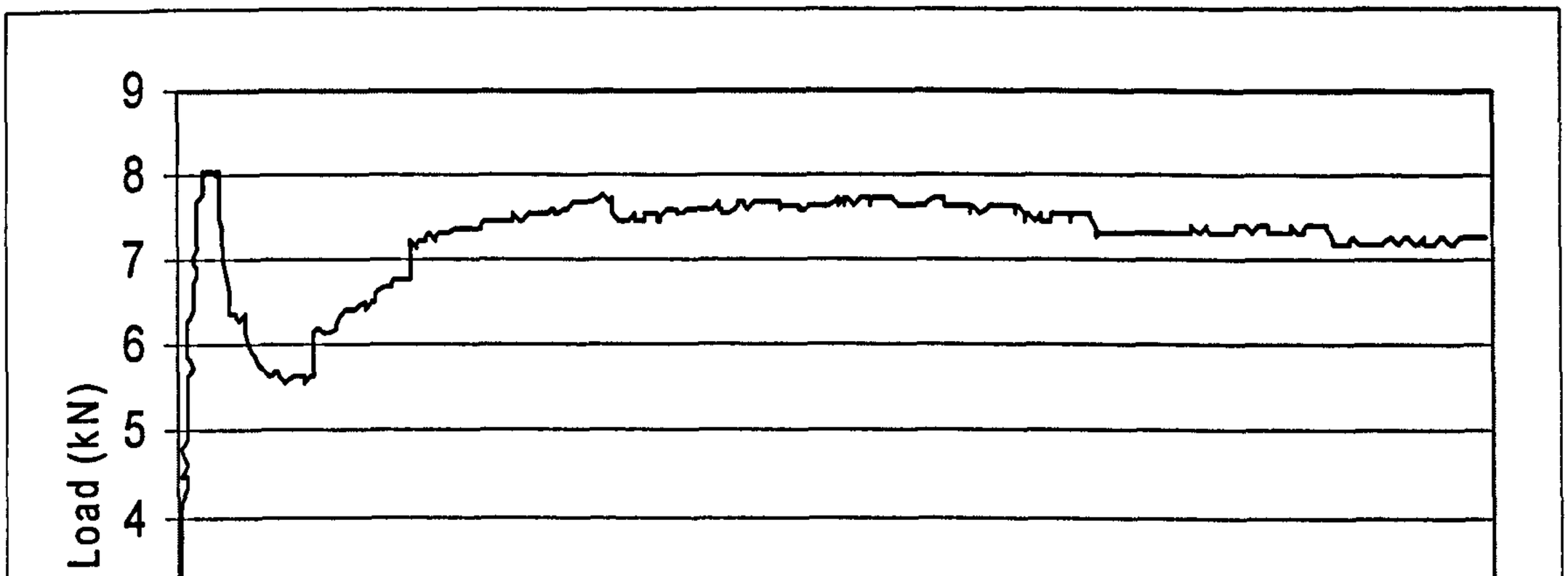

Figure 6.7a: Load-displacement curve of beam 1 - slab S4

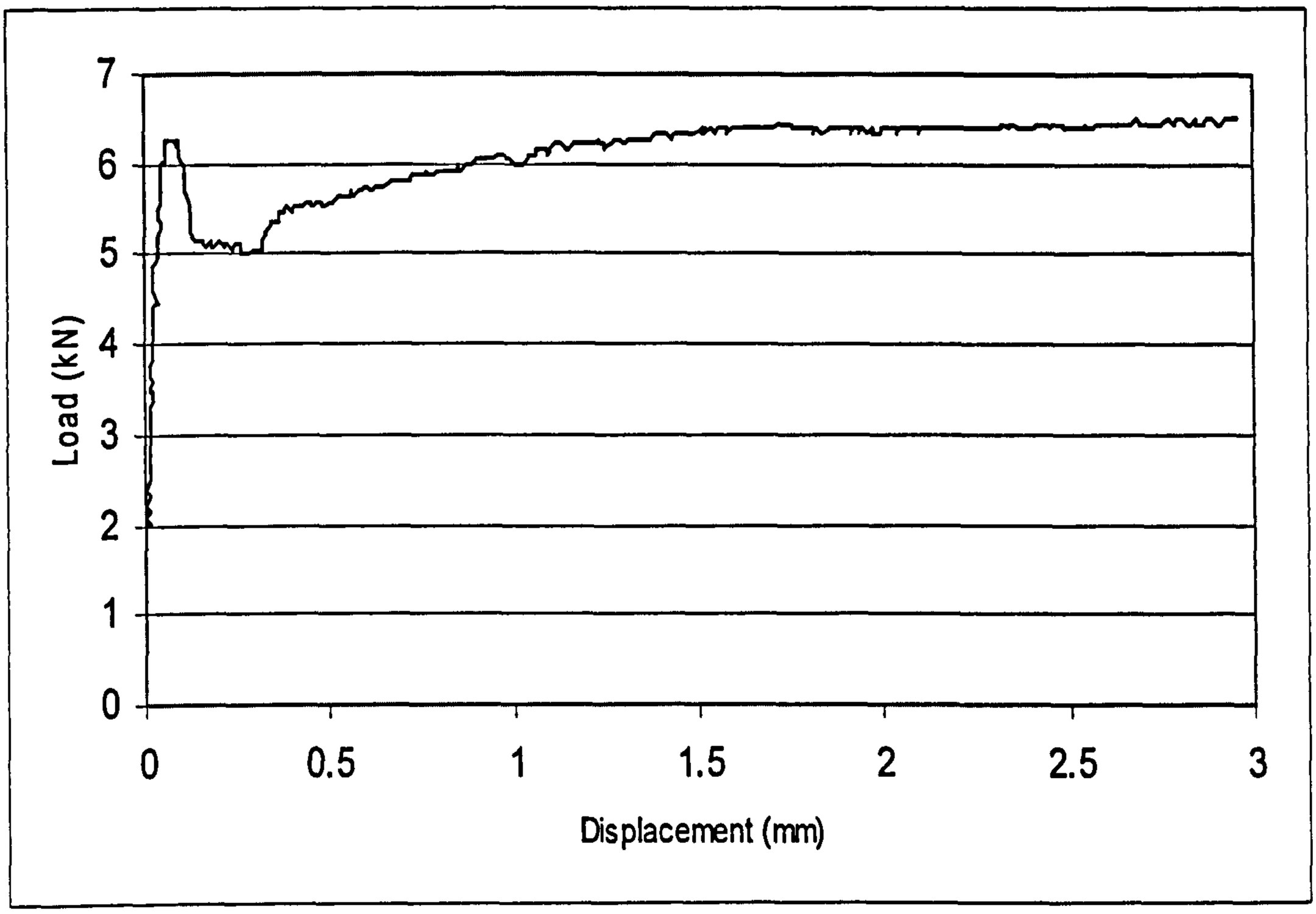

Figure 6.7b: Load-displacement curve of beam 2 - slab S4

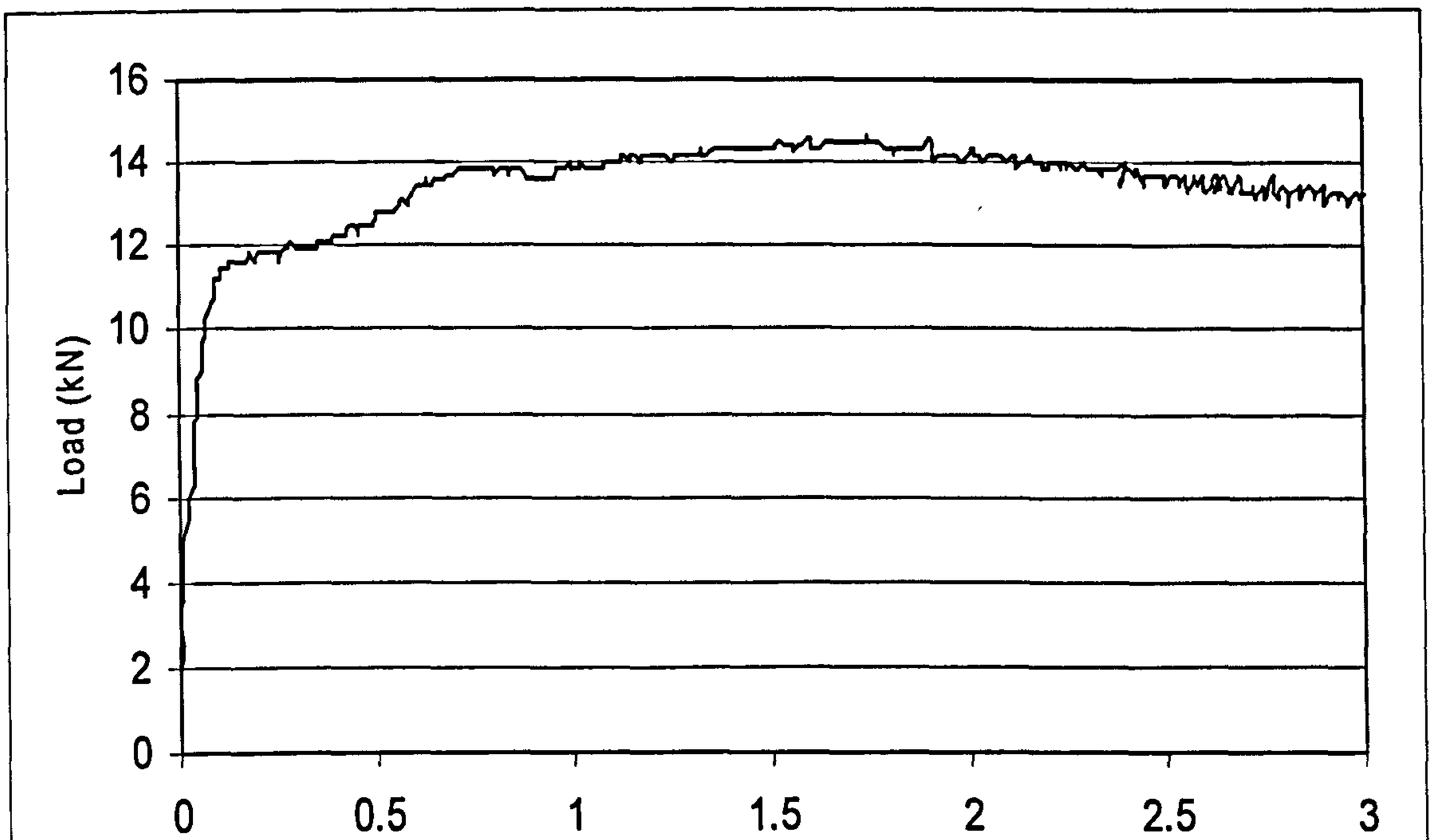

Figure 6.8a: Load-displacement curve of beam 1 - slab S5

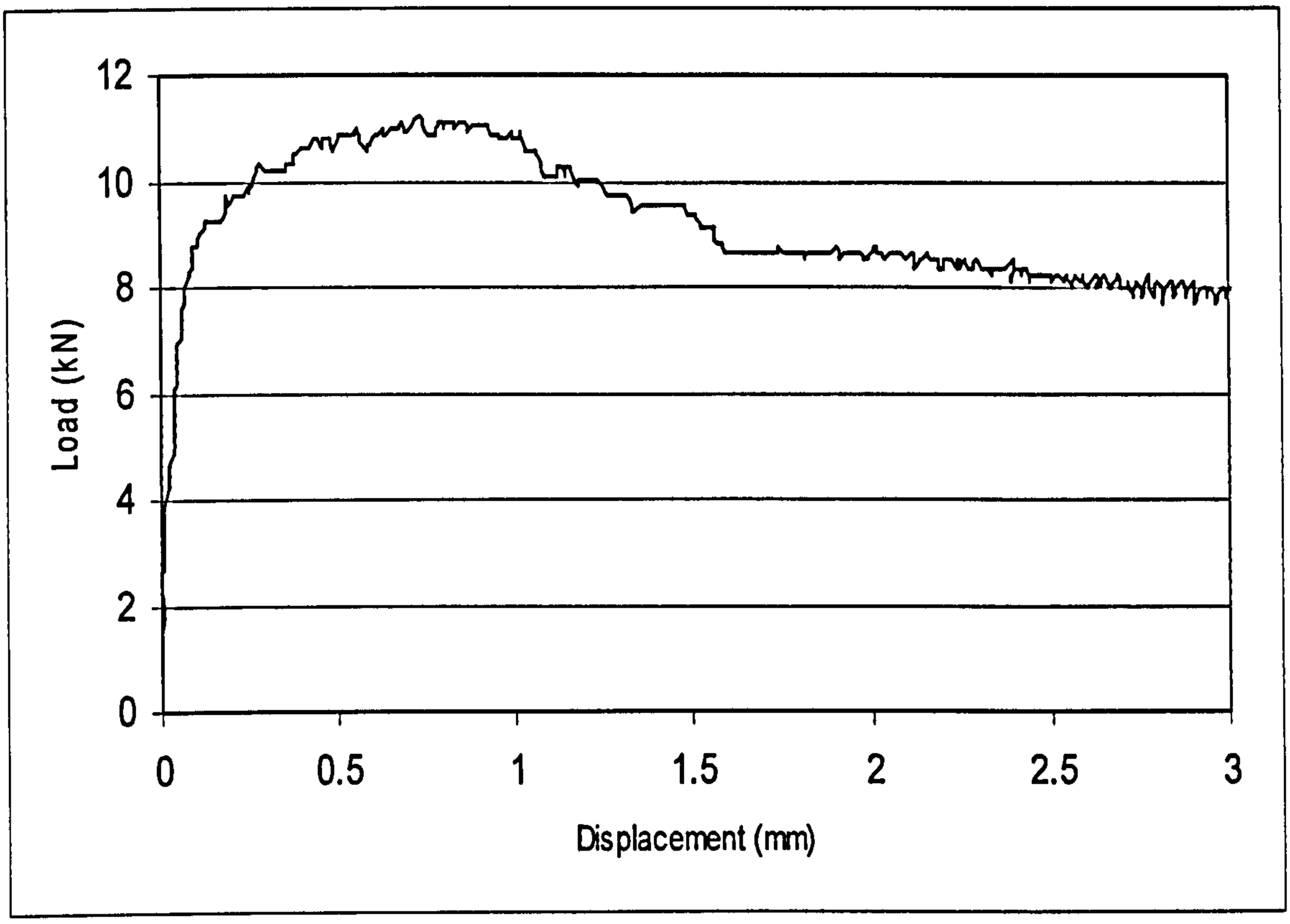

Figure 6.8b: Load-displacement curve of beam 2 - slab S5

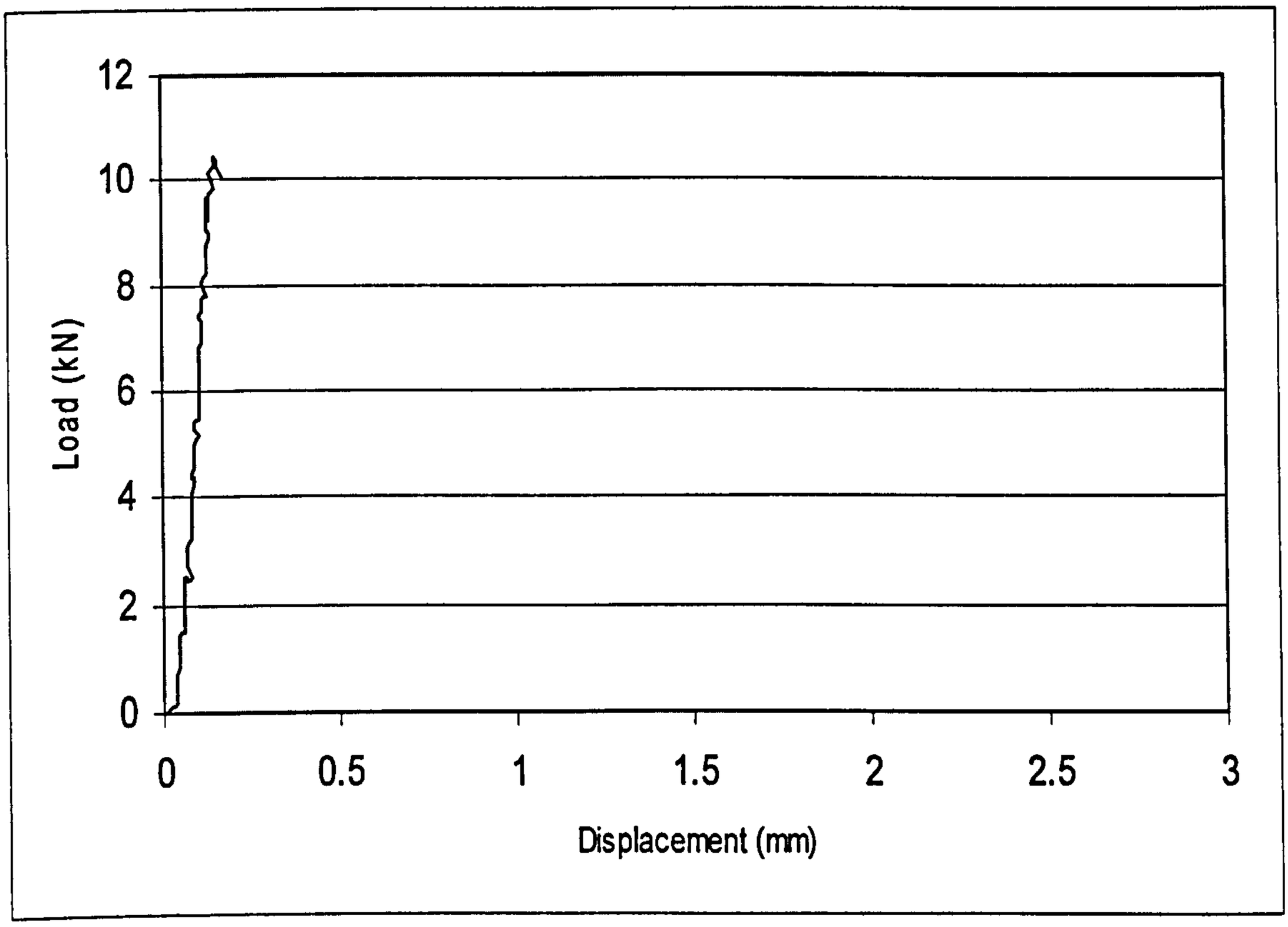

Figure 6.9a: Load-displacement curve of beam 1 - slab S6

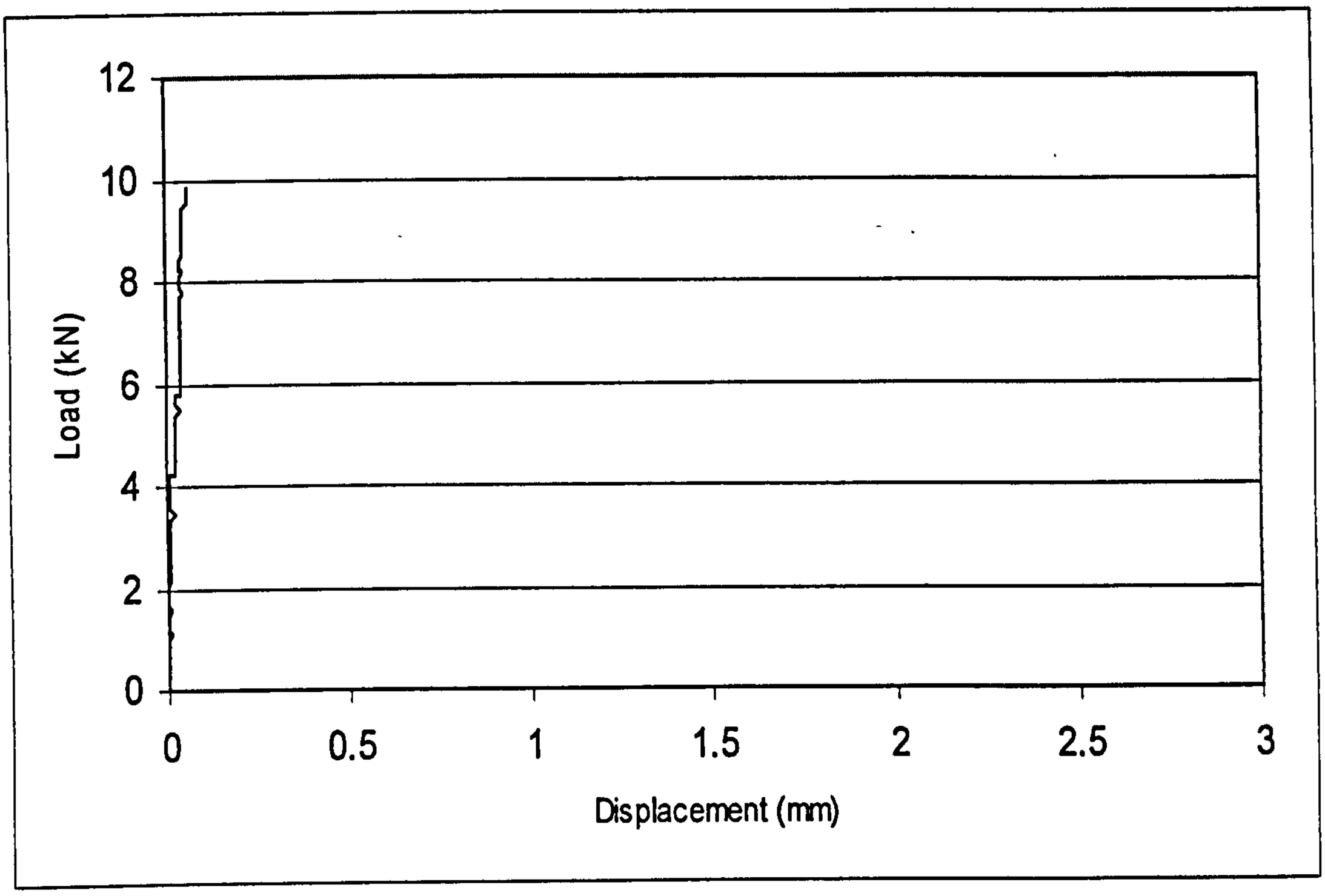

Figure 6.9b: Load-displacement curve of beam 2 - slab S6

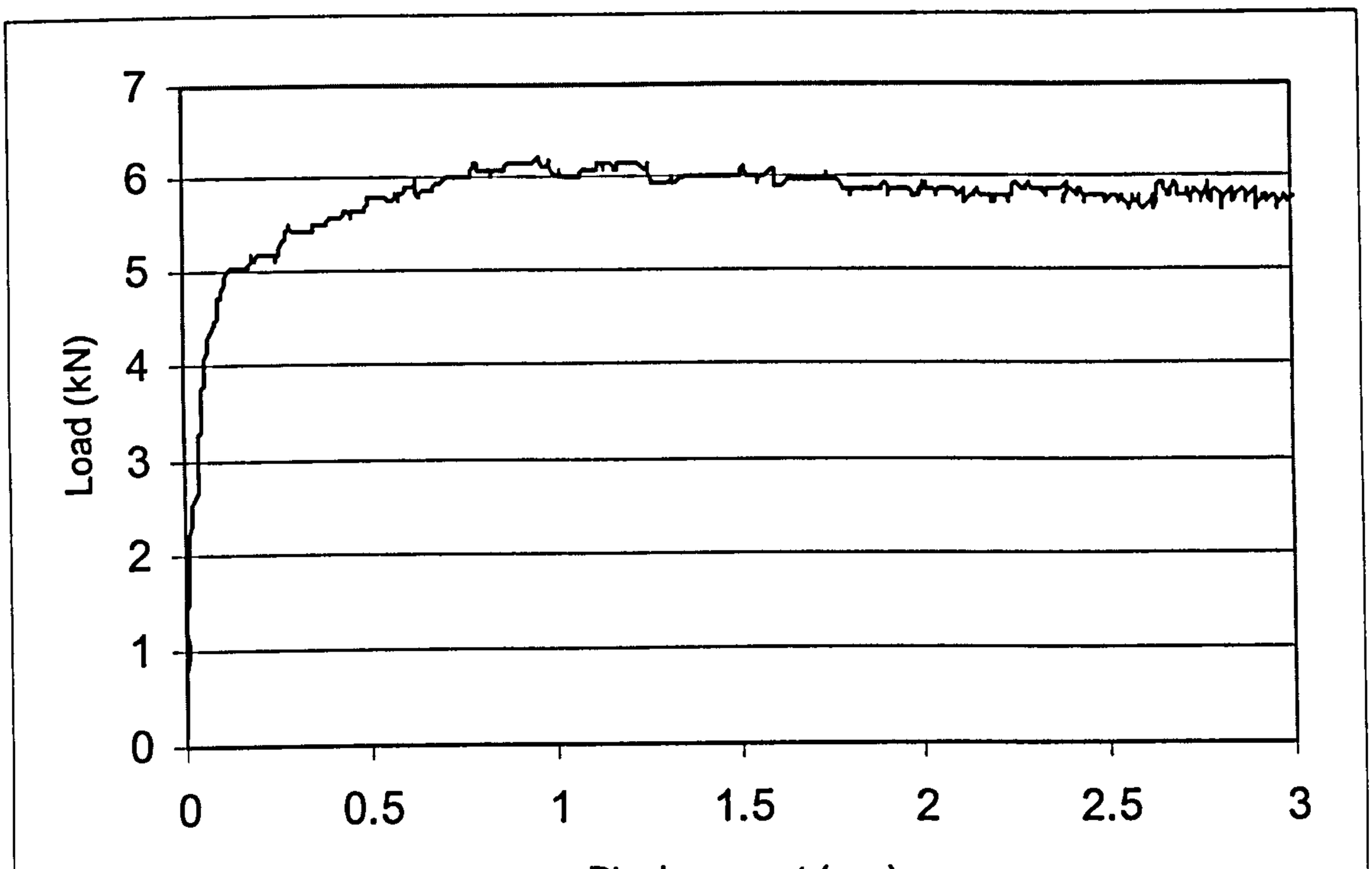

Figure 6.10a: Load-displacement curve of beam 1 - slab S7

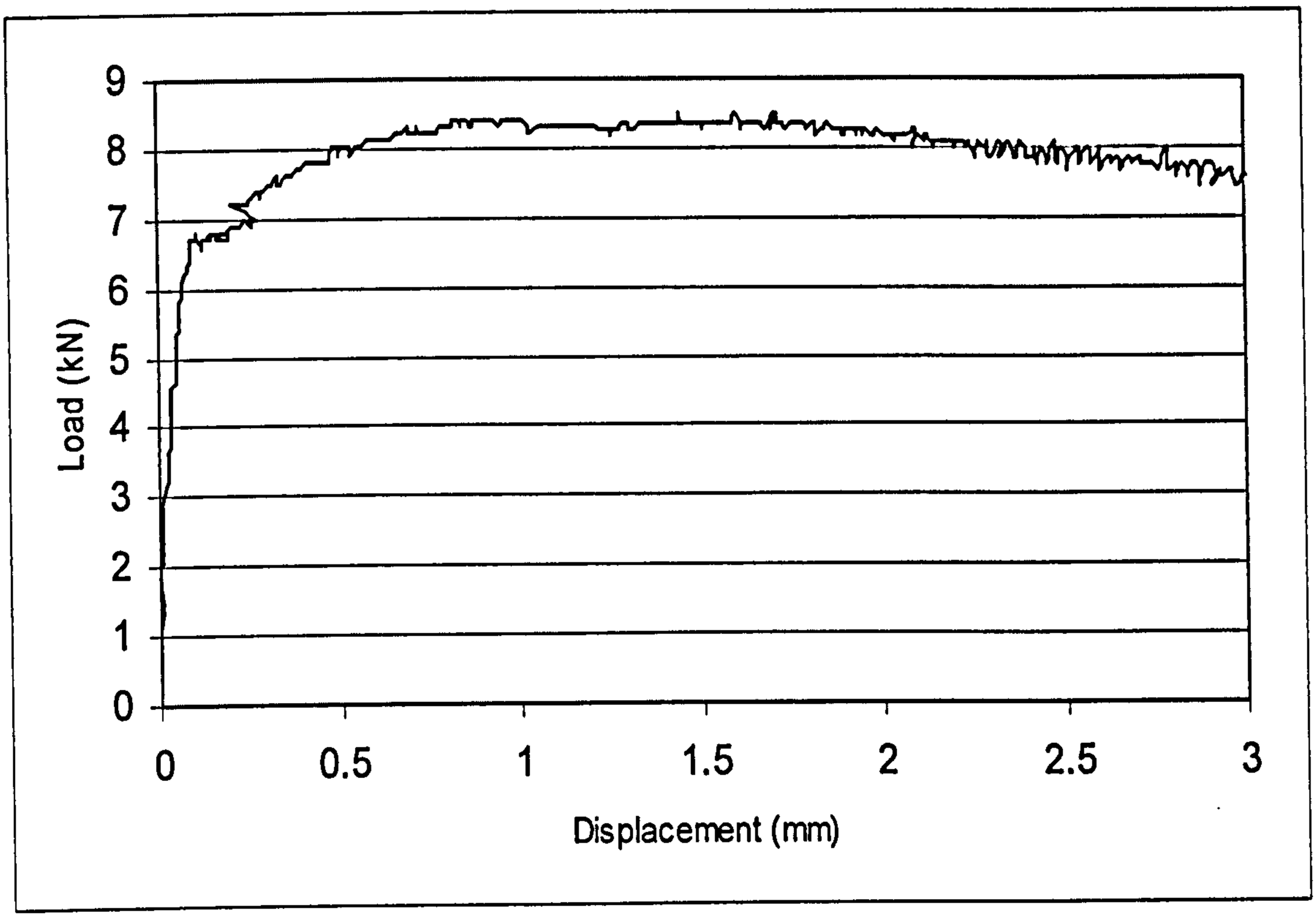

Figure 6.10b: Load-displacement curve of beam 2 - slab S7

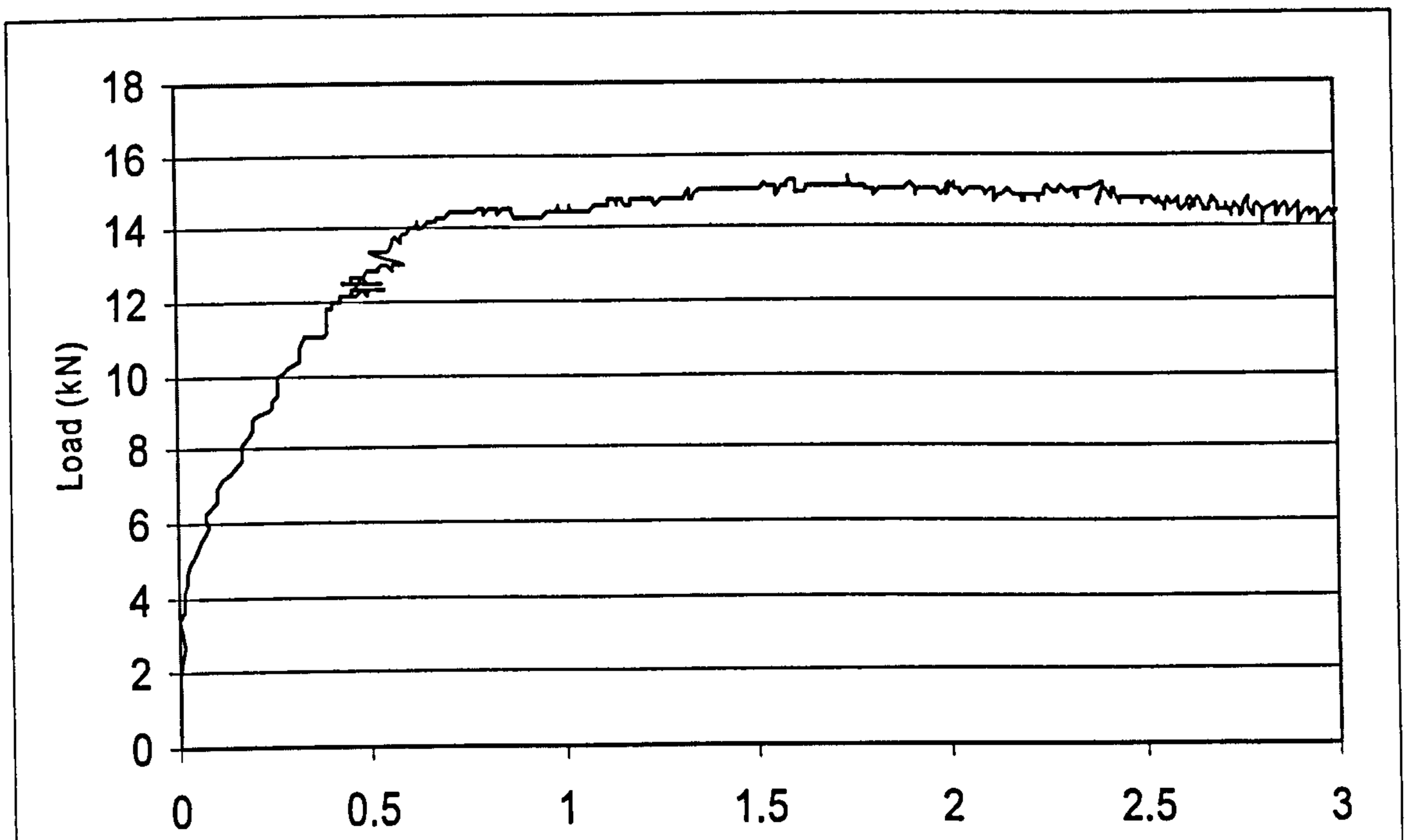

Figure 6.11a: Load-displacement curve of beam 1 - slab S8

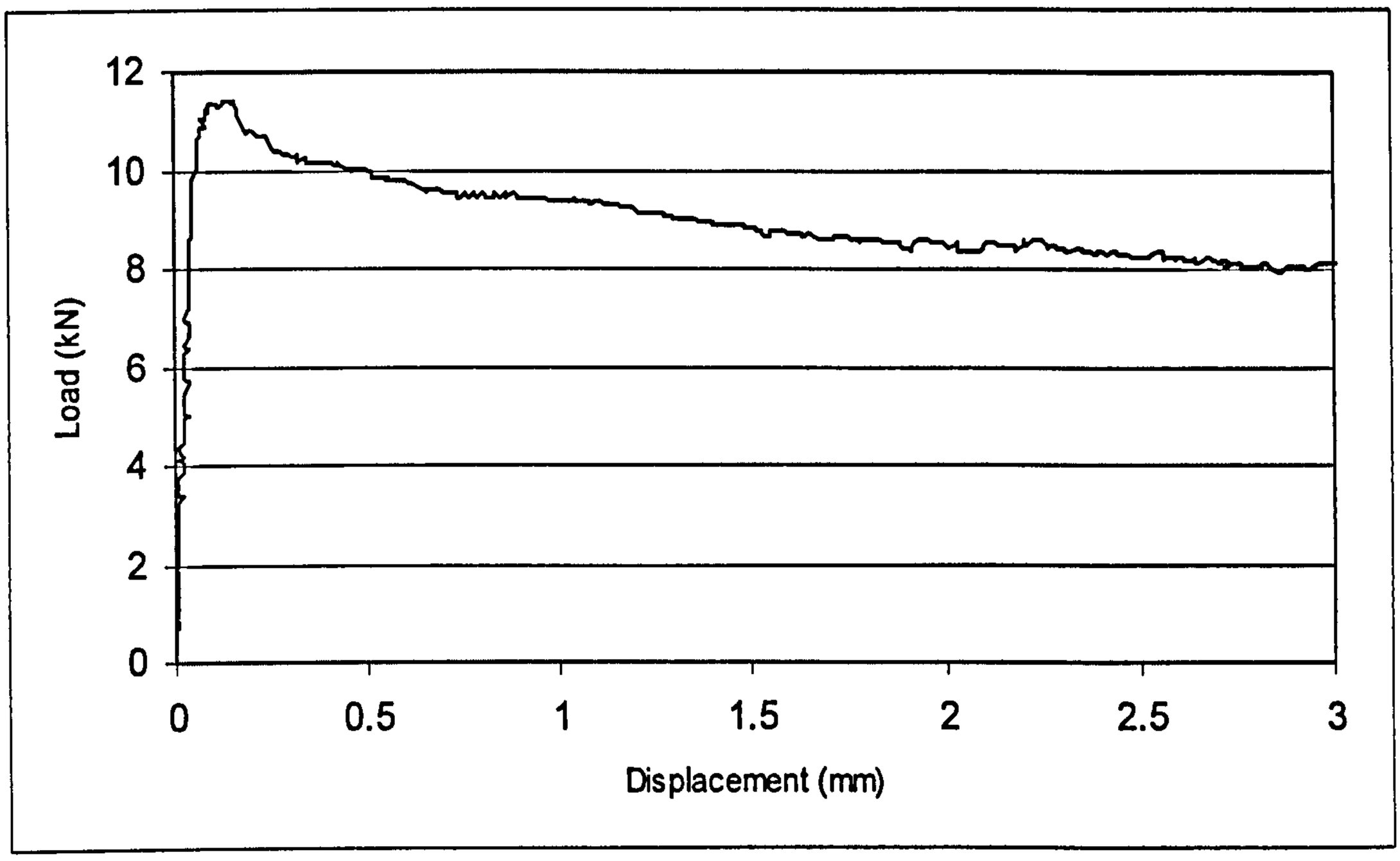

Figure 6.11b: Load-displacement curve of beam 2 - slab S8

6.5 Test Apparatus and Instrumentation

The instrumentation was designed to collect data on the applied loading, the slab deflection, and the concrete strains both in the radial and the circumferential directions. The applied load was monitored, in real time, by an accurately calibrated load cell. The test rig used, as well as instrumentations used to measure slab deflection and concrete strains, are discussed below.

6.5.1. Test Rig

The test rig used for the slabs mainly consisted of the slab supporting system and the loading system. The supporting system was designed to be able to best simulate the actual boundary conditions in the real structure and to have an adequate strength and stiffness to accommodate the loads likely to be encountered. The supporting system was composed of a steel ring with a radius of 550 mm and a piece of heavy metal base laid underneath the ring, as illustrated in Figure 6.12.

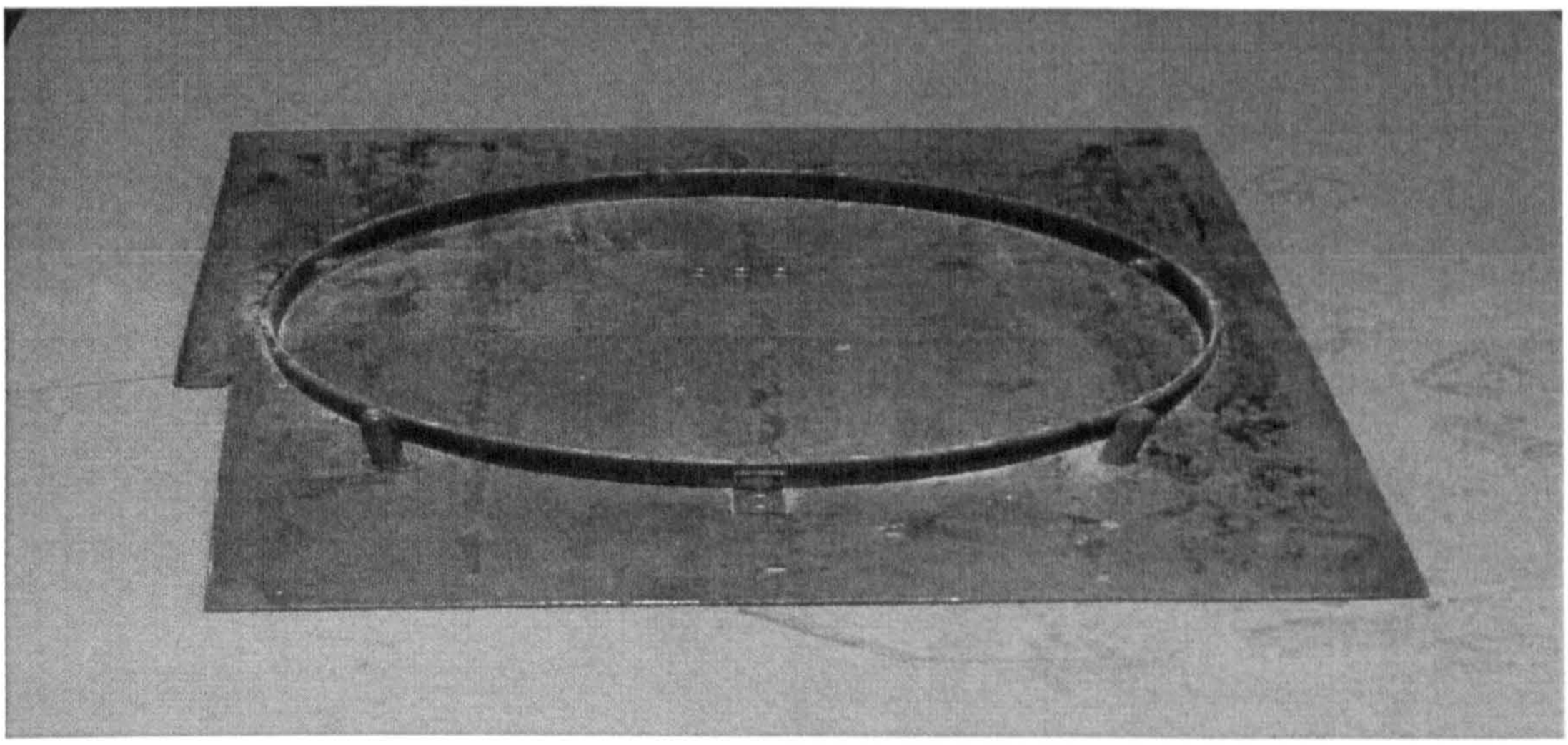

Figure 6.12: Slab supporting system

The slabs were tested in the inverted position to facilitate the setup of the loading arrangement and the supporting system. The loads were applied to the test slab through the 75 mm diameter steel column stub, which was used to model the action of an interior column and was placed at the centre of the test slabs. By loading the column stub the load was uniformly distributed on the slab along the steel ring perimeter by the supporting system. The Mayes testing machine was used as a test bid for slab tests. The details of the test rig and the test set-up are presented in Figure 6.13.

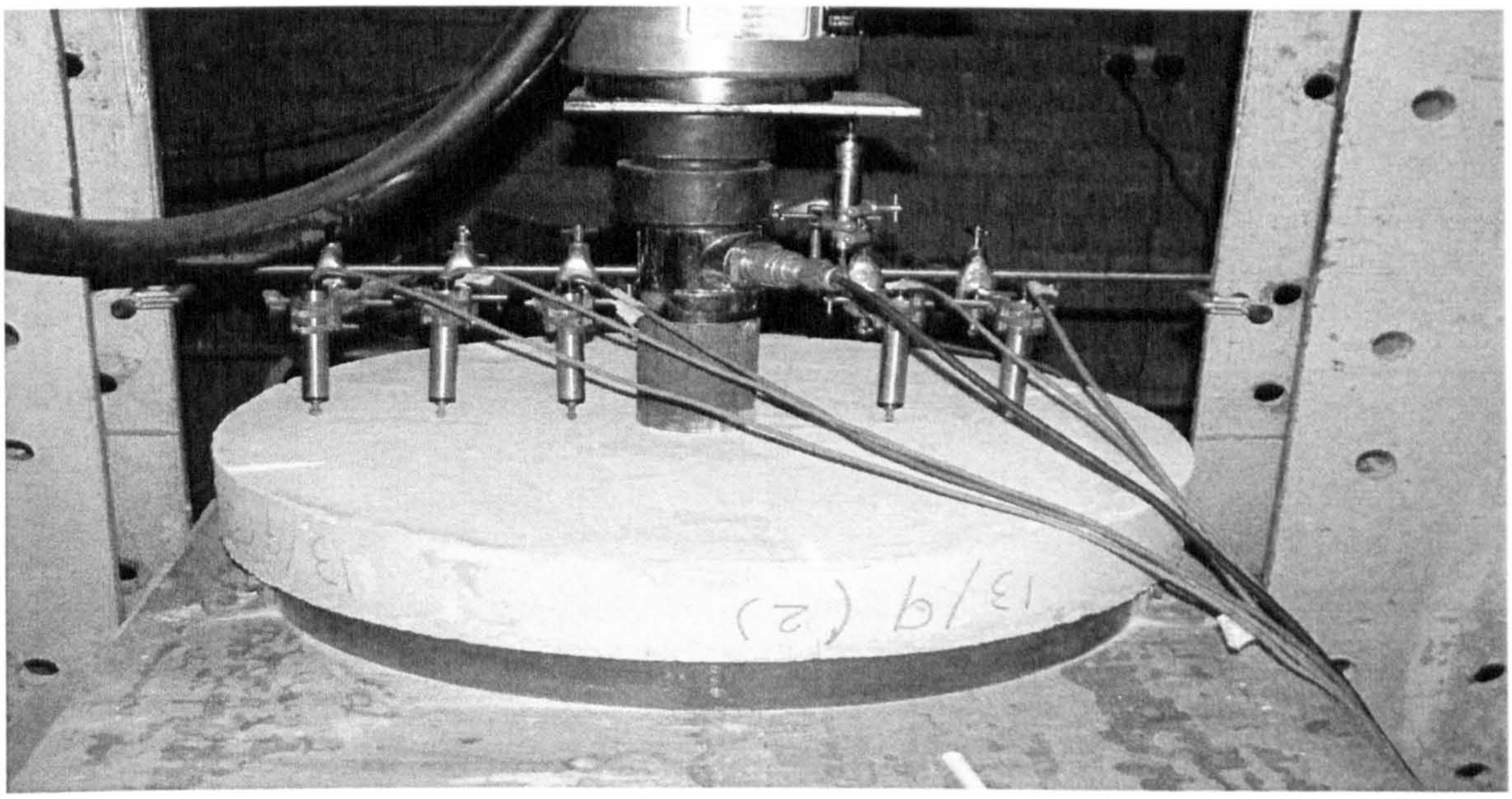

Figure 6.13: Test set-up

6.5.2 Deflection Measurement

The deflections of the slabs were measured with, six Linear Variable Differential Transformers (LVDT). The LVDTs were placed a long the diameter on the top side of the slabs (compression side). The transducers were fixed vertically against the slab surface. They were attached to rigid steel supporting system. Figure 6.14 shows the arrangement used to fix the transducers and their position across the slab surface.

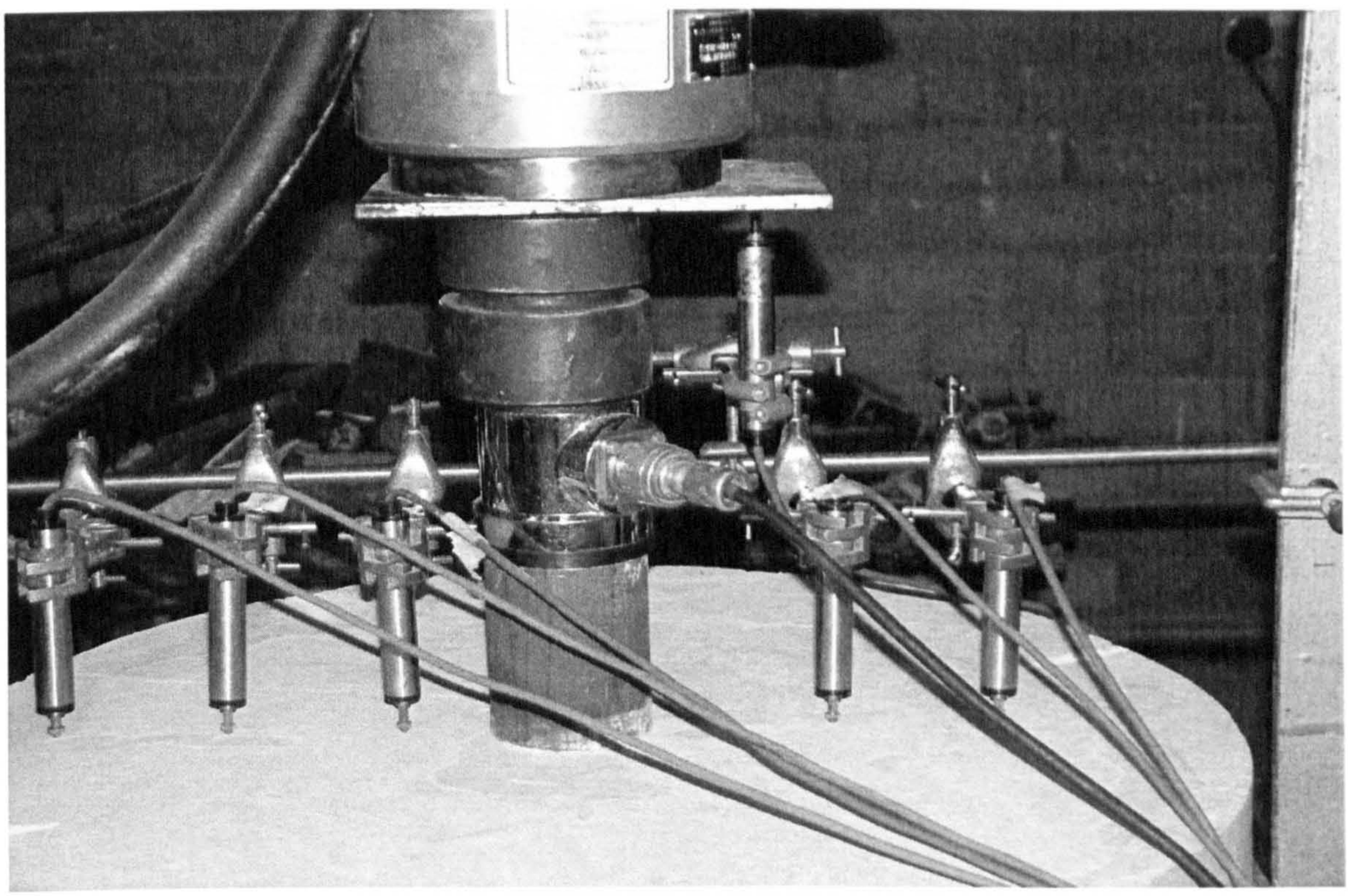

Figure 6.14: Position of the LVDTs across the slab surface

6.5.3 Strain Measurement

Concrete strains in the radial and tangential directions were measured on the bottom (tension) side of the slabs with electrical resistance strain gauges glued to the concrete surface at various distances from the column, see Figure 6.15. Slab S5 was strain gauged with 20 strain gauges to determine the best location of the strain gauges from the column. Based on the results obtained the strain values at eleven locations were believed to be

mandatory. Consequently, eleven strain gauges were used for the remaining slabs. These gauges were fixed on the concrete surface using an epoxy adhesive imported from China. The gauges were of 30 mm length. All the strain gauges readings were obtained using the data acquisition system

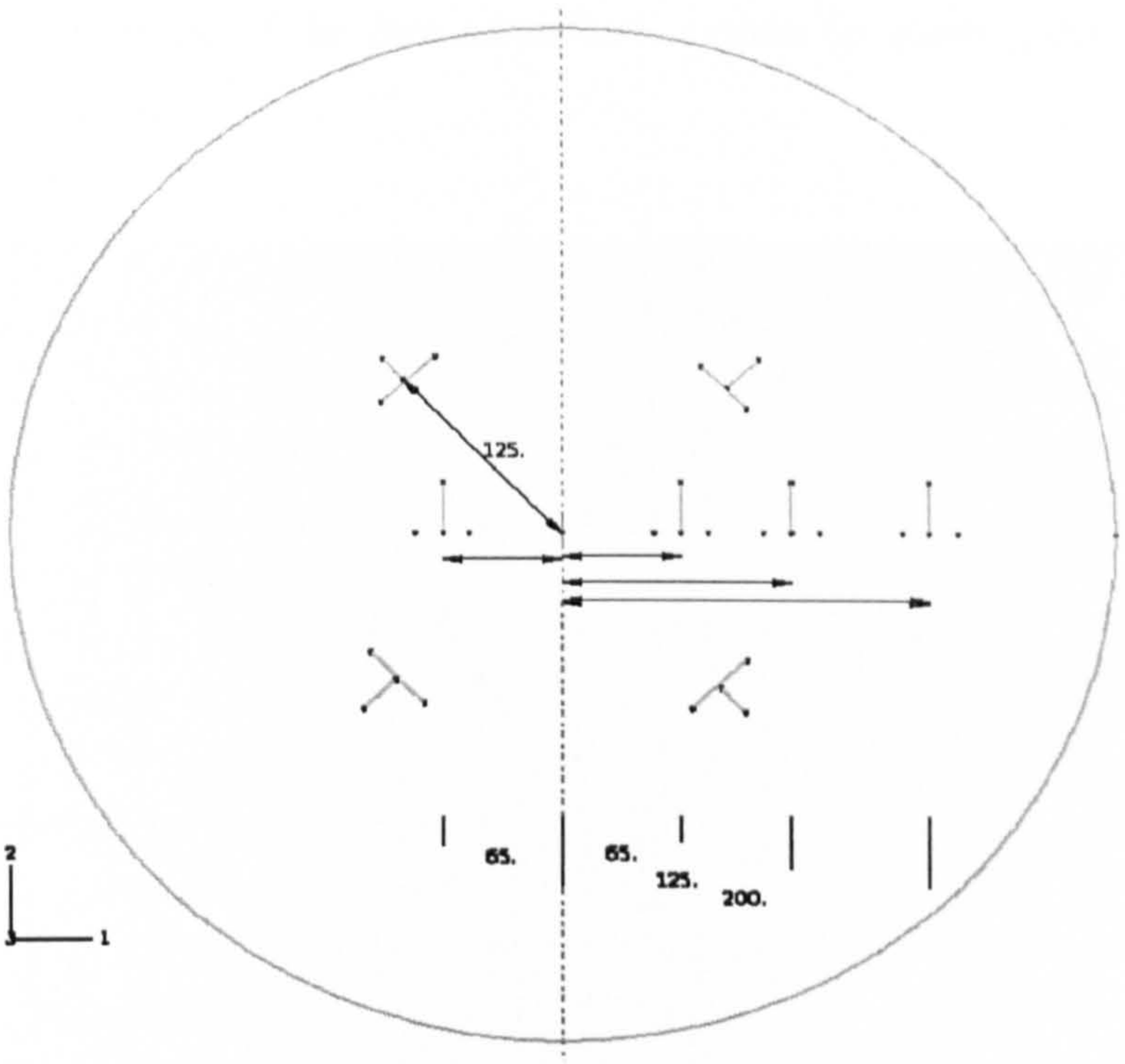

Figure 6.15 Strain gauges arrangement

6.6. Testing of Slabs

Approximately, four weeks after casting, the tested slab specimens and the corresponding control specimens were taken out from the curing room and were prepared for testing.

6.6.1 Preparation

After taking out the test slab specimens from the curing room and transporting them to the laboratory, some preparation work had to be done before carrying out the load test. First, the designed locations for fitting the strain gauges were marked and the strain gauges were fixed to the slab at the marked positions in a way similar to that described in section 6.5.3.

When all the strain gauges were properly fixed to the slab, the electrical connecting wires were soldered at the copper terminals together with the leads from the strain gauges, see Figure 6.16. Then the slab was lifted and positioned on the steel ring on the bid of the Mayes machine. Then the LVDTs for the measurement of the deflections were installed and the electrical connecting wires from loading cell, strain gauges and the LVDTs were connected to the extension of the data acquisition system for reading the load, strain and deflection measurement.

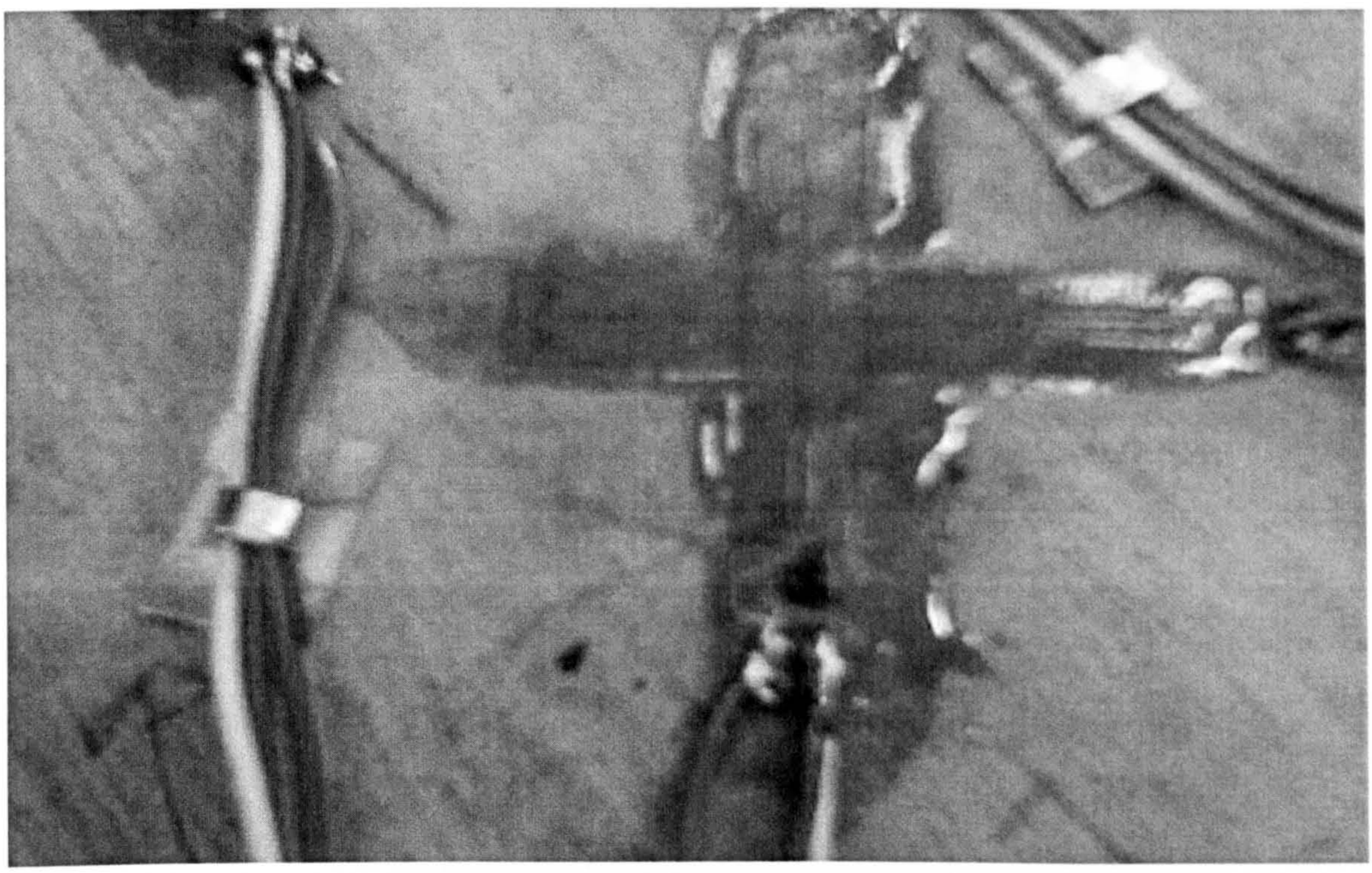

Figure 6.16: Strain gauges fixing

6.6.2 Testing

Before starting the test, all the measuring equipments, the supporting and loading systems were carefully checked to make sure that they had been properly installed and connected and the initial readings from the LVDTs and the strain gauges were recorded at the zero loading.

The slab tests were performed using a Mayes 334k-83 with 600 kN servo-hydraulic testing machine. The vertical displacement of the load cell at the column stub (75 mm diameter) was performed using the built-in LVDT displacement transducers, see Figure 6.14.

During the testing, the slabs were carefully inspected and the cracks were marked. The entire load-deflection response was also monitored using an X-Y recorder. All **the** specimens were loaded beyond the peak load in order to record the post-punching behaviour of the slabs. The tests were terminated when the column stub had penetrated so deep (5.5 cm) into the slab.

Loads, strains, and deflections were measured and recorded continuously throughout the test with an automatic data acquisition system without interrupting the load application. All the displacement transducers and the strain gauges were connected to the computer via a multi channel reader. Readings were recorded every three seconds. The Mayes testing machine and the arrangements of the data acquisition are shown in Figures 6.17 and 6.18 respectively.

Figure 6.17: Mayes testing machine

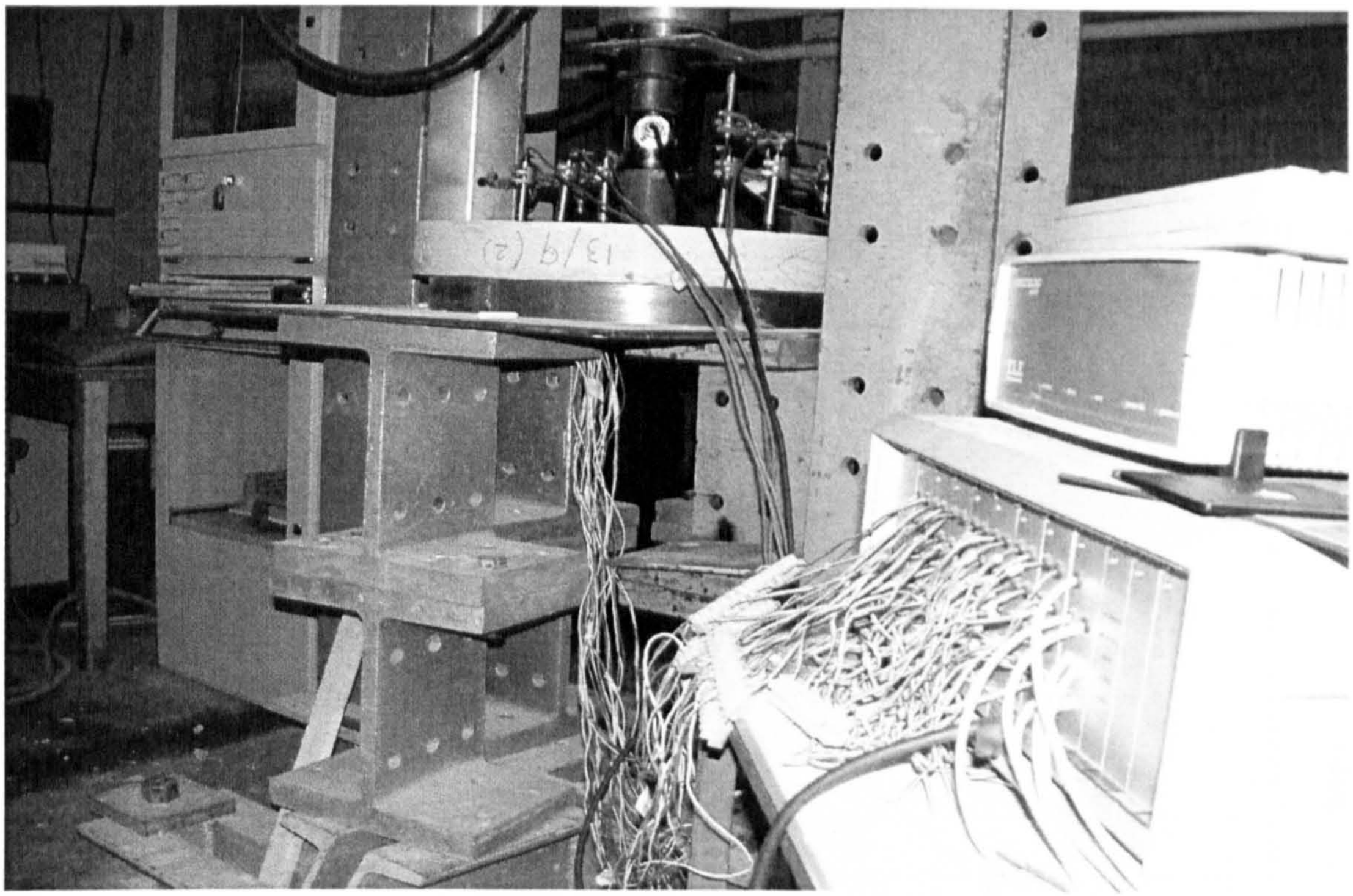

Figure 6.18: Data acquisition system

The test data was then stored in a personal computer and evaluated using the computer program Microsoft Excel (2003).

6.7 Results from Specimens Tests

In the following subsections, the physical observations and the experimental measurements of all of the test-specimens are reported. The behaviour in terms of the deflections, the response strains in concrete, crack pattern, cross sectional profiles of the slabs showing the profiles of the inclined failure surfaces, and the ultimate loads. Finally, the influences of the parameters considered in the test (i.e. the compressive strength, the fibre dosage and the aspect ratio) are discussed.

6.7.1 Slab Deflection

The load versus the centre-slab deflection plot of the six SFRC slabs and two plain concrete slabs can be seen in Figures 6.19-6.26. The load-deflection responses of the slabs were

linear up to the point where the first flexural crack occurred. Up to this point, making the end of elastic state, which occurs when the flexural stress in the tension face of the slab equals the cracking stress of the composite material, the composite material behaves elastically, in both tension and compression. Also stress and strain vary linearly across the slab thickness.

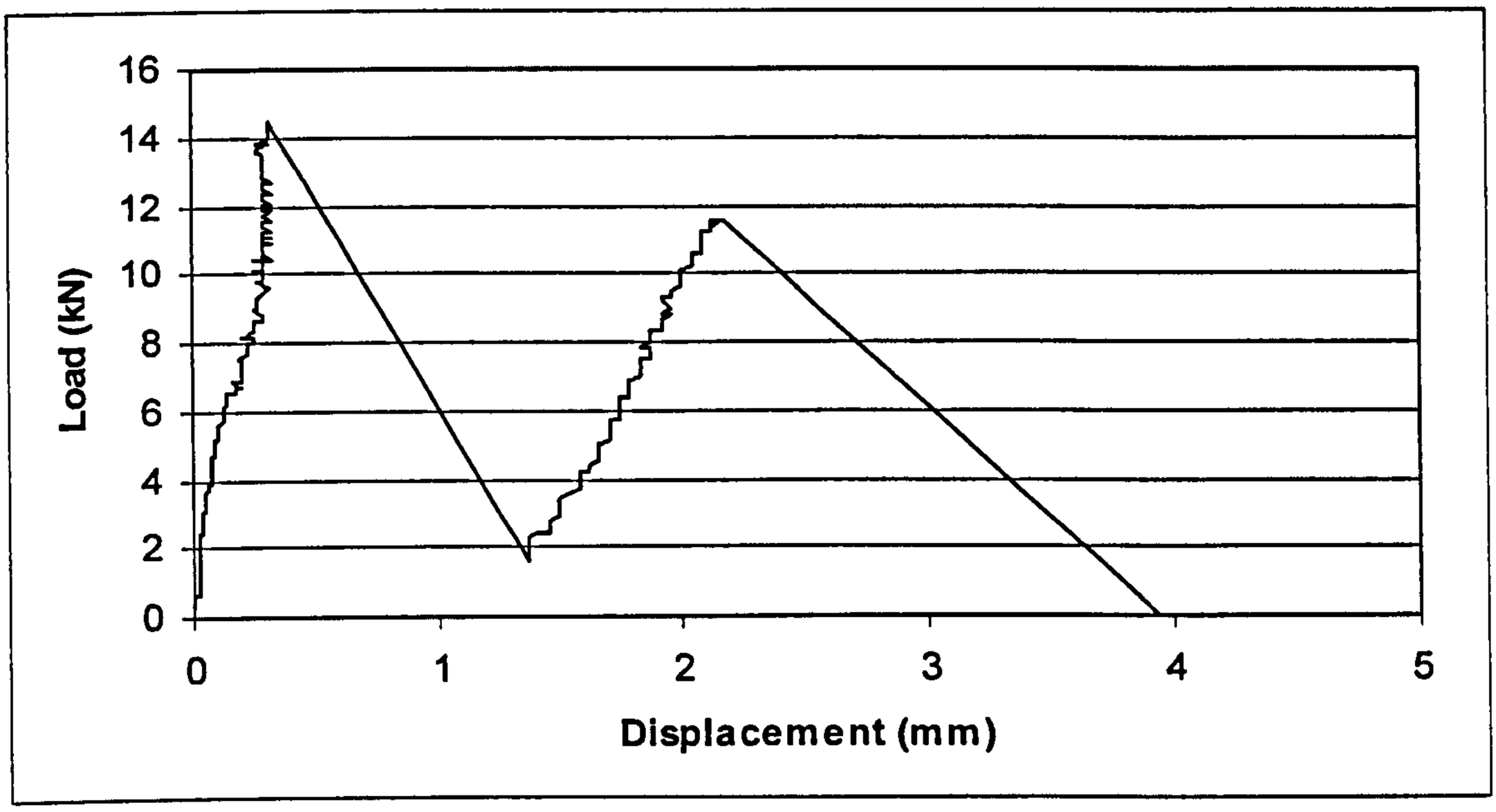

Figure 6.19: Load-displacement curve slab S1

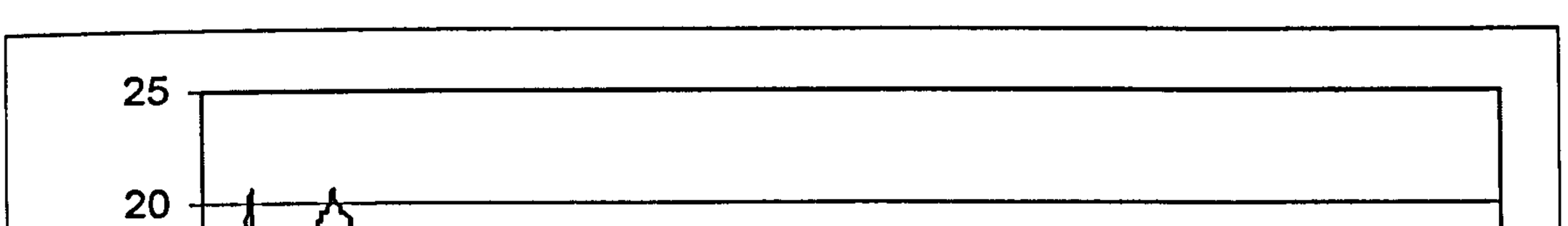

Figure 6.20: Load-displacement curve slab S2

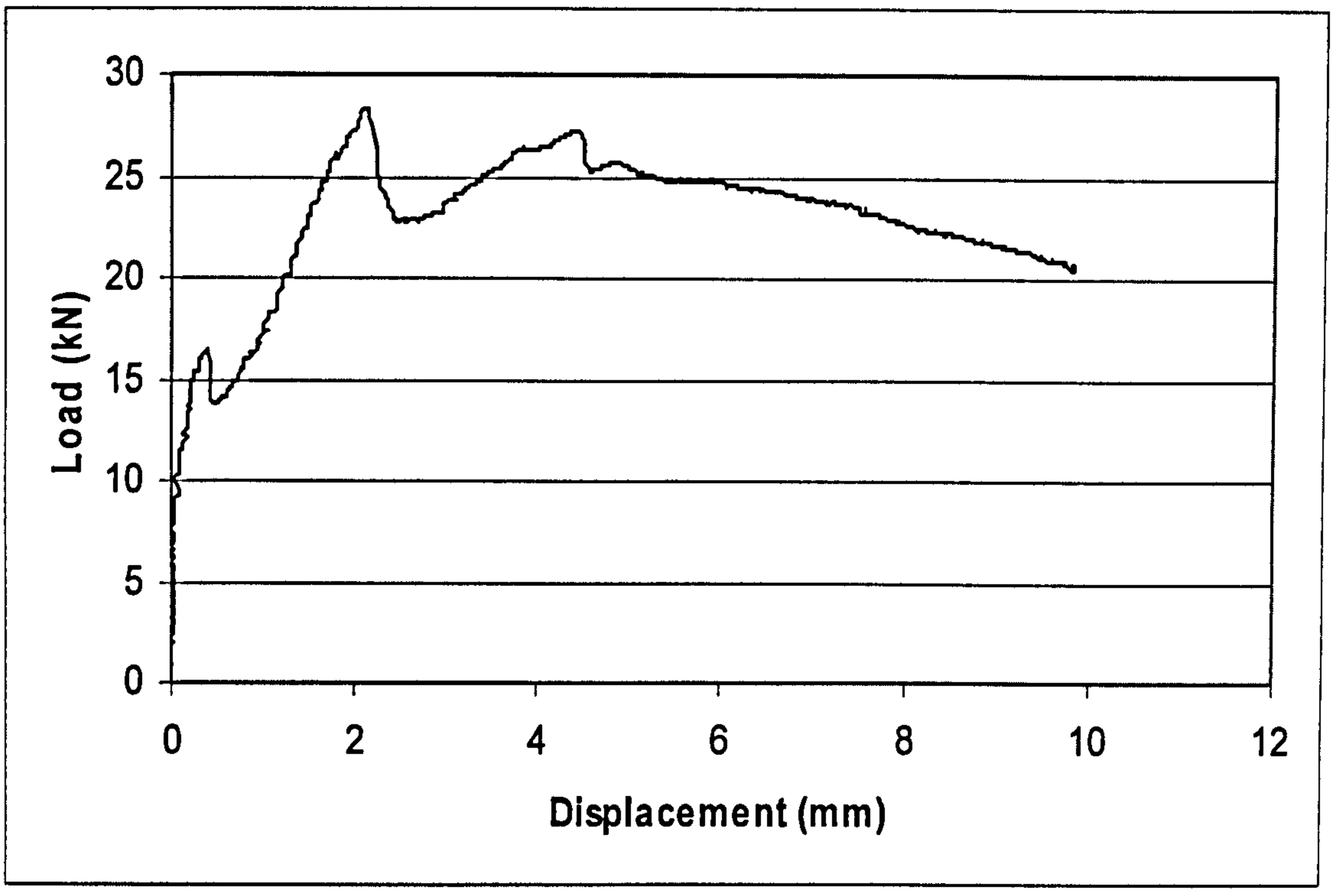

Figure 6.21: Load-displacement curve slab S3

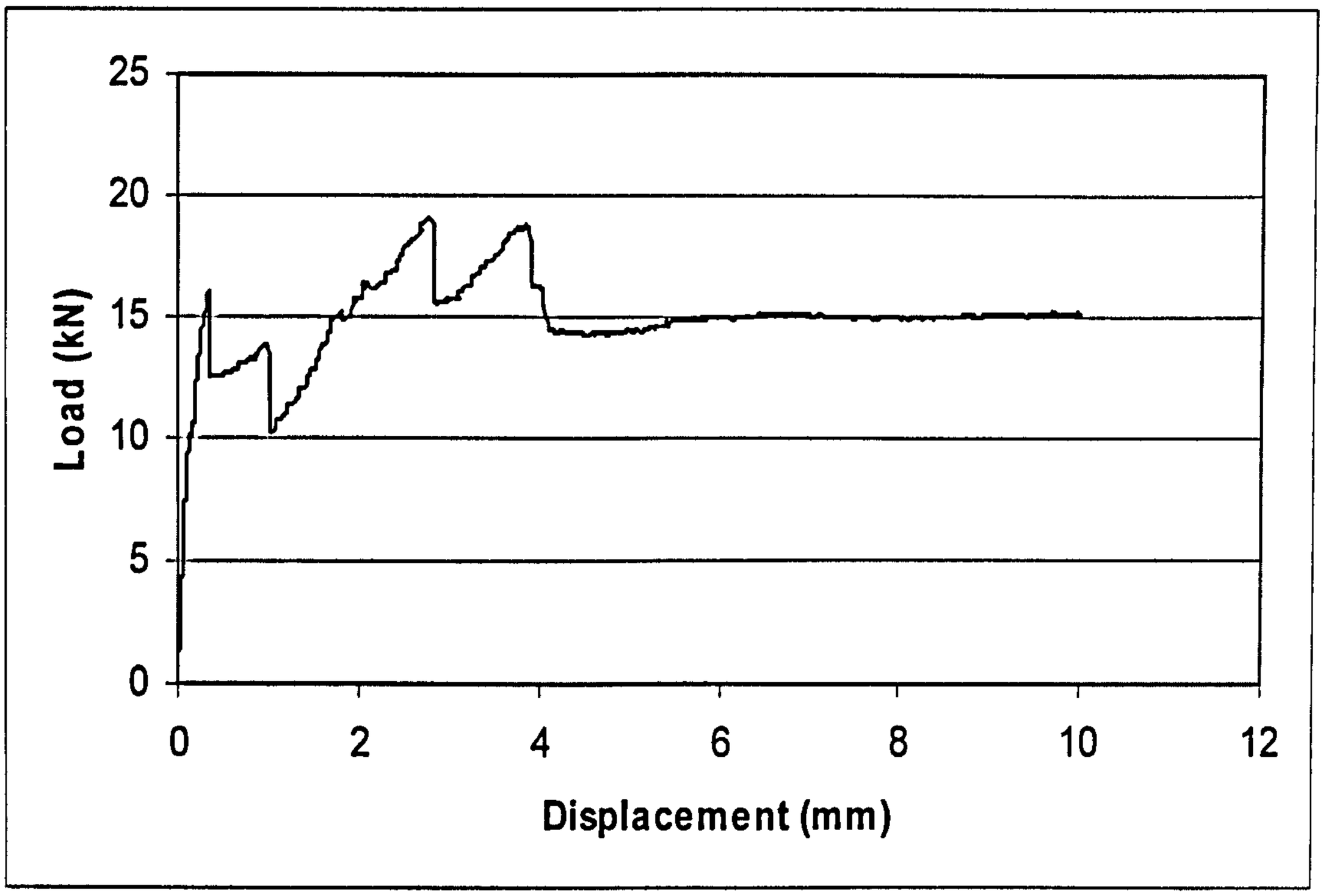

Figure 6.22: Load-displacement curve slab S4

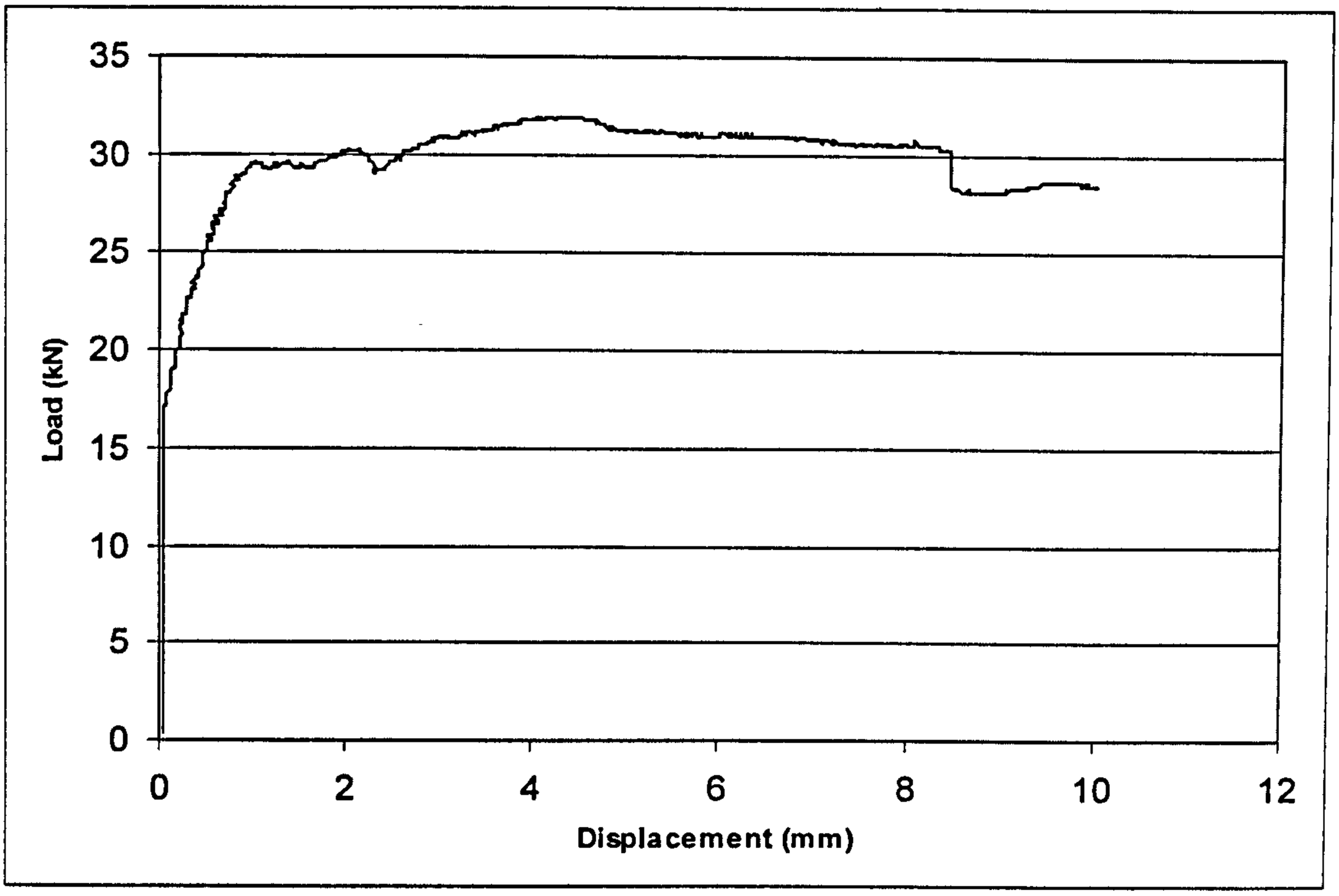

Figure 6.23: Load-displacement curve slab S5

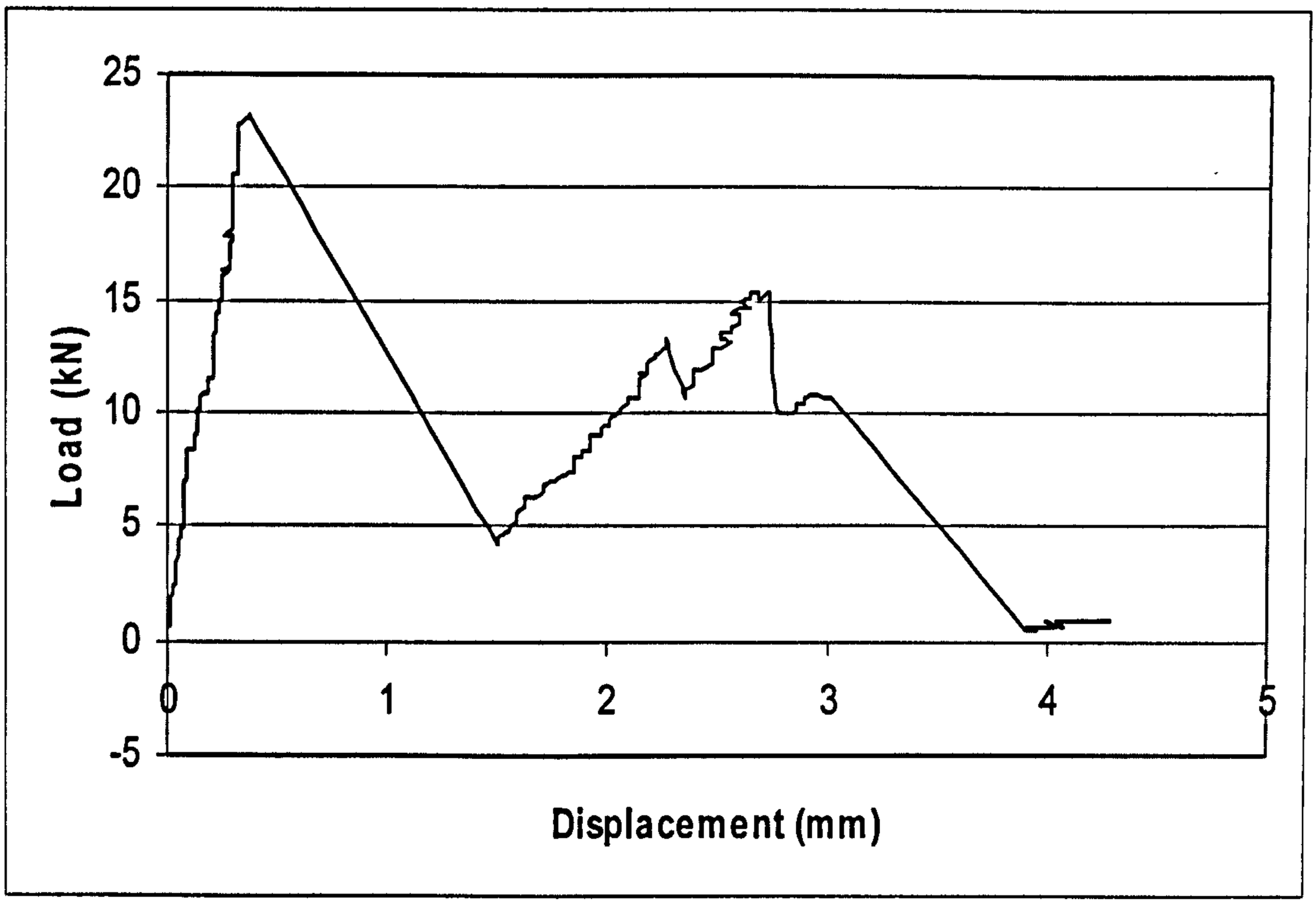

Figure 6.24: Load-displacement curve slab6

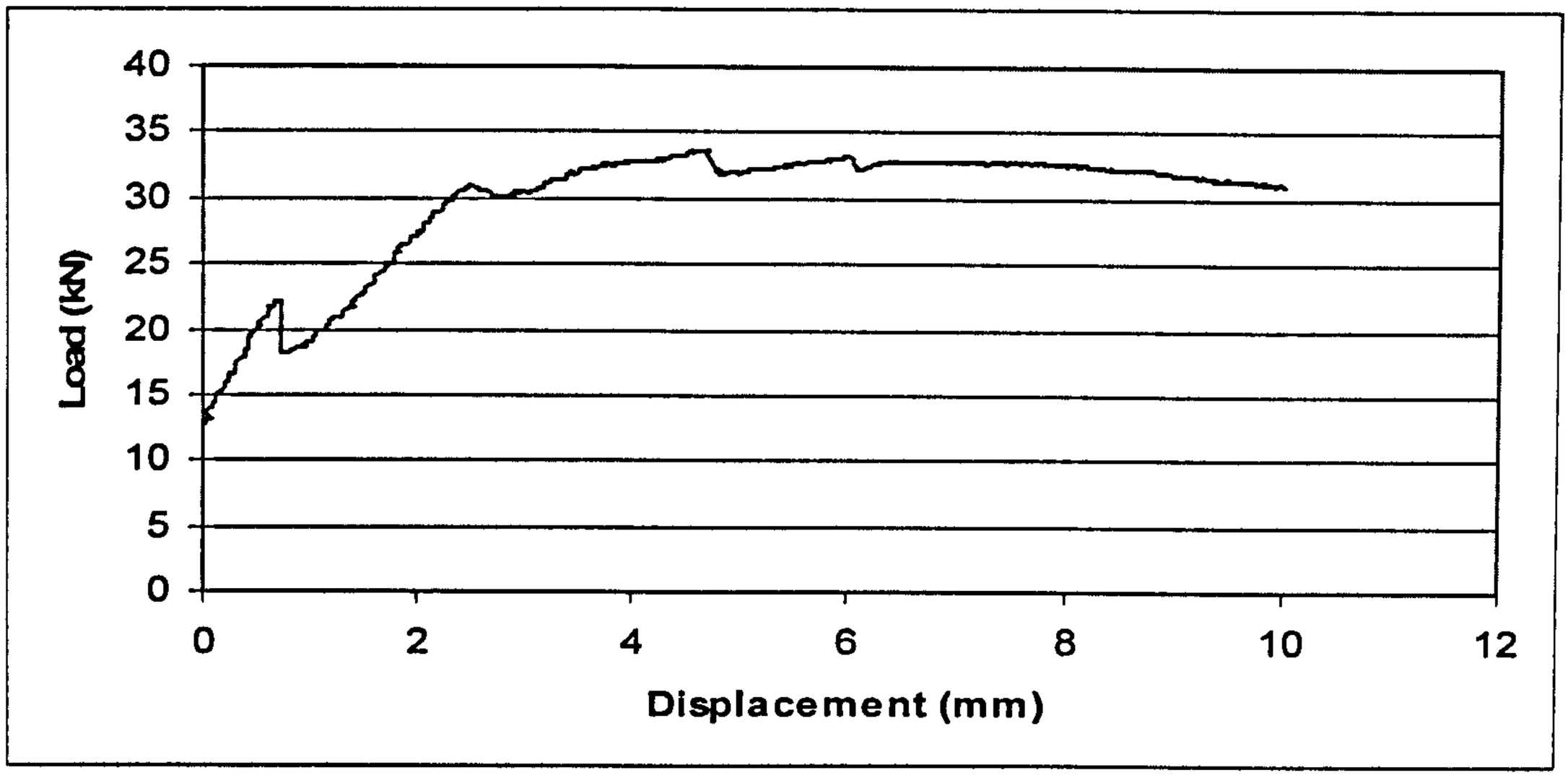

Figure 6.25: Load-displacement curve slab S7

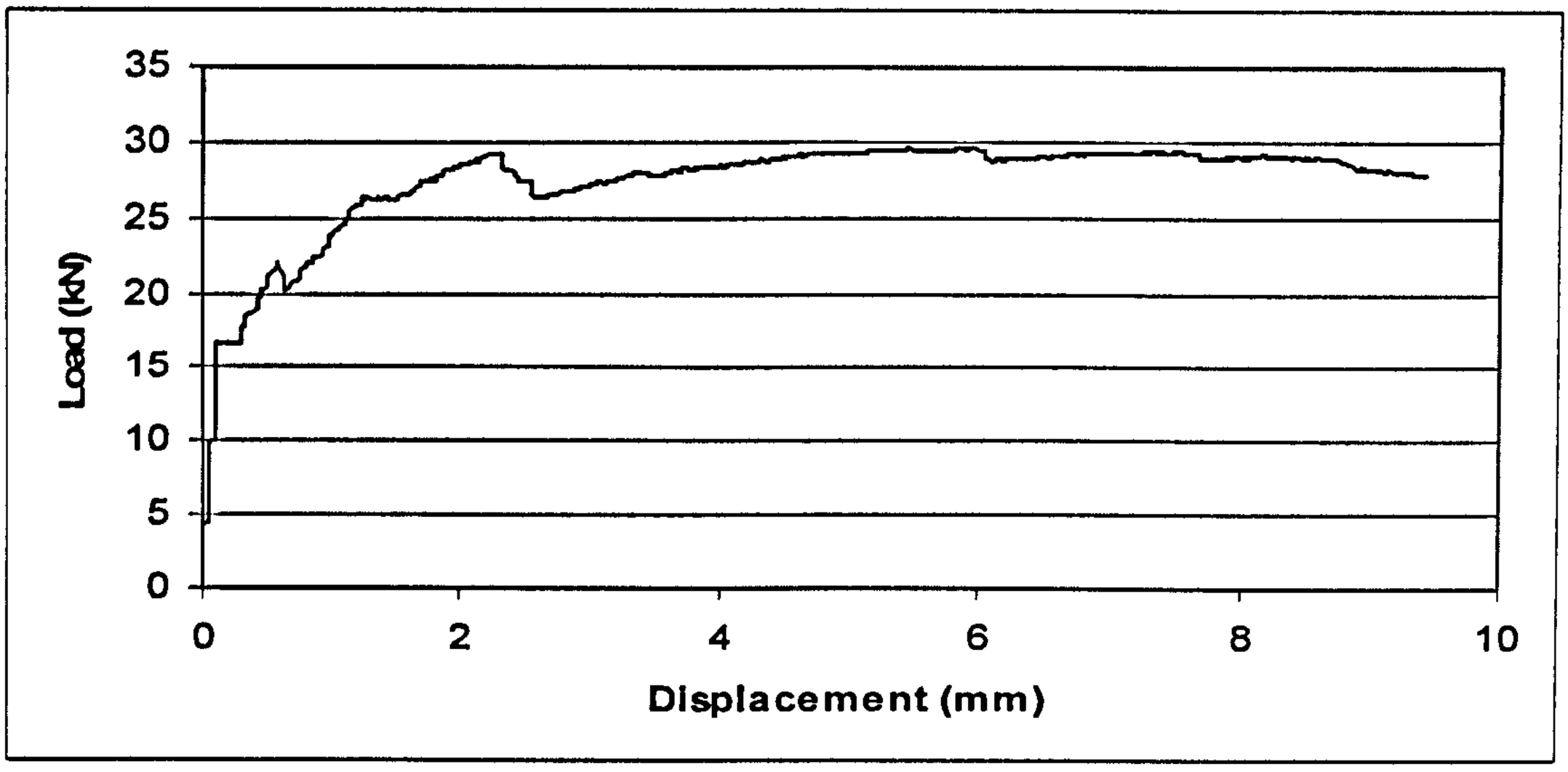

Figure 6.26: Load-displacement curve slab S8

The flexural crack or hinge was defined when there was a sudden reduction in the load-carrying capacity of the slab, as seen in the load versus deflection plots. The bending resistance of the slab decreased dramatically orthogonal to the flexural crack and a significant loss of stiffness was observed. This was more pronounced in the slabs with no fibres. For other slabs, an apparent delayed occurrence of stiffness degradation was evident. Upon increasing the loading, other load reductions were associated with secondary flexural cracks in directions approximately orthogonal to the first flexural crack. First and secondary flexural cracks always initiated on the bottom of the slab near the interior and

propagated vertically upward and toward the slab edges. The collapse or ultimate load of the slab can be seen in the plots as the level at which no further increase in load was reached with increasing magnitudes of slab deformation.

In the SFRC slabs, when the matrix cracks, the stress is transferred to the steel fibres crossing the propagating crack length, while the un-cracked part of the matrix still carries its share of the tensile strength. As a consequence of the crack propagation across the matrix, the neutral axis will shift toward the compression face of the slab. Due to these mechanisms of nonlinear tensile stress in the tension region, and the progressive shift in the neutral axis of the slab section, the curve representing the load-deflection relation has a flattening ascending shape; this demonstrates the improved structural response the steel fibres add to plain concrete slabs. Moreover, the benefit of the fibres could be seen immediately in the ultimate strength of the slab and the smaller reduction in load-carrying capacity after each cracking stage was attained. Furthermore the toughness, which is proportional to the area under the load-deflection curve shown in load-displacement plots, was another indicator of the benefit of fibres to slabs. Table 6.4 is a summary of the ultimate load of each slab.

Table 6.4: Ultimate load

Specimen no.	Ultimate load (kN)	Plain/SFRC ultimate load
S1	14.5	-
S2	20.7	1.43
S3	28.36	1.96
S4	19.07	1.32
S5	33.74	2.2
S6	23.55	-
S7	38.63	1.43
S8	33.08	1.26

As seen in the plots, the deformation at which each slab reached its ultimate load level was different. Figures 6.27 to 6.34 show the measured deflections along the diameter of each slab at various load levels. The lowest curve in each diagram in the figure is the deflection

distribution at the ultimate load. The maximum deflection at the ultimate load of slabs S1 and S6 without fibre reinforcement was 0.3mm. The maximum deflection at the ultimate load of slabs S2 and S4, with low fibre dosage, was 0.4 mm. The maximum deflection at the ultimate load of slabs S3, S5, S7 and S8 with high fibre dosage was in the range of 2.1 to 5.9 mm.

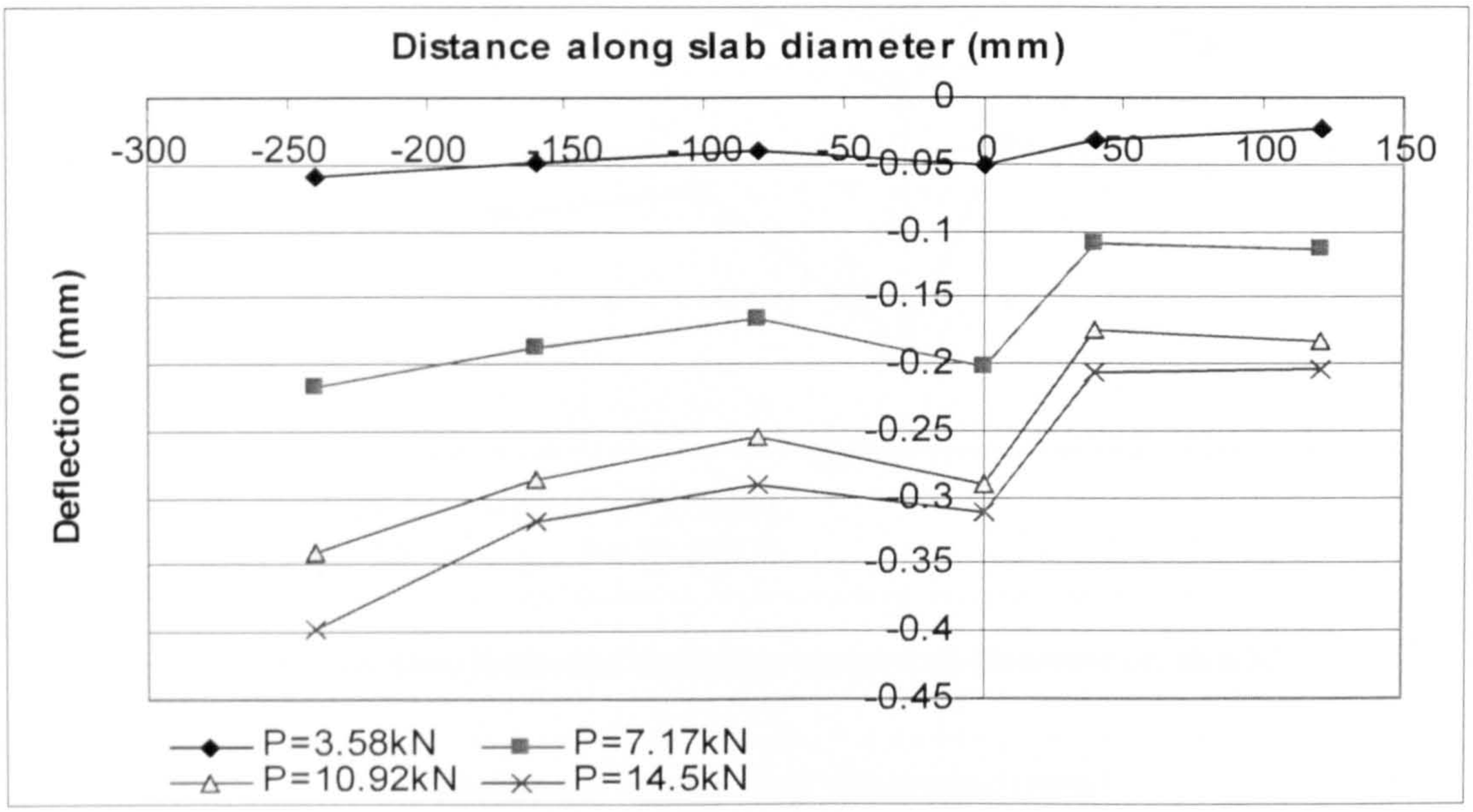

Figure 6.27: Distribution of deflection along slab diameter on slab S1

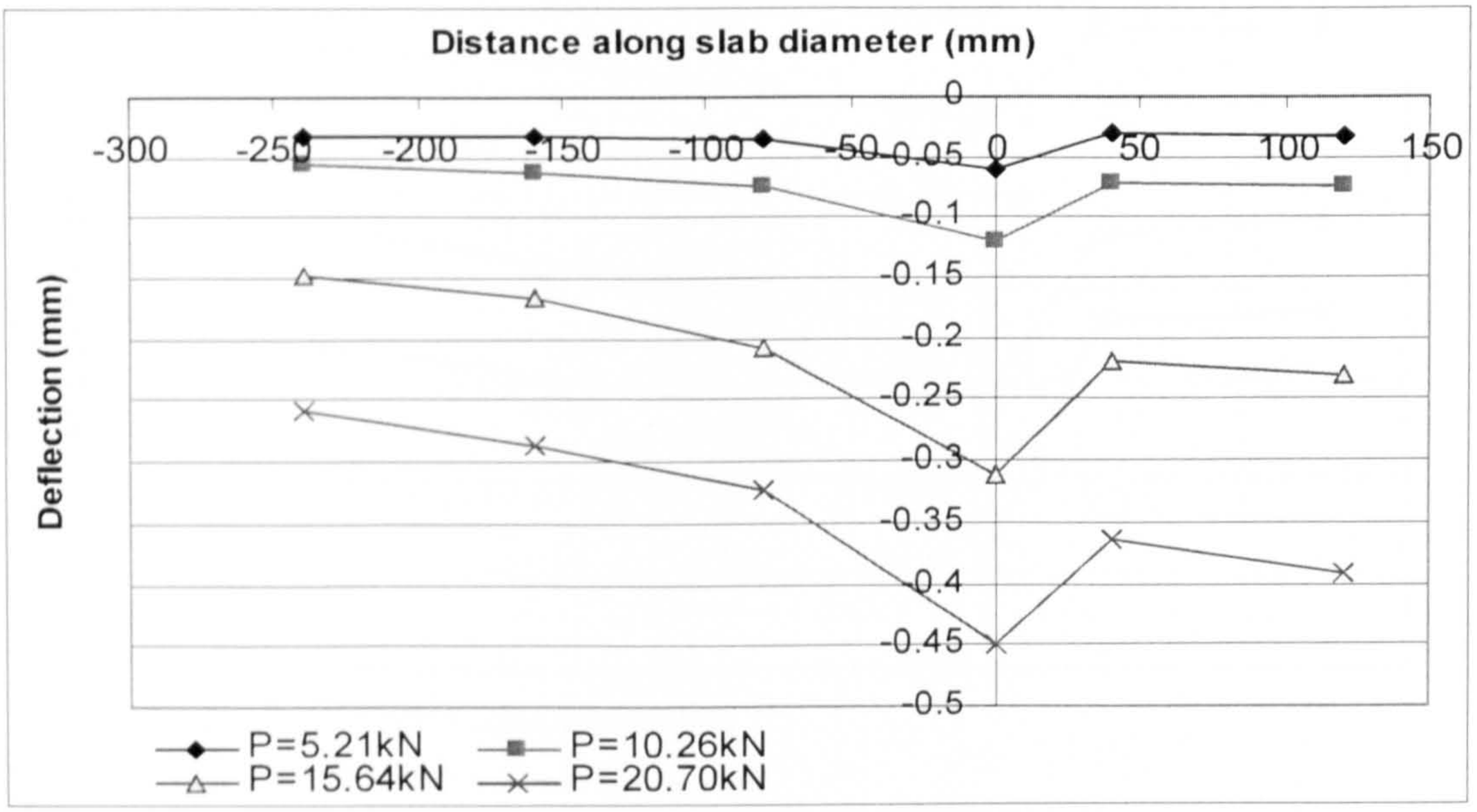

Figure 6.28: Distribution of deflection along slab diameter on slab S2

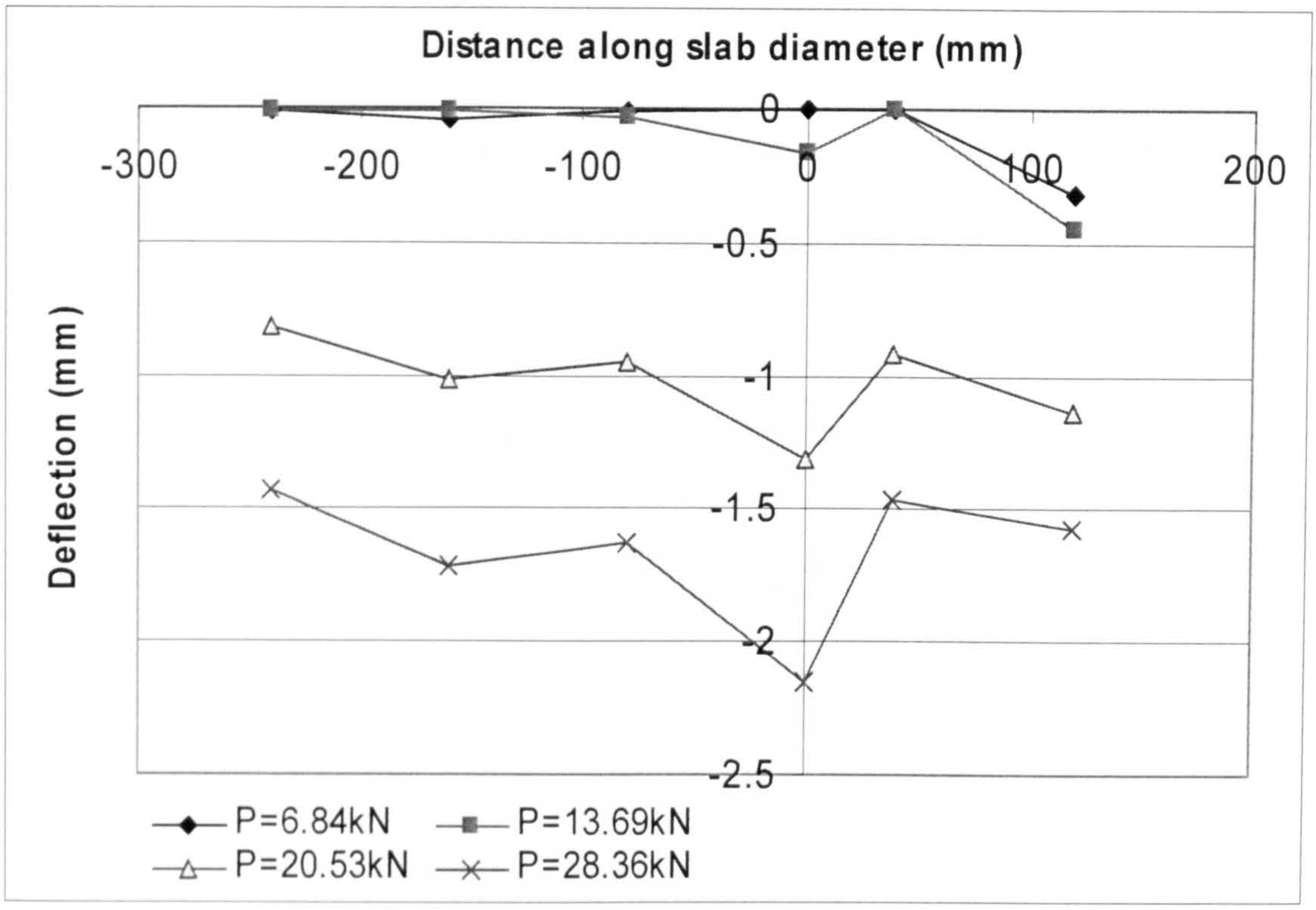

Figure 6.29: Distribution of deflection along slab diameter on slab S3

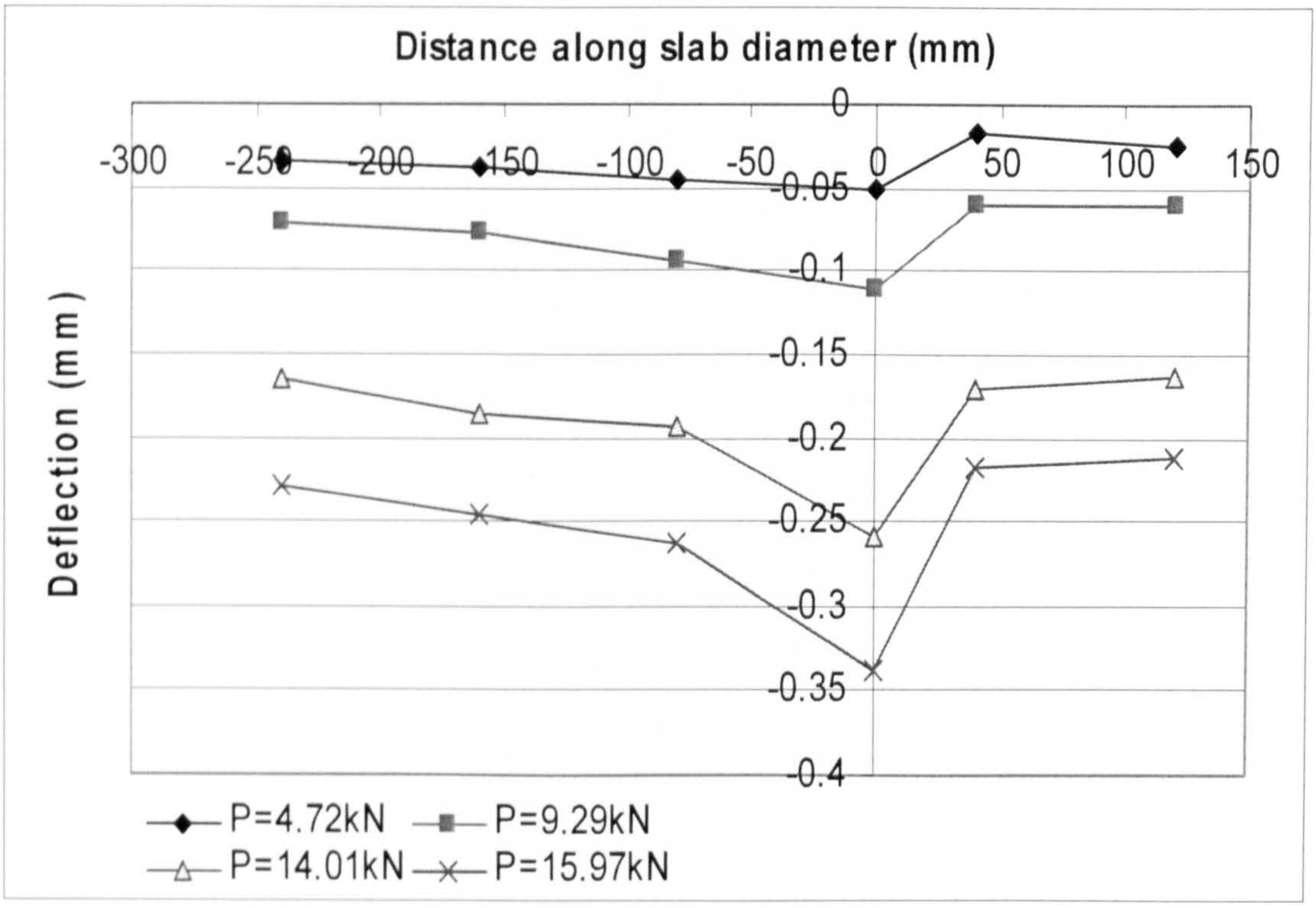

Figure 6.30: Distribution of deflection along slab diameter on slab S4

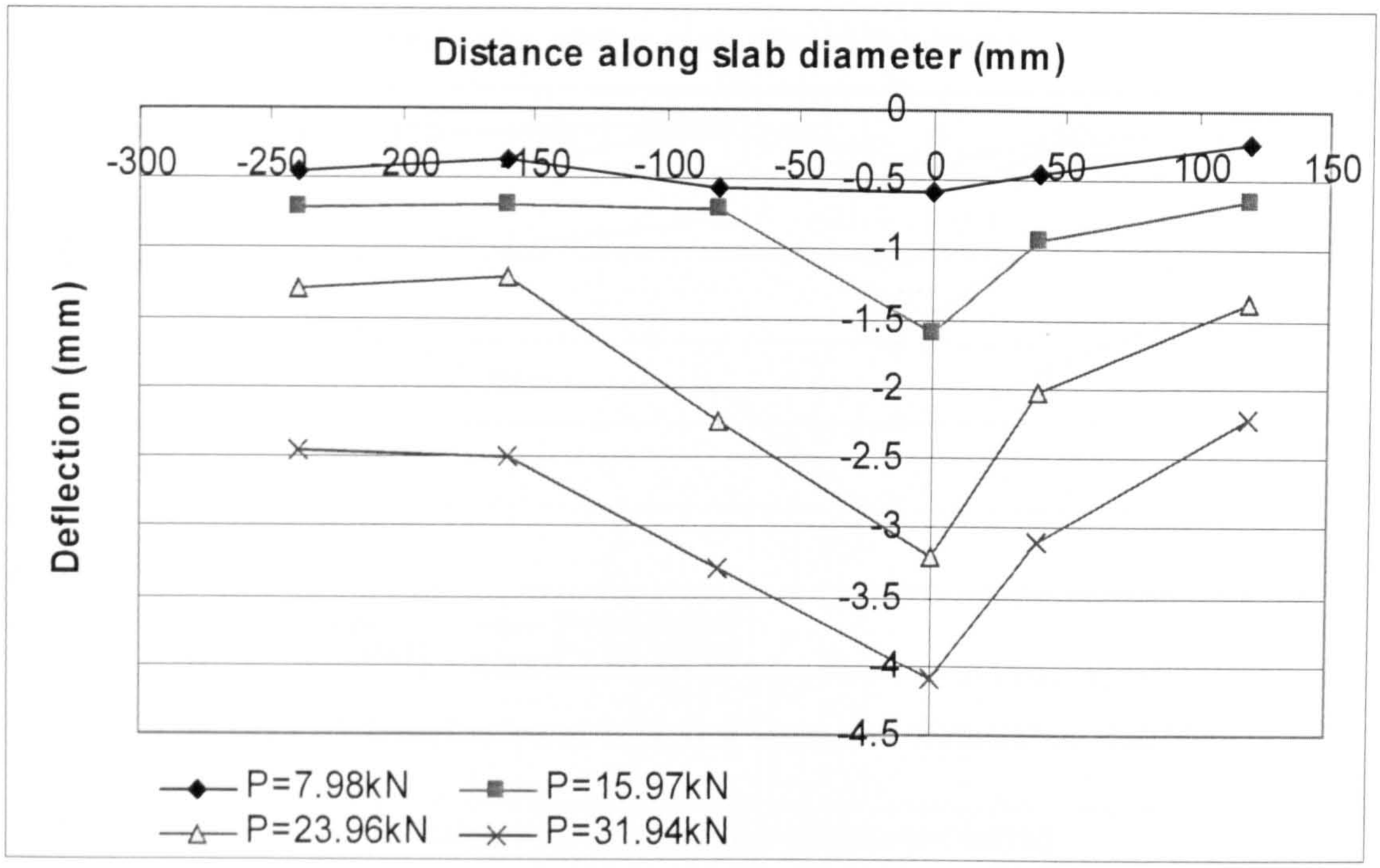

Figure 6.31: Distribution of deflection along slab diameter on slab S5

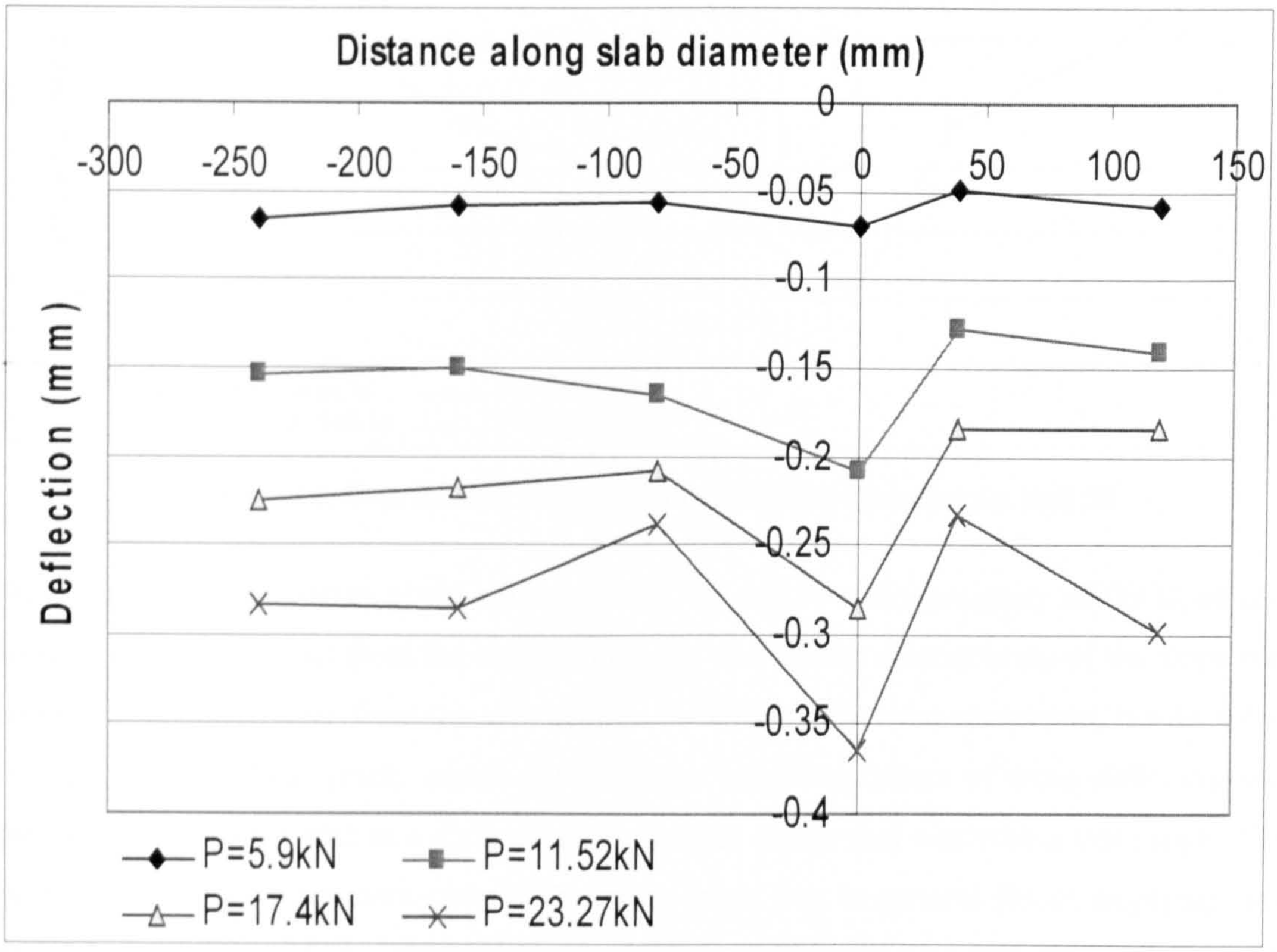

Figure 6.32: Distribution of deflection along slab diameter on slab S6

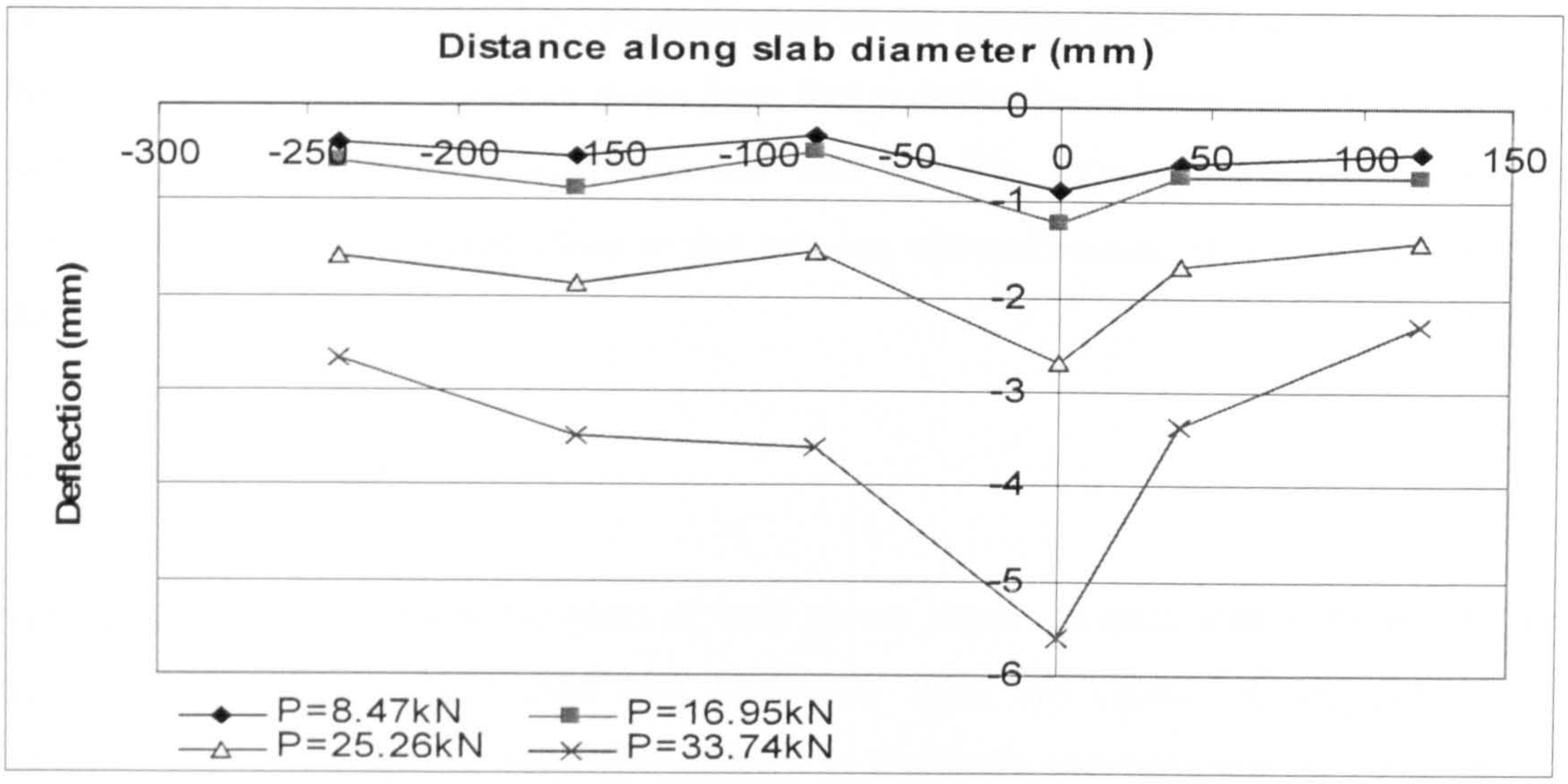

Figure 6.33: Distribution of deflection along slab diameter on slab S7

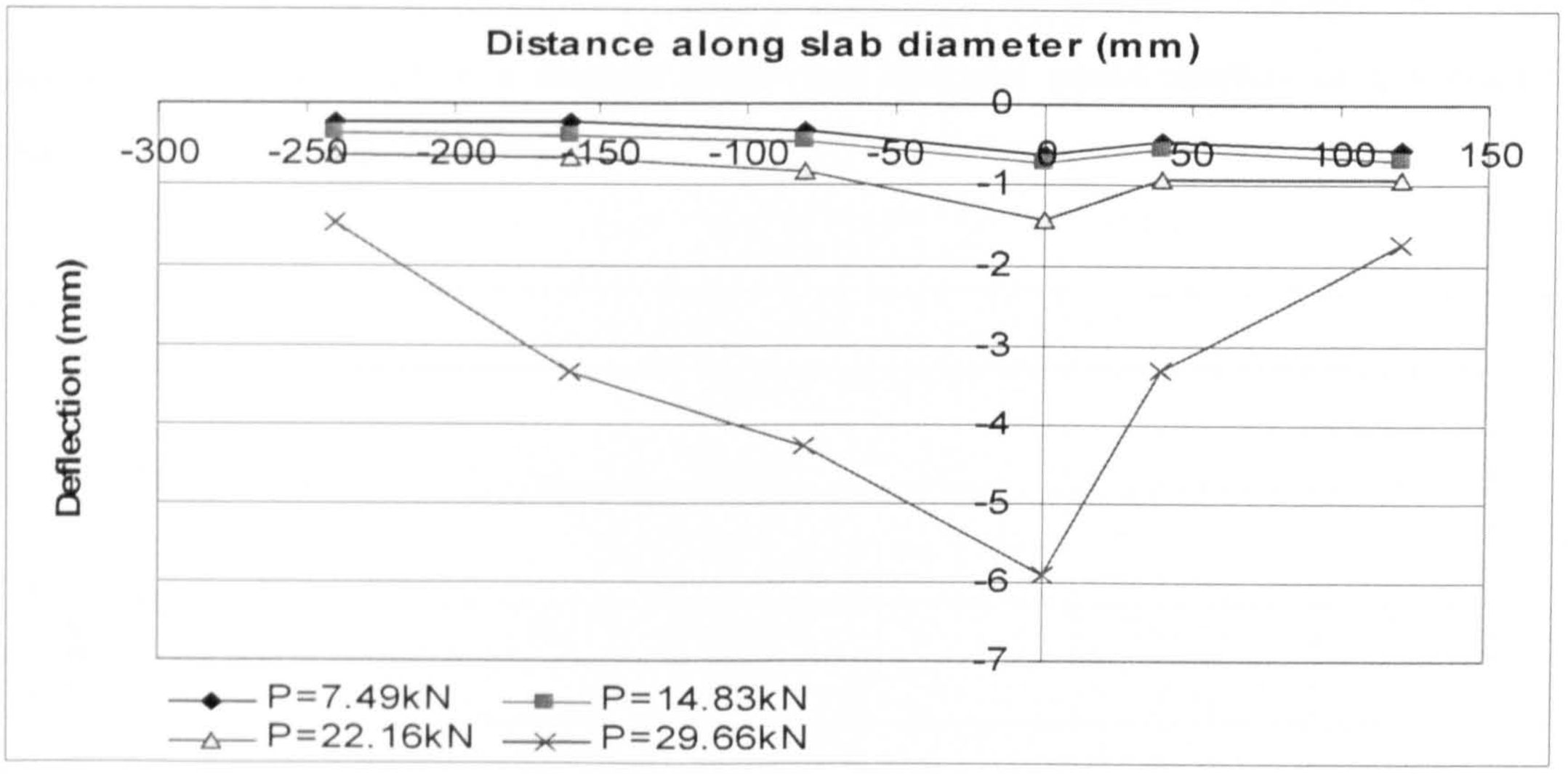

Figure 6.34: Distribution of deflection along slab diameter on slab S8

From the deflection curves of the slabs with S3, S7 and S8 a discontinuity of the slope can be seen at 80 to 160 mm from the slab centre. For slab S5 the discontinuity of the slope can be seen at about 160mm from the slab centre. After the tests were completed, it was noted that the inclined shear crack, which governed the punching failure of these slabs, crossed the top surface of the slab at a distance from the slab centre that was within this range. The distribution of the deflections outside the shear crack was in general linear, implying that the slab portion outside the shear crack rotated as a rigid body. The deflections of slabs S2

and S4 were linear from the slab circumference to the measuring point at 80 mm from the slab centre, followed by a steeper slope from that point to the column circumference. This implies that a crack, which divided the slab into a rigidly rotating portion and a portion within the crack, was located close to the column circumference. This was also verified after the tests.

6.7.2 Concrete Strains

Figures 6.35 to 6.42 present the plots of load versus strains in each slab at three different distances (i.e. 65 mm, 125 mm and 200 mm) from the centre of the slab. As is demonstrated in the figures, very little change in the strain measurement of concrete was recorded and that the strains were approximately in proportion to the load applied before any cracking in concrete took place. After cracking of the concrete occurred the strains increased with the load at a slightly faster rate and the strain reading at the cracked locations increased significantly.

Figure 6.35a: Distribution of radial strain on slab S1

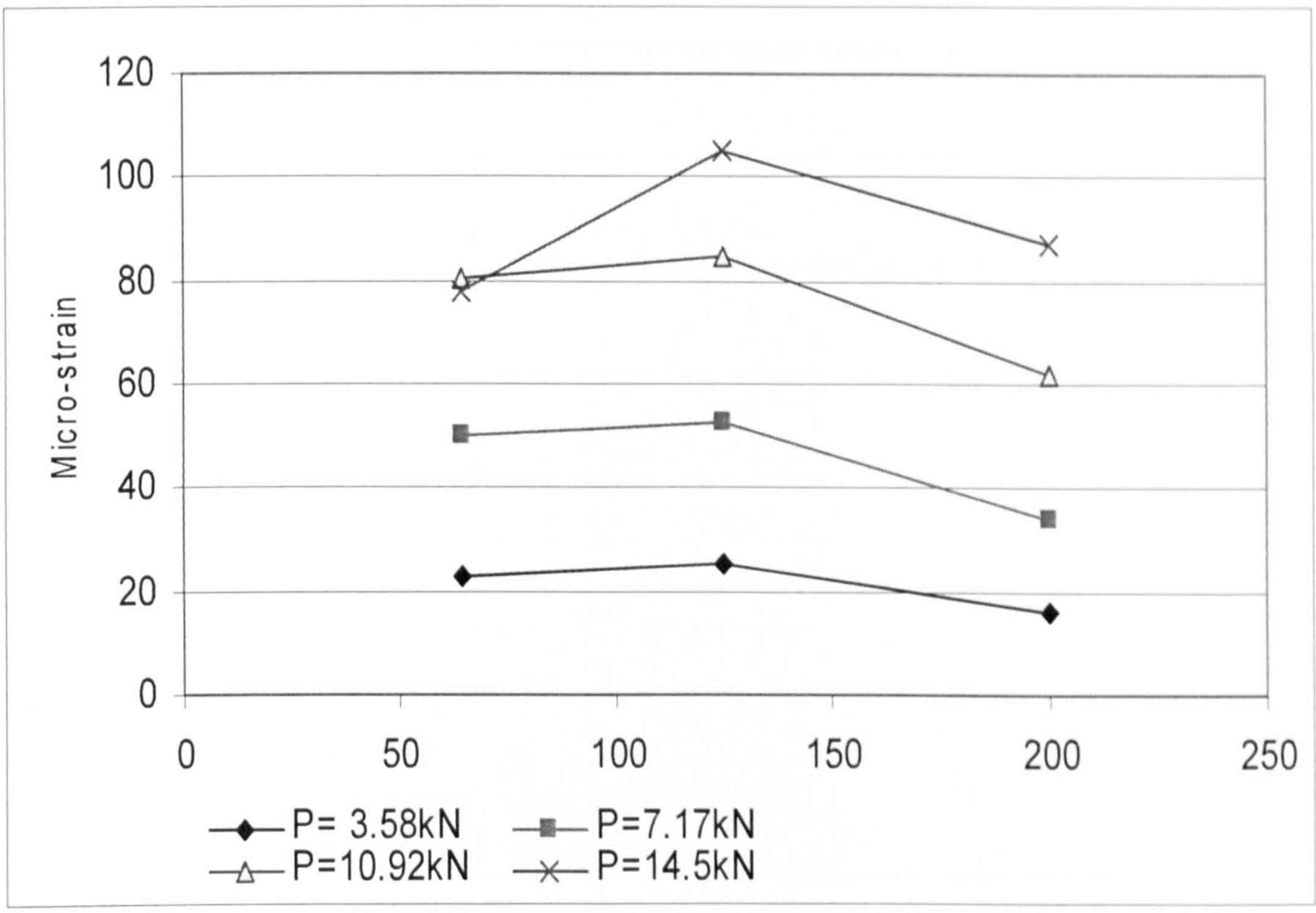

Figure 6.35b: Distribution of tangential strain on slab S1

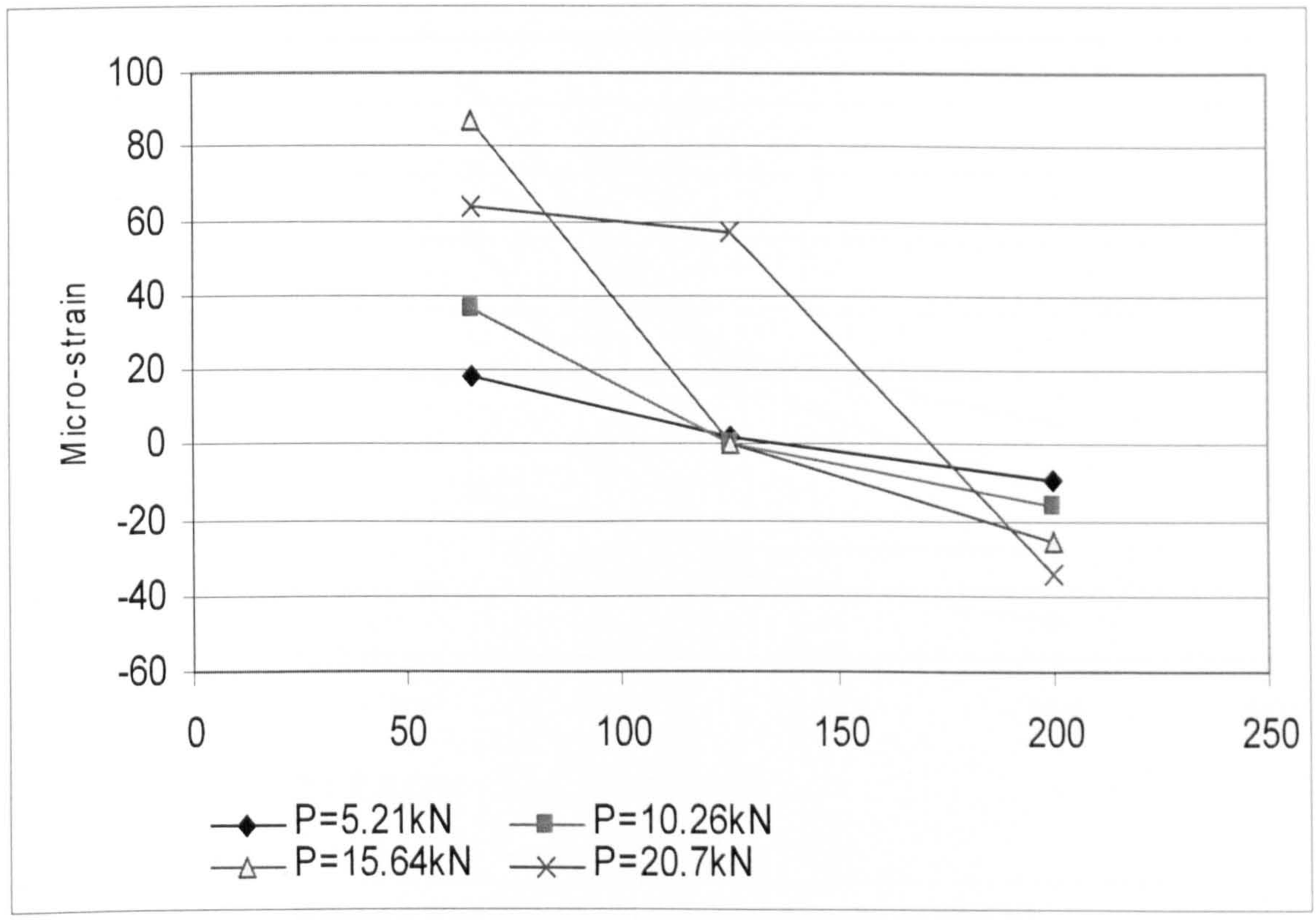

Figure 6.36a: Distribution of radial strain on slab S2

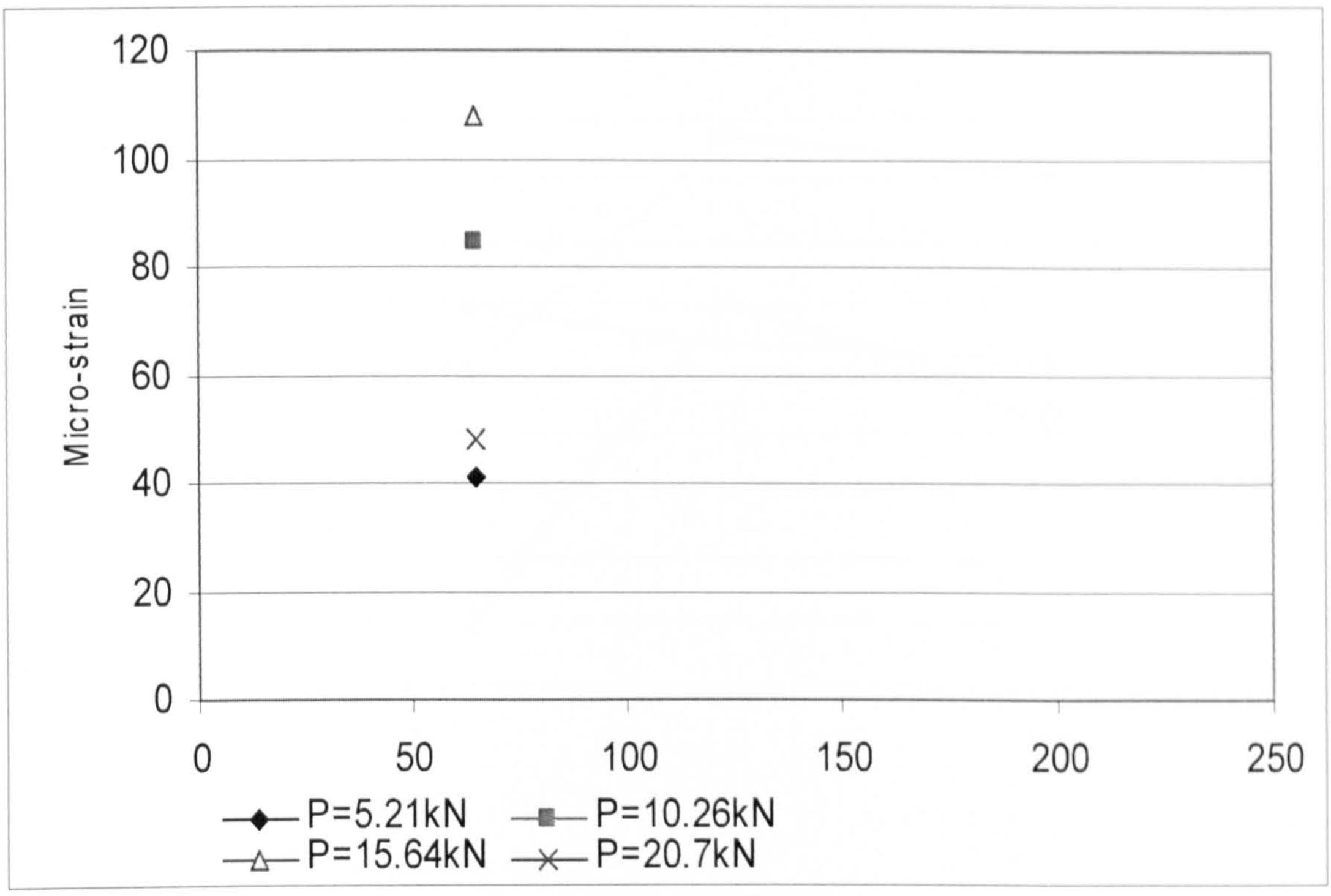

Figure 6.36b: Distribution of tangential strain on slab S2

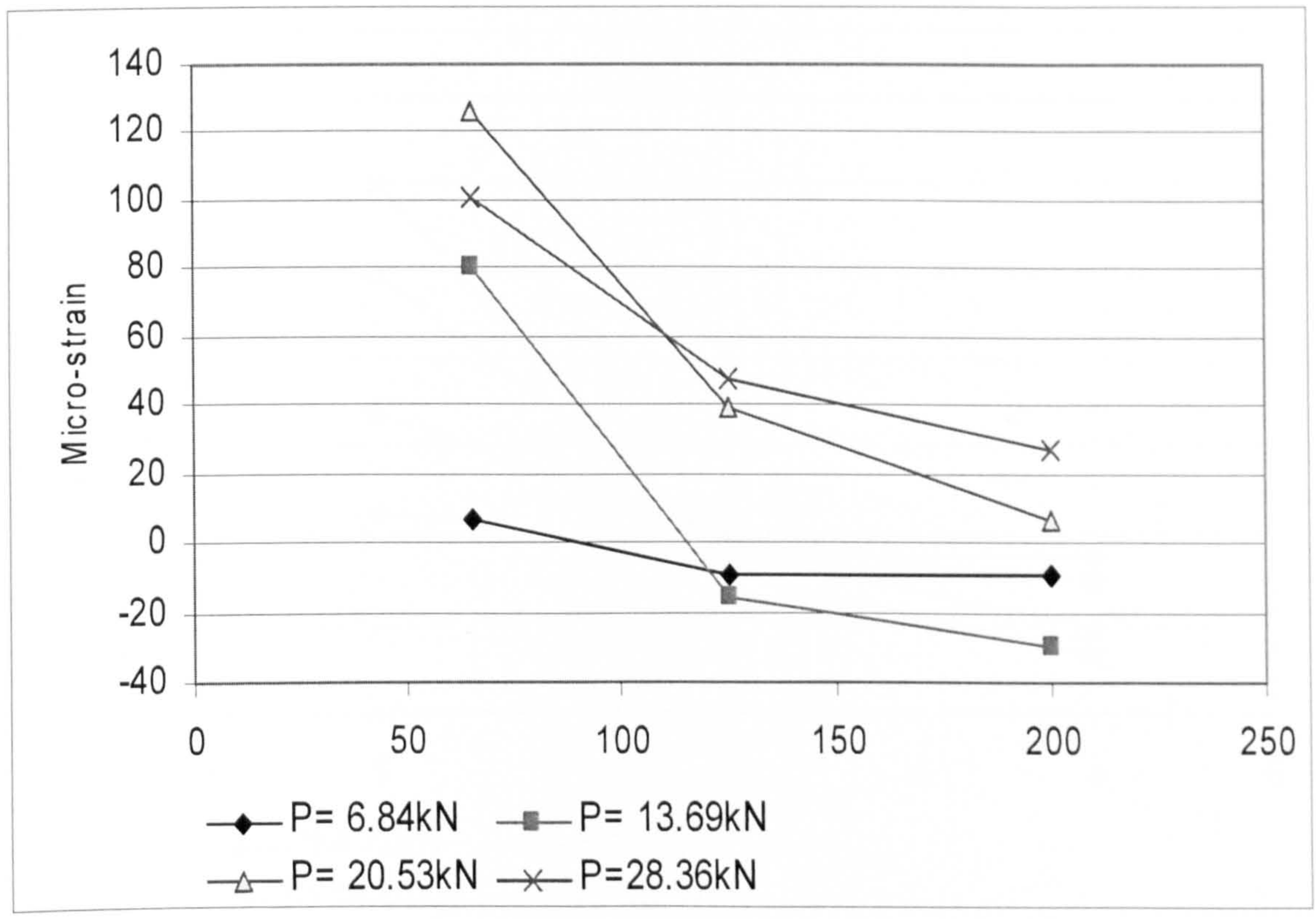

Figure 6.37a: Distribution of radial strain on slab S3

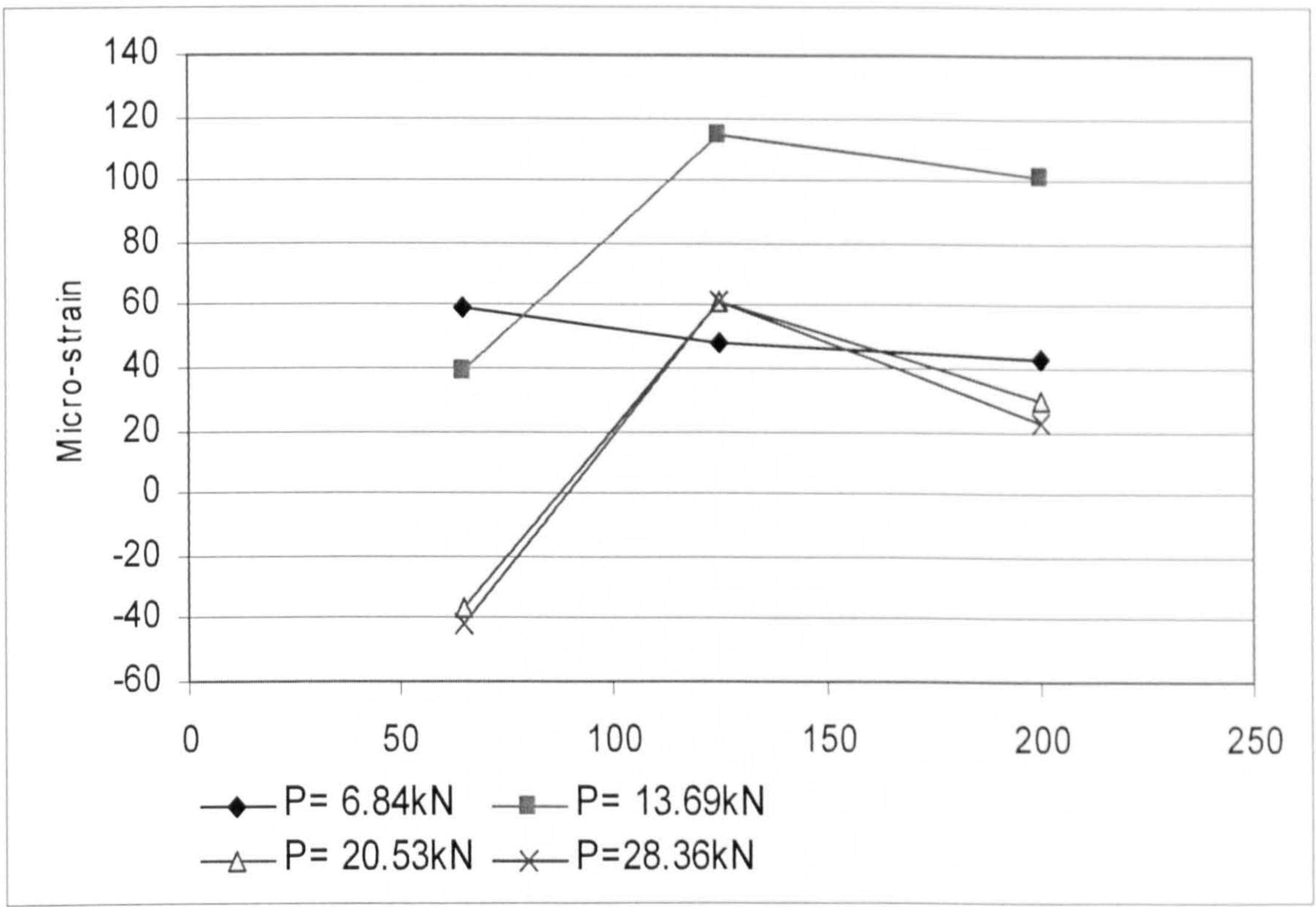

Figure 6.37b: Distribution of tangential strain on slab S3

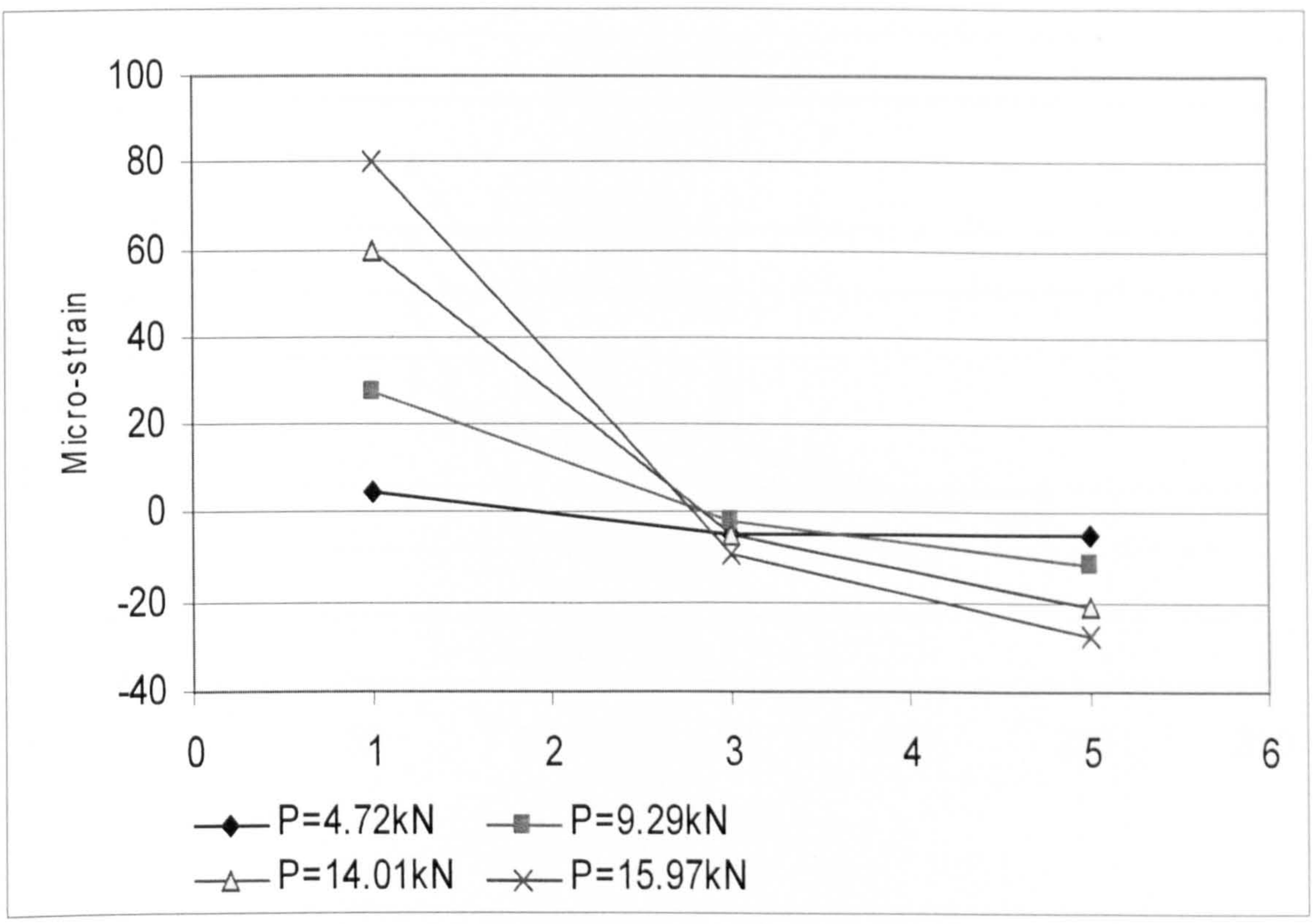

Figure 6.38a: Distribution of radial strain on slab S4

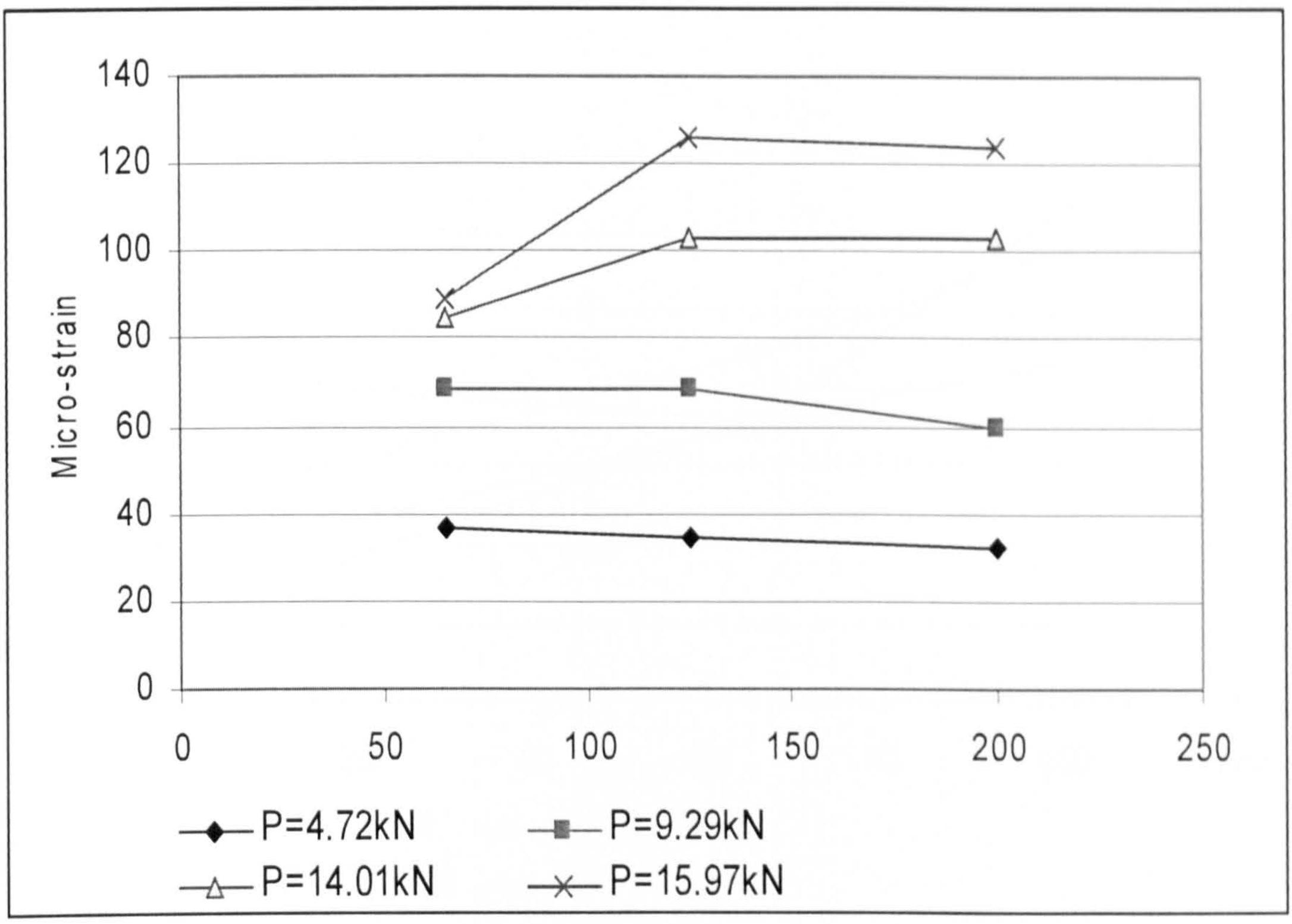

Figure 6.38b: Distribution of tangential strain on slab S4

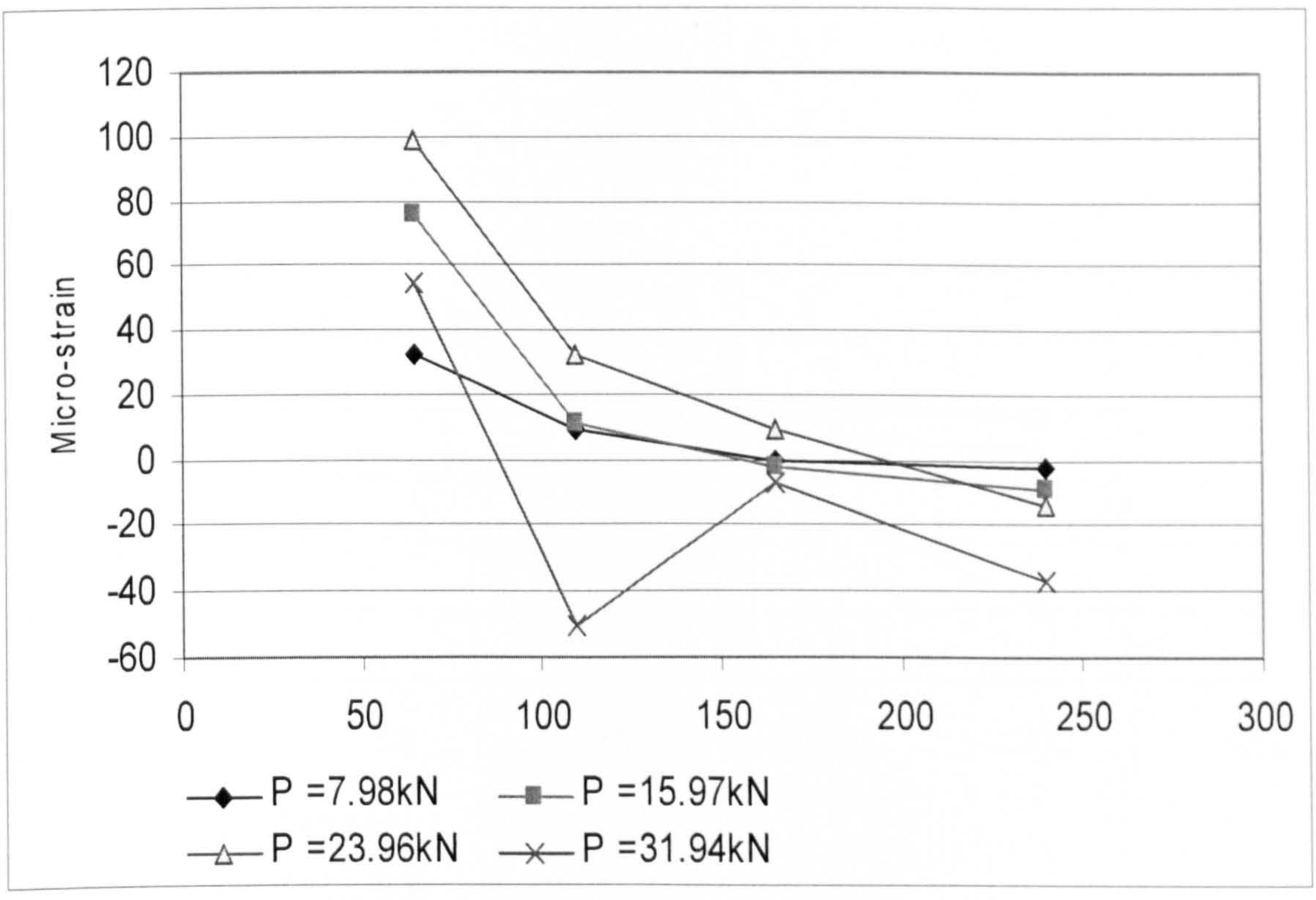

Figure 6.39a: Distribution of radial strain on slab S5

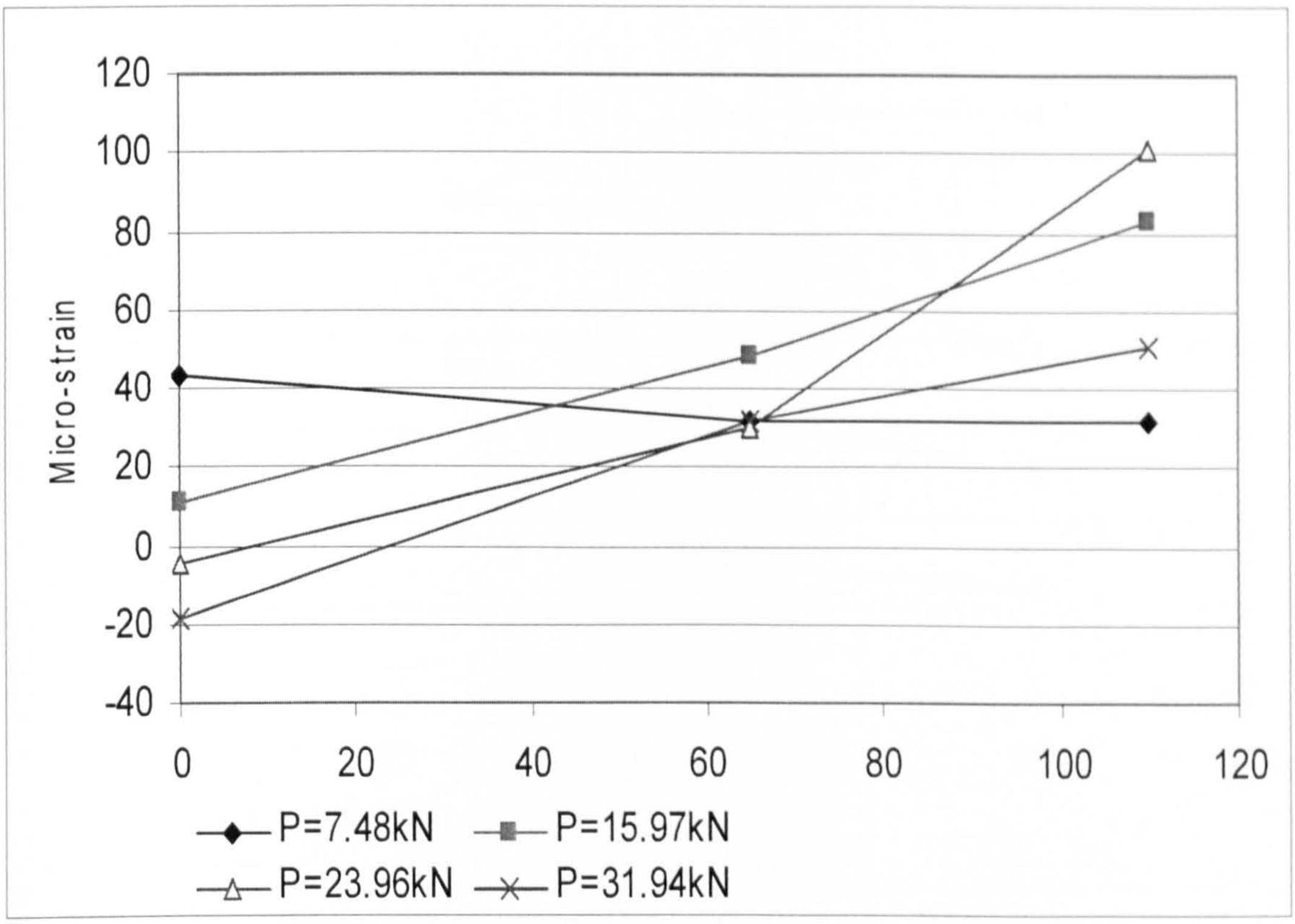

Figure 6.39b: Distribution of tangential strain on slab S5

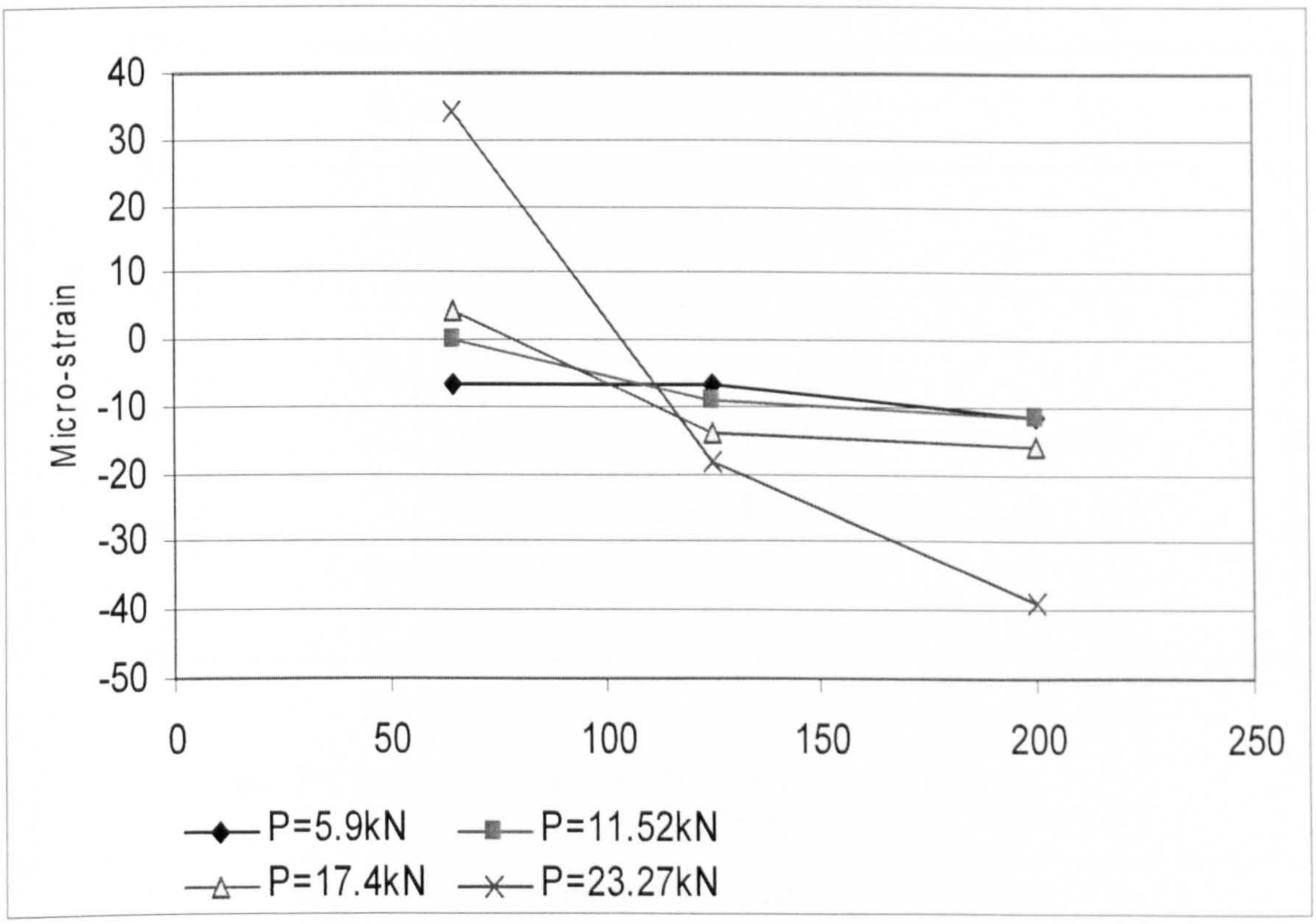

Figure 6.40a: Distribution of radial strain on slab S6

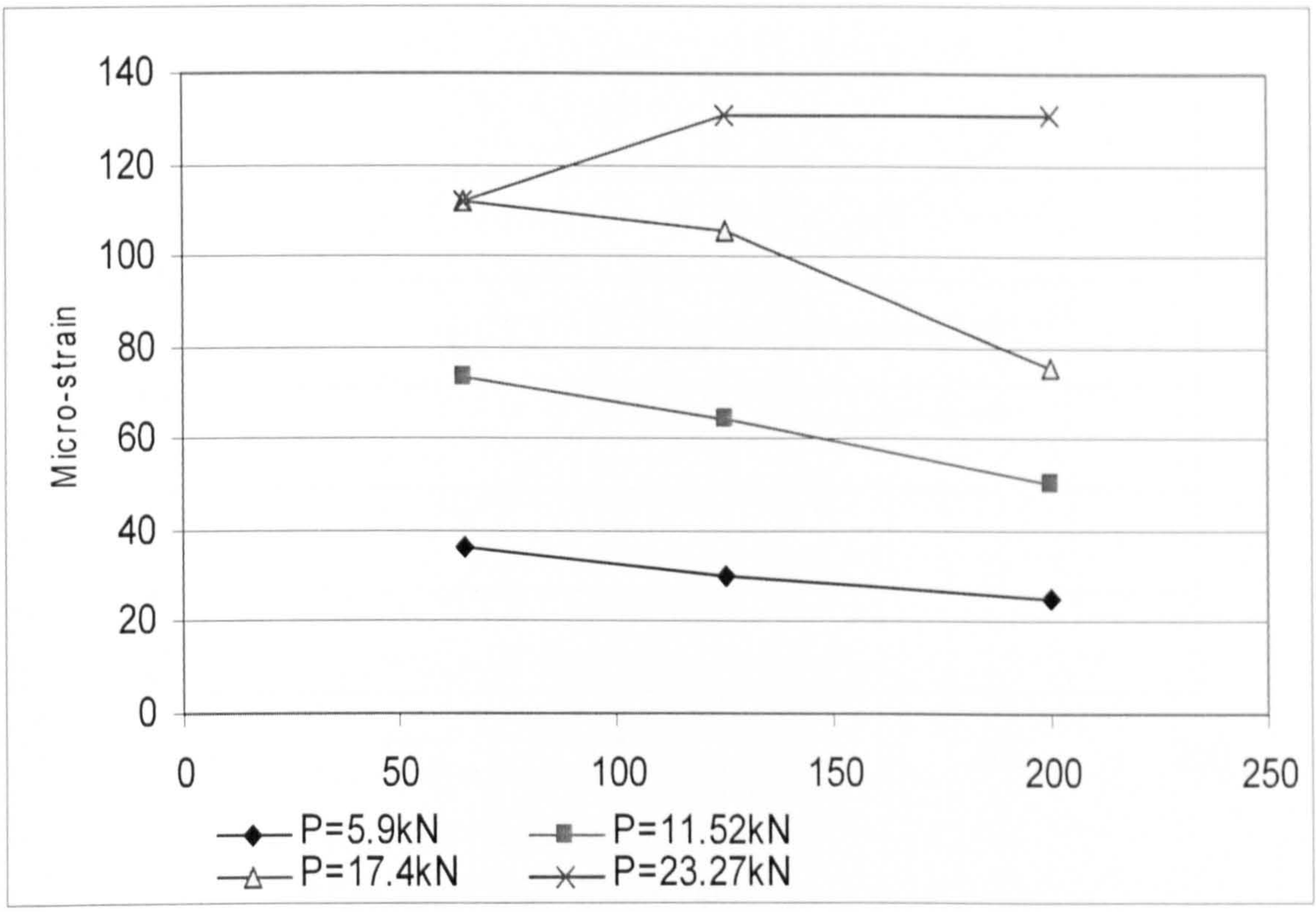

Figure 6.40b: Distribution of tangential strain on slab S6

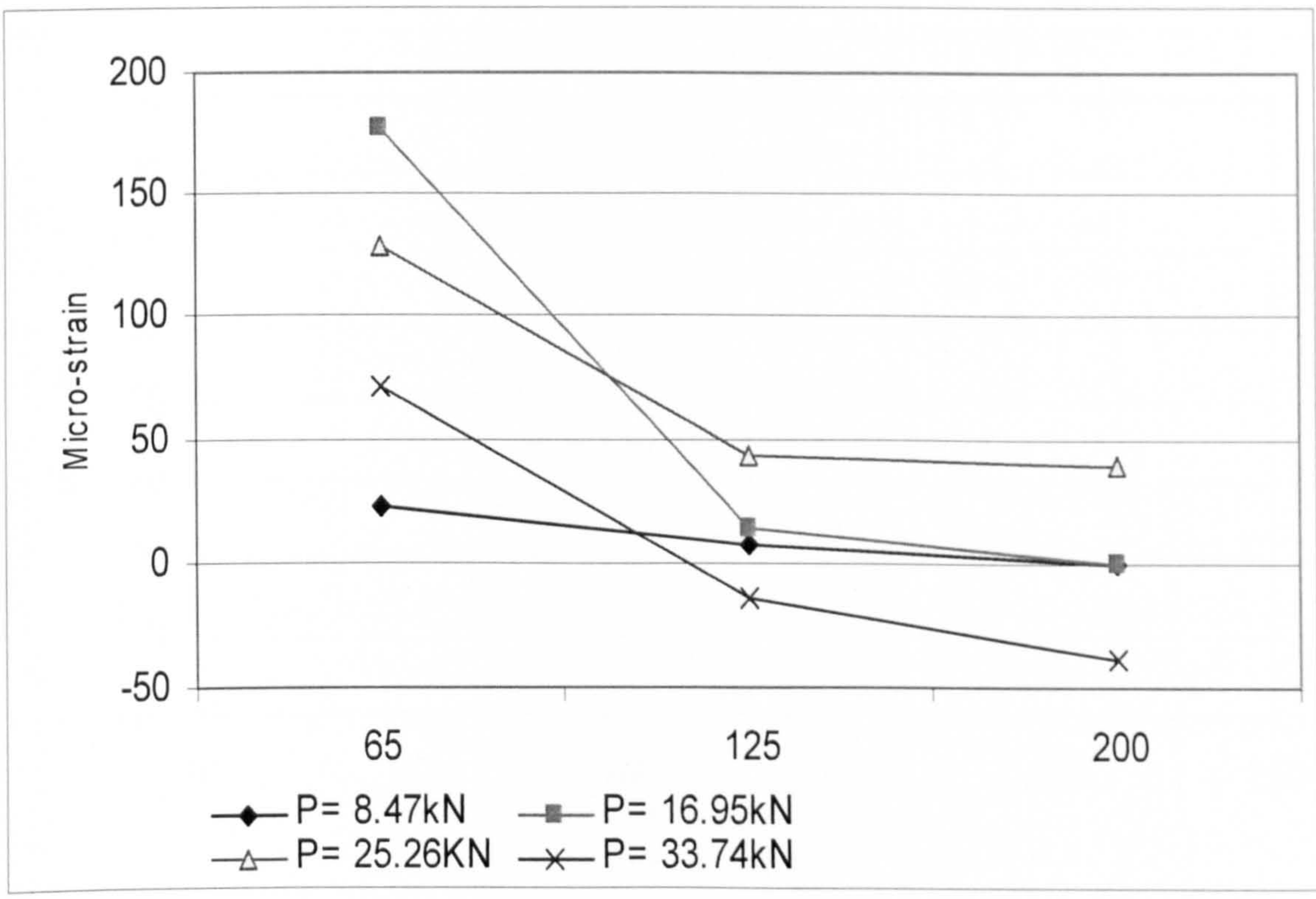

Figure 6.41a: Distribution of radial strain on slab S7

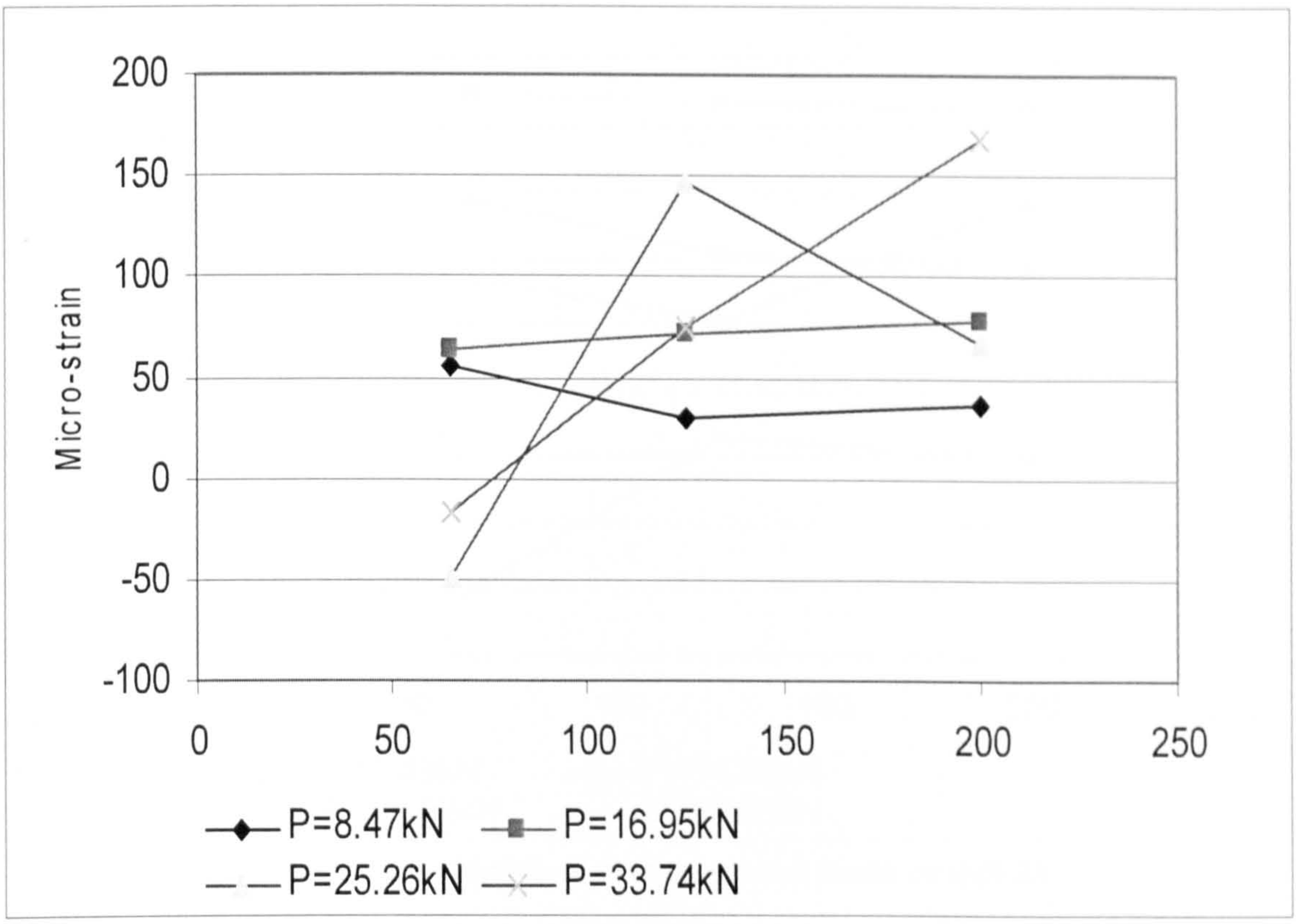

Figure 6.41b: Distribution of tangential strain on slab S7

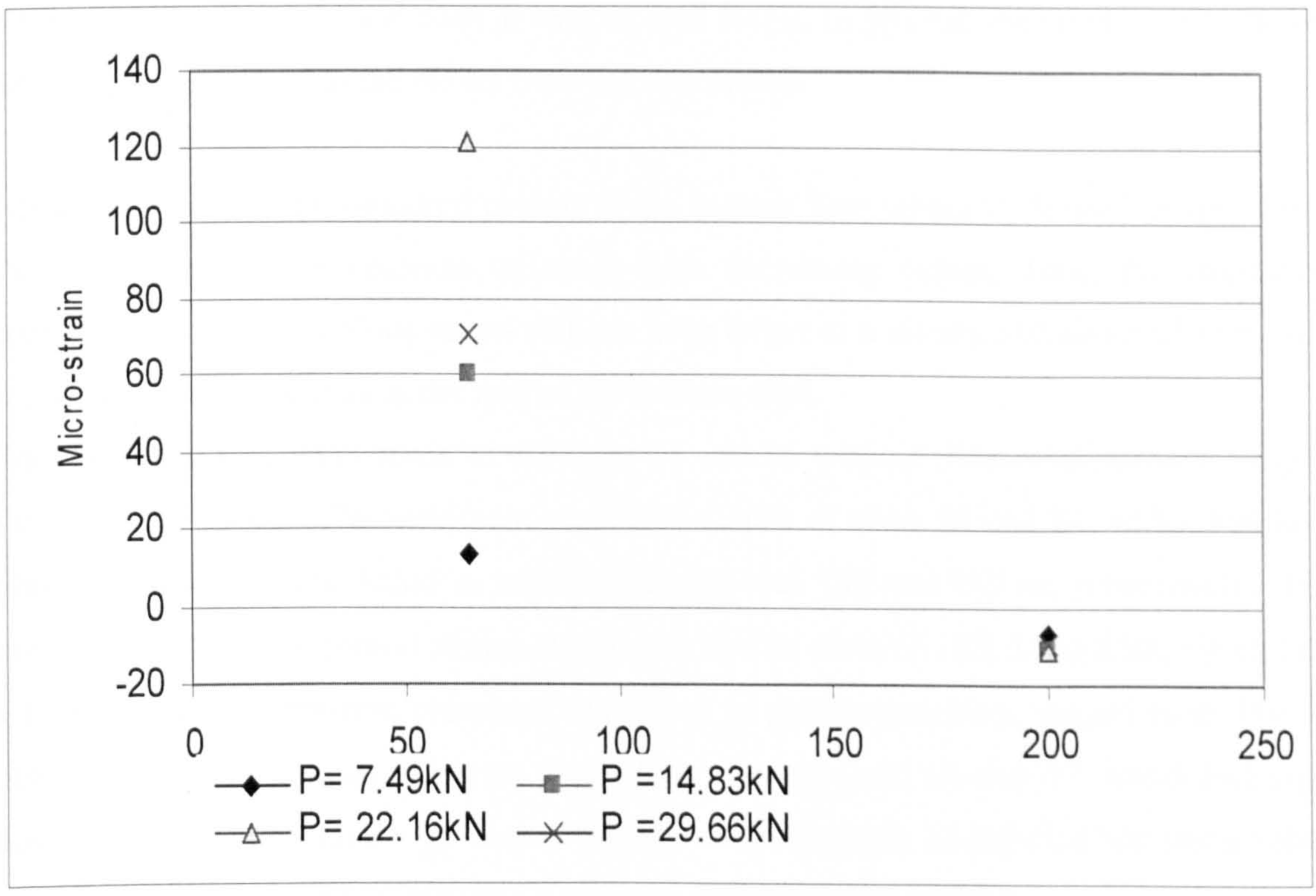

Figure 6.42a: Distribution of radial strain on slab S8

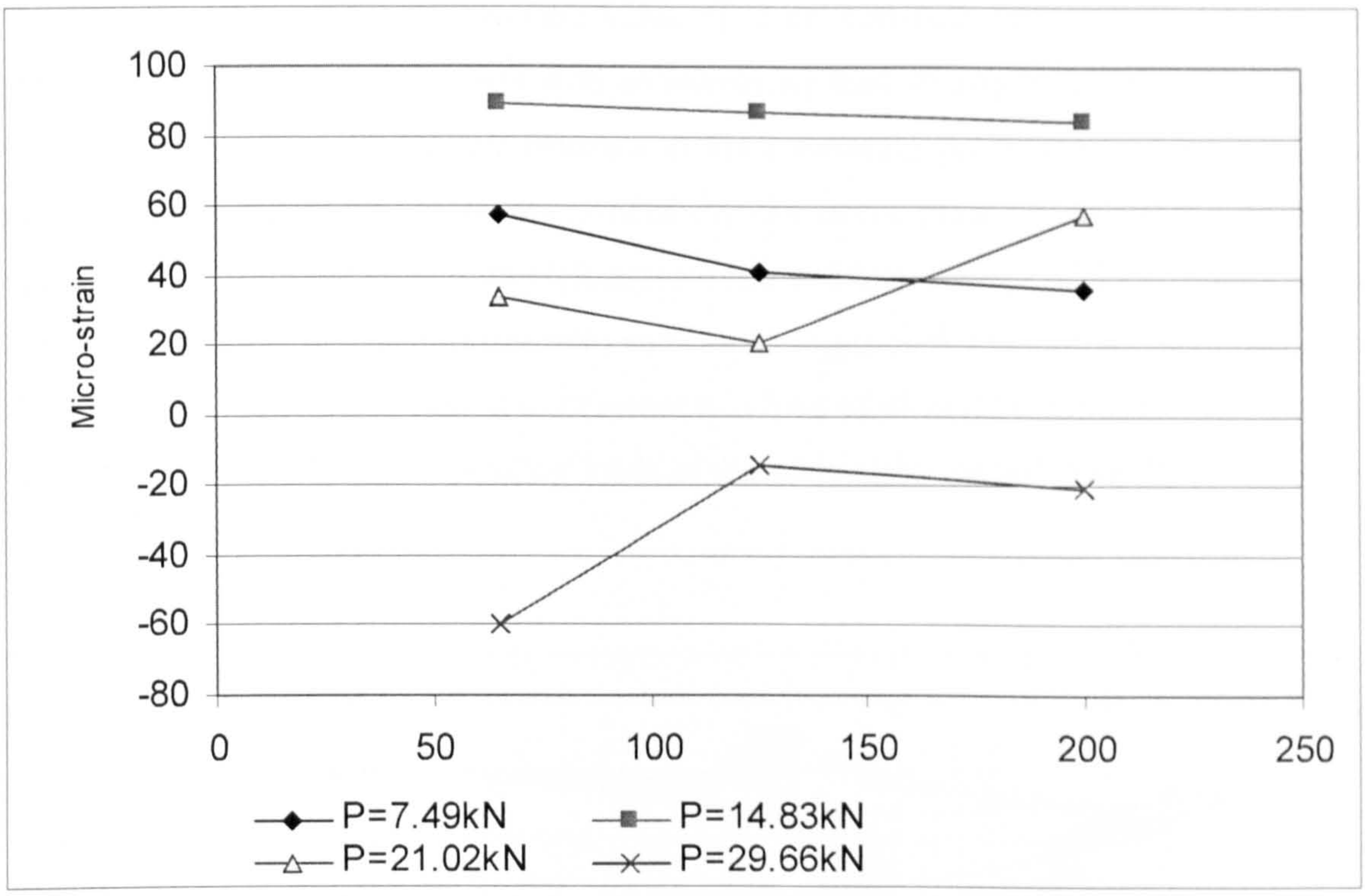

Figure 6.42b: Distribution of tangential strain on slab S8

Figures 6.35 to 6.42 show the distribution of measured radial and tangential concrete strains on the bottom surface of the slabs at various load levels. In general, the strain appears to be inversely proportional to the radius from the slab centre.

For all slabs the strain measured closest to the column face seems to deviate sharply from the trend, implying a decrease of strain with decreasing radius. Thus, the tangential concrete strain in these slabs seems to have been larger at a distance of about 85 mm (1d) from the column face than at the root of the column stub.

The maximum tangential strain of the slabs S1 and S6 without fibre reinforcement ranged from 119 to 135 με. The maximum tangential strains of slabs S2 and S4, which had low fibre-reinforcement and failed in brittle-punching, was 188 and 137 με, respectively. On the other hand, the tangential strains at ultimate load of slabs S3, S5, S7 and S8, which had a high dosage of fibre-reinforcement and failed in ductile-punching, ranged from 144 to 288 με. The lowest strain value for these slabs was measured on slab S7, which had high dosage of ZP30/.50 with a high concrete compressive strength, and the highest strain value was measured on slab S8, which had high fibre dosage of RC65/60BN.

As shown in Figure 6.43, the absolute value of radial concrete strain of all slabs, except slabs S1 and S6, started to decrease with an increasing load shortly before the ultimate load was reached. This means that the concrete at the measuring point was compressed in the radial direction before failure. It was noticed that the decompression started at a relatively higher load level for the slabs with high aspect ratio and high dosage of fibre-reinforcement than for the slabs with lower aspect ratio and low dosages of fibre-reinforcement. For slabs S5 and S8, the radial strain started to decrease at a load of 98 and 96 percent of the ultimate load, respectively. The corresponding loads of the other slabs ranged from 78 to 85 percent of the ultimate load.

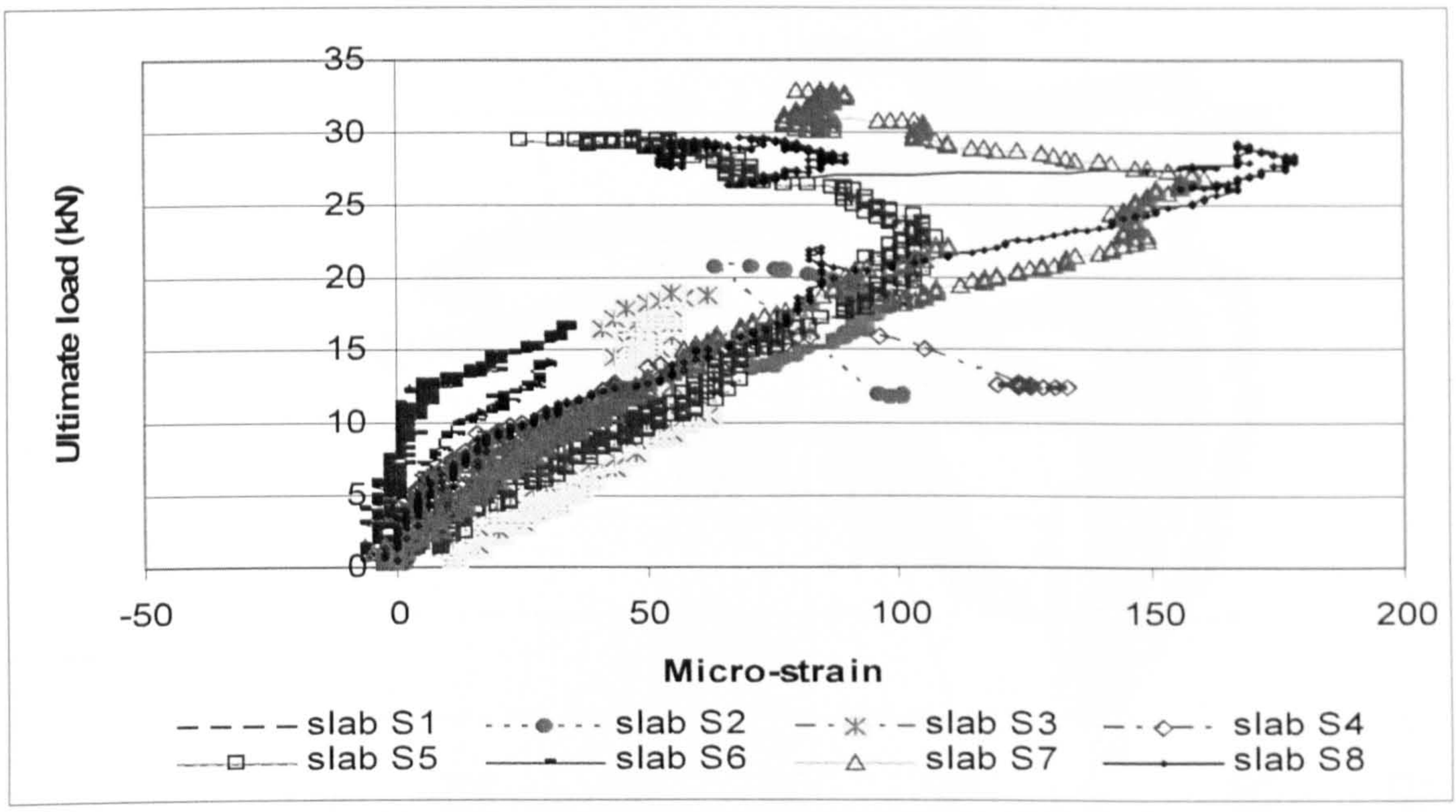

Figure 6.43: Distribution of radial strain

The radial strain at ultimate load ranged from 39 to 29 με for the slabs S1 and S6 without fibre-reinforcement. For slabs S2 and S4, the radial strains at ultimate load were 64 and 80 με, respectively. The radial strain at ultimate load of slabs S3, S5, S7 and S8 ranged from 55 and 100 με respectively.

Figure 6.44 to 6.46 show the tangential strains, at about 85 mm from the column face (125 mm from centre of slab), measured on the bottom surface of the slabs in relation to the load. The measured strains were also used to approximate tensile and flexural cracking loads of the concrete slabs and to further explain the difference in fracture behaviour

between the plain and fibre-reinforced concrete slabs. The unloading strain responses for slabs S1 and S6 of the plain concrete were different to those for the slabs with fibre-reinforcement. The plain concrete unloaded rapidly before becoming unstable, while fibre-reinforced slabs unloaded gradually before they became unstable, which suggested that the steel fibre continued to redistribute the stresses while cracking propagated upward, with slabs with higher fibre dosage exhibiting more stress redistribution.

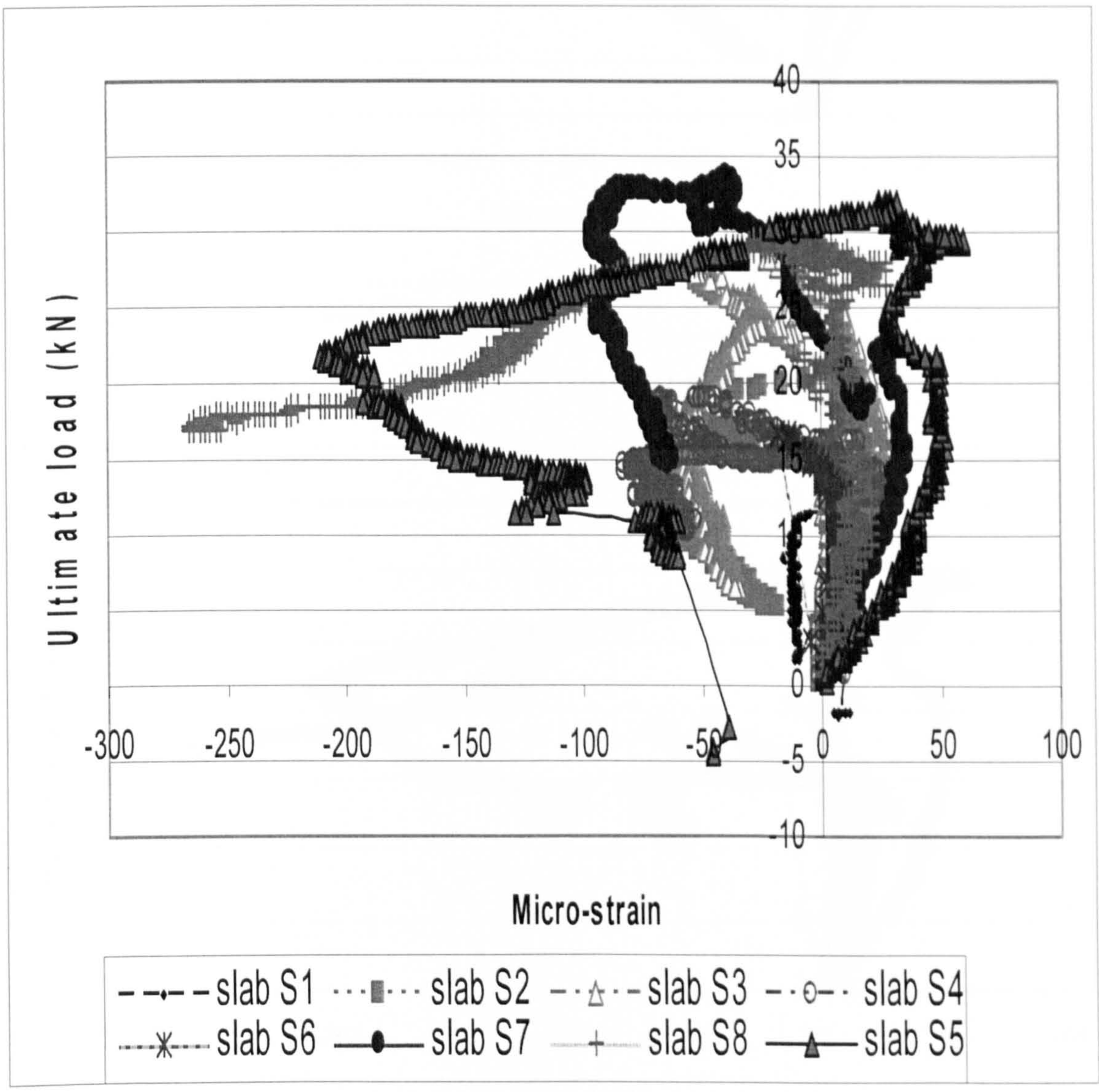

Figure 6.44: Distribution of tangential strain

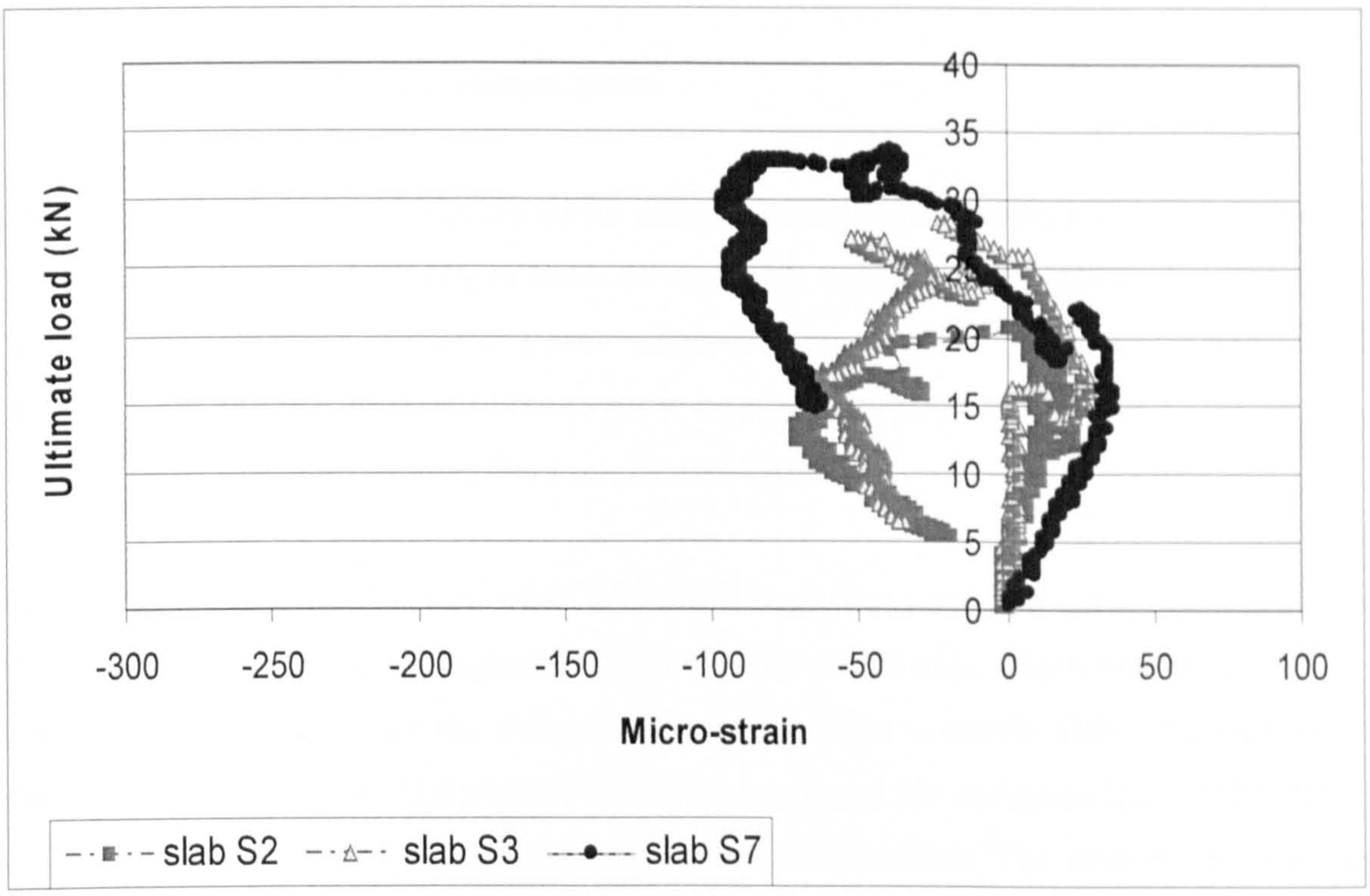

Figure 6.45: Distribution of tangential strain (ZP30/.50)

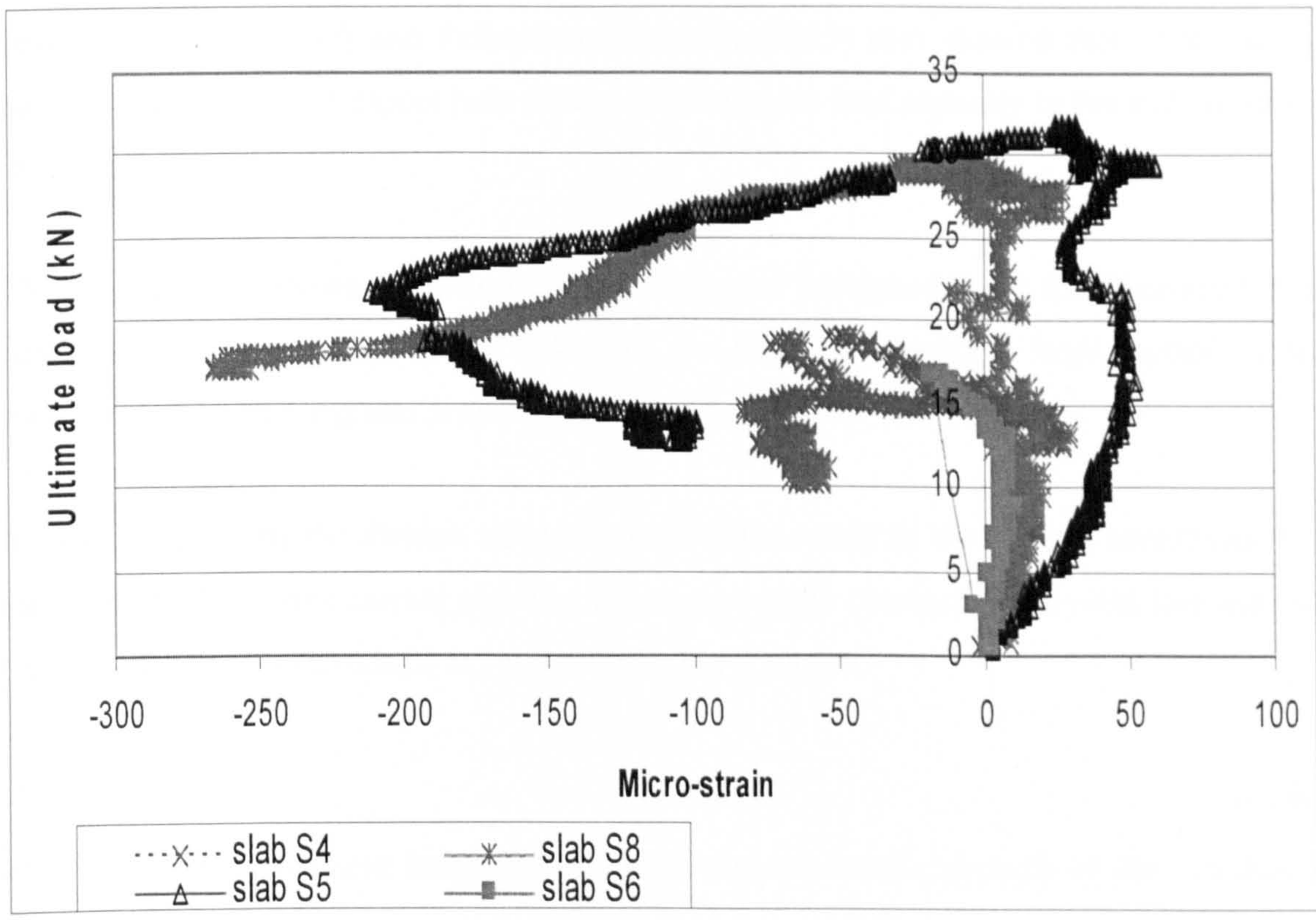

Figure 6.46:Distribution of tangential strain (RC65/60BN)

6.7.3 Ultimate Strength of Concrete Slabs

The ultimate load-carrying capacity of the slabs was defined as the peak load level attained. Table 6.4 summarises the collapse loads of each slab tested. In the plain concrete slab, the ultimate load-carrying capacity never exceeded the second flexural cracking load. However, the addition of steel fibres to plain concrete increased the ultimate load-carrying capacity of the concrete slabs by between 22 and 130%.

Slab S5 which contains 40kg/m^3 of RC65/60 BN steel fibres and had concrete compressive strength of 38.63 kN had the highest collapse load of (33.74 kN), which was more than two times (220 %) greater than the collapse load of the plain concrete slab. The addition of 20kg/m^3 of ZP30/.50 and RC65/60BN steel fibre increased the collapsed load of the slab by 43% and 32% respectively, compared to the plain concrete slab. The steel fibres increased the ultimate load-carrying capacity of the concrete slab which was similar to the results published by Beckett (1990) and Falkner and Teutsch (1995) for similar fibre types and dosages. Beckett (1990) and Falkner and Teutsch (1995) also showed that fibre quality, quantity, geometry, and aspect ratio affected the ultimate load capacity of the slab as shown in Table 6.4.

The primary mechanism allowing for an increased collapsed load for fibre-reinforced concrete slabs was related to the ability of the fibres to engage a large portion of the concrete slab in carrying and distributing the load even after cracking.

In order to evaluate the flexure strength of the slabs tested in the current investigation, a yield line analysis was carried out. The flexure strengths obtained from yield line analysis for each slab were determined using the following equation.

$$P_u = 2\pi M \qquad \text{.....6.1}$$

M = the moment per unit length at which the flexure tensile strength of the concrete is reached = $f_{ctk,fl}\left[\frac{h^2}{6}\right]$

Moreover the formula presented in TR34 (2003) and discussed in Chapter two was also implemented for comparison purposes with test results.

Table 6.5: Flexure strength according to yield-line theory

Specimen no.	Ultimate load (kN)	Flexure load (kN)
S1	14.5	21.2
S2	20.7	34.5
S3	28.36	37.9
S4	19.07	39.0
S5	33.74	41.3
S6	23.55	24.7
S7	38.63	53.1
S8	33.08	46.0

The results presented in Table 6.5 show that for all slabs, the flexure strength is greater than the actual failure load indicating that all the tested slabs failed in shear before the flexure strength was exhausted.

6.7.4 Slab Cracking Interpretation

Figures 6.47 to 6.54 show crack patterns on the top and bottom surface of all the tested slabs. The photographs were taken after the tests. It shows in the figures that for slabs with higher dosage of fibres (i.e. 40kg/m^3) the crack pattern of the slab was more intense.

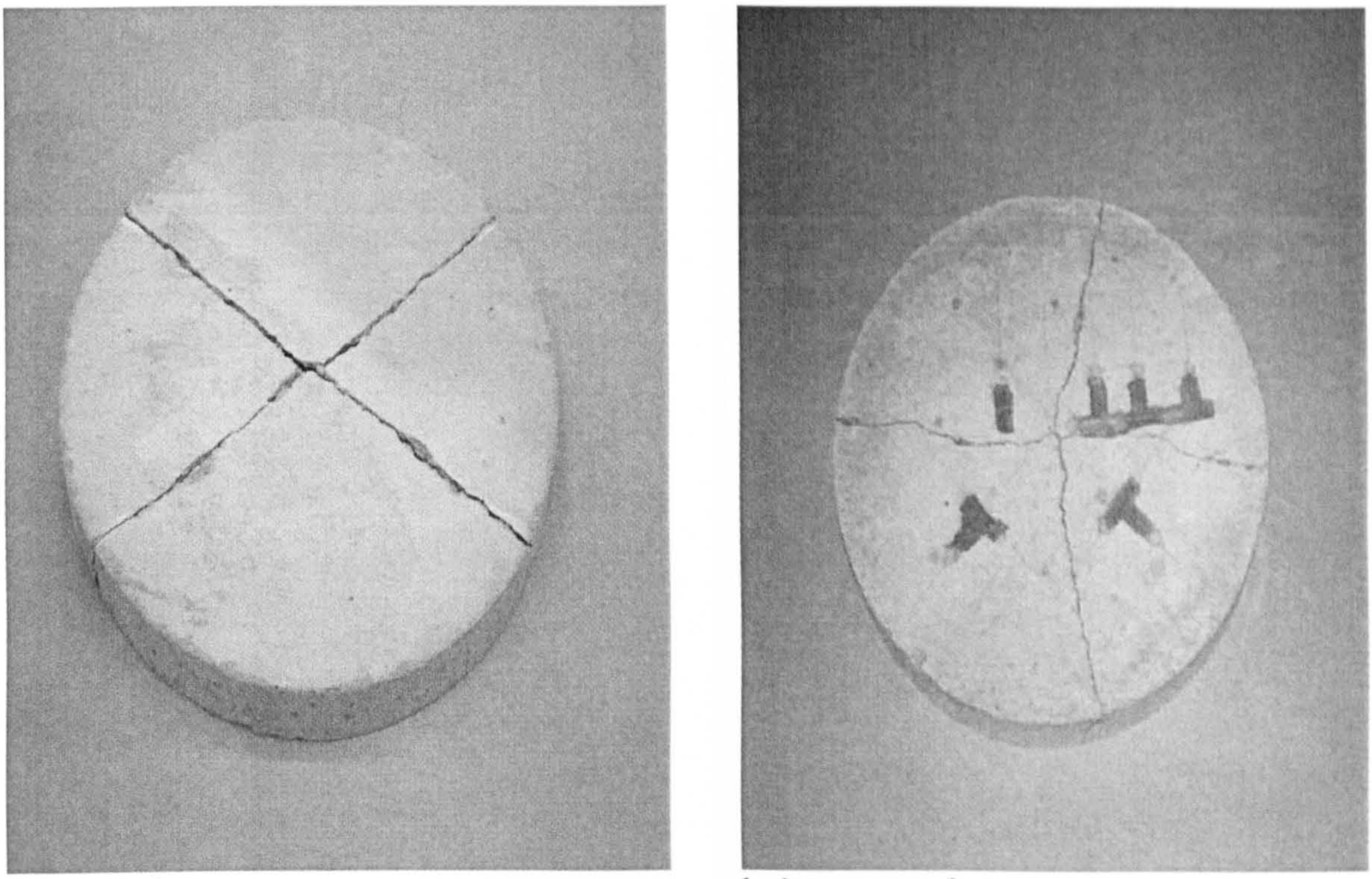

a. top surface b. bottom surface

Figure 6.47: crack patterns of slab S1 (a. top surface and b. bottom surface)

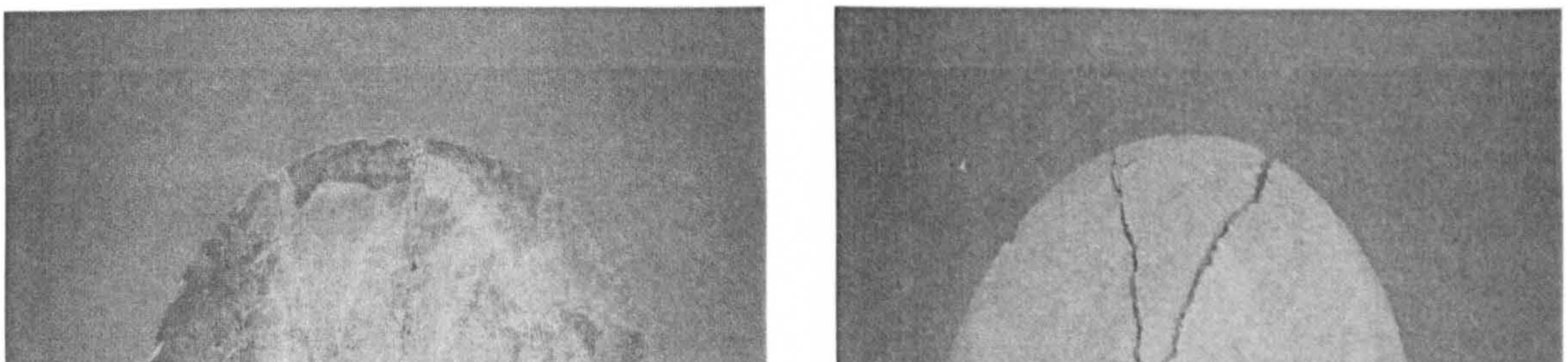

a. top surface b. bottom surface

Figure 6.48: crack patterns of slab S2 (a. top surface and b. bottom surface)

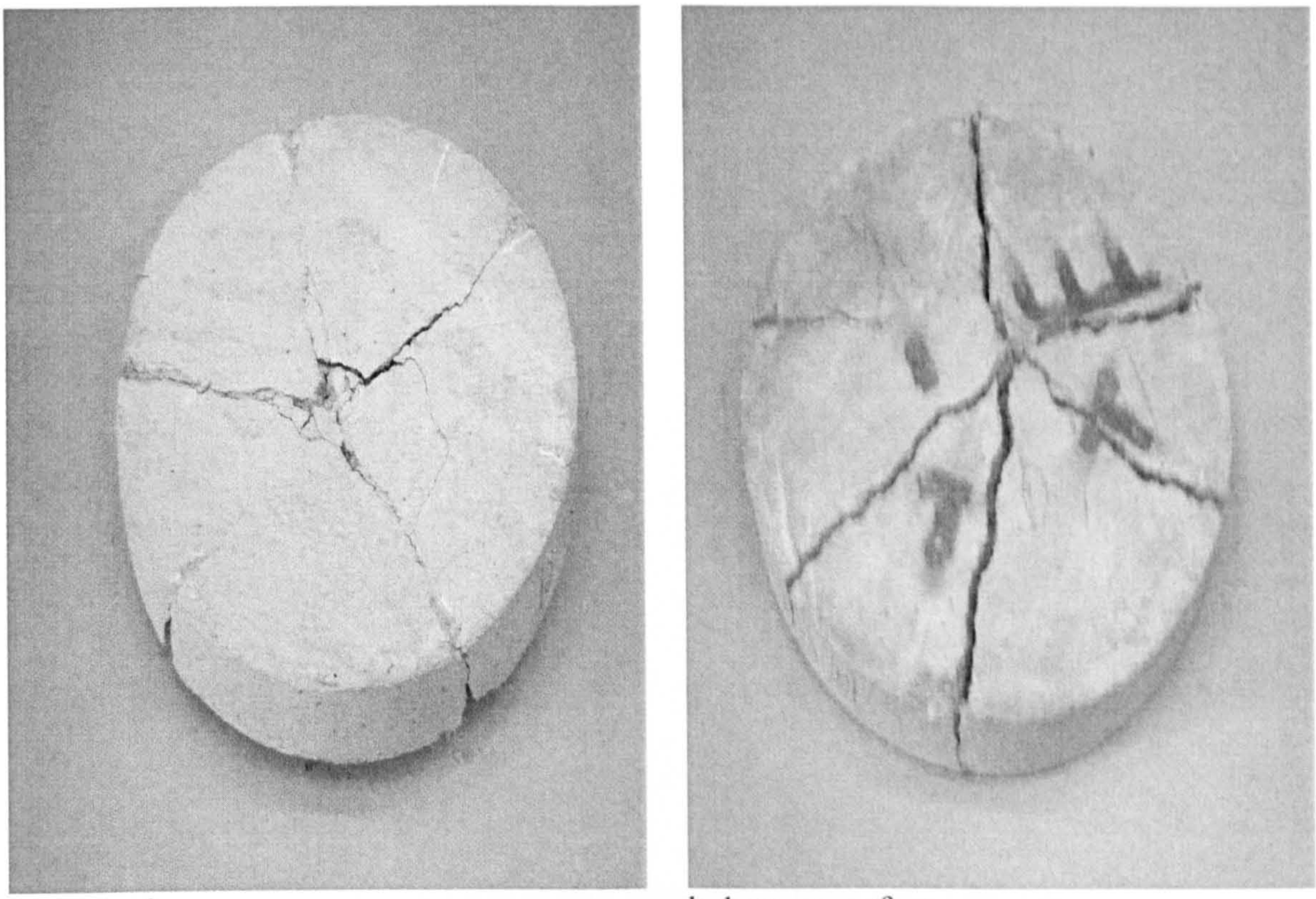

a. top surface b. bottom surface

Figure 6.49: crack patterns of slab S3 (a. top surface and b. bottom surface)

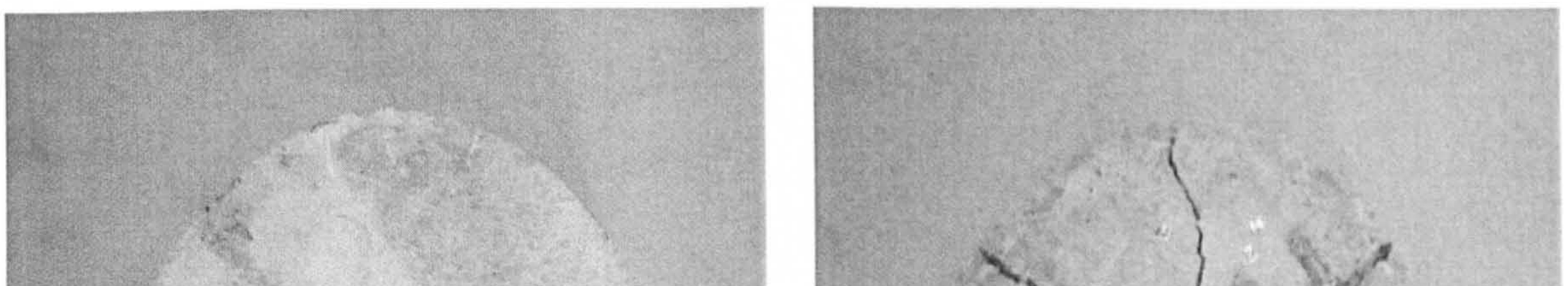

a. top surface b. bottom surface

Figure 6.50: crack patterns of slab S4 (a. top surface and b. bottom surface)

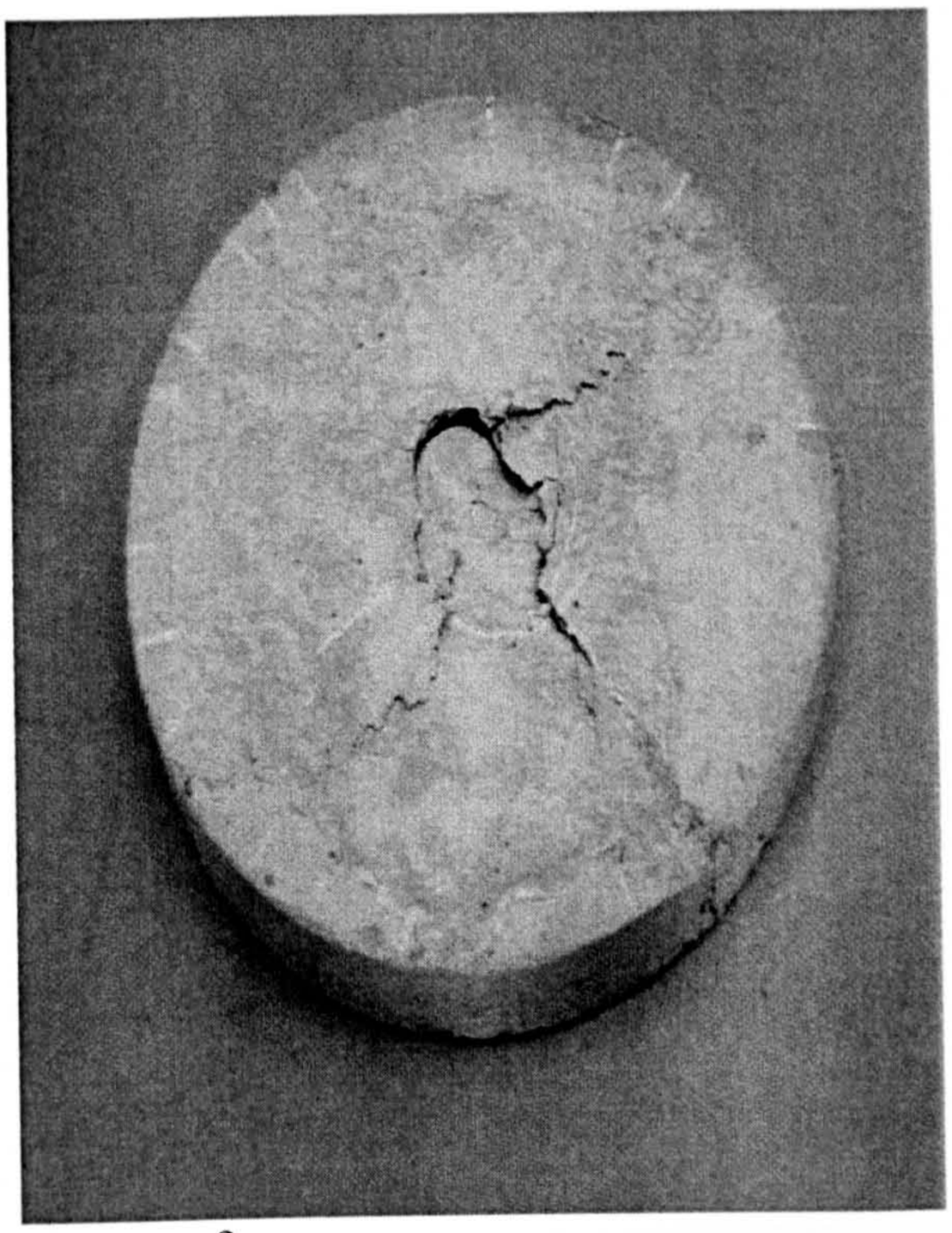

a. top surface

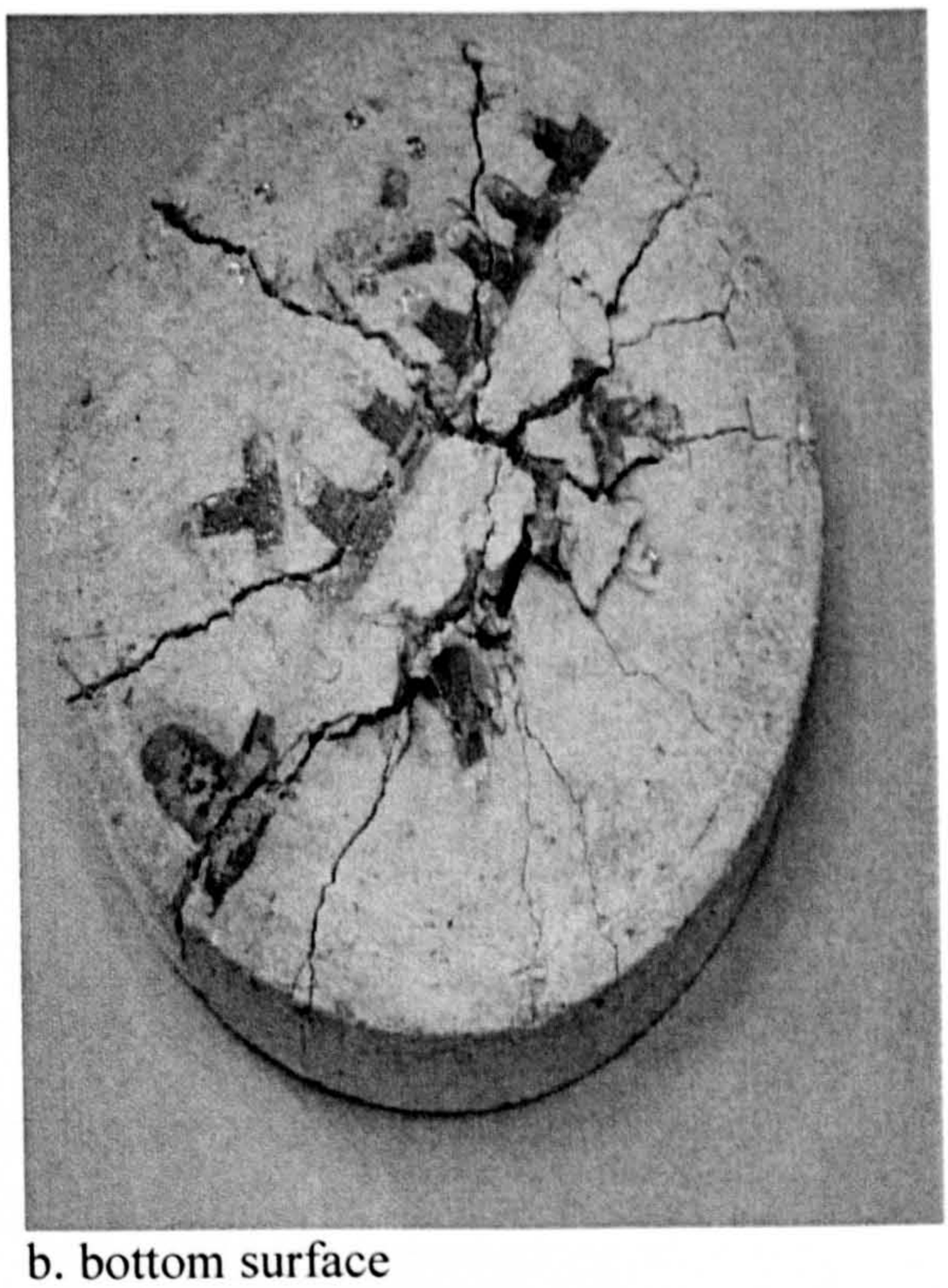

b. bottom surface

Figure 6.51: crack patterns of slab S5 (a. top surface and b. bottom surface)

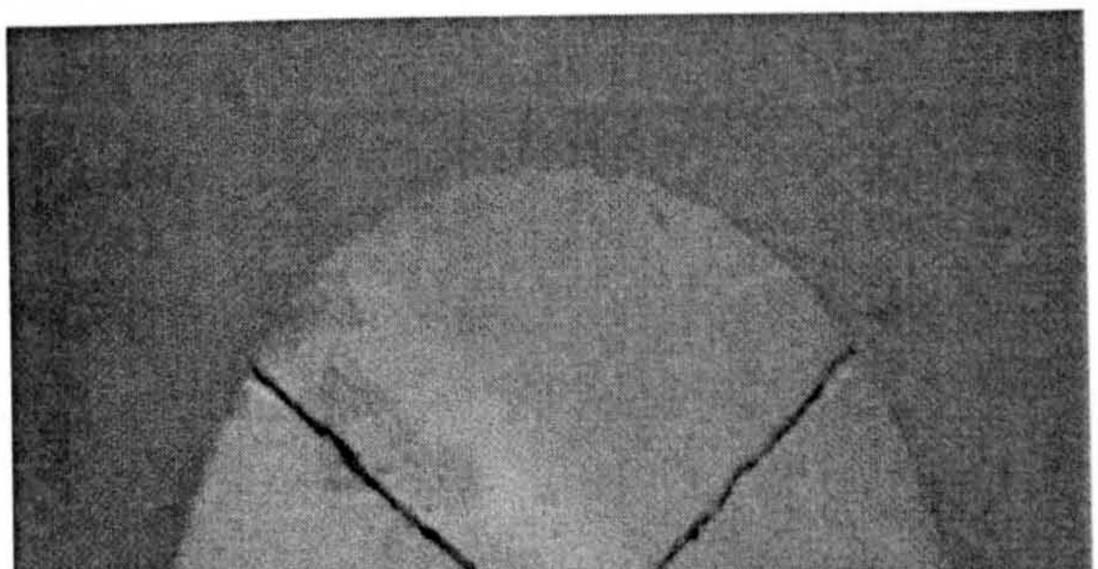

a. top surface

b. bottom surface

Figure 6.52: crack patterns of slab S6 (a. top surface and b. bottom surface)

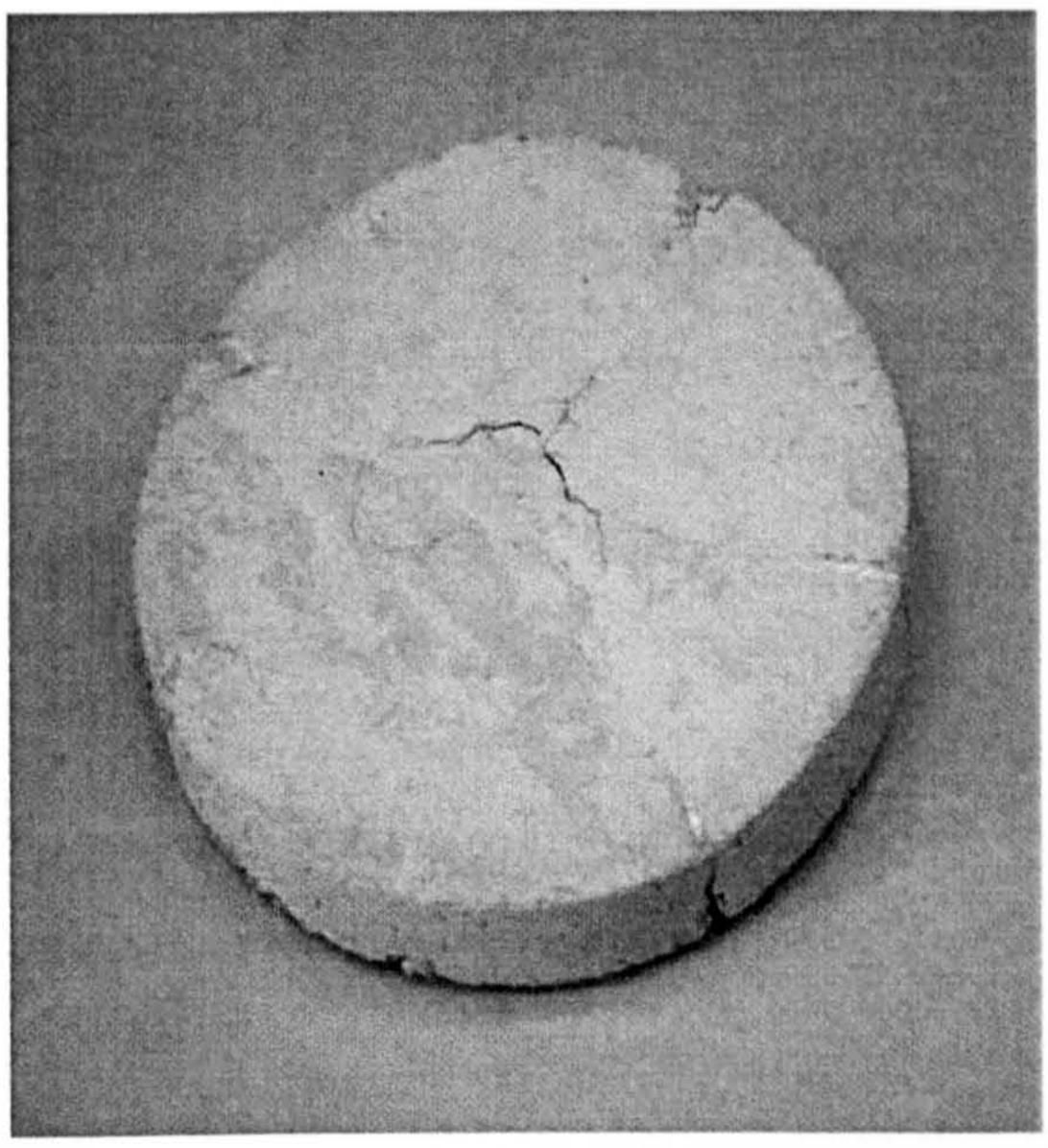

a. top surface

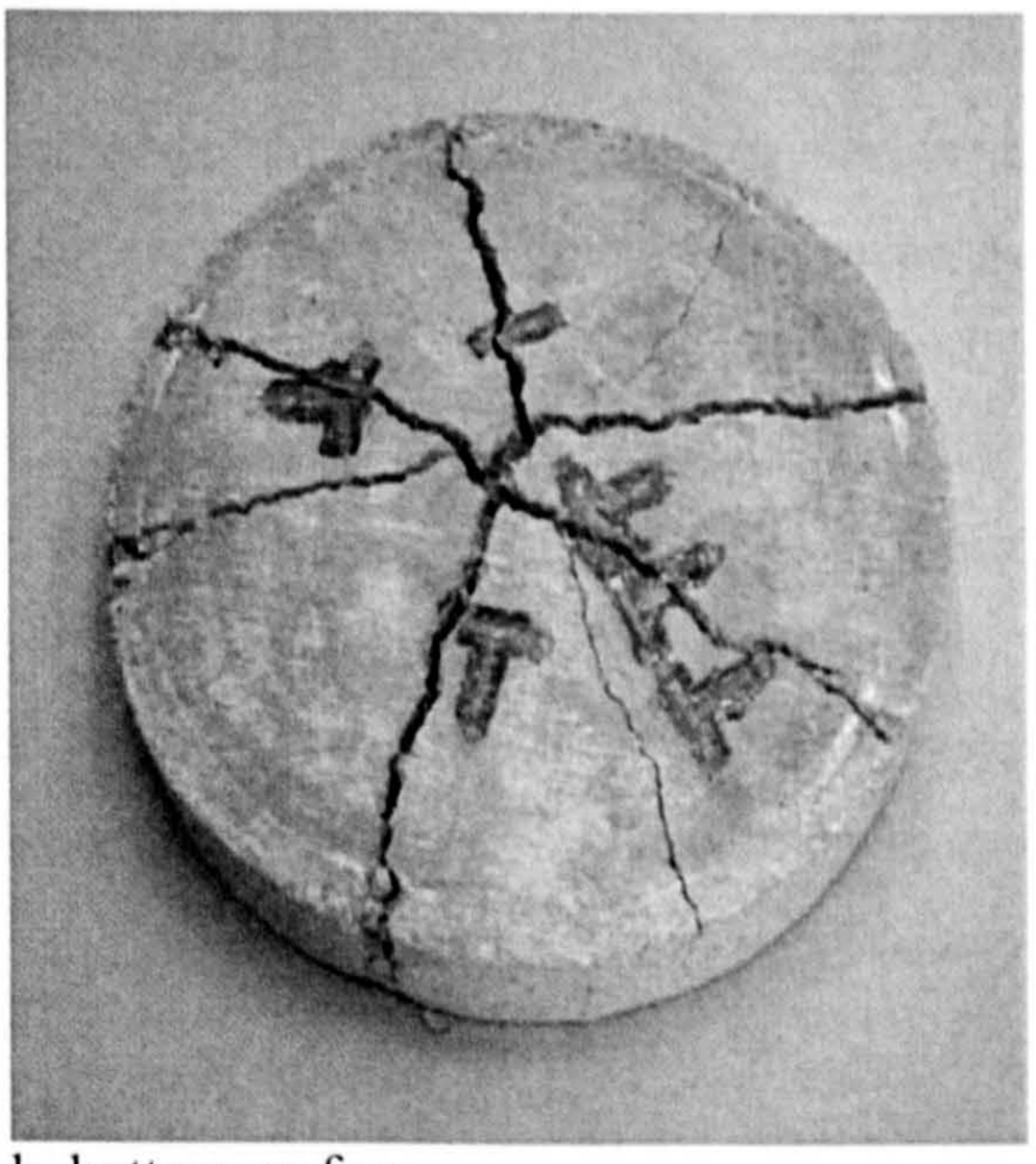

b. bottom surface

Figure 6.53: crack patterns of slab S7 (a. top surface and b. bottom surface)

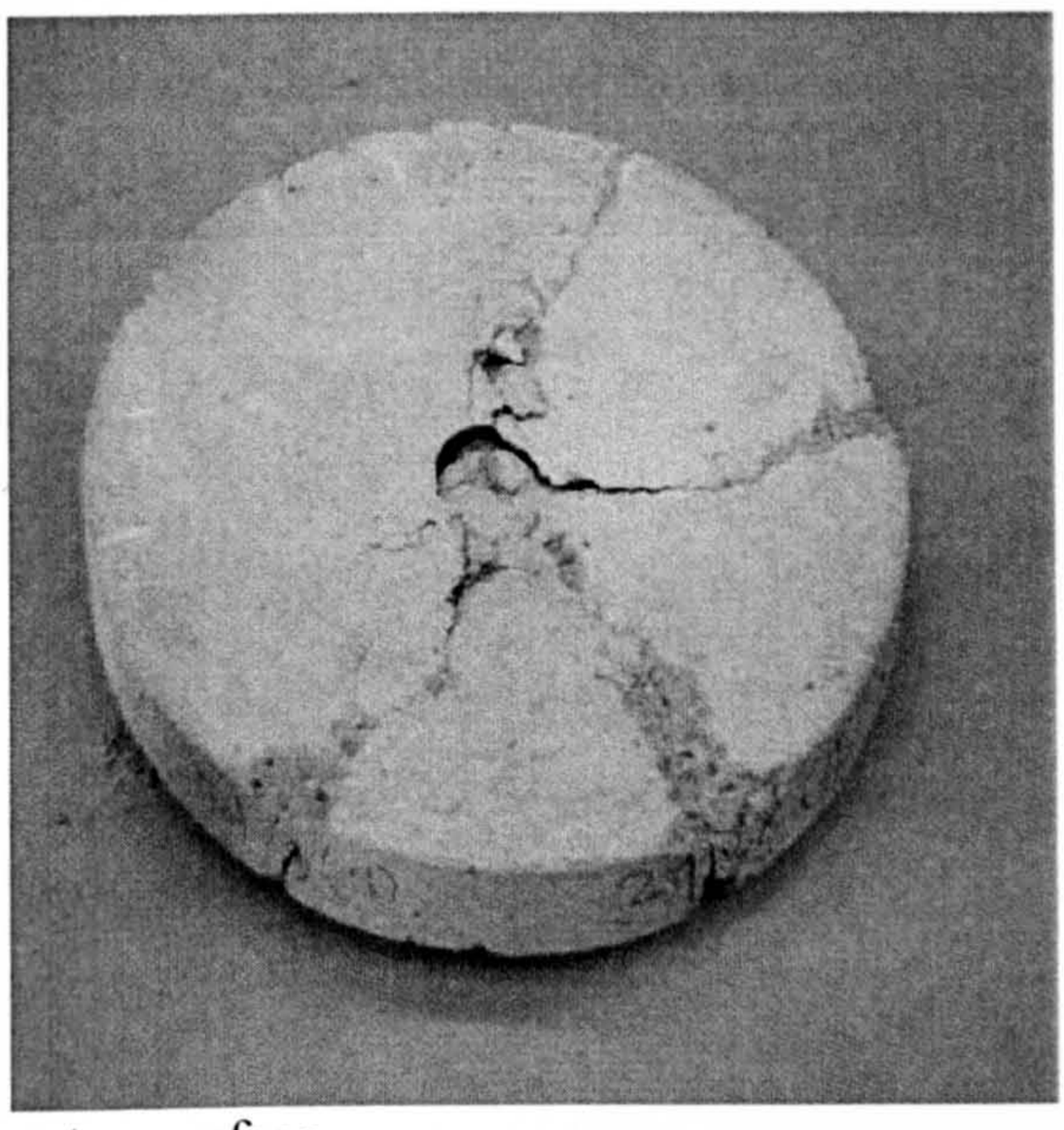

a. top surface

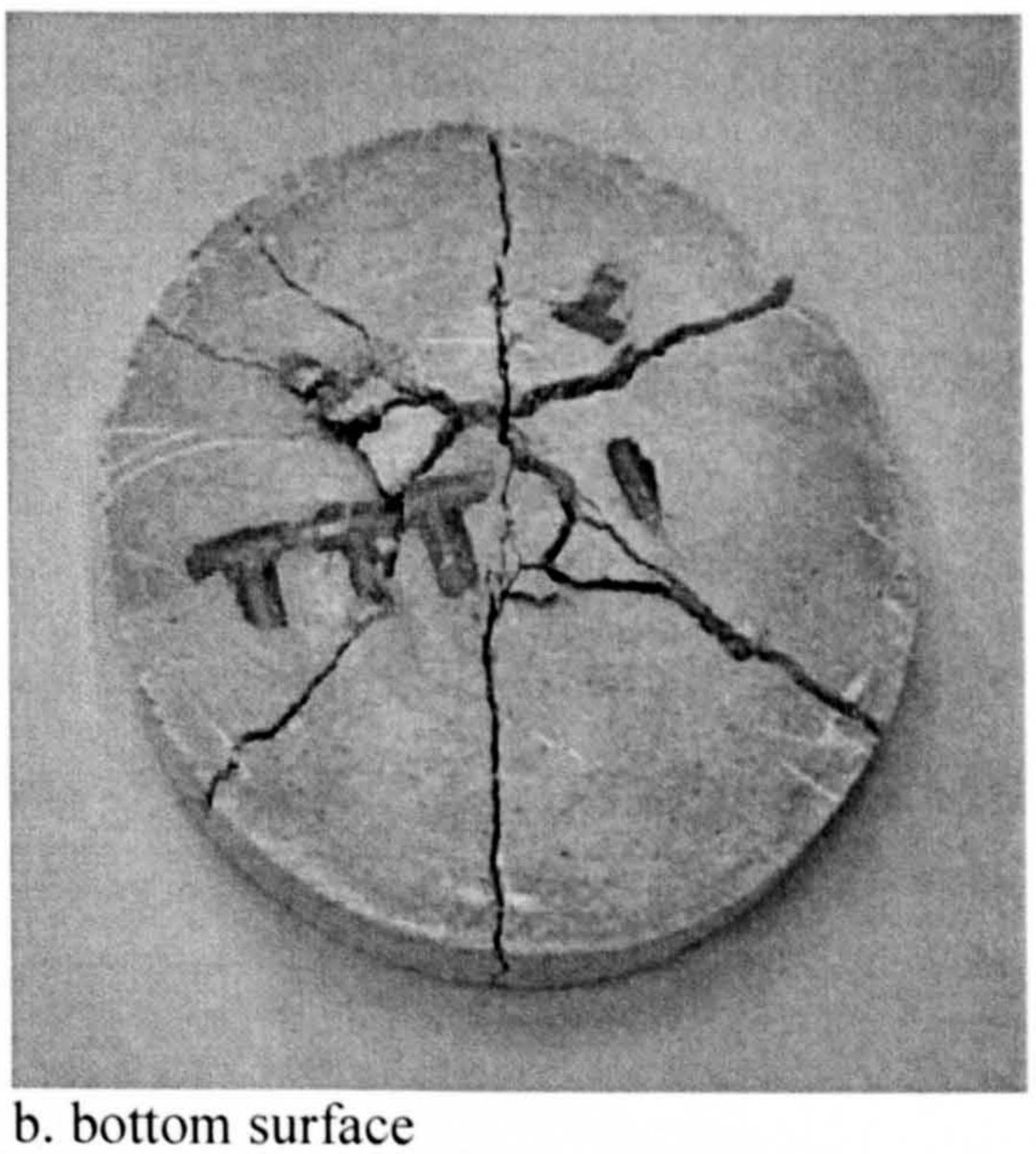

b. bottom surface

Figure 6.54: crack patterns of slab S8 (a. top surface and b. bottom surface)

Generally, the initial damage to the slab occurs in the form of tension cracking in the radial direction, but the crack propagation is lower due to increased fibre-reinforcement. With increasing load, cracks are also formed in the circumferential direction with accompanying degradation in the shear transfer mechanism. With increasing load, micro-cracks were formed across the slab thickness before failure occurred. This was reported by Regan

(1983) and Moe (1961) who observed visually the formation of inclined cracks across the slab thickness, which develops towards the compression zone, before failure occurs. With increase of load (vertical displacement of the column stub) this inclined crack expands towards the corner of the slab-column intersection. At the final stage, crack propagation is prevented by the compression zone above the top of the crack near the column face. It is this two way cracking in the radial and circumferential direction, accompanied by shear degradation in cracked zones that forms the failure mechanism in conjunction with crushing of concrete in compression zone. However, the presence and propagation of these cracks further reduced the stiffness of the slab on the other hand, the strains in the steel fibres and in the concrete increased significantly.

Based on the results, it was assumed that the shear resistance of the SFRC slab–column connections is provided mainly by the contribution of the intact concrete in the compression zone. This assumption is supported with many observations of other studies on normal concrete slab–column connections. However, the major difference in SFRC slab–column connections is that after cracking occurs, tensile stress is transferred across the crack surfaces by the fibres. During micro-crack formation, the fibres are crossed by various micro-cracks so that the tensile force inside the fibres is distributed along the micro-cracked zone and is transmitted beyond this micro-crack zone to the concrete by bond stresses. The tensile force in the fibres is transmitted by bond stresses to the concrete over the transmission length (defined as the length over which slip between the steel and the concrete occurs (Hannant and Spring, 1974). Therefore, unlike conventional concrete slab–column connections, the tension zone of SFRC slab–column connections contributes to the shear resistance by means of the post-cracking tensile strength. As would be expected, failure took place when fibre-pull-out reached its final stage; the cracks extended well into the compressive zone so that no further load could be carried and the slab collapsed.

Slabs S1 and S6 without fibres failed in a more violent way than other slabs, with extensive spalling of tension concrete and with cracks extending along both tensile and compressive faces (see Figures 6.47 and 6.54). Although Slabs S2 and S4 had low fibre contents, the cracks developed only on their tensile faces and the fibres controlled the cracking, even

after reaching maximum load, and maintained the integrity of the structure. There were more cracks in slabs with higher fibre contents and these were finer than the cracks in the plain concrete slabs or in slabs with small values of fibre dosage.

6.7.5. Angle of Punching Cone

After the tests, it was not possible to remove the punching cone of the slabs because the shear crack was intersected by steel fibres within the slab. An attempt to remove this punching cone would have caused too much damage to the failure surface. Slabs were, therefore, sawn into four symmetrical pieces. Figures 6.55 to 6.60 show a cross section of the slab after it had been divided. After that the failure surface of the slabs were carefully investigated and measured.

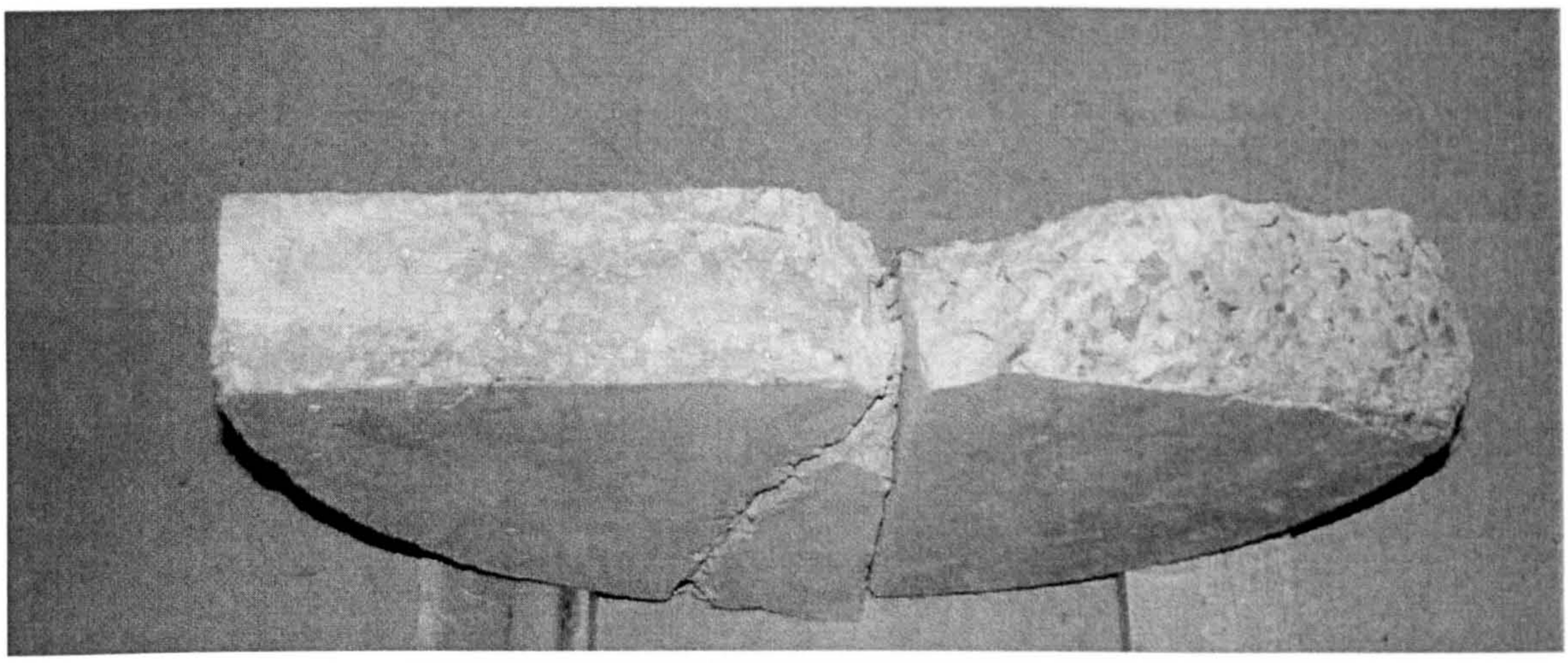

Figure 6.55: Cross section - slab S2

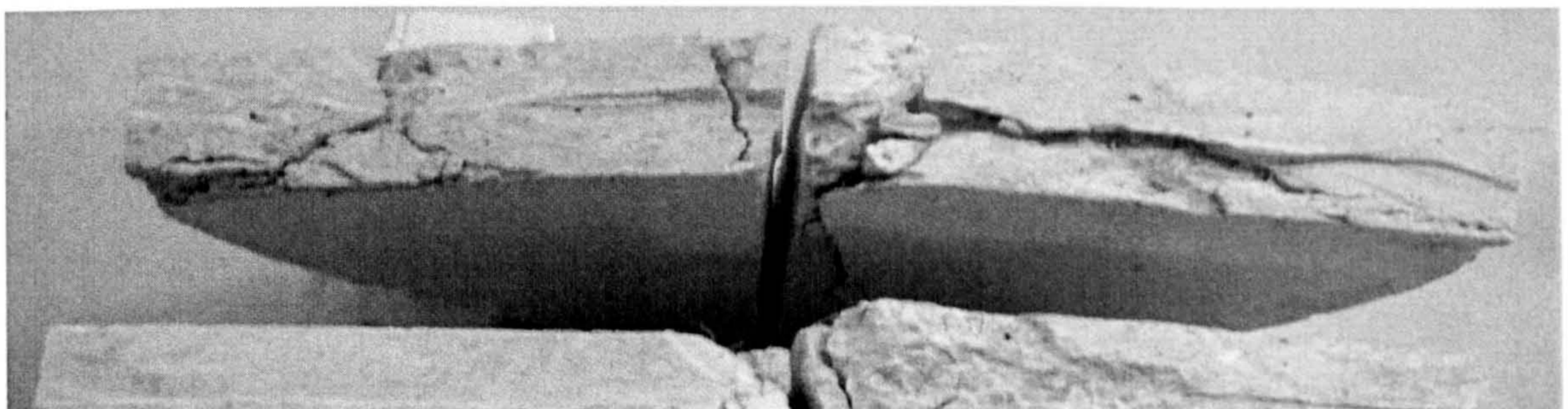

Figure 6.56: Cross section - slab S3

Figure 6.57: Cross section - slab S4

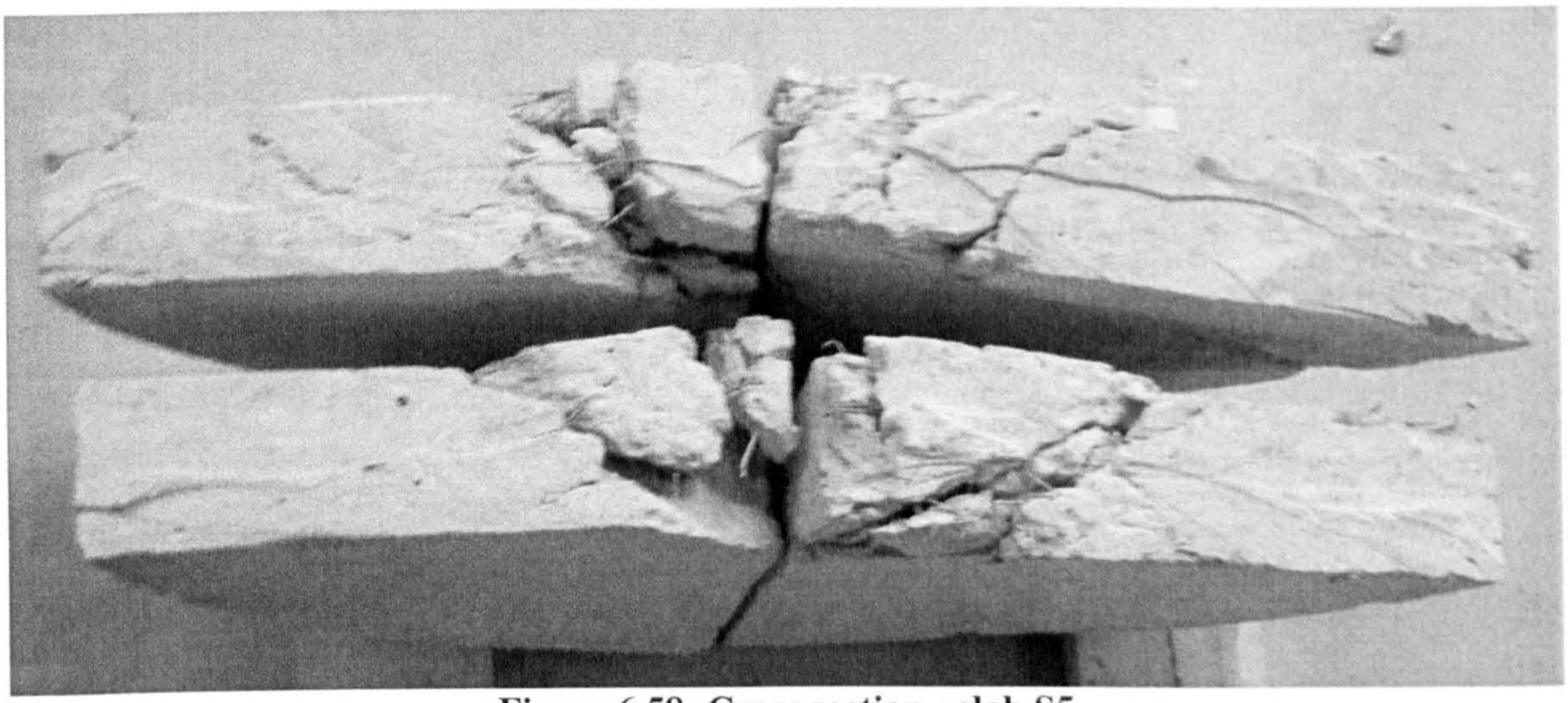

Figure 6.58: Cross section - slab S5

Figure 6.59: Cross section - slab S7

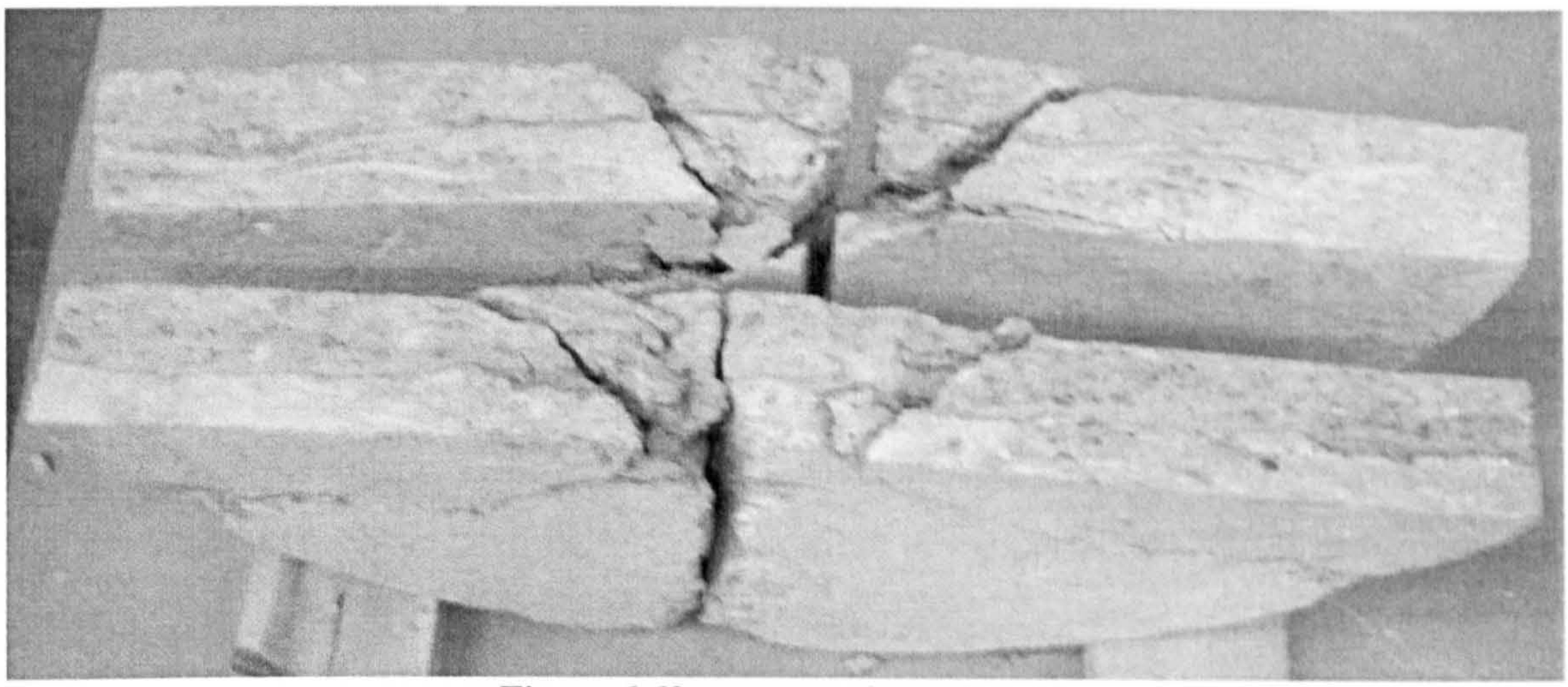

Figure 6.60: cross section - slab S8

The results indicated that the addition of steel fibres did significantly affect the shape of the failure surfaces. The sketches also indicated that the inclination of the failure surfaces relative to the horizontal ranged between 30 and 55 degree. This finding corroborates those of Tan and Paramasivam (1994) who also determined that the inclination of the punching surface with the horizontal for SFRC slabs varying from 20 to 60 deg.

In the slabs reinforced with RC65/60BN (i.e. slabs S4, S5 and S8) the inclination of the failure surfaces relative to the horizontal ranged between 30 and 42 degree. The inclination of the punching surface was less with increasing fibre dosages, with less inclination of 30° observed in slab S5. On the other hand, in the slabs which were provided with ZP30/.50 (i.e. slabs S2, S3 and S7) the failure crack was much steeper with inclination of the failure surfaces relative to the horizontal ranged between 40 and 55 deg. However, the inclination of the punching surface was less with increasing fibre dosages. Moreover, the inclination of the punching surface did not change greatly at different compressive strength.

The test results presented illustrate that for the same fibre type and aspect ratio, there is a dependence of punching resistance upon the angle θ between the failure surface and the mean plane of the slab with increasing in punching resistance with decreasing of the angle. Moreover, the presence of fibres resulted in decreasing the angle of shear failure plane of the slabs, hence stretched the failure surface on the tension face away from the column face. The use of steel fibre thus, increase the area of the failure surface, this resulted in an

increase of their punching shear resistance. This observation was also noticed in the work of Swamy and Ali (1982) who found that the inclusion of fibres pushed the failure surface away from the column face.

6.8 Influence of Tested Parameter on the Punching Behaviour of Slabs

In the test programme, three parameters considered in designing the test specimens included the compressive strength of concrete, fibre dosage and fibre aspect ratio. From the results of the tests it is demonstrated that all these parameters had some definite effects on the punching shear behaviour of the slabs.

6.8.1 Concrete Compressive Strength

Two concrete compressive strengths were used on the slab which was tested to determine the effect of this primary design parameter, these are 30 and 40 MPa. Slabs S3 and S7 with ZP30/.50 steel fibres and slabs S5 and S8 with RC65/60BN steel fibre are similar in the type of the fibre used but different in their compressive strength. Figure 6.21, 6.25, 6.23 and 6.26 show the load-displacement behaviour of slabs S3, S7, S5 and S8 respectively. However, inspection of Figure 6.21 and 6.25 shows that slabs S3 and S7 exhibit a very similar behaviour. Moreover, the behaviour of both slabs in terms of the concrete strain distribution, cracking mechanism and the angle of punching cone are almost identical. The same is true when comparing slabs S5 and S8, see Figures 6.23 and 6.26.

Generally, the uniaxial compressive strength has little influence on the punching shear failure. However, in order to confirm this, this parameter will be studied further using FEA as presented in section 7.5.1.

6.8.2. Fibre Dosage

Two fibre dosages were used in this research 20kg/m^3 and 40kg/m^3. The influence of hooked-end steel fibres on the ultimate punching shear strength of the slabs tested is illustrated by plotting the ultimate punching load for all the specimens tested as a function

of volume fraction, see Figures 6.61 and 6.62. As would be expected there is a definite increase in the load-carrying capacity as the volume fraction increases.

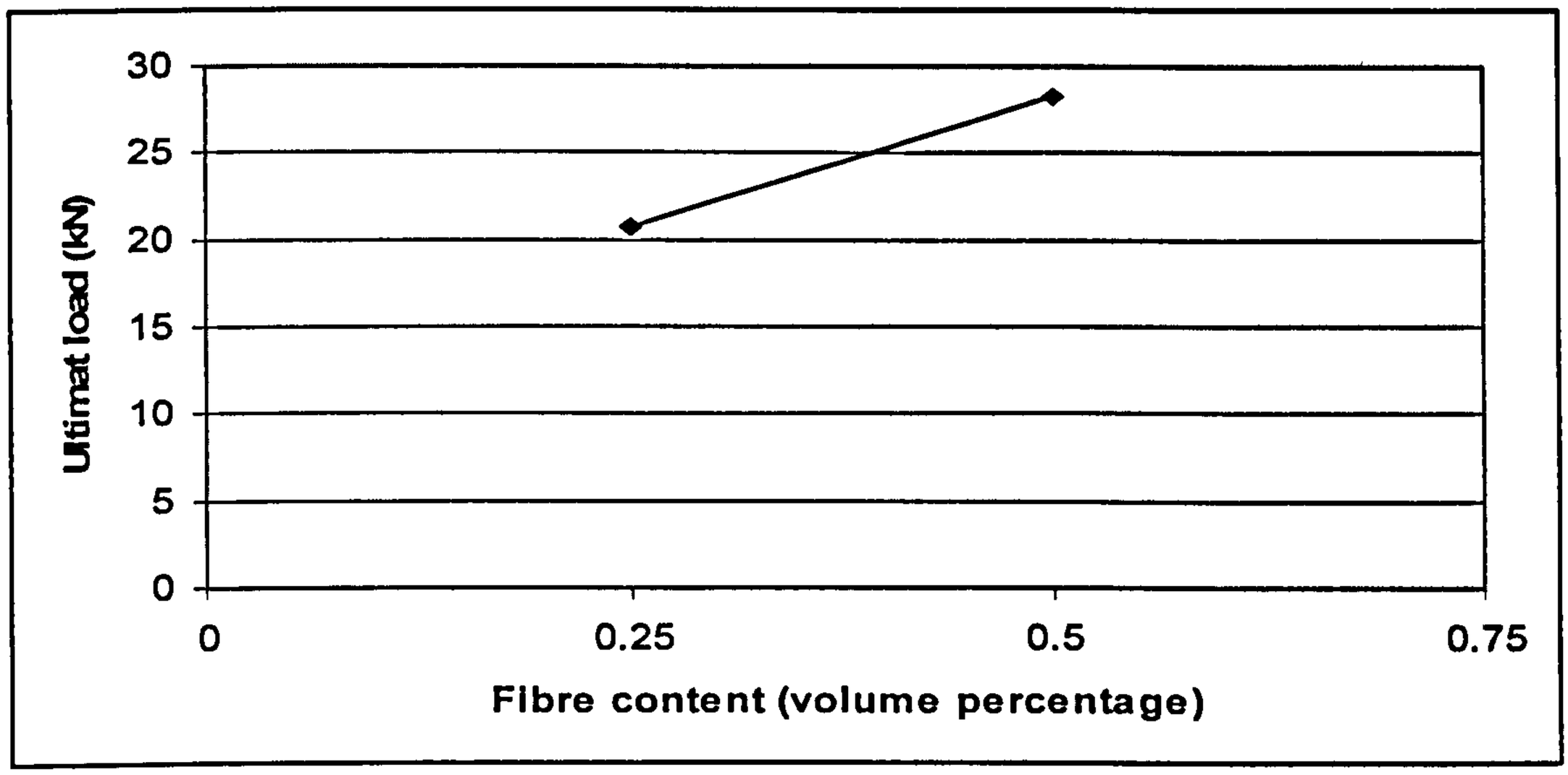

Figure 6.61: Variation of the punching shear strengths of SFRC slabs with the Fibre content (ZP30/0.50)

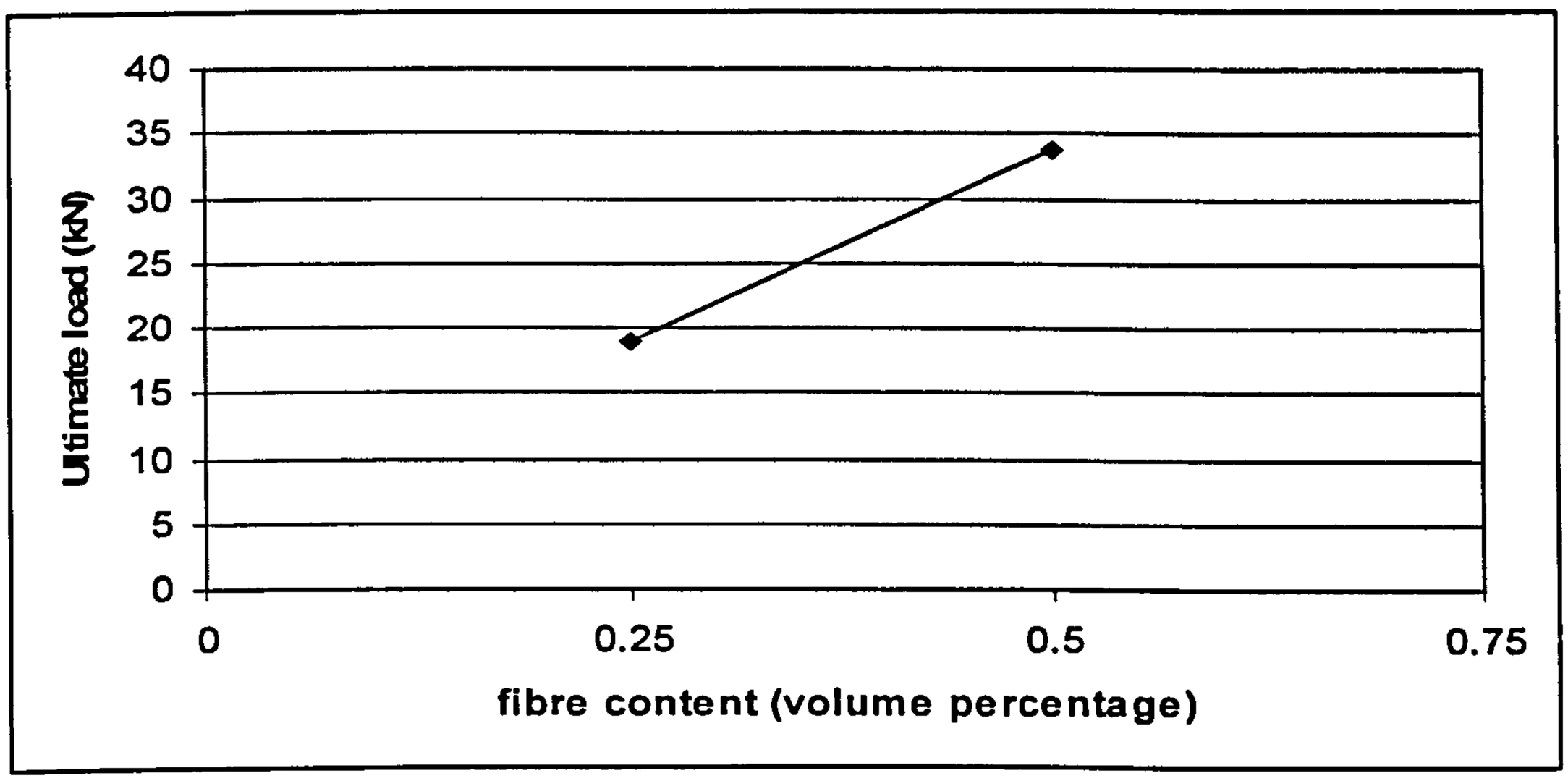

Figure 6.62: Variation of the punching shear strengths of SFRC slabs with the Fibre content (RC65/60BN)

From the load-deflection relationship recorded during the tests (see Figure 6.19 to Figure 6.27) it is shown that in all the slabs the load-deflection relationships were the same for the two different fibre dosages until the cracking of the concrete took place. After the concrete cracking occurred, the stiffness of the slab with more fibres is higher than the stiffness of

the slab with less fibre. The deflections of the slabs at the same loading level were smaller for higher fibre dosage. It was also demonstrated that the increase in the post-cracking stiffness of the slabs provided by the higher fibre dosage.

The provision of more steel fibres will tend to increase the ultimate load capacity of the slab. In other words, the punching shear strength can be enhanced by increasing the steel fibre dosage. This will also result in increase in the ductility of the slab. Unlike conventional reinforcement, more reinforcement will tend to increase the ultimate load; on the other hand the ductility of the slab will be decreased. It will make the failure of the slab more brittle with less warning which is a disadvantage as far as the punching shear is concerned.

The graphs of the failure load versus the steel fibre dosage for two different fibre dosages (i.e. 20 kg/m^3 and 40 kg/m^3) are presented in Figure 6.61 and Figure 6.62 respectively. The results summarised in Table 6.4 demonstrate that adding steel fibres in 0.25 and 0.5% by volume fraction increased the average ultimate punching resistance in comparison with the plain slabs by about 43 and 96%, respectively with fibre type ZP30/.50 and by about 31 and 132% with fibre type RC65/60BN. It was also demonstrated that an increase in the post-cracking stiffness of the slabs provided by the higher steel fibre dosage decrease the angle of the inclined punching shear failure surface of the slabs, and thus the ultimate load is increased. The increased in the fibre dosage has also some desirable effects. One of the desirable effects caused by increase of fibre dosage is that it causes a significant increase in the ductility of the slab. However, the ductility in the slab-column region is a very important characteristic in the flat slab systems. Sufficient ductility in the slab-column connections is necessary to allow the full bending moment redistribution to take place.

Generally, the punching shear capacity of flat slabs may be influenced by the amount of the steel fibres provided in the slabs in a number of different ways. Firstly, the increase of steel fibre dosage could effectively help to increase the load for first yielding of steel fibres and consequently reduce the crack width for a given loading. This would significantly increase the stiffness of the slabs at the post-cracking and improve the transfer of shear forces by interlock of aggregates. Secondly, the increase of the amount of steel fibres would lead to

the increase in the depth of compression area in the cross section at failure. Therefore, a greater uncracked concrete area would be available to resist the shear forces acting on the section.

6.8.3 Fibre Aspect Ratio

The influence of the fibre aspect ratio on the ultimate punching shear strength was studied by using two different fibre aspect ratios in the tested slabs, 60 and 67. Table 6.4 shows that increasing the fibre aspect ratio had little effect on the ultimate punching shear resistance. So that, for the range used in this test, the fibre aspect ratio (ratio of length-diameter of fibres) does not significantly influence the punching shear strength of the slabs. For instance, Specimens S2, S4, with same fibre dosage and different aspect ratio as well as Specimens S3 and S5, which have approximately equal fibre densities but much different fibre aspect ratios, mobilized almost equal ultimate shear resistance and their failure mode was very similar.

Another characteristic that can be seen from the load-deflection relationship is that, for the same fibre dosage, the stiffness of the slabs with RC65/60BN fibres was found to be almost the same as with ZP 30/.50 fibres.

6.9 Conclusions

In this Chapter, it was concluded that all the SFRC slab specimens tested failed in punching shear with maximum compressive strains at the bottom of the slab that were much smaller than the critical crushing strain of concrete. This implies that the failures of all the tested slabs were caused by tension rather than compression.

It was found that, the punching shear strengths of SFRC slabs are strongly dependent on the fibre dosage, with the inclusion of fibres into the concrete mix improved the punching shear strength of the concrete slabs by 22 and 130%. Moreover, the failure modes of SFRC slabs were affected by the dosage of steel fibres with two possible punching shear failure modes were noticed. For a smaller dosage of fibre-reinforcement (i.e. 20kg/m^3), the failure may

occur in a brittle manner, while for a larger dosage (i.e. 40 kg/m^3), failure occurs in a more ductile manner.

The results also show that for all slabs, the flexure strength is greater than the actual failure load indicating that all the tested slabs failed in shear before the flexure strength was exhausted. Moreover, the formula presented in TR34 (2003) over predict the punching shear capacity of SFRC slabs.

In addition, the experimental data clearly show that the punching shear strength and the angle of the punching cone are directly related. However, the angle of punching cone was reduced with increasing fibre dosage. So the presence of steel fibres decreased the angle of the shear failure plane of the slabs, hence they stretched the failure surface on the tension face away from the column face resulting in an increase in the area of the failure surface. This resulted in increasing their punching shear resistance.

The experimental data clearly show that the punching shear capacity was not significantly affected by the compressive strength and the fibre aspect ratio. Although the aspect-ratio of the steel fibres did not significantly affect the punching shear capacity of the slabs, the shorter fibre was most effective. This has been attributed to the reduction in workability with the longer fibres.

CHAPTER SEVEN

FINITE ELEMENT ANALYSIS

7.1 Introduction

Although the experimental results presented in chapter six provide a valuable insight into the punching shear behaviour of SFRC slabs, it is not practical to use laboratory testing to cover the range needed for a complete study. In order to extend the range of parameters covered, the most suitable tool available at present is the finite element method. Finite element simulations have become an important tool which can be used to gain a better understanding of the behaviour and characteristics of reinforced concrete structures under variety of loading and boundary conditions (Kotosovos and Pavlovic, 1995 and Chen, 1982). This chapter deals with finite element modelling of the punching shear behaviour of SFRC slabs. In the experimental programme, discussed and reported in Chapter six, six simply supported SFRC slabs were tested to failure under a concentrated load applied at the centre. These test specimens were analysed by the finite element method in order to, numerically demonstrate the possibility of reproducing the structural behaviour of the slabs, using measured material strengths as well as the constitutive model for SFRC developed earlier in Chapter Four.

Hence, finite element model implementing an axi-symmetrical element was developed in this research. Furthermore, parametric studies were carried out in which the influence of material and geometrical properties on the punching behaviour is studied. In order to conduct the parametric studies, the relevant parameters should be determined first by means of a sensitivity analysis. Therefore, a series of sensitivity analyses were carried out and the results and recommendations stemming from these analyses are described in this chapter.

In the present numerical study, the damaged plasticity approach implemented in a general purpose finite element code, ABAQUS (2006a), which offers a non-linear material model for reinforced concrete, was adopted. The applied model was presented in some more details in Chapter Three.

7.2 Finite Element Analysis

CEB/fib Task Group (2001) in the technical report of Punching of Structural Concrete slabs compared the existing mechanical models for punching shear with the test data bank and concluded that the development of mechanical models based on experimental data alone has limitations. These limitations include:

- The limited number of parameters that can be varied within comparable test programmes
- The relatively small (size effect) the slab thicknesses and column dimensions of the scaled test structures
- Important material properties of the concrete like fracture energy and tensile strength cannot be directly controlled and analysed
- The formation and propagation of internal cracks cannot be directly observed
- Punching tests are expensive
- The bandwidth of test setups and test results exhibiting in the existing punching tests are enormous.

Therefore and in order to address the above limitations, a realistic finite element model is mandatory for the development or improvement of mechanical models for the punching failure. The primary tasks of the numerical investigations should be the visualisation of the experimentally invisible fracture process inside the slab as well as the analysis of important geometrical and material parameters such as the concrete tensile properties and the slab thickness.

7.2.1 Finite Element Model

As this research focused on modelling circular slabs subjected to symmetrical punching shear without moment transfer and due to polar symmetry, the slabs were modelled using axisymmetric isoparametric eight-node solid elements (CAX8) with nine integration points (i.e. with full integration). It is defined as a three-dimensional body that is developed by

rotation of a planar section about an axis. Cylindrical coordinates r, θ and z provide a suitable reference frame.

Due to axi-symmetry, only one-half of the slab was taken, with the origin at the centreline. The punching load is applied by imposing vertical displacement restraints throughout the loaded area (at the bottom of the column stub) and then subjecting the structure to the edge reaction force; such a modelling is consistent with the notion that the punching pressure is usually due to a column. Figure 7.1 shows the boundary conditions adopted in the analysis.

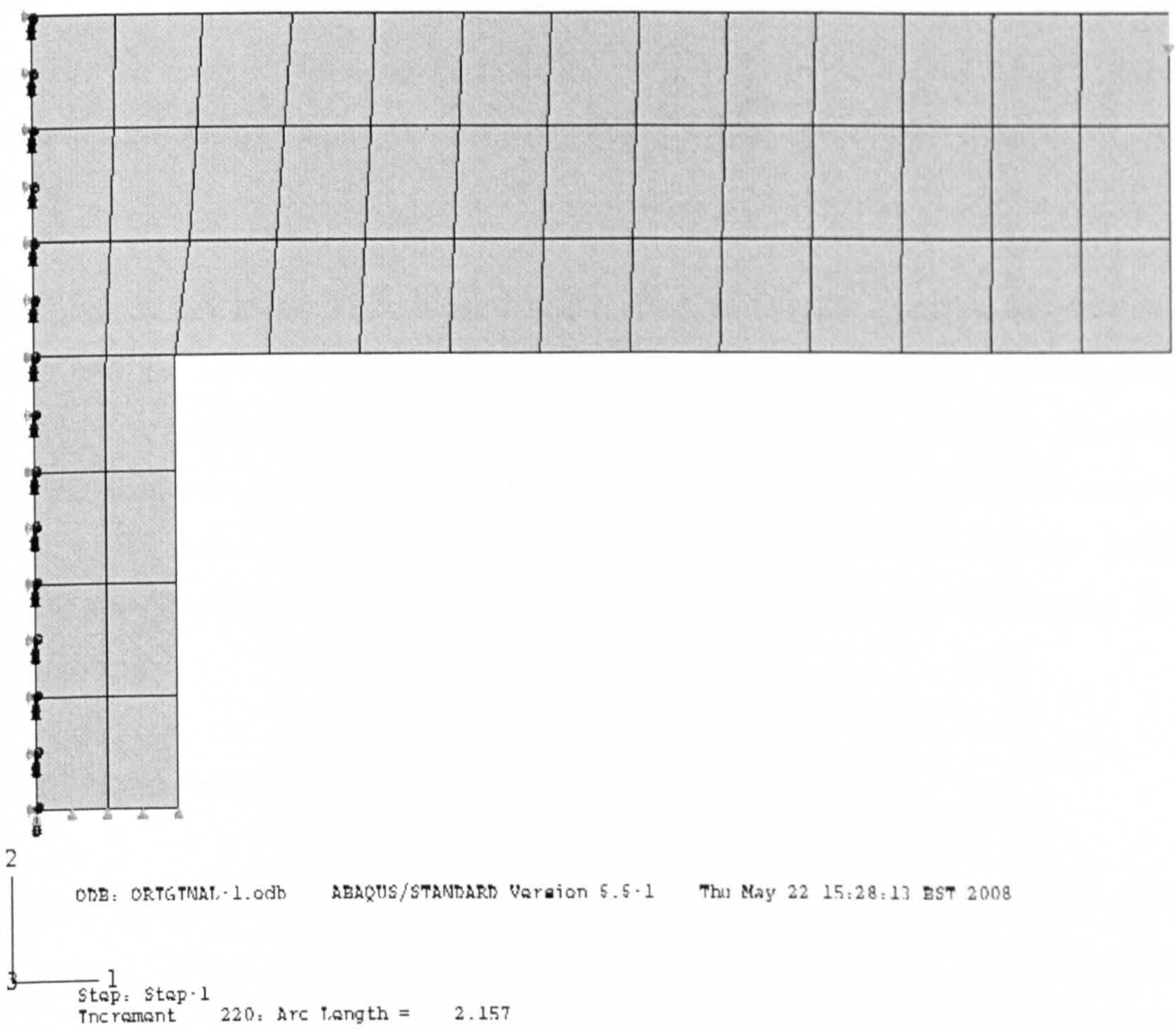

Figure 7.1: Boundary conditions adopted in the numerical model

7.2.2 Material Modelling

The damaged plasticity model was used in the current analysis. This concrete model is based on the classical concepts of the plasticity theory: a strain rate decomposing into elastic and inelastic strain rates; elasticity; yield; flow and hardening, which allow for strain-softening after both cracking and crushing. The smeared crack method based on the concept of stress discontinuity, while maintaining displacement continuity, was used in this investigation. Cracking is assumed to occur when the stress reaches a failure surface. Cracking is irrecoverable and remains throughout the rest of calculation. Once concrete has cracked, the tension stiffening is modelled by loosing the concrete strength through a softening mechanism. The strain softening after cracking reduces the stress in the concrete model.

As discussed in Chapter Four, modelling the effect of fibres in concrete has still not been taken into account in the FEA of SFRC structures in any of finite element programs. Therefore, a constitutive model for SFRC was developed in this research. The choice of material properties (i.e. the angle of dilation, the ratio of the ultimate biaxial compressive stress to the ultimate uniaxial compressive stress, the compressive damage d_c and the tensile damage d_t) were discussed and presented in full details in the material property section 4.5.2.

7.2.2.1 Input Parameter for the Model

Material sample test data (i.e. cubes and beams) is required to calculate the model parameters. Thus material testing should be performed with a great care, following prescribed procedures from taking samples, storing the samples, performing the tests with calibrated equipment until eventually assessing the resulting parameters.

The following mechanical properties are needed for the Damaged Plasticity Model implemented in the ABAQUS finite element code:

- Compression strength (cubes with side length of 150mm were tested as presented in Chapter Six)
- The cylinder compressive strength of concrete (f_c') was taken to be $0.8f_{cu}$, where f_{cu} is the compressive cube strength of concrete
- Young's modulus of concrete, $E_c = 21{,}500[f_c'/10]^{1/3}\ \text{N/mm}^2$, this formula was chosen as a result of sensitivity analysis (as presented earlier in section 4.5.2.1)
- Flexural tensile strength (beams under three-point bending were tested as presented in Chapter Six)
- The post crack stress-strain relationship in tension (tension-stiffening) was determined using the inverse method technique by means of numerical simulation of experiments performed on three-point bending beams. The beam test was discussed in details in section 6.4.2. Two SFRC beams, tested with each slab, were analysed using FEA and the results are shown in Figures 7.2 to7.7. Table 7.1 shows the basic material properties used in FE analysis for SFRC beams. The use of inverse analysis to determine the tension-stiffening behaviour for beams was discussed in Chapter Four.
- For each slab the tension stiffening behaviour was taken as the average results of the two corresponding beams. Table 7.2 shows the material properties used in the FE analysis for SFRC slabs.
- Angle of dilation, $\psi = 10^{\circ}$
- The ratio of the ultimate biaxial compressive stress to the ultimate uniaxial compressive stress = 1.15
- The compressive damage d_c and the tensile damage d_t were taken as presented in Chapter 4.

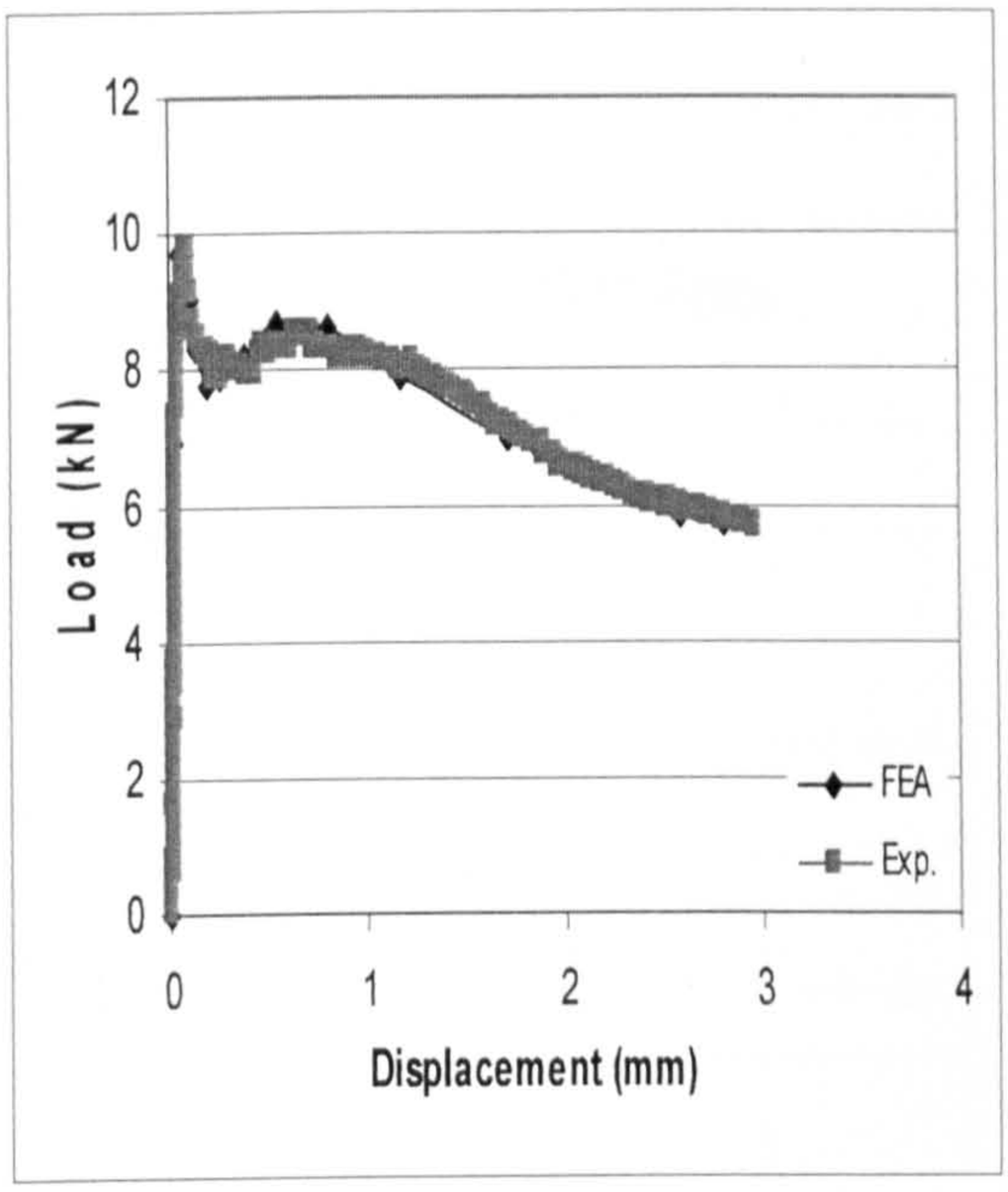

a. beam 1

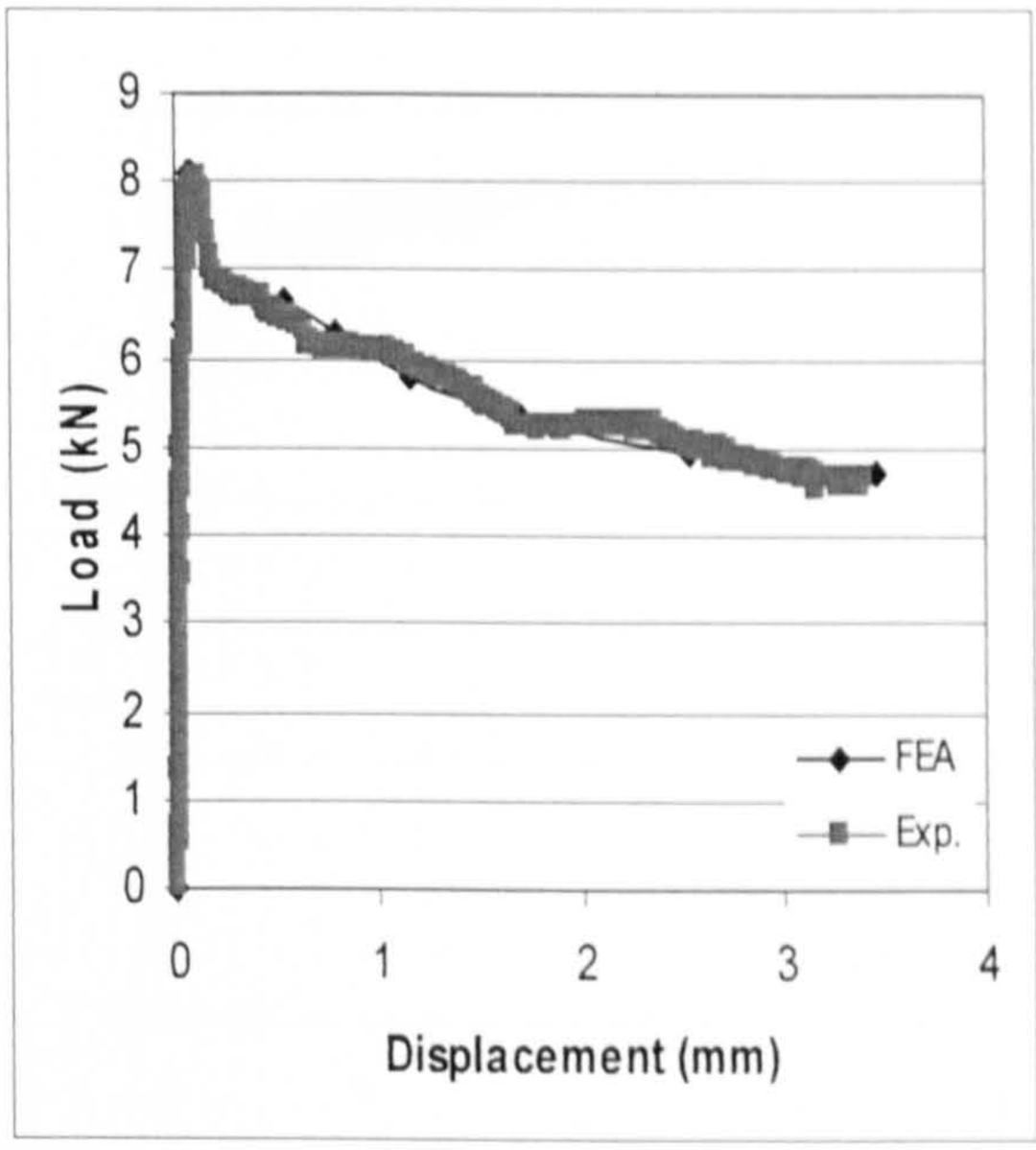

b. beam 2

Figure 7.2: Numerical load-deflection response of beams (slab S2) in comparison with the measured test values (a. beam 1 and b. beam 2)

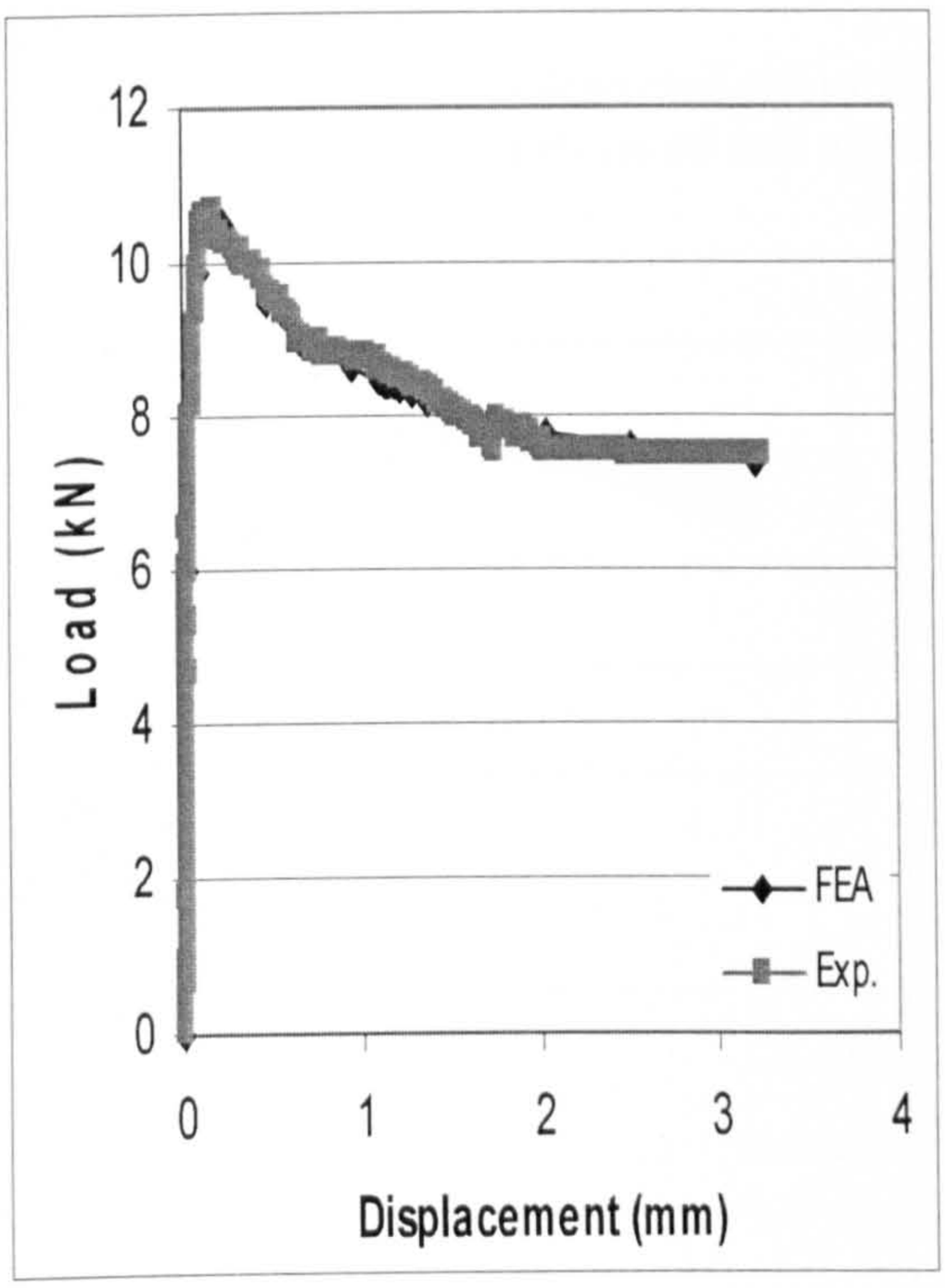

a. beam 1

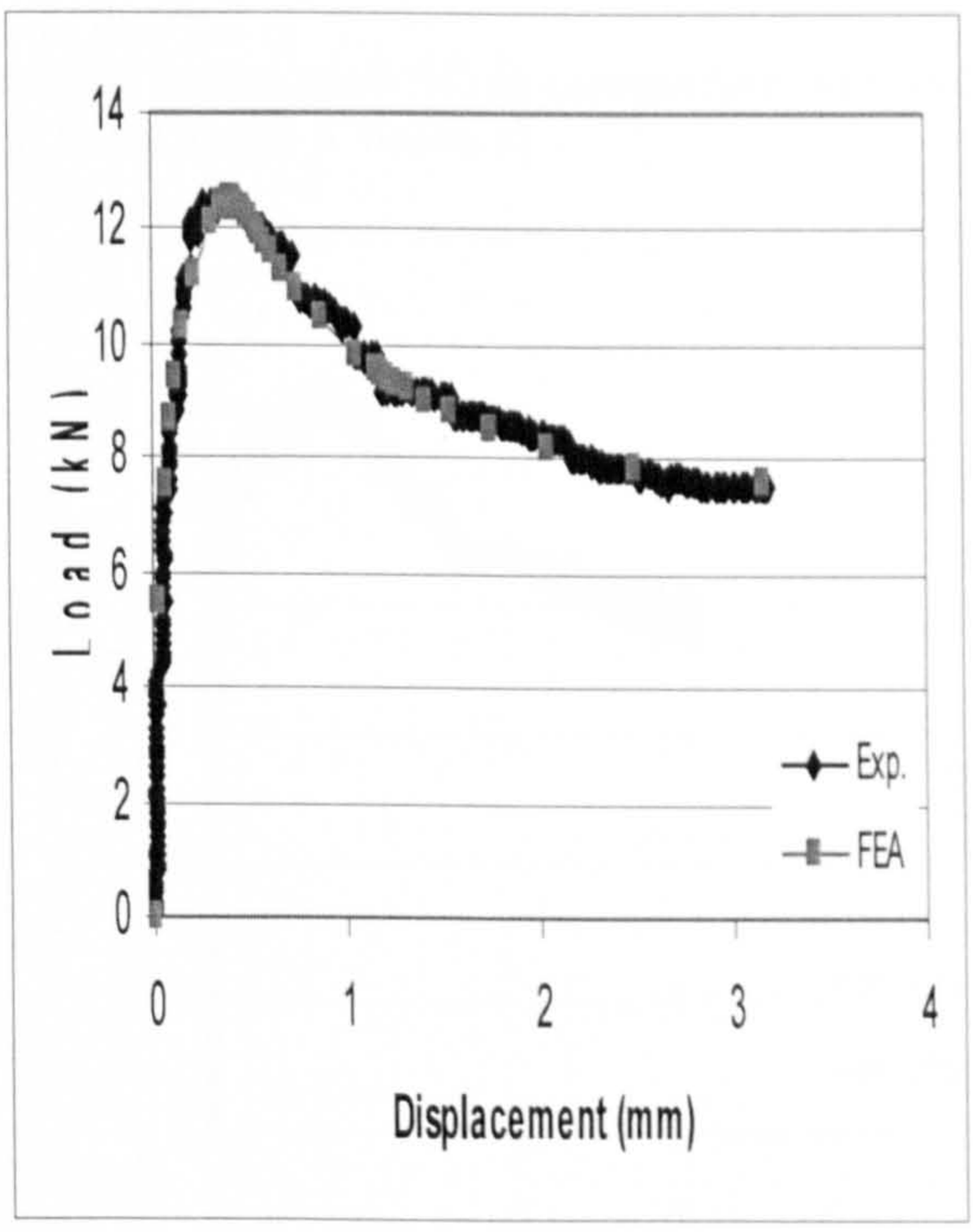

b. beam 2

Figure 7.3: Numerical load-deflection response of beams (slab S3) in comparison with the measured test values (a. beam 1 and b. beam 2)

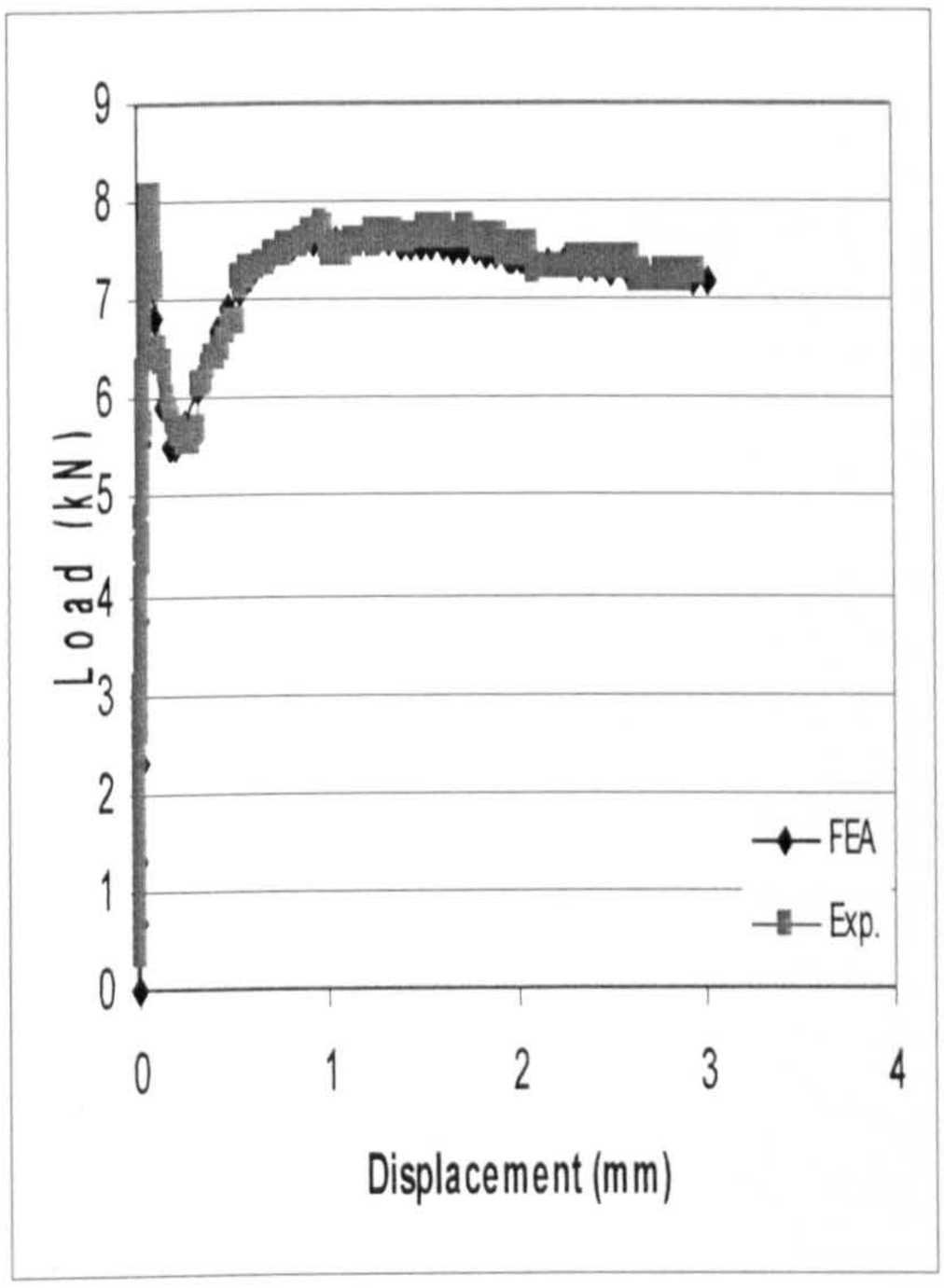

a. beam 1

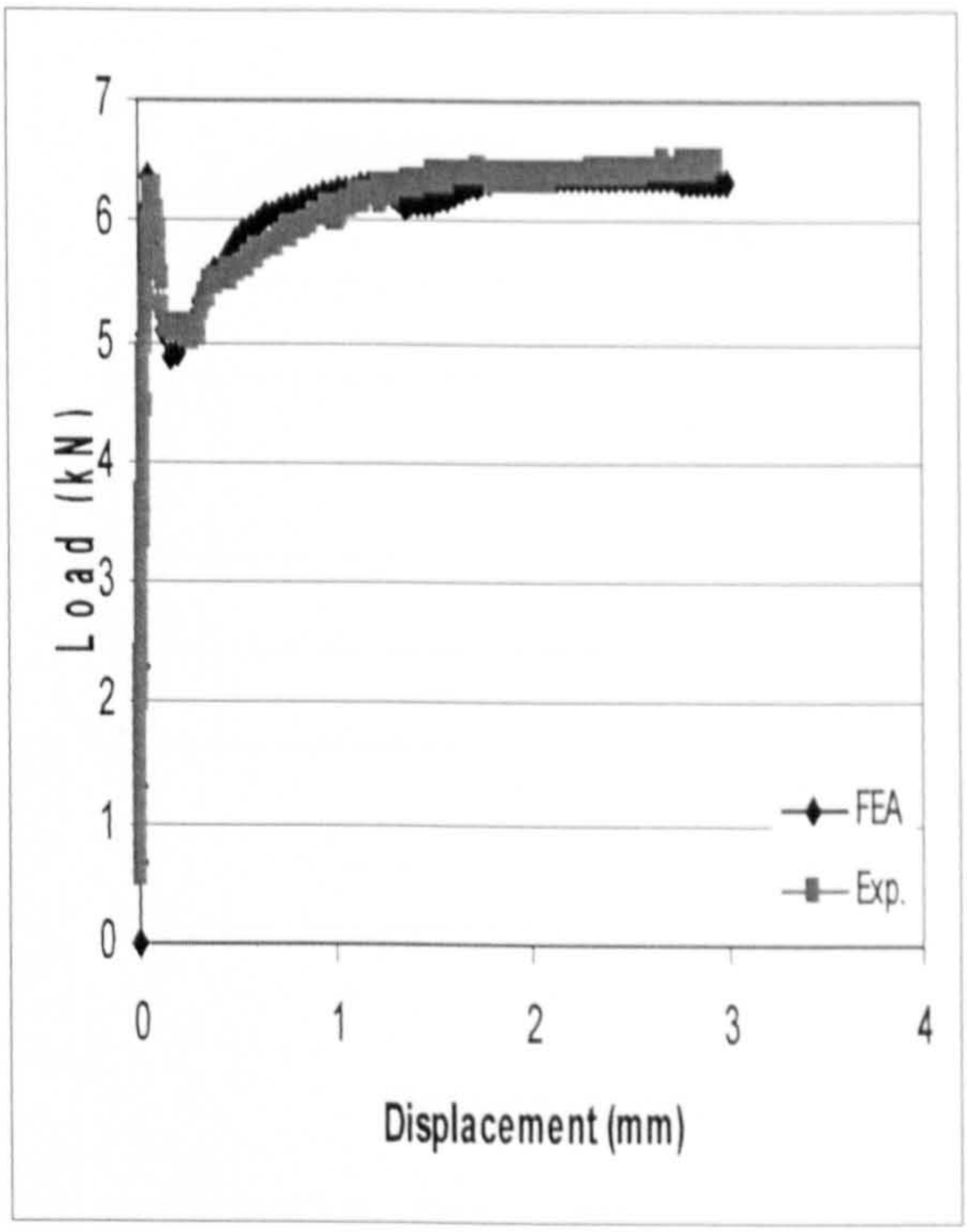

b. beam 2

Figure 7.4: Numerical load-deflection response of beams (slab S4) in comparison with the measured test values (a. beam 1 and b. beam 2)

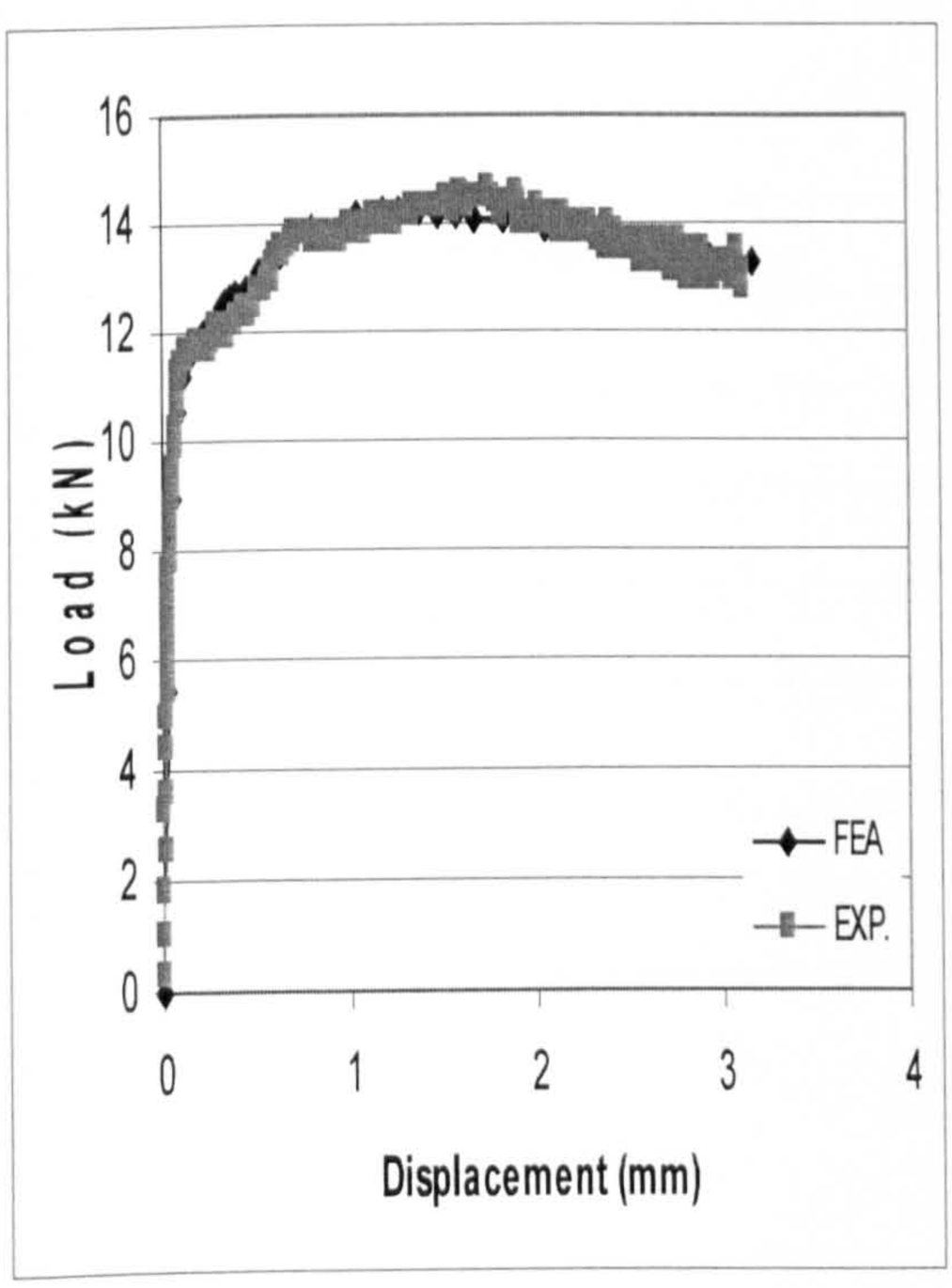

a. beam 1

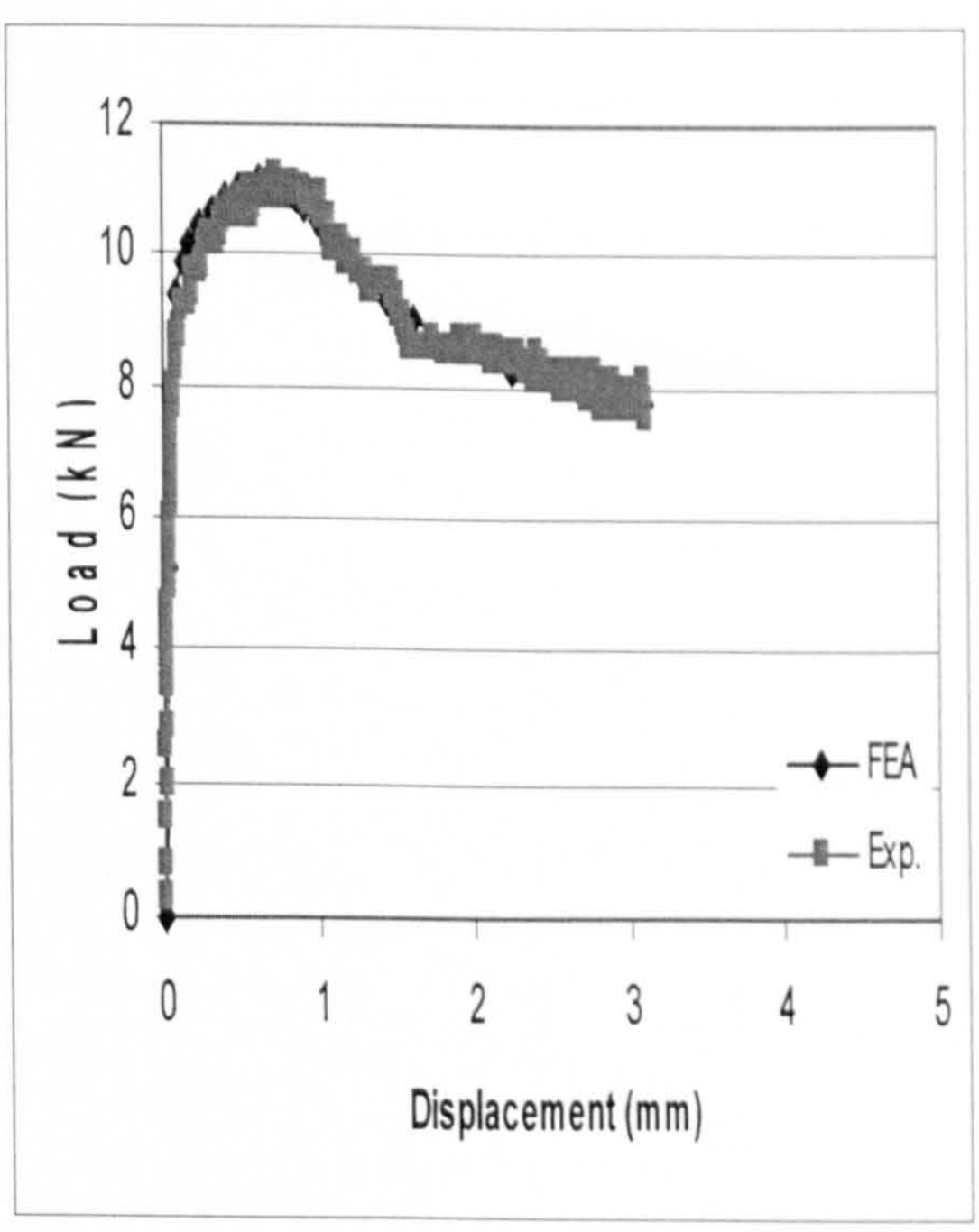

b. beam 2

Figure 7.5: Numerical load-deflection response of beams (slab S5) in comparison with the measured test values (a. beam 1 and b. beam 2)

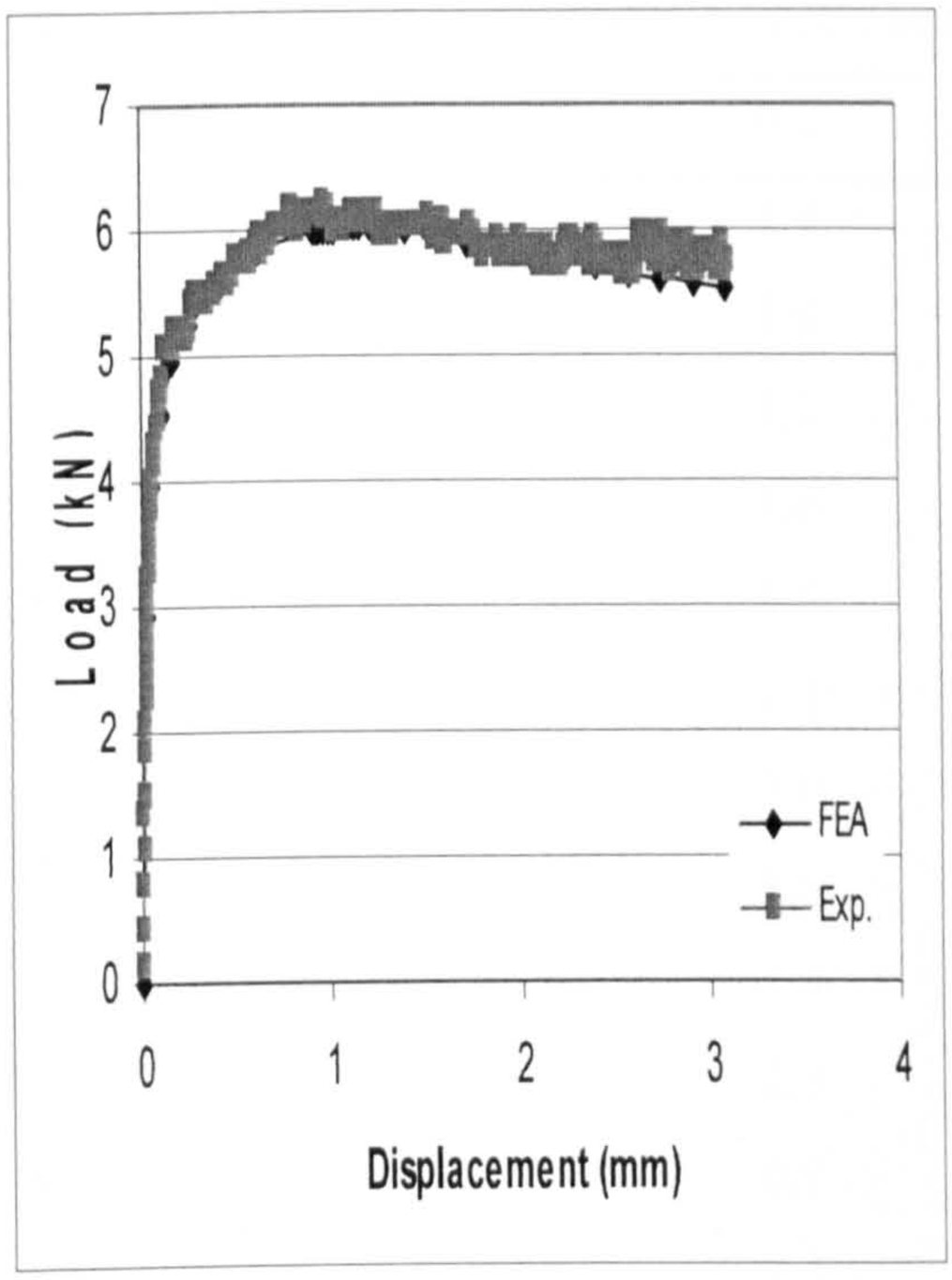

a. beam 1

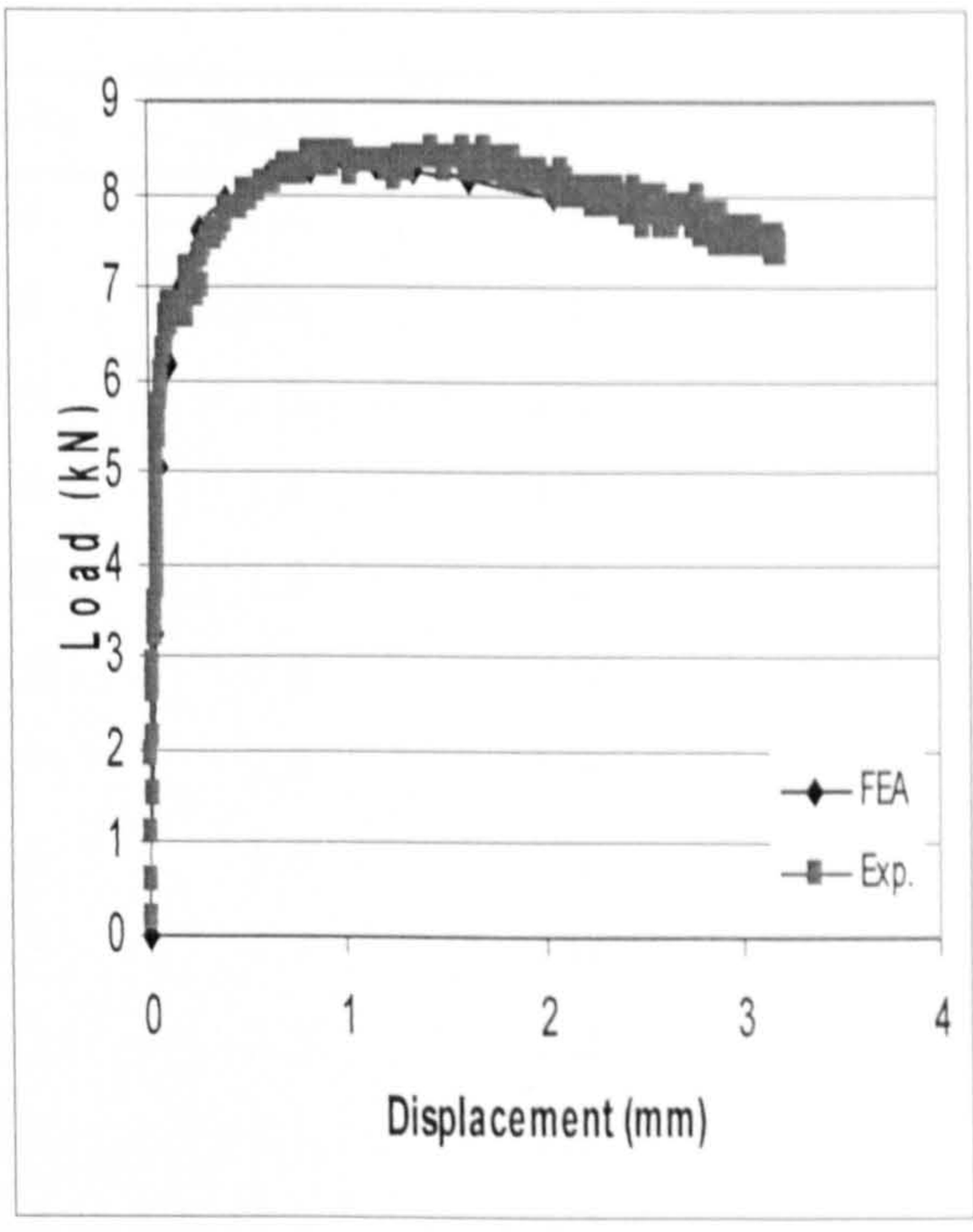

b. beam 2

Figure 7.6: Numerical load-deflection response of beams (slab S7) in comparison with the measured test values (a. beam 1 and b. beam 2)

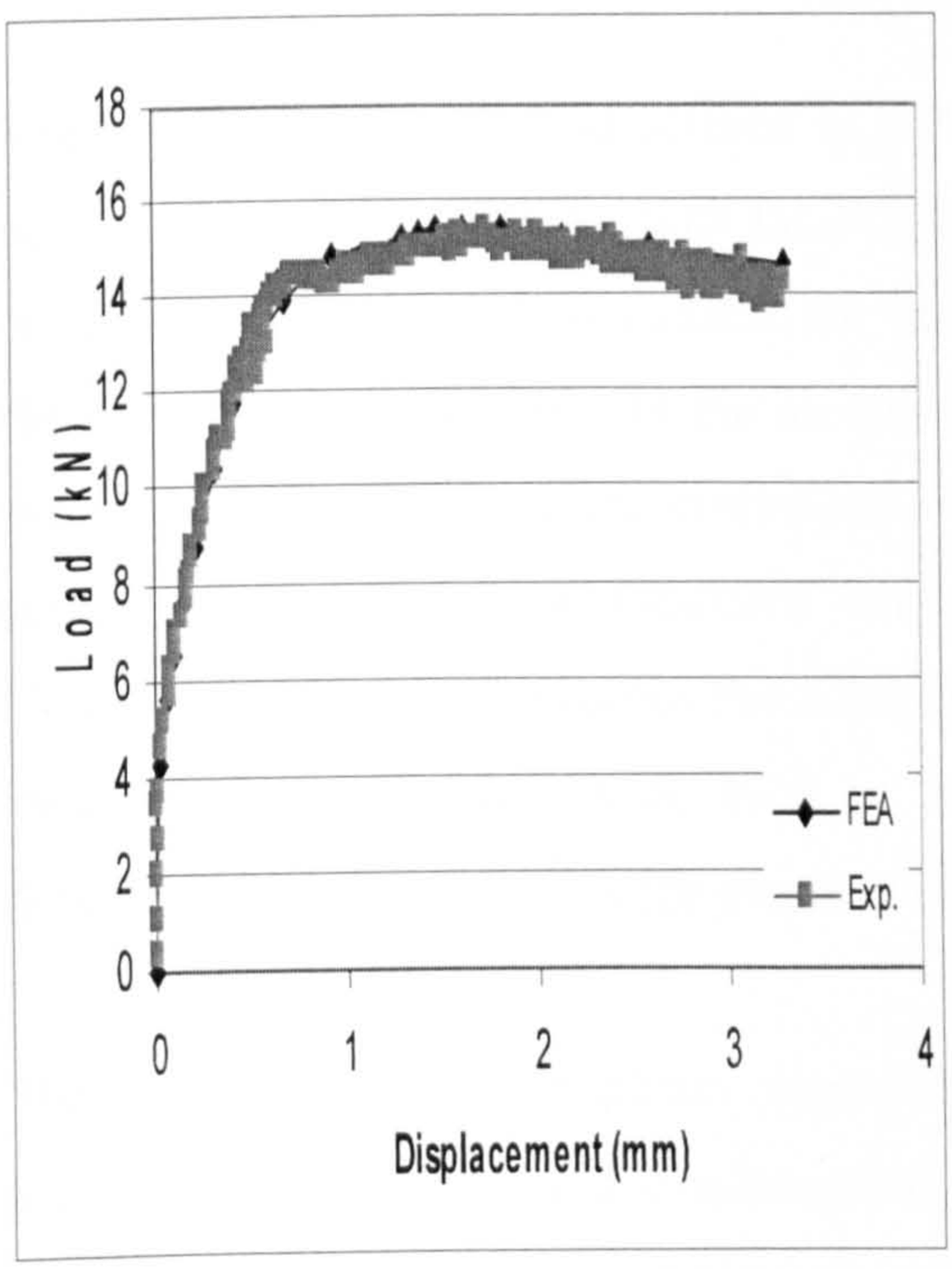

a. beam 1

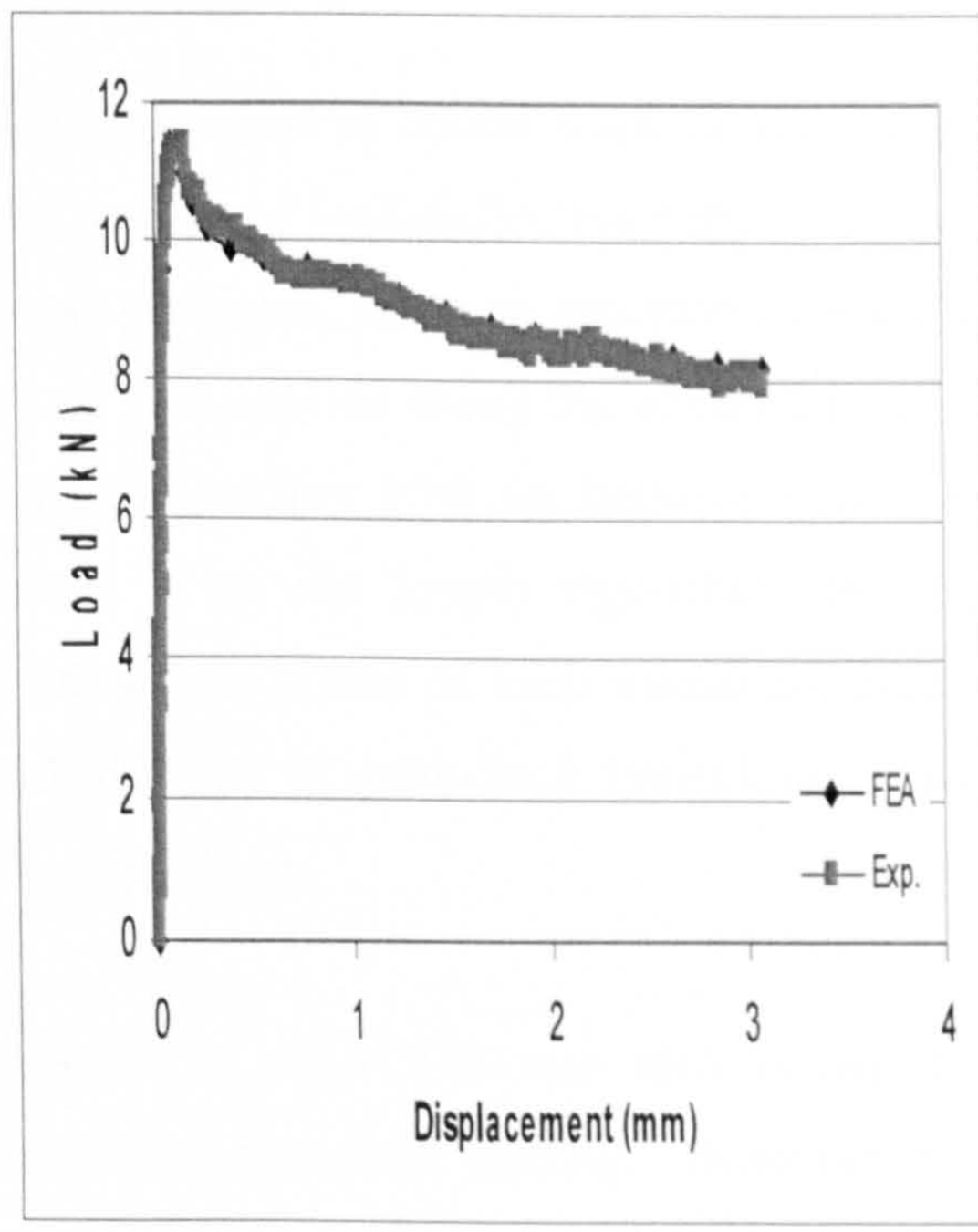

b. beam 2

Figure 7.7: Numerical load-deflection response of beams (slab S8) in comparison with the measured test values (a. beam 1 and b. beam 2)

Table 7.1: Material properties for SFRC beams

Slab no.	Beams	f_c'	σ_{tu}	$\sigma_{n1}/\varepsilon_1$	$\sigma_{n2}/\varepsilon_1$	$\sigma_{n3}/\varepsilon_1$	$\sigma_{n4}/\varepsilon_1$
S2	Beam1		1.8	0.8	1.2	0.8	0.65
	Beam2		1.4	0.8	0.8	0.6	0.55
S3	Beam1		1.2	2.0	1.3	1.1	1.0
	Beam2		1.6	1.6	1.1	1.1	1.0
S4	Beam1		1.5	0.5	1.0	1.0	0.95
	Beam2		1.1	0.5	0.8	0.8	0.85
S5	Beam1		2.0	1.7	2.0	1.9	1.8
	Beam2		1.6	1.5	1.6	1.1	1.0
S7	Beam1		1.4	1.5	1.7	1.6	1.5
	Beam2		2.0	2.3	2.3	2.2	2.1
S8	Beam1		0.7	2.2	2.1	2.0	1.9
	Beam2		2.3	1.4	1.3	1.2	1.1

7.2.3 Loading

The modified Riks Method offered in ABAQUS was used to obtain static equilibrium in non-linear unstable regions, thus facilitating the tracing of load-deflection behaviour up to collapse and beyond. It is suitable for non-linear problems, since an automatic control of time stepping is provided. In the model, the load was applied along the circumference of the slab using displacement controlled incremental loading with an iterative non-linear solution technique. The modified Riks method is an arc length algorithm (see, e.g. Crisfield 1991), which enables the solution to pass limit points of local maximum load or local maximum displacement, such as in snap-through or snap-back behaviour. More details about Riks method were presented in Chapter Three.

The standard Newton-Raphson algorithm offered in ABAQUS was also tested in a preliminary analysis, using displacement controlled incremental loading. However, with the standard Newton-Raphson algorithm, the process diverged before reaching a peak load. Newton–Raphson type methods did not converge even with a very small step size. With the modified Riks method a peak load was reached and the process did not diverge.

7.3 Sensitivity Analysis

As pointed earlier in section 4.5, there are many parameters which affect the FE prediction of the behaviour of slabs. Therefore, sensitivity analysis was carried out in order to arrive at a general strategy for the entire non-linear finite element analysis. The following parameters are considered for investigation to determine whether their influence on the results is significant and to determine their suitable values for the subsequent parametric studies.

Generally, these parameters can be classified into two categories. The first category contains numerical parameter such as the convergence tolerance, the size of initial arc length, the size of the arc length in the Riks method (initial arc length and arc length are discussed in details in section 3.2.1), the mesh size and the element type. The second category contains the material parameters such as compressive and tensile strengths, Young's modulus, Poisson's ratio. However, the effect of material parameters were studied earlier in section 4.5, therefore the obtained values will be used in the current FE analysis. For this, study material parameters were kept constant as shown in Table 7.2.

Table 7.2: Material properties for SFRC slabs

Slab no.	σ_{tu}	$\sigma_{n1}/\varepsilon_1$	$\sigma_{n2}/\varepsilon_1$	$\sigma_{n3}/\varepsilon_1$	$\sigma_{n4}/\varepsilon_1$
S2	1.6	0.8	1.0	0.7	0.6
S3	1.4	1.8	1.2	1.1	1.0
S4	1.3	.5	0.9	0.9	0.9
S5	1.8	1.6	1.8	1.5	1.4
S7	1.7	1.9	2.0	1.9	1.8
S8	1.5	1.8	1.7	1.6	1.5

In sensitivity analysis, the parameters are varied one at a time. As the number of variations is large, the comparison will be confined to one typical slab, i.e. slab S5. The values of the parameters chosen are based upon those giving the best comparison with the experimental

results. The comparison between the experiments and predicted values was based on the following aspects of structural behaviour:

- The ultimate load capacity of the slab
- The load-deflection response
- The mode of failure

A set of general rules were laid down for the classification of the modes of failure based on the following structural responses from experimental observations:

- Load-deflection response
- Principal compressive stress and strain in concrete
- Crack pattern

a) Load Deflection Response/Load-Rotation Response

Slabs which display large ductility, basically fail in flexural mode, while brittle behaviour represents slabs failing by primary punching. However, this is only rough classification. The experimental load-deflection curve response shows that the gradient of the curve prior to failure is low for slabs which, fail in flexural mode and is steep for slabs which fail in shear mode. Therefore, if the gradient prior to failure is low, the slab is said to have failed in flexural mode. Conversely, if the slope is very steep, the slab is said to have failed in shear mode.

b) Principal Compressive Stress and Strains

Kinnunen-Nylander's model, presented earlier in Chapter Two, indicates that slabs failing in punching shear mode are highly stressed. It assumes that punching occurs when the stress and strain in the conical shell reaches critical values. In the present study, concrete crushing is assumed to occur when the maximum compressive strain exceeded 0.0035. Therefore, when either principal compressive stress greater than f_c' or principal compressive strain reaches or exceeds 0.0035, the slab is said to fail in punching.

c) Crack Pattern

In ductile-type behaviour, radial cracks spread throughout the top face of the slab and increase in-depth with increasing load. In contrast to radial cracks, circumferential cracks only spread to about half the span (at the tension face), and increase in-depth with increasing load, but at a lower rate than was the case with radial cracks. However, for the case of brittle behaviour, radial cracking occurs at a lower rate and the crack depth is smaller than that for the slab exhibiting ductile behaviour. In contrast with radial cracks, circumferential, cracks increase in-depth in the periphery of the column; beyond that region their depth is small and the cracks do not extend to the region of the supports.

7.3.1 Numerical Parameters

The main purpose of the study of the effect of numerical parameters on slabs behaviour is to choose the values of the parameters to achieve an accurate and at the same time economical solution for the non-linear analysis. Six parameters which have significant effect on the computational cost and Finite Element prediction were studied. These parameters are:

1. Convergence tolerance
2. Arc length
3. Size of initial load increment
4. Mesh density
5. Element type

After having chosen the best values for the concrete model, all the analysis will use this set parameters for the analysis of the remaining tested slabs.

7.3.1.1 Effect of Convergence Tolerance

In the numerical procedure, convergence tolerance is used to monitor the gradual elimination of the out-of-balance residual forces until desired accuracy is achieved. Theoretically, a small tolerance is required but it can be very expensive because it requires a large number of iterations. For this study, three tolerance factors were studied 1%, 5% and 10%. Figures 7.8 to 7.10 show that the results for load-deflection and strain in compression zone, the structural response are very similar for different values of tolerance factor except that the smaller value of tolerance predicted lower ultimate load. Table 7.3 shows the variation of the ratio of predicted/experimental failure load and deflection at failure load with the tolerance limits. The ultimate load and deflection predicted for the three tolerances are almost same (see Table7.3), but using tolerance of 10% will increase the radial and tangential strain in the compression zone at the column face by 5.73% and 10.10%. Whereas, 1% and 5% are almost same but the computational cost increased by 40% and the number of iterations increased by 20% when using 1% tolerance (as measured by the solution time). The above study indicates that smaller tolerances do not show much difference in the structural behaviour other than increasing the computational cost. Therefore, a 5% tolerance will be used throughout the present investigation.

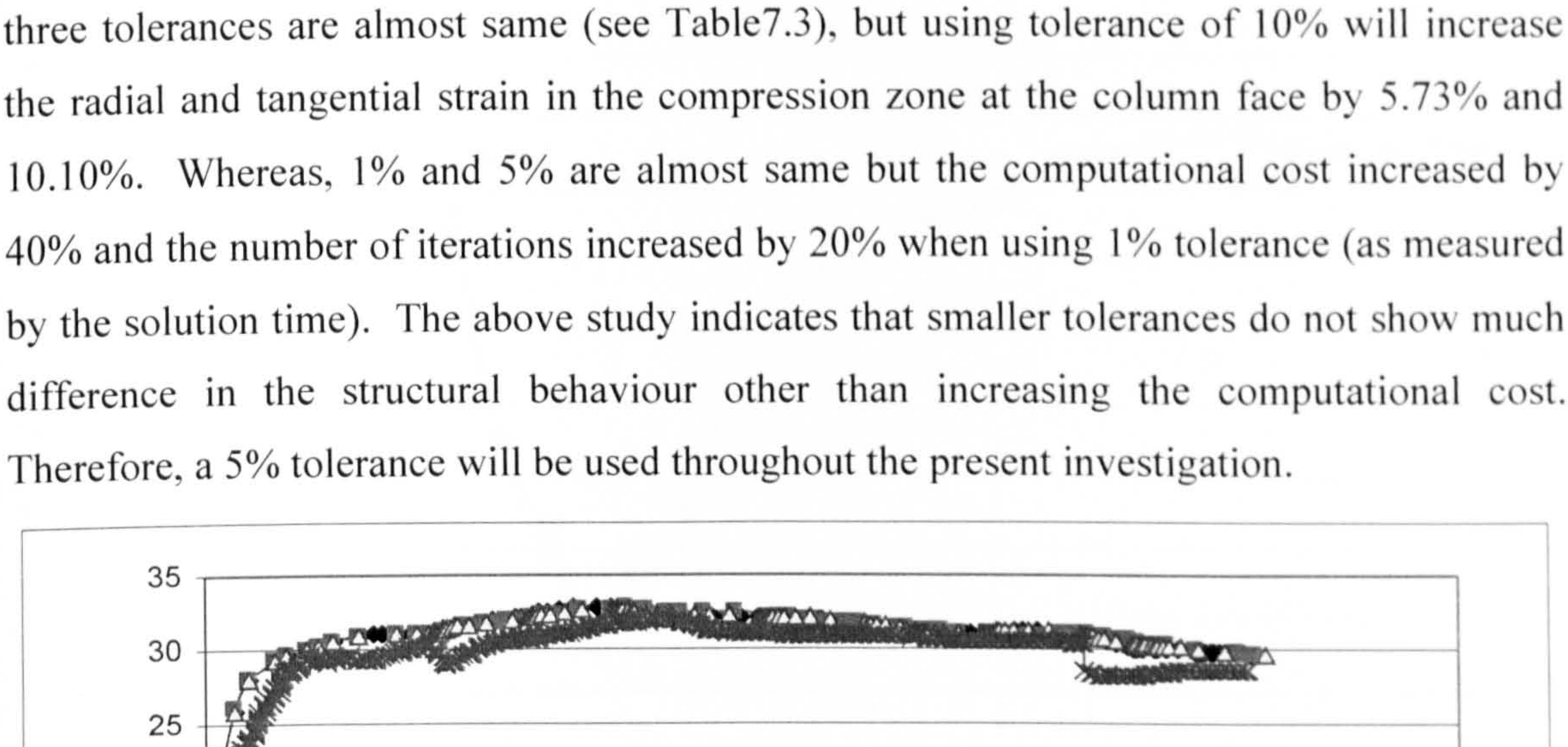

Figure 7.8: Effect of convergence tolerance on the load-displacement behaviour

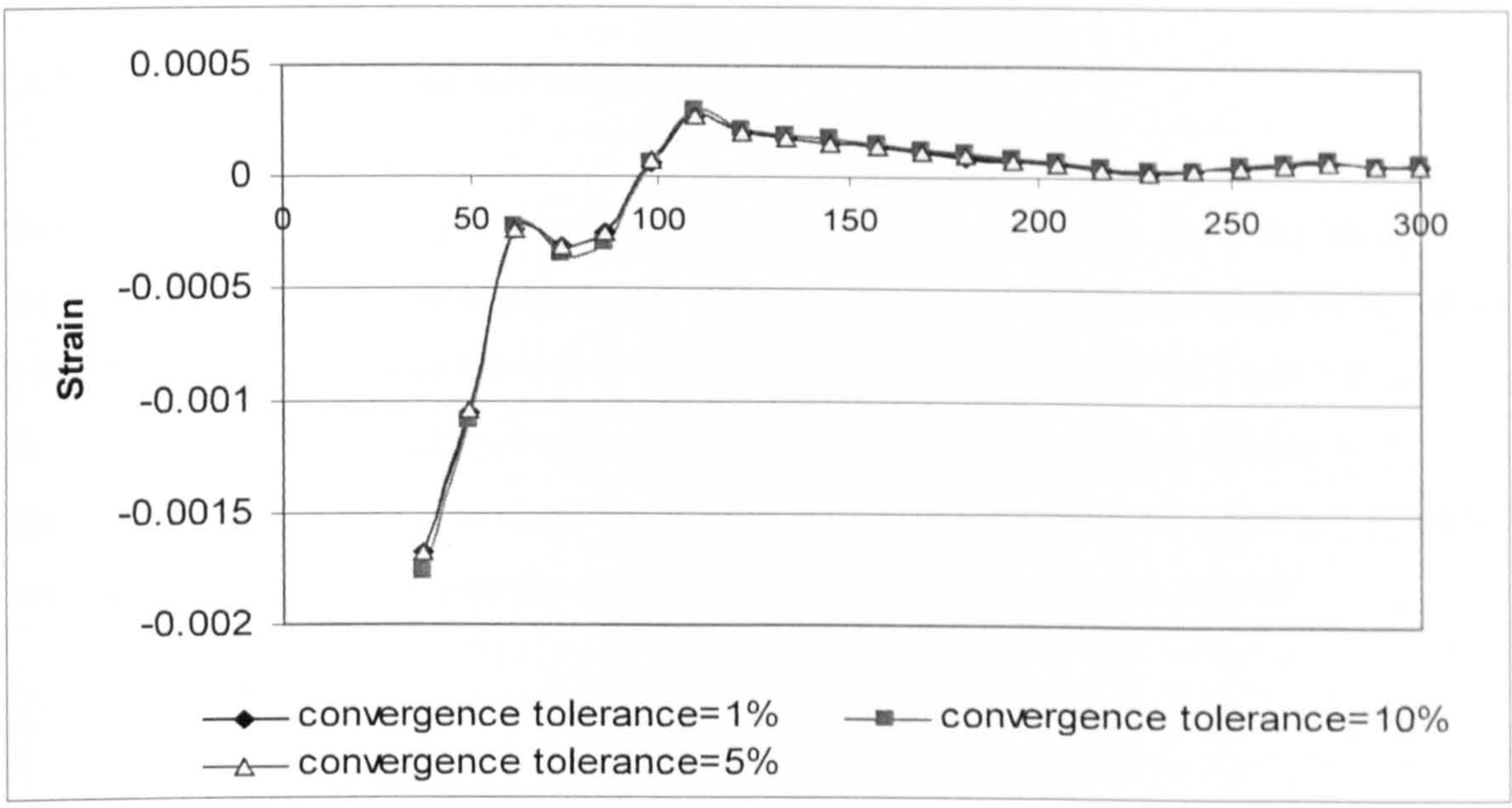

Figure 7.9: Effect of convergence tolerance on the radial strains in the compression zone

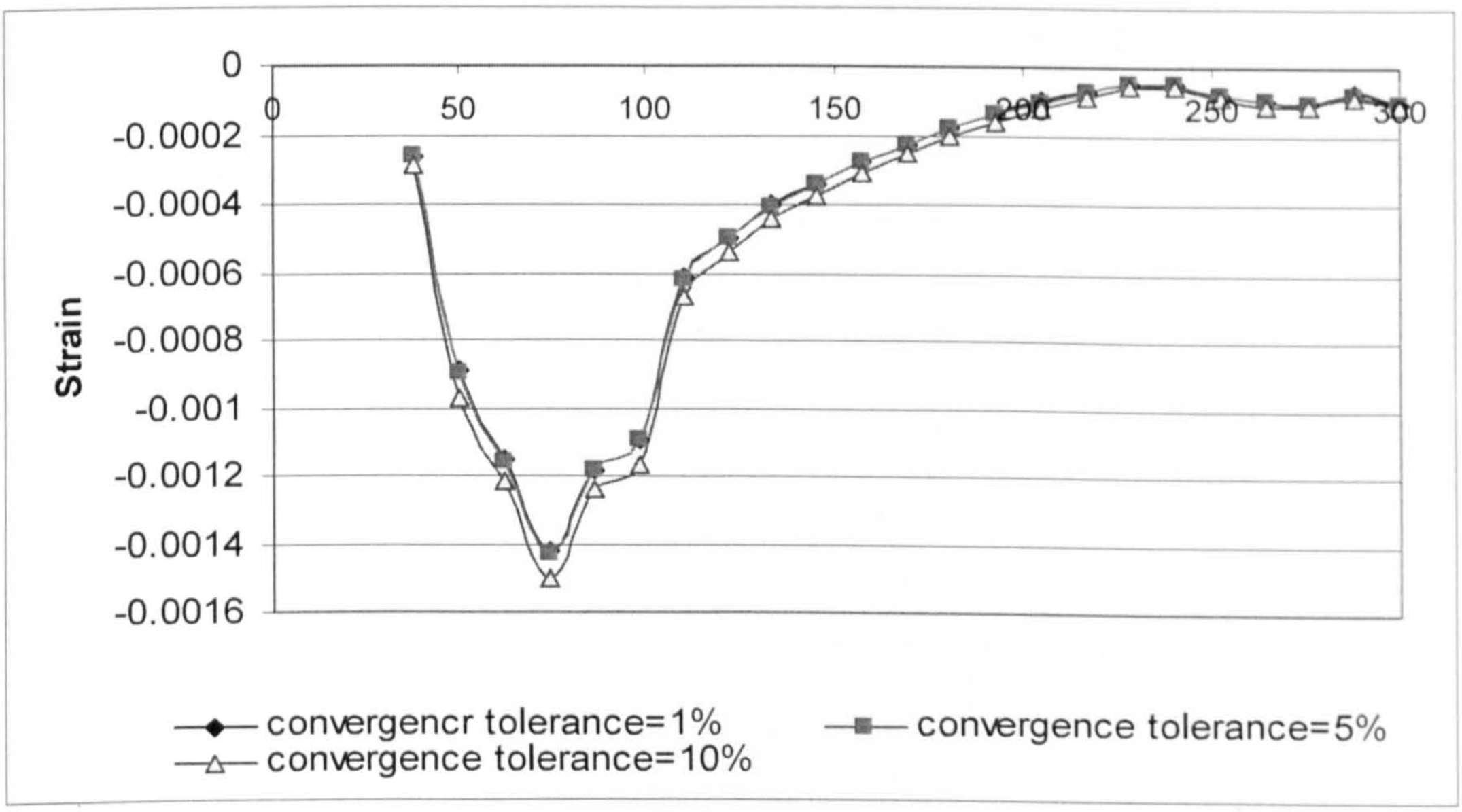

Figure 7.10: Effect of convergence tolerance on the tangential strains in the compression zone

Table 7.3: Effect of convergence tolerance

TOL	Ultimate-load (kN)	Deflection (mm)	Numerical/Exp. Ultimate load	Numerical/Exp. Deflection	Radial strain	Tangential strain	No.of inc.	Total time (secs)
1%	32.86	3.772	1.030	0.921	-0.00167	-0.00026	183	81
5%	32.76	3.900	1.027	0.953	-0.00168	-0.00026	153	58
10%	32.75	3.910	1.027	0.956	-0.00177	-0.00028	155	60

7.3.1.2 Effect of the Size of Arc Length

Three different sizes of arc length were studied: 0.01, 0.1, 1.0, in order to keep the computational cost at a reasonable level. The results obtained from the analysis are shown in Figures 7.11 to 7.13 and Table 7.4. From Table 7.4, arc length of 0.01 and 1.0 predicted the highest value of the ratio of numerical to experimental ultimate load along with almost same radial and tangential strains. In contrast by using arc length of 1 the computational cost is increased by 11.5 times the computational cost using arc length of 0.01.

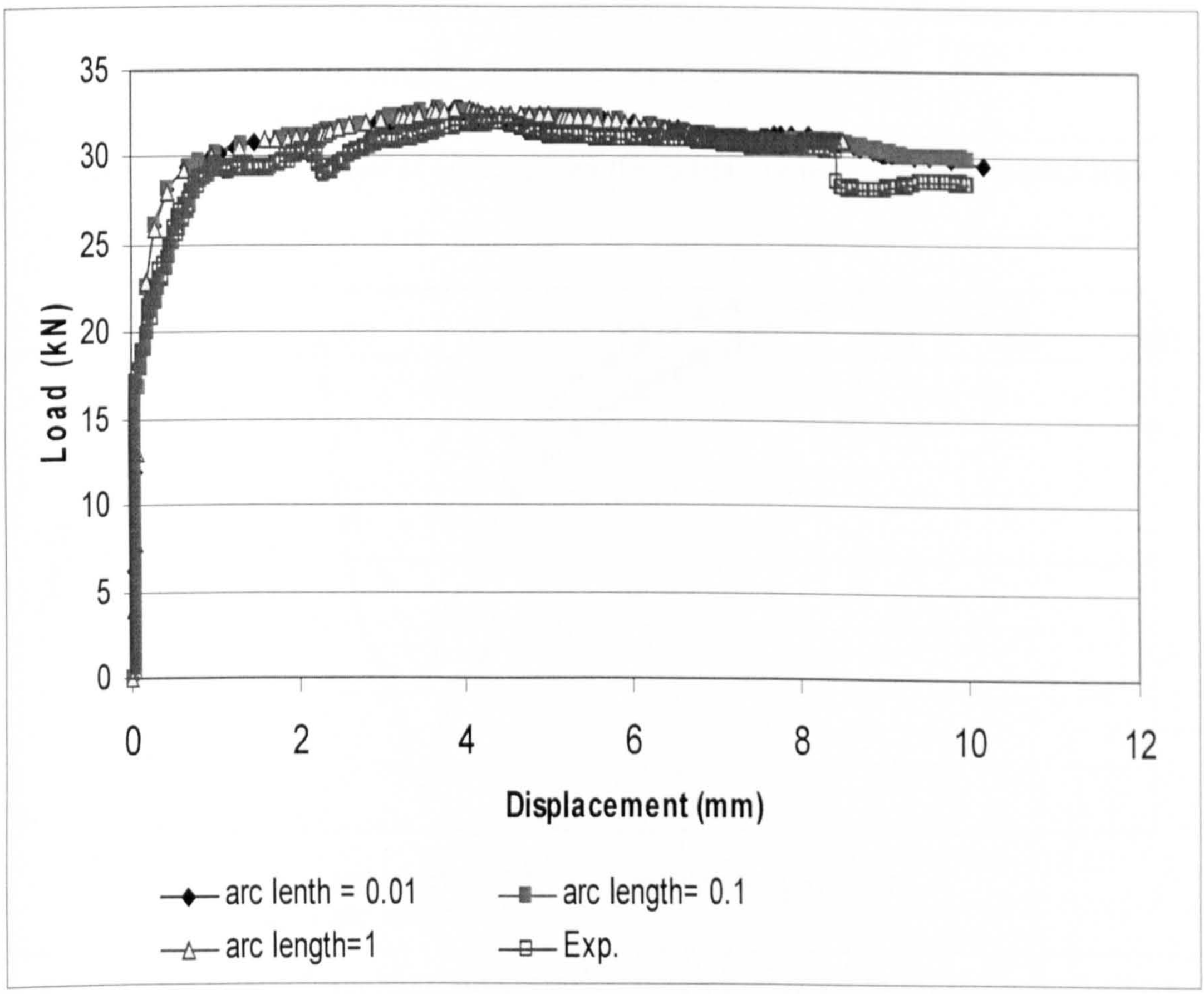

Figure 7.11: Effect of size of arc length on the load-displacement behaviour

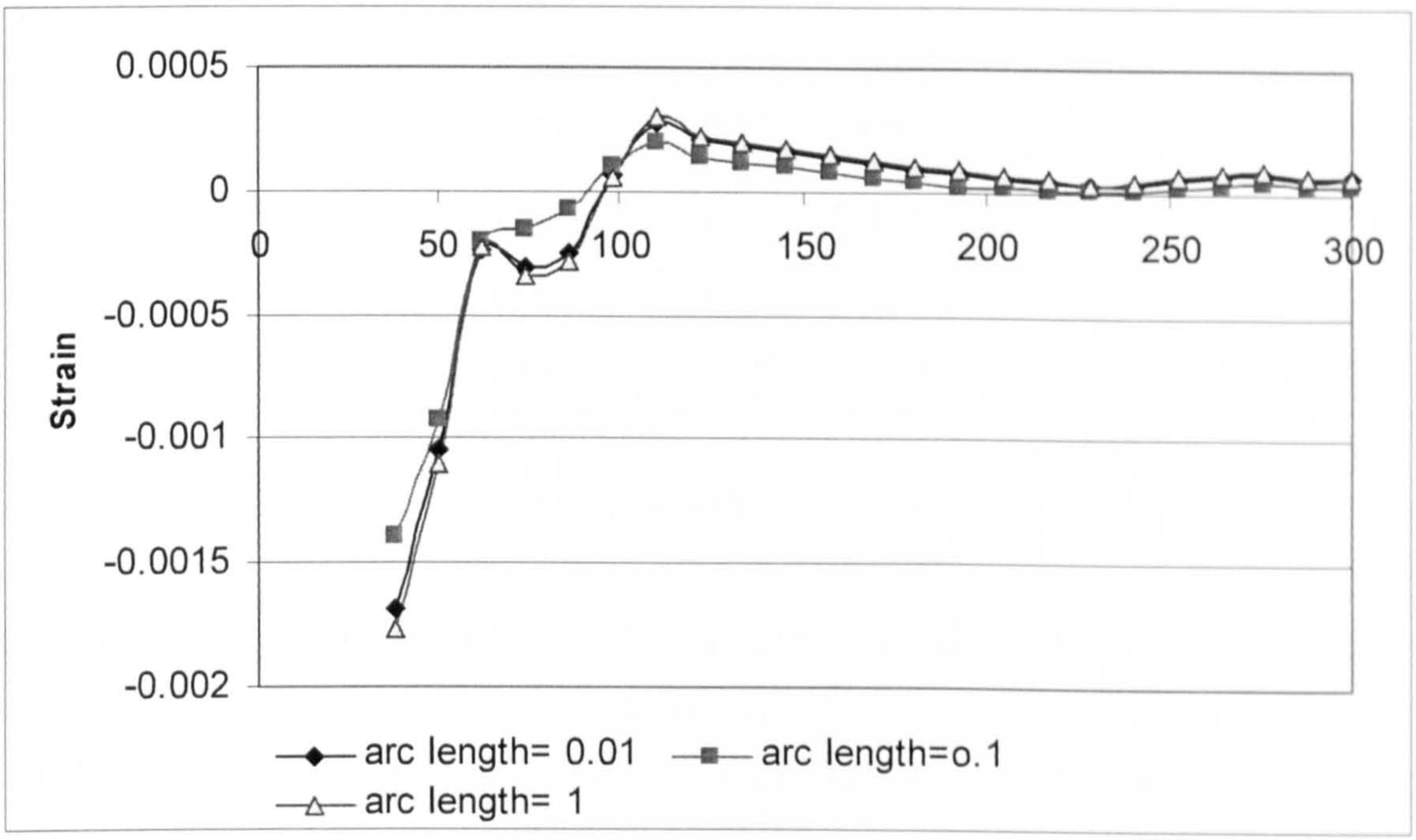

Figure 7.12: Effect of size of arc length on the radial strains in the compression zone

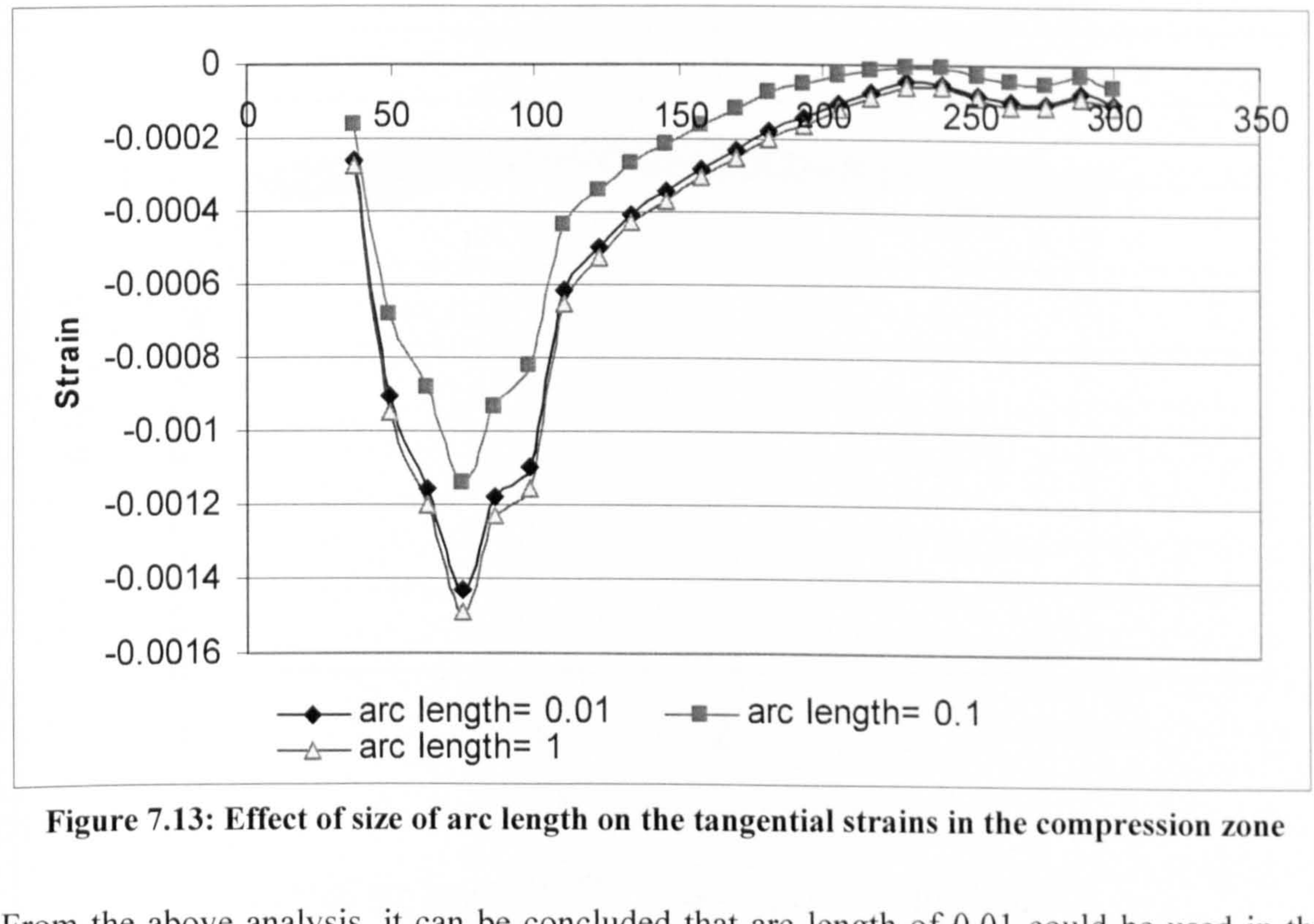

Figure 7.13: Effect of size of arc length on the tangential strains in the compression zone

From the above analysis, it can be concluded that arc length of 0.01 could be used in the current analysis, in order to get reasonably good results and to reduce the computational cost.

Table 7.4: Effect of arc length

Arc length	Ultimate -load (kN)	Deflection (mm)	Numerical/Exp Ultimate load	Numerical/Exp Deflection	Radial strain	Tangential strain	No.of inc.	Total time (secs)
0.01	32.76	3.900	1.027	0.953	-0.00168	-0.00026	153	58
0.1	32.803	3.676	1.027	0.898	-0.00139	-0.00016	634	187
1	32.653	3.673	1.022	0.897	-0.00177	-0.00027	1451	681

7.3.1.3 Effect of the Size of Initial Arc Length

In the numerical procedure, three initial arc lengths were studied 0.01, 0.001 and 0.0001. Figures 7.14 to 7.16 show that the structural responses are similar for different values of initial arc length except that smaller value of initial arc length predicted lower deflection at ultimate load.

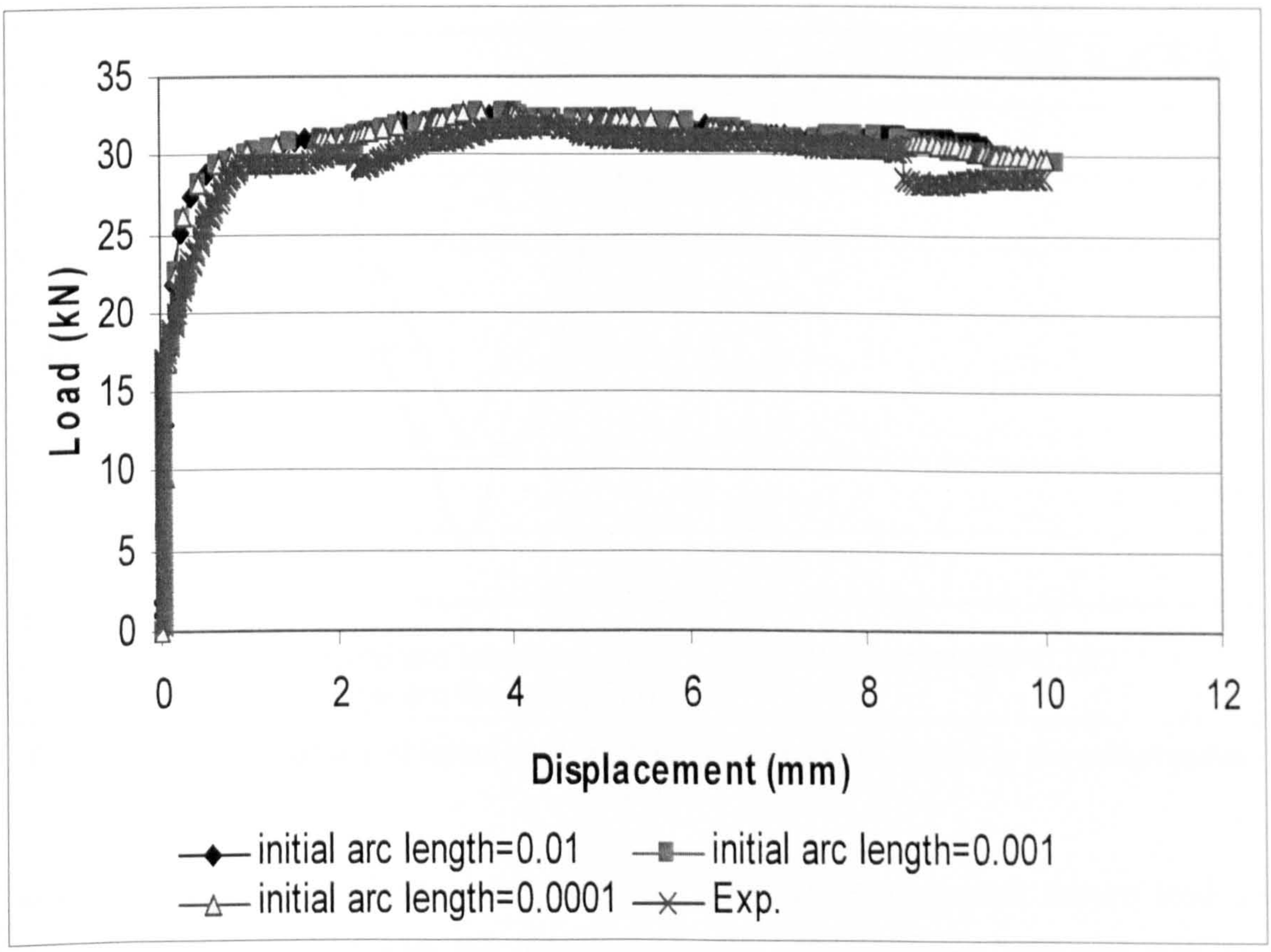

Figure 7.14: Effect of size of initial arc length on the load-displacement behaviour

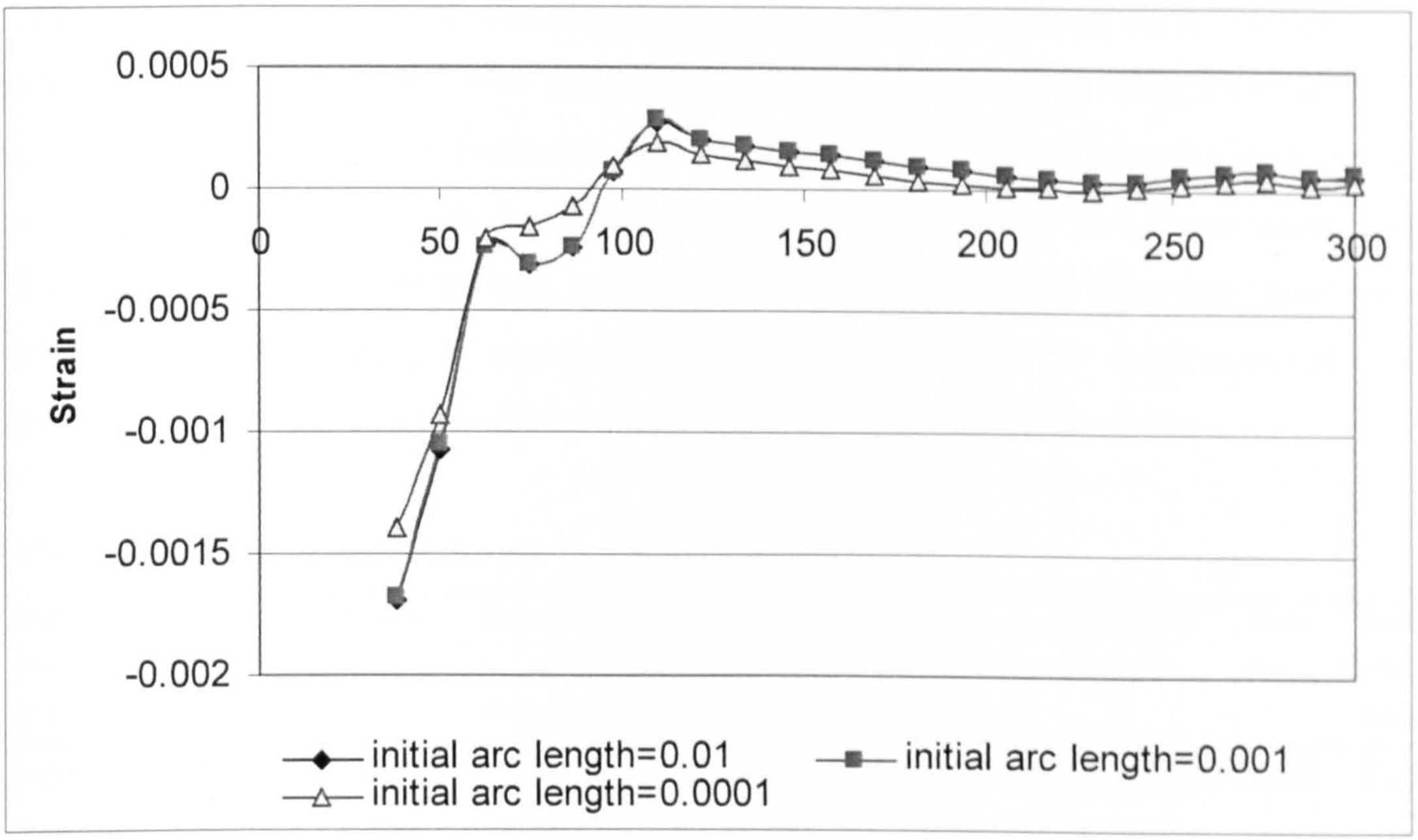

Figure 7.15: Effect of size of initial arc length on the radial strains in the compression zone

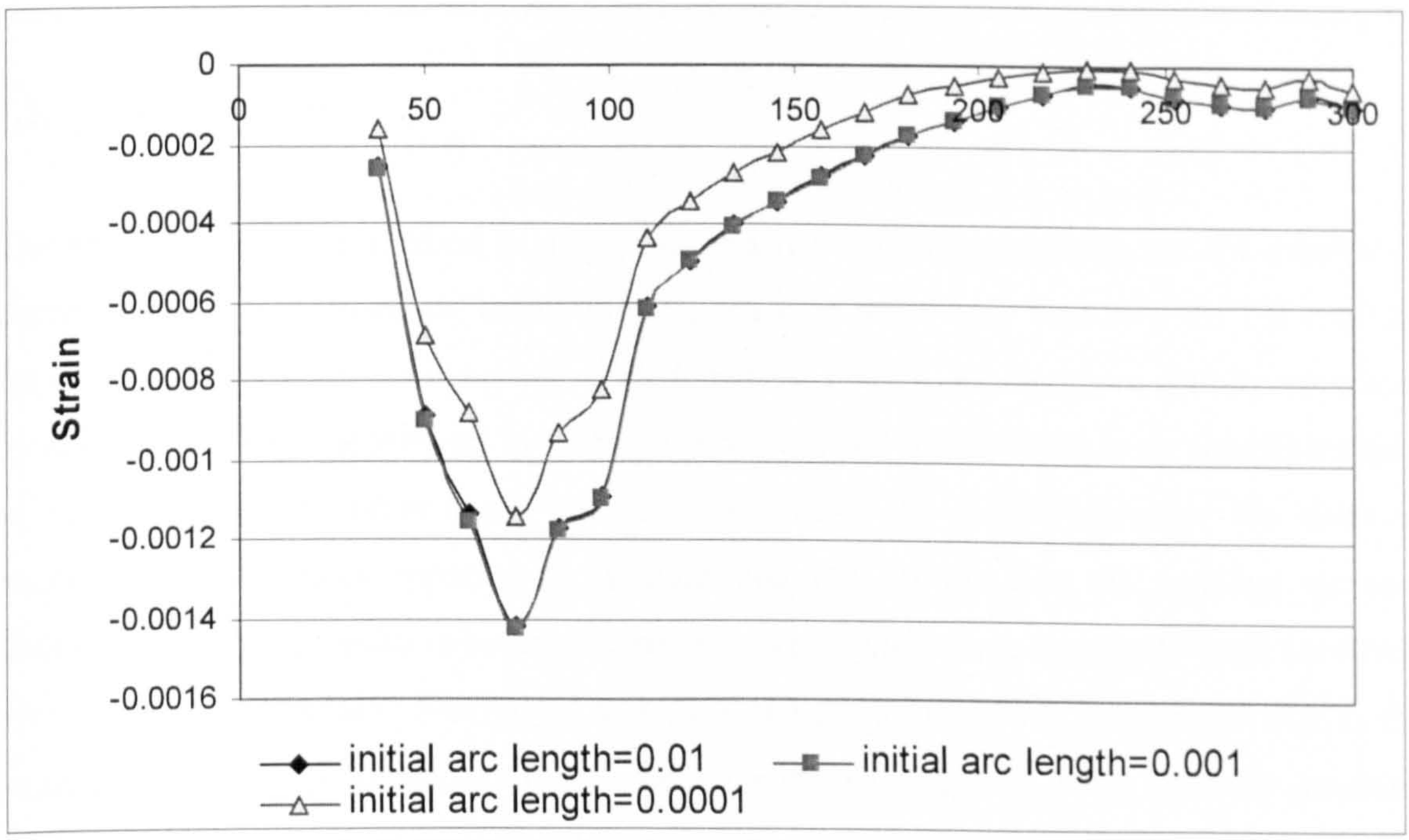

Figure 7.16: Effect of size of initial arc length on the tangential strains in the compression zone

Table 7.5 shows the variation of the ratio of predicted/experimental failure load and deflection at failure load with the initial arc length. The ultimate load and deflection predicted for the three initials arc length are almost the same (see Table 7.5), but using

initial arc length of 0.0001 will reduce the radial and tangential strain in the compression zone at the column face by 5.73% and 10.10%. Whereas, the strains using 0.01 and 0.001 are almost same but the computational cost increased by about 8.5 times (as measured by the solution time) and the number of iteration increased by about 14.6 times when using 0.01 initial arc length. Therefore, using smaller initial arc length does not show much difference in the structural behaviour other than increasing the computational cost. Therefore, a 0.001 arc length will be used throughout the present investigation.

Table 7.5: Effect of initial arc length

Initial arc Length	Ultimate -load (kN)	Deflection (mm)	Numerical/Exp. Ultimate load	Numerical/Exp. Deflection	Radial strain	Tangential strain	No.of inc.	Total time (secs
0.01	32.56	3.818	1.019	0.933	-0.00169	-0.00025	2235	1276
0.001	32.76	3.900	1.027	0.953	-0.00168	-0.00026	153	58
0.0001	32.803	3.676	1.027	0.898	-0.00139	-0.00016	155	53

7.3.1.4 Mesh Density

The accuracy of the FE method is largely dependent on the mesh density, i.e. the number of elements used. It is, therefore extremely important to asses how sensitive the FE analysis for the present problem is to varying mesh densities. The FE solutions are usually improved by refining the mesh density up to a certain limit, beyond which there is no significant gain in accuracy. On the other hand, the finer the mesh the more expensive the solution becomes. It has been reported by Bazant and Oh (1983) that the smallest element dimension in an FE model is controlled by the size of the coarse aggregate used i.e.10mm used in the present study. Moreover, Kotsovos and Pavlovic (1995) pointed out that as the experimental conditions under which the constitutive relations were derived involved measurements taken from strain gauges that were approximately two to three times larger than the maximum aggregate size used in the concrete mix, it is clear that a lower-bound limit to the size of an FE is provided by such a gauge length. The mesh employed in this study was arrived at taking into account these considerations along with the computational effort involved. Thus, the present study was set up to obtain an economical FE mesh density that ensures convergence of the values of ultimate load, stresses and deflections.

Furthermore, in the present study the mesh sensitivity was not to some extent taken into consideration by modelling the tensile behaviour of concrete with a stress-strain relation rather than with a stress-displacement relation. However, it was of interest to check how the model used in the present analysis, would respond to a change of the mesh density. Hence, a dense mesh and coarse mesh were checked in the additional analysis. The dense mesh has 60 elements instead of 39 elements in the original mesh. The coarse mesh has 30 elements. For both the dense and the coarse mesh, the same type of elements was used as in the original mesh i.e. axi-symmetric solid elements with eight nodes. All the FE meshes are shown in Figure 7.17. In Figures 7.18 to 7.20 the load-deflection curves and radial and tangential strains in the compression zone obtained with the three different meshes are compared.

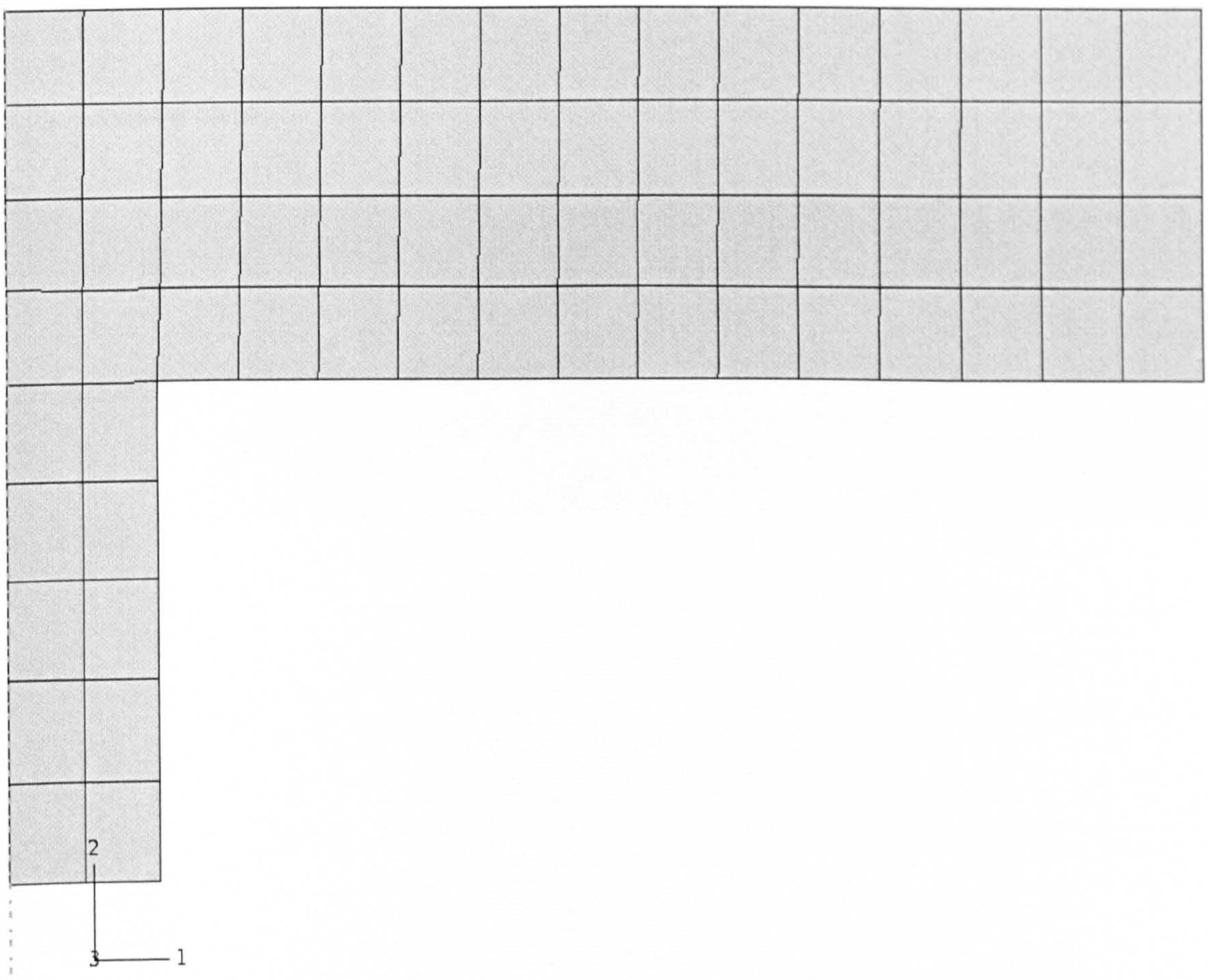

a. dense mesh

b. original mesh

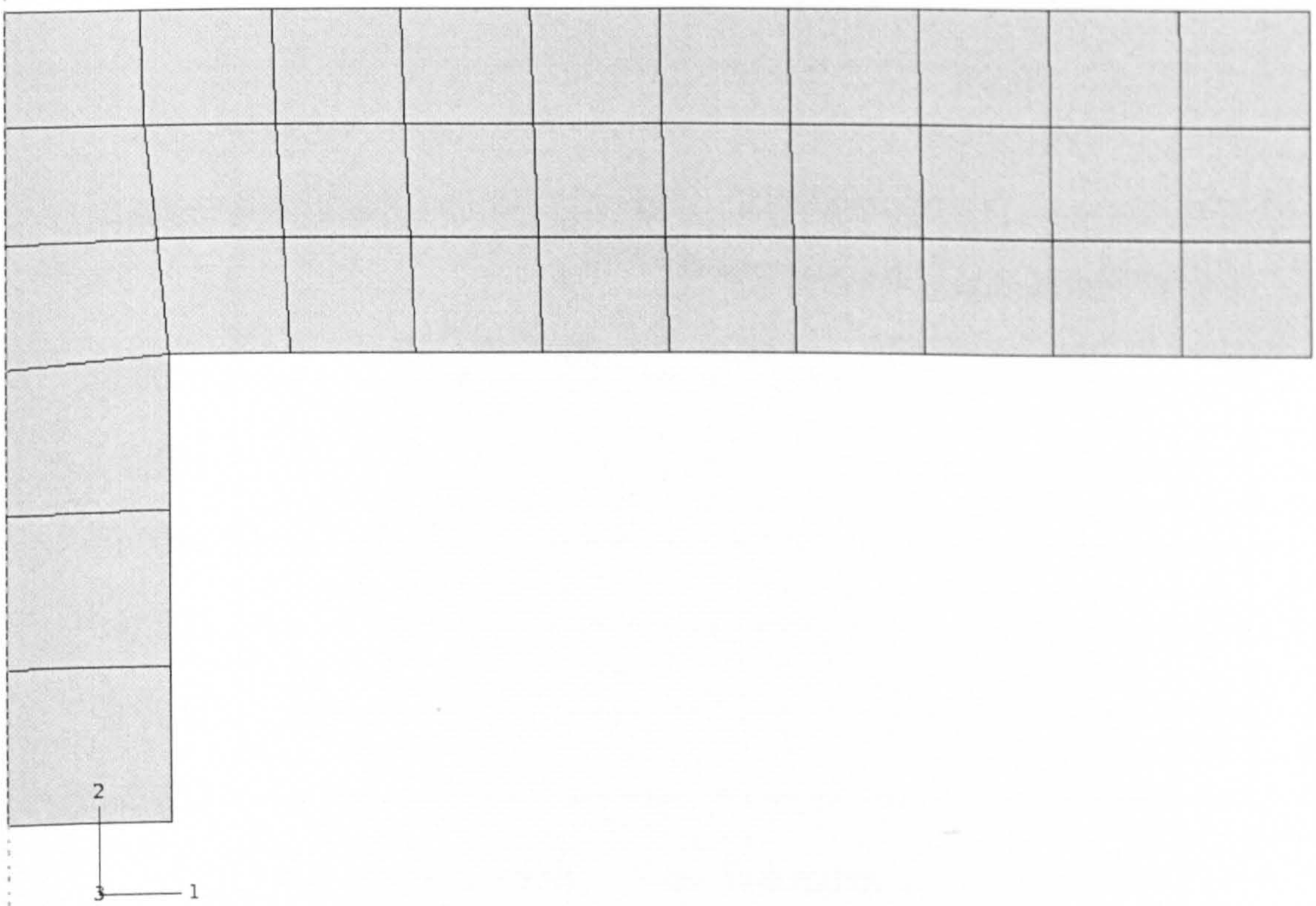

c. coarse mesh

Figure 7.17: FE meshes (a. dense mesh, b. original mesh and c. coarse mesh)

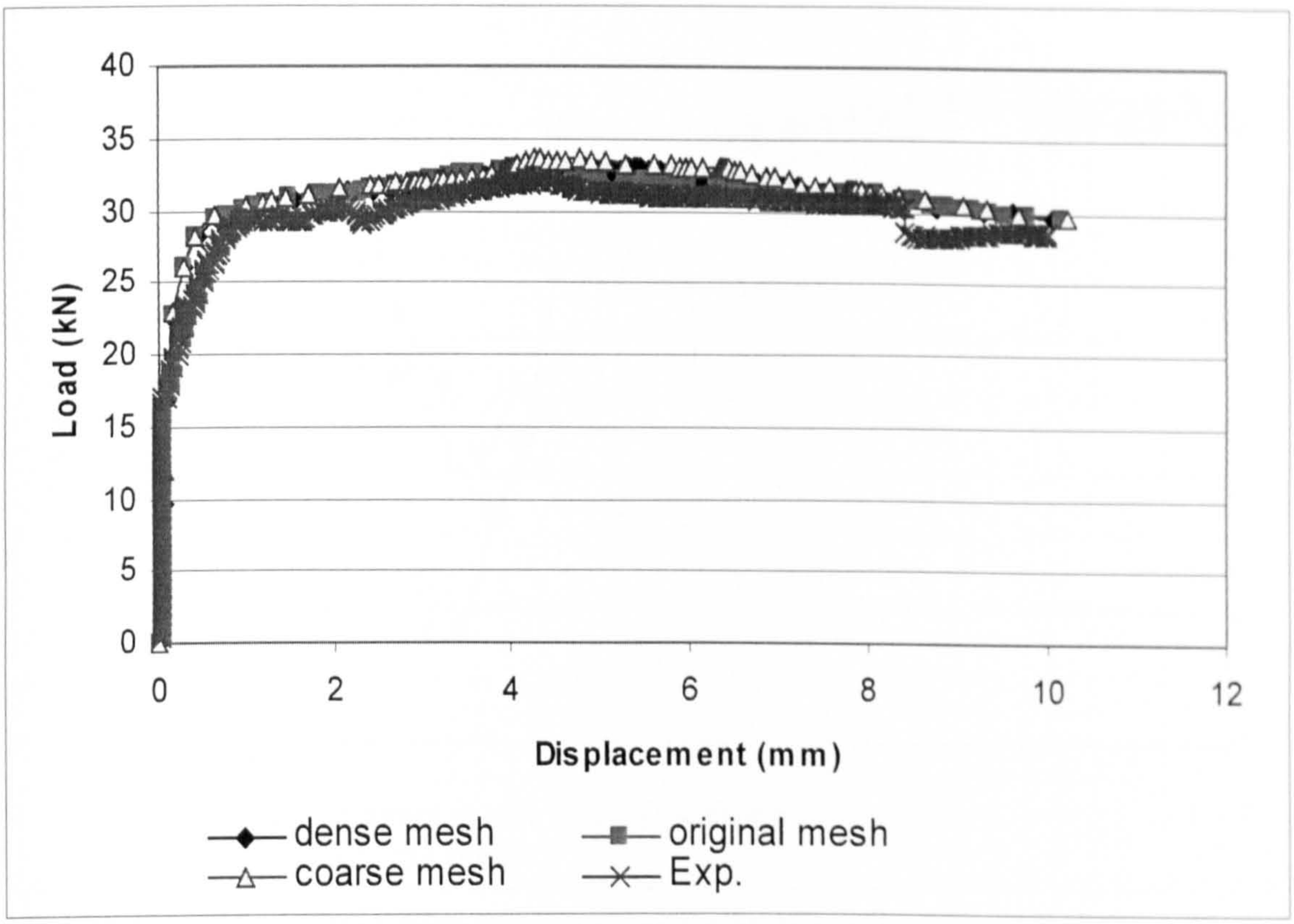

Figure 7.18: Effect of mesh size on the load-displacement behaviour

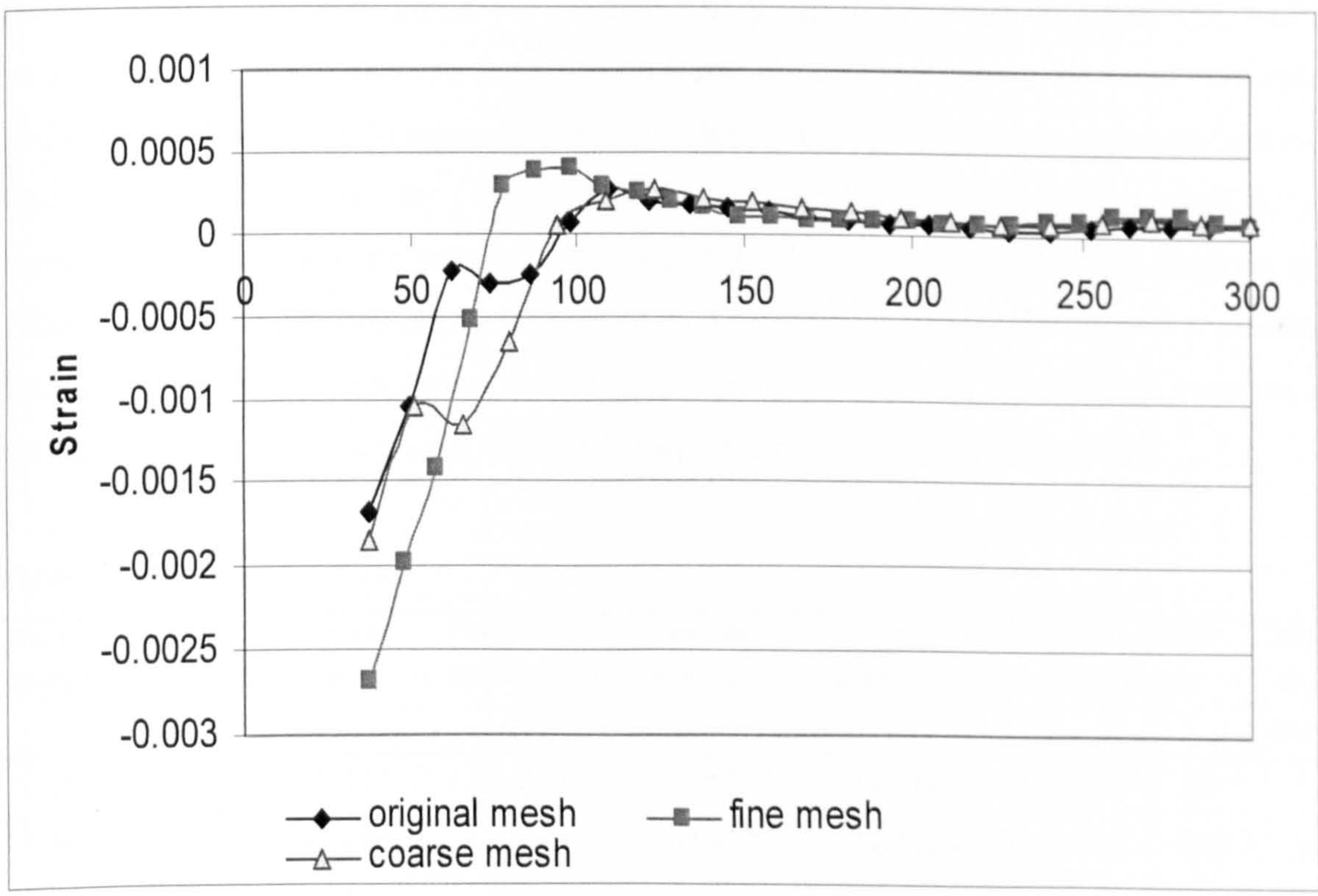

Figure 7.19: Effect of mesh size on the radial strains in the compression zone

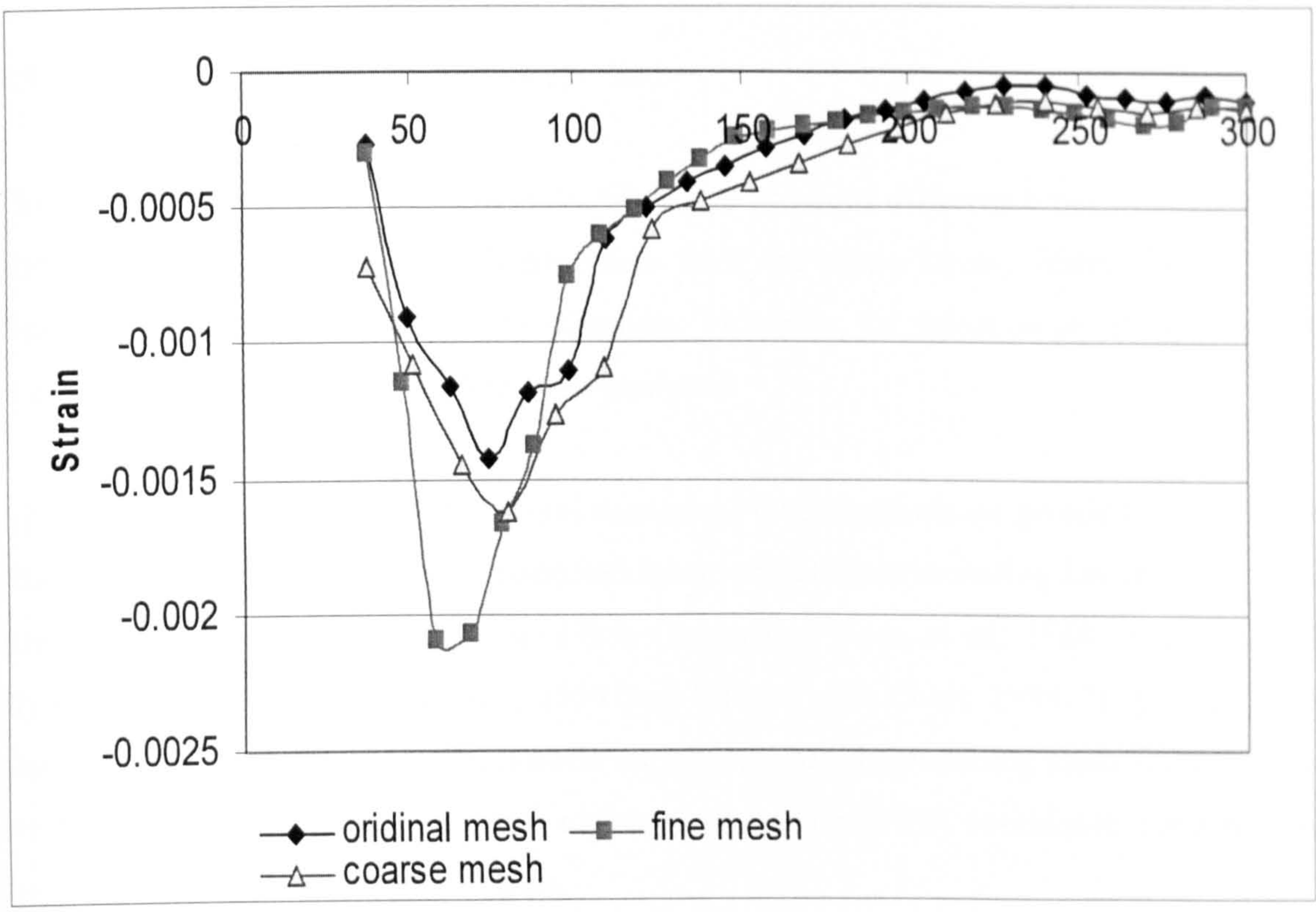

Figure 7.20: Effect of mesh size on the tangential strains in the compression zone

The results of the analysis are shown in Table 7.6. It can be seen that the mesh size, within the range of the chosen meshes, have a little influence on the ultimate load and behaviour of the slab (i.e. strains in compression zone). Hence, the results are not particularly mesh dependent. Furthermore, the convergence was practically achieved with a mesh of 39 elements, as increasing the number of elements to 60 did not significantly improve the solution but only increased computational cost. Therefore, in order to achieve a consistent, accurate and economical solution, the adopted mesh in the present FE analysis, consists of square axi-symmetrical elements with a plan square area with a width of 25mm.

Table 7.6: Effect of mesh size

No. of elements	Ultimate -load (kN)	Deflection (mm)	Numerical/Exp Ultimate load	Numerical/Exp Deflection	Radial strain	Tangential strain	No.of inc.	Total time (secs)
30	33.67	4.351	1.055	1.063	-0.00183	-0.00070	86	37
39	32.76	3.900	1.027	0.953	-0.00168	-0.00026	153	58
60	32.96	5.366	1.033	1.309	-0.00268	-0.00030	163	68

7.3.1.5 Element Type for Modelling the Slab

The general purpose finite element code ABAQUS provides different types of elements for one- two- and three-dimensional problems such as plane stress, plane strain, three-dimensional solid elements, and shell elements. However, the selection of the element type is always related to type of problem to be analysed.

As presented in Chapter Three, several numerical investigations on punching of concrete slabs, using the FEM, have been conducted by several authors including Loesth et al, 1982; Andra, 1982; De Borst and Nauta, 1985; Gonzalez-Vidosa et al, 1988, Malvam,1992; Dyngel and et al, 1994, Menetrey, 1994 and Marzok and Chen, 1993. In general, three element types are used for the FE models which simulate the punching shear failure. These are two dimensional shell and plate elements, axi-symmetrical continuum elements and three-dimensional continuum elements.

a) Plate and Shell Element

In this case the slab is modelled as two-dimensional (2-D) and thus the stresses and the strains in the direction normal to the surface are neglected. The degrees of freedom are the vertical translation and the rotations associated with the bending. This element type is suitable for modelling structures when one dimension is much smaller than the other dimensions, as it simplifies a 3-D problem into a 2-D one. It is therefore, a convenient tool for modelling the general bending behaviour of a structure and that is why it is popular for suspended slabs with uniform distributed load. On the other hand, as the problem of pile-supported slabs under punching load distributed over small areas is of a local nature, the 2-D state of stress is not suitable. This was confirmed by Marzouk and Chen (1993) who noted that, although with shell/plate elements acceptable numerical predictions for the experimental results were achieved, the agreement with experimental results was less accurate for slabs which failed in brittle punching than for slabs which failed in more ductile mode. This was due to the fact that the formulation of plate/shell elements is based on the in-plane stresses and not the transverse shear stresses for the failure criteria. This

implies that there is no triaxial effect and hence the inclined crack growth within the slab cannot be observed, which is of a considerable interest in this research. Moreover, the formulation of plate/shell elements assumes that the distribution of strain through the thickness is linear. The actual distribution of strain through the thickness of plate is not necessarily linear.

b) Axi-Symmetrical Element

In this case, the element is essentially axisymmetric, which produces axial, radial and tangential stresses. The degrees of freedom are only translational. Rotational symmetric problems can be simulated with a small number of elements, and therefore, a minimum numerical effort, using axisymmetrical elements. It is effective for problems involving symmetry, e.g. single central load, where the origin of co-ordination is at the load location. However, it is less favourable for modelling asymmetrical loading configurations, e.g. a group of adjacent loads. In addition, slabs with orthogonal reinforcement as well as punching with moment transfer or punching at edge and corner columns cannot be modelled using axi-symmetrical two-dimensional elements. Therefore, this element type was used in the current numerical analysis.

c) Three-Dimensional Element (3-D)

This element models the slab as a 3-D solid rather than a 2-D surface and thus allows for the true triaxial state of stress to be modelled. The element is capable of detecting the direct and shear stresses and strains in three orthogonal directions. The degrees of freedom are the translations in the 3-D space. These elements offer high flexibility and accuracy in the modelling of reinforced concrete structure and generally lead to the most realistic results but the FE-mesh becomes more difficult and the numerical effort is high.

7.4 Validation of Numerical Results

This section presents the results of the analysis of SFRC internal slab-column connection without moment transfer subjected to symmetrical punching load. Experimental data for

SFRC slabs failing in punching, as presented in Chapter Six, have been used to validate a nonlinear finite element programme for concrete. These slabs cover the important parameters governing punching shear strength such as: fibre dosage, fibre aspect ratio, and concrete compressive strength. The analysis used material parameters as shown in Table7.2 while the numerical parameters used were held constant as follows:

- The size of the initial load increment is 0.001
- The maximum number of iterations per increment is 50
- The size of arc length is 0.01
- The convergence criteria based on the residual forces tolerance of 5%
- The study is based on the mesh arrangement of 39 elements
- Axi-symmetrical elements were used, and the analysis was extended to cover a three-dimensional elements

The analysis will look into the predicted behaviour and mode of failure to validate the mathematical model. The validation was based on the correlation between the experimental and predicted values on five aspects of observed structural behaviour:

- The ultimate load capacity of the slab
- The load-deflection response
- The distribution of strains and stresses in concrete within the compression zone
- The crack pattern
- The mode of failure

7.4.1 Ultimate Loads

The finite element and experimental values of ultimate loads and the associated deflections at the centre of the test slabs are summarised in Table 7.7 along with the comparison between the two sets of values. It can be observed that the finite element method overestimates the ultimate load compared with the experimental predictions. This was pointed out by Kwon and Spacone (2002), who noted that although the smeared crack approach is consistent with the FE philosophy, it may lead to an overestimation of the shear strength of structural members.

Table 7.7: Ultimate load predicted using FEA

Slab no.	Ultimate load Experimental results (kN)	Ultimate load (FEA) (kN)	Predicted/ experimental ultimate load
S2	20.70	23.78	1.15
S3	28.36	31.54	1.11
S4	19.07	19.36	1.02
S5	31.94	32.76	1.03
S7	33.74	36.85	1.09
S8	29.34	32.96	1.12

The agreement between the analysis and the experiment results is generally close with the mean value of the ratio between the analytical and experimental results being 1.102 and the standard deviation being 0.054 respectively. The maximum deviation is 14.9% as in the case of the specimen slab S2.

In view of the approximations involved in the analysis the prediction by the finite element modelling was in close agreement with the test observation.

7.4.2 Load-Deflection Curve

In Figure 7.21 to Figure 7.26, the load-deflection curves obtained from the FE analysis are compared with the curves obtained from the test of SFRC slabs. The load and deflection before crack and at first crack in the analysis were very much in agreement with the experimental values. At the peak load the values of load obtained from FE analysis were close to the test results. However, the deflection obtained from FEA was less than those in the test. One possible reason for the lower deflection may be due to the fact that the effect of bond-slip between concrete and fibres being neglected in the FE model. The loads are in good agreement with the test observations in all stages (first linear behaviour up to first crack, ultimate load and unloading path after having reached a peak load).

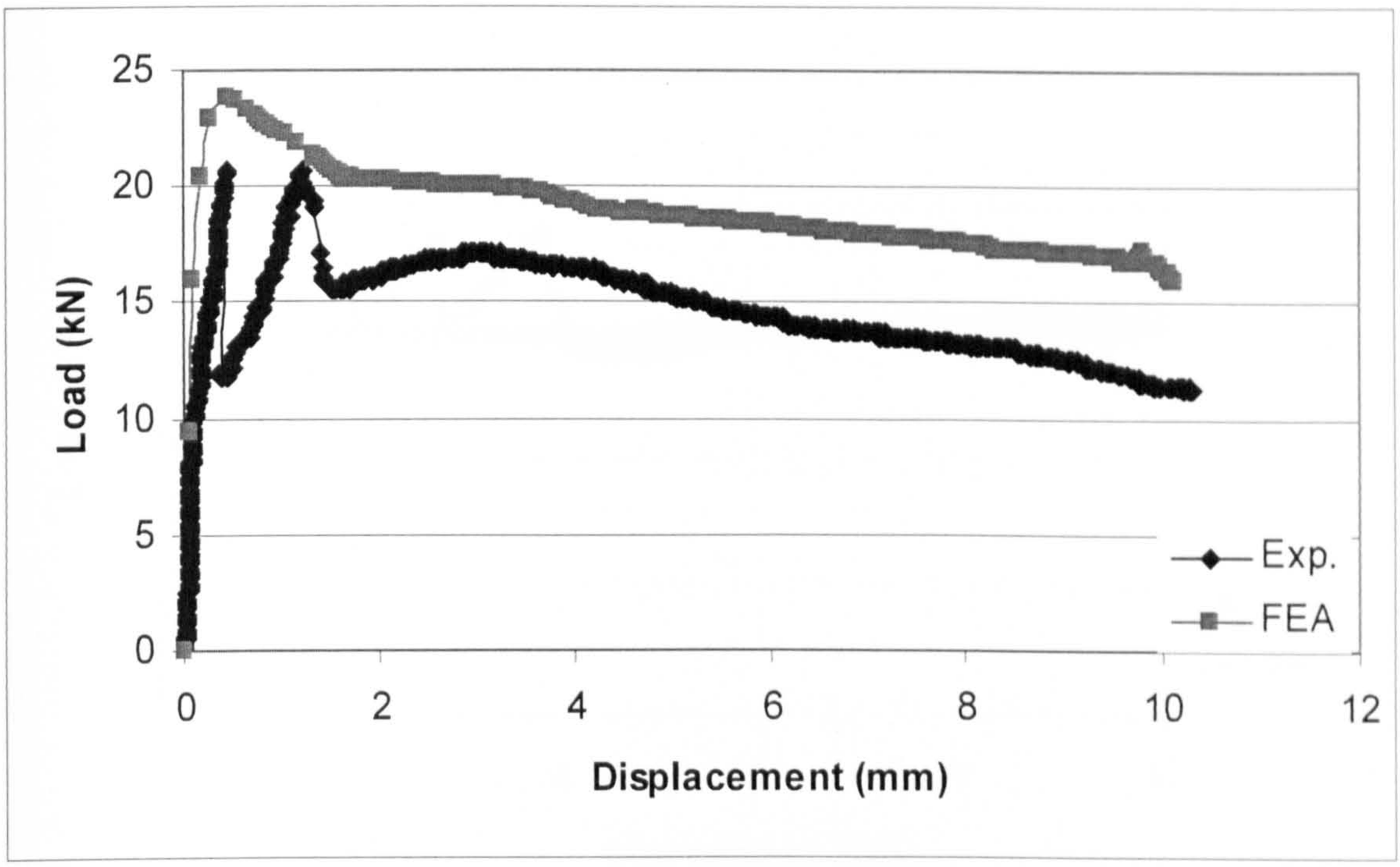

Figure 7.21: Numerical load-deflection response for slab S2

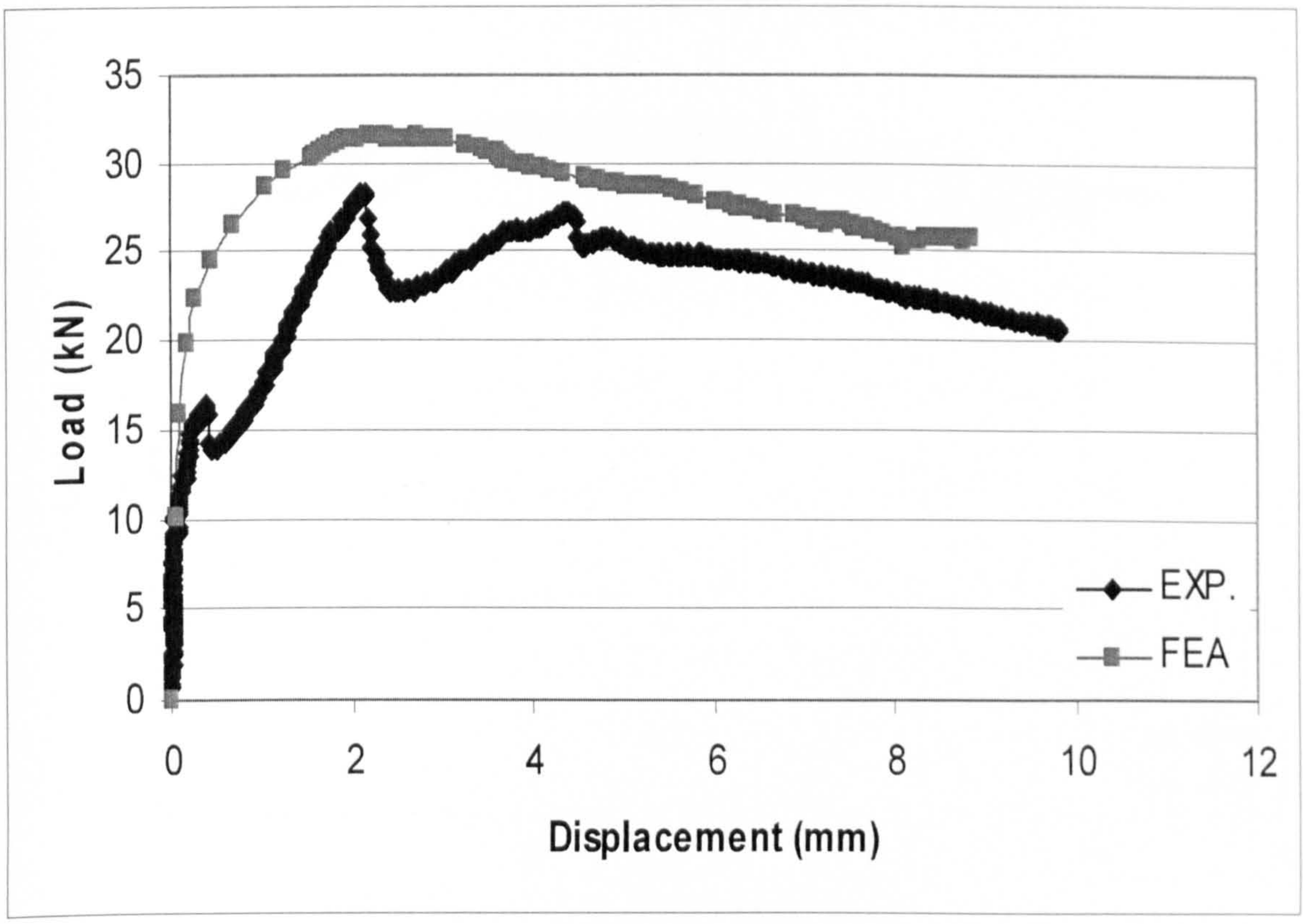

Figure 7.22: Numerical load-deflection response for slab S3

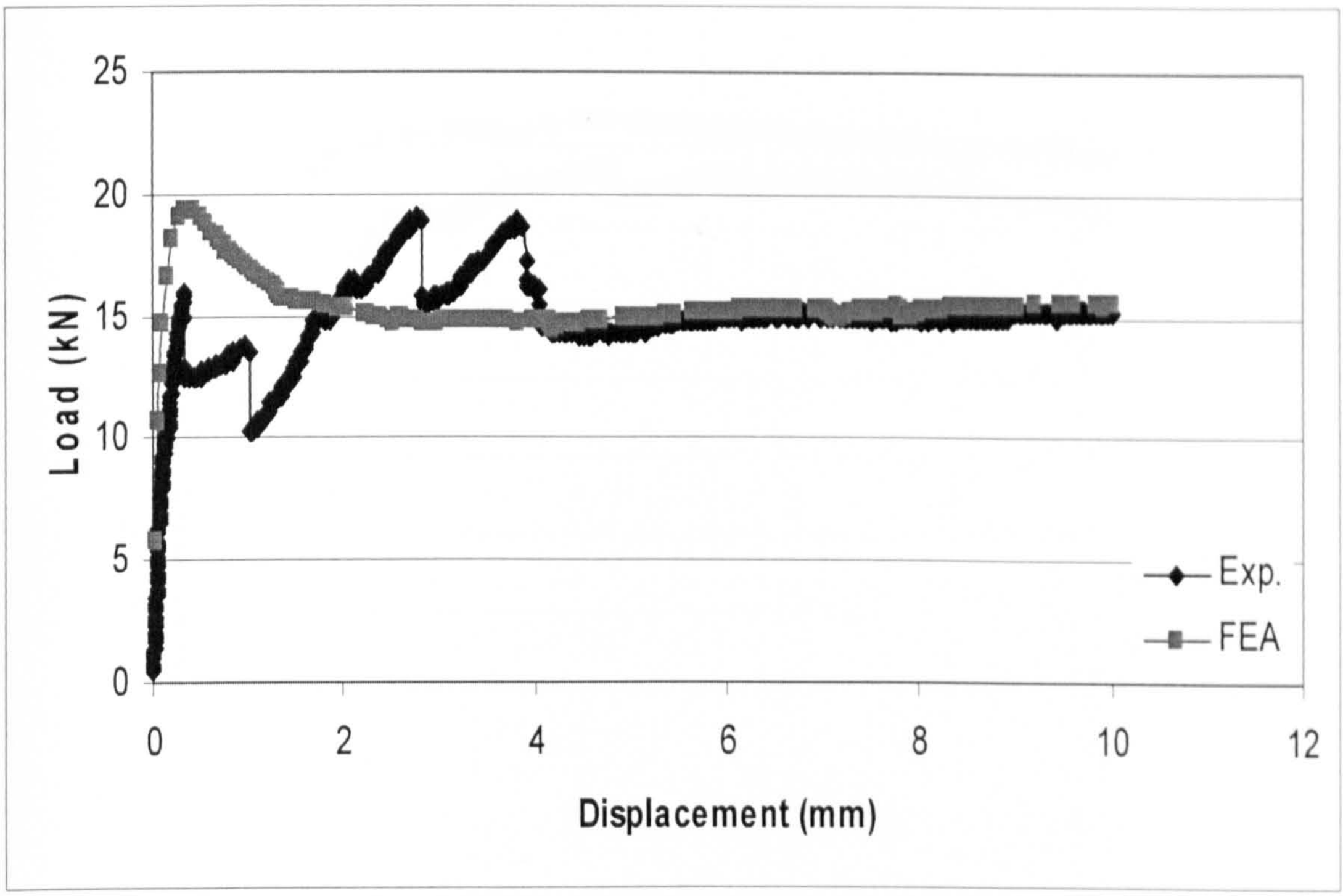

Figure 7.23: Numerical load-deflection response for slab S4

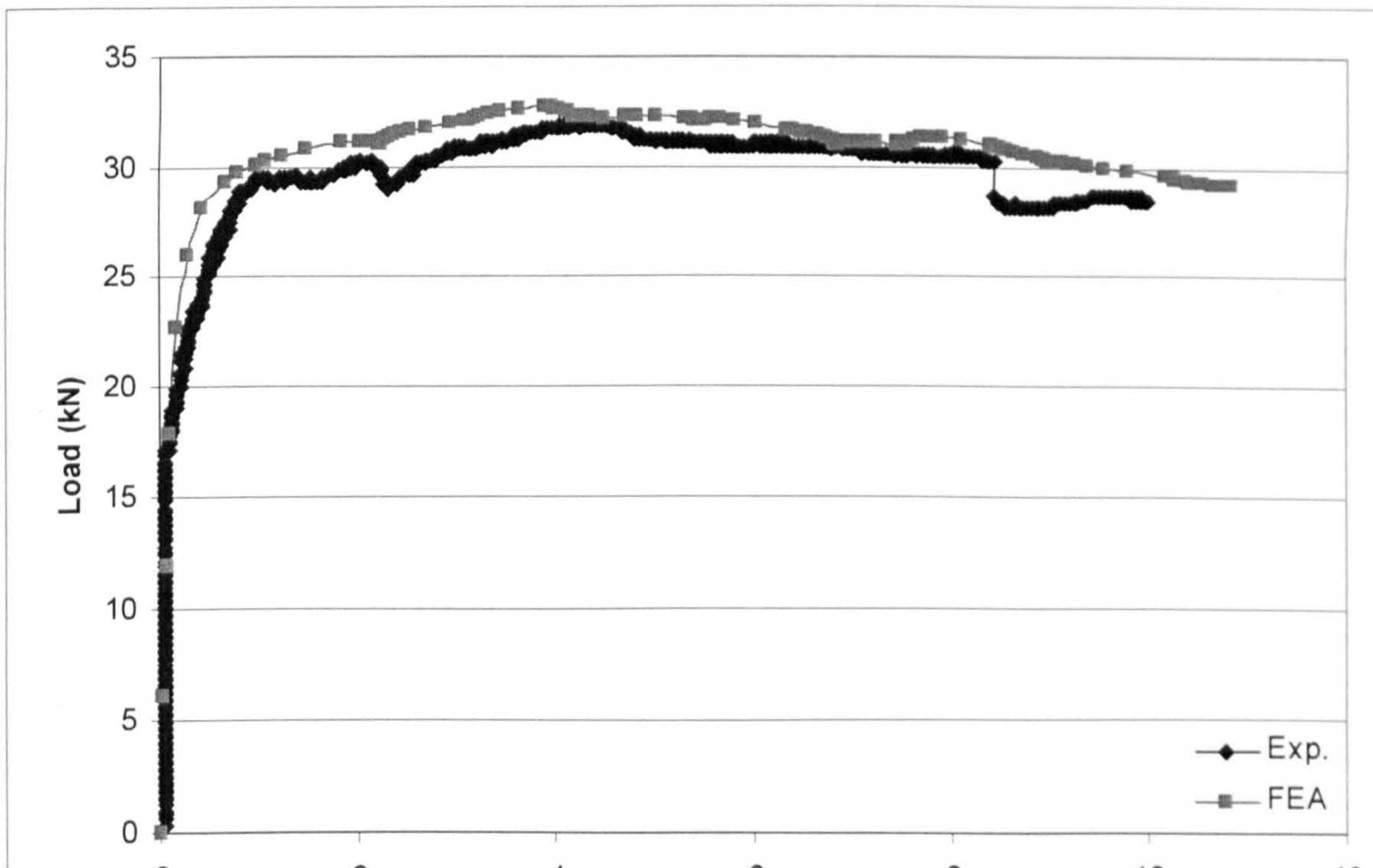

Figure 7.24: Numerical load-deflection response for slab S5

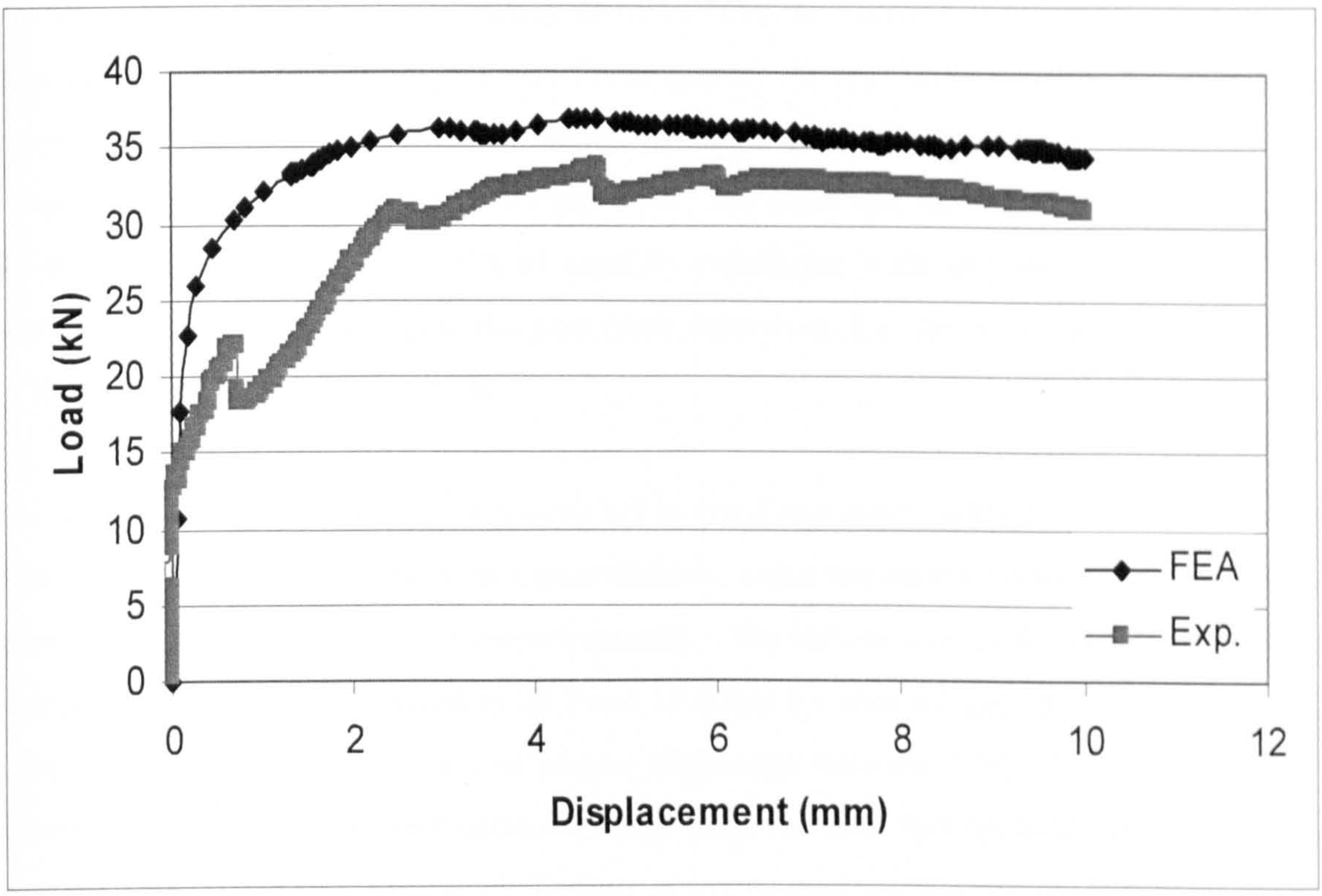

Figure 7.25: Numerical load-deflection response for slab S7

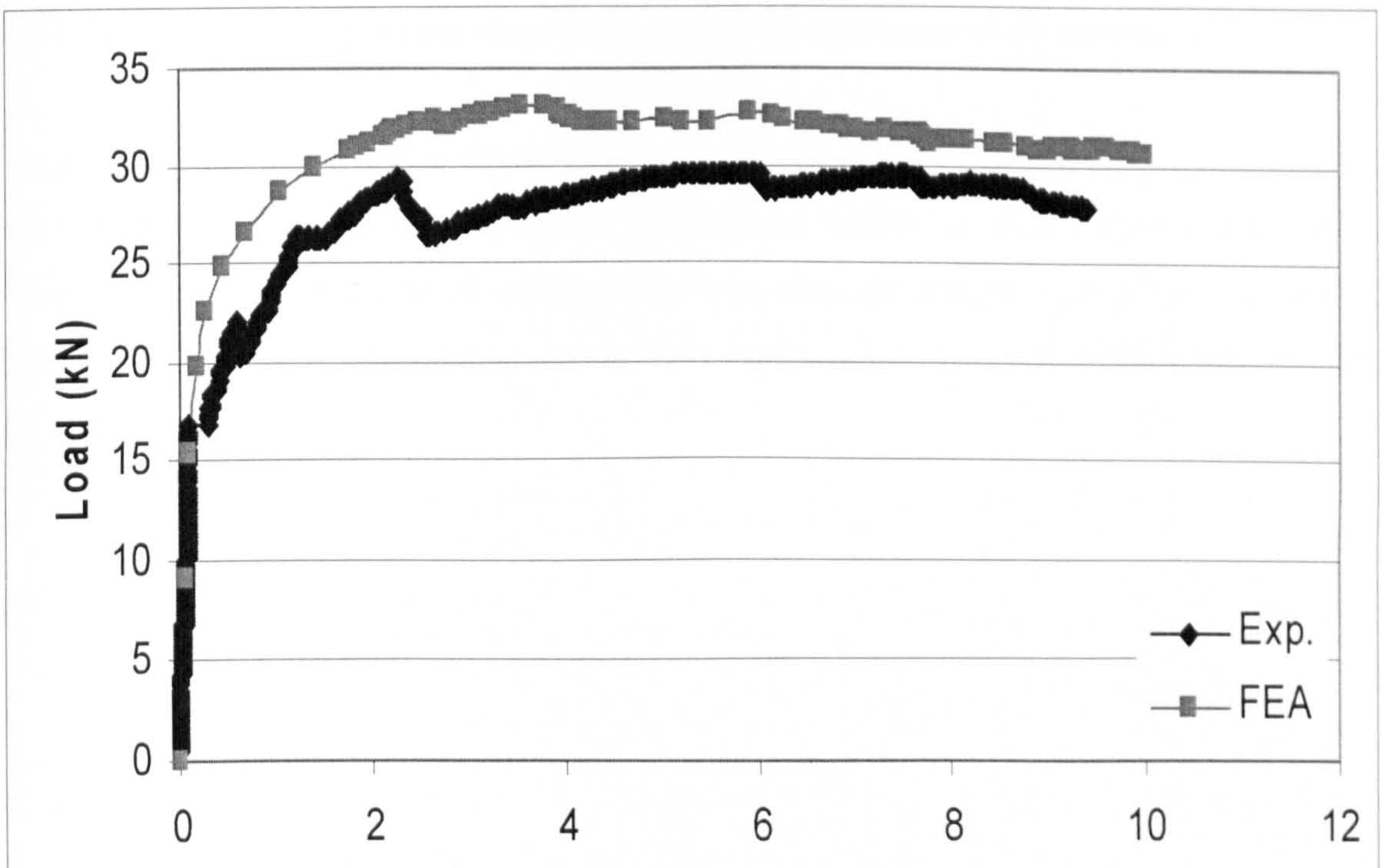

Figure 7.26: Numerical load-deflection response for slab S8

For slab S5, the load increased linearly up to 16.46kN at which the first crack was detected. The curve now continued in the non-linear phase. At the load 29.34kN initial inclined cracking, i.e. shear cracking, was detected. At the load 32.7kN the load reached its peak value. The ultimate load was in agreement with the observed ultimate load of slab S3, S5, S7 and S8 a gradual decrease of load capacity was found with increasing displacement. It was hence, possible to simulate the post-peak behaviour, i.e. the post punching behaviour of the slabs in the present analysis.

For slabs S2 and S4, the FE models were not in good agreement with the test results. These slabs performed experimentally in a poor fashion, since the added fibres did not contribute to extra punching shear capacity experimentally. The failure load of the reference slab (i.e. slab S1) was 16.78kN compared to 20.7 and 19.07kN for slab S2 and S4, respectively. The poor behaviour was due to lack of proper anchorage between fibres and concrete. The presence of instability in load-deflection plot indicates that this volume fraction is lower than the critical volume fraction V_c. Indeed, if the volume fraction of the fibres is less than V_c, the stress sustainable by the composite drops either when the matrix cracks, or when some stable de-bonding occurs immediately after the extension of the matrix crack.

Figure 7.27 shows a typical deformed mesh at ultimate load. The deformation of the slab is concentrated to the slab portion above the column within an area between the vertical symmetry line and an about 30 inclined line from the slab-column root to the top surface. Outside this area, the slab seems to rotate as a rigid body. This is in good agreement with the test observations.

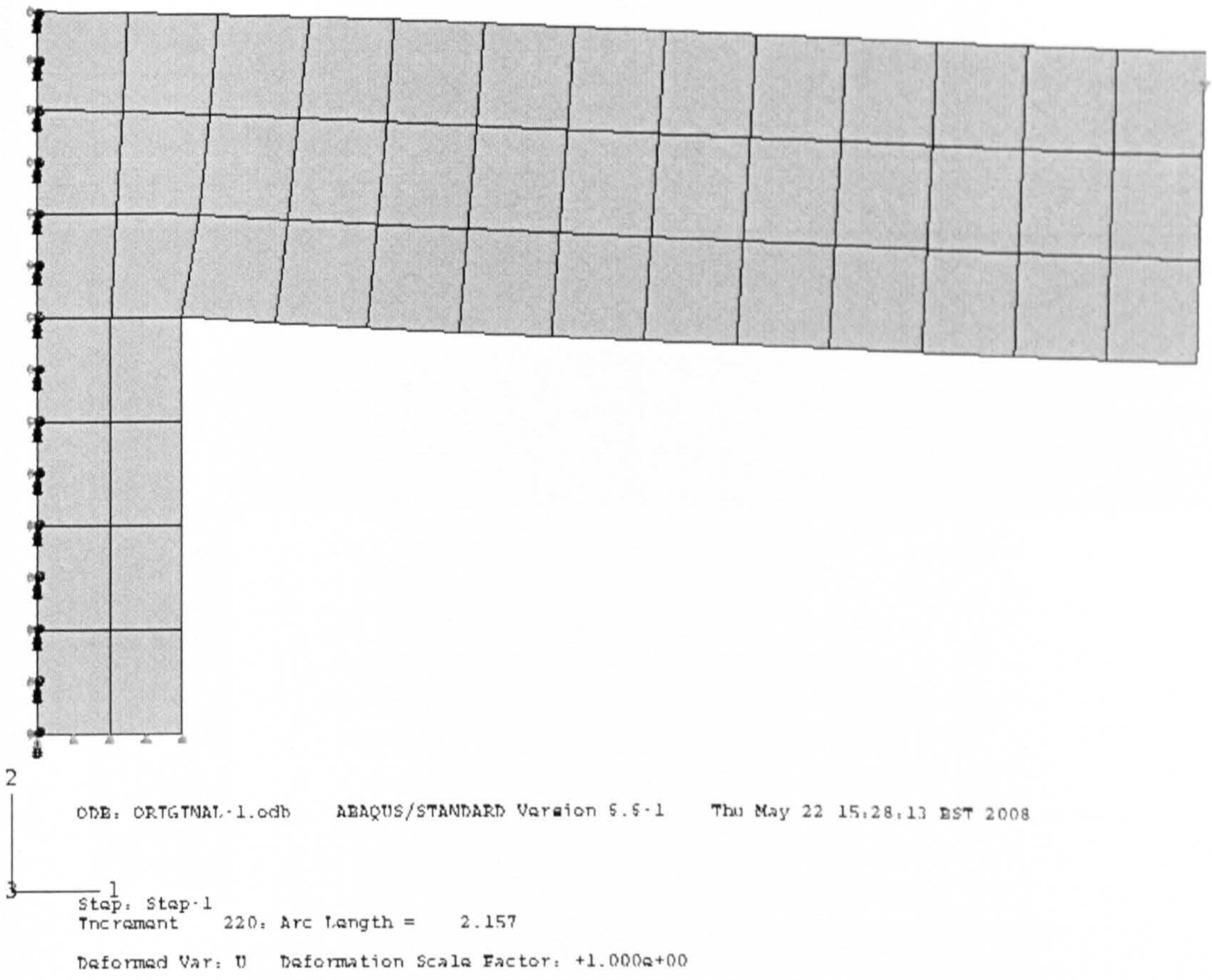

Figure 7.27: Typical deformed mesh at ultimate load

7.4.3 Stresses and Strains

Figure 7.28 shows a typical vector plot of principal stresses obtained with the FE analysis. In the analysis, stresses are actually element properties which are associated to the integration points of the finite elements. In the plot, the stresses are extrapolated to and averaged at the nodes. The plot clearly shows the inclined strut of compressive stresses from the slab-column root to the top side of the slab. As expected, the highest compressive stresses were found immediately above the slab-column root. At this area and towards the circumference of the slab, the state of stress in the compression zone turns into a bi-axial state.

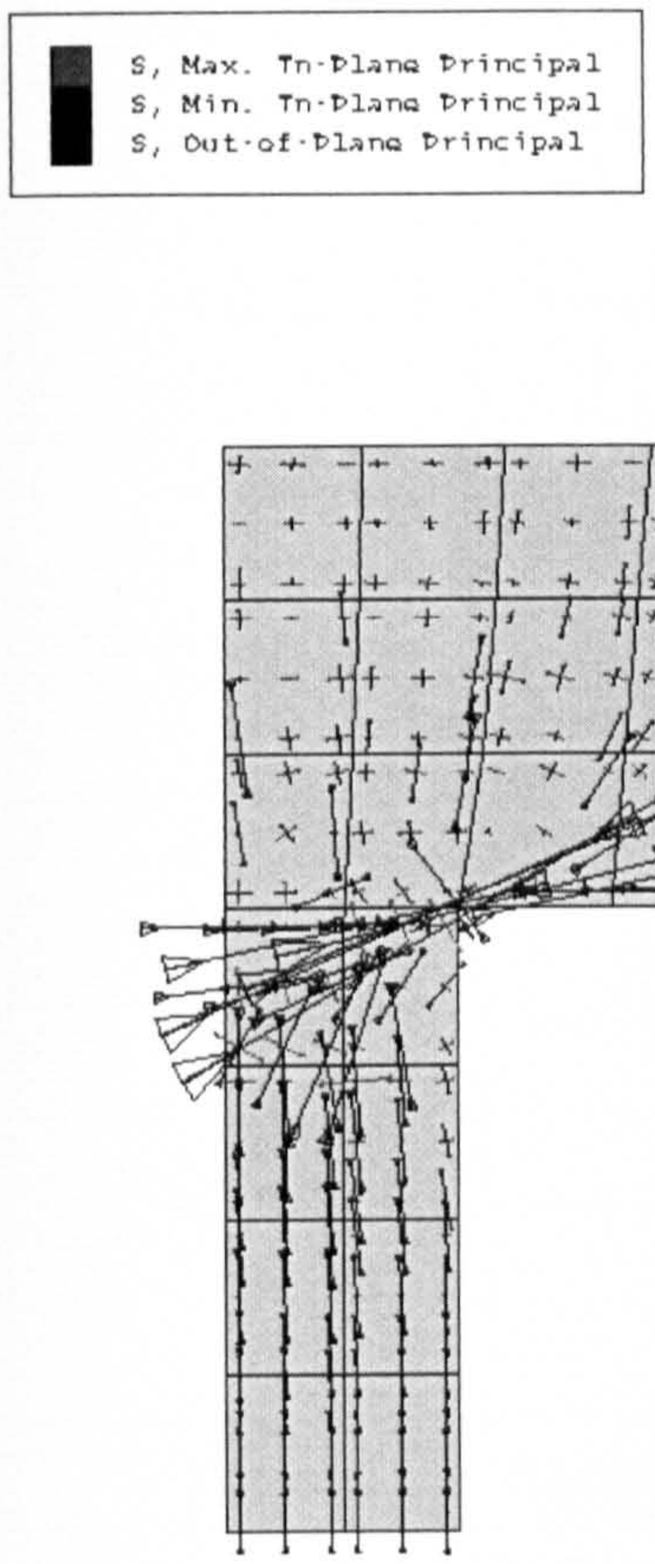

Figure 7.28: Typical vector plot of principal stresses

Figure 7.29 to 7.34 show the predicted distribution of strains and stresses sustained by concrete within the compressive zone (at the Gauss points closest to the surface of the slab), for all the slabs. In the figures the stresses are normalised to the uniaxial compressive stress of concrete. Two types of failure were noticed; brittle failure (brittle-punching) as in slab S2 and slab S4 and more ductile failure (ductile-punching) as in slabs S3, S5, S7 and S8.

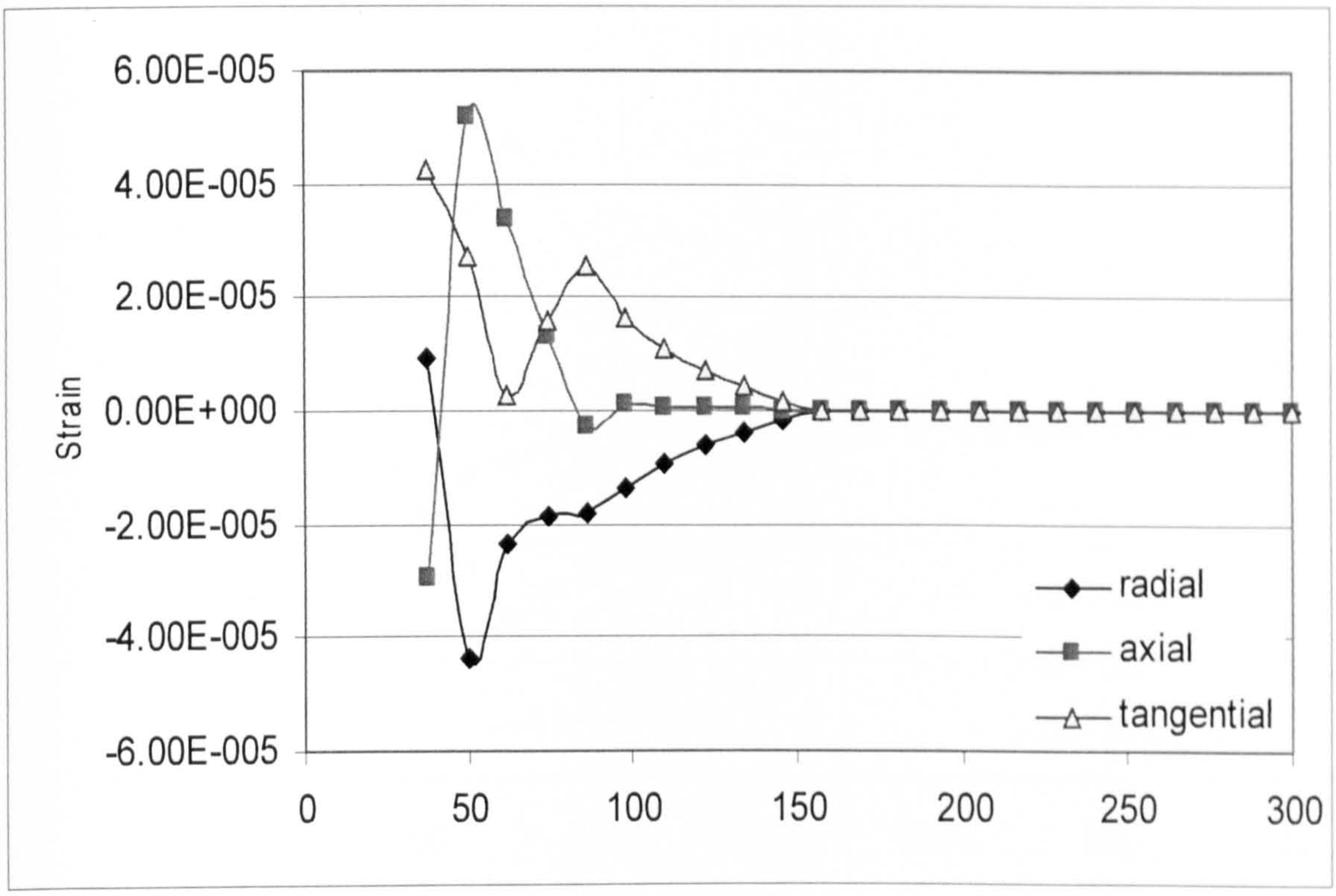

Figure 7.29a: Numerical results for the concrete strain distribution in slab S2

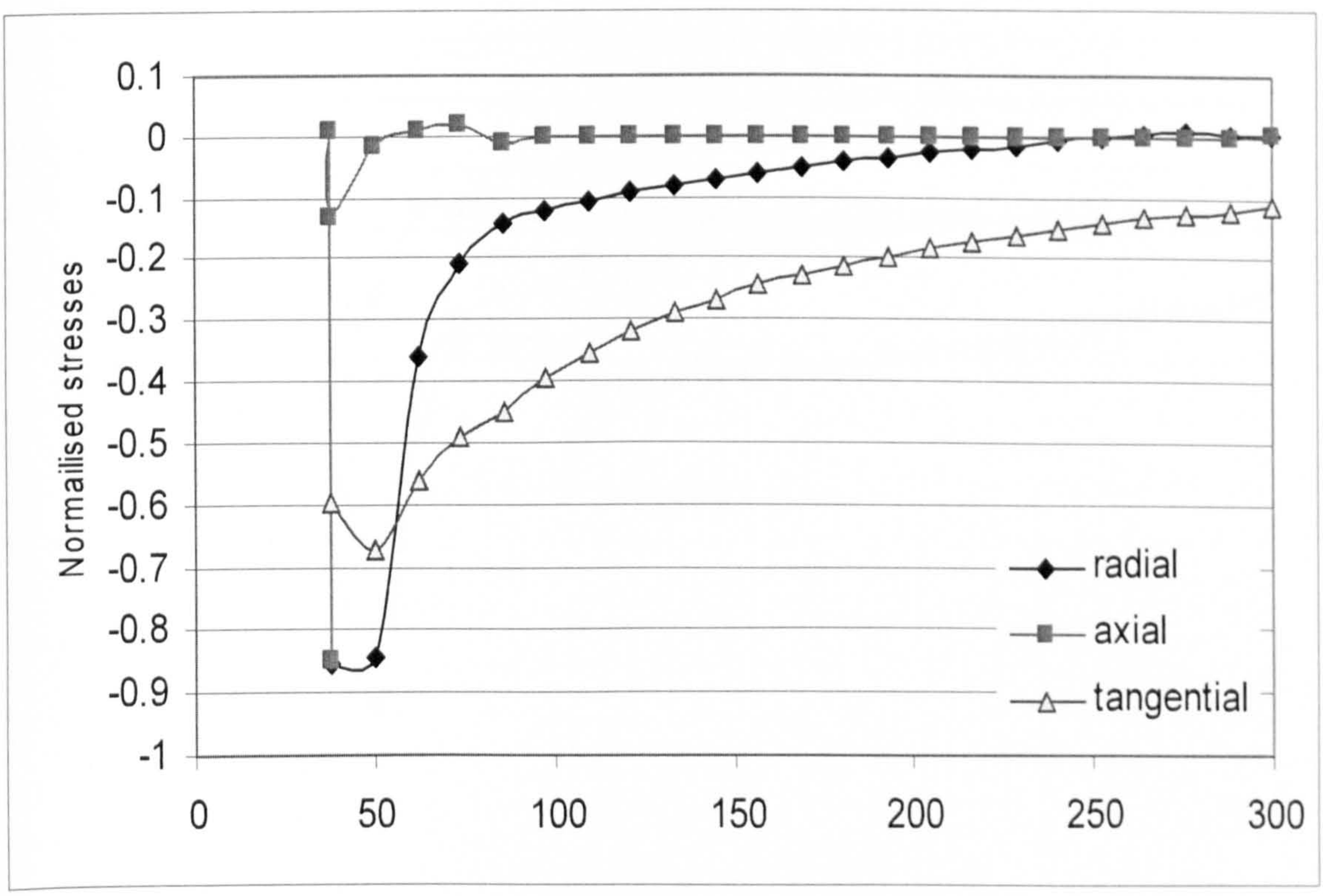

Figure 7.29b: Numerical results for the concrete stress distribution in slab S2

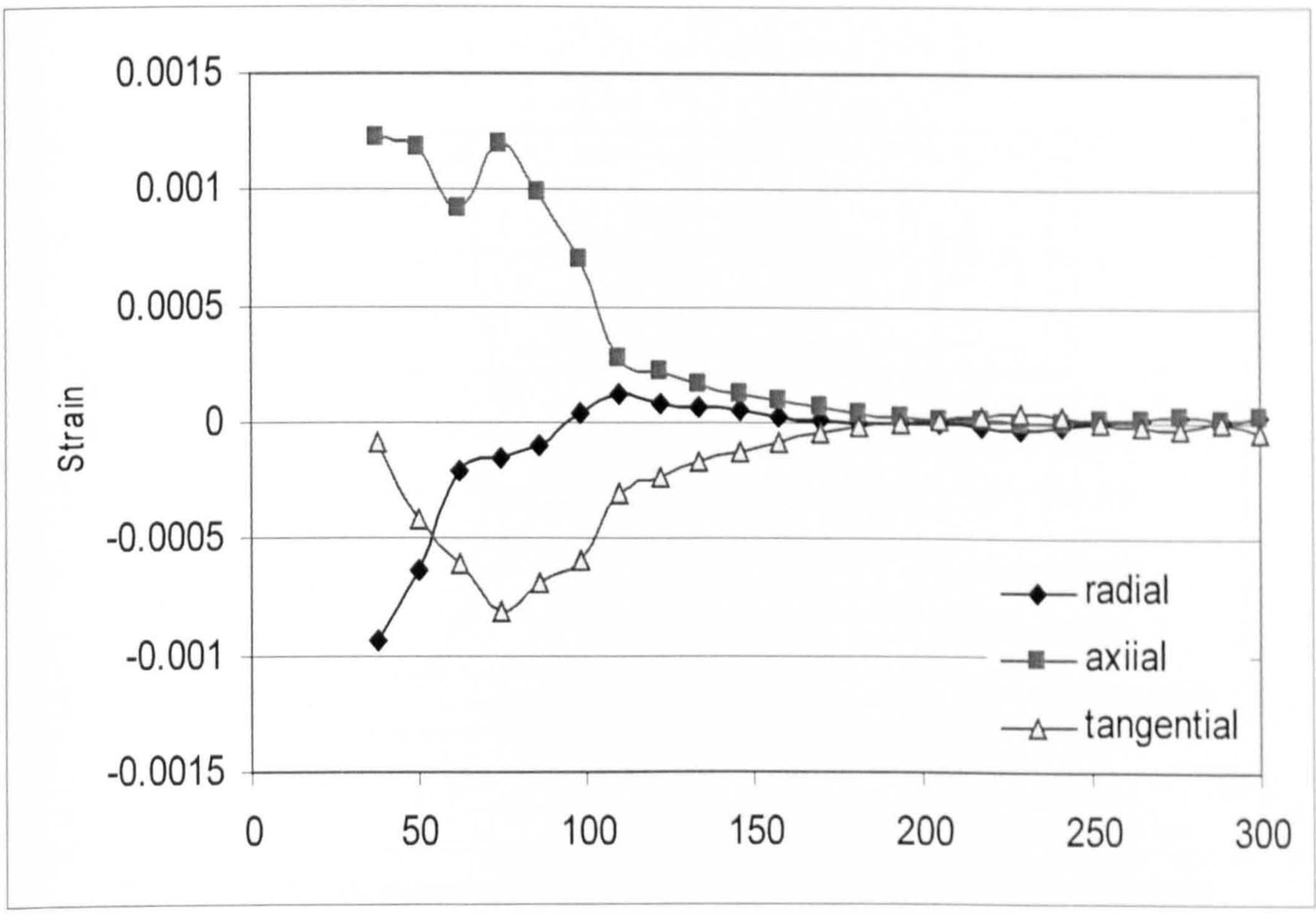

Figure 7.30a: Numerical results for the concrete strain distribution in slab S3

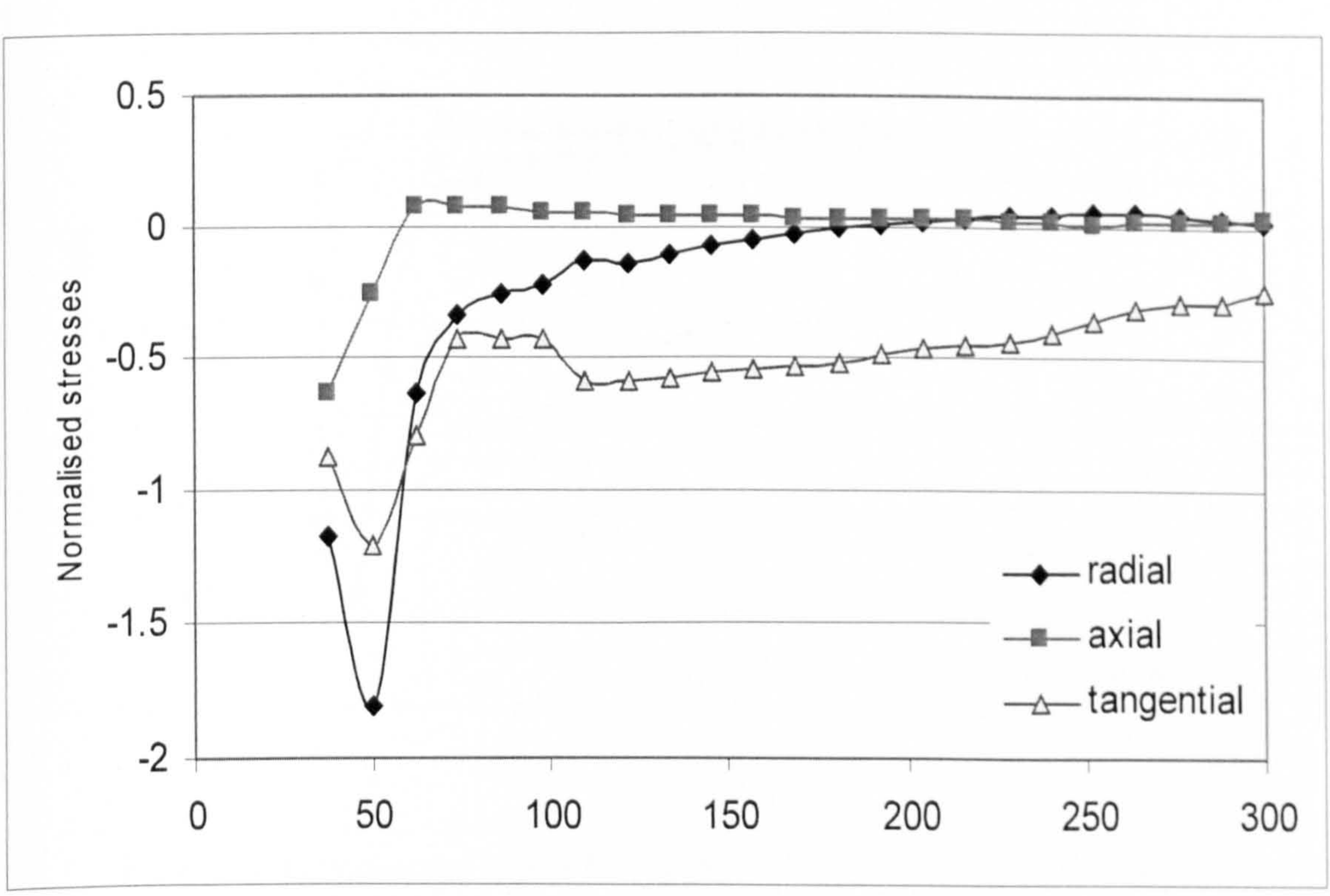

Figure 7.30b: Numerical results for the concrete stress distribution in slab S3

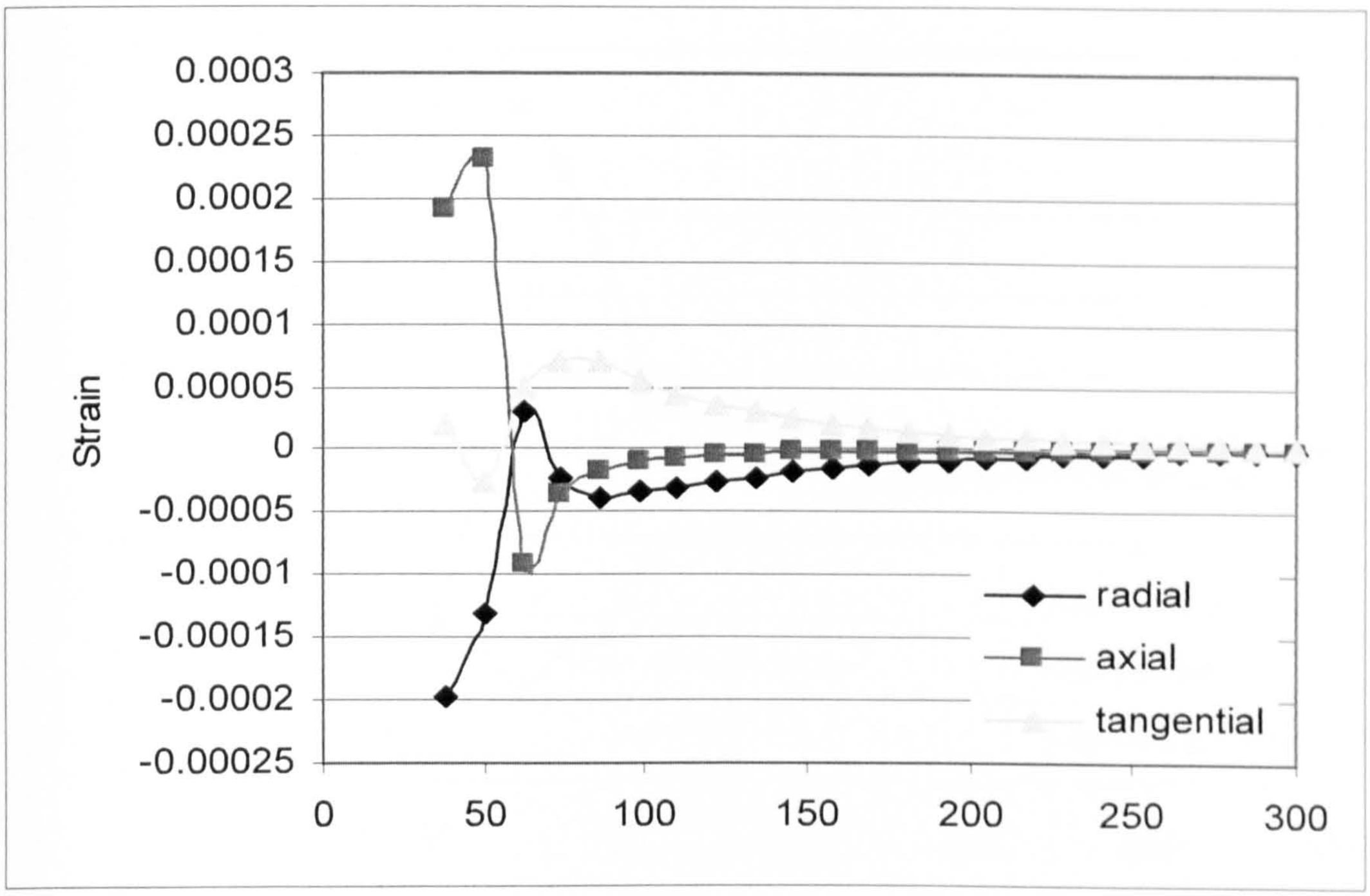

Figure 7.31a: Numerical results for the concrete strain distribution in slab S4

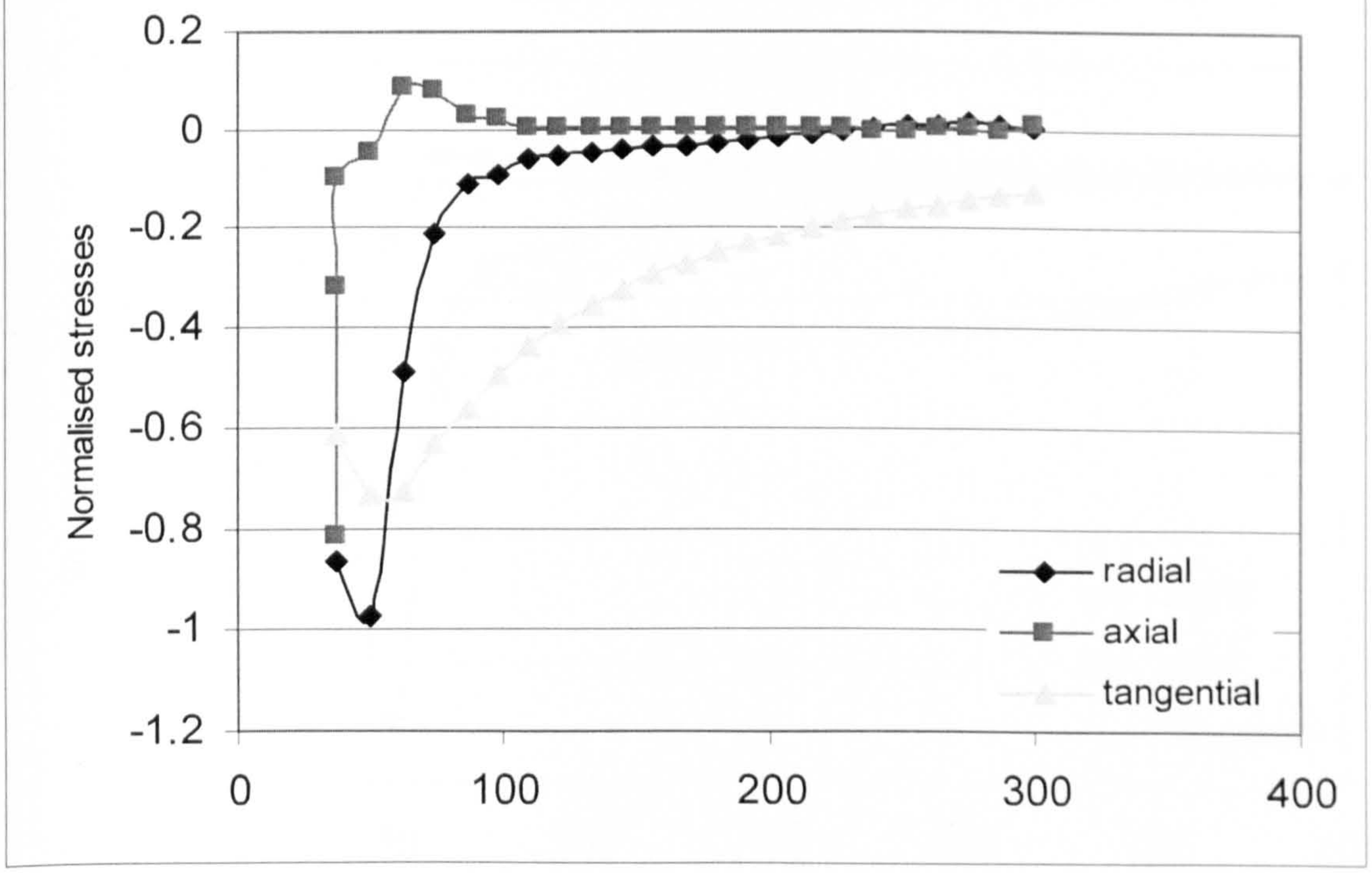

Figure 7.31b: Numerical results for the concrete stress distribution in slab S4

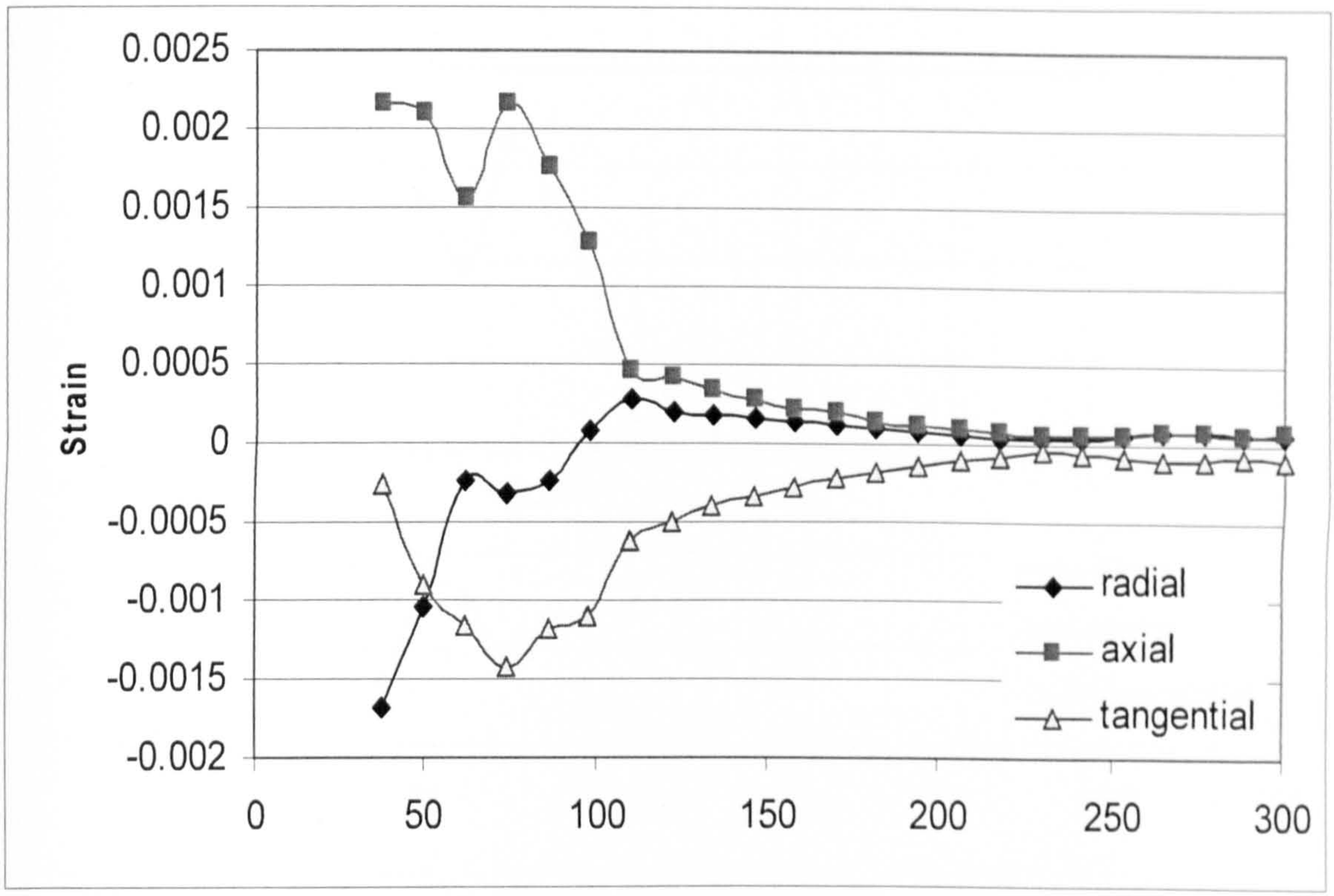

Figure 7.32a: Numerical results for the concrete strain distribution in slab S5

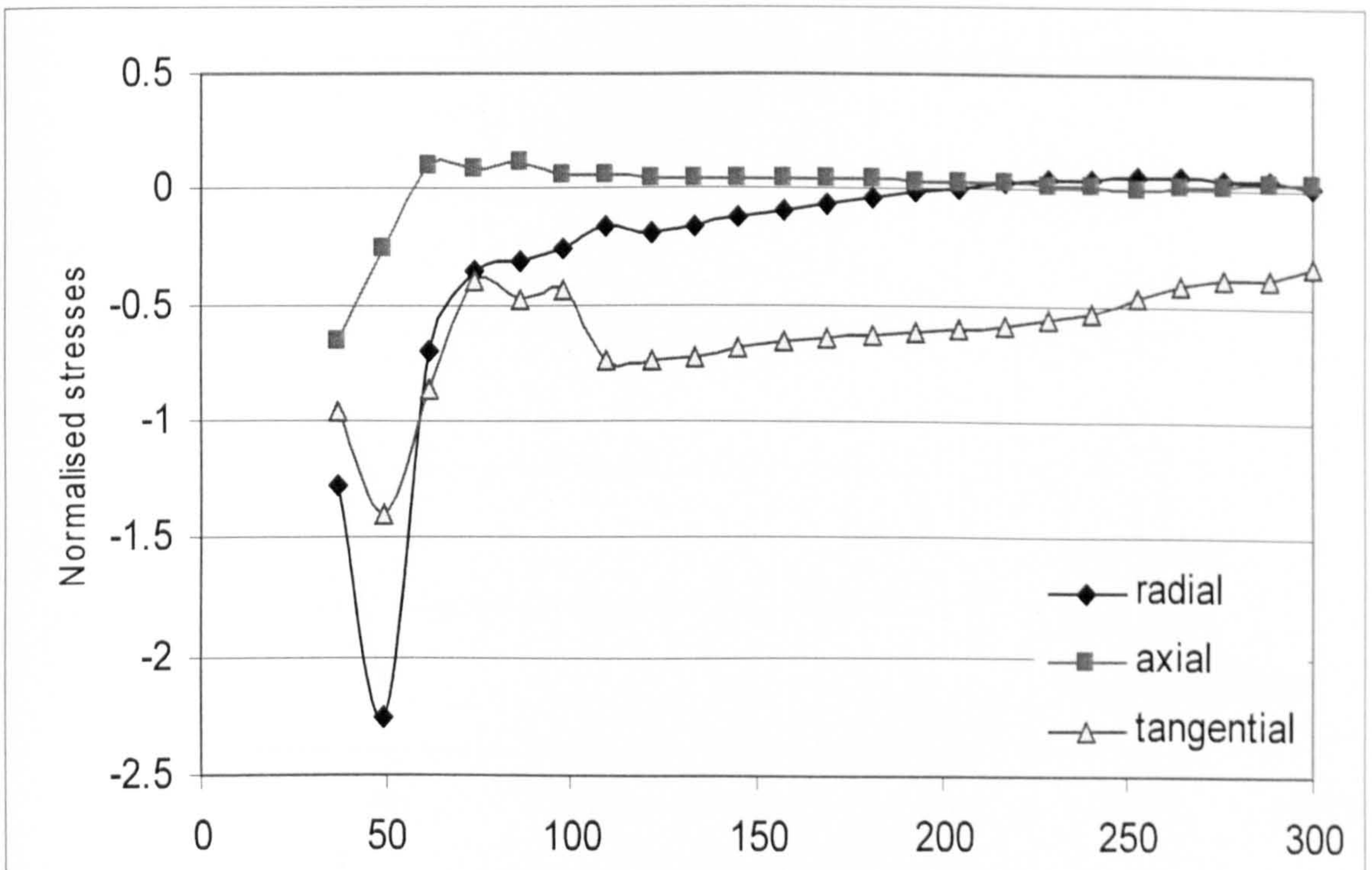

Figure 7.32b: Numerical results for the concrete stress distribution in slab S5

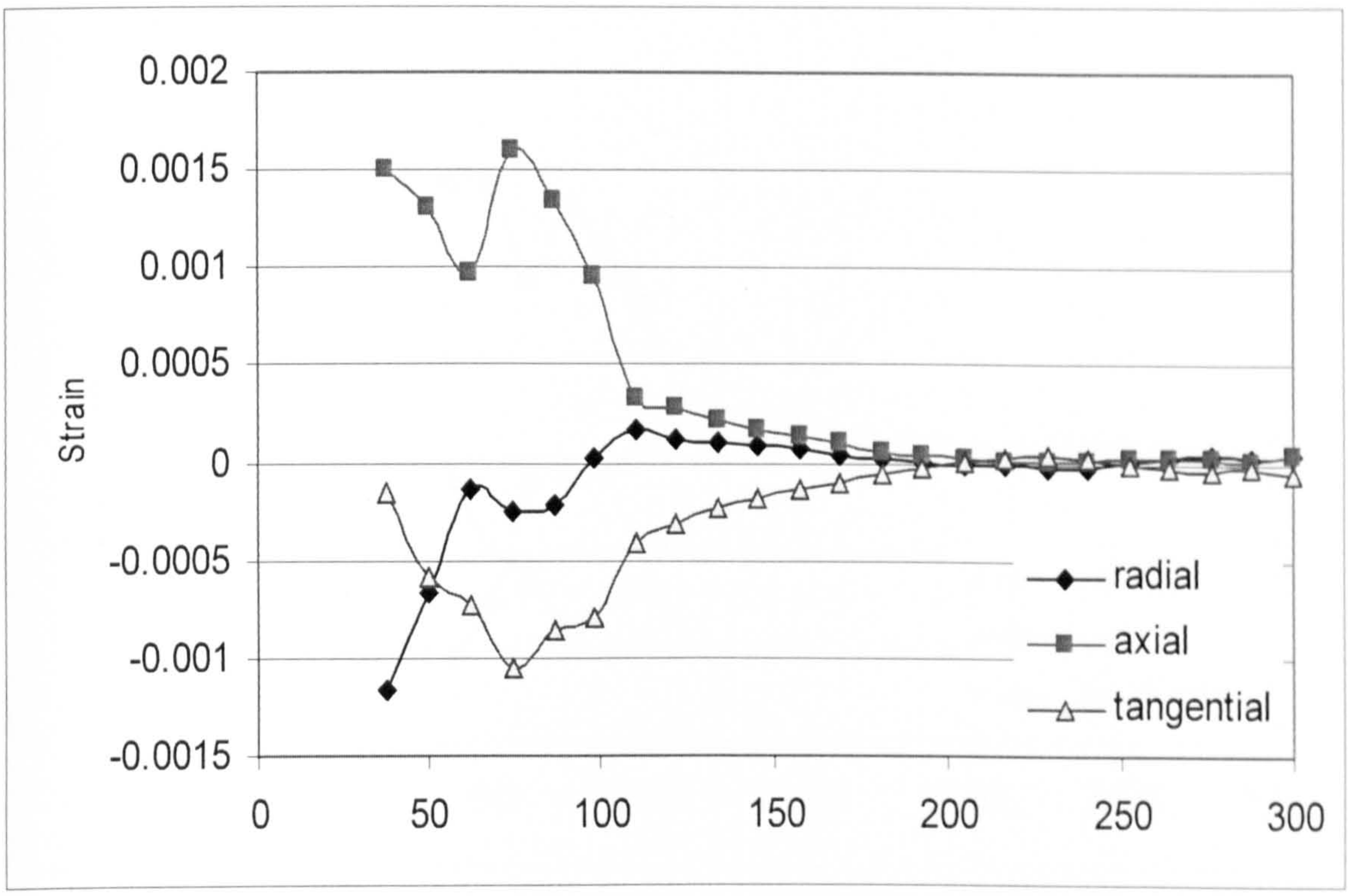

Figure 7.33a: Numerical results for the concrete strain distribution in slab S7

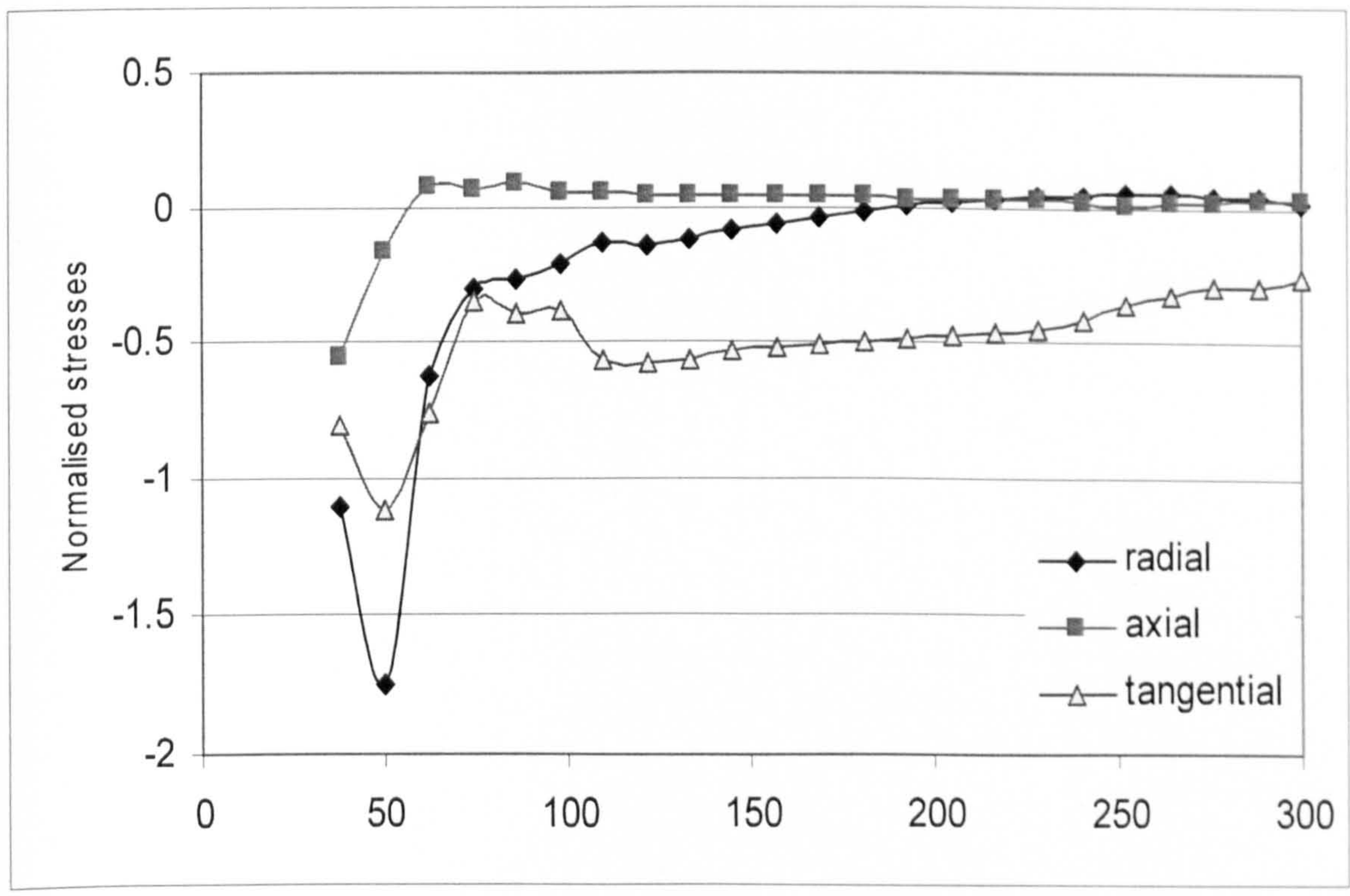

Figure 7.33b: Numerical results for the concrete stress distribution in slab S7

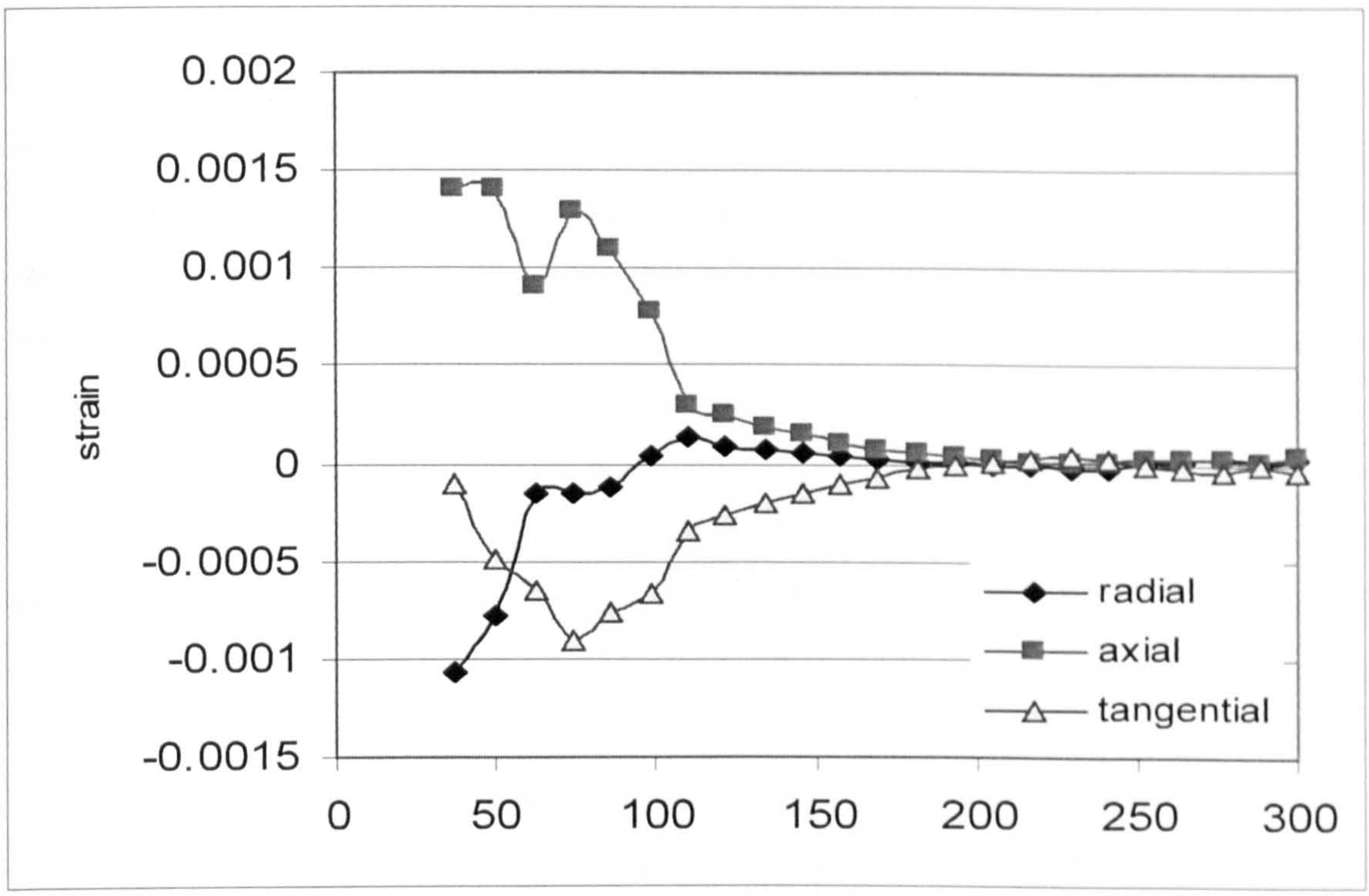

Figure 7.34a: Numerical results for the concrete strain distribution in slab S8

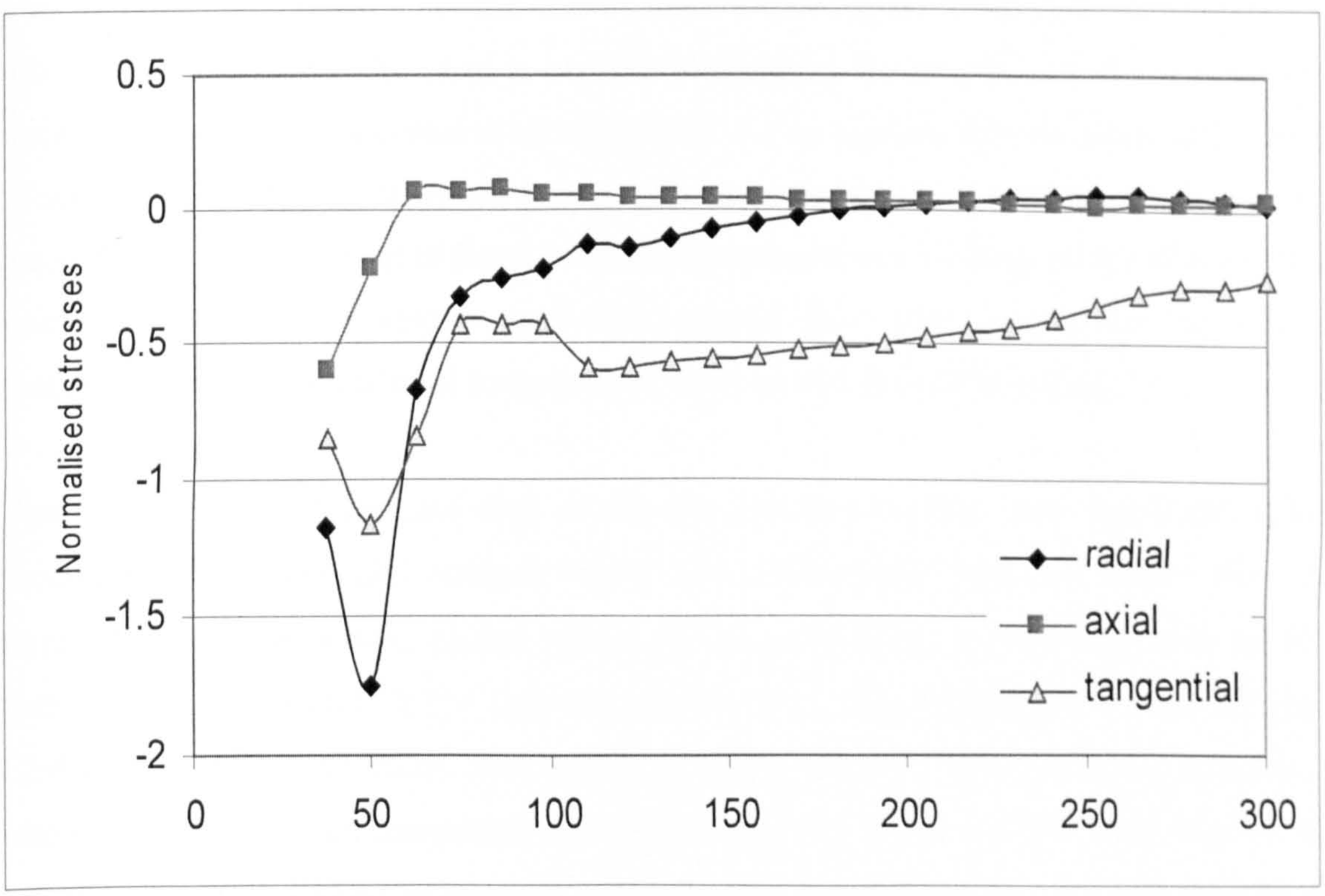

Figure 7.34b: Numerical results for the concrete stress distribution in slab S8

As Figures 7.30 and 7.32 to 7.34 indicates, it appears that circumferential strains and stresses are higher than the corresponding radial values, except within the area extending to a distance of approximately 0.5d from the column face. It is interesting to note that a high triaxial compressive state of stress occurs in the vicinity of the column face, where the maximum principal compressive stress σ_1 reaches a value nearly twice that of the uniaxial cylinder compressive strength f_c. Also interesting is the fact that the direct tensile strains in the z (axial) direction exhibited by the concrete in the compressive zone remain low throughout the load history, except for those occurring within a distance of 0.5 to 1.0d from the column face when horizontal cracking takes place at the last load step. As shown in Figures 7.30 and 7.32 to 7.34, it appears that a high radial strain of up to 0.002 develops within the compressive zone by the column face. It is important to point out that a triaxial compressive state of stress exists in the vicinity of the column face; however, as the axial stress diminishes rapidly away from this location, the stress state becomes one of nearly biaxial compression at a distance of about 0.5d from the column face. However this triaxial stress state is reduced to a nearly biaxial compressive stress state from a distance of about 0.5d from the column face. For the case of slabs with 40kg/m3 fibres (i.e. slabs S3, S5, S7 and S8), it appears that the fibre is capable of delaying the occurrence of the horizontal cracking. Once such horizontal cracking occurs, it also appears that the fibres are capable of controlling the spread of tensile axial strains towards adjacent locations. However, it is found that the development of these horizontal cracks causes yielding of the fibres so that tensile axial strains eventually reach the column face area, leading to the loss of confinement of the high triaxial compressive stress conditions in that region.

Figure 7.29 and 7.31 indicate that, as for the ductile-punching case described earlier, circumferential strains and stresses within the compressive zone are larger than the corresponding radial values, except within the area extending, in this case, only up to a distance of approximately 0.25d from the column face. It is interesting to note in Figure 7.29b and 7.31b that the lowest principal compressive stress σ_1 sustained by the concrete in relation to the uniaxial compressive strength, which is close to but below that of the uniaxial cylinder compressive strength, are found for slabs S2 and S4. This can be defined as the most brittle slabs; high brittleness reduces the ability to deform and, thus, reduces the load capacity of the slab. The same observation was noticed elsewhere (Hallgren, 1996).

However this triaxial stress state is reduced to a nearly biaxial compressive stress state from a distance of about 0.5d from the column face. It is also interesting that no horizontal (i.e. circumferential) cracking occurs within the compressive zone upto the ultimate load. The occurrence of such horizontal cracking is considered to cause the brittle collapse of the structure by removing the previously mentioned triaxial stress conditions. The latter holds right up to collapse; hence, the horizontal cracks in the compression zone appear suddenly just beyond the ultimate load, so that they cannot be seen. This is due to the immediate loss in load-carrying capacity in this area; hence, the loss of confinement of the triaxial compressive state is so catastrophic. Such a high triaxial stress state, therefore, can no longer be sustained nor redistributed. The presence of fibres does lead to yielding of the fibres but such fibre dosages are not sufficient to increase the ductility of the member to a noticeable (overall) structural level, and there is no significant deflection warning at failure. On the other hand, unlike this case of low fibre dosages where horizontal cracking in the compression zone near the support led to immediate failure, the slabs with high fibre dosages exhibit a somewhat more gradual crack development.

For slabs S3, S5, S7 and S8, a maximum value of the tangential strain obtained with the analyses is found at a radius of about 75mm, i.e. at the distance of about 0.5d from the column face. From this point, the tangential strain decreases towards the column face. This tendency was also observed in the tests on slabs with lower fibre dosages (i.e. slabs S2 and S4), where the strain was measured at a radius smaller than 0.5d. The smaller tangential strain at the column face was most likely caused by the constraining effect of the column in tangential direction.

7.4.4 Cracks

Unlike concrete models based on the smeared crack approach, the concrete damaged plasticity model does not have the notion of cracks developing at the material integration point. However, it is possible to introduce the concept of an effective crack direction with the purpose of obtaining a graphical visualisation of the cracking patterns in the concrete structure. Different criteria can be adopted within the framework of scalar-damage plasticity for the definition of the direction of cracking. Following Lubliner et al. (1989),

we can assume that cracking initiates at points where the tensile equivalent plastic strain is greater than zero and the maximum principal plastic strain is positive. Fixed crack mode is used in the present study. Once a crack occurs, its direction is fixed and remains constant during subsequent loadings. Crack direction is perpendicular to the direction of first principal strain.

When the ultimate-strength level of an element of concrete subjected to a state of stress with at least one tensile stress is exceeded, then a macro-crack is thought to form on the plane of the maximum and intermediate principal compressive stresses, with concrete suffering a complete and immediate loss of load-carrying capacity in the orthogonal direction. If, on reaching the failure envelope, the stress state is wholly compressive (either under uniaxial or triaxial conditions), then a complete loss of load-carrying capacity occurs.

Crack pattern was simulated in terms of maximum principal strains and in the vector plot diagram; the crack length is plotted as proportional to the magnitude of first principal strain. This direction can be viewed in the visualisation module of ABAQUS.

Figure 7.41 and 7.42 show the crack patterns at various load level obtained from the finite element analysis of slabs S2 (typical crack pattern for brittle-punching) and S5 (typical crack pattern for ductile-punching failure). The plots show the extension of the radial and tangential crack across the section. The radial cracks appear to have propagated in a triangular shape from the slab centre towards the circumference of the slab. The crack propagation at the slab centre stopped at about half the effective depth. In the plots, the integration points at which tangential cracks were detected are marked with short lines, which also indicate the direction of the cracks. Initial inclined shear cracking was detected at the tip of a vertical flexural crack above the slab-column root at a level about one third of the effective depth. At higher loads, it appears that inclined cracks propagated from that level both up towards the top surface and down towards the slab-column root. Simultaneously, and as the loading proceeded, bands of new inclined cracks were detected outside the previous cracks. At ultimate load P_u, the outermost complete band of inclined cracks had a slope of about 45°.

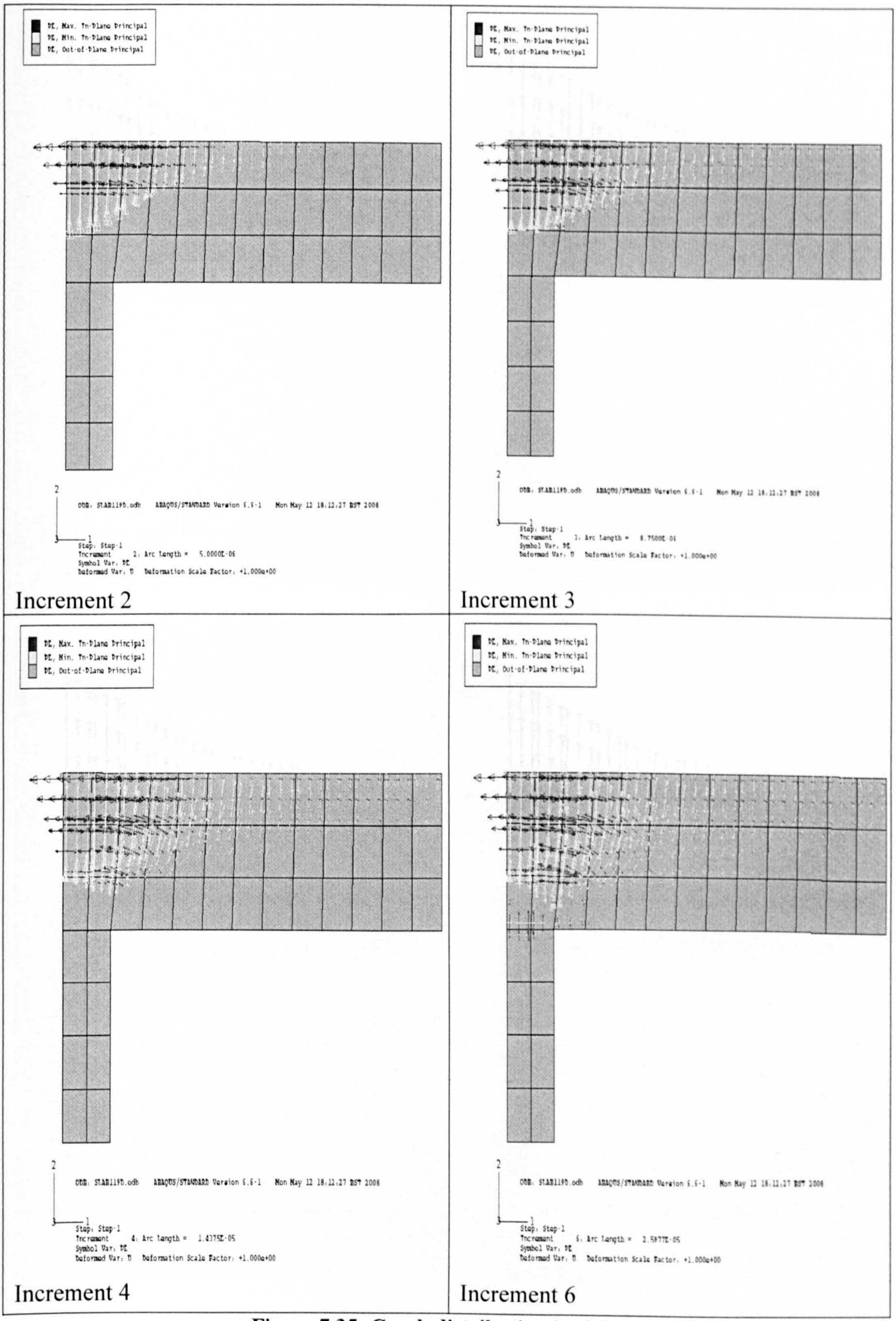

Figure 7.35: Crack distribution in slab S2

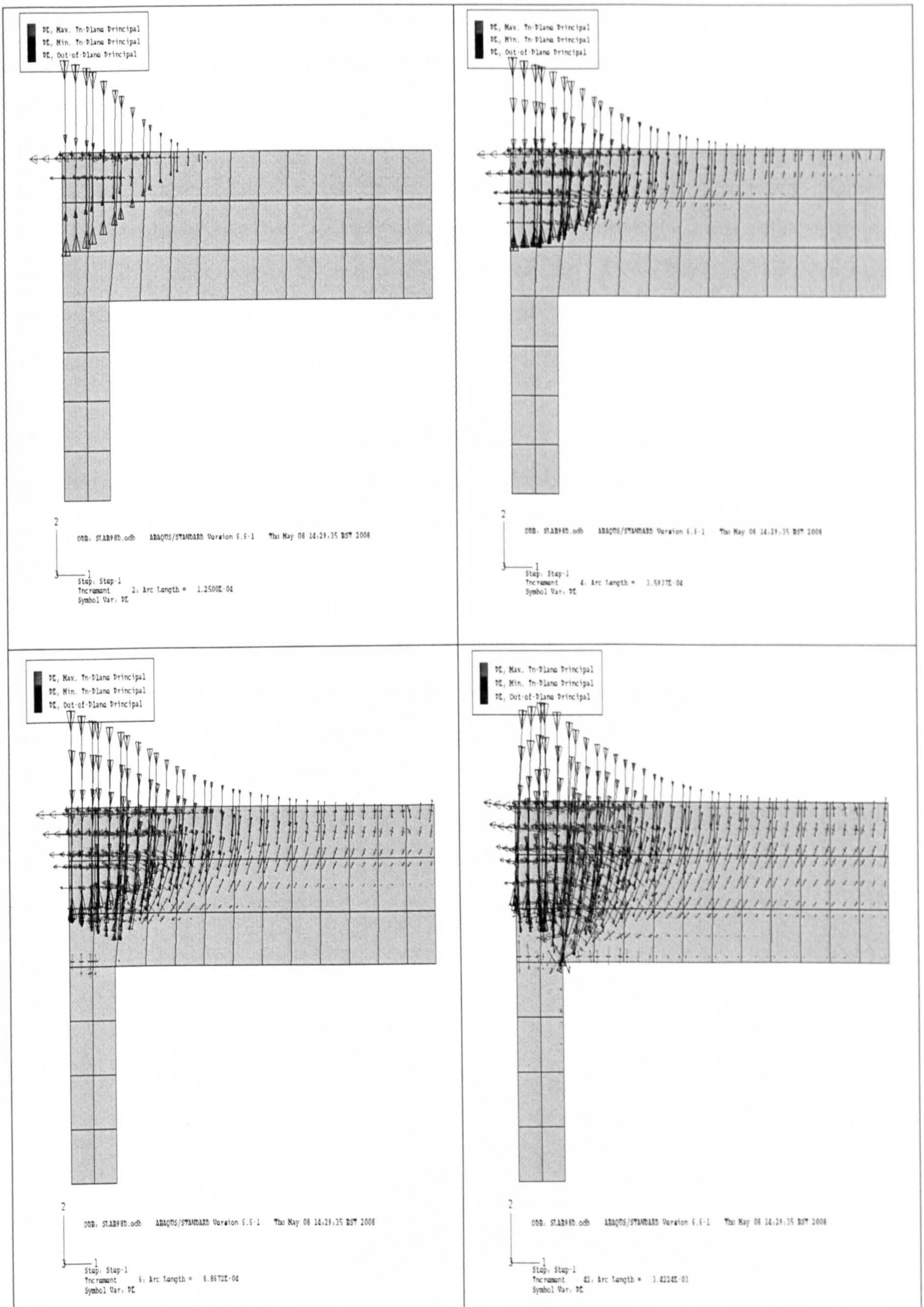

Figure 7.36: Crack distribution in slab S5

On the other hand, for the case of ductile-punching (i.e slabs S3, S5, S7 and S8), radial cracks spread throughout the top face of the slab and increase in depth with increasing load up to a five-sixths of the slab depth (at ultimate conditions) so that the tension zone is divided into radial segments. In contrast to radial cracks, circumferential cracks only spread to about half the span (at the tension face), and increase in depth with increasing load, but at a lower rate than the case with radial cracks. Radial cracking occurs at a higher rate and the crack depth is larger than that for the slab exhibiting brittle-punching behaviour. In contrast with radial cracks, circumferential cracks increase in depth at a lower rate.

In all finite element analyses, tangential cracks were detected only inside an imaginary punching cone. Outside this cone, the slab portion rotated as a rigid body (see Figure 7.41 and 7.42) and no tangential cracks were found there. This is in good agreement with the test observation.

The punching cone is in very close agreement with the experiment. In the plots on Figure 7.43 the outermost complete band of inclined cracks had a slope of about 30 to 55°. This is in good agreement with the slope and position of the failure shear crack observed in the test, see section 6.7.5. But, the diameter of the cone influenced by the two steep formation of the punching crack is somewhat too small on the top side of the slab. This can be traced back to smeared crack approach which, in the period just prior to failure, is no longer able to simulate the crack precisely.

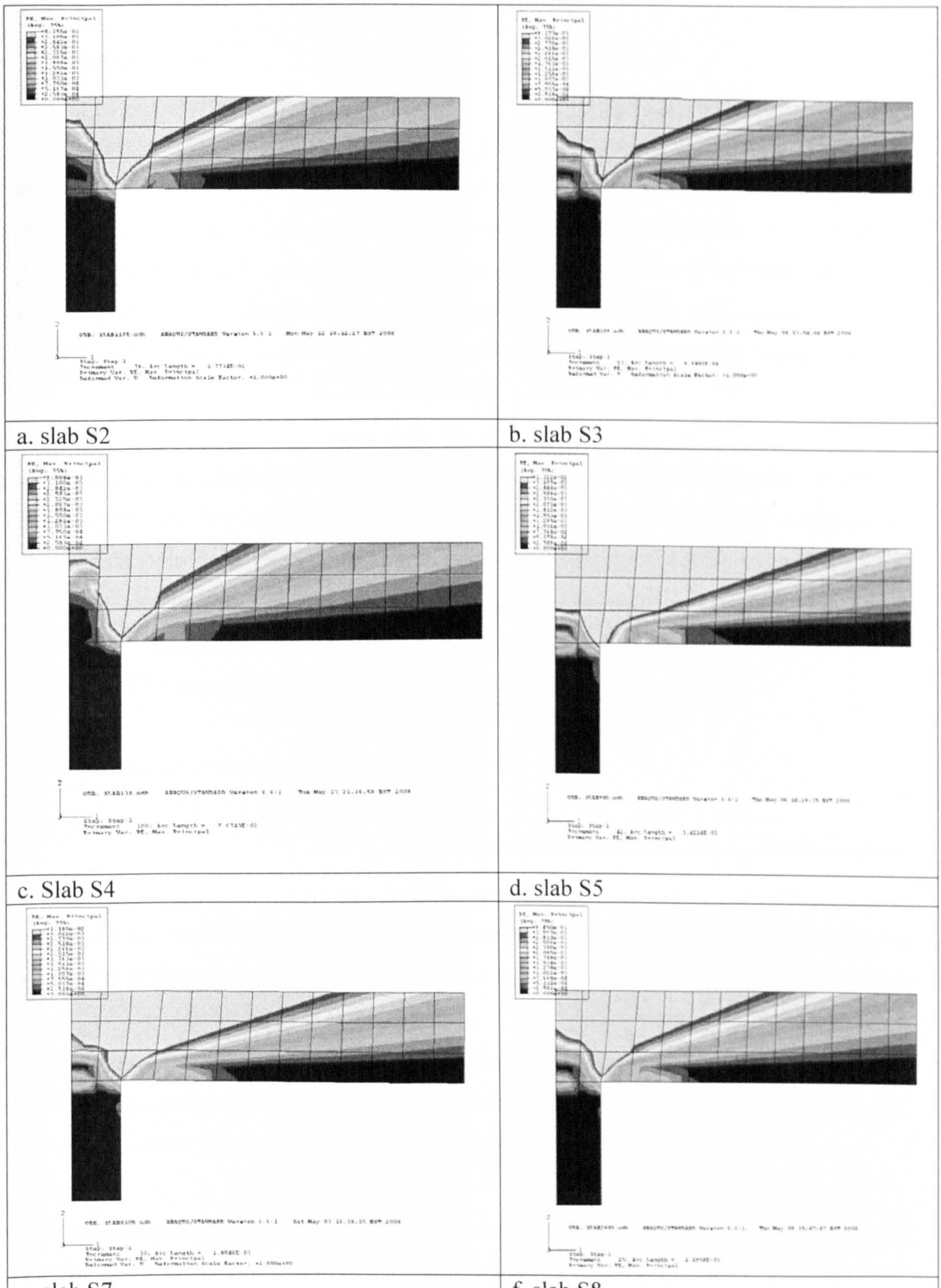

a. slab S2

b. slab S3

c. Slab S4

d. slab S5

e. slab S7

f. slab S8

Figure 7.37: Angle of punching cone of slabs (a. slab S2, b. slab S3, c. slab S4, d. slab S5, e. slab S7 and f. slab S8)

7.4.5 Failure Mode

In the finite element analyses of the slabs, the concrete between the tip of the shear crack and the slab-column root was found to be in a tri-axial state of compressive stress. The strain corresponding to the smallest compressive stress was tensile and orientated approximately normal to the shear crack. The compressive stress in this direction had a confining effect, preventing the shear crack progressing through the compression zone. The punching shear failure is assumed to occur when the confining stress is reduced due to horizontal cracking in the tangential compression zone at the distance slightly longer than one depth of the compression zone from the column face. The shear crack then breaks through the radial compression zone, causing a sudden loss of the load capacity. However, in slabs with low fibre dosage (i.e. slabs S2 and S4) the fibres were not able to prevent the shear crack to progress through the compression zone, whereas the fibres in the slabs with high fibre dosage (i.e. slabs S3, S5, S7 and S8) were more able to prevent such crack progressing through the compression zone. It can be concluded that the current axi-symmetrical FE model can predict the mode of failure of the slabs correctly.

7.4.6 Discussion of the Results

In all cases the ultimate load carrying capacity predicted by finite element modelling agrees closely with the corresponding experimental values and the load-deformational characteristics obtained from the FE solution were also close to the experimental results for all slabs at all critical stages of loading with closer agreement found in slabs S3, S5, S7 and S8. The computationally simulated response of the load-displacement exhibits a close match to the experimental behavior at early stages of loading. Near the peak load response, the simulated behavior exhibits slightly higher stiffness and then softens afterwards. The simulated softening is only slightly less brittle than experimentally observed.

The comparative analysis of test and the numerical results showed a good correlation between the non-linear FE analysis and the experimental data, not only on the global level of load–deflection behaviour, but also in the relation with local strains and stresses in the

concrete. Strain and stress states obtained with this analysis could serve as a basis for studying and better understanding of the punching failure mechanism.

The crack pattern at both the initial and the failure stages predicted by the FEM was in close agreement with the experiment results, indicating that the effect of fibres on the concrete strength and ductility and its bridging effect in arresting crack propagation have been suitably captured. Moreover, the layout and inclination of the failure surface were well approached with this numerical analysis.

It can be concluded that the use of the damaged plasticity model and proper material properties is able to realistically predict the behaviour of flat slab-column connection subjected to punching shear.

7.5 Parametric Study

The FE analysis offers a reliable and very cost-effective alternative to full-scale laboratory testing as a way of generating results. The punching failure in SFRC slabs were successfully simulated allowing the parametric analysis to be performed. Therefore, the FE analysis was repeated twice for each parameter, in order to study the influence of relevant materials and geometrical parameters on the punching shear behaviour of the tested slab (i.e. slab 5). For the first repeated analysis the parameter was decreased and the second repeated analysis the parameter was increased in comparison with the value in the original analysis. The finite element model was used in 31 parametric slab studies to show the effects of changes in compressive strength, tensile strength, tension stiffening and slab size. In general, the calculations were carried out by varying one parameter while all other parameters, which were the same as in the experiment, were kept constant.

7.5.1. Influence of the Compressive Strength of Concrete

The concrete parameters such as the tensile and compressive strengths are known to be interrelated. However, for the following parametric analysis, they are considered independently in order to determine their effects on the punching failure process.

The influence of the compressive strength of concrete was checked by performing the analysis of slab S5 twice with f'_c set to 25MPa and to 40MPa, respectively. The compressive strength was hence, decreased and increased by about 30%, respectively, compared with the measured values 32.7Mpa. All other parameters and material properties had the same values as in the original analysis.

Figure 7.44 shows the obtained load-deflection curves. The uniaxial concrete compressive strength has little influence on the punching failure as neither the cracking mechanism nor the response curve are modified for slabs with different uniaxial compressive strengths (when the tensile strength is held constant). It can be concluded that the punching failure is due to tensile failure of the concrete along the inclined punching crack and is not due to compressive failure of the concrete. This was also observed in the experimental work as presented in section 6.8.1.

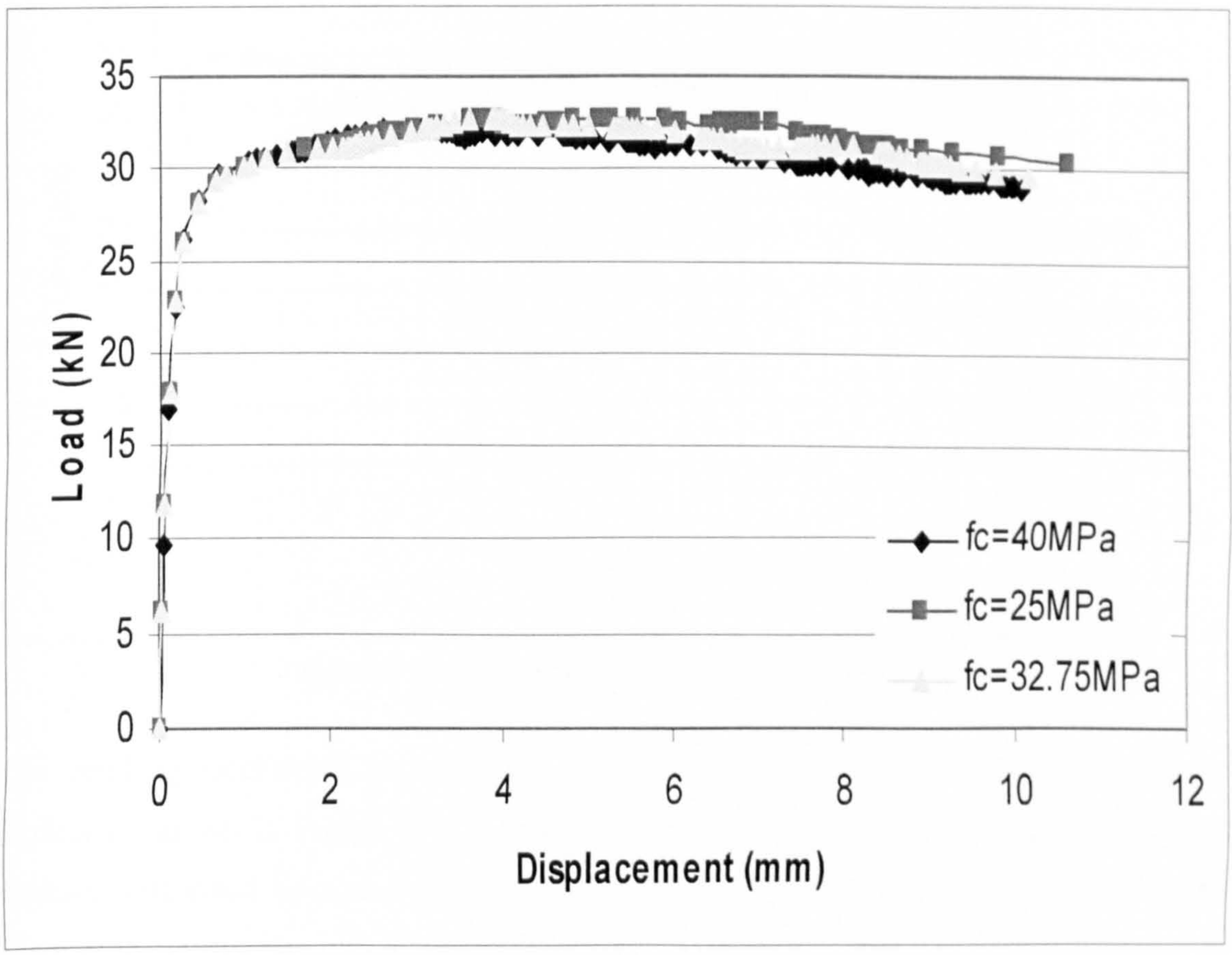

Figure 7.38: Effect of compressive strength

This conclusion was confirmed earlier by Menetrey (1994). Based on numerical study he concluded that the compressive strength has no influence on the punching shear. However, in his parametric study the compressive strength varied from 22.5 MPa to 33.7 MPa.

7.5.2 Influence of the Tensile Strength of Concrete

The influence of tensile strength of concrete was investigated by simulating the test of slab S5 with three different values of tensile strength f_{ct} 1.26 and 2.34MPa, where 1.8MPa was the value used in the original analysis. All other parameters, including the tensile stiffening, had the same value as in the original analysis. Figure 7.45 shows the obtained load-deflection curves, in both the additional cases the simulation ended with a ductile-punching failure similar to the one obtained in the original analysis.

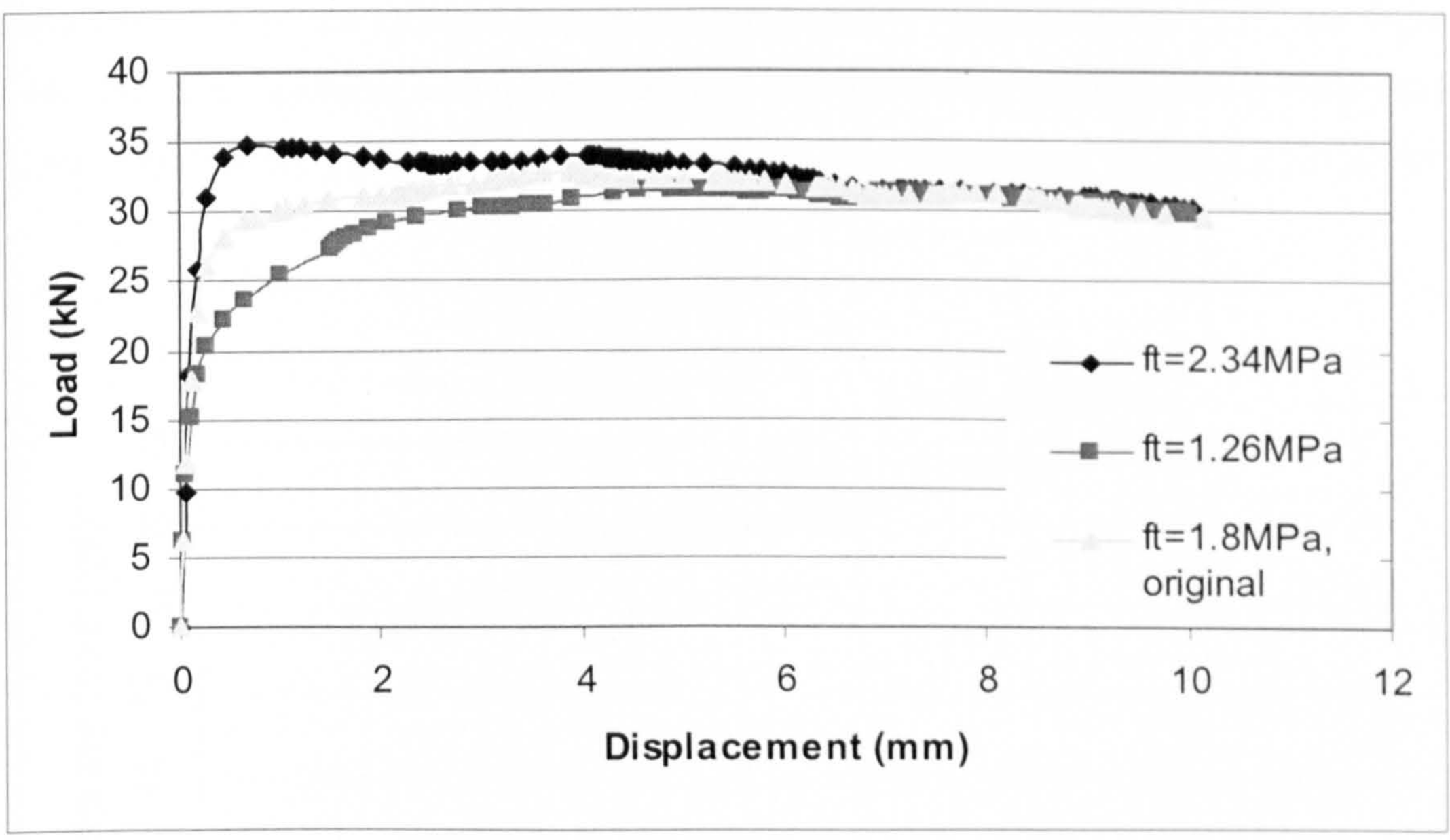

Figure 7.39: Effect of tensile strength of concrete

The cracking mechanism is analogous for the three slabs but the response curves are distinct as shown in Figure 7.45. The load at which the first tangential flexural crack appears (illustrated by a discontinuity of the response curves) increases with increasing value of the tensile strength. Once the tangential flexural crack has formed, the slope of the

response is similar for all slabs. The failure occurs first in the slab with the lowest tensile strength.

The tensile strength of concrete seems to have a major influence on the punching shear capacity. The influence of the tensile strength was already suggested by Moe (1961) who observed that the punching failure is very often of a splitting type, and it is comparable to the type of failure observed in specimens under tension. As expected, slabs with higher tensile strength initially have a stiffer response due to the higher cracking load. However, the ultimate deflection, i.e. the deformation capacity, increases with increasing tensile strength. Higher tensile strength also clearly increases the ultimate load. The increase of load capacity is, however, not linearly proportional to the tensile strength. The ultimate loads obtained with f_{ct} = 1.26MPa and f_{ct} = 2.34MPa were 23.69kN and 34.91 kN, respectively. The ultimate load obtained from the original analysis was 32.67kN. Based on these three results; the ultimate load P_u is approximately proportional to $f_{ct}^{0.6}$, see Figure 7.46. This is in agrement with the findings by Menetrey (1994) and Hallgren (1996), where P_u was approximately proportional to $f_{ct}^{2/3}$ when f_{ct} was varied from 2.1 MPa to a 3.9 MPa.

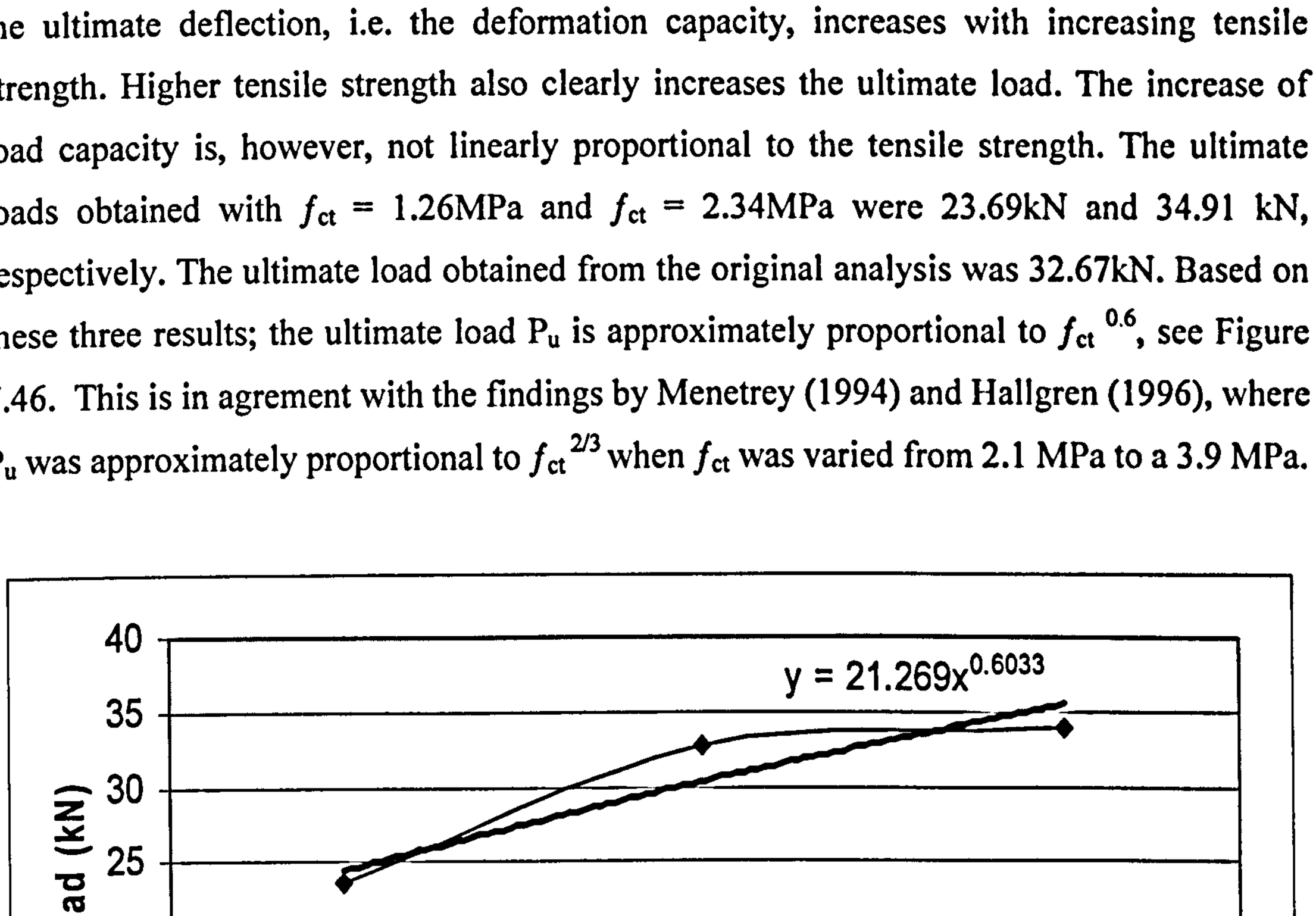

Figure 7.40: Relationship between tensile strength of concrete and ultimate strength of slab

7.5.3 Influence of the Tension Stiffening of Concrete

The influence of the tension stiffening of concrete was checked by simulating the test of slab S5 with three different tension stiffening curves (see Figure 7.47) where curve B was the curve used in the original analysis. All other parameters and material properties had the same values as in the original analysis.

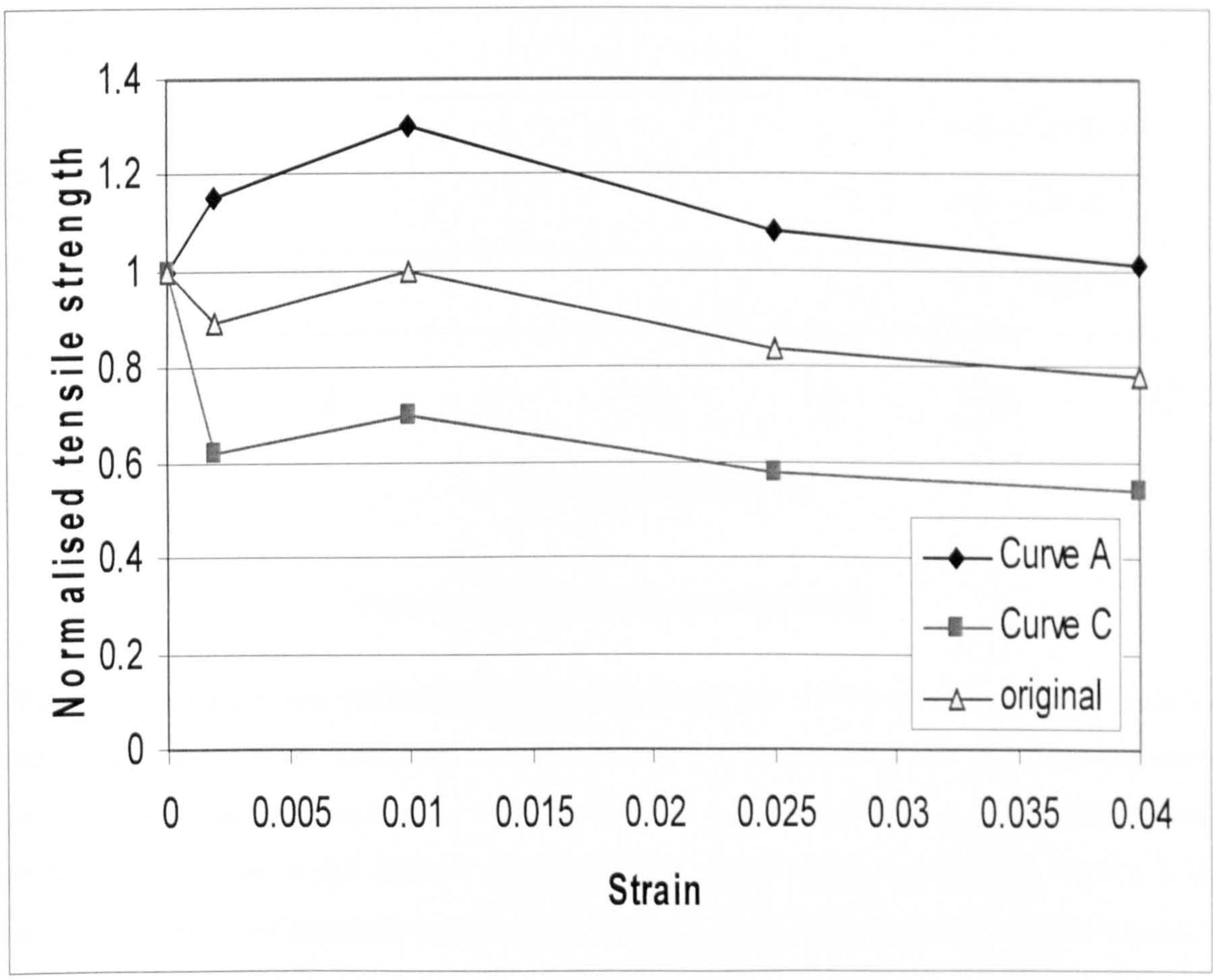

Figure 7.41: Tension stiffening curves

Figure 7.48 shows the load deflection curves obtained. In both the additional cases, the simulation ended with a ductile-punching failure similar to the one obtained in the original analysis

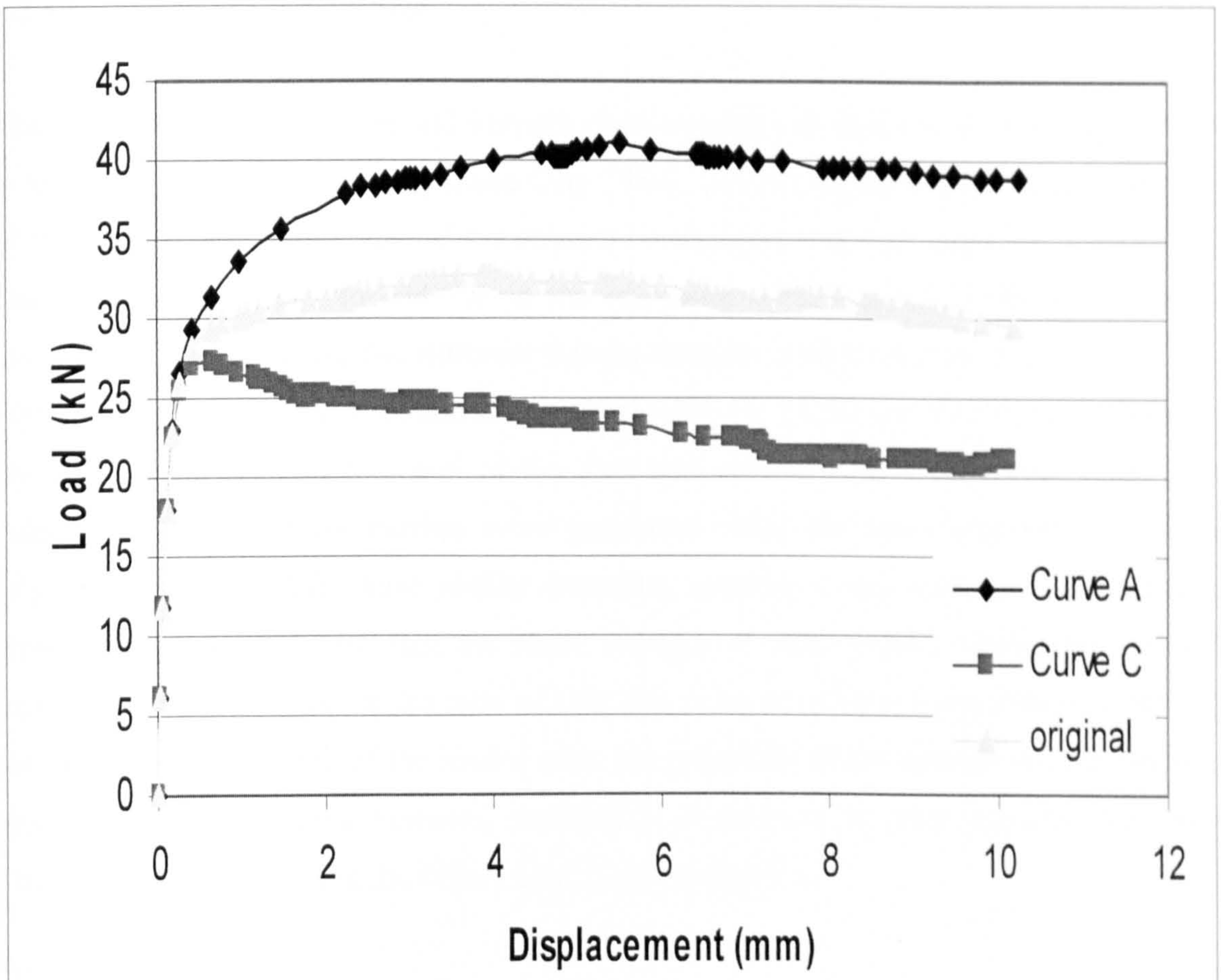

Figure 7.42: Effect of tension stiffening

The increase of tension stiffening slightly increased the stiffness of the slab. The main influence of the tension stiffening is on the deformation capacity of the slab. Consequently, the ultimate load also increases with increasing tension stiffening. The ultimate load obtained with curve A and curve C were 41.02kN and 27.18kN respectively. Hence, if the tension stiffening of concrete is increased, the punching shear capacity can be improved considerably, provided that the action made to increase the tension stiffening does not decrease the strength of the concrete. An increase in the tension stiffening can be obtained by e.g. changing the type of aggregate, increasing the aggregate size, or by adding fibre reinforcement to the concrete mix.

7.5.4 Influence of the Slab Size

The phenomenon that the nominal strength decreases with an increase of the structural size is known as the size effect (Bazant and Cao, 1987). To investigate the influence of the size of the slab and the dimensions of the column on the punching load capacity, a parametric study was carried out. In addition to the reference slab (Figure7.1), the size effect is investigated by simulating five different slab thicknesses (slab thickness: 50, 65, 75, 85 and 100 mm) and five different column diameters D = 55, 65, 75, 85 and 95 mm were analysed. By geometrical scaling, the span of the slab was related to the thickness of the slab. Additional finite element meshes were generated using the same element sizes as in original mesh. All slabs have similar boundary conditions and material characteristics. However, the results show that the shear strength of slab-column connection tends to increase with the increase of the ratio of D/h; this is because for a given effective depth of the slab and given shape of the loaded area, the perimeter of the critical section becomes greater as the loaded area increases, resulting in an increase in shear strength. However, The nominal shear stress at the failure load P_u is computed as

$$\tau_{12} = \frac{P_u}{\pi(D+h)h}$$

Where the diameter of the column is denoted by D and h is the slab effective depth. As presented in Table 7.8 and in Figures 7.49 and 7.50, the nominal shear stress increases with increasing thickness of the slab and decreases with increasing the radius of the column.

Table 7.8: Ultimate load (kN) predicted by finite element model for different slab and column sizes

Slab thickness (mm)	Column size (diameter-circular cross-section) (mm)				
	55	65	75	85	95
50	14.9	15.7	16.1	17.2	17.7
65	24.5	25.2	25.3	26.2	27.3
75	31.3	32.6	32.7	34.1	34.7
85	39.0	40.2	41.1	41.7	43.5
100	51.6	53.6	54.4	55.9	58.1

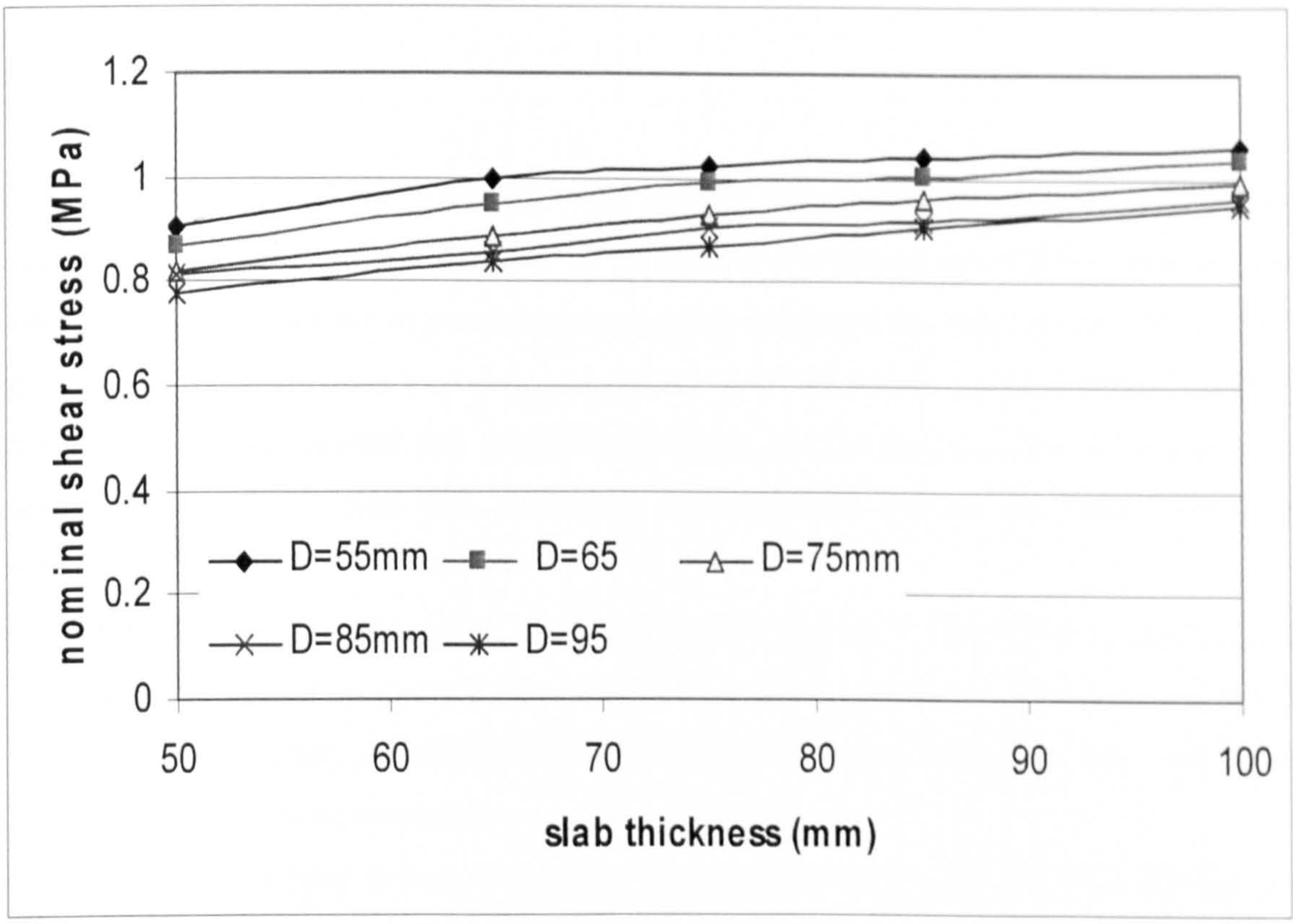

Figure 7.43: Effect of slab thickness with different column diameter (D)

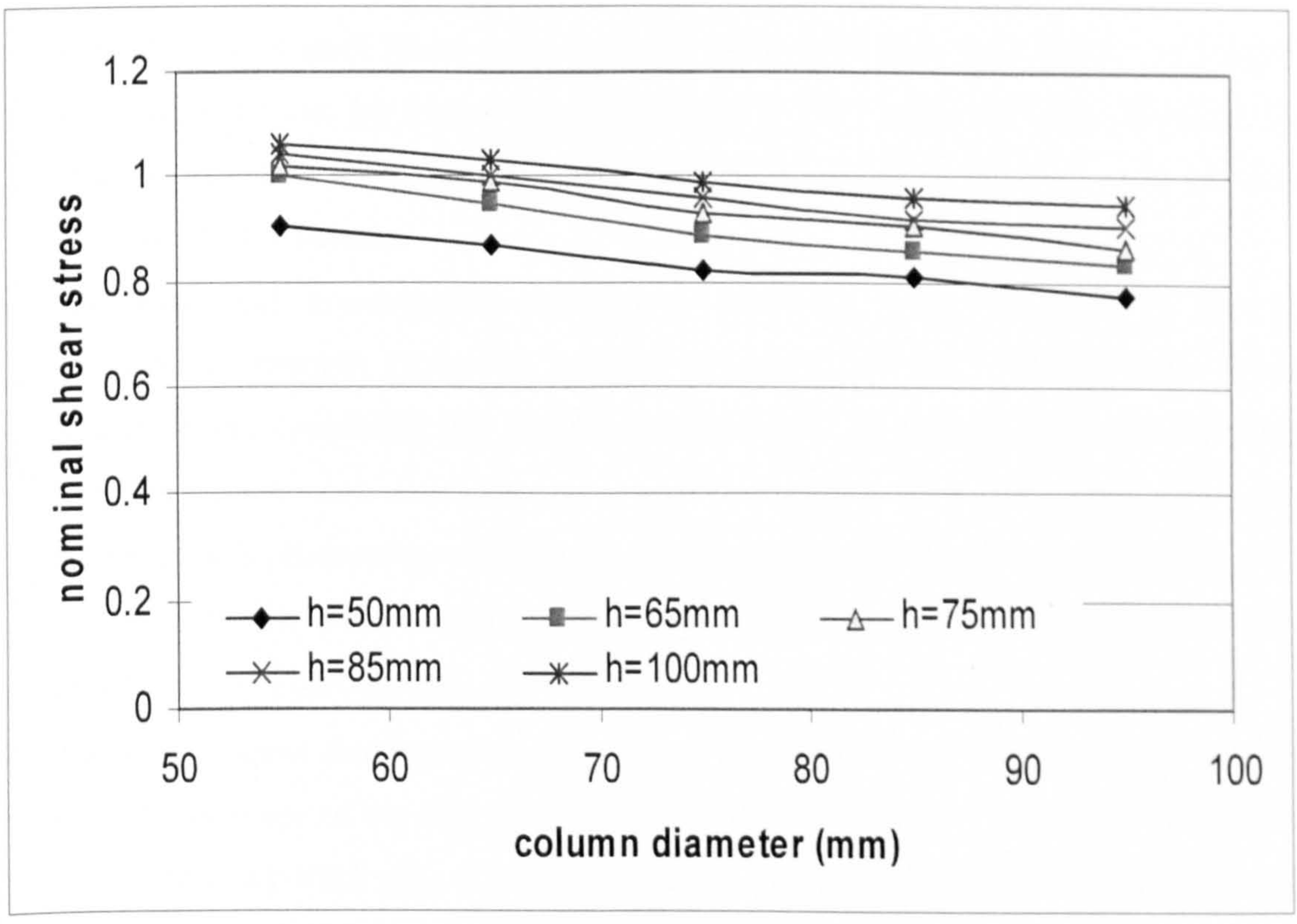

Figure 7.44: Effect of column size with different slab thicknesses (h)

7.6 Conclusions

The finite element package ABAQUS was used to extend the scope of the experimental work, by demonstrating the possibility of predicting the behaviour of SFRC internal slab-column connection subject to punching shear using an axisymmetrical model. On the basis of the comparison between experimental results obtained in testing the isolated specimen that represented the internal slab-column connection and the results of the non-linear finite element analysis performed with ABAQUS finite element System, the following can be concluded:

- The FEA with the Damaged Plasticity Model based on the Mohr–Coulumb yield condition with non-associated flow rule and smeared cracking approach for the tensile regime in concrete are efficient tools for modeling the behaviour and strength of internal slab-column connection.
- The brittle-punching failure which was observed in slabs with low fibre dosage (i.e. slabs S2 and S4) was stiffer than the real slab in non-linear range of response, with lower strains compared to the measured strains.
- The addition of steel fibres improve the tension stiffening, as a result, the punching shear capacity can be improved. Moreover, it was found that, the ultimate shear strength increases with increasing thickness of the slab and increases with increasing the radius of the column.
- The numerical investigations indicate a relatively small influence of the pure compressive strength (assuming constant tensile properties). On the basis of these results, it was concluded that punching failure was primarily a failure by splitting of concrete which was followed by concrete crushing as a secondary phenomena. However, this observation shall not lead to the conclusion that the punching failure was a purely tensile failure and a simplified modelling of the compressive concrete properties e.g. elasto-plastic, was sufficient.
- The results show that the shear strength of slab-column connection tends to increase with the increase of the ratio of D/h. Moreover, the ultimate shear strength increases with increasing thickness of the slab and increases with increasing the radius of the column.

CHAPTER EIGHT

CONCLUSIONS AND RECOMMENDATIONS FOR FUTURE WORK

8.1 Introduction

In spite of the fact that SFRC ground-suspended floor slabs have become a popular structural form in the concrete structure industry, it is still true that the information and data on many aspects of their behaviour are not complete. The behaviour of SFRC slabs at the ultimate limit state, particularly the behaviour under shear loading, is still not clear. This results in the situation that appropriate design methods that can take into account the real behaviour of this type of structures are not yet available. Therefore, in most of the current design codes for concrete structures, they fail to mention the design of SFRC at all, and simply treat ground-suspended slab structure in the same way as suspended slab structures. To this end, the overall aim of the current study is to investigate the structural effect of using steel fibre-reinforcement on the punching shear behaviour of ground-suspended slabs with internal columns.

The study was carried out in four stages. In the first stage, a constitutive model for SFRC, namely, the tension stiffening behaviour was developed, in order to capture the main characteristics induced by steel fibre-reinforcement. In the second stage, a preliminary FEA of concrete slabs was carried out. The main objectives at this stage were to determine the test set-up (i.e. the size of the tested specimen and the effect of the presence of the underlying soil on the ultimate load capacity of the slabs). In the third stage, an experimental study into the punching shear behaviour of SFRC slabs was carried out. The main objective of the fourth stage was to analyse the tested specimens by the finite element method in order to, numerically demonstrate the possibility of reproducing the structural behaviour of the slabs. A finite element model for predicting the punching shear behaviour of SFRC slabs was developed, using experimental results obtained from stage three and the constitutive model for SFRC developed in stage one.

This chapter concludes the thesis by identifying the research's major conclusions. However, considering the fact that there are still no sufficient data with respect to the

punching shear behaviour of SFRC slabs and the investigation undertaken here is only a preliminary study in this area, further work on the behaviour of SFRC under loading is necessary, they are listed for future work.

8.2 General Conclusions

The literature review presented in Chapter Two revealed that there was no theoretical or analytical models developed to predict the punching shear behaviour of SFRC slabs with no longitudinal reinforcement. It also indicated that there are no systematic experimental studies conducted on punching shear failure of SFRC slabs with no longitudinal reinforcement. According the main contributions of this research are:

1. Systematic experimental studies on punching shear failure of SFRC slabs with no longitudinal reinforcement were carried out in terms of the following parameters: concrete compressive strength, fibre dosage, and fibre aspect ratio.

2. A Finite Element Model that has the capability to predict the punching shear behaviour of SFRC slabs with no longitudinal reinforcement. This model was validated using the results obtained from the experimental studies based on the following factors ultimate load capacity, load-deflection behaviour, crack pattern, and mode of failure. This model was also used as a supplement in order to predict the effect of concrete compressive strength, tensile strength, tension stiffening, slab size and column size on the punching shear failure of SFRC slabs.

Moreover, one of the main findings of this research is the constitutive model for SFRC in the post-cracking stage. This model enables one to estimate the tension-stiffening behaviour of SFRC based on the results of a simple beam bending test and a statistical model developed in this research. However, the use of this model, represented by the bellow equations, is limited to the type and content of steel fibres which were used in the current investigation. In an attempt to obtain generic equations that could be used for different types of fibres the same methodology (i.e. the inverse method with the finite element

analysis) which was used in developing these equations should be used and the resulting equations should be compared against these equations. These equations are:

$$\sigma_{n1} = 0.055 - 0.14\,\sigma_{tu} + 0.486 f_{R1}$$

$$\sigma_{n2} = 0.193 - 0.082 f_L + 0.46 f_{R2}$$

$$\sigma_{n3} = 0.347 - 0.236 f_L + 0.489 f_{R3} + 0.17\,\sigma_{tu}$$

$$\sigma_{n4} = 0.344 - 0.076 f_L + 0.378 f_{R4}$$

In addition, the following conclusions could be drawn from this research:

- From the FEA results of beams under bending it was found that the structural response of the SFRC beams was not altered by the inclusion of post-peak response in compression; this is expected because the peak stress in compression is never actually reached in the structure. Whereas, the post-peak response in tension (tension-stiffening) has a significant effect on the structural response of the SFRC beams.

- The preliminary FEA results show that the locations of the contra-flexure lines in the flat slabs vary with the panel span lengths, whereas, the column size has little influence on the positions of contra-flexure lines.
- The preliminary FEA results show that the value of the ratio of the distance between the zero bending moment and centre of the column, α_o should lie somewhere between 0.203 and 0.213. This definition and value are very similar to those proposed by CEB-fib (2001) for flat slabs in which α_o is defined as 0.2.

- It was found that the presence of very poor soil with modulus of sub-grade reaction of 10 and 27 MN/m^3, respectively have minimal effect on the ultimate load capacity of the slab although more at the early age of casting (before 28 days).

- In the experimental tests of SFRC slab specimens, it was found that the failure mode of SFRC slabs is affected by the dosage of steel fibres. There are two possible punching shear failure modes controlled by the dosage of steel fibre-reinforcement. The failure may occur in a brittle-punching manner when using smaller dosage of fibre-

reinforcement (i.e. 20 kg/m^3), while the ductile-punching mode of failure occurs with a larger fibre dosage (i.e. 40 kg/m^3). Therefore, there is a need to define a critical value for the fibre dosage, which could be used to distinguish between a brittle and ductile mode of failure in order to arrive at ductile mode of failure.

- The experimental data clearly show that the inclusion of steel fibres into the concrete mix improved the punching shear strength of concrete slabs by 22 and 130%. It also shows that the punching shear capacity was not significantly affected by the compressive strength.

- While the aspect- ratio of the steel fibres did not significantly affect the punching shear capacity of the slabs, the shorter fibre was most effective. This has been attributed to the reduction in workability with the longer fibres.

- Of particular note is the observation that the punching shear strength and the angle of the punching cone are directly related. The angle of the punching cone was reduced with increasing fibre dosage. The presence of steel fibres resulted in decreasing the angle of shear failure plane of the slabs, hence, stretched the failure surface on the tension face away from the column face resulting in increasing the area of failure surface. This resulted in increasing their punching shear resistance.

- From the results of the FEA, it was concluded that axi-symmetrical model is a good model for analysis of punching shear problem.

- From the results of the FEA, it was concluded that axi-symmetrical finite element model generally agree with the experimental results for all the tested slabs in terms of ultimate load, load-displacement behaviour, mode of failure, crack pattern and angle of punching cone, with correlation between the experimental and the numerical prediction of 90% in the ultimate load. Of the two different mode of failure, better agreement with experimental results was obtained with the model in which the ductile-punching was observed. The deviation from ultimate capacity was only about 4%.

- The trend of parameters governing the punching shear strength predicted by the present model correlates very well with test data.

- The numerical investigations indicate a relatively small influence of the pure compressive strength (assuming constant tensile properties). However, this observation shall not lead to the conclusion that the punching failure was a purely tensile failure and a simplified modelling of the compressive concrete properties e.g. elasto-plastic, was sufficient. The material model should be able to stimulate the tensile splitting as well as failure of concrete in compression.

- The finite element results show that the shear strength of the slab-column connection tends to increase with an increase in thickness of the slab and decreases when the radius of the column increases.

8.3 Recommendations for Future Work

Further aspects of analysis and design are of interest for the future research. The following work is recommended:

- Using the same methodology utilized in chapter four, further laboratory work should be undertaken on fibre-reinforced beams bending test in order to analyse it using FEA and get a more generalised model to describe the tension-stiffening behaviour of fibre-reinforced concrete.

- There is no systematic study of the factors governing the punching shear for SFRC slab column connections with no longitudinal reinforcement. More extensive experimental studies are needed to investigate the effects of other parameters, such as the size effect (span-depth ratio), the size of loaded area, the shape and the type of loaded area and in-plane restraints.

- The work can clearly be extended to the analysis of punching shear for slab-column connection subjected to combination of shear and unbalanced moment especially for edge and corner slab-column connections.

- It would be interesting to compare the performance of specimens reinforced with structural synthetic fibres with the specimens tested during this study. This should include the same fibre volume used in the current study but with different types of fibre.

- The proposed finite element model was only tested on slabs subjected to a concentrated loading on circular areas, therefore, it would be useful to extend and verify the method to enable the analysis of slabs subjected to loadings on rectangular areas with different boundary condition to simulate the edge effect.

REFERENCES

ABAQUS ANALYSIS MANUAL (2006a) HiBBITT, KARLSSON AND SORENSEN, INC, Warrington, Cheshire, version 6.6.1, pp. 1–13.

ABAQUS THEORY MANUAL (2006b) HiBBITT, KARLSSON AND SORENSEN, INC, Warrington, Cheshire, version 6.6.1, pp. 1–13.

Abbas, A. A. (2002) *Analysis and Design of Industrial Ground-Floor Slabs Using The Finite Element Method*, PhD Thesis, University of London, London.

Abbasi, M., Baluch, M., Azad, A. and Adbel Rahman, H. (1992) Nonlinear finite element modelling of failure modes in RC slabs, *Computers and Structures*, **42**(5), 815-823.

ACI 318-89 (1989) *Building Code of Requirements for Reinforced Concrete*, American Concrete Institute, Detroit.

ACI Committee 544 (1988a) Design considerations for steel fibre reinforced concrete, in ACI manual of concrete practice, Part 5-1990, *American Concrete Institute*, Michigan, USA.

ACI Committee 544 (1993) Guide for proportioning, mixing, placing and finishing steel fibre reinforced concrete, *ACI Materials Journal*, **90**(1), 94-101.

ACI Committee 544, (1986) *State-of-art report on fibre reinforced concrete, in ACI manual of concrete practice*, part 5 – 1990, American concrete institute, Michigan, USA.

ACI Committee 544.1R (1996) Fibre reinforced concrete, *American Concrete Institute*, Michigan, USA.

ACIFC, Association of Concrete Industrial Flooring Contractors (1999) An Introduction Guide: Steel fibre reinforced concrete industrial ground floors, ACIFC, Warwickshire.

Allen, H. G. (1975) Glass-fibre reinforced cement, strength and stiffness, *CIRIA Report*, **55**.

Alexander, S. and Simmonds, S. (1992) Punching shear tests of concrete- Column joints containing fibre-reinforcement, *ACI Structural Journal*, **89**(4), 425-432.

Al-Nasra, M. (1997), Finite element analysis of floor slabs under warping effect, *Engineering Structures*, **19**(7), 533-539.

Andersson, J. (1963) Punching of concrete slabs with shear reinforcement, *Meddelande Nr.47*, Institutionen for Byggnadsstatik, Kungliga Tekniska Hogskolan, Stockholm.

ASCE (1982) Task Committee on Concrete and Masonry Structures, *ASCE*, State of the art report on finite element analysis of reinforced concrete.

Aveston, J., Cooper, G. A. and Kelly, A. (1971) Conference Proceedings, National Physical Laboratory. In: *The Properties of Fibre Composites*, IPC Science and Technology Press Ltd, London, p. 15.

Aveston, J.; Mercer, R. and Sillwood, J. (1974) *Fibre-reinforced cements- Scientific Foundations for Specifications, Composites Standard Testing and Design*, NPL Conference Proceedings, 93-103.

Balakrishnan, S. and Murray, D.W. (1988) Concrete constitutive model for NLFE analysis of structures, *ASCE Journal of Structural Engineering,* **114**(7), 1449–1466.

Bangash, M. Y. H. (1989) *Concrete and Concrete Structures: Numerical Modelling and Applications,* Elsevier Science Publisher, London.

Balaguru, P. and Ramakrishnan, V. (1986) Freeze-thaw durability of fibre reinforced concrete, *ACI Journal Proceedings*, **83**(3), 374-382.

Banthia, N. and Trottier, J. (1994) Concrete reinforced with deformed steel fibres: Part I. Bond–slip mechanism, *ACI Material Journal,* **91**(5), 435–446.

Barros, J. A. O., and Figueiras, J. A. (2001) Model for the analysis of steel fibre reinforced concrete slabs on grade, *Computers and Structures*, **79**(1), 97-106.

Barros, J. and Figueiras, J. (1999) Flexural behaviour of SFRC: Testing and Modelling, *Journal of Materials in Civil Engineering ASCE*, **11**, 331-339.

Barros, J. and Figueiras, J. (1998) Experimental behaviour of fibre concrete slabs on soil, *Mechanics of Cohesive-Frictional Materials*, **3**(3), 277-290.

Bathe, K. J. (1996) *Finite Element Procedures*, Prentice-Hall, London

Bazant, Z. P. (1978) On endochronic inelasticity and incremental plasticity, *International Journal of Solids Structures,* **14**, 691–714.

Bazant, Z. P. and Cao, Z. (1987) Size effect in punching shear failure of slabs, *ACI Structural Journal*, **84**, January-February, 44-53.

Bazant, Z. P. and Oh, B. H. (1983) Crack band theory for fracture of concrete, *Materials and Structures, RILEM 93*, **16**, 155-177.

Beckett, D. (1990) Comparative tests on plain, fabric reinforced and steel fibre reinforced concrete ground slabs, *Concrete*, **24**(3), 43-45.

Beckett, D. (1999) Corner and edge loading on concrete industrial ground floors reinforced with steel fibres, *Concrete*, **33**(3), 22-24.

Beckett, D. (2004) The performance of concrete slabs, *Concrete*, 38(9), 30-33.

Bekaert, (1990) *Industrial Floors with Dramix Steel Wire Fibre Reinforced Concrete*, NV Bekaert S. A. Zwevegem.

Bekaerts NV Ltd (1998) Trade literature on Dramix®, 8550 Zwevegem, Belgium.

Benture, A. and Mindess, S. (1990) *Fibre Reinforces Cementitious Composites*, Elsevier Applied Science, London.

Beutel, R. and Hagger, J. (1998) Punching shear resistance of shear reinforced flat slabs, *Research Programme No. 10644-N, DBV 185.*

Biryukovich, K., Yu, L. and Yu, D. L. (1965) Glass fibre reinforced concrete, Kiev, Budivel'nik, translated by G. L. Cairns as CERA Translation No. 12, *Civil Engineering Research Association*, 41, London.

Boussinesq, J. (1878) Equilibre d'elasticite d'un solide isotrope sans pesanteur, supporttant differents poids, C. Rendus Acad. Sci., Paris, **86**, 1260-1263.

Branson, D. E. (1968) Design procedures for computing deflection, *ACI Journal,* **65** (8), 730–742.

Brooms, C. (1990) Punching of flat plates-A Question of concrete properties in biaxial compression and size effect, *ACI Structural Journal*, **87**(3), 292-304.

BS EN 12390-3; 2002 (2002) British Standard Institution, Testing hardened concrete – Copressive strength of test specimens, BSI, London.

BS EN 12350-2; 2000 (2000) British Standard Institution, Testing fresh concrete – Slump test, BSI, London.

BS 5930 (1999) British Standard Institution, British Standard Code of Practice for Site Investigations, London.

BS 8110 (1985) British Standard Institution, Structural Use of Concrete, Part2: Code of Practice for Special Circumstances, London.

BS 8110 (1997) British Standard Institution, Structural Use of Concrete, British Standard Code of Practice for Design and Construction: Part 1, London.

Budiansky, B., Hutchinson, J. W. and Evans, A. G. (1986) *Journal of Mech. Phys. Solids,* **34**, 167.

Candappa, D.P. Setunge S. and Sanjayan, J.G. (1999) Stress versus strain relationship of high strength concrete under high lateral confinement, *Cement and Concrete Research,* **29**(12),1977–1982.

Cao, J. and Chung, D. D. L. (2001) Improving the dispersion of steel fibres in cement mortar by the addition of silane, *Cement and Concrete Research*, **31**, 39-311.

CEB-fib, (2001) Punching of Structural Concrete Slabs, *Technical Report*, Bulletin 12, Sprint-Druck Stuttgart, Switzerland.

CEB-FIP MC 90 (1993), Design of concrete structures. CEB-FIP-Model-Code 1990, Thomas Telford, London.

Chandler, J. W. E. and Neal, F. R. (1988) The design of ground supported concrete industrial floor slabs, *British Cement Association, Interim Technical Note 11.*

Chen, A. C. T. and Chen, W. F. (1975) Constitutive relations for concrete, *Journal of the Engineering Mechanical Division, ASCE,* **101**, 465–481.

Chen, E. S. and Buyukozturk, O. (1985) Constitutive model for concrete in cyclic compression, *Journal of the Engineering Mechanics Division, ASCE,* **111**, 797–814.

Chen, W. F. (1982) *Plasticity in Reinforced Concrete*, McGraw-Hill, London.

Chern, J. C., Yang, H. J. and Chen, H. W. (1992) Behaviour of steel fibre reinforced concrete in multiaxial loading, *ACI Materials Journal,* **89**(1), 32–40.

Choi, C. K. and Cheung, S. H. (1996) Tension stiffening model for planar reinforced concrete members, *Computers and Structures,* **59**(1), 179–190.

Clarke, J. L., Garas, F. K. and Armer, G. S. T. (1985) *Design of Concrete Structures, The Use of Model Analysis*, Elsevier Applied Science Publishers.

Collins, M. P. and Vecchio, F. J. (1986) The modified compression-field theory for reinforced concrete elements subjected to shear, *ACI Journal*, **83**(2), 219–231.

Cosenza, E. (1990) Finite element analysis of reinforced concrete elements in a cracked state, *Computers and Structures* **36** (1), 71–79.

Crisfield, M. (1981) *A fast incremental/iteration solution procedure that handles snap-through*. Computers and Structures, Vol.13, Issues 1-3, pp. 55–62.

Criswell, M. (1974) Static and dynamic response of reinforced concrete slab-column connections, *Publication SP-42, ACI*, **2**,721-746.

Davis, R. O. and Selvadurai, A. P. S. (1996) *Elasticity and Geomechanics*, University Press, Cambridge.

De Borst, R. and Nauta, P. (1984) Smeared crack analysis of reinforced concrete beams and slabs failing in shear, *Proceedings of International Conference on Computer Aided Analysis and Design of Concrete Structure- Part1*, Split, Yugolavia, pp.261-273.

Destree, X. (2005) Concrete free suspended elevated slabs reinforced with only steel fibres: full scale testing results and conclusions – Design Examples.

Dragon, A. and Mroz, Z. (1979) A continuum model for plastic-brittle behaviour of rock and concrete, *International Journal of Engineering Science,* **17**, 121–137.

Dyngeland, T., Hoiseth, K., Ophein, E. and Hole, A. (1994) Nonlinear analyses of reinforced concrete members subjecte to punching shear, In Computer Modelling of Concrete Structures, *Proceedings of EURO-C conference*, Innsbruck.

Eddy, D. (2003) New guide for suspended concrete ground floor slabs, *Concrete*, **37**(9), 26-27.

Edgington, J. and Hannant, D. J. (1972) Steel fibre reinforced concrete. The effect on fibre orientation of compaction by vibration, *RILEM Materials and Structures*, **5**(25), 41-44.

Edgington, J., Hannant, D. J. and Williams, R. I. T. (1974) Steel fibre reinforced concrete, *Building Research Establishment*, Current paper 69/74.

Elstner, R. and Hognestad, E. (1956) Shearing strength of reinforced concrete slabs, *ACI Proceedings*, **53**(1), 29-58.

Este, G. and Willam, K. J. (1994) A fracture-energy based constitutive formulation for inelastic behaviour of plain concrete, *Journal of Engineering Mechanics, ASCE,* **120**, 1983–2011.

Euro code 2 (2004) BE EN 1992-1-1, *Design of concrete structures- Part 1:General rules and rules for buildings*, British Standards Institution, London.

Ezeldin, A. and Balaguru, P. (1992) Normal- and high-strength fibre-reinforced concrete under compression, *Journal of Materials in Civil Engineering*, **4**(4), 415-429.

Ezeldin, A. and Lowe, S. (1991) Mechanical Properties of Steel Fiber Reinforced Rapid-Set Materials, *ACI Materials Journal*, **88**(4), 384-389.

Falkner, H. and Teutsch, M. (1993) Comparative investigations of plain and steel fibre reinforced industrial ground slabs, *Institut Fur Baustoffe*, Massivbau und Brandschutz, 102.

Fanella, D. and Naaman, A. (1985) Stress-strain properties of fibre reinforced concrete in compression, *Journal of American Concrete Institute*, **82**, 475-483.

Farhang, A. and Vogt, C. (2005) Residual flexural tensile strength of SFRC beams – an experimental comparison between DRAMIX and TABIX fibres, *Report No. 2005-95, Swedish Cement and Concrete Research Institute.*

Febrillet, N., Kido, A., Ito, Y. and Ishibashi, K. (2000) Strength and abrasion resistance of ultra high strength steel fibre reinforced concrete, *Transactions of the Japan Concrete Institute*, **22**, 243-252.

Floegl, H. and Mang, H. A. (1982) Tension stiffening concept based on bond slip, *Journal of the Structural Division, ASCE,* **108**(12), 2681–2701.

Gasser, T. and Holzapfel, G. (2005) Modelling 3D crack propagation in un-reinforced concrete using PUFEM, *Computer Methods in Applied Mechanics and Engineering*,**194**(25-26), 2859-2896.

Gatuingt, F. and Pijaudier-Cabot, G. (2002) Coupled damage and plasticity modelling in transient dynamic analysis of concrete, *International Journal of Numerical and Analytical Methods in Geomechanics,* **26**, 1–24.

Goldfein, S. (1963) Plastic fibrous reinforcement for Portland Cement, *Technical report No. 1757-TR, US Army Engineer Research and Development Laboratories*, Fort Belvoir, Va. October, 16.

Gomes, R. and Regan, P. (1999) Punching resistances of RC slabs with shear reinforcement, *Journal of Structural Engineering*, **125**(6), 684-692.

Gonzalez, V., Kotsovos, M. and Pavlovic, M. (1991) Three-dimensional non-linear finite element model for structural concrete. Part2: generality study, *Proceedings of Institution of Civil Engineers*, **91**(2), 545-560.

Gonzalez, V.; Kotsovos, M and Pavlovic, M. (1988) Symmetrical punching of reinforced concrete slab: An analytical investigation based on nonlinear finite element modelling. *ACI Structural Journal*, **85**(3), 241-250.

Goparalatnam, V. S. and Wecharatana, M. (1991) Fracture toughness of fibre reinforced concrete, *ACI Material Journal,* **88**(4), 339–353.

Grassl, P., Lundgren, K. and Gylltoft, K. (2002) Concrete in compression: a plasticity theory with a novel hardening law, *International Journal of Solids and Structures,* **39**, 5205–5223.

Gray, B. H. and Rice, J. L. (1972) Pavement performance investigation, Fibrous concrete: construction material for the seventies, *CERL Conference Proceeding*, M. 28, December, Champing, Illinois 61820, 147-157.

Gregory, J., Galloway, J.W. and Raithby, K. D. (1975) Full scale trials of a wire fibre reinforced concrete overlay on a motorway, *Fibre Reinforced Cement and Concrete, RILEM Symposium*, Construction Press Ltd, 383-394.

Grimer, F. J. and Ali, M. A. (1969) The strengths of cements reinforced with glass fibres, *Magazine of Concrete Research*, **21**(66), 23-30.

Gupta, A. and Maestrini, S. R. (1990) Tension-stiffness model for reinforced concrete bars, *ASCE Journal of Structural Engineering*, **116**(3), 769–791.

Hallgren, M. (1996) Punching shear capacity of reinforced high strength concrete slabs, *Bulletin,* **No 23**. *Department of Structural Engineering, KTH*, Stockholm.

Hallgren, M. and Bjerke, M. (2002) Non-linear finite element analysis of punching shear failure of column footings, *Cement and Concrete Composites*, **24**(6), 491-496.

Hannant, D. (1978) *Fibre Cements and Fibre Concretes*, John Wiley & Sons, New York.

Hannant, D. J. and Spring, N. (1974) Steel fibre reinforced mortar, A technique for producing composites with uniaxial fire alignment, *Magazine of Concrete Research*, **26**(86), 47-48.

Harajli, M., Maalouf, D. and Khatib, H. (1995) Effect of fibres on the punching shear strength of slab-column connections, *Cement and Concrete composites*, **17**, 161-170.

Hawkins, N. (1971a) Progress Report on NSF Grant No.Gk.16375, Shear and moment transfer between concrete flat plates and columns, Department of Civil Engineering, University of Washington.

Hawkins, N. M., Criswell M. E. and Roll, F. (1974) Shear strength of slabs without shear reinforcement, *ACI Publication SP-42*, **2**, 677-720.

Hawkins, N. M., Falssen, H. B. and Hinojosa, R. C. (1971) Influence of column rectangularity on the behaviour of flat plate structures, *American Concrete Institute*, Publication SP-30, Detroit, 127-146.

Hemmy, O. (2002) Recommendations for finite element analysis of FRC, report of subtask 3.5, Brite-EuRam Project BRPR-CT98-0813: Test and design methods for steel fibre reinforced concrete, project funded by the European Community under the Industrial & Materials Technologies Programme (Brite-Euram II).

Hetenyi, M. (1946) *Beams on Elastic Foundation*, The University of Michigan Press, Ann Arbor.

Hillerborg, A. (1985) Results of three comparative test series for determining the fracture energy G_f of concrete, *Materials and Structures, Research and Testing (RILEM, Paris)*, **18**(107), 407-413.

Hillerborg, A., Modeer, M. and Petersson, P. (1976) Analysis of crack formation and crack growth in concrete by means of fracture mechanics and finite element, *Cement and Concrete Research*, **6**,773-782.

Hinton, E. and Owen, D. R. J. (1989) Finite Element Programming, Academic Press, London.

Hu, X. D., Day, R. and Dux, P. (2003) Biaxial failure model for fibre reinforced concrete, ASCE, *Journal of Materials and Civil Engineering,* **15**(6), 609–615.

Hughes, B. and Fattuhi, N. (1977) Stress-strain curves for fibre reinforced concrete in compression, *Cement and Concrete Research*, **7**, 173-184.

Hull, D. (1981) *An Introduction to Composite Materials*, Cambridge Solid State Science Series, Cambridge University press, Cambridge.

Ioannides, A. and Korovesis, G. (1992) Analysis and design of doweled slab-on-grade pavement systems, *Journal of Transportation Engineering*, **118**(6), 745-768.

Jason, L., Pijaudier-Cabot, G., Huerta, A., Crouch, R., Ghavamian, S. (2004) An elastic plastic damage formulation for the behaviour of concrete. In: Li, V., Leung, C.K.Y., William, K.J., Billington, S.L. (Eds.), *Fracture Mechanics of Concrete Structures, Ia-FraMCos-5*, Vail, Colorado, USA, pp. 549–556.

Jiang, D. H and Shen, J. H. (1986) Strength of concrete slabs in punching shear, *ASCE Journal of structural Engineering*,**112**(12), 2578-2591.

Jofriet, J. and McNeice, G. (1971) Finite element analysis of reinforced concrete slabs, *Journal of the Structural Division, Proceedings of ASCE*, **97**(ST3), 785-806.

Johanson, and Nephew, (1975) *Trade Literature on Wirand Concretes*, Ambergate Ltd, Derbyshire.

John, S. and David, I. (1990) Punching shear behaviour of slabs with varying span-depth ratios, *ACI Structural Journal*, **87**, (5), 507-511.

Johnston, C. (1974) Steel fibre reinforced mortar and concrete: A review of mechanical properties, in Fibre Reinforced Concrete, *ACI SP – 44, American Concrete Institute*, Detroit, 127-142.

Karabinis A. I. and Kiousis, P. D. (1994) Effects of confinement on concrete columns: a plasticity theory approach, *ASCE Journal of Structural Engineering*, **120**, 2747–2767.

Keer, J. (1984) *Fibre Reinforced Concrete, in Concrete Technology and Design*, New reinforced concretes, Ed. Swamy RN, Surry University Press, London.

Kelley, E. F. (1939b) Application of the results of research to the structural design of concrete pavement, *Public Roads*, **20**(5), 83-104.

Kelly, A. (1973) *Strong Solids*, Clarenden press, Oxford

Killen, P., and Dalgleish, P. (1997) Practical applications of steel fibre reinforced concrete floor slabs for industrial projects in Australia, *Proceedings of the Asia-Pacific Specialisty Conference on Fibre reinforced Concrete*, August 28-29, 137-144, Singapore.

Killu, B. (2002) *Punching Shear in High Strength Steel Fibre Reinforced Concrete Slabs*, MPhil thesis, University of Cambridge, Cambridge.

Kinnunen, S. (1963) Punching of concrete slabs with two-way reinforcement with special reference to dowel effect and deviation of reinforcement from polar symmetry, *Meddelande Nr.45*, Institutionen for Byggnadsstatik, Kungliga Tekniska Hogskolan, Stockholm.

Kinnunen, S. and Nylander, H. (1960) Punching of concrete slabs without shear reinforcement, Meddelande Nr 38, Institutionen for Byggnadsstatik, KTH, Stockholm.

Kinnunen, S., Nylander, H. and Tolf, P. (1978) Investigation of punching at the building statics institute KTH, *Nordisk Betong*, **3**, 25-27.

Knapton, J. (1999) *Single Pour Industrial Floor*, Thomas Telford, London.

Knapton, J. (2003) *Ground Bearing Concrete Slabs*, Thomas Telford, London

Kotsovos, M. and Pavlovic, M. (1995) *Structural Concrete. Finite Element analysis for Limit-state Design*, Thomas Telford, London.

Krajcinovic, D. (1983) Continuum damage mechanics, *Applied Mechanics Reviews*, **37**, 1–6.

Krajcinovic, D. (1985) Continuous damage mechanics revisited: basic concepts and definitions, *Journal of Applied Mechanics*, **52**, 829–834.

Krenchel, H. (1974) Fibre-reinforced brittle matrix materials, *Fibre-Reinforced Concrete, ACI Publication*, **SP-44**, 45-77.

Kuang, J. and Morley, C. (1993) A plasticity model for punching shear of laterally restrained slabs with a compressive membrane action, *International Journal of Mechanical Sciences*, **35**(5), 371-385.

Kurihara, N., Kunieda, M., Kamada, T., Uchida, Y. and Rokugo, K. (2000) Tension softening diagrams and evaluation of properties of steel fibre reinforced concrete, *Engineering Fracture Mechanic*, **65**(2-3), 235-245.

Kwak, H. G. and Song, J. Y. (2002) Cracking analysis of RC members using polynomial strain distribution function, *Engineering Structures*, **24**, 455–468.

Kwon, M. and Spacone, E. (2002) Three-dimensional finite element analyses of reinforced concrete columns, *Computers and Structures*, **80**(2), 199-212.

Lange-Kornbam, D. and Karihaloo, B.L. (1997) Tension softening of fibre-reinforced cementitious composites, *Cement Concrete Composites*, **19**, pp. 315–328.

Laws, V. (1971) The efficiency of fibrous reinforcement of brittle matrices, *Journal of Physics; Applied Physics*, **4**, 1737-1746.

Lee, J. and Fenves, G. L. (1998) A plastic-damage model for cyclic loading of concrete structures, *Journal of Engineering Mechanics, ASCE*, **124**, 892–900.

Leibengood, L. Darwin, D. and Dodds, R. (1986) Parameters affecting FE analysis of concrete structures, *Journal of Structural Engineering ASCE*, **12**(2), 326-341.

Leung, C. and Geng, Y.P. (1998) Micromechanical modelling of softening behaviour in steel fibre reinforced cementitious composites, *International Journal of Solids Structures.* **35**, 4205–4222.

Li, V., Stang, H. and Krenchel H. (1993) Micromechanics of crack bridging in fibre reinforced concrete, *Journal of Materials and Structures*, **26**, 486-494.

Li, V., Wang, Y. and Backer, S. (1991) A micromechanical model of tension-softening and bridging toughening of short random fiber reinforced brittle matrix composites, *Journal of the Mechanics and Physics of Solids*, **39**(5), 607-625.

Li, V. C. (1998) Influence of fibre bridging on structural size-effect, *International Journal of Solids Structures.* **35**, 4223–4238.

Lin, C. S. and Scordelis, A. C. (1975) Nonlinear analysis of RC shells of general form, *Journal of the Structural Division ASCE,* **101**(3), 523–538.

Loesth, S., Slatto, A. and Syvertsen, T. (1982) Finite element analysis of punching shear failure of reinforced concrete slabs, *Nordic Concrete Research*, 1, Oslo.

Loland, K. E. (1980) Continuous damage model for load-response estimation of concrete, *Cement and Concrete Research,* **10**, 395–402.

Long, A. (1973) Punching failure of slabs-transfer for moment and shear, *Journal of Structural Division, ASCE*, **99** (ST4), 665-685.

Long, A. and Bond, D. (1967) Punching failure of Reinforced concrete slabs, *Proceedings Institution of Civil Engineers*, 109-136.

Lubarda, V. A., Kracjinvovic, D. and Mastilovic, S. (1994) Damage model for brittle elastic solids with unequal tensile and compressive strength, *Engineering Fracture Mechanics,* **49**, 681–697.

Lubliner, J., Oliver, J., Oller, S. and Onate, E. (1989) A plastic-damage model for concrete, *International Journal of Solids and Structures*, **25**, 299-329.

Maidl, B. (1995) *Steel Fibre Reinforced Concrete*, Ernst & Sohn, Berlin.

Majumdar, A. J. and Ryder, J. F. (1968) Glass fibre reinforcement of cement products, *Journal of Glass Technology*, **9**(3), 78-84.

Majumdar, A. J. and Ryder, J. F. (1970) Reinforcement of cement and gypsum plasters by glass fibre, *Science of Ceramics*, **5**, 539-564.

Majumdar, A. J. (1970) Glass fibre reinforced cement and gypsum products, Proceedings, *Royal Society of London*, **319**, 69-78.

Marzouk, H. and Chen, Z. (1993) Finite element analysis of high strength concrete slabs, *ACI Structural Journal*, **90**(5), 505-513.

Marzouk, H. and Hussein, A. (1991a) Punching shear analysis of reinforced high-strength concrete slabs, *Canadian Journal of Civil Engineering*, **18**, 954-963.

Marzouk, H. and Hussein, A. (1991b) Experimental investigation on the behaviour of high strength concrete slabs, *ACI Structural Journal*, **88**(6), 505-513.

Marzouk, H. and Jiang, D. (1996) Finite element evaluation of shear enhancement of high-strength concrete plates, *ACI Structural Journal*, November-December, 667-673.

Marzouk, H., Osman, M. and Hussien, A. (2002) Punching shear of slabs: crack size and size effects, *Magazine of Concrete Research*, **54**(1), 13-21.

Massicote, B., Elwi, A. E. and MacGregor, J. G. (1990) Tension-stiffening model for planar reinforced concrete members, *ASCE Journal of Structural Engineering*, **106**(11), 3039–3058.

Mazars, J. and Pijaudier-Cabot, G. (1989) Continuum damage theory- Application to concrete, *Journal of Engineering Mechanics*, **115**, 345–365.

McCurrich, L. H. and Adams, M. A. J. (1973) Fibres in cement and concrete, *Current Practice Sheets, Concrete*, **5**, 51-53.

Mebarkia, S., and Vipulanandan, C. (1992) Compressive behaviour of glass-fibre reinforced polymer concrete, *Journal of Materials in Civil Engineering, ASCE*, **4**(1), pp.91-105.

Menetrey, P. (2002) Synthesis of punching failure in reinforced concrete, *Cement and Concrete Composite*, **24**(6), 497-507.

Menetrey, P. and Willam, K. (1995) A triaxail failure criterion for concrete and its generalization, *ACI Structural Journal*, **92**(2), 311-318.

Menetrey, Ph. (1994) Numerical analysis of punching failure in reinforced concrete structures, *PhD Thesis*, Lausanne.

Moe, J. (1961) Shearing strength of reinforced concrete slabs and footings under concentrated load, Bulletin D47, *Portland Cement Association*, Research and Development Laboratories, Skokie, Illinois.

Monfore, G. E. (1968) A review of fibre reinforcement of Portland Cement paste, mortar and concrete, *Journal of Portland Cement Association, Research and Development Laboratories*, **10**(3), 36-42.

Namman, A. (1987) High performance fibre reinforced composites, *Concrete Structures for the Future, IABSE Symposium*, Paris, pp.371-376.

Narayanan, R. and Darwish, I. Y. S. (1987) Punching shear tests on steel-fibre-reinforced micro-concrete slabs, *Magazine of Concrete Research*, **39**(138), 42-50.

Nataraja, M. C. (1999) Stress–strain curves for steel-fibre reinforced concrete under compression, *Cement Concrete Composites,* **21**, 383–390.
Nawy, G. E. (1996) *Fundamentals of High Strength High Performance Concrete*, Uk

Neville, A. (1995) *Properties of Concrete*, Longman, London.

Neville, A. and Brook, J. (1994) *Concrete Technology*, Longman Scientific and Technology, 193-261.

Newman, J. and Choo, B. (2003) *Advanced Concrete Technology (processes)*, Elsevier Ltd, Oxford.

Nielsen, C. V. (1998) Triaxial behaviour of high-strength concrete and mortar, *ACI Materials Journal,* **95**(2), 144–151.

Nielsen, M. (1999) *Limit Analysis and Concrete Plasticity*, 2nd edition, CRC Press, Boca Raton, FL.

Nielsen, M., Braestrup, M., Jenson, B. and Bach, F. (1978) Concrete plasticity, Beam shear-shear in joints- Punching shear, *Structural Research Laboratory*, Technical University of Denmark.

Oh, B. H. (1992) Flexural analysis of reinforced concrete beams containing steel fibres, *ASCE Journal Structural Engineering,* **118**(10), 2691–2698.

Ohama, Y., Miyara, M. and Endo, M. (1985) Properties of steel and polyethylene fibre hybrid reinforced polymer modified concrete, *Proceedings of 28th Japan Congress on Materials research,* March, 151-155.

Onate, E. Oller, S. Oliver, S. and Lubliner, J. (1988) A constitutive model of concrete based on the incremental theory of plasticity, *Engineering Computations,* **5**, 309–319.

Ortiz, M. and Popov, E.P. (1982) Plain concrete as a composite material, *Mechanics of Material,* **1**, 139–150.

Ostergaard, L., Olesen, J. F., Stage, H. and Lange, D. (2002) A method for fast and simple interpretation and inverse analysis of the wedge splitting test, Report of sub-tank 3.5, Brite-EuRam Project BRPB-CT98-0813: Test and design methods for steel fibre reinforced concrete, project funded by the European Community under the Industrial and Materials Technologies Programme (Brite-EuramII).

Pan, A. and Moehle, J. (1992) An experimental study of slab-column connections, *ACI Structural Journal*, **89**(6), 626-638.

Panak, J. and Rauhut, J. (1975) Behaviour and design of industrial slabs on grade, *Journal of the ACI, Proceedings of the American Concrete Institute*, **72**(5), 219-224.

Pantazopoulou S. J. and Zanganeh M. (2001) Triaxial tests of fibre-reinforced concrete, *Journal of Materials in Civil Engineering,* **September/October,** 340-348.

Park, H. and Kim, J. Y. (2005) Plasticity model using multiple failure criteria for concrete in compression, International Journal of Solids and Structures, **42**, 2303-2322.

Park, K. (1975) An improved stiffly stable method for direct integration of nonlinear structural dynamics, *Journal of Applied Mechanics*, **42**, 464–470.

Patel, S. (1970) Effectiveness of steel fibres as shear reinforcement in concrete slabs, Ms Thesis, Clarkson college of Technology, New York, USA.

Polak, M. A. (1998) Modelling punching shear of RC slabs using layered finite elements, *ACI Structures Journal*, **95**(1), 71-80.

Powell, G. and Simons, J. (1981) *Improved iterative strategy for nonlinear structures.* International Journal for Numerical Methods in Engineering, **17**(10), 1455–1467.

Prisco, M. and Felicetti, R. (1997) Some results on punching shear in plain and fibre-reinforced micro-concrete slabs, *Magazine of Concrete Research*, 49(**180**), 201-219.

Qian, C. X. and Stroeven, P. (2000) Development of hybrid polypropylene-steel fibre reinforced concrete, *Cement and Concrete Research*, **30**, 63-69.

Ramakrishnan, V. (1988) Materials and properties of fibre reinforced concrete, *Civil Engineering,* **April**, 29-40, London.

Ramm, E. (1981) *Strategies for tracing the nonlinear response near limit points.* In: Wunderlich, E., Stein, E. and Bathe, K. (1981) *Nonlinear Finite Element Analysis in Structural Mechanics*, Springer, Berlin.

Ramu, S. (1983) Fibre reinforced concrete-What it has to offer?, *Journal of the Institute of Engineers*,**64-S**, 61-64.

Rashid Y (1968) Analysis of prestressed concrete vessels, *Nuclear Engineering and Design*, pp. 334-344

Regan, P. E. (1983) Punching shear in prestressed concrete slab bridges, *Technical Report, Engineering Structural Research Group*, Polytechnic of Central Londol.

Regan P. E. (1986), Symmetric Punching of Reinforced Concrete Slabs, *Magazine of Concrete Research*, **38**(136), 115-128.

Regan, P. E. (1984) The dependence of punching resistance upon the geometry of the failure surface, *Magazine of Concrete Research*, **36**(126), pp.3-8.

Regan, P. E. and Braestrup, M. W. (1985) Punching shear in reinforced concrete. A State of the Art Report. *Comite Euro-International, Lausanne, CEB-Bulletin* No **168.**

Regan P. E. (1971) Behaviour of Reinforced and Prestressed Concrete Subjected to Shear Forces, *Proceedings of ICE*, **50**, London England.
Resende, L. and Martin, J. B. (1984) A progressive damage continuum model for granular materials, *Computer Methods in Applied Mechanics and Engineering*, **42**, 1–18.

Riks, E. (1972) The application of Newton's method to the problem of elastic stability, *Journal of Applied Mechanics*, **39**, 1060–1066.

RILEMTC162-TDF (2002) Test and design methods for steel fibre reinforced concrete, Design of steel fibre reinforced concrete using the σ-w method: principles and applications, *Materials and Structures*, **35**(249), 262-278.

RILEMTC162-TDF (2003) Test and design methods for steel fibre reinforced concrete σ-ε design method, Final recommendation, *Materials and Structures*, **36**(262), 560-567.

RMC Admixtures (2007) CSP313 Concrete Superplasticising Admixture, *Technical Information*.

Robinson, D., Taylor, S. E. and Rankin, B. (2004) Finite element simulation of arching action in restrained slabs, *Proceedings of the Seventh International Conference on Computational Structures Technology*, September, Lisbon, Portugal.

Romualdi, J. and Baston, G. (1963) Mechanics of crack arrest in concrete, *Proceedings ASCE*, **89**(EM3),147-168.

Romualdi, J. P. and Mandel, J. A. (1964) Tensile strength of concrete as affected by uniformly distributed and closely spaced short lengths of wire reinforcement, *ACI Journal*, **61**(6), 650–670.

Russo, G. and Romano, F. (1992) Cracking response of RC members subjected to uniaxial tension, *ASCE Journal of Structural Engineering*, **118**(5), 1172–1190.

Scanlon, A. and Murray, D. W. (1874) Time-dependent reinforced concrete slab deflections, *Journal of the Structural Division*, **100**(8), 1911–1924.

Schrader, E. K. (1989) Fibre reinforced concrete, *ICOLD Buletin 40*, International Committee on Large Dams, Paris, 22.

Schrader, E. K. and Munch, A. V. (1976) Deck slab repaired by fibrous concrete overlay, *Proceedings ASCE*, **102**, 179-196.

Schreyer, H. L. (1983) Third-invariant plasticity theory for frictional materials, *Journal of Structural Mechanics,* **11,** 177–196.

Schupack, M. (1986) Durability of SFRC exposed to severe environments, *Steel Fibre Concrete*, Elsevier Applied Science Publishers, Ltd, 479-496.

Selvadurai, A. P. S. (1979) *Elastic Analysis of Soil-foundation Interaction, Developments in Geotechnical Engineering, Vol. 17*, Elsevier Scientific Publishing, New York.

Shaaban, A. and Gesund, H. (1994) Punching shear strength of steel fibre, *ACI Structural Journal*, **91**(3), 406-414.

Shehata, I. and Regan, P. (1989) Punching in reinforced concrete slabs, *Journal of the Structural Division, ASCE*, **115**(7), 1726-1740.

Shentu, L., Jiang, D. and Hsu, C. (1997) Load-carrying capacity for concrete slabs on grade, *Journal of Structural Engineering*, **123**(1), 95-103.

Sherif, A. G. and Dilger, W. H. (1998) Analysis and deflections of reinforced concrete flat slabs, *CJCE*, **25**, 451-466.

Simo, J. C. and Ju, J. W. (1987a) Strain and stress-based continuum damage. Model. Part I: formulation, *International Journal of Solids and Structures*, **23**, 821–840.

Simo, J. C. and Ju, J. W. (1987b) Strain- and stress-based continuum damage models. Part II: computational aspects, *International Journal for Solids and Structures,* **23**, 841–869.

Simpson, D. (2004) Suspended floors for industrial use: an overview, *Concrete*, **38**(2), 16-18.

Snežana, B. M. and Alendar, V. H. (2008) Punching failure mechanism at edge columns of post-tensioned lift slabs, *Engineering Structures, In Press, Corrected Proof*, Available on line 28 April 2008.

Soroushian, P. and Bayasi, Z. (1991) Fibre type effects on the performance of steel fibre reinforced concrete, *ACI Materials Journal*, **88**(2), 129-134.

Soroushian, P. and Lee, C. (1990a) Distribution and orientation of fibres in steel fibre reinforced concrete, *ACI Materials Journal,* **87**(5), 433–439.

Soroushian. P. and Lee, C. (1990b) Tensile strength of steel fibre reinforced concrete: Correlation with some measures of fibre spacing, *ACI Materials Journal,* **87**(5), 542–546.

Sri Ravindrarajah, R. and Tam, C. (1984) Flexural strength of steel fibre reinforced concrete beams, *International Journal of Cement Composites and Lightweight Concrete*, **6**, 273-278.

Stang, H. (2002) *Finite element modelling using discrete crack elements*, report of subtask 3.5, Brite-EuRam Project BRPR-CT98-0813: Test and design methods for steel fibre reinforced concrete, project funded by the European Community under the Industrial & Materials Technologies Programme (Brite-Euram II).

Stevens, N. J., Uzumeri, S. M., Collins, M. P. (1987) Analytical modelling of reinforced concrete subjected to monotonic and reversed loadings. Report. Canada: University of Toronto.

Swamy, R. (1974) The technology of steel fibre-reinforced concrete for practical applications, *Proceedings of the Institution of Civil Engineers*, London, May 1994, **56**(1), 143-159.

Swamy, R. and Ali, S. (1982) Punching shear behaviour of reinforced slab-column connections made with steel fibre concrete, *ACI Journal*, **79**(41), 392-405.

Swamy, R. and Al-Noori, K. (1975) Flexural behaviour of fibre reinforced concrete with conventional steel reinforcement, *RILEM Symposium, Fibre Reinforced Cement and Concrete*, The Construction Press Ltd, Hormby, pp.187-196.

Swamy, R. N. and Stavrides, H. (1975) Some properties of high workability steel fibre reinforced concrete, *Fibre Reinforced Cement and Concrete, RILEM Symposium*, Construction Press Ltd, 197-208.

Swamy, R. N. and Stavrides, H. (1979) Influence of fibre reinforcement in restrained shrinkage and cracking, *Journal of American Concrete Institute*, **76**, 443-460.

Tan, K.H. and Paramasivam, P. (1994) Punching shear strength of steel fibre reinforced concrete slab, *Journal of Materials in Civil Engineering*, **6**(2), 240-253.

Taylor, R. and Hayes, B. (1965) Some tests on the effect of edge restraints on punching shear in reinforced concrete slabs, *Magazine of Concrete Research*, **17**(S), 39-44.

Taylor, S. E. and Robinson, D. (2004) Modelling of arching action in FRP reinforced concrete slabs, *Proceeding of the Second International Conference on FRP Composites in Civil Engineering – CICE*, December, Adelaide, Australia, 757-763.

Tebbett, I. E. and Harrop, J. (1979) Analytical design of ribbed flat slabs, *The Structural Engineer*, **57A**(7), 223-229.

Theodorakopoulos, D. and Swamy, R. (1999) Ultimate punching shear strength analysis of slab-column connections with steel fibre, *ACI Publications*, American Technical Publishers LTD.

Tho, K. K., Seow, P. E. C. and Swaddiwudhipong, S. (2003) Numerical method for analysis of concrete under multi-axial loads, *Magazine of Concrete Research*, **55**(6), 537–547.

Tlemat, H., Pilakoutas, K. and Neocleous, K. (2006) Modelling of SFRC using inversefinite element analysis, *Materials and Structures*, **39**, 197-207.

TR 34 (1994) Concrete industrial ground floors – A guide to their design and construction, *Technical Report No. 34*, The Concrete Society, Slough.

TR 34 (2003) Concrete industrial ground floors – A guide to their design and construction, *Technical Report No. 34*, The Concrete Society, Slough.

TR 63 (2006) Concrete industrial ground floors – A guidance for the design of steel-fibre-reinforced concrete, *Technical Report No. 63*, The Concrete Society, Slough.

Traina, L. A. and Mansour, S. A. (1991) Biaxial strength and deformational behaviour of plain and steel fibre concrete, *ACI Materials Journal,* 88(4), 354–362.

Unwalla, B. (1982) Steel fibre reinforced concrete, *Chemical Age of India*, 33(7), pp.C-1/1-4.

Vassou, V. (2003) Abrasion resistance of fibre reinforced concrete floors, *PhD Thesis*, Aston University, Birmingham.

Vecchio, F. J. and Collins, M. P. (1986) The modified compression-field theory for reinforced concrete elements subjected to shear, *ACI Journal*, March-April, 219-231.

Vitali, R. and Zanotelli, G. (1994) User element for Crack Propagation in Concrete-like Materials, *ABAQUS User's Conference*, Habbitt Karlsson and Sorensen Italia, Milan, Italy.

Voyiadjis, G. Z. and Abu-Lebdeh, T. M. (1994) Plasticity model for concrete using the bounding surface concept, *International Journal of Plasticity,* **10**, 1–21.

Wang, Y., Li, V. C. and Backer, S. (1990a) Experimental determination to tensile behavior of fibre reinforced concrete, *ACI, Material Journal,* **87**, 461-468.

Wang, Y., Li, V. C. and Backer, S. (1990b) Tensile properties of synthetic fiber reinforced mortar, *Journal of Cement and Concrete Composites,* **12**, 29-40.

Westergaard, H. (1925) Computation of stresses in concrete roads, *Proceedings of the 4th Annual Meeting of the Highway Research Board*, National Research Council, Washington D. C., 60-61.

William, K.J., Warnke, E.P., (1975) Constitutive model for the triaxial behavior of concrete. International Association of Bridge and Structural Engineers, Seminar on Concrete Structure Subjected to Triaxial Stresses, Paper III-1, Bergamo, Italy, May IABSE Proceedings 19.

Williamson, G. (1974) The effect of steel fibres on the compressive strength of concrete, in Fibre Reinforced Concrete, *ACI SP-44, American Concrete Institute*, Detroit, 195-207.

Williamson, G. R. (1965) The use of Fibrous reinforced concrete in structures exposed to explosives hazards, *Miscellaneous Paper,* **No. 5-5,** U.S Army Ohio River Division Laboratories.

Winkler, E. (1867) Die Lehre von der Elastizitat und Festigkeit, Prague.

Wu, J. U., Li, J. and Faria, R. (2006) An energy release rate-based plastic-damage model for concrete, *International Journal of Solids and Structures,* **43,** 583–612.

Wu, Z. Yoshikawa, H. and Tanabe, T. (1991) Tension stiffness model for cracked reinforced concrete, *ASCE Journal of Structural Engineering,* **117**(3), 715–732.

Xiang, Z. X. (1993) Punching Shear Strength of Waffle Slabs at Internal Columns, *PhD Thesis*, The University of Leeds, Leeds.

Yankelevsky, D. and Leibowitz, O. (1999) Punching shear in concrete slabs, *International Journal of Mechanical Sciences*, **41**(1), 1-15.

Yazdani, S, and Schreyer, H. L. (1990) Combined plasticity and damage mechanics model for plain concrete, *Journal of the Engineering Mechanics Division, ASCE,* **116,** 1435–1450.

Yin, W. S., Su, E. C. M., Mansur, M. A. and Hsu, T. T. C. (1989) Biaxial tests of plain and fibre concrete, *ACI Materials Journal,* **86**(3), 236–243.

Zia, P. et al (1995) High performance concretes: A State of Art Report (1989-1994), Strategic highway program, National research Council, SHRP.

Zienkiiewiez, O. and Taylor, R. (1989) The Finite Element Method, Volume 1: Basic Formulation and Linear Problem, McGraw-Hill Book Company.

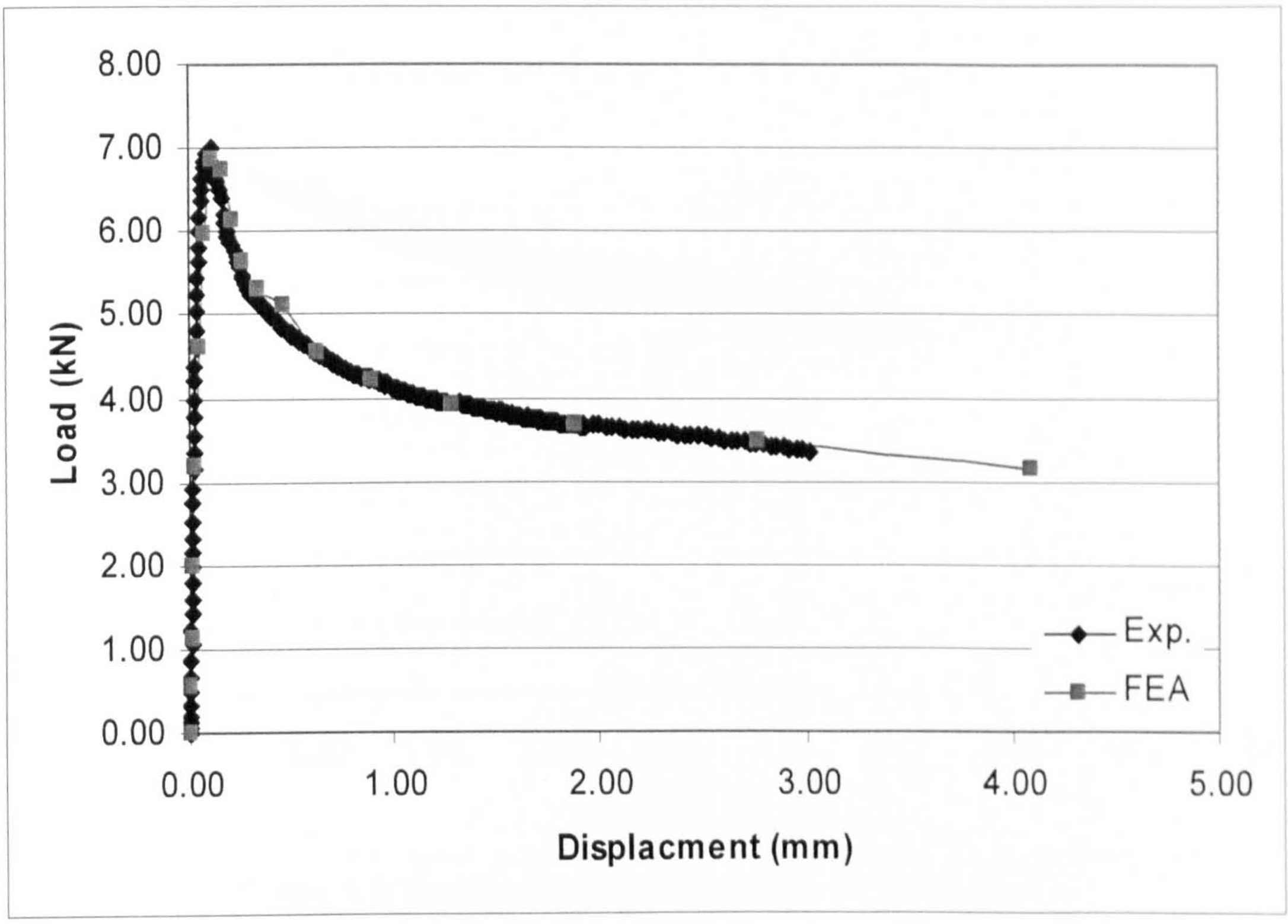

Figure A.1: Experimental and numerical results (beam B1)

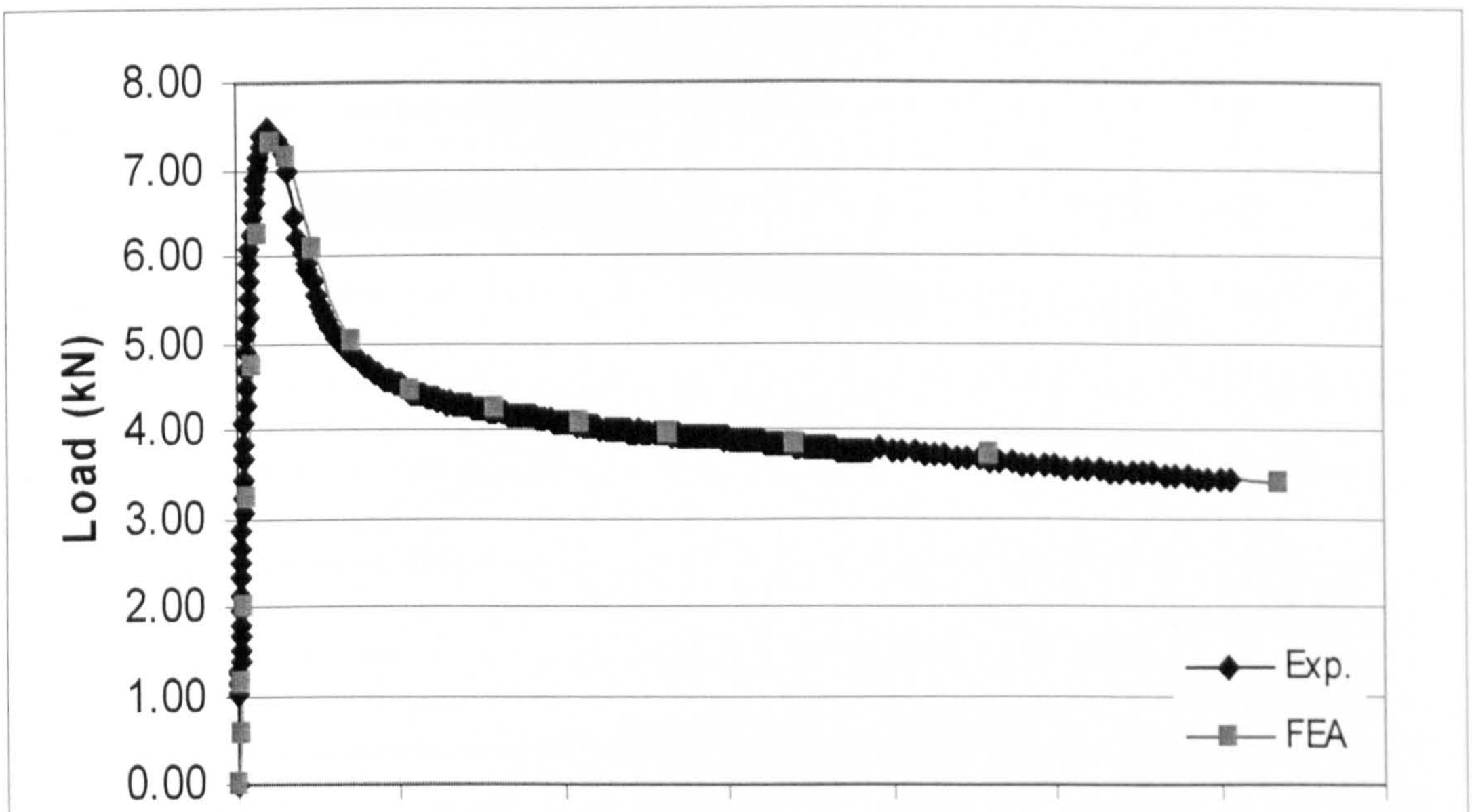

Figure A.2: Experimental and numerical results (beam B2)

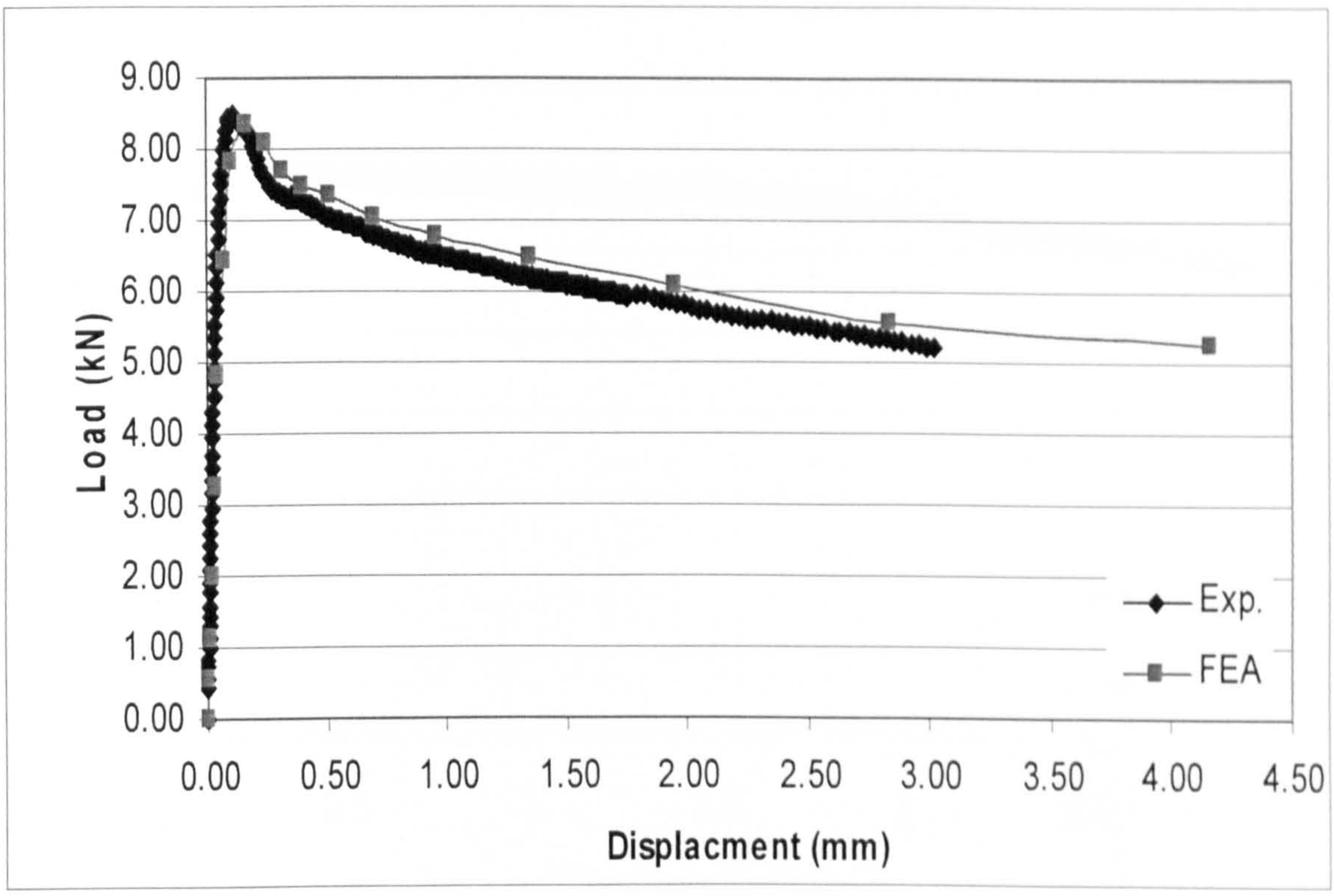

Figure A.3: Experimental and numerical results (beam B3)

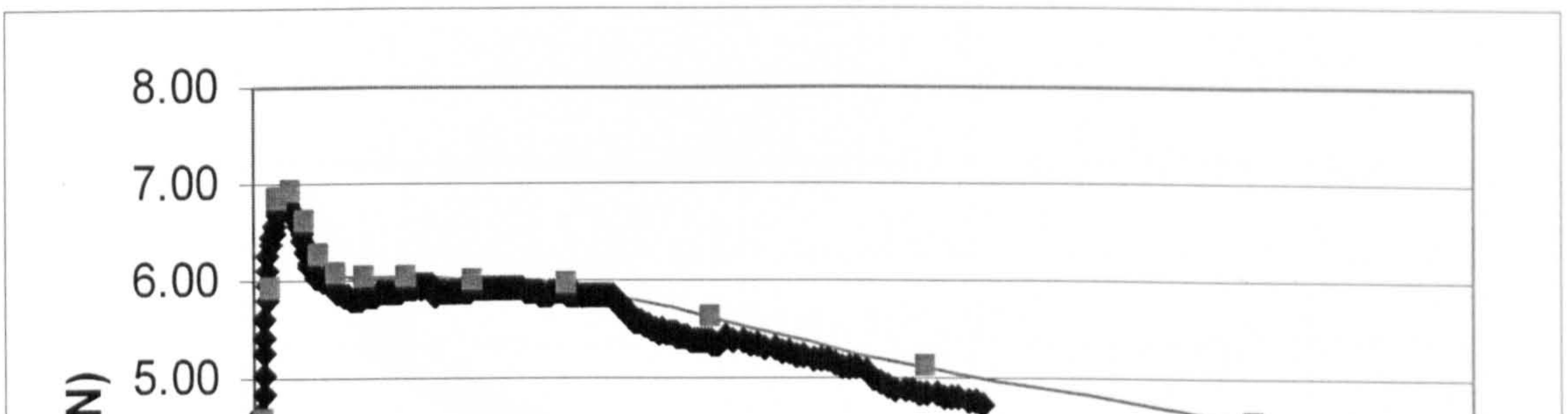

Figure A.4: Experimental and numerical results (beam B4)

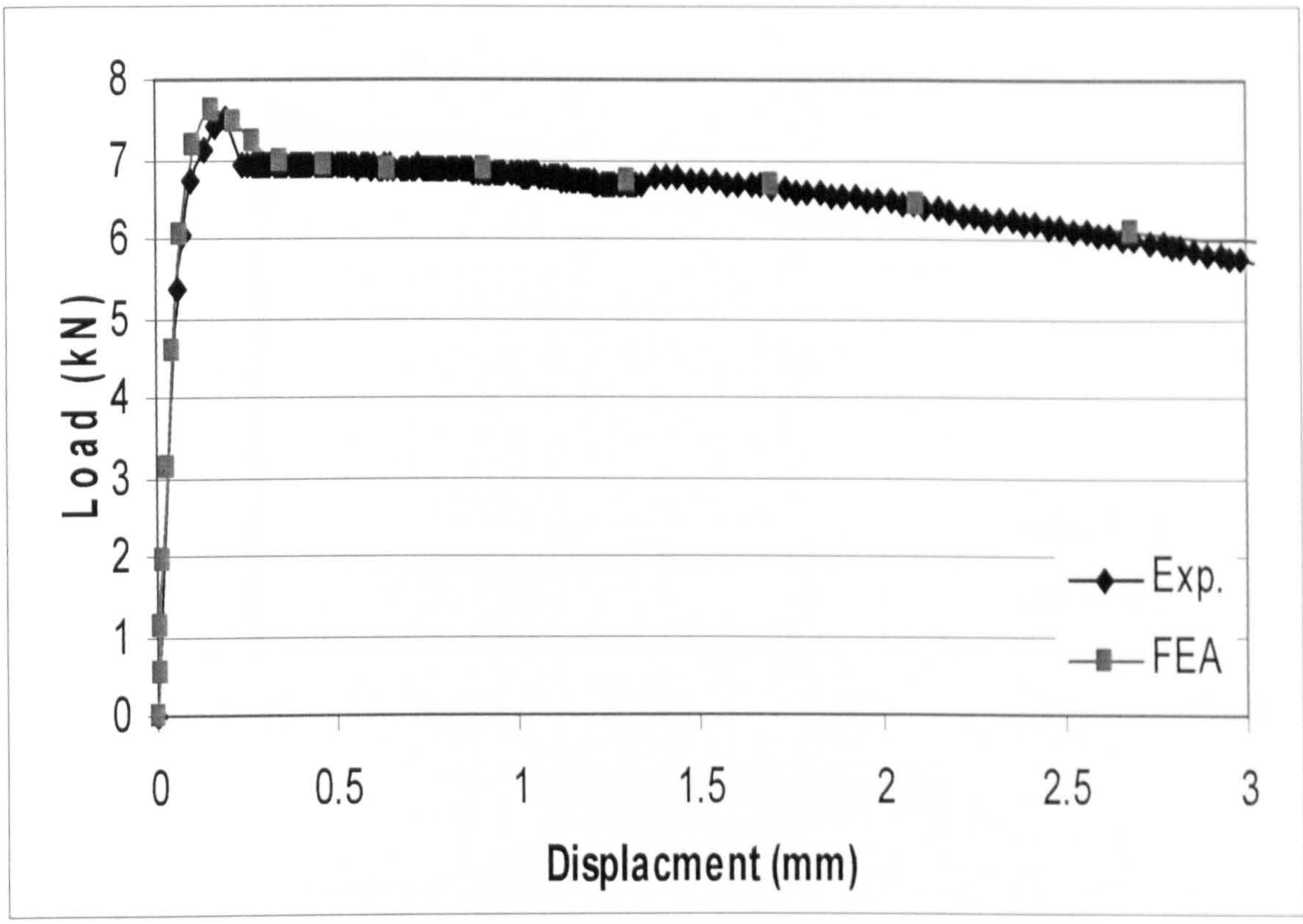

Figure A.5: Experimental and numerical results (beam B5)

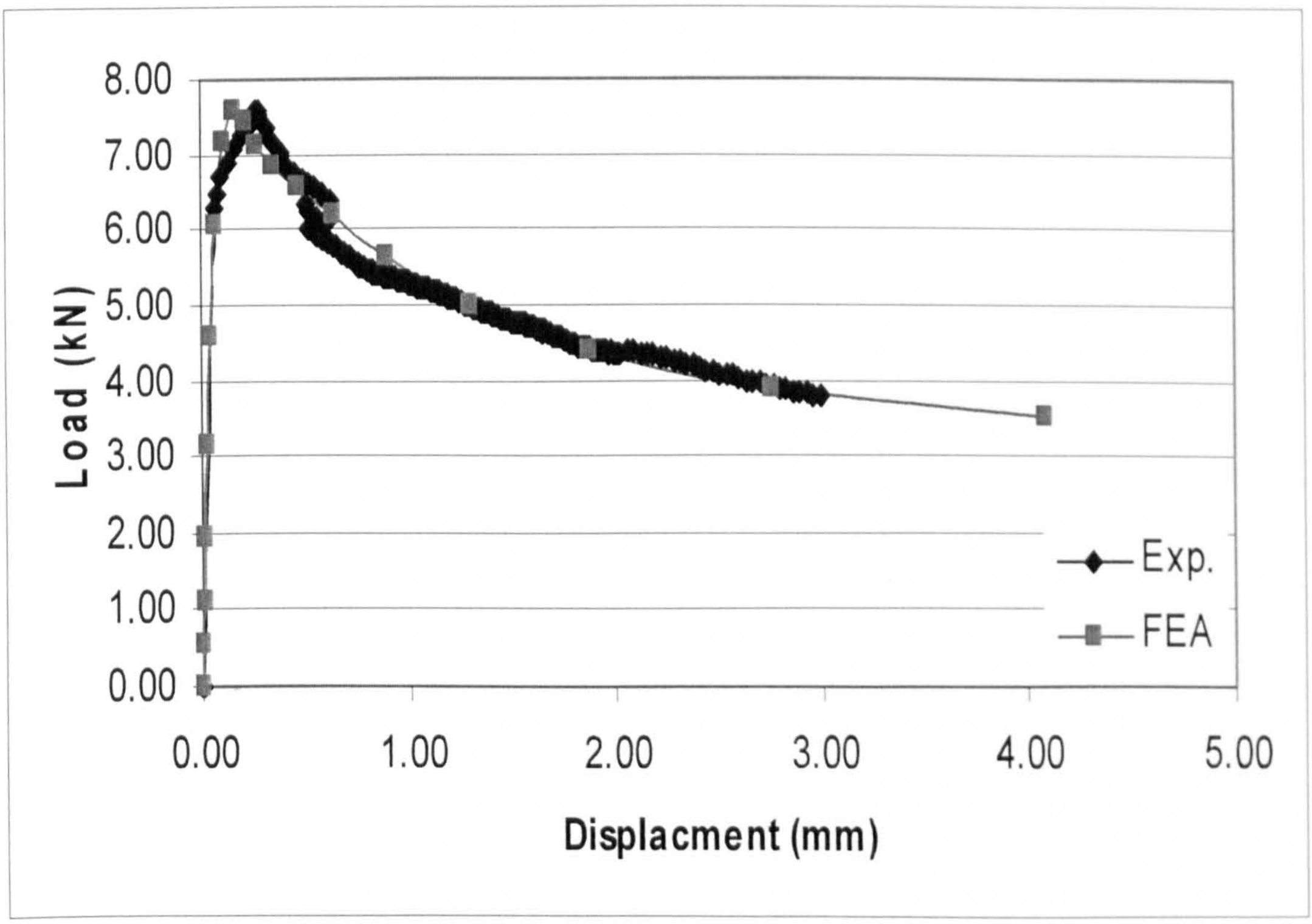

Figure A.6: Experimental and numerical results (beam B6)

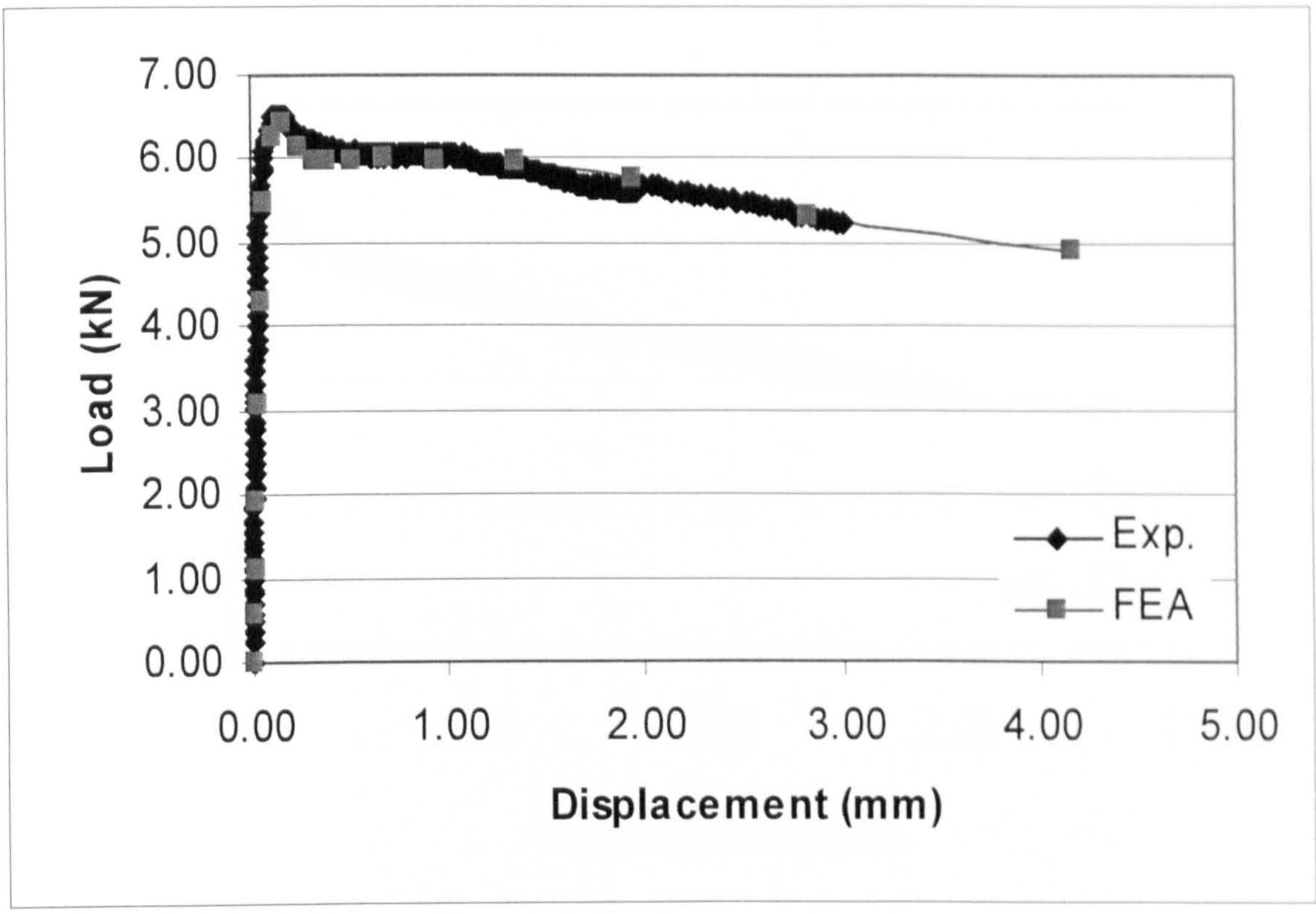

Figure A.7: Experimental and numerical results (beam B7)

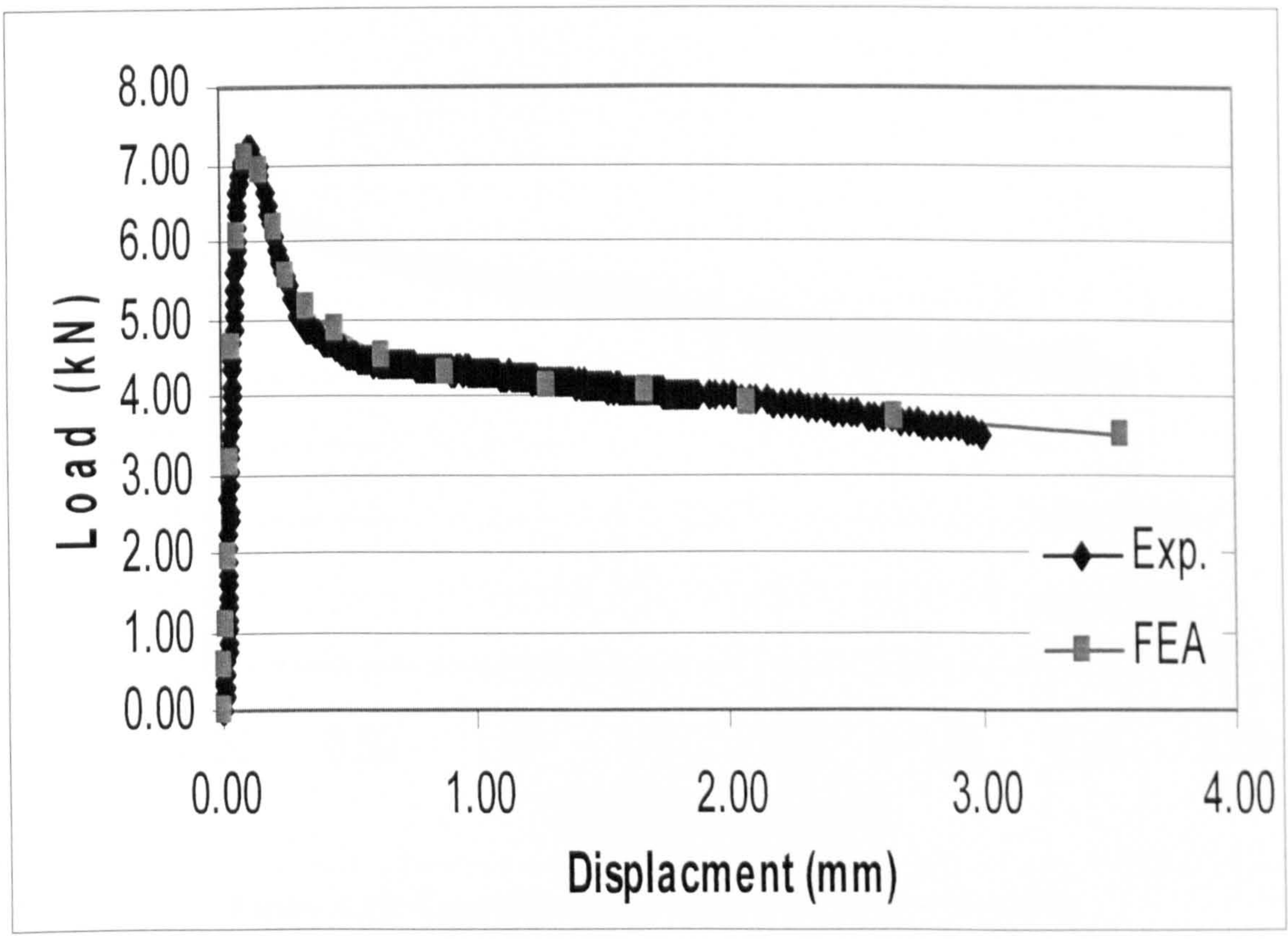

Figure A.8: Experimental and numerical results (beam B8)

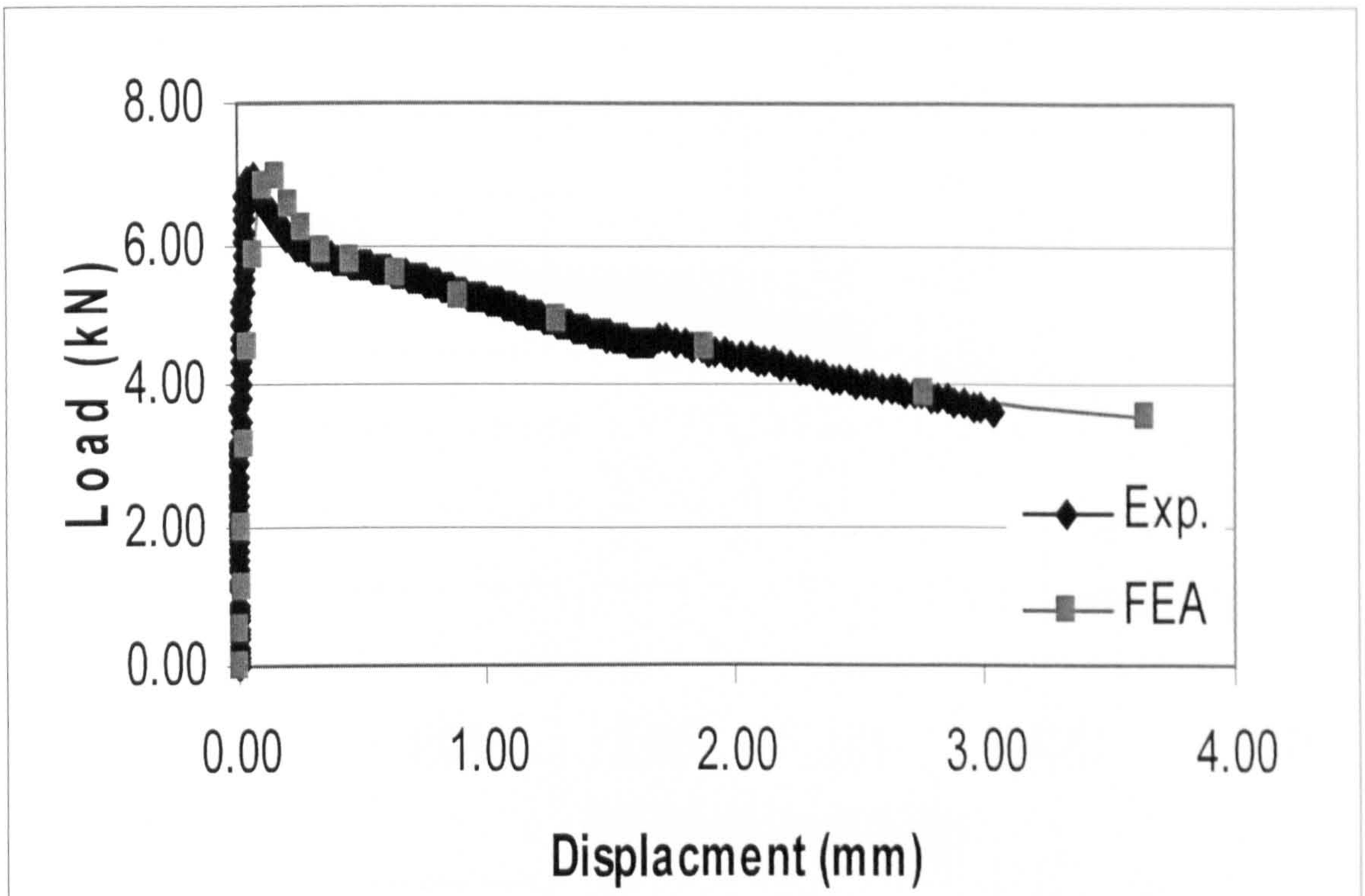

Figure A.9: Experimental and numerical results (beam B9)

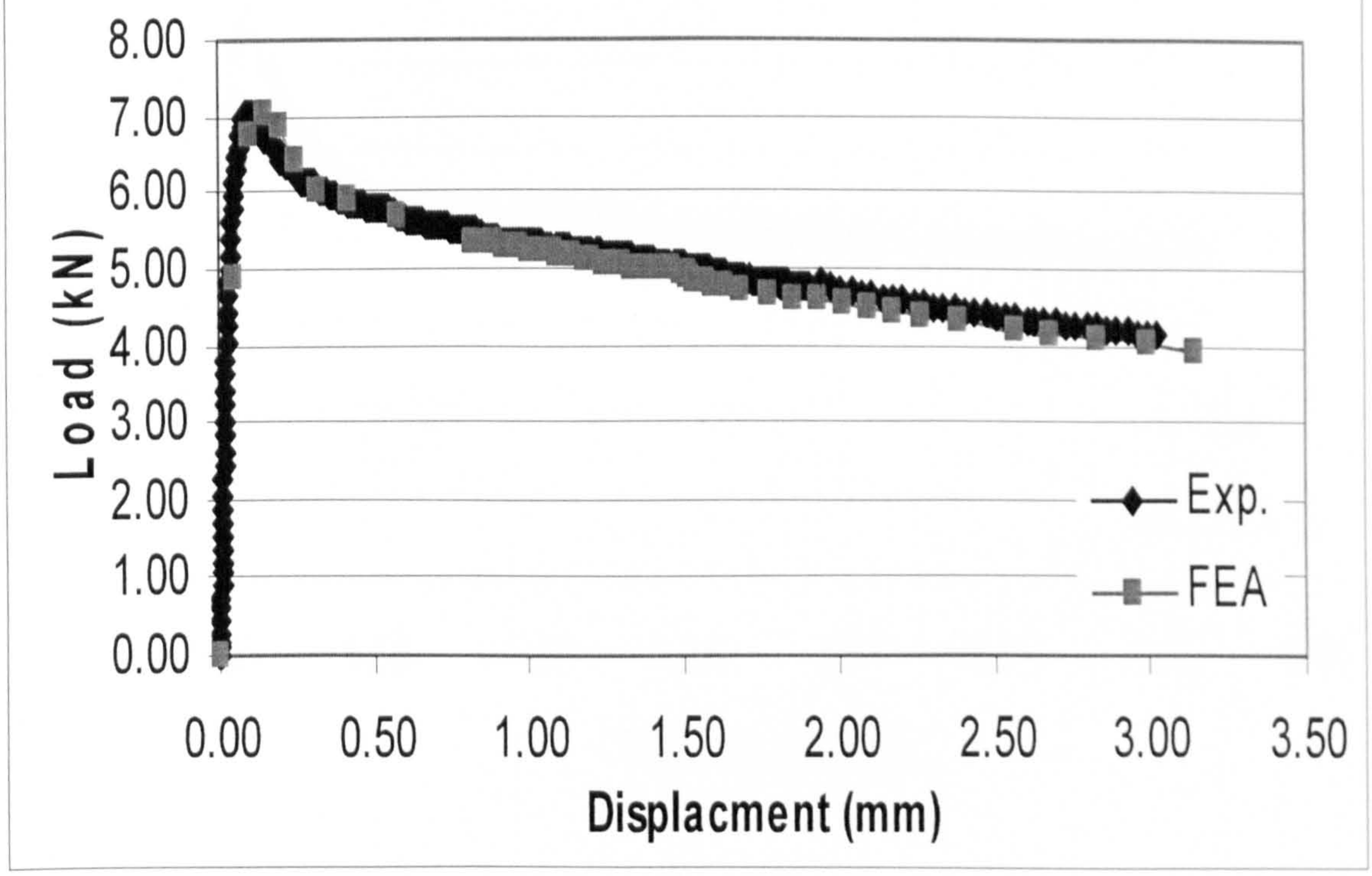

Figure A.10: Experimental and numerical results (beam B10)

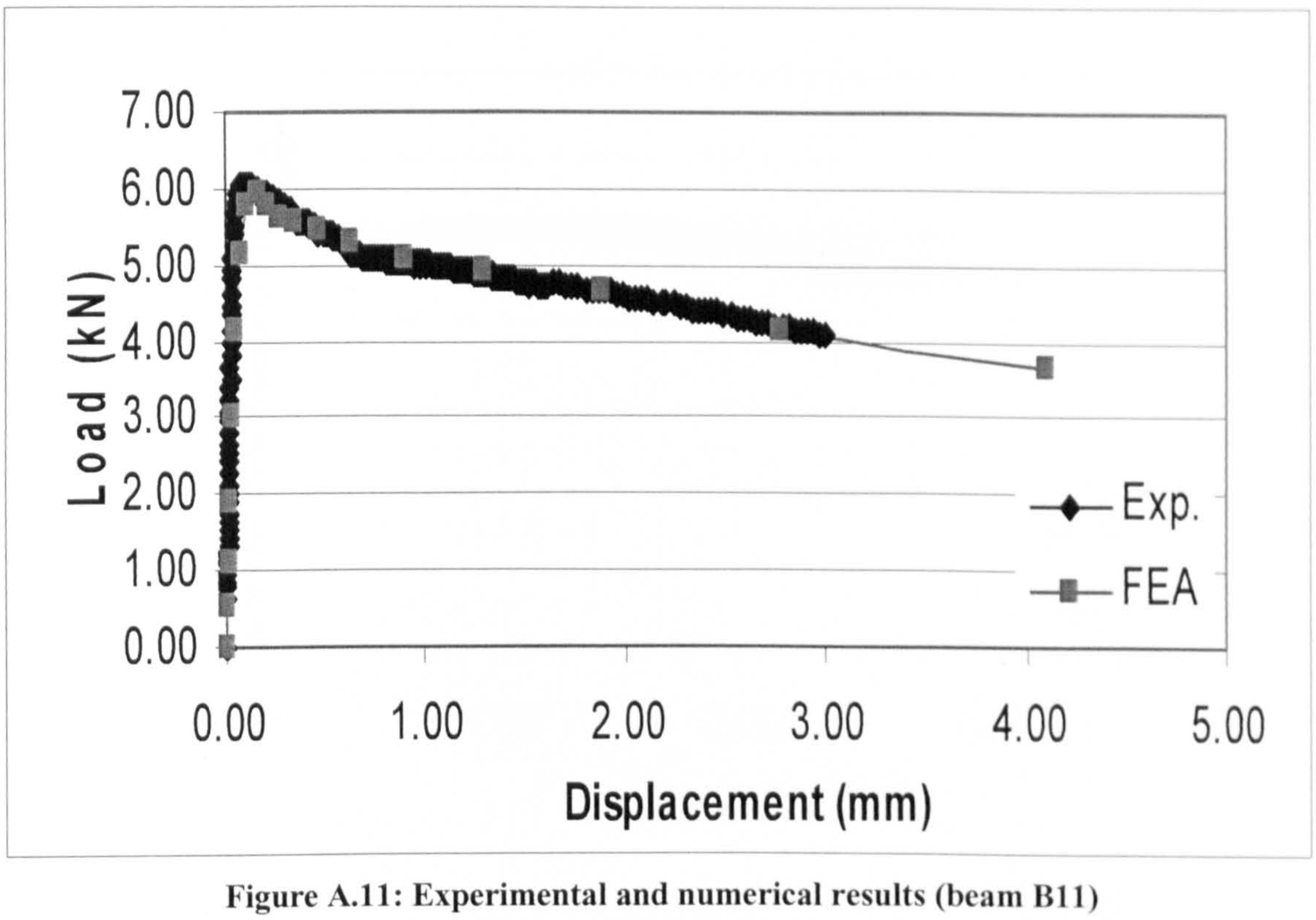

Figure A.11: Experimental and numerical results (beam B11)

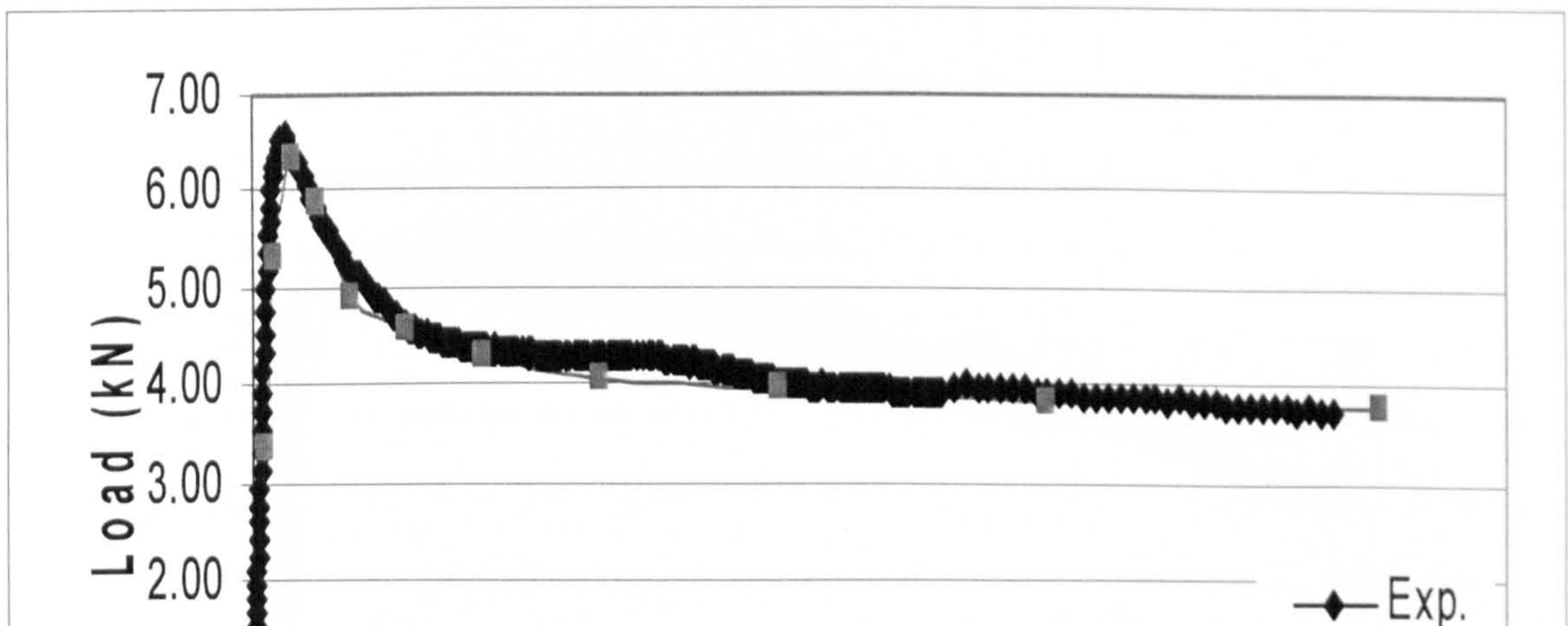

Figure A.12: Experimental and numerical results (beam B12)

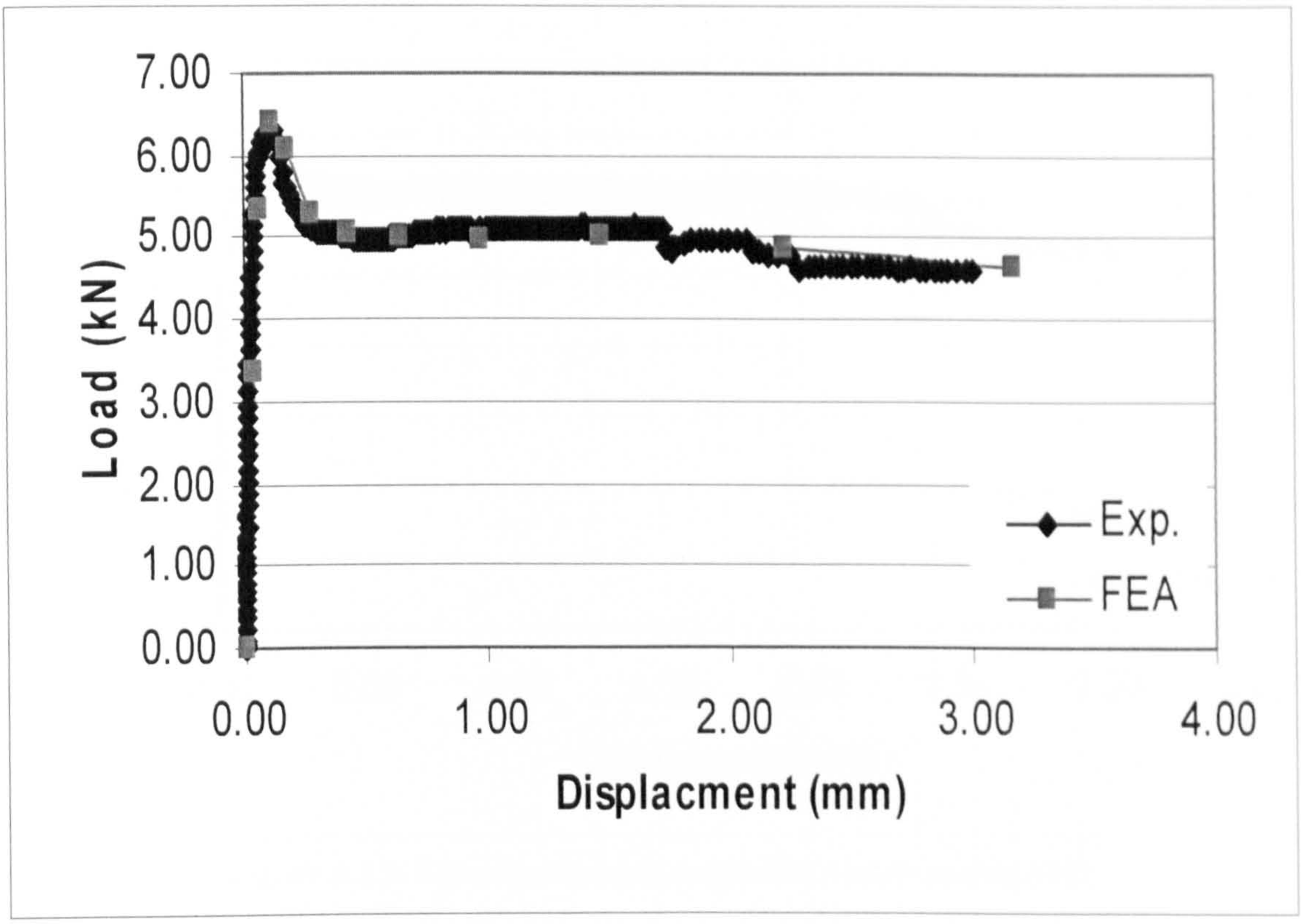

Figure A.13: Experimental and numerical results (beam B13)

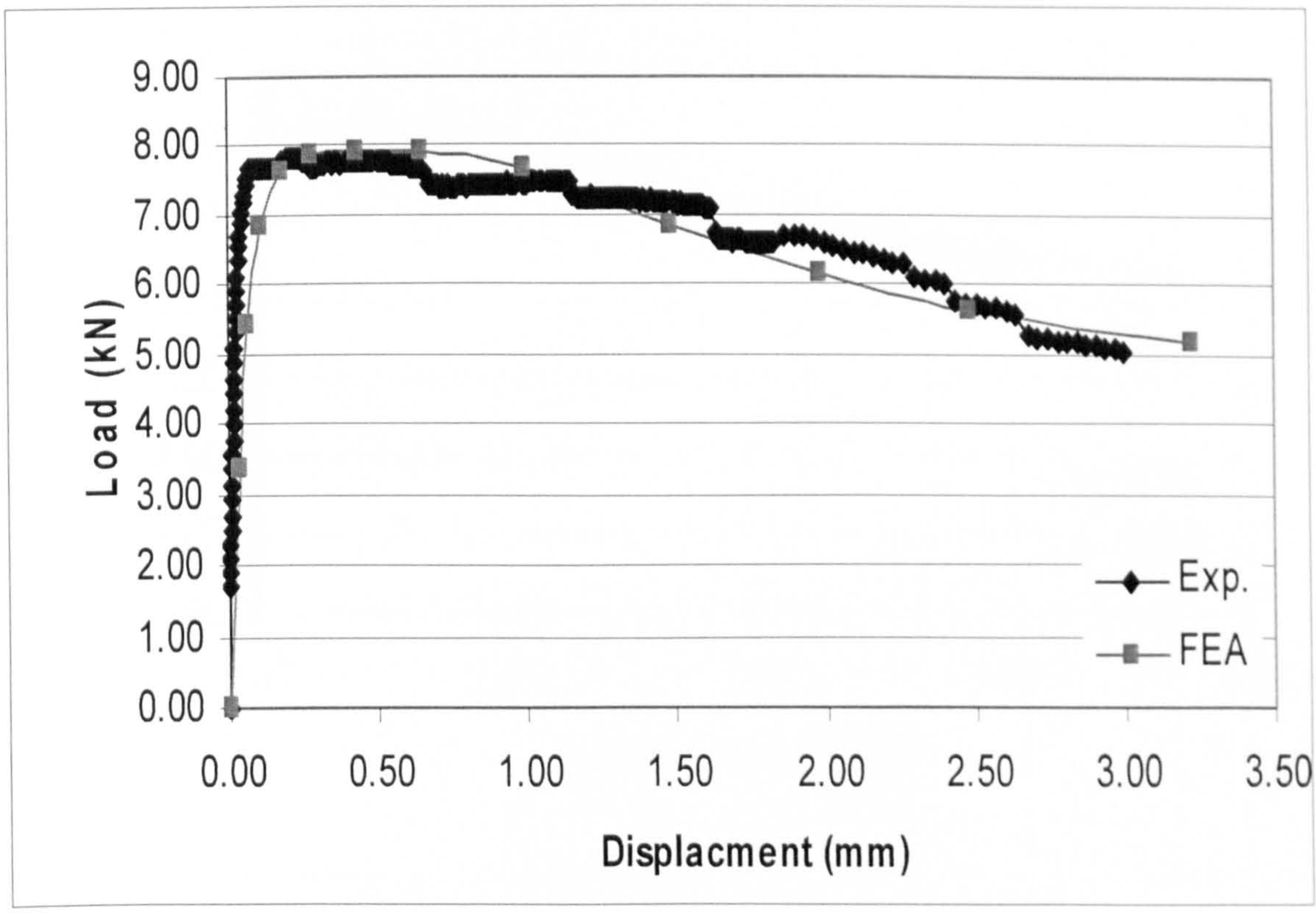

Figure A.14: Experimental and numerical results (beam B14)

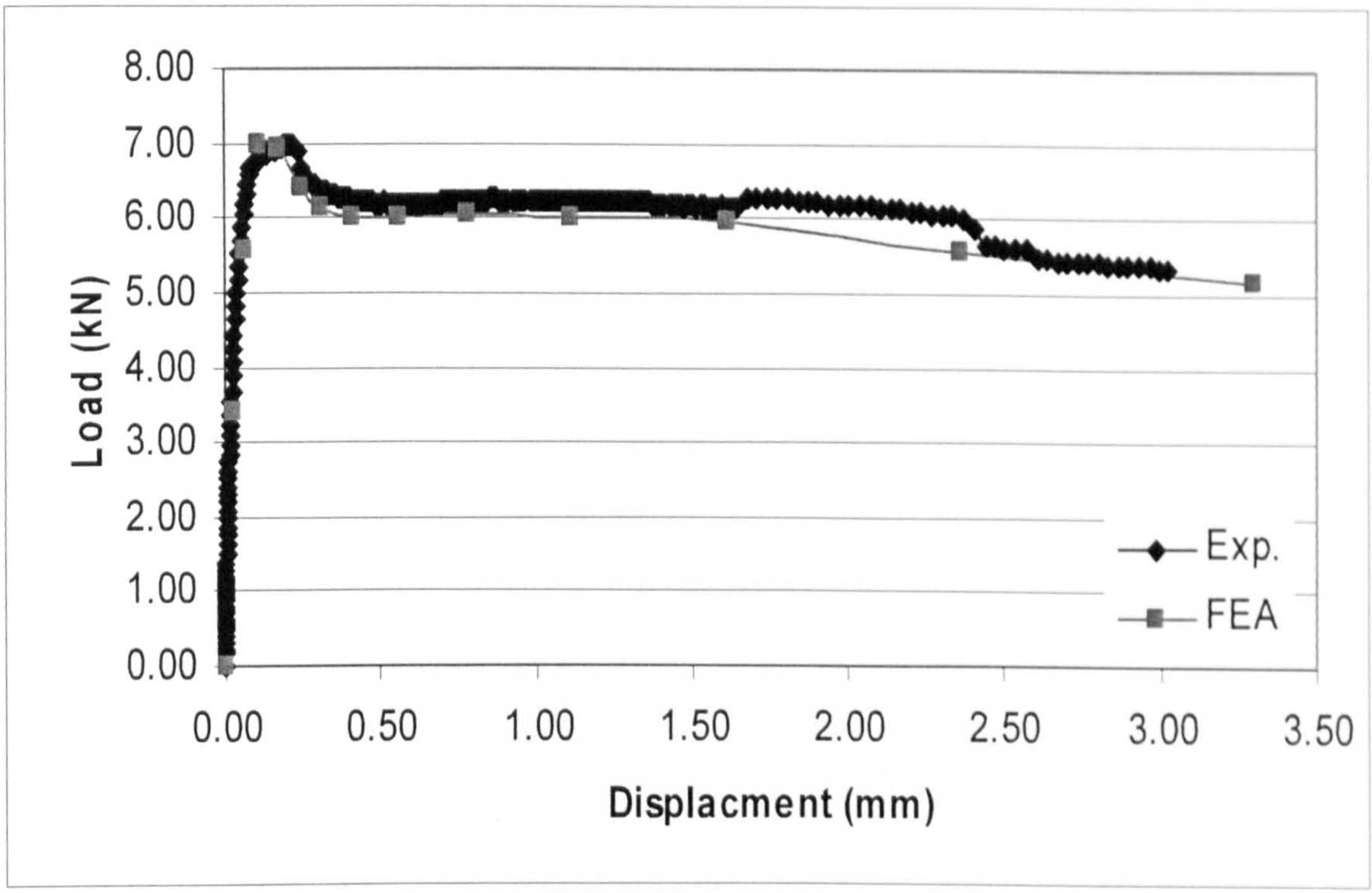

Figure A.15: Experimental and numerical results (beam B15)

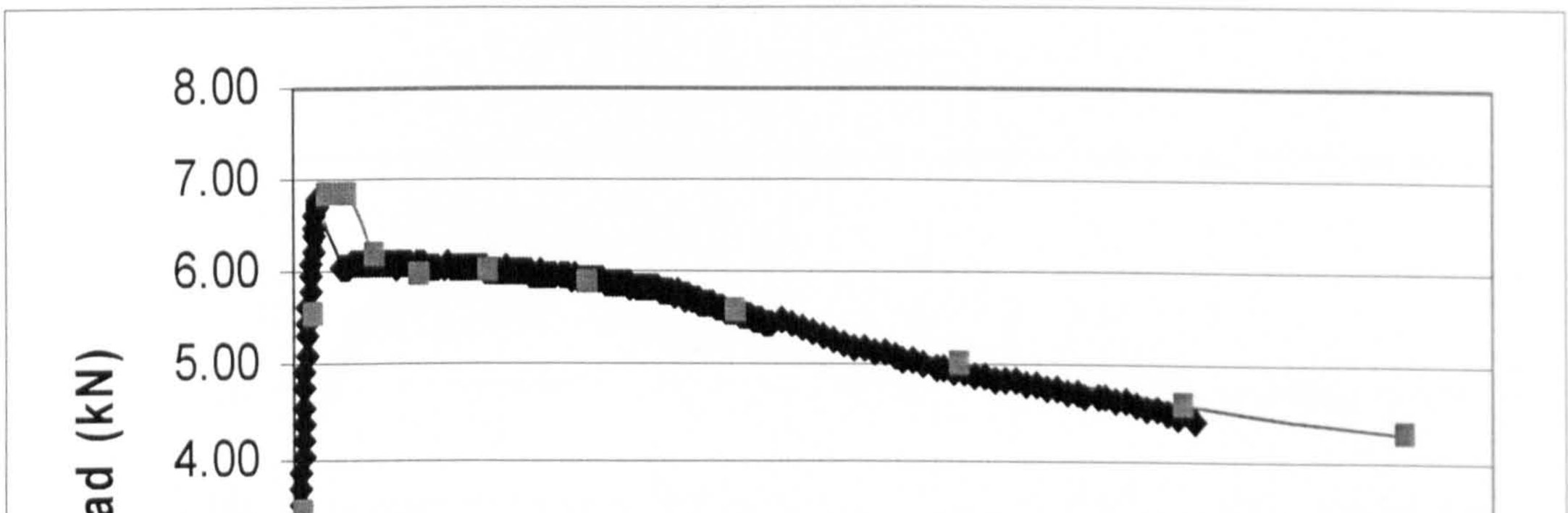

Figure A.16: Experimental and numerical results (beam B16)

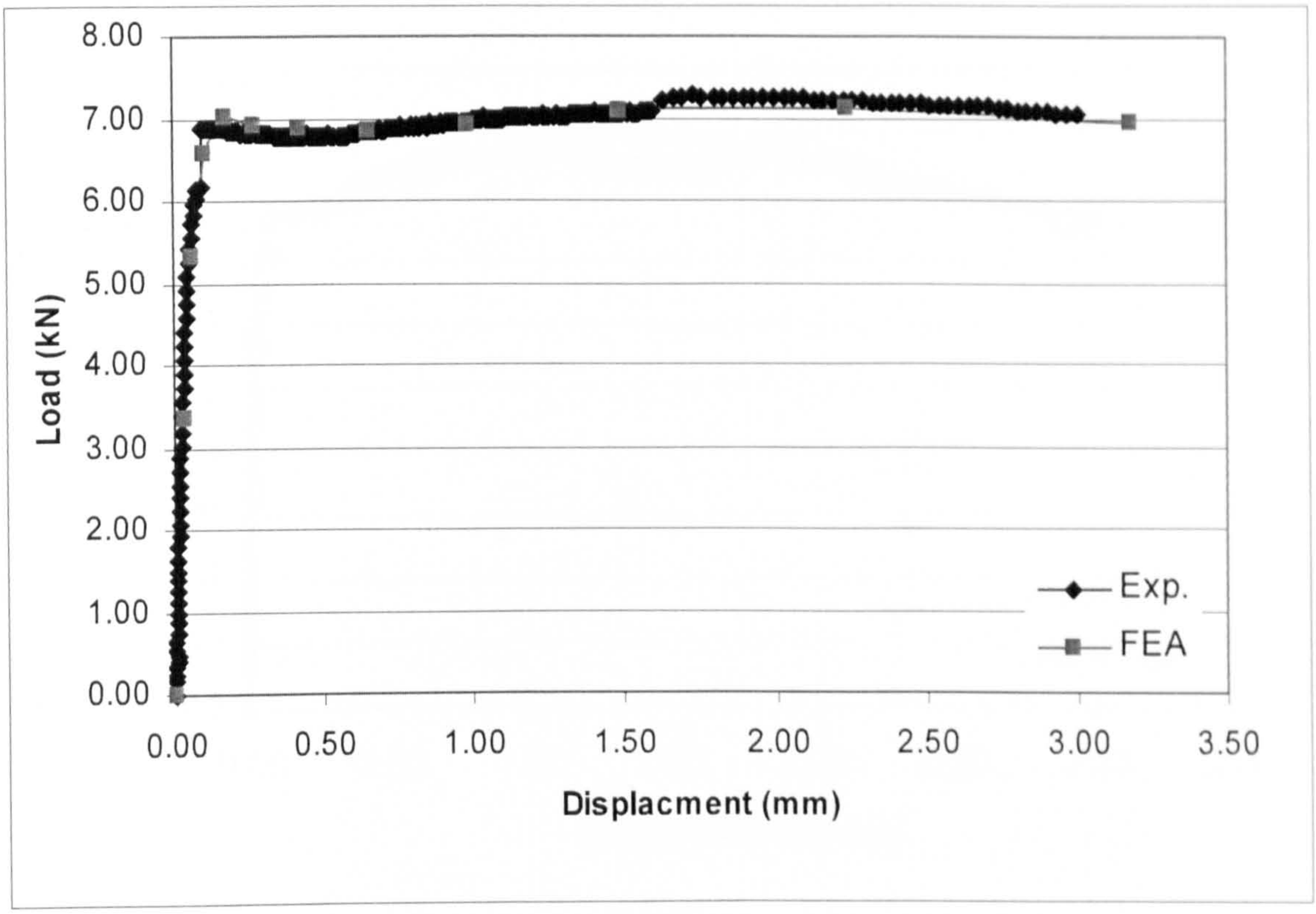

Figure A.17: Experimental and numerical results (beam B17)

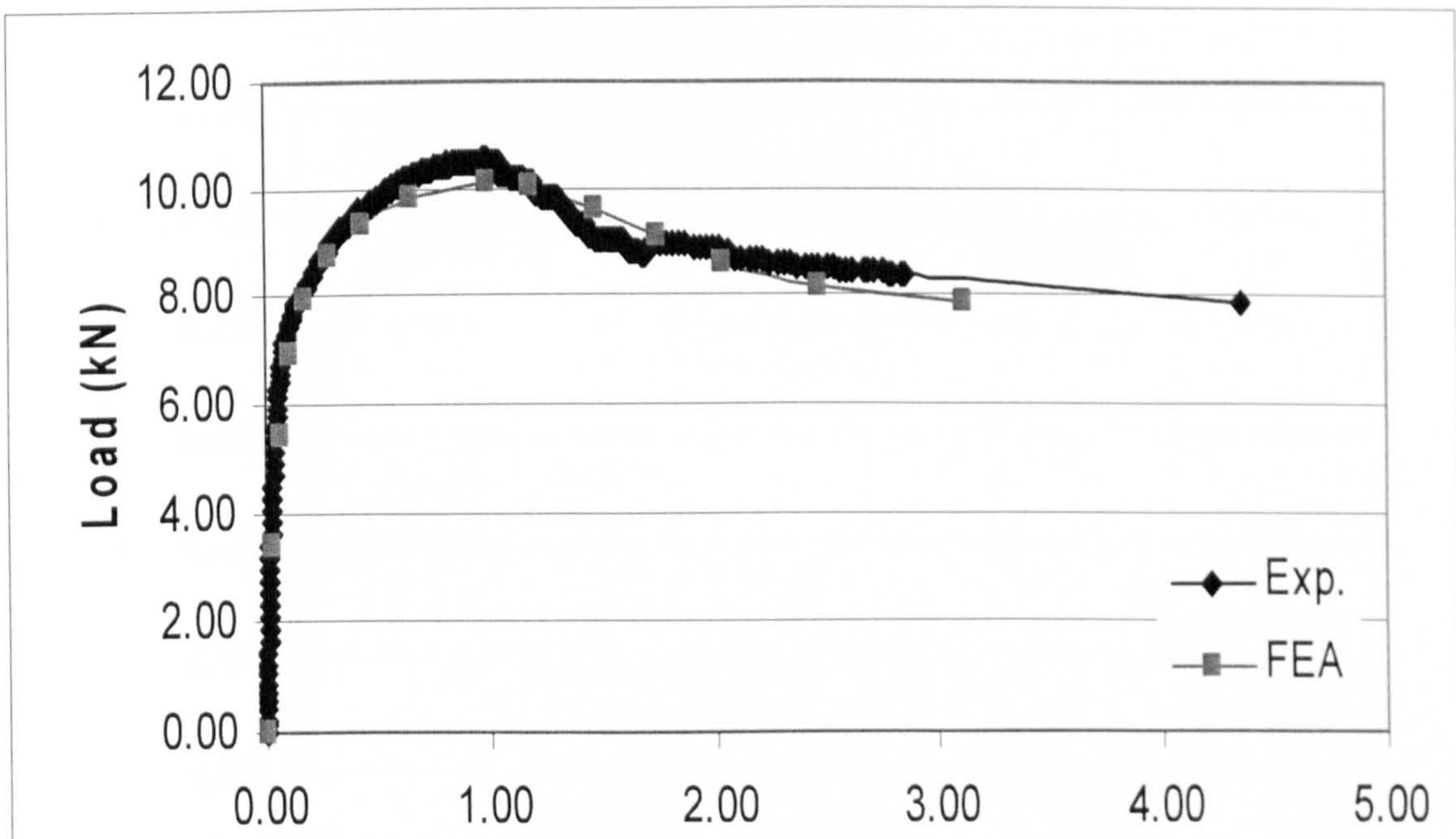

Figure A.18: Experimental and numerical results (beam B18)

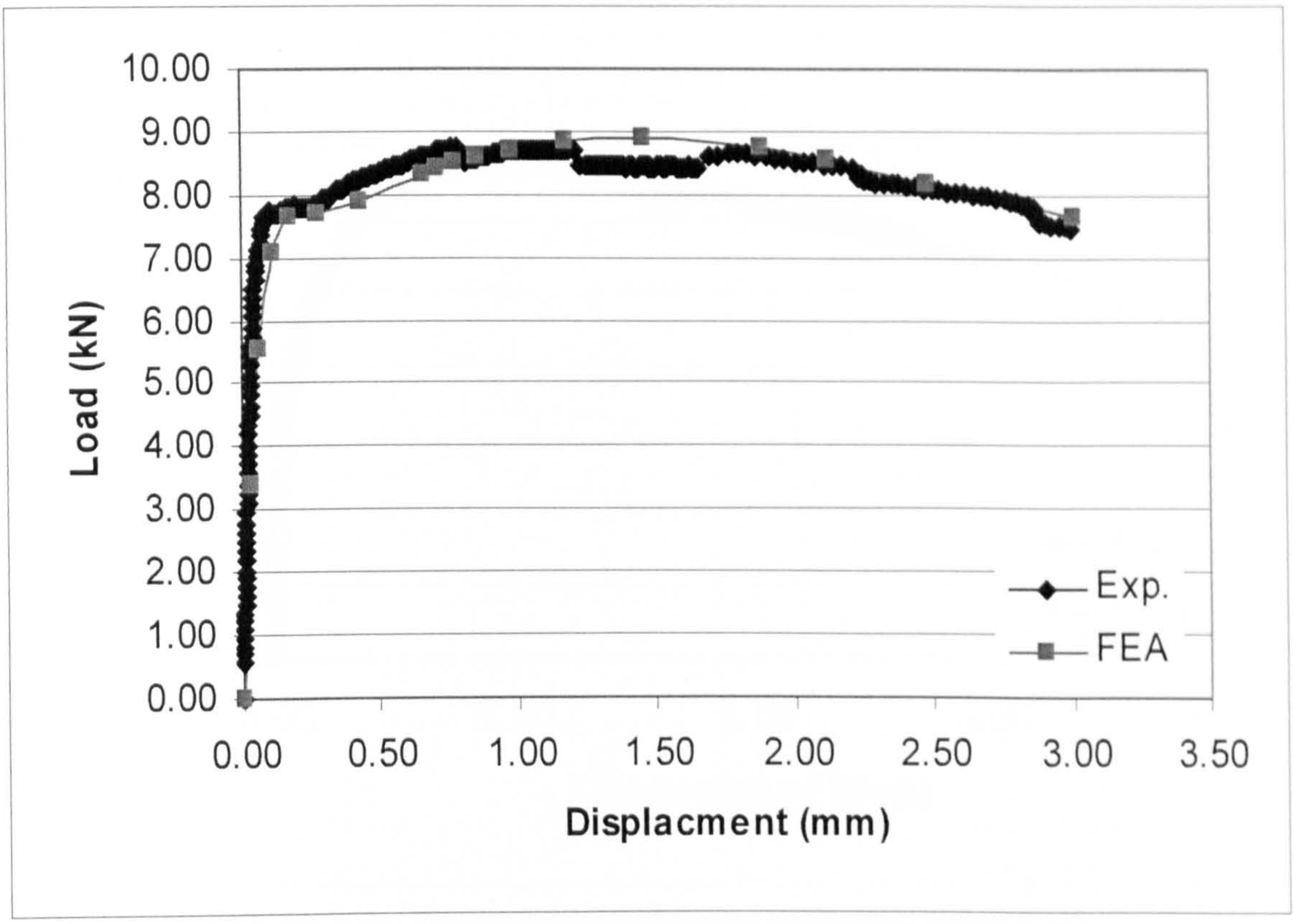

Figure A.19: Experimental and numerical results (beam B19)

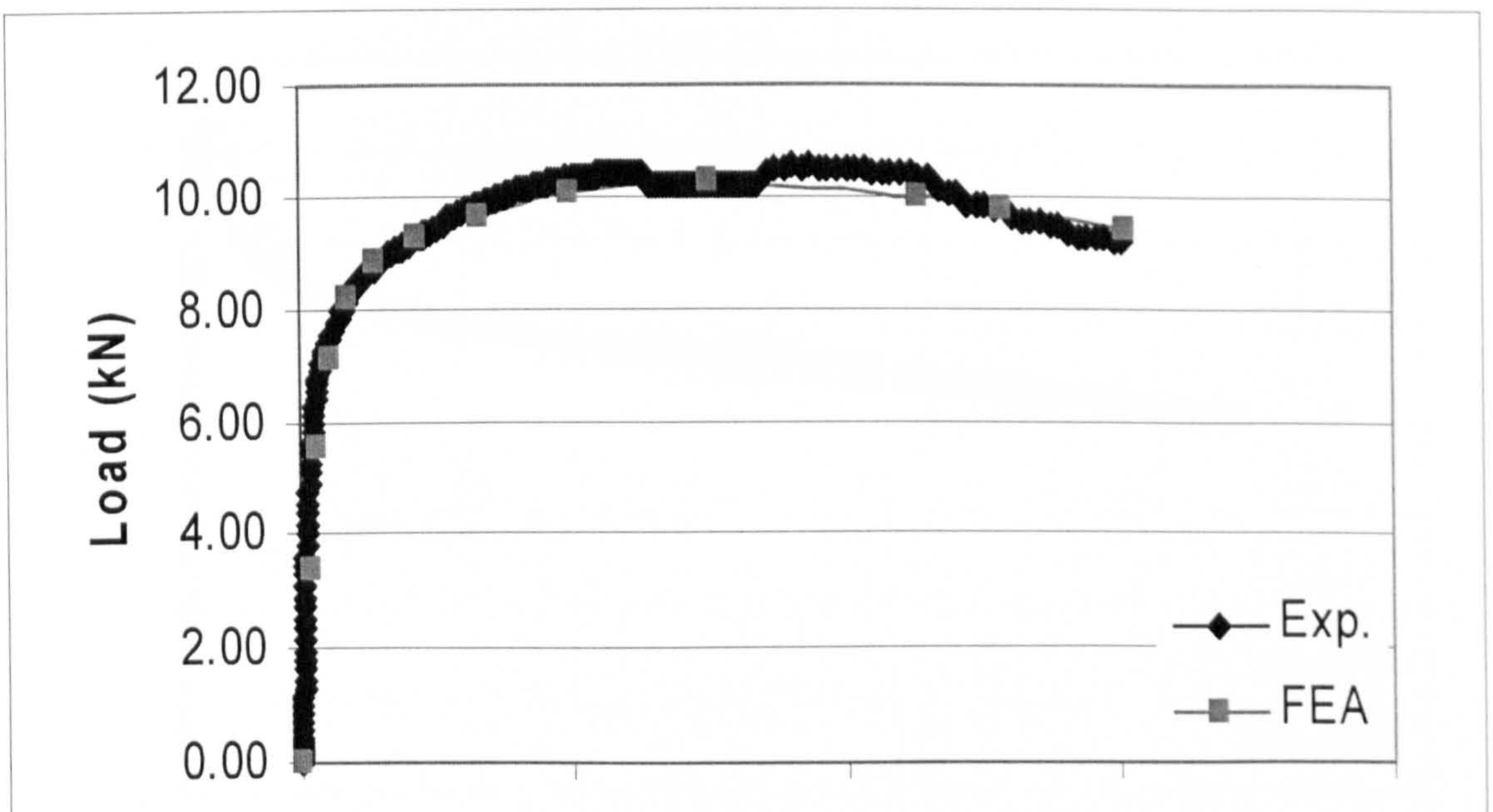

Figure A.20: Experimental and numerical results (beam B20)

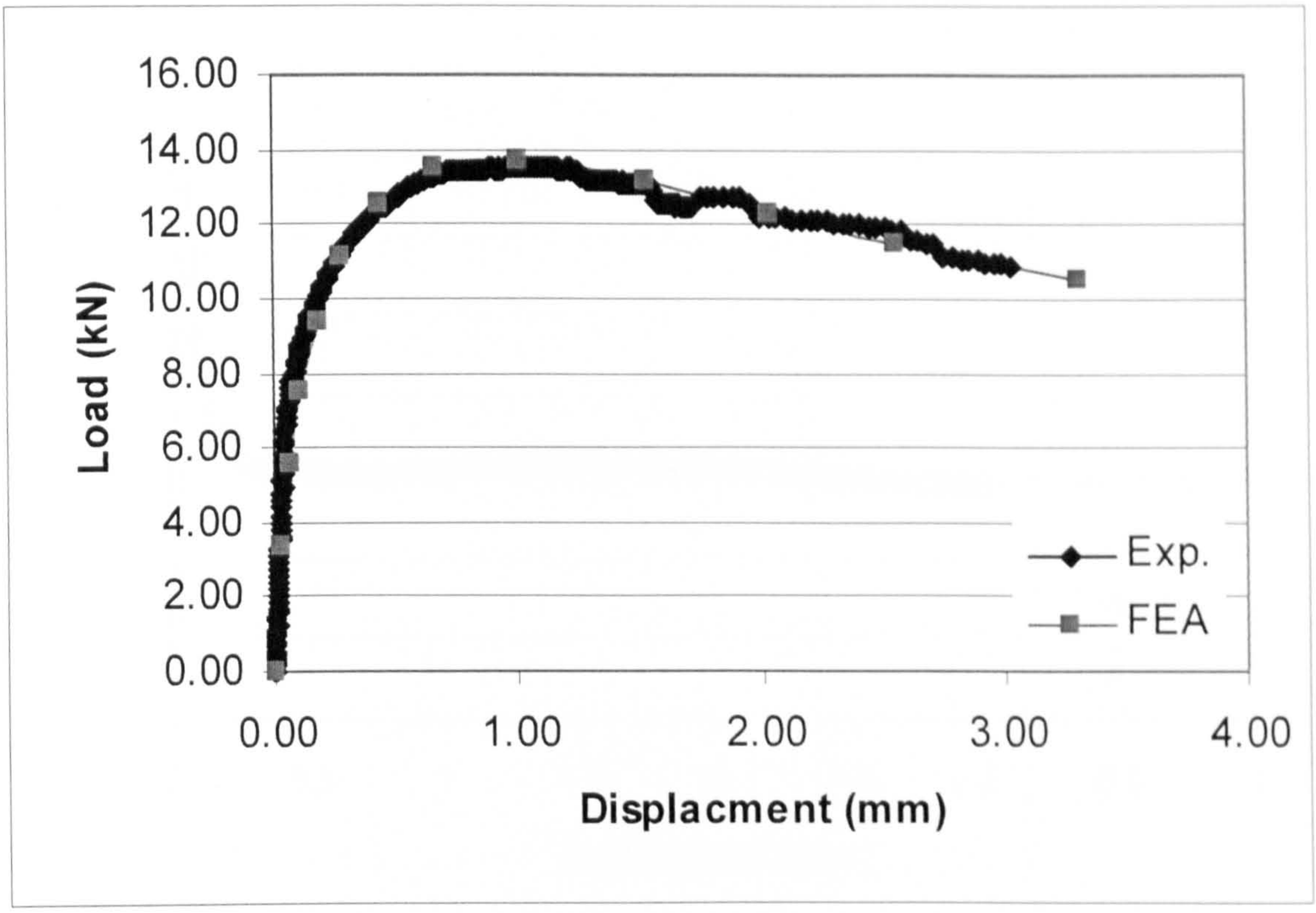

Figure A.21: Experimental and numerical results (beam B21)

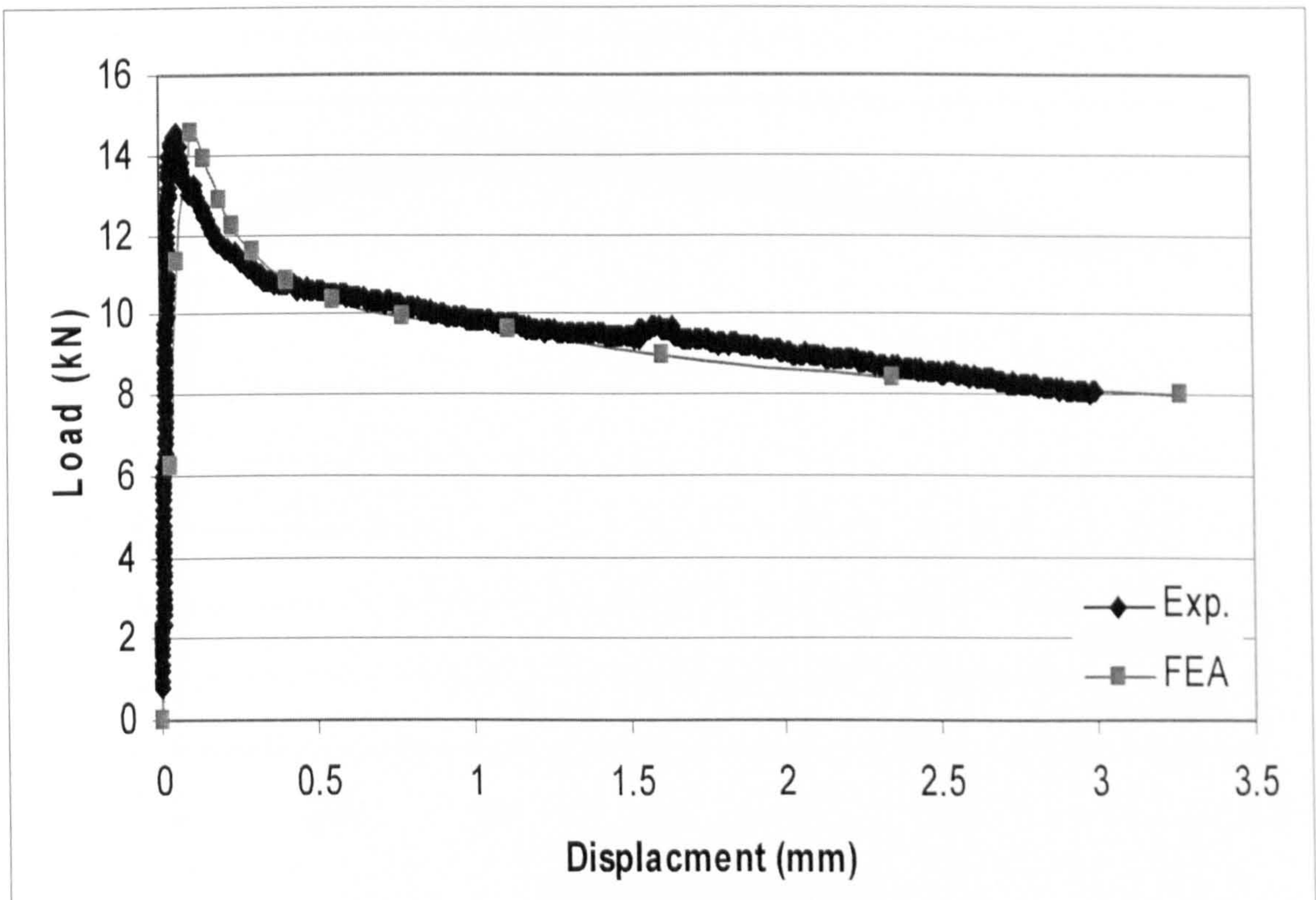

Figure A.22: Experimental and numerical results (beam B22)

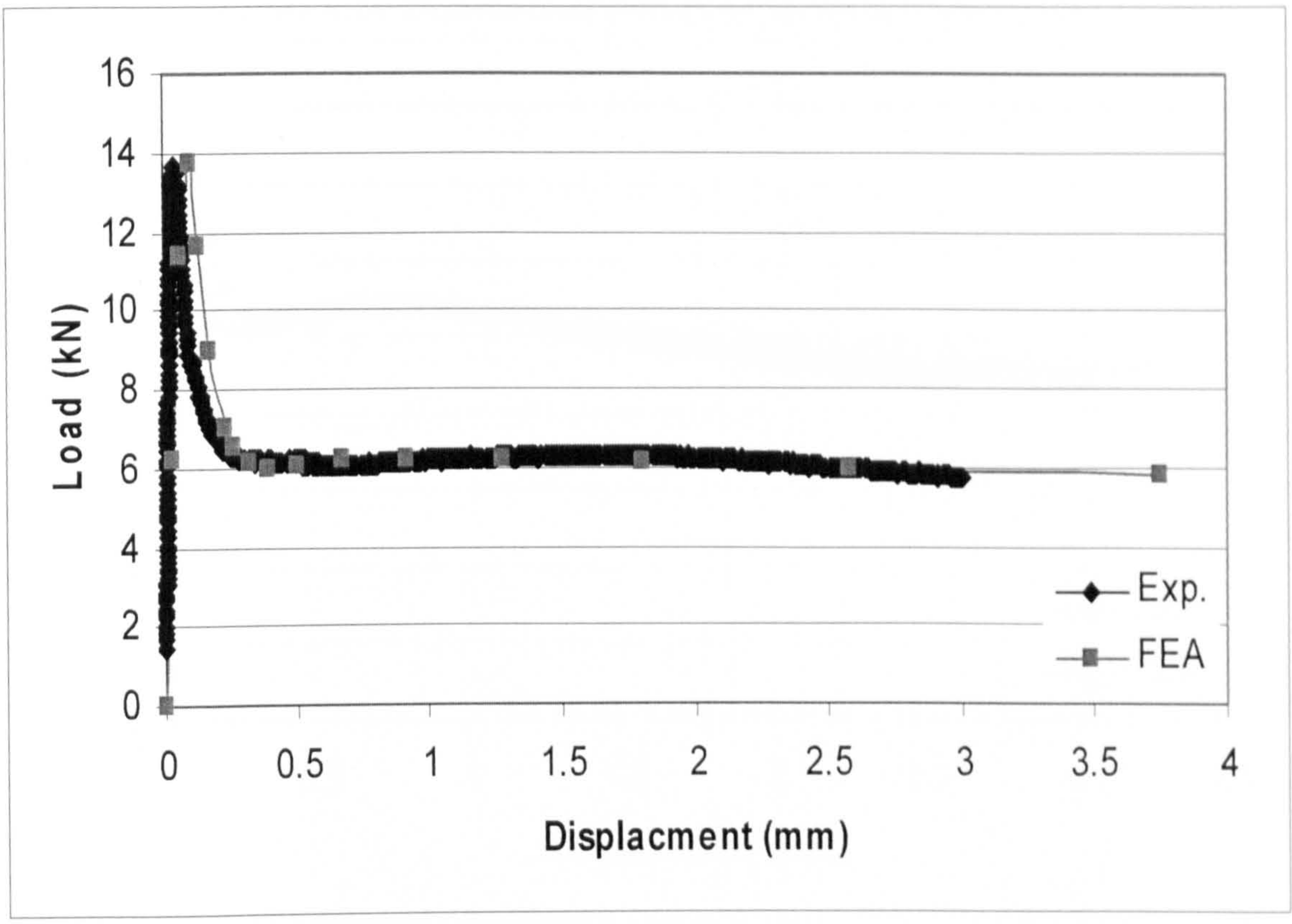

Figure A.23: Experimental and numerical results (beam B23)

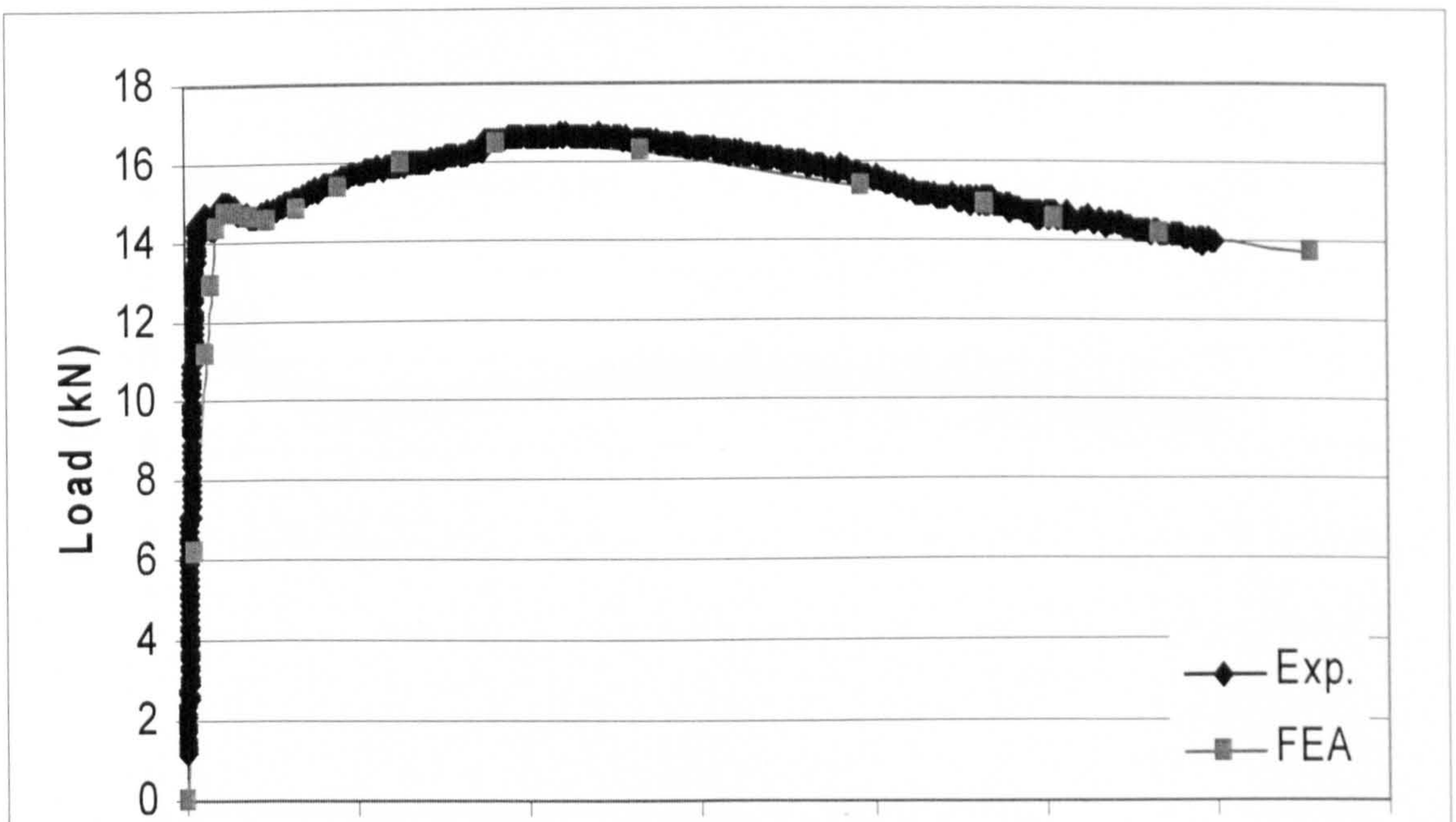

Figure A.24: Experimental and numerical results (beam B24)

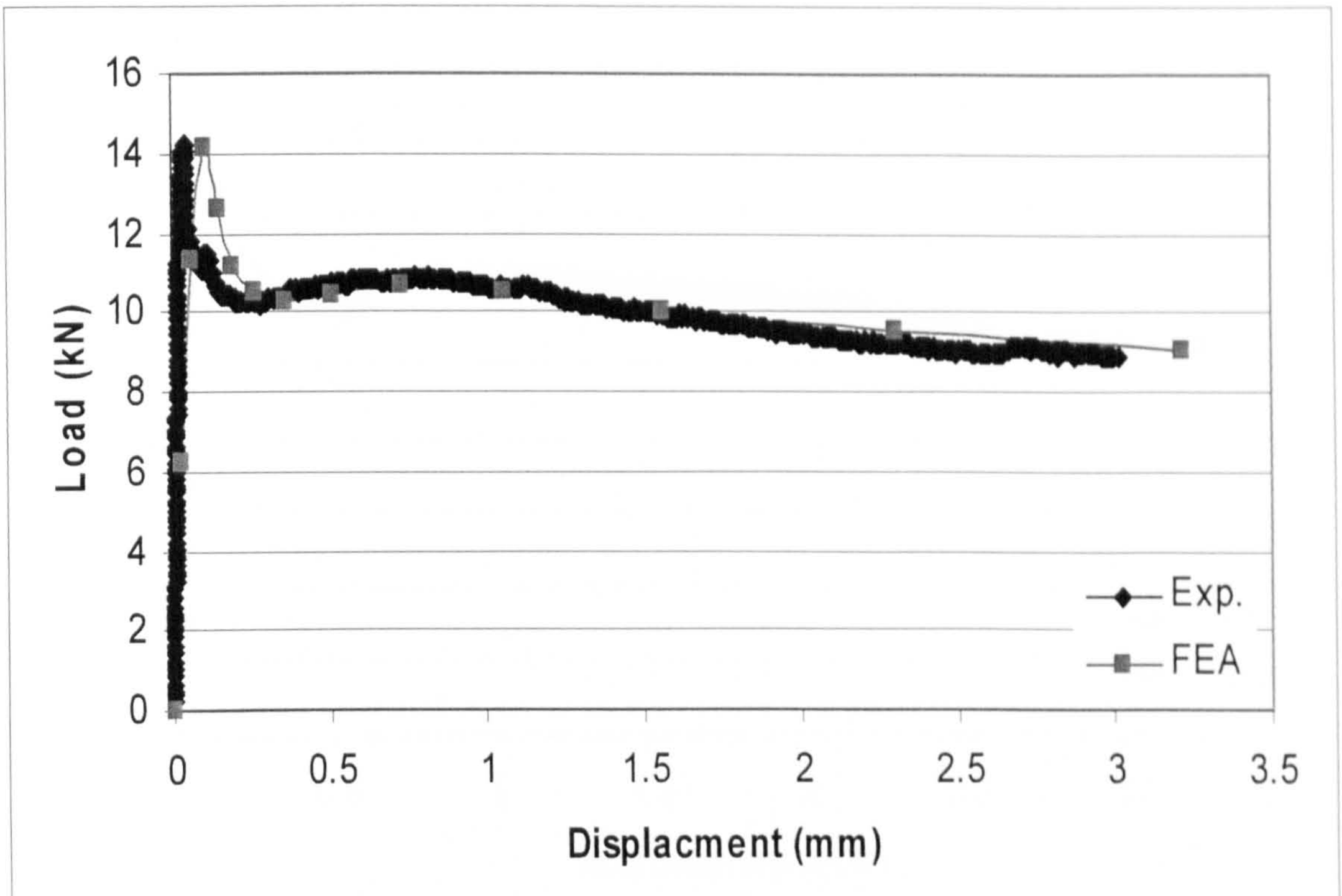

Figure A.25: Experimental and numerical results (beam B25)

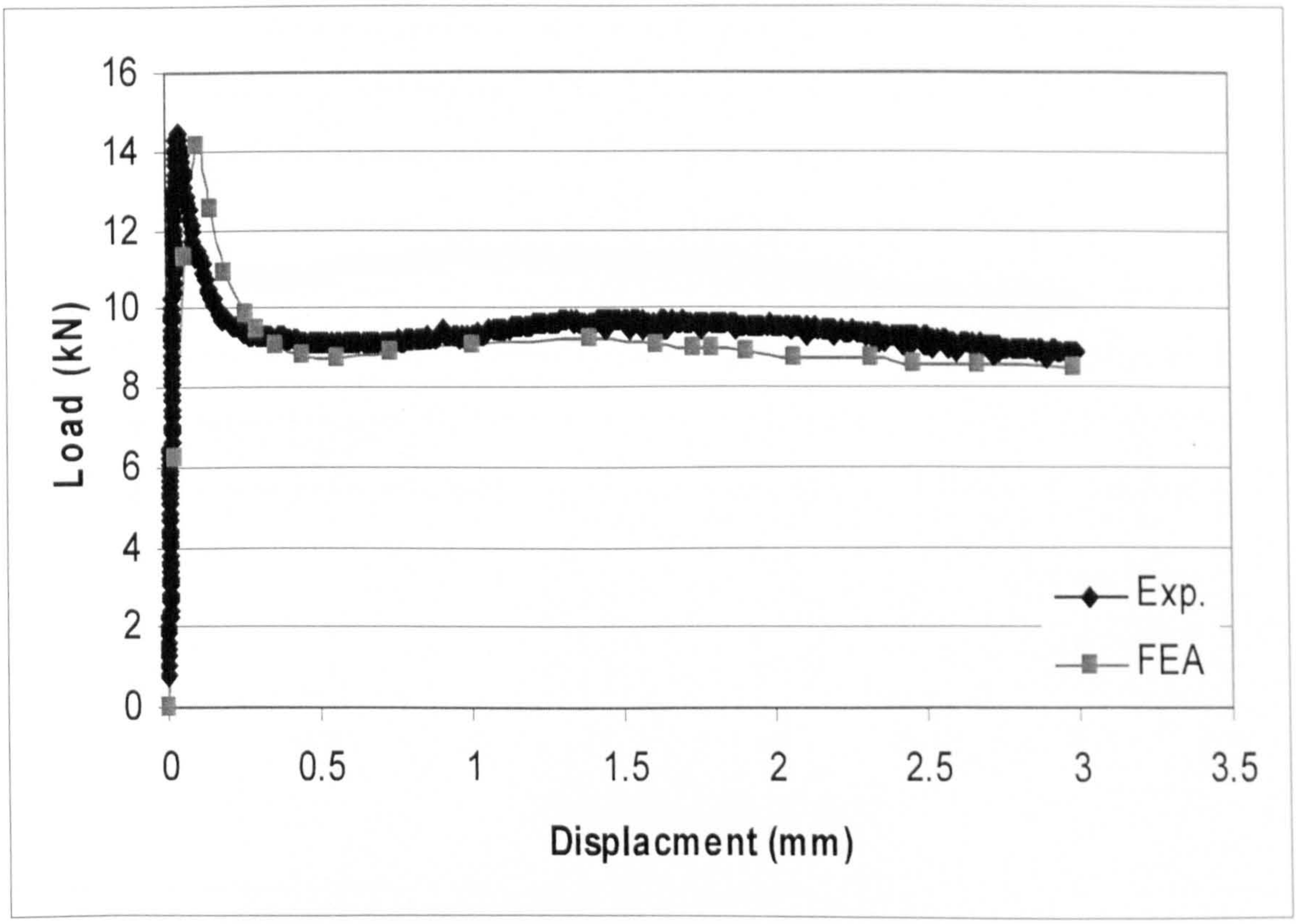

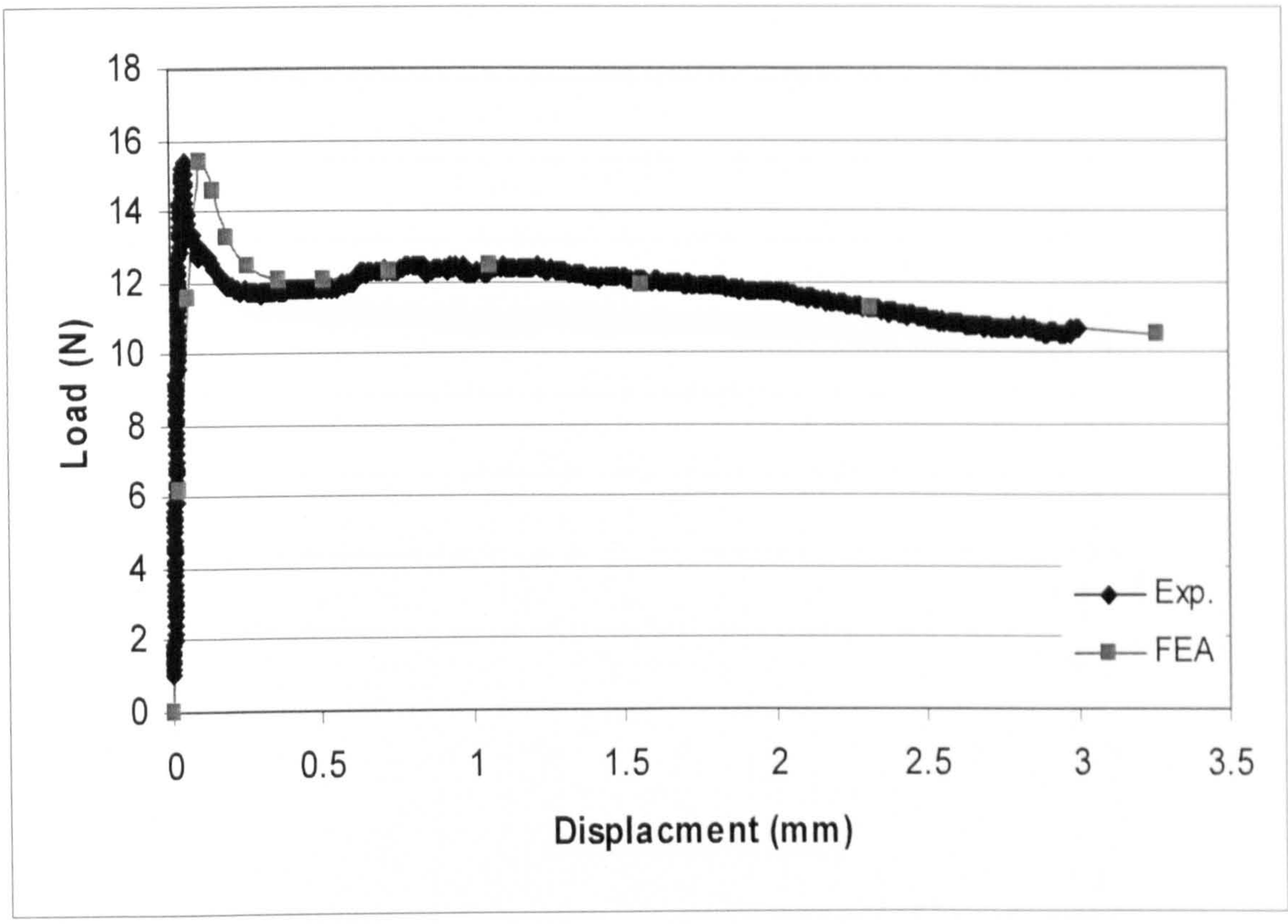

Figure A.26: Experimental and numerical results (beam B26)

Figure A.27: Experimental and numerical results (beam B27)

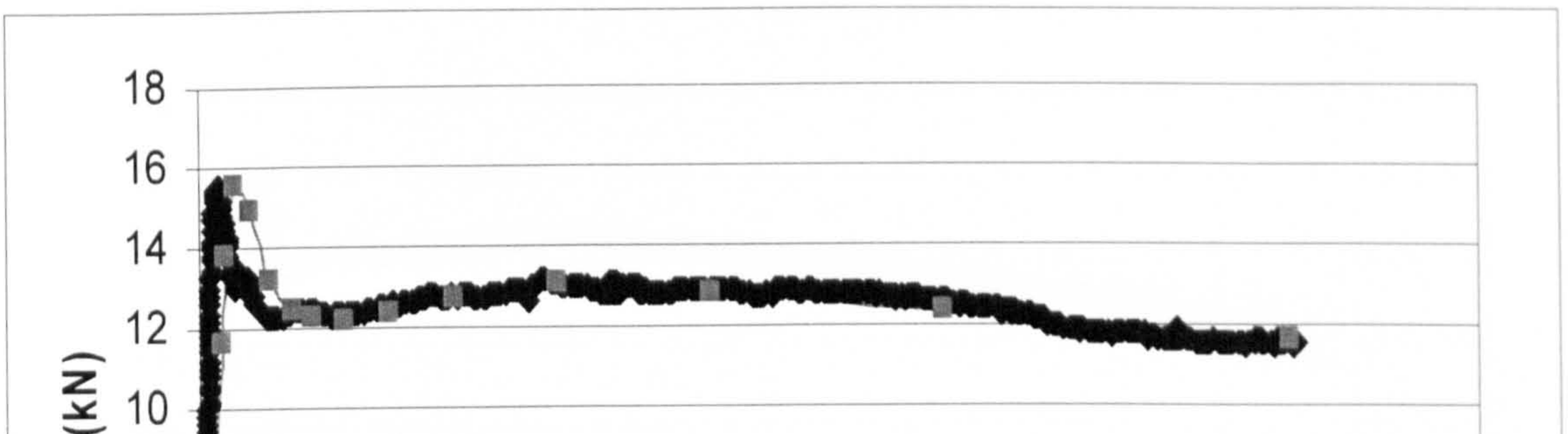

Figure A.28: Experimental and numerical results (beam B28)

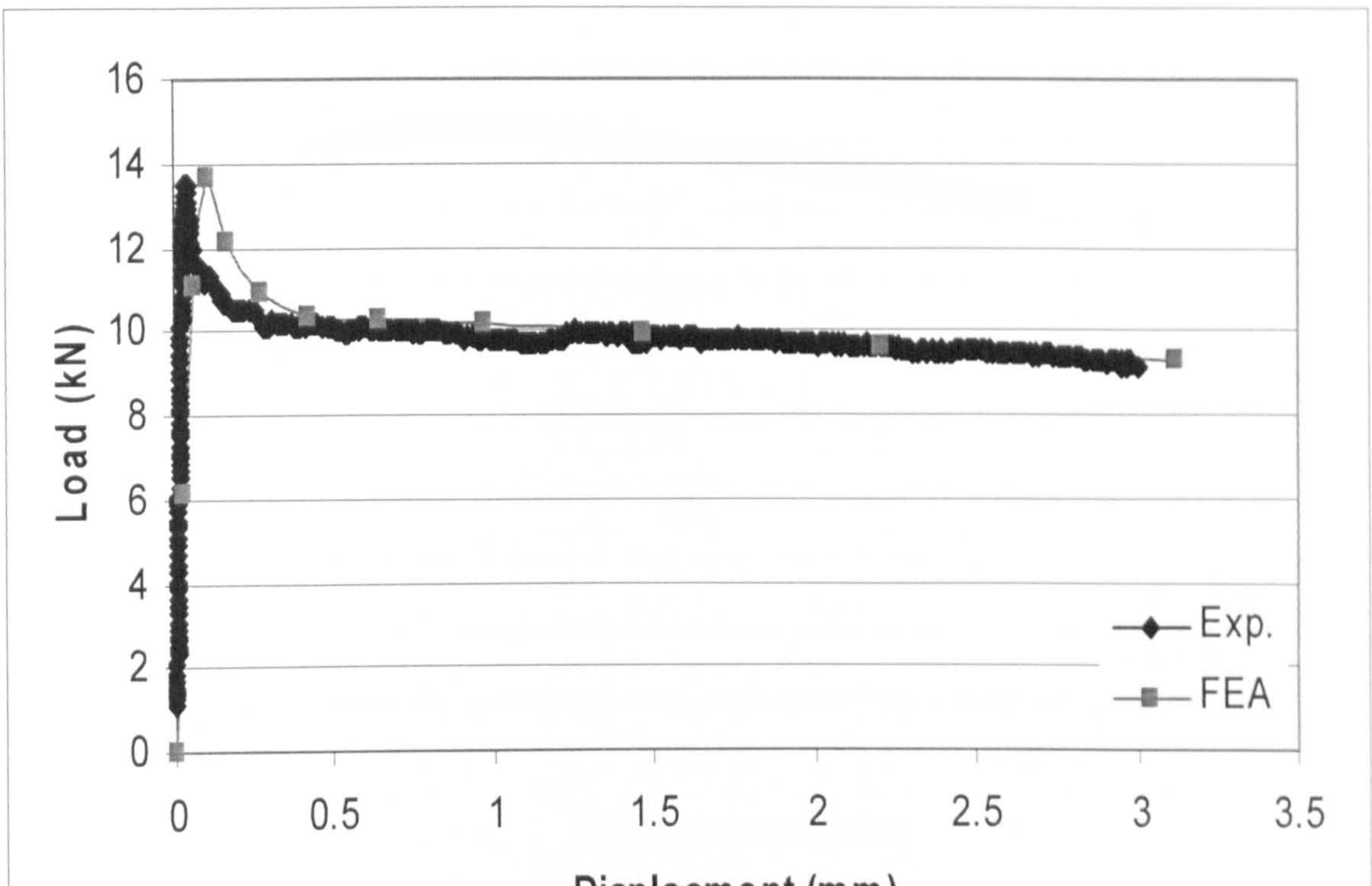

Figure A.29: Experimental and numerical results (beam B29)

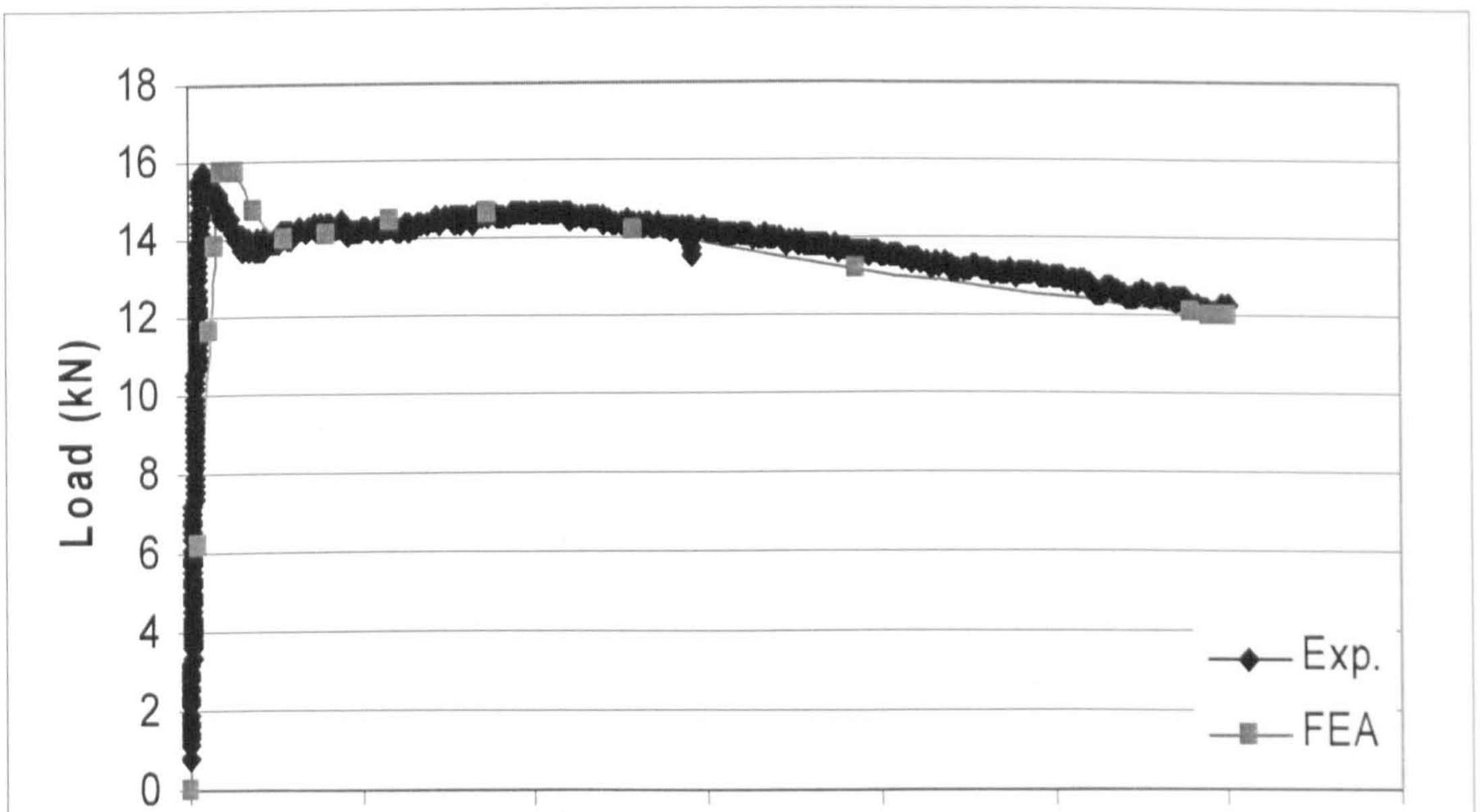

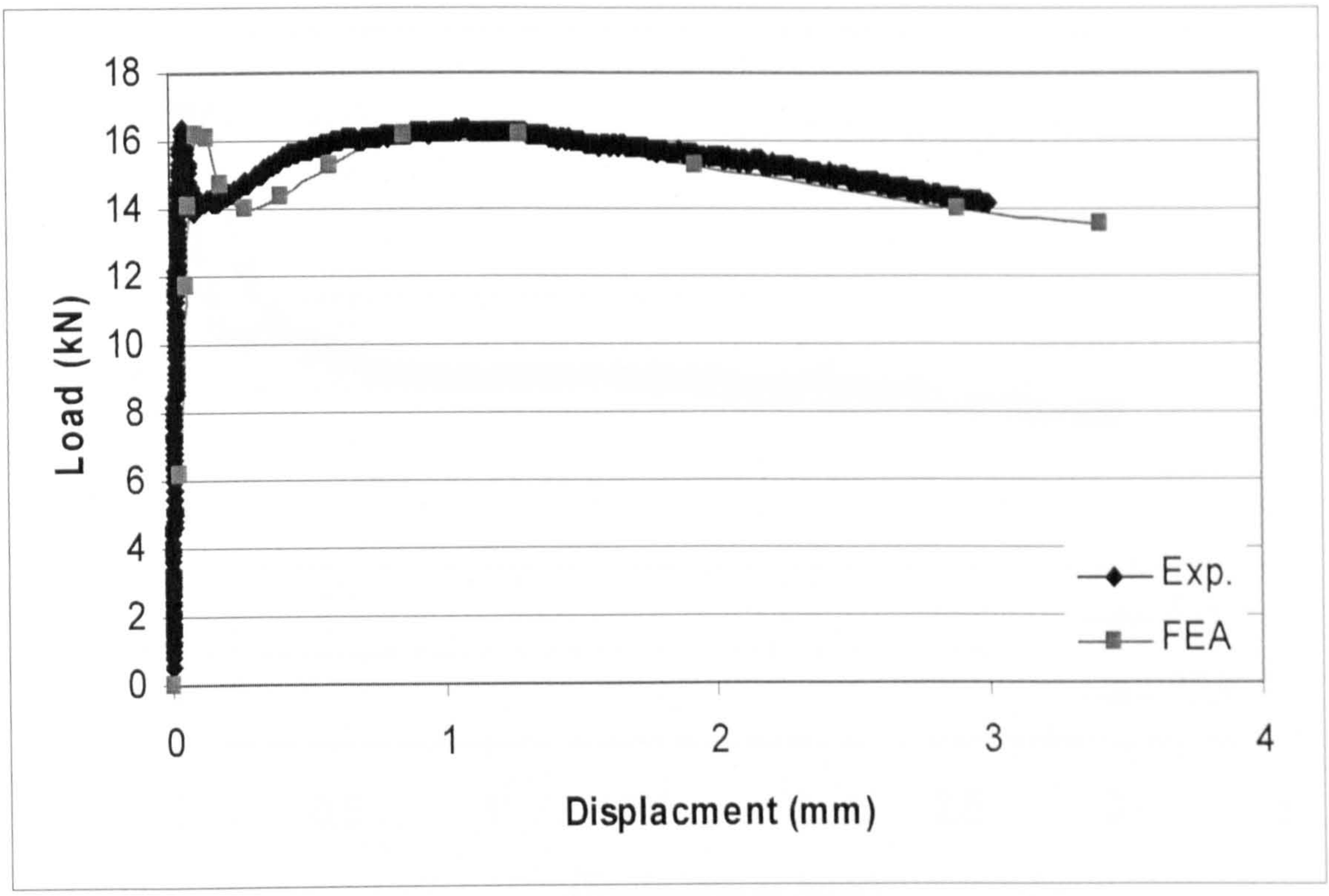

Figure A.30: Experimental and numerical results (beam B30)

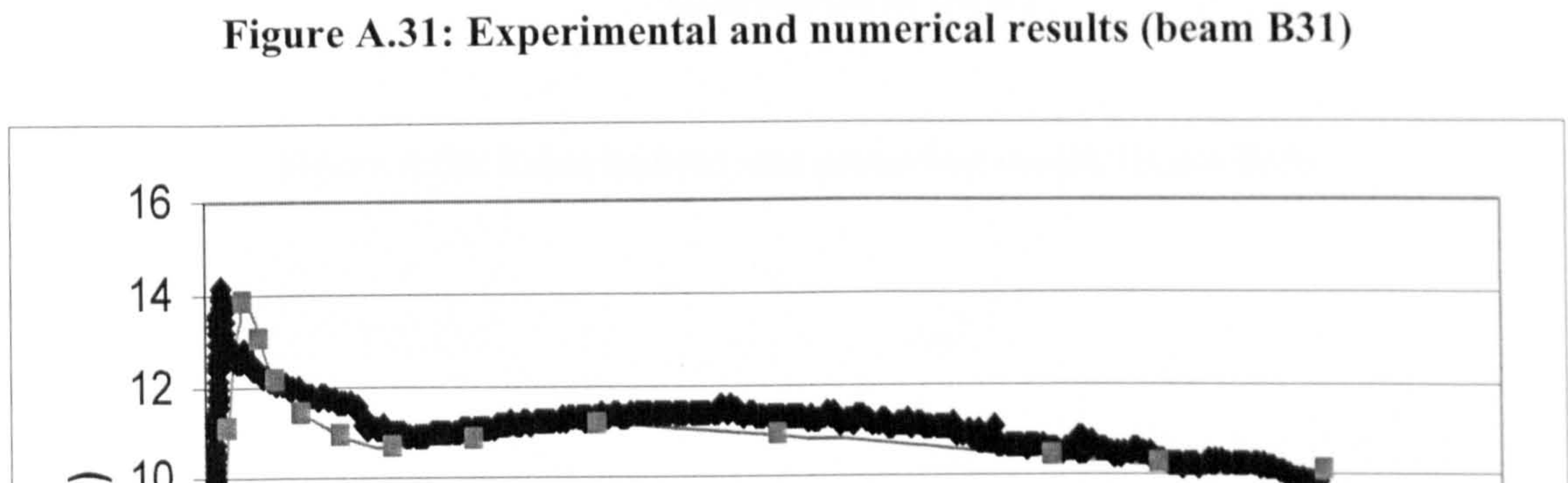

Figure A.31: Experimental and numerical results (beam B31)

Figure A.32: Experimental and numerical results (beam B32)

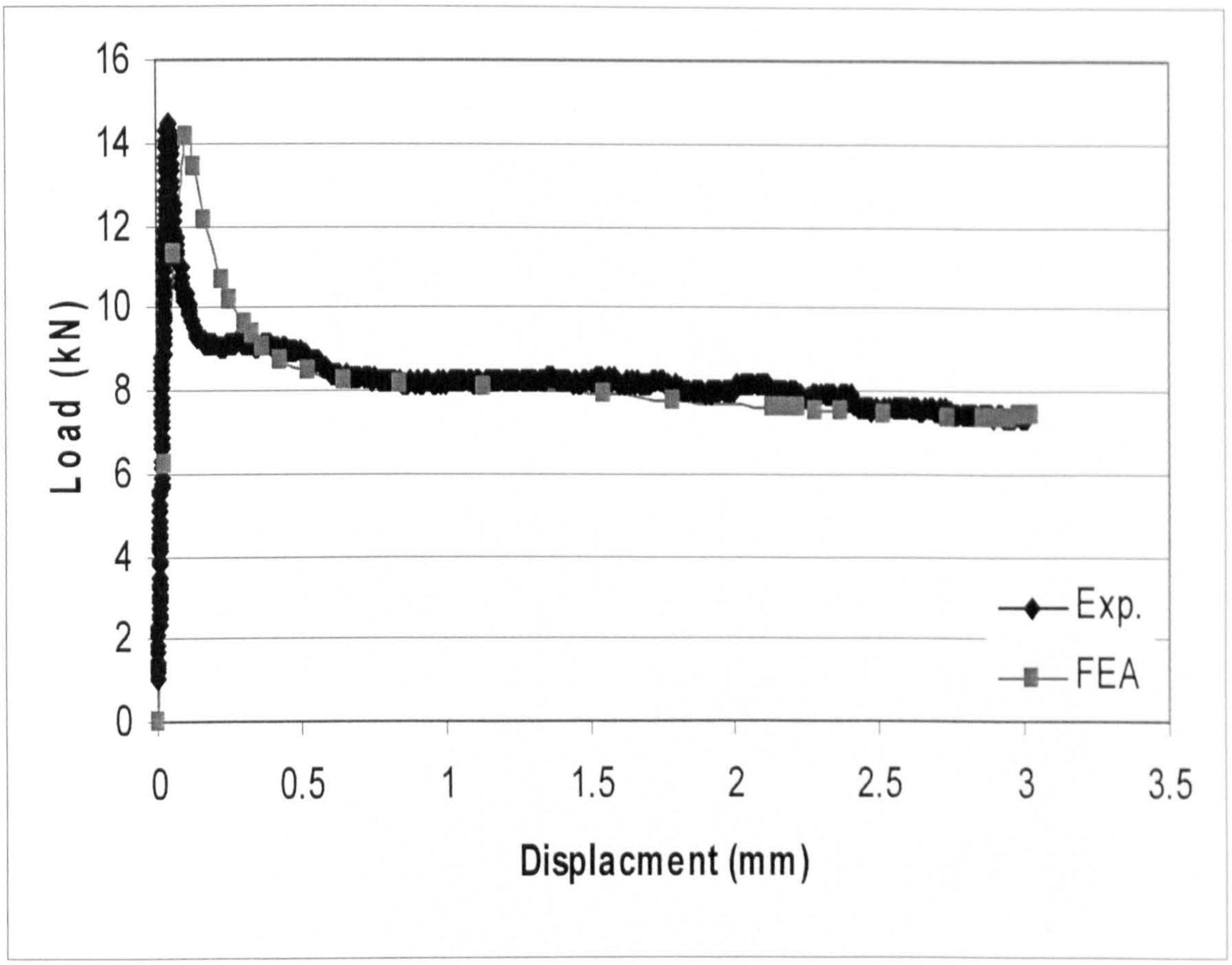

Figure A.33: Experimental and numerical results (beam B33)